TRANSACTIONS
OF THE ASME
Series E

Journal of APPLIED MECHANICS

June 1960

DYNAMICS • VIBRATIONS • ELASTICITY • LUBRICATION AND WEAR
RHEOLOGY • FRACTURES • STRUCTURES • HYDRAULICS • AERODYNAMICS
INTERNAL FLOW • MECHANICAL PROPERTIES OF METALS • THERMODYNAMICS
TURBULENCE • HEAT TRANSFER • COMPUTING DEVICES AND METHODS
BOUNDARY LAYERS • AEROELASTICITY • EXPERIMENTAL STRESS ANALYSIS

Published Quarterly by
THE AMERICAN SOCIETY OF MECHANICAL ENGINEERS

TRANSACTIONS OF THE ASME
Series E

EDITORIAL DEPARTMENT

Editor, J. J. JAKLITSCH, JR.
Consulting Editor, LEO BLODGETT
Art Editor, HENRY BALFOUR
Production, HILDA K. WILGUS

APPLIED MECHANICS DIVISION

Chairman, S. B. BATDORF
Secretary, A. M. WAHL
Technical Editor, D. C. DRUCKER
Technical Editor, J. KESTIN
Honorary Editor, JOHN M. LESSELLS

OFFICERS OF THE ASME

President, W. L. CISLER
Secretary, O. B. SCHIER, II
Treasurer, E. J. KATES
Assistant Treasurer, H. J. BAUER

PUBLICATIONS COMMITTEE

Chairman, B. G. A. SKROTZKI
HENDLEY M. BLACKMON
R. D. MINDLIN
MARTIN GOLAND
VITO L. SALERNO

Junior Representatives
A. S. GOLDSTEIN
J. W. FOLLANSBEE

REGIONAL ADVISORY BOARD

Region I, H. B. ROGERS, JR.
Region II, GLENN R. FRYLING
Region III, F. J. HEINZE
Region IV, FRANCIS C. SMITH
Region V, H. M. CATHER
Region VI, C. R. EARLE
Region VII, M. S. UMBENHAUER
Region VIII, CARL J. ECKHARDT

Published quarterly by The American Society of Mechanical Engineers. Publication office at 20th and Northampton Streets, Easton, Pa. The editorial department is located at the headquarters of the Society, 29 West Thirty-Ninth Street, New York 18, N. Y. Cable address, "Mechaneer," New York. Price $3.00 a copy, $10.00 annually; to members, $1.50 a copy, $5.00 annually. Add 50 cents for postage to all countries outside the United States and Canada. Changes of address must be received at Society headquarters seven weeks before they are to be effective on the mailing list. Please send old as well as new address. . . . By-Law: The Society shall not be responsible for statements or opinions advanced in papers or . . . printed in its publications (B13, Par. 4). . . . Second-class mail privileges authorized at Easton, Penna. . . . This publication is authorized to be mailed at the special rates of postage prescribed by Section 132.122. © Copyrighted, 1960, by The American Society of Mechanical Engineers. Reprints from this publication may be made on condition that full credit be given the Transactions of the ASME, Series E—Journal of Applied Mechanics, and the author, and that date of publication be stated.

TRANSACTIONS OF THE ASME
is indexed by the Engineering Index, Inc.

Journal of APPLIED MECHANICS

VOLUME 27 • SERIES E • NUMBER 2
June 1960

CONTENTS

TECHNICAL PAPERS

223 **Note on the Assessment of Flow Disturbances at a Blunt Body Traveling at Supersonic Speeds Owing to Flow Disturbances in Free Stream**
M. V. Morkovin

230 **Possible Similarity Solutions for Laminar Free Convection on Vertical Plates and Cylinders**
Kwang-Tzu Yang

237 **On the Annular Damper for a Freely Precessing Gyroscope**
G. F. Carrier and J. W. Miles

241 **Heat Transfer for Laminar Flow in Ducts With Arbitrary Time Variations in Wall Temperature**
Robert Siegel

250 **A Study of the Stability of Externally Pressurized Gas Bearings**
Lazar Licht and Harold Elrod

259 **On the Theoretical Analysis of a Dynamic Thermocouple: 2—The Continuous Area Interface**
W. F. Hughes and E. W. Gaylord

263 **Normal Modes of Nonlinear Dual-Mode Systems**
R. M. Rosenberg

269 **Classical Normal Modes in Damped Linear Dynamic Systems**
T. K. Caughey

272 **The Vibration Response of a Linear Undamped System Resting on a Nonlinear Spring**
P. R. Paslay and M. E. Gurtin

275 **The Approximate Analysis of Certain Boundary-Value Problems**
H. D. Conway

278 **Stresses in a Slab Having a Spherical Cavity Under Circular Bending**
Chih-Bing Ling and Chen-Peng Tsai

283 **Elastic Equilibrium of a Plate With a Reinforced Elliptical Hole**
Eugene Levin

289 **A Method of Solution for the Elastic Quarter-Plane**
M. Hetényi

297 **Thermal Stress in a Viscoelastic-Plastic Plate With Temperature-Dependent Yield Stress**
H. G. Landau, J. H. Weiner, and E. E. Zwicky, Jr.

303 **Prediction of Creep Failure Time for Pressure Vessels**
F. P. J. Rimrott, E. J. Mills, and Joseph Marin

309 **On the Plastic Behavior of Rotating Cylinders**
F. P. J. Rimrott

316 **On the Optimum Design of Shells**
R. T. Shield

323 **Yield Conditions for Rotationally Symmetric Shells Under Axisymmetric Loading**
P. G. Hodge, Jr.

332 **An Approximate Analysis of the Influence of Aerodynamic Heating and Initial Twist on the Torsional Stiffness of Thin Wings**
L. S. Han

CONTENTS

335 **Postbuckling Behavior of Rectangular Plates With Small Initial Curvature Loaded in Edge Compression—(continued)**
Noboru Yamaki

343 **The Junction Problem of Solid-Slotted Cylindrical Shells**
D. H. Cheng and N. A. Weil

BRIEF NOTES

Method of Numerical Evaluation of a Large Determinant 350
F. R. E. Crossley and U. Germen

On the Griffith-Irwin Fracture Theory 352
J. L. Sanders, Jr.

On the Flexure of Plastic Plates 353
S. Lerner and W. Prager

Induced Velocities in Two-Dimensional Cascade Theory 355
J. Polasek

Relation Between Stress Concentration and Boundary Displacement 356
J. S. Brock

Bending of an Isotropic Triangular Plate 357
B. D. Aggarwala

Simplified Analysis of a Thrust-Augmentation System 358
K. L. Bergman

Stress Concentration in a Rotating Disk 359
Ta-Cheng Ku

DISCUSSION

361 Discussion of previously published papers by *M. V. Newman; M. V. Morkovin; P. G. Hodge, Jr., and R. Sankaranarayanan; Joseph Marin; R. R. Berlot; Norman Davids; T. Gillespie and A. W. Gunter; J. W. Dally, W. F. Riley, and A. J. Durelli; T. K. Caughey; H. H. Bleich and O. W. Dillon, Jr.; H. D. Conway; P. S. Theocaris; D. S. Johnson; R. P. Kanwal; Yu-Yuan Yi; C. W. Nelson; A. E. Bryson*

BOOK REVIEWS

Compact Heat Exchangers 377
Hyperstatic Structures 377
Mechanism and Motion 377
Hypersonic Flow Theory 378
Hypersonic Aerodynamics 378
Plastic Analysis of Structures 378
Practical Photoelasticity 379
Statistical Physics 379
Turbulent Flows and Heat Transfer 379

TRANSACTIONS OF THE ASME Series C

Journal of HEAT TRANSFER

Vol. 82 • Series C • No. 2

CONTENTS FOR MAY, 1960

77 Heat Transfer From Transverse and Yawed Cylinders in Continuum, Slip, and Free Molecule Air Flows, by L. V. Baldwin, V. A. Sandborn, and J. C. Laurence. (58—A-202 and 59—HT-5)

87 Magnetohydrodynamic Effects Upon Heat Transfer for Laminar Flow Across a Flat Plate, by R. D. Cess. (59—HT-14)

94 Conical Turbulent Boundary Layer Experiments and a Correlation With Flat Plate Data, by W. S. Bradfield. (59—HT-6)

101 The Influence of Free Stream Turbulence on the Local Heat Transfer From Cylinders, by R. A. Seban. (59—HT-3)

108 Heat Transfer to Fully Developed Laminar Flow in a Circular Tube With Arbitrary Circumferential Heat Flux, by W. C. Reynolds. (59—HT-13)

113 Steam Slip—Theoretical Prediction From Momentum Model, by S. Levy. (59—HT-15)

125 Pressure Drop and Heat Transfer in a Duct With Triangular Cross Section, by E. R. G. Eckert and T. F. Irvine, Jr. (59—HT-10)

139 Heat Transfer in Flow Through Rotating Ducts, by C. Y. Kuo, H. T. Iida, J. H. Taylor, and F. Kreith. (59—HT-12)

TECHNICAL BRIEF

152 Comparison of Turbulent Heat-Transfer Results for Uniform Wall Heat Flux and Uniform Wall Temperature, by R. Siegel and E. M. Sparrow.

TRANSACTIONS OF THE ASME Series B

Journal of ENGINEERING FOR INDUSTRY

Volume 82 • Series B • Number 2

CONTENTS FOR MAY, 1960

87 Simplified Approach to Understanding the Suction Problems for Reciprocating Mud Pumps, by W. E. Liljestrand. (59—Pet-23)

93 Prevention of Sulfide-Stress Cracking in Sour-Condensate Well Equipment, by W. J. McGuire and L. W. Vollmer. (59—Pet-36)

103 Overstrain Tests on Thick-Walled Cylinders, by S. M. Jorgensen. (59—Pet-1)

122 An Analytical Study of Drill-String Vibration, by J. J. Bailey and I. Finnie. (59—Pet-15)

129 An Experimental Study of Drill-String Vibration, by I. Finnie and J. J. Bailey. (59—Pet-16)

136 The Theory of the Ideal Design of a Compound Vessel, by S. J. Becker and L. Mollick. (59—A-125)

143 The Strength of Thick Cylinders Subjected to Repeated Internal Pressure, by J. L. M. Morrison, B. Crossland, and J. S. C. Parry. (59—A-167)

154 The Interaction of Textile Structures and High-Speed Textile Processes, by H. M. Morgan. (59—A-115)

159 Effect of Transient Loads on the Refrigerated-Space Temperature of a Cooling Complex, by C. F. Kayan. (59—A-181)

167 Uniform Two-Way Orientation of Plastic Films, by M. O. Longstreth and Turner Alfrey, Jr. (59—1-113)

TRANSACTIONS OF THE ASME Series A

Journal of
ENGINEERING FOR POWER

Volume 82 • Series A • Number 2

CONTENTS FOR APRIL, 1960

83 Critical Flow Velocities for Collapse of Reactor Parallel-Plate Fuel Assemblies, by D. R. Miller.
96 The Propeller Turbines of the St. Lawrence Power Project, by G. G. Fintak. (59—Hyd-11)
103 Influence of Trailing-Edge Geometry on Hydraulic-Turbine-Blade Vibration Resulting From Vortex Excitation, by Gunnar Heskestad and D. R. Olberts. (59—Hyd-7)
111 Water-Hammer Damage to Oigawa Power Station, by C. C. Bonin. (59—Hyd-8)
120 An Experimental Investigation of Radial Thrust in Centrifugal Pumps, by A. Agostinelli, D. Nobles, and C. R. Mockridge. (59—Hyd-2)
127 Design and Test of Mixed-Flow and Centrifugal Impellers, by J. J. Kramer, W. M. Osborn, and J. T. Hamrick. (59—Hyd-20)
136 Volute Pressure Distribution, Radial Force on the Impeller, and Volute Mixing Losses of a Radial Flow Centrifugal Pump, by H. W. Iversen, R. E. Rolling, and J. J. Carlson. (59—Hyd-10)
145 Relationship of Coal-Ash Viscosity to Chemical Composition, by W. L. Sage and J. B. McIlroy. (59—Fu-4)
156 Pressurization of Granular Solid Fuels, by M. N. Arafat. (59—A-150)

TRANSACTIONS OF THE ASME Series D

Journal of
BASIC ENGINEERING

Vol. 82 • Series D • No. 2

CONTENTS FOR JUNE, 1960

251 The Fluids Engineering Laboratory at the University of Michigan, by G. V. Edmonson. (59—Hyd-16)
257 Flow Parameters in Hydrostatic Lubrication for Several Bearing Shapes, by S. Raynor and A. Charnes. (59—SA-61)
265 A General Method for Correlating Labyrinth-Seal Leak-Rate Data, by F. E. Heffner. (59—Lub-7)
276 Hydrostatic Gas Bearings, by J. H. Laub. (59—Lub-1)
287 Effect of Hardness, Surface Finish, and Grain Size on Rolling-Contact Fatigue Life of M-50 Bearing Steel, by R. A. Baughman. (59—Lub-11)
295 The Importance of Spinning Friction in Thrust-Carrying Ball Bearings, by G. S. Reichenbach. (59—Lub-9)
302 The Effect of Ball Bearing Steel Structure on Rolling Friction and Contact Plastic Deformation, by R. C. Drutowski and E. B. Mikus. (59—Lub-2)
309 A General Theory for Elastically Constrained Ball and Radial Roller Bearings Under Arbitrary Load and Speed Conditions, by A. B. Jones. (59—Lub-10)
321 A Sommerfeld Solution for Finite Bearings With Circumferential Grooves, by J. V. Fedor. (59—Lub-4)
327 Bearing Oil-Ring Performance, by D. C. Lemmon and E. R. Booser. (59—Lub-5)
335 Torque Produced by Misalignment of Hydrodynamic Gas-Lubricated Journal Bearings, by J. S. Ausman. (59—Lub-3)
342 Friction Characteristics of Sliding Surfaces Undergoing Subsurface Plastic Flow, by M. C. Shaw, A. Ber, and P. A. Mamin.
347 Machining Characteristics of Leaded Steel, by F. L. Bagley, Jr., and R. Mennell.
360 A General Flow Graph Technique for the Solution of Multiloop Sampled Systems, by R. Ash, W. H. Kim, and G. M. Kranc. (59—NAC-1)
371 Control System Analysis and Design Via the "Second Method "of Lyapunov, Part I, by R. E. Kalman and J. E. Bertram. (59—NAC-2)
394 Control System Analysis and Design Via the "Second Method" of Lyapunov, Part II, by R. E. Kalman and J. E. Bertram. (59—NAC-3)
401 Relations Between the Notch Tensile Strength of Cylindrical and Prismatic Specimens of Titanium Alloys and Heat-Treated Steels, by G. Sachs, J. G. Sessler, R. F. Pray, and T. H. Yeh. (59—Met-2)
411 Nonmetallic Inclusions and Fracture Behavior of Steels, by S. Yukawa. (59—Met-10)
417 Fracture Mode Transition for a Crack Traversing a Plate, by G. R. Irwin.
426 Use of the Moiré Effect to Measure Plastic Strains, by A. Vinckier and R. Dechaene. (59—Met-7)
435 A Generalization of Cumulative Damage, by R. M. Mains. (59—Met-1)
441 Effect of Relaxation on the Behavior of Materials Under Combined Alternating and Static Stress, by F. H. Vitovec. (59—Met-3)
447 Cyclic Operation of Pressure Piping With γ Heating, by K. R. Merckx. (59—Met-4)
453 Creep Rupture Tests for Design of High-Pressure Steam Equipment, by E. A. Davis. (59—Met-14)
462 Steady Creep of a Tube Under Combined Bending and Internal Pressure, by Iain Finnie. (59—Met-5)
465 Effect of Wall Thickness on Stress-Rupture Life of Tubular Specimens, by J. T. Tucker, Jr., E. E. Coulter, and L. F. Kooistra. (59—Met-11)
477 Design of Pressurized Cylinders for High-Temperature Applications, by J. F. Traexler. (59—Met-8)
482 The Response of a Pressure-Sensing System, by R. P. Benedict. (59—A-289)
489 Dynamics of Heat Exchangers and Their Models, by Herman Thal-Larsen. (59—A-117)

Note on the Assessment of Flow Disturbances at a Blunt Body Traveling at Supersonic Speeds Owing to Flow Disturbances in Free Stream[2]

M. V. MORKOVIN[1]
Department of Aeronautics,
The Johns Hopkins University,
Baltimore, Md.
Mem. ASME

For the purposes of assessing the magnitude of flow disturbances which would affect conditions on a blunt nose of a body moving at supersonic speeds, the detached shock is approximated by a purely normal shock. The disturbances downstream of the shock are expressed in terms of the "free-stream" disturbances by considering sinusoidal fluctuations. Pressure fluctuations generated by interactions of entropy-temperature disturbances with the normal shock may be considerable at high Mach numbers, but their effect on the transition of a laminar boundary layer to a turbulent one is a matter of speculation. However, conjectures that reflections of such pressure waves between the body and the shock wave might lead to high resonant amplifications are definitely disproved.

Introduction

When a strong shock wave is perturbed from its equilibrium configuration, the field downstream of the shock can be thought of as being composed of the original field plus perturbation fields of (*a*) entropy, (*b*) vorticity, and (*c*) pressure and irrotational velocity ("sound"). If the perturbations are small, the three resulting fields are computable from separate systems of linear partial differential equations, connected only through the boundary conditions on the shock wave and solid boundaries.[3] Because of the linearity of these equations it is convenient to represent the perturbation field as a three-dimensional Fourier integral (see Batchelor [1][5]), and reduce the problem by treating individual Fourier "components." This approach, for instance, has been applied successfully to the problem of the interaction of a single vortex and a shock wave by Ram and Ribner [2].

The present note is concerned with assessing the magnitude of flow disturbances outside of the viscous layer which would affect conditions on a blunt nose of a body moving at supersonic speeds. For this limited objective it is permissible to approximate the detached shock by a normal shock wave. Nonuniformities in the atmosphere ahead of a missile or in the air upstream of a model in a wind tunnel or shock tube constitute the disturbing fields which interact with the shock wave. The Fourier components, simulating this field, are characterized by their amplitude, frequency, and orientation. From studies of the work of Chang [3, 9], Ribner [4, 5], and Moore [6], one can assess the general effects of the orientation of the disturbing (incoming) waves. For the problem at hand, i.e., estimate of magnitudes, it then appears conservative to consider the disturbing waves to be parallel to the normal shock wave. The problem then reduces to

[1] Also, Principal Scientist, Aerophysics Research Staff, The Martin Company, Manned Vehicle Division, Baltimore, Md.

[2] A revised version of a 1957 report prepared for the Missile and Ordnance Systems Department of the General Electric Company, Philadelphia, Pa.

[3] The decomposition into the separate perturbation fields and their governing equations are derived rather simply in the first section of reference [8].[4]

[4] Numbers in brackets designate References at end of paper.

[5] Reference [1], pp. 28, et seq.

For presentation at the Summer Conference of the Applied Mechanics Division, University Park, Pa., June 20–22, 1960, of THE AMERICAN SOCIETY OF MECHANICAL ENGINEERS.

Discussion of this paper should be addressed to the Secretary, ASME, 29 West 39th Street, New York, N. Y., and will be accepted until July 22, 1960, for publication at a later date. Discussion received after the closing date will be returned.

NOTE: Statements and opinions advanced in papers are to be understood as individual expressions of their authors and not those of the Society. Manuscript received by ASME Applied Mechanics Division, February 27, 1959. Paper No. 60—APM-10.

Nomenclature

$a_{(7a)}$ = amplitudes of dimensionless sinusoidal disturbances identified by subscript
A = speed of sound
C_p = specific heat at constant pressure
C_v = specific heat at constant volume
d = detachment distance of shock from body, Fig. 4.
F = multiplying factor, expressing damping of sound wave due to reflection from body
M = local mean Mach number
k = wave number of entropy fluctuations, Equations (5)
l = wave number of sound fluctuations, Equations (5)
j_2, k_2, l_2, m_2 = phase shifts of fluctuations due to body presence, Equation (9)
$P_{\Sigma 2} = \Pi_{\Sigma 2} - \Pi_{\Sigma 1}$
p = pressure fluctuation, nondimensionalized, Equation (1*a*); also known as condensation
p_m = local mean absolute pressure

(Continued on next page)

an algebraic one. For this normal orientation, the vorticity field[6] vanishes, of course.

In the first part of the note, the ratio of amplitudes of the (downstream) generated pressure waves and entropy waves to the amplitude of the disturbing or "forcing" wave (upstream) are found as if the body causing the shock wave were absent. However, there are reflections and rereflections from any body (or conditions at downstream infinity) which influence the shock-wave distortion and hence the level of disturbances. Such reflected field could have an attenuating or an enhancing effect. The second half of the note is then concerned with the possibility of having resonance by reflection from a flat front of the body to the shock. For this purpose, upstream traveling pressure waves in the subsonic detached flow are introduced. They are again assumed parallel to the shock wave. The expectation is that the deviation from flatness and normality will cause scattering of the waves (rather than focusing) so that the assumed simplified case would represent the most conservative estimate. Since this special reflection will be seen incapable of producing resonance, the more realistic models should yield more moderate results.

Finally, the missile or model may be vibrating, as a result of earlier fast application of forces. Should the blunt surface oscillate about its mean position, pressure waves would be generated and propagated upstream toward the head shock. Once more, reflections and rereflections will be seen incapable of building up resonances in the (conservative) case of plane waves.

For the purposes of the present assessment, real gas effects can be neglected. Consequently, the computations were based on tables of reference [7].

Transfer Relations Across a Normal Shock Wave

It is most convenient to nondimensionalize the perturbation fields on either side of the shock with respect to the local mean flow properties, which are denoted by subscripts m_1 and m. In what follows we shall use Chang's notation [3] and denote the upstream perturbation variables by subscripts minus and the downstream ones by plus, Fig. 1.

If the perturbation fields are represented as increments δp, δS, δu, and so on, from the mean values, we have for the nondimensional perturbation fields[7]

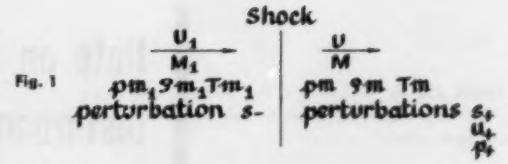

Fig. 1

$$p(x, t) = \frac{\delta p}{\gamma p_m}, \qquad \gamma = \text{adiabatic exponent} = \frac{C_p}{C_v} \tag{1a}$$

$$s(x, t) = \frac{\delta S}{C_p} \qquad C_p = \text{specific heat at constant pressure} \tag{1b}$$

$$u(x, t) = \frac{\delta u}{A_m} \qquad A = \text{speed of sound} \tag{1c}$$

Furthermore, let the yz-plane be located on the mean position of the shock so that the displacement perturbation of the shock is the "small" quantity $x_s = \psi(t)$. Then the linearized equations for conservation of mass, of momentum in the x-direction, and of energy for the unsteady shock can be solved for the perturbations immediately downstream of the shock:

$$s_+ = \Lambda_{11}s_- + \Lambda_{12}p_- + \Lambda_{13}u_- + \Pi_{11}\frac{1}{A_m}\frac{\partial \psi}{\partial t} \tag{2a}$$

$$p_+ = \Lambda_{21}s_- + \Lambda_{22}p_- + \Lambda_{23}u_- + \Pi_{21}\frac{1}{A_m}\frac{\partial \psi}{\partial t} \tag{2b}$$

$$u_+ = \Lambda_{31}s_- + \Lambda_{32}p_- + \Lambda_{33}u_- + \Pi_{31}\frac{1}{A_m}\frac{\partial \psi}{\partial t} \tag{2c}$$

where all quantities are evaluated at $x = 0-$ or $0+$, and

$$\Lambda_{11} = \left(\frac{\rho_m}{\rho_{1m}}\right)^3\left(\frac{M}{M_1}\right)^2 - (\gamma - 1)\left(1 - \frac{\rho_m}{\rho_{1m}}\right)M^2$$

$$\Lambda_{21} = \frac{M^2}{1 - M^2}\left\{\left(1 - \frac{\rho_m}{\rho_{1m}}\right)[1 + (\gamma - 1)M^2] + \left[1 - \left(\frac{\rho_m}{\rho_{1m}}\right)^2\left(\frac{M}{M_1}\right)^2\right]\right\}$$

$$\Lambda_{31} = -\frac{M}{1 - M^2}\left\{\left[1 - \left(\frac{\rho_m}{\rho_{1m}}\right)^3\left(\frac{M}{M_1}\right)^2\right] + \left(1 - \frac{\rho_m}{\rho_{1m}}\right)\gamma M^2\right\}$$

[6] For amplification of vorticity fields see Ribner [4] and Werner [10]. Vorticity oriented normally to the shock wave remains unaltered since velocity components parallel to the shock plane are preserved. For sinusoidal vorticity fields parallel to the shock wave, equations (38) of Ribner [4] indicate amplification factors 1 to 3, depending upon the orientation of the shear wave and the Mach number. According to Werner [10], this factor may be somewhat higher when transient rather than uniform sinusoidal disturbances are considered. While such vorticity amplifications through the shock wave do not appear critical, one cannot rule out further amplification (instability) in the stagnation region of the body such as conjectured by Kuethe [11].

[7] Reference [3], p. 2.

Nomenclature

s = dimensionless entropy fluctuation, Equation (1b)
S = entropy
t = time
T = absolute temperature
u = dimensionless velocity fluctuation, Equation (1c)
U = mean flow velocity, Fig. 1
x = co-ordinate in direction of flow, normal to shock and body face; origin at shock
γ = adiabatic exponent, C_p/C_v
Δ_{22} = $\Pi_{21}\Lambda_{31} - \pi_{31}\Lambda_{31}$
Λ_{ij} = transfer functions across shock, defined by Equations (2) and (3)
Π_{ij} = transfer functions across shock, defined by Equations (2) and (3)
ρ = absolute density
ψ = displacement of shock from mean position
ω = circular frequency of fluctuations

Subscripts

1 = undisturbed free stream
$-$ = upstream of shock
$+$ = downstream of shock (including reflections), Fig. 4
m = local mean flow property
prime = pertaining to upstream moving sound wave

$$\Lambda_{12} = (\gamma - 1)\left(1 - \frac{\rho_m}{\rho_{1m}}\right)\left(1 - \frac{1}{M_1^2}\frac{\rho_m}{\rho_{1m}}\right)M^2$$

$$\Lambda_{22} = -\frac{M^2}{1 - M^2}\left\{\left(1 - \frac{\rho_m}{\rho_{1m}}\right) + \left(1 - \frac{1}{M_1^2}\frac{\rho_m}{\rho_{1m}}\right)\left[1 + (\gamma - 1)\left(1 - \frac{\rho_m}{\rho_{1m}}\right)M^2\right]\right\}$$

$$\Lambda_{32} = \frac{M}{1 - M^2}\left\{\left[1 - \left(\frac{\rho_m}{\rho_{1m}}\right)^2\left(\frac{M}{M_1}\right)^2\right] + \gamma\left(1 - \frac{\rho_m}{\rho_{1m}}\right)\left(1 - \frac{1}{M_1^2}\frac{\rho_m}{\rho_{1m}}\right)M^2\right\}$$

$$\Lambda_{13} = (\gamma - 1)\left(1 - \frac{\rho_m}{\rho_{1m}}\right)^2\frac{M^2}{M_1^2} \qquad (3)$$

$$\Lambda_{23} = -\frac{M}{1 - M^2}\left(1 - \frac{\rho_m}{\rho_{1m}}\right) \times \left\{2 + (\gamma - 1)\left(1 - \frac{\rho_m}{\rho_{1m}}\right)M^2\right\}\frac{M}{M_1}$$

$$\Lambda_{33} = \frac{1}{1 - M^2}\frac{M}{M_1}\left\{1 - \left(\frac{\rho_m}{\rho_{1m}}M\right)^2 + \gamma\left(1 - \frac{\rho_m}{\rho_{1m}}\right)^2 M^2\right\}$$

$$\Pi_{11} = -(\gamma - 1)\left(1 - \frac{\rho_{1m}}{\rho_m}\right)^2\left(\frac{\rho_m}{\rho_{1m}}\right)M$$

$$\Pi_{21} = -\frac{M}{1 - M^2}\left(1 - \frac{\rho_{1m}}{\rho_m}\right) \times \left[2 + (\gamma - 1)\left(1 - \frac{\rho_m}{\rho_{1m}}\right)M^2\right]$$

$$\Pi_{31} = \frac{1}{1 - M^2}\left(1 - \frac{\rho_{1m}}{\rho_m}\right) \times \left[1 + M^2 + (\gamma - 1)\left(1 - \frac{\rho_m}{\rho_{1m}}\right)M^2\right]$$

It should be clear from the algebraic complexity of the coefficients in this simplified case why the simplification is desirable and why we take over Chang's complete expressions of the transfer relationships. (When the perturbing waves are not parallel to the original shock, dependence on a lateral dimension (say y) enters with additional terms in equation (2), proportional to $\partial\psi/\partial y$, the local slope of the perturbed shock.[9])

Now, in accordance with our discussion in the introductory section, we can consider single Fourier components of the disturbing field, and the "response" to them. As an illustration we take a shock wave (missile) moving at speed U_1 through an atmosphere which has small variations in absolute static temperature, δT. Placing the origin of the co-ordinates on the shock wave, we see entropy disturbances approaching as function of time:

$$s_- = \frac{\delta S}{C_p} = \frac{\delta T}{T_{1m}} = -\frac{\delta\rho}{\rho_{1m}} \qquad (4)$$

The last parts of equation (4) stem from the linearization of the equation of state for constant pressure. In this co-ordinate system the linearized differential equations of motion tell us that the entropy wave is convected with the apparent speed U_1 toward the shock so that we may set for our forcing function:

$$s_- = a_{s-}e^{i(x - U_1 t)k_-} \qquad (5a)$$

where k_- is a measure of the "size" of the temperature (wave number) spots and a_{s-} is the "driving amplitude." There being no motion or sound disturbance in the "atmosphere" upstream of the shock, p_- and u_- in equation (2) disappear. Thus one expects that the responses s_+, p_+, u_+, and $\partial\psi/\partial t$ evaluated at the shock wave, $x = 0_+$, will have the time variation $e^{-iU_1 t k_-}$. The entropy disturbance s_+ downstream of the shock is again convected with the mean stream, now denoted U without subscript, so that it must have the form

$$s_+ = a_{s+}e^{i(x - Ut)k_+} \qquad (5b)$$

The scale of the entropy spots is given by k_+ which is related to k_- by $k_+U = k_-U_1$. The response amplitude a_{s+}, however, cannot be found without solving for the derivative of the shock displacement, $\partial\psi/\partial t$. The displacement $\psi(t)$ must have the form

$$\psi = ia_\psi e^{-iU_1 k_- t} \qquad (5c)$$

Since the amplitude a_ψ is unknown, we must use all three equations (2) simultaneously. For pressure velocity waves traveling downstream the velocity of propagation is $(A_m + U)$ relative to the shock so that the nondimensional sound perturbation downstream should have the form

$$p_+ = a_{p+}e^{i[x - (1+M)A_m t]l_+} \qquad (5d)$$

$$u_+ = a_{u+}e^{i[x - (1+M)A_m t]l_+} \qquad (5e)$$

Here, the conditions on the shock, $x = 0$, relate the scale factor l_+ of the sound response to the scale factor of the driving perturbations: $U_1 k_- = (1 + M)A_m l_+$. At first glance, substitution of equations (5) into equations (2) would appear to lead to three equations in four unknowns, a_{s+}, a_ψ, a_{p+}, a_{u+}. However, one must remember that (5d) and (5e) must satisfy the linearized differential equations of motion in the downstream region [as (5b) already does]. For downstream[10] moving waves, both the continuity and the momentum equations yield the same additional piece of information, namely

$$a_{p+} = a_{u+} \qquad (6)$$

In other words, the dimensional form of this equation is the well-known sound relation $\delta p = \rho_m A_m \delta u$. Algebraic manipulations then yield for the amplitude of the sound response:

$$\frac{a_{p+}}{a_{s-}} = \frac{a_{u+}}{a_{s-}} = \frac{\Pi_{23}\Lambda_{31} - \Pi_{31}\Lambda_{23}}{\Pi_{21} - \Pi_{11}} = \frac{\Delta_{23}}{P_{23}} \qquad (7a)$$

$$\frac{a_{s+}}{a_{s-}} = \Lambda_{13} + \frac{\Pi_{11}(\Lambda_{21} - \Lambda_{23})}{\Pi_{21} - \Pi_{31}} \qquad (7b)$$

The important functions

$$\Lambda_{13},\ -\Lambda_{23},\ -\Pi_{21},\ -\Pi_{31} \quad \text{and} \quad \Pi_{21} - \Pi_{11} = P_{23},$$

are shown in Fig. 2, as they vary with Mach number. It can be seen that rapid changes in these functions (or their inverses) occur only in the neighborhood of Mach number unity (where they have no physical significance since the linearized perturbation of the weak shock relations has no meaning). The ratio (7a) is seen to decrease rapidly with Mach number in Fig. 3. We must re-

[8] Here a misprint in Chang's equations was removed.

[9] Reference [3], pp. 10–11.

[10] We note that for waves moving against the stream such as those reflected from a flat body, the space-time factor in (5d) and (5e) would be $e^{i[x - (M-1)A_m t]l}$ and that the amplitudes in (6) would have opposite signs; i.e., there is 180-deg phase shift between the velocity and the pressure waves, since velocity possesses an orientation.

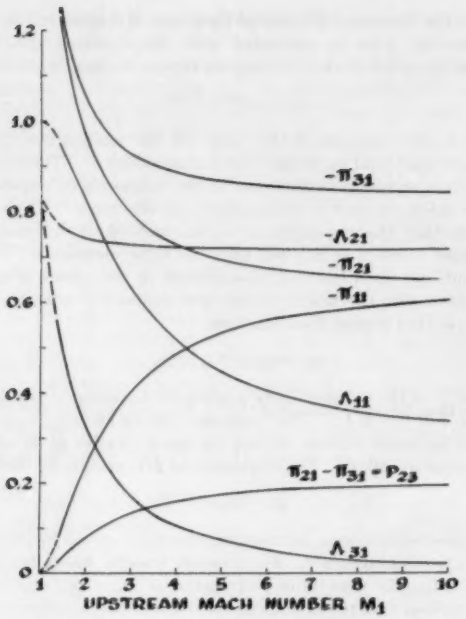

Fig. 2 Transfer functions across shock wave, Equations (2) and (3)

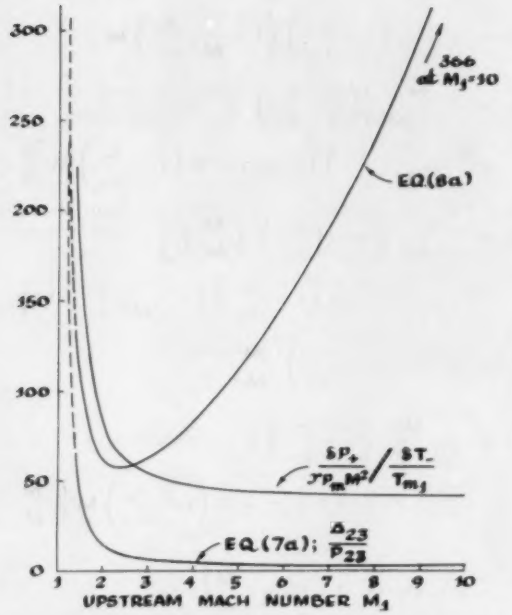

Fig. 3 Sound fluctuations resulting from oncoming entropy fluctuations; various representative ratios

member, however, that the driven amplitudes in equations (7), e.g., a_{p+}, are nondimensionalized with respect to the downstream mean properties, whereas the "driving" amplitude, a_{s-}, is nondimensionalized with respect to upstream conditions. Since conditions in the free stream ahead of the shock are usually used as reference, the additional large ratio of pressure p_m/p_{1m} would enter as a multiplier in equation (7a):

$$\frac{\left|\frac{\delta p_+}{\gamma p_{1m}}\right|}{\left|\frac{\delta T_-}{T_{1m}}\right|} = \frac{\left|\Pi_2\Lambda_{31} - \Pi_{31}\Lambda_{21}\right|}{\left|\Pi_{31} - \Pi_{11}\right|}\frac{p_m}{p_{1m}} \tag{8a}$$

The ratio of the "percentage" disturbances in equation (8a) rises steadily from the values of 57.5 at $M_1 = 2.5$ to 148 at $M_1 = 6$ and to 365 at $M_1 = 10$ (using Burcher's [7] tables), largely because of the increasing pressure ratio p_m/p_{1m}, Fig. 3. However, the ratio in (7a) can, in the case of sound-fluctuation response to entropy disturbances be better interpreted as the ratio of the percentage density variations (often called condensation) in the resulting sound and in the "driving" entropy spots:

$$\frac{\delta p_+}{\gamma p_m} = \frac{\delta p_+}{\rho_m} = \frac{\delta \rho_+}{\rho_{1m}}\frac{\rho_{1m}}{\rho_m}, \quad \text{(isentropic)}$$

$$\frac{\delta s_-}{C_p} = -\frac{\delta \rho_-}{\rho_{1m}}, \quad \text{(isobaric)}$$

$$\frac{a_{p+}}{a_{s-}} = \frac{\left|\frac{\delta p_+}{\gamma p_m}\right|}{\left|\frac{\delta s_-}{C_p}\right|} = \left|\frac{\frac{\delta \rho_+}{\rho_m}}{\frac{\delta \rho_-}{\rho_{1m}}}\right| \tag{7a'}$$

This ratio decreases from 8.1 at $M_1 = 2.5$ to 3.5 at $M_1 = 6$ and to 3.1 at $M_1 = 10$. It appears, therefore, that unless unusually large density variations are encountered in the "free stream," the resulting perturbation of density (or particle velocities obtainable via sound relations) will not be excessive. However, if effects on transition to turbulent boundary layer were being considered, one must remember that much lower sound levels promote transition in regions of slow velocity as occur on a blunt nose. Reference of δp_+ to the local dynamic pressure $(\gamma/2)(p_m M^2)$, is then probably more significant, or perhaps $\delta M_+/M_m$. From Fig. 3 we can see that

$$\left|\frac{\delta p_+}{\frac{\gamma}{2}\,p_m M^2}\Big/\frac{\delta T_-}{T_{1m}}\right|$$

is a decreasing function of M_1, approaching 40+ as an asymptote. The actual mechanism through which sound promotes turbulence in a laminar boundary layer is undoubtedly nonlinear in character and is still unknown. And so is the proper parameter or criterion.

Returning to equations (2), one can ask for possible free-stream disturbances other than those of entropy. Significant sound disturbances as such are unlikely to occur (except in wind tunnels where their orientation, however, is not parallel to the shock wave). Variations δu_- at constant pressure or variations in δp_- without motion are both rather artificial. However, solutions similar to (7) are easily obtained. The nondimensional ratios a_{p+}/a_{u-} or a_{p+}/a_{p-} again decrease with M_1, the first similarly to (7a') and the second much faster. (Response to free-stream sound would be a linear superposition of the foregoing.) Thus it appears that the entropy disturbances in free stream represent the significant case.

Effects Due to the Body

Having obtained an estimate of the disturbances downstream of a strong shock for given perturbations of the free stream, the next question is whether the presence of a blunt body can enhance these disturbances through reflections. The entropy and the vorticity perturbations are merely transported downstream in the first-order approximations so that we need be concerned only with reflections of the correlated disturbances of pressure,

density, temperature, and irrotational velocity, designated as sound. In a duct where there are identifiable reflecting areas, such as openings, or bends, resonance may be set up irrespective of the presence of a steady flow through the duct. Since an upstream traveling sound wave does reflect from a shock wave and is in turn rereflected from the blunt part of the body, a similar resonance cannot be ruled out *a priori*. Should such a resonance be possible for the simplified one-dimensional model, a more realistic analysis would be called for. The curvature of the body would tend to scatter the sound, but the curvature of the shock might help to focus it. The variation of free-stream velocity U between the shock and the body (which is safely neglected in the one-dimensional model, since generally U is considerably smaller than the speed of sound A_m) would be likely to spoil the phasing along the wave front and hence diminish any tendencies toward resonance.

We proceed then to set up the equations for the system summarized in Fig. 4. The upstream moving, reflected sound wave is represented by the (correlated) pressure and velocity waves of equal nondimensional amplitude a_{u+}' but opposite sign as mentioned previously.[10] It will be convenient to modify the form of the space-time dependence factor to

$$e^{i\omega\left[\frac{x}{A_m(1-\mathbf{M})}+t\right]},$$

which emphasizes the circular frequency ω rather than the wave number. An additional factor e^{il_2} is introduced in order to account for the phase of the upstream moving sound wave, while e^{il_2} and e^{ik_2} indicate phases of the downstream moving sound and entropy disturbances. The phase of the displacement of the shock wave may also shift from 90 deg., and we shall allow for that by the factor e^{ij_2}. Again, we shall use the important case of the upstream monochromatic entropy disturbance (with zero phase at the shock)

$$s_- = a_{s-}e^{i\omega\left(t-\frac{x}{U_1}\right)} \tag{8}$$

as the principal illustration. The combined response then is represented as

$$s_+ = a_{s+}e^{im_2+i\omega\left(t-\frac{x}{U}\right)} \tag{9a}$$

$$u_+ = a_{u+}e^{il_2+i\omega\left[t-\frac{x}{A_m(1+\mathbf{M})}\right]} + a_{u+}'e^{ik_2+i\omega\left[t+\frac{x}{A_m(1-\mathbf{M})}\right]} \tag{9b}$$

$$p_+ = a_{u+}e^{il_2+i\omega\left[t-\frac{x}{A_m(1+\mathbf{M})}\right]} - a_{u+}'e^{ik_2+i\omega\left[t+\frac{x}{A_m(1-\mathbf{M})}\right]} \tag{9c}$$

$$\psi = ia_\psi e^{ij_2+i\omega t} \tag{9d}$$

Since these expressions already satisfy the governing differential equations, it remains to put down the boundary conditions at the shock and on the body. Substitution of equations (9) into the transfer equations (2) across the shock at $x = 0$ yield the conditions

$$a_{u+}e^{il_2} - a_{u+}'e^{ik_2} + \Pi_{21}\frac{\omega}{A_m}a_\psi e^{ij_2} = \Lambda_{21}a_{s-} \tag{10a}$$

$$a_{u+}e^{il_2} + a_{u+}'e^{ik_2} + \Pi_{31}\frac{\omega}{A_m}a_\psi e^{ij_2} = A_{21}a_{s-} \tag{10b}$$

for the velocity and pressure unknowns which form a special subset. The condition on the reflecting body is for the velocity perturbation to vanish at $x = d$:

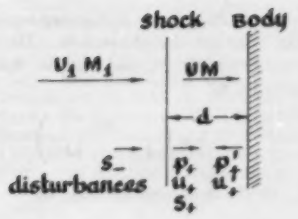

Fig. 4

$$a_{u+}e^{il_2}e^{-\frac{i\omega d}{A_m(1+\mathbf{M})}} + a_{u+}'e^{ik_2}e^{+\frac{i\omega d}{A_m(1-\mathbf{M})}} = 0 \tag{10c}$$

The boundary conditions thus form a system of three complex equations in three complex unknowns or six real equations in the three unknown real amplitudes a_{u+}, a_{u+}', and a_ψ, and the three real relative phases l_2, k_2, and j_2. The condition on the body requires that the amplitudes of the opposite moving sound waves be equal in magnitude

$$a_{u+} = -a_{u+}' \tag{11a}$$

and puts a clamp on their relative phases:

$$l_2 = k_2 + \frac{2\omega d}{A_m(1-\mathbf{M}^2)} + 2n\pi \tag{11b}$$

where n is an arbitrary integer. Elimination of $a_\psi e^{ij_2}$ from (10a) and (10b) leads to the solution equivalent to (7a) of the preceding section, with the body effect added:

$$\frac{a_{u+}e^{ik_2}}{a_{s-}} = \frac{\Delta_{23}}{P_{23}e^{\frac{2i\omega d}{A_m(1-\mathbf{M}^2)}} - P_{23}^+} \tag{11c}$$

where P_{23}^+ represents $\Pi_{21} + \Pi_{31}$ and P_{23} again $\Pi_{21} - \Pi_{31}$. We can now use equations (11) to evaluate the pressure on the body at $x = d$ by substitution into (9c):

$$\frac{p_+(d)}{a_{s-}}e^{-i\omega t}e^{-\frac{i\omega d}{A_m(1-\mathbf{M})}} = \frac{2\Delta_{23}}{P_{23}e^{\frac{2i\omega d}{A_m(1-\mathbf{M}^2)}} - P_{23}^+} \tag{12a}$$

The real part of the equation gives us the desired criterion for the possibility of resonance:

$$\left|\frac{p_+(d)}{a_{s-}}\right| = \frac{2\Delta_{23}}{\left[P_{23}^2 + P_{23}^{+2} - 2P_{23}P_{23}^+\cos\left(\frac{2\omega d}{A_m(1-\mathbf{M}^2)}\right)\right]^{1/2}} \tag{12b}$$

Taking the ratio of this solution in presence of the body to that of (7a) without the body, we can "graft" the body-factor F onto the computed results of the last section:

$$F = \frac{2P_{23}}{\left[P_{23}^2 + P_{23}^{+2} - 2P_{23}P_{23}^+\cos\left(\frac{2\omega d}{A_m(1-\mathbf{M}^2)}\right)\right]^{1/2}}, \tag{13a}$$

As the parameter in the problem, the circular frequency ω changes, the factor F varies between a maximum and a minimum, but never increases without bounds. This can be seen by observing from (12a) that the denominator [proportional to the determinant of the system of equations (10)] represents a vectorial difference of two vectors of magnitude of P_{23} and P_{23}^+ at a relative angle (phase)

$$\frac{2\omega d}{A_m(1-\mathbf{M}^2)}$$

For a duct with flow-through, solved along similar lines, the

vectors are of equal magnitude and resonance corresponds to the frequency which makes the phase zero. Here, the vectors are always of unequal length, P_{22} and $P_{22}{}^{+}$, so that the maxima and minima correspond to

$$\cos\left(\frac{2\omega d}{A_m(1-M^2)}\right)$$

becoming ± 1 in the denominator; i.e., to

$$F_{max} = \frac{P_{22}}{-\Pi_{21}} \tag{13b}$$

$$F_{min} = \frac{P_{22}}{-\Pi_{21}} \tag{13c}$$

A glance at Fig. 5, where F_{max} and F_{min} are plotted, shows us that the pressure fluctuations are heavily damped due to the presence of the body. This effect can be traced to the fact that $|P_{22}{}^{+}|$ is very much larger than P_{22} (sevenfold even at $M_1 = 10$). This in turn is a result of the presence of the shock-displacement terms in equations (10*a*) and (10*b*). Because of this "yielding" of the shock wave, the conditions at the shock are radically different from those at an open or closed end of a duct (which would correspond to vanishing Π_{21} or Π_{21}, respectively). The shock wave in yielding makes impossible a phasing favorable to unlimited build-up of energy in the sound disturbances.

It is of course possible to solve for the rest of the unknowns, but that is now of little interest. Instead, we can surmise from the foregoing physical causes of the damping that no resonance should occur when the body vibrates in such a manner that the blunt face oscillates perpendicularly to itself. The boundary conditions (10*a*) and (10*b*) would be homogeneous with a_{r-} vanishing. The solution, however, would be "driven" by the nonvanishing right side of the boundary condition at the body, namely B, the nondimensional amplitude of the velocity oscillation (now taken as having zero relative phase). The solution then proceeds as before, and

$$\left|\frac{p_+(d)}{B}\right| = \frac{\delta p(d)}{\delta u(d)}\frac{A_m}{\gamma p_m} = \frac{\delta p(d)}{\delta u(d)}\frac{1}{\rho_m A_m}$$

$$= \left|\frac{P_{22}{}^{+} + P_{22}e^{i\frac{\omega d}{A_m(1-M^2)}}}{P_{22}{}^{+} - P_{22}e^{i\frac{\omega d}{A_m(1-M^2)}}}\right| \tag{14}$$

For sound without reflection, the ratio (14) would be unity, according to the usual relation between pressure and velocity in a plane sound wave. Hence the ratio (14) is again a factor which accounts for the reflections and rereflections. The denominator, as expected, is the same as in the preceding case, equation (11*c*). The vector argument then leads to the maxima of (14), namely Π_{21}/Π_{21}, and the minima, namely, Π_{21}/Π_{21}. The first is plotted in Fig. 5. There is little enhancing or damping in this case.

Conclusions

1 The significant disturbances that can be experienced at the body are coupled pressure-density-temperature-velocity disturbances, i.e., sound. In absence of reflections from the body, temperature variations δT_- upstream of a normal shock wave produce sound disturbances according to equivalent equations (7*a*), (7*a'*), (8*a*), and Fig. 3. Free-stream variations of pressure or velocity generate sound of comparable magnitude.

2 For assessment of the actual disturbances in a given case, adequate knowledge of the free-stream disturbances is necessary. Such information can come only from actual measurements in the atmosphere or in the wind tunnel. Furthermore, the effect of the sound disturbance on the boundary layer in the low-speed regions of the blunt body forms a separate problem, concerning which there is scanty experimental[11] and theoretical information.

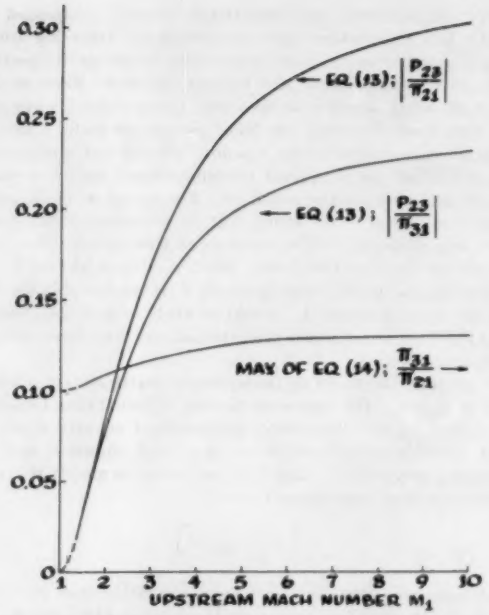

Fig. 5 Multiplying factors resulting from reflections of sound from body, Equation (13), and from longitudinal vibrations of body, Equation (14)

3 The blunt body reflects the sound generated by the shock oscillation and modifies the results of the first section by the factor F of equation (13*a*). The maxima and minima of this factor are displayed in Fig. 5. The phasing of the outgoing and incoming disturbances at the shock, and the phasing of the shock displacement preclude the build-up of resonance.

4 Similar conclusions are valid for the case of the oscillating body, generating pressure waves which are reflected back from the shock wave. The generated waves are then modified by the factor (14) with maxima and minima shown in Fig. 5; i.e., very little.

References

1 G. K. Batchelor, "The Theory of Homogeneous Turbulence," Cambridge University Press, Cambridge, England, 1953.

2 G. S. Ram and H. S. Ribner, "The Sound Generated by Interaction of a Single Vortex With a Shock Wave," 1957 Heat Transfer and Fluid Mechanics Institute, California Institute of Technology, June, 1957.

3 C. T. Chang, "On the Interaction of Weak Disturbances and a Plane Shock of Arbitrary Strength in a Perfect Gas," PhD thesis, The Johns Hopkins University, June 1955, available from SQUID.

4 H. S. Ribner, "Convection of a Pattern of Vorticity Through a Shock Wave," NACA TR 1164, 1954.

[11] At the present time apparently there exist no instruments capable of recording atmospheric disturbances at high altitudes on a scale as small or smaller than the radius of the body; i.e., relevant to the transition and heating problems. For information on free-stream disturbances in supersonic wind tunnels pertinent to the transition problem, see Morkovin [12, 13].

5 H. S. Ribner, "Shock Turbulence Interaction and the Generation of Noise," NACA TR 1233, 1954.

6 F. K. Moore, "Unsteady Oblique Interaction of a Shock Wave with a Plane Disturbance," NACA TR 1165, 1954.

7 M. A. Bureher, "Compressible Tables for Air," NACA TN 1592, 1948.

8 M. V. Morkovin, "Fluctuations and Hot-Wire Anemometry in Compressible Flows," AGARDograph No. 24, 1956.

9 C. T. Chang, "Interaction of a Plane Shock and Oblique Plane Disturbances, With Special Reference to Entropy Waves," *Journal of the Aeronautical Sciences*, vol. 24, 1957, pp. 675–682.

10 J. E. Werner, "Shock Wave-Turbulence Interaction, Investigations in a Shock Tube," AFOSR TR 59–46, AD 214847, Department of Aeronautics, The Johns Hopkins University, May 1959.

11 A. M. Kuethe, "On the Character of the Instability of the Laminar Boundary Layer Near the Nose of a Blunt Body," *Journal of the Aeronautical Sciences*, vol. 25, 1958, pp. 338–339.

12 M. V. Morkovin, "On Supersonic Wind Tunnels With Low Free-Stream Disturbances," JOURNAL OF APPLIED MECHANICS, vol. 26, TRANS. ASME, series E, vol. 81, September, 1959, pp. 319–324.

13 M. V. Morkovin, "On Transition Experiments at Moderate Supersonic Speeds," *Journal of the Aeronautical Sciences*, vol. 24, 1957, pp. 480–486.

Possible Similarity Solutions for Laminar Free Convection on Vertical Plates and Cylinders

KWANG-TZU YANG
Associate Professor,
Department of Mechanical Engineering,
University of Notre Dame,
Notre Dame, Ind.
Assoc. Mem. ASME

In this paper, a study is made of the unsteady laminar boundary-layer equations for free convection on vertical plates and cylinders to establish necessary and sufficient conditions under which similarity solutions are possible. On the basis of these conditions, all possible cases are derived, including those for unsteady conditions. And it is found that the available similarity solutions in the literature have essentially covered all steady cases, except that the present analysis shows that somewhat more general conditions may also be taken in account.

RECENTLY, theoretical studies on laminar free convection on vertical plates and cylinders have received wider attention, especially in dealing with nonuniform surface temperature and heat-flux distributions. However, available in the literature are only a few exact solutions, which have all been derived by using the technique of similarity solution. In such a technique, the pertinent boundary-layer equations, under a suitable transformation, are reduced to a set of ordinary differential equations in terms of a "similarity variable," which is a function of the original independent variables. Then, these simultaneous ordinary equations with proper boundary conditions are solved numerically, yielding velocity and temperature profiles, from which important boundary-layer characteristics are determined.

However, because of the nature of the transformation, these similarity solutions are only valid for certain specific surface conditions. For the vertical-plate problem, Pohlhausen's solution for steady uniform surface temperature is well known [1].[1] More recently, Sparrow and Gregg [2, 3] have provided three more similarity solutions; i.e., steady uniform heat flux at plate surface, plate temperature varying as a power of the distance along the plate, and a surface-temperature variation according to an exponential function of the same distance. In the vertical-cylinder case, there is only one similarity solution available in the literature, and it is recently given by Millsaps and Pohlhausen [4] for a linear variation of cylinder surface temperature with distance along the cylinder.

Since these authors have only dealt with specific cases, it is still uncertain whether or not these authors have exhausted all possible similarity solutions. If they have not, then it is very desirable to find the rest of all possible cases, since they not only would represent additional exact solutions in laminar boundary-layer theory, but could as well be used as a basis for checking the accuracy of other approximate solutions, which are normally applicable to more general problems. Thus it is the purpose of this paper (*a*) to present a unified analysis of the unsteady laminar boundary-layer equations for free convection on vertical plates and cylinders for establishing necessary and sufficient conditions under which similarity solutions are possible, and (*b*) to indicate all possible cases which include not only those which already have appeared in the literature, but also additional new ones. No numerical solutions for these new cases, however, are attempted at the present time. Similar treatments of certain other laminar boundary-layer problems may be found in references [5, 6, and 7]. In the following sections, the problems of vertical plates and vertical cylinders will be dealt with separately.

[1] Numbers in brackets designate References at end of paper.

Contributed by the Applied Mechanics Division and presented at the Annual Meeting, Atlantic City, N. J., November 29–December 4, 1959, of THE AMERICAN SOCIETY OF MECHANICAL ENGINEERS.

Discussion of this paper should be addressed to the Secretary, ASME, 29 West 39th Street, New York, N. Y., and will be accepted until July 10, 1960, for publication at a later date. Discussion received after the closing date will be returned.

NOTE: Statements and opinions advanced in papers are to be understood as individual expressions of their authors and not those of the Society. Manuscript received by ASME Applied Mechanics Division, February 20, 1959. Paper No. 59—A-86.

Nomenclature

$A(x)$, $B(x)$, $C(t)$, $D(t)$, $E(x)$ = arbitrary functions

a_1, a_2, a_3, a_4, a_5, a_6, a_7 = constant parameters for vertical plate

a_8, a_9, a_{10}, a_{11}, a_{12}, a_{13}, a_{14}, a_{15} = arbitrary constants of integration

b_1, b_2, b_3 = constant parameters for vertical cylinder

b_4, b_5 = arbitrary constants of integration

F = dimensionless stream function for cylinder case

f = dimensionless stream function for vertical-plate case

$G \equiv g\beta L^3(\bar{T} - \bar{T}_\infty)/\nu^2$

g = gravitational acceleration

k = thermal conductivity

L = characteristic length of vertical plate

m, n, p = constant parameters

$\bar{Q}$ = cylinder surface heat flow per unit height

$Q \equiv \bar{Q}g\beta\bar{r}_0^3/2\pi\nu^2k$

$\bar{q}$ = vertical-plate surface heat flux

$q \equiv \bar{q}g\beta L^4/\nu^2k$

$\bar{r}$, r = radius variable for cylinder

r_0 = radius of cylinder

$\bar{T}$, T = temperature variable

(*Continued on next page*)

Vertical Plate

Laminar free convection on a vertical plate under the condition of constant properties may be described adequately by the following boundary-layer equations:

$$\frac{\partial \bar{u}}{\partial \bar{t}} + \bar{u}\frac{\partial \bar{u}}{\partial \bar{x}} + \bar{v}\frac{\partial \bar{u}}{\partial \bar{y}} = g\beta(\bar{T} - \bar{T}_\infty) + \nu\frac{\partial^2 \bar{u}}{\partial \bar{y}^2} \tag{1}$$

$$\frac{\partial \bar{u}}{\partial \bar{x}} + \frac{\partial \bar{v}}{\partial \bar{y}} = 0 \tag{2}$$

$$\frac{\partial \bar{T}}{\partial \bar{t}} + \bar{u}\frac{\partial \bar{T}}{\partial \bar{x}} + \bar{v}\frac{\partial \bar{T}}{\partial \bar{y}} = \alpha\frac{\partial^2 \bar{T}}{\partial \bar{y}^2} \tag{3}$$

The space co-ordinates $\bar{x}$ and $\bar{y}$ are shown in Fig. 1, which indicates only the case where $\bar{T}_w$ is higher than $\bar{T}_\infty$. This is the case to which the present analysis is directed. However, it should be clear that, by means of a simple change of the co-ordinate system, the results are also applicable when $\bar{T}_w$ is lower than $\bar{T}_\infty$. The initial condition generally depends on the particular problem, while the boundary conditions are

$$\bar{y} = 0 \quad \bar{u} = \bar{v} = 0 \quad \bar{T} = \bar{T}_w(\bar{x}, \bar{t}) \quad \text{or} \quad \frac{\partial \bar{T}}{\partial \bar{y}} = -\frac{\bar{q}(\bar{x}, \bar{t})}{k}$$
$$\bar{y} = \infty \quad \bar{u} = 0 \quad \bar{T} = \bar{T}_\infty \text{ (const)} \tag{4}$$

By introducing the following dimensionless quantities

$$x = \frac{\bar{x}}{L} \qquad y = \frac{\bar{y}}{L} \qquad t = \frac{\nu \bar{t}}{L^2}$$

$$u = \frac{\bar{u}L}{\nu} \qquad v = \frac{\bar{v}L}{\nu} \qquad G = \frac{g\beta L^3}{\nu^2}(\bar{T} - \bar{T}_\infty)$$

where L is a characteristic length of the plate and G a generalized Grashof number, Equations (1), (2), and (3) become, respectively

$$\frac{\partial u}{\partial t} + u\frac{\partial u}{\partial x} + v\frac{\partial u}{\partial y} = G + \frac{\partial^2 u}{\partial y^2} \tag{5}$$

$$\frac{\partial u}{\partial x} + \frac{\partial v}{\partial y} = 0 \tag{6}$$

$$\frac{\partial G}{\partial t} + u\frac{\partial G}{\partial x} + v\frac{\partial G}{\partial y} = \frac{1}{\sigma}\frac{\partial^2 G}{\partial y^2} \tag{7}$$

with boundary conditions

$$y = 0 \quad u = v = 0 \quad G = G_w(x, t) \quad \text{or} \quad \frac{\partial G}{\partial y} = -q(x, t)$$
$$y = \infty \quad u = 0 \quad G = 0 \tag{8}$$

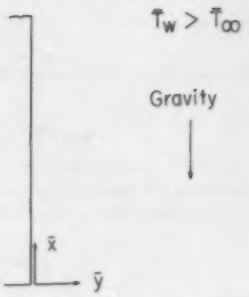

Fig. 1 Space co-ordinate system for vertical plate

The continuity equation (6) is automatically satisfied when a dimensionless stream function ψ is introduced, i.e.

$$u = \frac{\partial \psi}{\partial y} \qquad v = -\frac{\partial \psi}{\partial x}$$

If now we choose a similarity variable η in the form

$$\eta = y\phi_1(x, t) \tag{9}$$

and the following corresponding dependent variables

$$f(\eta) = \frac{\psi(x, y, t)}{\phi_2(x, t)} \qquad \theta(\eta) = \frac{G(x, y, t)}{G_w(x, t)} \tag{10}$$

the present problem reduces to one of determining functions $\phi_1(x, t)$, $\phi_2(x, t)$, and $G_w(x, t)$ such that Equations (5) and (7) are reducible to two ordinary differential equations for $f(\eta)$ and $\theta(\eta)$ with proper boundary conditions from (8). In the analysis to follow, the plate-surface condition is to be restricted to a prescribed temperature variation. However, when later possible similarity solutions are discussed, the corresponding cases for prescribed surface-flux distribution will also be indicated.

With the following identities from Equations (9) and (10)

$$u = \frac{\partial \psi}{\partial y} = \phi_1\phi_2 f' \tag{11}$$

$$v = -\frac{\partial \psi}{\partial x} = -\left[\left(\frac{\partial \phi_2}{\partial x}\right)f + \frac{\phi_2}{\phi_1}\left(\frac{\partial \phi_1}{\partial x}\right)\eta f'\right] \tag{12}$$

$$G = G_w\theta \tag{13}$$

substituted in Equations (5) and (7), where the prime indicates derivative with respect to η, we obtain

$$f''' - a_2\eta f'' - (a_2 + a_5)f' + a_5 ff'' - (a_4 + a_5)(f')^2 + a_1\theta = 0 \tag{14}$$

$$\frac{1}{\sigma}\theta'' - (a_2\eta - a_5 f)\theta' - (a_4 + a_7 f')\theta = 0 \tag{15}$$

Nomenclature

$\bar{l}, l$ = time variable
$\bar{U}, U$ = velocity component in $\bar{Z}$-direction
$\bar{V}, V$ = velocity component in $\bar{r}$-direction
$\bar{u}, u$ = velocity component in $\bar{x}$-direction
$\bar{v}, v$ = velocity component in $\bar{y}$-direction
$\bar{x}, x$ = co-ordinate along plate
$\bar{y}, y$ = co-ordinate normal to plate
$\bar{z}, z$ = co-ordinate along cylinder
α = thermal diffusivity
β = coefficient of volumetric expansion
β, γ = constant parameters
$\Gamma \equiv g\beta\bar{r}_0{}^3(\bar{T} - \bar{T}_\infty)/\nu^2$
$\epsilon \equiv a_3/a_4$
η = similarity variable for vertical-plate case
$\Theta \equiv \Gamma/\Gamma_w$
$\theta \equiv G/G_w$
ν = kinematic viscosity
σ = Prandtl number
Φ, ϕ_1, ϕ_2 = unknown functions
Ψ, ψ = stream functions
$\omega = a_3/a_2$

Subscripts

w = surface conditions
∞ = conditions in the ambient

Superscript:

($'$) = derivatives with respect to the independent variable

where

$$a_1 = \frac{G_w}{\phi_1^5 \phi_2} \tag{16}$$

$$a_2 = \frac{1}{\phi_1^5}\left(\frac{\partial \phi_1}{\partial t}\right) \tag{17}$$

$$a_3 = \frac{1}{\phi_1^5 \phi_2}\left(\frac{\partial \phi_2}{\partial t}\right) \tag{18}$$

$$a_4 = \frac{\phi_2}{\phi_1^4}\left(\frac{\partial \phi_1}{\partial x}\right) \tag{19}$$

$$a_5 = \frac{1}{\phi_1}\left(\frac{\partial \phi_2}{\partial x}\right) \tag{20}$$

$$a_6 = \frac{1}{G_w \phi_1^4}\left(\frac{\partial G_w}{\partial t}\right) \tag{21}$$

$$a_7 = \frac{\phi_2}{G_w \phi_1}\left(\frac{\partial G_w}{\partial x}\right) \tag{22}$$

The boundary conditions (8) with prescribed surface-temperature variation now become, according to Equations (11), (12), and (13)

$$\begin{aligned} f(0) = f'(0) &= 0 \qquad & f'(\infty) &= 0 \\ \theta(0) &= 1 \qquad & \theta(\infty) &= 0 \end{aligned} \tag{23}$$

It is now evident from Equations (14) and (15) that similarity solutions are possible when and only when a_1, a_2, a_3, a_4, a_5, a_6, and a_7 are all constants. Consequently, Equations (16) to (22) inclusive may be regarded as necessary and sufficient conditions for similarity solutions. Since there are more conditions than unknowns, the constants are not all arbitrary. For instance, it may be easily shown that

$$a_6 = 3a_2 + a_3 \qquad a_7 = 3a_4 + a_5 \tag{24}$$

A general method of determining the unknown functions ϕ_1, ϕ_2, and G_w is first to solve for ϕ_1 and ϕ_2 from differential equations (17), (18), (19), and (20). Then Equation (16) yields immediately the surface-temperature variation for which a similarity solution is possible.

Possible Similarity Solutions for Vertical Plates

In this section, all possible similarity solutions for the vertical-plate problem, including those already known in the literature, are to be derived from the afore-established conditions. First treated will be the steady problems, which are then to be followed by unsteady cases.

Case 1—Steady Free Convection With Prescribed Constant Surface Temperature. For this simple case, $a_2 = a_3 = a_4 = a_7 = 0$ and $a_5 = -3a_4$. By eliminating ϕ_2 from Equtions (16) and (19), we have

$$\frac{1}{\phi_1^5}\frac{d\phi_1}{dx} = \frac{a_4 a_1}{G_w}$$

which has a general solution

$$\phi_1 = \left(a_8 - 4\,\frac{a_4 a_1}{G_w}\,x\right)^{-1/4} \tag{25}$$

where a_8 is a constant of integration. Then Equation (16) yields

$$\phi_2 = \frac{G_w}{a_1}\left(a_8 - 4\,\frac{a_4 a_1}{G_w}\,x\right)^{5/4} \tag{26}$$

Even though constants a_1, a_4, and a_8 are all arbitrary, they may, however, be absorbed conveniently in G_w, which is to be specified in the problem. Thus, in letting $a_1 = 1$, $a_4 = -1$, $a_8 = 3$, and $a_8 = 0$, Equations (25) and (26) reduce, respectively, to

$$\phi_1 = \left(\frac{4x}{G_w}\right)^{-1/4} \qquad \phi_2 = G_w\left(\frac{4x}{G_w}\right)^{5/4}$$

and finally we have

$$\begin{aligned} f''' + 3ff'' - 2(f')^2 + \theta &= 0 \\ \frac{1}{\sigma}\,\theta'' + 3f\theta' &= 0 \end{aligned} \tag{27}$$

with boundary conditions indicated in Equations (23). This obviously is the well-known classical solution of Pohlhausen [1].

Case 2—Steady Free Convection with Surface Temperature Varying With Any Power of a Linear Function of x. Since the condition is still steady, $a_2 = a_3 = a_6 = 0$. For this case, it is possible to obtain a general solution to Equations (19) and (20). A combination of these two equations yields

$$\frac{1}{\phi_2}\frac{d\phi_2}{dx} = \frac{\epsilon}{\phi_1}\frac{d\phi_1}{dx}$$

where $\epsilon = a_5/a_4$, and it has a general solution

$$\phi_2 = a_9 \phi_1^{\epsilon} \tag{28}$$

where a_9 is another constant of integration. With Equation (28) substituted in Equation (19), we obtain for the case $\epsilon \neq 1$

$$\begin{aligned} \phi_1 &= \left[a_{10} + \frac{a_4}{a_9}(\epsilon - 1)x\right]^{\frac{1}{\epsilon-1}} \\ \phi_2 &= a_9\left[a_{10} + \frac{a_4}{a_9}(\epsilon - 1)x\right]^{\frac{\epsilon}{\epsilon-1}} \end{aligned} \tag{29}$$

and finally G_w is determined from Equation (16) as

$$G_w = a_1 a_9\left[a_{10} + \frac{a_4}{a_9}(\epsilon - 1)x\right]^{\frac{\epsilon+3}{\epsilon-1}} \tag{30}$$

The case of $\epsilon = 1$ will be treated later. Here constants a_1, a_4, ϵ, a_9, and a_{10} are all arbitrary. However, without loss of any generality, simplification is still possible. Since a_9 is entirely arbitrary and does not appear in the ordinary equation, it is practical to assign a value of positive unity to a_1 without restricting G_w in any way, as indicated in Equation (30). By a similar reasoning, the value of a_4 may also be assigned, leaving ϵ, a_9, and a_{10} as arbitrary constants.[2] For convenience, a new constant n defined by $n = (\epsilon + 3)/(\epsilon - 1)$ is now introduced. Since ϵ is directly related to n by $\epsilon = (n + 3)/(n - 1)$, it is convenient to let

$$a_4 = n - 1 \qquad a_5 = n + 3$$

according to the definition of ϵ. From Equation (24), a_7 is then equal to $4n$. Now the functions ϕ_1, ϕ_2, and G_w have the following final forms:

$$\begin{aligned} \phi_1 &= \left(a_{10} + \frac{4}{a_9}\,x\right)^{\frac{n-1}{4}} \qquad \phi_2 = a_9\left(a_{10} + \frac{4}{a_9}\,x\right)^{\frac{n+3}{4}} \\ G_w &= a_9\left(a_{10} + \frac{4}{a_9}\,x\right)^{n} \end{aligned} \tag{31}$$

Furthermore, Equations (14) and (15) reduce to

[2] Note that the characteristic length L included in x is also arbitrary.

$$f''' + (n+3)ff'' - (2n+2)(f')^2 + \theta = 0$$
$$\frac{1}{\sigma}\theta'' + (n+3)f\theta' - 4nf'\theta = 0 \tag{32}$$

which are to be solved numerically with the boundary conditions in Equations (23). Some boundary-layer characteristics may now be written:

$$u = a_9\left(a_{10} + \frac{4}{a_9}x\right)^{\frac{n+1}{2}} f' \tag{33}$$

$$v = -\left(a_{10} + \frac{4}{a_9}x\right)^{\frac{n-1}{4}} [(n+3)f + (n-1)\eta f'] \tag{34}$$

$$G = a_9\left(a_{10} + \frac{4}{a_9}x\right)^{n} \theta \tag{35}$$

$$q = -\left(a_{10} + \frac{4}{a_9}x\right)^{\frac{5n-1}{4}} \theta'(0) \tag{36}$$

Several special cases are of interest. With $n = a_{10} = 0$, the present solution reduces identically to that of Case 1. Sparrow and Gregg [2] have dealt with the case of uniform surface heat flux and have shown that the resulting surface temperature varies with one-fifth power of the distance away from the leading edge. That this is the case is evident when Equations (35) and (36) are considered with $a_{10} = 0$ and $n = 1/5$. Recently, the same authors [3] have studied a more general problem, which is identical to the present case with $a_{10} = 0$ and arbitrary value of n. This same similarity solution also has been given by Finston [8]. However, only Sparrow and Gregg [3] have carried out the numerical solutions to Equations (32) for several distinct values of n and two values of σ. The present analysis reveals that these numerical results are also directly applicable to cases where a_{10} is nonzero and positive. The physical implication of a nonzero a_{10} is that the surface temperature at the leading edge of the plate is different from that in the ambient, a feature which is certainly more realistic, since it is difficult physically to heat the plate without raising the temperature of its leading edge. However, it should be noted from Equation (33) that for such a case of nonzero a_{10} the velocity component u is not identically zero along $x = 0$, but is only zero at $y = 0$ and $y = \infty$.

It is also of interest to note that, when $n = 1$, and $a_{10} = 0$, a_4 becomes zero, indicating that the similarity variable η is now a pure function of y and the plate-surface temperature varies linearly with the distance from the leading edge. This is analogous to the well-known case of steady forced flow in the neighborhood of the stagnation point of a blunt-nosed cylinder, since the free-stream velocity and the corresponding similarity variable behave in a similar manner.

In view of Equation (36), it is not difficult to notice that the present similarity solution, as has also been remarked by Sparrow and Gregg [3], is equally possible when the plate-surface heat flux, instead of the temperature variation, is prescribed. The condition is that now the surface heat flux q must be of the form

$$q = \left(a_{10} + \frac{4}{a_9}x\right)^{\beta}$$

where β is another constant parameter. If we let $\beta = (5n-1)/4$ or $n = (4\beta+1)/5$, these two problems then become identical.

Case 3—Steady Free Convection With Surface Temperature Varying With an Exponential Function of x. Here again $a_2 = a_5 = a_6 = 0$. With $\epsilon = 1$, Equation (28) becomes $\phi_2 = a_9\phi_1$. Then, Equation (19) may be simply solved, resulting in

$$\phi_1 = a_{11}e^{\frac{a_9}{a_9}x} \tag{37}$$

from which the plate-temperature variation may be written as

$$G_w = a_1 a_9 a_{11}{}^4 e^{\frac{4a_4}{a_9}x} \tag{38}$$

Since the integration constants a_9 and a_{11} are entirely arbitrary, values of a_1 and a_4, without loss of generality, may be assigned. With $a_1 = 1$, $a_4 = 1$, $a_5 = 1$, $a_7 = 4$, Equations (14) and (15) become, respectively,

$$f''' + ff'' - 2(f')^2 + \theta = 0$$
$$\frac{1}{\sigma}\theta'' + f\theta' - 4f'\theta = 0 \tag{39}$$

Boundary conditions are again those given by Equations (23). To put the present case in a final form, we introduce a new constant m such that $m = 4/a_9$ or $a_9 = 4/m$. Then we have

$$\phi_1 = a_{11}e^{\frac{mx}{4}} \qquad \phi_2 = \frac{4}{m}a_{11}e^{\frac{mx}{4}} \qquad G_w = \frac{4}{m}a_{11}{}^4 e^{mx} \tag{40}$$

and

$$u = \frac{4}{m}a_{11}{}^2 e^{\frac{mx}{2}} f' \qquad v = -a_{11}e^{mx}(f + \eta f') \tag{41}$$

$$G = \frac{4}{m}a_{11}{}^4 e^{mx}\theta$$

$$q = -\frac{4}{m}a_{11}{}^5 e^{\frac{5mx}{4}}\theta'(0) \tag{42}$$

This case is identical to that also treated in reference [3] by Sparrow and Gregg.[3] Since in the physical problem m is indeed a parameter, they have expressed surprise that m does not occur in Equations (39). The present analysis shows the exact reason in two ways. One is simply that from Equation (38) values of a_1 and a_4, which do occur in the ordinary equations, may be arbitrarily assigned without restricting G_w in any way. The other reason is that, since it has already been shown in Case 2 that ϵ is a parameter, once the value of ϵ is fixed, this parameter certainly should drop out of the ordinary equations. As pointed out at the beginning of this section, for the present case $\epsilon = 1$.

According to Equation (42), the present similarity solution is again seen to be identical to that of prescribed plate-surface heat flux given by

$$q = \frac{5}{\gamma}a_{11}{}^5 e^{\gamma x}$$

where γ is to be equal to $5m/4$.

Case 4—Unsteady Free Convection With Surface Temperature Varying Inversely as a Linear Combination of x and t. As far as the author is aware, no similarity solution for unsteady free convection on vertical plates exists in the literature. In fact, there are available only a very few analytical studies [9], [10], which, however, all deal with transient problems; i.e. problems with stepwise change in plate temperature or heat flux. The conditions for possible similarity solutions established previously enable us to determine several possible cases under unsteady conditions.

A general solution to Equation (17) is

$$\phi_1 = [A(x) - 2a_9 t]^{-1/2} \tag{43}$$

[3] There is a mistake in their Equation (11*b*), as the constant m should appear in the numerator for the expression of the dimensionless stream function.

where $A(x)$ is yet to be determined. Also, combining Equations (17) and (18) yields

$$\phi_2 = B(x)\phi_1^{\omega}$$

where $B(x)$ is an arbitrary function and $\omega = a_2/a_2$. Thus

$$\phi_2 = B(x)[A(x) - 2a_2 t]^{-\omega/2} \tag{44}$$

A similar combination of Equations (19) and (20) results in

$$\phi_2 = C(t)\phi_1^{\epsilon}$$

where $\epsilon = a_5/a_4$ and $a_4 \neq 0$. The case of $a_4 = 0$ will be treated later. Then Equation (19) may be solved generally, yielding

$$\phi_1 = \left[\frac{a_4(\epsilon - 1)}{C(t)}\, x + D(t)\right]^{\frac{1}{\epsilon-1}} \tag{45}$$

and then ϕ_2 becomes

$$\phi_2 = C(t)\left[\frac{a_4(\epsilon - 1)}{C(t)}\, x + D(t)\right]^{\frac{\epsilon}{\epsilon-1}} \tag{46}$$

When Equations (43), (44), (45) and (46) are compared, a convenient solution is obtainable if the following identities hold:

$$\epsilon = \omega = -1 \qquad A(x) = -\frac{2a_4}{a_{12}}\, x$$

$$B(x) = C(t) = a_{12} \qquad D(t) = -2a_2 t$$

The corresponding G_w may now be written as

$$G_w = \frac{a_1 a_{12}}{\left(-\dfrac{2a_4}{a_{12}}\, x - 2a_2 t\right)} \tag{47}$$

Since a_{12} and the characteristic length L in x are both arbitrary, constants a_1 and a_4 may be arbitrarily assigned. However, a_2 must remain as a parameter in the ordinary equations. With $a_1 = 1$, $a_2 = a_2$, $a_3 = -a_2$, $a_4 = 1$, $a_5 = 1$, $a_6 = 2a_2$, and $a_7 = -2$, Equations (14) and (15) now reduce, respectively, to

$$\begin{aligned} f''' - a_2\eta f'' + ff'' + \theta &= 0 \\ \frac{1}{\sigma}\,\theta'' - (a_2\eta - f)\theta' - (2a_2 - 2f')\theta &= 0 \end{aligned} \tag{48}$$

which are to be solved with the usual set of boundary conditions. Final forms of functions ϕ_1, ϕ_2, and G_w, and boundary-layer characteristics may now be shown:

$$\phi_1 = \left(\frac{2}{a_{12}}\, x - 2a_2 t\right)^{-1/2} \qquad \phi_2 = a_{12}\left(\frac{2}{a_{12}}\, x - 2a_2 t\right)^{1/2}$$

$$G_w = \frac{a_{12}}{\left(\dfrac{2}{a_{12}}\, x - 2a_2 t\right)} \tag{49}$$

$$u = a_{12} f' \qquad v = -\left(\frac{2}{a_{12}}\, x - 2a_2 t\right)^{-1/2}(f - \eta f')$$

$$G = \frac{a_{12}\theta}{\left(\dfrac{2}{a_{12}}\, x - 2a_2 t\right)} \qquad q = -a_{12}\left(\frac{2}{a_{12}}\, x - 2a_2 t\right)^{-3/2}\theta'(0) \tag{50}$$

It should be noted that this similarity solution is only valid when the quantity $[(2/a_{12})x - 2a_2 t]$ is positive, and therefore in numerical calculations care should be taken to choose the parameter a_2 and to specify the range of validity of x and t. This restriction is necessary to keep both the surface-temperature distribution and surface heat flux finite. Evidently, at $t = 0$ the leading edge of the plate must be excluded from consideration with respect to this similarity solution. Otherwise, at any finite $x \neq 0$ the surface temperature decreases monotonically with time for $a_2 \leqslant 0$, and increases with time for $a_2 > 0$ and $t < (x/a_2 a_{12})$. This time limit, however, is not too restrictive because of the arbitrary constants a_2 and a_{12}. Since physically the parameter a_2 is an indication of the unsteadiness of surface-temperature variation, this similarity solution could prove useful in determining the validity of quasi-steady solutions. Furthermore, similar to the previous steady cases, this similarity solution is also applicable to the problem with surface heat flux prescribed by

$$q = a_{12}\left(\frac{2}{a_{12}}\, x - 2a_2 t\right)^{-3/2}$$

Case 5—Unsteady Free Convection With Surface Temperature Varying Directly With a Linear Function of x and Inversely With the Square of a Linear Function of t. The case of $a_4 = 0$ is here considered. Equation (43) now becomes

$$\phi_1 = (a_{13} - 2a_2 t)^{-1/2} \tag{51}$$

where a_{13} is a constant of integration. Then Equation (18) may be readily solved, yielding

$$\phi_2 = E(x)(a_{13} - 2a_2 t)^{-\omega/2} \tag{52}$$

where $E(x)$ is determined by introducing Equations (51) and (52) into Equation (20), which becomes

$$a_5(a_{13} - 2a_2 t)^{-1/2} = \frac{dE(x)}{dx}\,(a_{13} - 2a_2 t)^{-\omega/2}$$

With $\omega = 1$, $E(x)$ assumes the form

$$E(x) = a_5 x + a_{14}$$

and consequently

$$\begin{aligned} \phi_2 &= (a_5 x + a_{14})(a_{13} - 2a_2 t)^{-1/2} \\ G_w &= \frac{a_1(a_5 x + a_{14})}{(a_{13} - 2a_2 t)^2} \end{aligned} \tag{53}$$

In this case, constants a_1, a_2, and a_5 all have to remain as parameters in the ordinary equations, which now become

$$\begin{aligned} f''' - a_2\eta f'' - 2a_2 f' + a_5 ff'' - a_5(f')^2 + a_1\theta &= 0 \\ \frac{1}{\sigma}\,\theta'' - (a_2\eta - a_5 f)\theta' + (4a_2 + a_5 f')\theta &= 0 \end{aligned} \tag{54}$$

The usual boundary conditions also apply here. Finally, we have

$$\begin{aligned} u &= \frac{a_5 x + a_{14}}{(a_{13} - 2a_2 t)} f' \qquad v = -\frac{a_5}{(a_{13} - 2a_2 t)^{1/2}} f \\ G &= \frac{a_1(a_5 x + a_{14})}{(a_{13} - 2a_2 t)^2}\,\theta \qquad q = -\frac{a_1(a_5 x + a_{14})}{(a_{13} - 2a_2 t)^{5/2}}\,\theta'(0) \end{aligned} \tag{55}$$

Physically, a_1 represents level of Grashof number in the problem, while a_2 and a_5 indicate degrees to which G_w depends on t and x, respectively. Similar to that in the preceding case, constants a_{13} and a_2 should be so chosen that the quantity $(a_{13} - 2a_2 t)$ remains always positive. It is again seen that for $a_2 < 0$ the surface temperature at any x changes directly with time, and this trend is reversed for $a_2 > 0$. For this latter case, a limit on t, in fact, is not necessary, since the arbitrary constant a_{13} may assume any large value. A corresponding similarity solution for prescribed surface heat flux given by the last equation in (55) is also possible.

Case 6—Unsteady Free Convection With Uniform but Unsteady Surface Temperature Variation at Large Distance x. This case represents an asymptotic solution valid at large distances away from the leading edge. Therefore, all derivatives with respect to x may be neglected; i.e., $a_4 = a_5 = a_7 = 0$. Then solutions to Equations (17) and (18) are simply given by

$$\phi_1 = (a_{13} - 2a_2 t)^{-1/2} \qquad \phi_2 = a_{15}(a_{13} - 2a_2 t)^{-\omega/2}$$

from which

$$G_w = a_1 a_{15}(a_{13} - 2a_2 t)^{-\frac{3+\omega}{2}} \tag{56}$$

Without loss of any generality, we let $a_1 = 1$, $a_2 = -1$, $p = -(3 + \omega)/2$, $a_3 = 3 + 2p$, and $a_5 = 2p$, since constants a_{13}, a_{15}, and the characteristic length L in t are all entirely arbitrary. Consequently, we have for this similarity solution, the following equations:

$$\phi_1 = (a_{13} + 2t)^{-1/2} \qquad \phi_2 = a_{15}(a_{13} + 2t)^{\frac{3+2p}{2}}$$

$$G_w = a_{15}(a_{13} + 2t)^p \tag{57}$$

$$f''' + \eta f'' - (2 + 2p)f' + \theta = 0$$

$$\frac{1}{\sigma}\theta'' + \eta\theta' - 2p\theta = 0 \tag{58}$$

$$u = a_{15}(a_{13} + 2t)^{p+1} f' \qquad v = 0 \tag{59}$$

$$G = a_{15}(a_{13} + 2t)^p \theta \qquad q = -a_{15}(a_{13} + 2t)^{\frac{-1+2p}{2}} \theta'(0)$$

Here again Equations (58), which are uncoupled, are to be solved with boundary conditions (23). The fact that v is identically zero is evident from the continuity equation. This solution is only valid for positive values of a_{13} and a_{15}. It is interesting to note that, for $p = 0$ and $a_{13} = 0$, we have the special case of G_w undergoing a stepwise change from zero to a_{15}, and thus this similarity solution provides the transient-response behavior in the boundary layer. The solution to the second ordinary differential equation in (58) is elementary, as has been discussed by Siegel [10]. Finally, a corresponding similarity solution is again possible for prescribed unsteady surface heat flux. For $p = 1/2$ and $a_{13} = 0$, we have another transient case in which the surface heat flux undergoes a stepwise change.

In view of the generality of the present analysis, it is now believed that the six cases[4] indicated in the foregoing represent all possible similarity solutions for laminar free convection on a two-dimensional vertical plate.

Vertical Cylinder

The dimensionless differential equations describing laminar free convection on the outer surface of a vertical circular cylinder with constant properties are as follows:

$$\frac{\partial U}{\partial t} + U\frac{\partial U}{\partial z} + V\frac{\partial U}{\partial r} = \Gamma + \frac{\partial^2 U}{\partial r^2} + \frac{1}{r}\frac{\partial U}{\partial r} \tag{60}$$

$$\frac{\partial (rU)}{\partial z} + \frac{\partial (rV)}{\partial r} = 0 \tag{61}$$

$$\frac{\partial \Gamma}{\partial t} + U\frac{\partial \Gamma}{\partial z} + V\frac{\partial \Gamma}{\partial r} = \frac{1}{\sigma}\left(\frac{\partial^2 \Gamma}{\partial r^2} + \frac{1}{r}\frac{\partial \Gamma}{\partial r}\right) \tag{62}$$

where

[4] Basically, there are only five cases, since Case 1 is a special case of Case 2.

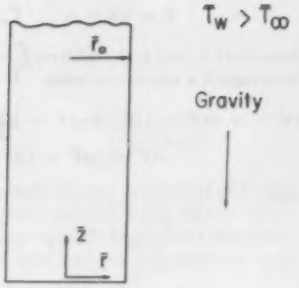

Fig. 2 Space co-ordinate system for vertical circular cylinder

$$r = \frac{\bar{r}}{\bar{r}_0} \qquad z = \frac{\bar{z}}{\bar{r}_0} \qquad t = \frac{\nu \bar{t}}{\bar{r}_0^2}$$

$$U = \frac{\bar{U}\bar{r}_0}{\nu} \qquad V = \frac{\bar{V}\bar{r}_0}{\nu} \qquad \Gamma = \frac{g\beta\bar{r}_0^3(\bar{T} - \bar{T}_\infty)}{\nu^2}$$

where $\bar{r}_0$ is the cylinder radius. The physical co-ordinates $(\bar{z}, \bar{r})$ are shown in Fig. 2 for the case $\bar{T}_w > \bar{T}_\infty$. The corresponding boundary conditions are

$$r = 1 \qquad U = V = 0 \qquad \Gamma = \Gamma_w(z, t) \quad \text{or} \quad \frac{\partial \Gamma}{\partial r} = -Q(z, t)$$

$$r = \infty \qquad U = 0 \qquad \Gamma = 0 \tag{63}$$

The analysis to follow is again restricted to the prescribed surface-temperature case, even though the results, as will be shown, are also applicable to the case of prescribed surface heat flow.

This continuity Equation (61) is first eliminated by introducing another stream function Ψ with

$$U = \frac{1}{r}\frac{\partial \Psi}{\partial r} \qquad V = -\frac{1}{r}\frac{\partial \Psi}{\partial z} \tag{64}$$

Because of the nature of the boundary condition at the cylinder surface, we shall choose r itself as the similarity variable. Even though this may seem rather restricted, it, however, appears to be the only convenient form to use, since during the course of this study the author utilized a number of other more general forms without any success. The dependent variables are now assumed to be

$$F(r) = \frac{\Psi(z, r, t)}{\Phi(z, t)} \qquad \Theta(r) = \frac{\Gamma(z, r, t)}{\Gamma_w(z, t)} \tag{65}$$

When Equations (64) and (65) are subtituted in Equations (60) and (62), we obtain

$$r^3F''' + r^2(b_3F - 1)F'' + r(b_3F - b_2r^2 + 1)F' + b_1r^4\Theta = 0 \tag{66}$$

$$r\Theta'' + (\sigma b_3 F + 1)\Theta' - \sigma(b_3F' + b_2 r)\Theta = 0 \tag{67}$$

where

$$b_1 = \frac{\Gamma_w}{\Phi} \qquad b_2 = \frac{1}{\Phi}\left(\frac{\partial \Phi}{\partial t}\right) \qquad b_3 = \left(\frac{\partial \Phi}{\partial z}\right) \tag{68}$$

The corresponding boundary conditions are

$$F(1) = F'(1) = 0 \qquad F'(\infty) = 0$$

$$\Theta(1) = 1 \qquad \Theta(\infty) = 0 \tag{69}$$

There are only two possible solutions for Φ as indicated by conditions (68) for similarity solution.

Case 7—Steady Free Convection on Cylinder With Surface Temperature Varying Linearly With z. For this case, $b_2 = 0$ and the other two conditions become

$$\Phi = b_2 z + b_4 \qquad \Gamma_w = b_1(b_2 z + b_4)$$

Since both b_1 and b_2 are arbitrary, one of these two constants may be assigned a numerical value. If we let $b_2 = 1$, then we have

$$r^3F''' + r^2(F - 1)F'' + r(F - 1)F' + b_1 r^4\Theta = 0$$
$$r\Theta'' + (\sigma F + 1)\Theta' - \sigma F'\Theta = 0 \tag{70}$$

and

$$U = \frac{z + b_4}{r} F' \qquad V = -\frac{1}{r} F$$
$$\Gamma = b_1(z + b_4)\Theta \qquad Q = -b_1(z + b_4)\Theta'(1) \tag{71}$$

With $b_4 = 0$, this similarity solution reduces to that recently treated by Millsaps and Pohlhausen [4] who, however, absorbed the parameter b_1 into the boundary conditions for Θ at the cylinder surface. Similar to Case 2, the present analysis reveals a somewhat more general solution in the inclusion of an arbitrary constant b_4 in the surface-temperature variation. Physically, this corresponds to a nonzero temperature difference at the cylinder tip. Furthermore, the present analysis also shows another similarity solution for which the prescribed surface heat flow varies linearly with z, as indicated by the last equation in (71).

Case 8—Unsteady Free Convection on Cylinder With Uniform But Unsteady Surface Temperatures at Large Values of z. This case, like Case 6, also represents an unsteady asymptotic solution for large values of z. With $b_2 = 0$, we have from (68)

$$\Phi = b_3 e^{b_3 t} \qquad \Gamma_w = b_1 b_3 e^{b_3 t}$$

Now if we choose $b_1 = 1$, Equations (66) and (67) become, respectively

$$r^3F''' - r^2F'' + r(1 - b_3 r^2)F' + r^4\Theta = 0$$
$$r\Theta'' + \Theta' - \sigma b_3 r\Theta = 0 \tag{72}$$

and

$$U = \frac{b_3}{r} e^{b_3 t} F' \qquad V = 0$$
$$\Gamma = b_3 e^{b_3 t}\Theta \qquad Q = -b_3 e^{b_3 t}\Theta\,(1) \tag{73}$$

It is of interest to note that when b_3 is imaginary the surface temperature undergoes periodic variation. The solution then provides phase relations between U, Q, and Γ_w. This similarity solution is again also valid when the unsteady surface heat flow is prescribed to be proportional to a similar exponential function.

Conclusion

An analysis is here made of the two-dimensional unsteady laminar boundary-layer equations for free convection on vertical plates and circular cylinders for establishing necessary and sufficient conditions under which similarity solutions are possible. On the basis of these conditions, all eight possible cases have been derived. Even though all similarity solutions available in the literature have essentially exhausted all cases under steady conditions, the present analysis shows that somewhat more general conditions actually could also be taken into account. The other new possible cases all deal with unsteady problems which, when numerically solved, are believed to be significant and useful, especially for checking the accuracy of other approximate, but more general, procedures such as quasi-steady solution, integral procedure, and method of series expansion. Numerical calculations for these new cases have already been initiated and results will be reported at a future date.

References

1 E. Schmidt and W. Beckman, "Das Temperatur- und Geschwindigheitsfeld von einer Wärme abgebenden senkrechten platte bei natürlicher Konvektion," *Technische Mechanik und Thermodynamik*, October, 1930, pp. 341–349; November, 1930, pp. 391–406.

2 E. M. Sparrow and J. L. Gregg, "Laminar Free Convection From a Vertical Plate With Uniform Surface Heat Flux," TRANS. ASME, vol. 78, 1956, pp. 435–440.

3 E. M. Sparrow and J. L. Gregg, "Similar Solutions for Free Convection From a Nonisothermal Vertical Plate," TRANS. ASME, vol. 80, 1958, pp. 379–386.

4 K. Millsaps and K. Pohlhausen, "The Laminar Free-Convective Heat Transfer From the Outer Surface of a Vertical Circular Cylinder," *Journal of the Aeronautical Sciences*, vol. 25, 1958, pp. 357–360.

5 H. Schuh, "Uber die ähnlichen Lösungen der instationären laminaren Grenzschichtgleichung in inkompressibler Strömung," Festschrift "50 Jahr Grenzschichtforschung," herausgeg von H. Görtler und W. Tollmein, Verlag Vieweg, Braunschweig, Germany, 1955, pp. 147–152.

6 T. Geis, "Bemerkung zu den Ähnlichen instationaren laminaren Grenzschichtströmungen," *Zeitschrift für angewandte Mathematik und Mechanik*, vol. 36, 1956, pp. 396–398.

7 A. G. Hansen, "Possible Similarity Solutions of the Laminar, Incompressible, Boundary-Layer Equations," TRANS. ASME, vol. 80, 1958, pp. 1553–1559.

8 M. Finston, "Free Convection Past a Vertical Plate," *Zeitschrift für angewandte Mathematik und Physik*, vol. 7, 1956, pp. 527–529.

9 S. Sugawara and I. Michiyoshi, "The Heat Transfer by Natural Convection in the Unsteady State on a Vertical Flat Wall," Proceedings of the First Japan National Congress for Applied Mechanics, 1951, National Committee for Theoretical and Applied Mechanics, Science Council of Japan, May, 1952, pp. 501–506.

10 R. Siegel, "Transient Free Convection From a Vertical Flat Plate," TRANS. ASME, vol. 80, 1958, pp. 347–359.

G. F. CARRIER[2]
Professor of Mechanical Engineering, Harvard University, Cambridge, Mass. Mem. ASME

J. W. MILES
Professor of Engineering, University of California, Los Angeles, Calif.[2]

On the Annular Damper for a Freely Precessing Gyroscope[1]

The dynamics of a damper that has been used to eliminate the free precession of flying, spinning objects are analyzed. There are three regimes in which the details of the mechanisms by which the viscous fluid dissipates the precessional energy differ markedly, and the fluid motion and energy-dissipation rate are described quantitatively for each regime.

1 Introduction

When the liquid contained in a symmetrically disposed annular cavity has a mass that is very small compared with that of the otherwise rigid gyroscope to which it is attached,[3] its presence cannot affect appreciably the free precession rate of that gyroscope but can only provide a source of energy dissipation that results in the damping of its precession. We shall explain here the manner in which this damping can occur and shall estimate the damping rate as a function of the parameters of the system.

Let the gyroscope be rotating initially about its axis of symmetry with an angular momentum H_0 and let the moment of inertia about this axis be the largest of the three principal moments of inertia. We assume that this initial motion is completely steady, so that the viscous liquid in the annular cavity ($A-A$ in Fig. 1; note that $\theta = 0$ for the assumed initial motion) moves with the body as though it were rigid. Now let an impulse of angular momentum H_1, small compared with H_0, be applied about an axis perpendicular to the axis of symmetry. The assumption $|H_1/H_0| \ll 1$ implies that the resulting angle of tilt, θ (between the axis of symmetry and the vertical, Fig. 1) must be small, while the assumption that the mass of liquid in the annulus is small implies that the rate of change of this angle $\dot{\theta}$ also will be small. The latter fact permits us to neglect the transient motion of the liquid (or, more to the point, the energy dissipation during this transient motion) and consider only the quasi-steady motion of the nonrigid system as a freely precessing gyroscope; i.e., we may treat the motion at each instant as if it were steady and then use the resulting solution to calculate the dissipation rate.

Let Ω and μ denote the angular velocities of spin and precession of the tilted gyroscope, as shown in Fig. 1, and assume the center of gravity of the system and the point of support to coincide (as implied by "freely precessing") at the point O. The momentum equations then are

$$H = J(\Omega + \mu \cos\theta)\cos\theta + I\mu \sin^2\theta \tag{1a}$$

and

$$0 = J(\Omega + \mu \cos\theta)\sin\theta - I\mu \sin\theta \cos\theta, \tag{1b}$$

where J and I denote the spin and transverse moments of inertia with respect to axes through O, and H is the total angular momentum. $\mathbf{H}$ is directed vertically and is a constant of the motion. It follows from Equations (1a, b) that $H = I\mu$ (exactly). If we invoke the requirement $\theta \ll 1$, we may approximate the total angular velocity ω and angular momentum by

$$\omega = (\Omega + \mu)[1 + O(\theta^2)] \tag{2}$$

and

$$H = J\omega[1 + O(\theta^2)] \tag{3}$$

We also find it convenient to express the spin angular velocity according to

$$\Omega \doteq -\alpha\omega, \qquad \alpha = (J/I) - 1 \tag{4a, b}$$

We recall that, by hypothesis, $J > I$, whence $\alpha > 0$.

The kinetic energy of the rigid-body motion is given by

$$E = \frac{1}{2}[J(\Omega + \mu\cos\theta)^2 + I(\mu \sin\theta)^2] \tag{5a}$$

$$= (H^2/2J)[1 + \alpha\theta^2 + O(\theta^4)] \tag{5b}$$

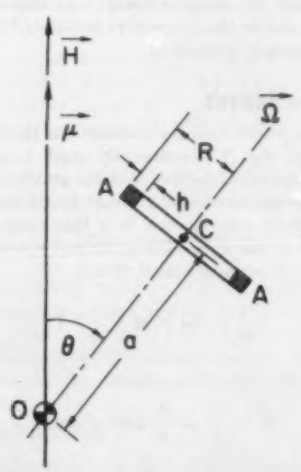

Fig. 1 Schematic diagram of freely precessing gyroscope carrying annulus (A-A) of fluid

---

[1] This paper is a revised version of Report GM-TM-0165-00265, Space Technology Laboratories, a division of The Ramo-Wooldridge Corporation.

[2] Also Consultant, Space Technology Laboratories, Inc., Los Angeles, Calif.

[3] Such a device has been exploited successfully by the U. S. Naval Ordnance Test Station, China Lake, Calif., and may be used to remove the wobble in flying objects such as satellites.

Contributed by the Applied Mechanics Division and presented at the Annual Meeting, Atlantic City, N. J., November 29–December 4, 1959, of The American Society of Mechanical Engineers.

Discussion of this paper should be addressed to the Secretary, ASME, 29 West 39th Street, New York, N. Y., and will be accepted until July 10, 1960, for publication at a later date. Discussion received after the closing date will be returned.

Note: Statements and opinions advanced in papers are to be understood as individual expressions of their authors and not those of the Society. Manuscript received by ASME Applied Mechanics Division, March 11, 1959. Paper No. 59—A-44.

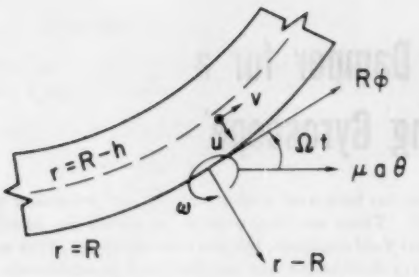

Fig. 2 Element of annulus

We observe that a decrease in E implies a decrease in θ in consequence of $\alpha > 0$ and $H = \text{const}$.

We shall assume that the annulus ($A - A$ in Fig. 1) is rectangular in cross section and that its depth D (measured along the spin axis) is sufficiently small compared with both its radius R and the distance a of its plane from O to justify a two-dimensional treatment of the fluid motion. Introducing (see Fig. 2) a set of polar co-ordinates, r and ϕ, in a reference frame moving with the outer wall of the annulus ($r = R$) and letting u and v denote the radial and tangential components of relative velocity in this reference frame, we may write

$$[u, v] = \mu a\theta \Re\{[-i, 1]e^{i(\Omega t+\phi)}\} \text{ at } r = R, \quad (6a, b)$$

for the fluid motion at the wall.

In Section 2 we shall analyze the motion of the fluid when θ is so small that the fluid may be assumed to be in contact with the outer wall over its complete circumference and to have a free surface at the inner face, $r = R - h$; in Section 3 we shall determine the fluid motion that occurs when θ is sufficiently large (but not so large that terms of order θ^2 are important compared with unity) that the fluid moves as a slug filling the annular cross section over an incomplete portion of the annulus; and in Section 4 we shall discuss that situation in which θ takes values intermediate to these extremes.

We emphasize that the effects of surface tension are ignored in each of the analyses of Sections 2 and 4. It has been noted, in experiments performed at the U. S. Naval Ordnance Test Station (China Lake, Calif.), that surface tension may delay or prevent the transition from the geometry of Section 3 to that of Section 2 or 4. Thus the question as to which of the regimes described here will dominate the damping history may depend not only on the initial state and on the parameters introduced herein but also on the surface tension of the fluid.

2 The Small-θ Analysis

We shall seek u and v on the assumptions that the motion is two dimensional, that θ is sufficiently small to permit linearization of the equations of motion, that the gravitational acceleration is negligible compared with the centripetal acceleration, and that viscous effects are confined to a thin (compared with h) boundary layer at the wall. The linearized equation of relative motion outside this boundary layer then is

$$\frac{\partial \mathbf{q}}{\partial t} + 2\boldsymbol{\omega} \times \mathbf{q} = -\nabla X, \quad (7a)$$

where

$$X = \frac{p}{\rho} - \frac{1}{2}\omega^2 r^2 + \text{const} \quad (7b)$$

is an acceleration potential, $\mathbf{q}$ fluid velocity, p pressure, and ρ density; the angular velocity $\boldsymbol{\omega}$ is approximately normal to the plane of motion (because θ is small).[4] Taking the curl of Equation (7a), we have (and here it is essential that $\boldsymbol{\omega}$ and $\mathbf{q}$ be approximated as mutually perpendicular)

$$\nabla \mathbf{q} = 0; \quad (8)$$

hence, within our approximations, the inviscid component of the motion is irrotational.

We shall assume that the additional viscous motion inside the boundary layer is governed by Stokes' equation[5]

$$v_t = \nu v_{rr}, \quad (9)$$

where ν denotes the kinematic viscosity. We emphasize that the solutions to Equations (7) and (9) must be superimposed to obtain the total velocity near the wall and that this total velocity must satisfy the continuity equation

$$\nabla \cdot \mathbf{q} = r^{-1}[(ru)_r + v_\phi] = 0 \quad (10)$$

We now complete the statement of our boundary-value problem by posing the boundary conditions at the free surface in the form

$$u = \eta_t \text{ and } p = \text{const at } r = R - h + \eta, \quad (11a, b)$$

where η denotes the radial displacement of the surface. Linearizing Equations (11a, b) and making a suitable choice of the constant in Equation (7b), we obtain

$$u = \eta_t \text{ and } X = -\omega^2(R - h)\eta, \quad r = R - h \quad (12a, b)$$

We shall satisfy the continuity Equation (10) by deriving the velocity from a stream function according to

$$ru = -\psi_\phi \text{ and } v = \psi_r; \quad (13a, b)$$

moreover, by virtue of the assumed linearity, the t- and ϕ-dependence of ψ must be as in Equations (6a, b). Then, remarking that that part of ψ corresponding to the irrotational motion must satisfy Laplace's equation, while that part corresponding to the shear flow must satisfy Equation (9), we may pose the total solution in the form

$$\psi = R\mu a\theta[A(r/R) + B(R/r) + Ce^{\lambda(r-R)/R}]e^{i(\Omega t+\phi)}, \quad (14)$$

where A, B, and C are dimensionless constants,

$$\lambda = (i\Omega R^2/\nu)^{1/2}, \ \Re\{\lambda\} > 0, \quad (15a, b)$$

and it is implicit, following the usual convention, that only the real parts of the complex quantities derived from ψ are to be retained.

The velocities and potential derived from Equations (13a, b) and (14) are

$$u = -i\mu a\theta[A + B(R/r)^2 + C(R/r)e^{\lambda(r-R)/R}]e^{i(\Omega t+\phi)}, \quad (16a)$$

$$v = \mu a\theta[A - B(R/r)^2 + \lambda Ce^{\lambda(r-R)/R}]e^{i(\Omega t+\phi)}, \quad (16b)$$

and

$$X = \mu a\theta R[(2\omega - \Omega)A(r/R) + (2\omega + \Omega)B(R/r)]e^{i(\Omega t+\phi)}, \quad (16c)$$

where we have derived X from the ϕ-component of Equation (7a), neglecting the contribution of the viscous solution. We remark that this last approximation is consistent with our separation of the inviscid and viscous solutions, and we now see that the restriction implied by this separation is

$$|\lambda(h/R)| = |\Omega h^2/\nu|^{1/2} \gg 1, \quad (17)$$

[4] There is a centripetal acceleration of approximately $\mu\omega R\theta$ along the spin axis, but, being approximately constant through the fluid, this results only in a hydrostatic pressure gradient.

[5] H. Lamb, "Hydrodynamics," Dover Publications, New York, N. Y., sixth edition, 1945, section 345.

in consequence of which the viscous solution is exponentially negligible outside of a boundary layer having a thickness of the order of $|\nu/\Omega|^{1/2}$ (essentially the result enunciated by Stokes).

Imposing on Equations (16*a*, *b*) the boundary conditions (6*a*, *b*) and the free-surface boundary condition obtained by eliminating η between Equations (12*a*, *b*), we obtain the matrix equation

$$[M]\{A, B, C\} = \{1, 1, 0\}, \tag{18a}$$

$$[M] = \begin{bmatrix} 1 & 1 & 1 \\ 1 & -1 & \lambda \\ m & n & 0 \end{bmatrix} \tag{18b}$$

where

$$m = (1 + \alpha)^2(1 - \beta)^2, \quad n = 1 + 2\alpha - \alpha^2, \tag{19a, b}$$

$$\beta = h/R, \tag{19c}$$

and α is given by Equation (4*b*). Solving Equation (18*a*), we obtain

$$\{A, B, C\} = \Delta^{-1}\{-n(\lambda - 1), m(\lambda - 1), 2m\}, \tag{20a}$$

$$\Delta = (m - n)\lambda + (m + n), \tag{20b}$$

where Δ is the determinant of the matrix $[M]$. Subsequently, we shall approximate $\lambda - 1$ by λ except in Δ.

The rate at which energy is dissipated in the fluid is given by[6]

$$-\dot{E} = \rho\nu \iiint (\nabla \times \mathbf{q})^2 dV, \tag{21}$$

where dV denotes an element of volume. Now, by definition, the irrotational component of the fluid motion cannot contribute to the integrand, and we have [consistently with the approximations implied by Equation (9)]

$$-\dot{E} = \rho\nu \iiint v_r^2 dV, \tag{22}$$

where only the viscous solution is to be included in evaluating v_r. From Equation (16*b*), we obtain (now exhibiting the $\Re$ operator explicitly)

$$v_r = (\mu a\theta/R)\Re\left\{\lambda^2 C \exp\left[\lambda\left(\frac{r - R}{R}\right) + i(\Omega t + \phi)\right]\right\} \tag{23}$$

Substituting Equation (23) in Equation (22) and carrying out the integrations over ϕ and over the depth D of the annulus, we obtain

$$-\dot{E} = \rho\nu(\mu a\theta/R)^2|\lambda^2 C|^2\pi D \int_{R-h}^{R} \exp\left[2\Re\{\lambda\}\left(\frac{r - R}{R}\right)\right] r\, dr \tag{24a}$$

$$\doteq \rho\nu(\mu a\theta/R)^2|\lambda^2 C|^2\pi DR^2 \int_0^\infty \exp\left[-2\Re\{\lambda\}x\right] dx \tag{24b}$$

$$= 2^{3/2}\pi DR^2\rho(\mu a\theta)^2|\Omega|m^2|\lambda|/|\Delta|^2, \tag{24c}$$

where we have neglected the variation of the radial weighting factor r in Equation (24*a*), introduced the change of variable $x = 1 - (r/R)$, replaced the upper limit $x = h/R$ by ∞ on virtue of Equation (17), and substituted λ and C from Equations (15*a*) and (20*a*), respectively.

The total energy to be absorbed is given by Equations (3) through (5) as

$$\delta E = E(\theta) - E(0) = \tfrac{1}{2}\alpha(\alpha + 1)^{-1}I\mu^2\theta^2 \tag{25}$$

Defining the time constant for the decay of θ as

$$T = \delta E/(-\dot{E}) \tag{26}$$

and substituting Equation (24*c*) and Equation (25), we obtain

$$T = \Gamma I/DR^2a^2\rho|\Omega|, \tag{27a}$$

$$\Gamma = \alpha[(m - n)^2|\lambda|^2 + 2^{1/2}(m^2 - n^2)|\lambda| + (m + n)^2]/2^{5/2}\pi(\alpha + 1)m^2|\lambda|, \tag{27b}$$

where, in evaluating Γ, we have substituted $|\Delta|^2$ from Equation (20*b*).

We now observe that Γ exhibits a strong minimum (maximum energy absorption or resonance) in the neighborhood of $m = n$; specifically,

$$\Gamma_{\min} = \alpha/2^{3/2}\pi(\alpha + 1)|\lambda| \tag{28}$$

at

$$m = n[1 - 2^{1/2}|\lambda|^{-1} + O(\lambda^{-2})] \tag{29a}$$

or

$$h \doteq R\left[\left(\frac{\alpha}{1 + \alpha}\right)^2 + 2^{-1/2}|\lambda|^{-1}\right], \tag{29b}$$

where we have assumed $\beta^2 \ll 1$ in obtaining Equation (29*b*). Away from this resonant neighborhood, on the other hand,

$$\Gamma \doteq \alpha(m - n)^2|\lambda|/2^{5/2}\pi(\alpha + 1)n^2, \quad |(m - n)\lambda| \gg 1 \tag{30}$$

The Q of the resonance is of the order of $|\lambda|$; in particular, if $m = n$, $\Gamma = 2\Gamma_{\min}$.

In assessing the resonance specified by Equations (28) and (29), we must recall that we have assumed the free-surface displacement η to be small compared with h. From Equations (12*a*), (16*a*) and (20*a*), we have

$$\eta = (i\Omega)^{-1}u|_{r=R-h} = 2\alpha(1 + \alpha)a\theta\lambda/\Delta \tag{31}$$

Evaluating Δ and h in accordance with Equations (28) and (29*b*) and neglecting terms of order β compared with one, we obtain

$$\left|\frac{\eta}{h}\right|_{\max} \doteq 2^{1/2}\left(\frac{1 + \alpha}{\alpha}\right)\left(\frac{|\Omega|a^2}{\nu}\right)^{1/2}\theta, \tag{32}$$

while the counterpart of Equation (30) is

$$\left|\frac{\eta}{h}\right| = \left(\frac{1 + \alpha}{\alpha}\right)\left(\frac{a}{h}\right)\theta, \quad |(m - n)\lambda| \gg 1 \tag{33}$$

We consider the specific example for which $R = 10$ cm, $a = 10$ cm, $D = 0.25$ cm, $h = 0.05$ cm, $I = 1.3$ kg-m^2, $\alpha = 1/3$, $\omega = 12$ rad/sec, $\rho = 13.6$ gm/cc, and $\nu = 10^{-3}$ cm^2/sec. Substituting these data in the foregoing formulas we obtain

$$|\lambda| = 632, \quad T = 14 \text{ sec}, \quad \text{and} \quad |\eta/h| = 8 \times 10^2\,\theta$$

Resonance would require $h = 0.637$ cm and would yield

$$T = 4.4 \times 10^{-3} \text{ sec} \quad \text{and} \quad |\eta/h| = 3.6 \times 10^3\,\theta$$

If we arbitrarily specify $|\eta/h| = 1/4$ as indicative of nonlinear effects, the respective, critical values of θ would be 3×10^{-4} radians and 7×10^{-5} radians. For θ appreciably in excess of these values we should expect gaps to appear in the fluid annulus, and our analysis then would cease to be significant.

3 The Large-θ Analysis

When θ is sufficiently large ($\theta > 0.02$ radian for the foregoing parameters), an inviscid fluid would undergo a rigid-body rotation at the angular velocity $\vec{\mu}$ depicted in Fig. 1. The free surface

[6] H. Lamb, ibid., p. 581. (Note: This result is not complete at large distances from the wall, but we are concerned only with dissipation near the wall.)

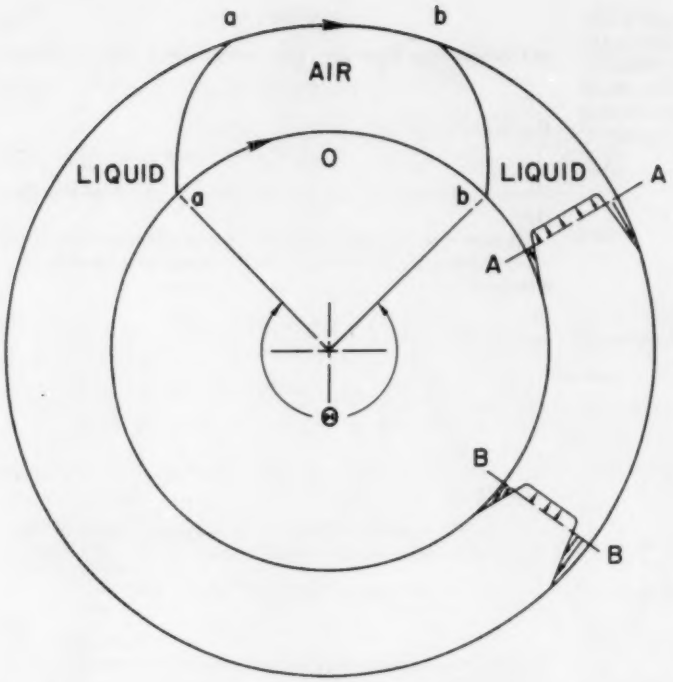

Fig. 3 Motion of fluid and solid relative to a co-ordinate system rotating at speed ω about O. The boundary-layer thickness increases as one proceeds in the clockwise direction.

of the fluid would be an equipotential surface; i. e., it would consist of a piece of a cylindrical surface with an axis that is directed along $\vec{\mu}$ and that passes through the center of gravity. The motion of the solid object would be a superposition of that rigid-body motion and another rigid-body rotation at speed Ω about the symmetry axis. This superimposed motion at speed Ω cannot influence the motion of the hypothetical inviscid fluid because it has a vanishing normal component of velocity at its interface with the fluid.

However, since the fluid is not inviscid its rigid-body motion must be supplemented by a thin boundary layer along the wall and a negligibly slow back flow down the center of the tube, Fig. 3. This boundary layer is intrinsically the same as that formed when a shock wave travels down a shock tube at speed ΩR. It is very thin at the front end and grows in thickness in precisely the same way with distance from this edge as a conventional boundary layer grows along a flat plate. The energy-dissipation rate, computed on a laminar basis, is

$$-\dot{E} = 2|\Omega|^{2.5}R^3\rho\nu^{1/2}P\Theta^{1/2}, \tag{34}$$

where Θ is the angle indicated in Fig. 3, and P is the perimeter of the cross section of the annulus. The energy to be removed is found from Equation (25) and is given by

$$\delta E \simeq I|\mu||\Omega|\theta^2/2 \tag{35}$$

The energy removal time T then is given by (26) as

$$T = I|\mu|\theta^2/4|\Omega|(|\Omega|\nu)^{1/2}R^4\rho P\Theta^{1/2} \tag{36}$$

For the parameters of the previous section, and for an initial angle $\theta = 1/6$ radian, $\Theta = 5$, and $P = 1$ cm, T is given by

$$T = 200 \text{ sec}$$

For the values of the parameters, however, the Reynolds number of the flow R_s is 1.5×10^6. At this Reynolds number the boundary layer must be turbulent over most of its length, and the increased skin friction so implied would reduce the time T to the order of 70 sec.

4 The Intermediate Values of θ

When θ has decreased from some large initial value to some smaller value such that the tube is not entirely empty at any angular co-ordinate ϕ, but such that the free surface is interrupted by contact with the inner wall, the fluid motion may well consist of a smooth flow (which is a combination of the rigid-body rotation plus approximately a Poiseuille flow) on which is superimposed some wave motion over that portion of the fluid whose surface is exposed. The dissipation of energy associated with the Poiseuille flow is small compared with the boundary-layer flow but, of course, the energy to be removed has also decreased markedly when this phase of the motion has been reached. If, for example, it is reached when θ becomes 0.02 radian, the remaining energy is about 1 per cent of the original; the dissipation rate is decreased by a factor of about 12. The time required to go to $\theta = 10^{-6}$ radians would be about $^1/_8$ of the large motion damping time or, in our illustrative example, about 10 more sec. This is almost surely an upper bound on the intermediate time since it completely ignores the damping associated with the wave motion.

5 Conclusions

It is quite clear that a very lightweight device of the type analyzed here can be so designed that the precessional motion of an otherwise rigid gyroscope can be damped out in a matter of seconds. The foregoing gives a good estimate of the decay times associated with each of the three regions of interest, and the results can be used to guide the selection of optimum-design parameters.

Heat Transfer for Laminar Flow in Ducts With Arbitrary Time Variations in Wall Temperature

ROBERT SIEGEL
National Aeronautics and Space Administration, Lewis Research Center, Cleveland, Ohio.
Assoc. Mem. ASME

An analysis is made for laminar forced-convection heat transfer in a circular tube or a parallel plate channel whose walls may undergo arbitrary time variations in temperature. The time-varying process can begin from an already established steady-state situation with heat transfer taking place, or the fluid and walls can be initially at the same uniform temperature. The fluid velocity distribution is fully developed and unchanging with time. At any instant during the transient the wall temperature is spatially uniform, that is, all portions of the wall simultaneously undergo the same temperature-time variation. The greater part of the analysis is concerned with the response to a step change in wall temperature, and the time required to reach steady state is given for this type of transient. Then the results are generalized to apply for arbitrary variations with time.

THE behavior of heat-transfer equipment during transient temperature changes has, in recent years, received greater attention especially in connection with the use of nuclear reactors as power sources. Since nuclear properties are often temperature dependent, it is sometimes necessary to consider in detail the thermal transients within the system, to be assured that proper control will be maintained during power changes. The present paper is concerned with studying the heat-transfer behavior associated with a thermal transient in a forced-convection channel flow.

Two geometries which are commonly encountered in practice are selected for analysis, the circular tube, and the parallel-plate channel. The flow in the tube or between the parallel plates is assumed to be laminar, incompressible, and fully developed. The last assumption implies that a hydrodynamic entrance length is

Presented at the West Coast Conference of the Applied Mechanics Division, Stanford, Calif., September 9–11, 1959, of THE AMERICAN SOCIETY OF MECHANICAL ENGINEERS.

Discussion of this paper should be addressed to the Secretary, ASME, 29 West 39th Street, New York, N. Y., and will be accepted until July 10, 1960, for publication at a later date. Discussion received after the closing date will be returned.

NOTE: Statements and opinions advanced in papers are to be understood as individual expressions of their authors and not those of the Society. Manuscript received by ASME Applied Mechanics Division, March 17, 1959. Paper No. 59—APMW-21.

Nomenclature

a = half width of spacing between parallel plates
a_n = the ratio, β_n^2/γ_n
C_n = coefficients in series expansion of temperature distribution in a circular tube
c_p = specific heat at constant pressure
D = tube diameter, $2r_0$
F_n = a function of X and Θ in Equation (9)
f_n = ratio, τ_n/σ_n
G_n = a function of X and Θ in Equation (35)
k = thermal conductivity
Pr = Prandtl number, $c_p\mu/k = \nu/\alpha$
q = local heat addition per unit area at channel wall
R = dimensionless radial co-ordinate, r/r_0
r = radial co-ordinate measured from circular tube center line; r_0, tube radius
Re = Reynolds number; $\bar{u}D/\nu$ for a circular tube; $\bar{u}4a/\nu$ for a parallel-plate channel
T = dimensionless temperature, $(t - t_0)/(t_w - t_0)$
t = temperature; t_0, temperature of fluid entering channel (a constant); t_w, wall temperature
t' = temperature difference, $t_w - t_0$
u = fluid velocity in x-direction; $\bar{u}$, mean fluid velocity; u_{max}, maximum fluid velocity in channel cross section
X = dimensionless axial co-ordinate; $(x/r_0)/\text{Re Pr}$ for a circular tube, $(8/3)[(x/a)/\text{Re Pr}]$ for a parallel-plate channel
x = axial distance from entrance of channel
Y = dimensionless co-ordinate, y/a
y = normal co-ordinate measured from center line of parallel-plate channel
α = thermal diffusivity, $k/\rho c_p$
β_n^2 = steady-state eigenvalues for circular tube
γ_n = exponential constants in transient solution for circular tube, Equation (17)
Θ = dimensionless time; $\theta\nu/r_0^2\text{Pr}$ for circular tube; $\theta\nu/a^2\text{Pr}$ for parallel-plate channel
θ = time
Θ^* = dummy integration variable
λ_n^2 = steady-state eigenvalues for parallel-plate channel
μ = absolute viscosity
ν = kinematic viscosity
ρ = fluid density
σ_n = exponential constants in solution for parallel-plate channel, Equation (36a)
τ_n = exponential constants in solution for parallel-plate channel, Equation (36b)
φ_n = eigenfunctions for solution in circular tube
χ = function of X in steady-state solution for circular tube, Equation (5)

Subscript

s, refers to steady-state condition

present which allows the flow to establish a fully developed velocity distribution before reaching the heated section of the channel. The transient heating process is such that the wall temperature can be specified to have an arbitrary time variation. Initially the system can be either at steady state with heat transfer taking place, or the whole system can be initially isothermal with the fluid and bounding walls all at the same temperature. At any instant of time the wall temperature is uniform, that is, all positions along the wall simultaneously undergo the same temperature-time variation.[1]

Most previous analyses of transient forced-convection heat transfer in passages have been treated by one-dimensional approximations; that is, velocity and temperature variations over the channel cross section have been neglected. A good review of work using this approach can be found, for example, in references [1][2] and [2]. The present work employs a two-dimensional analysis and thus includes the variations in velocity and temperature over the cross sections of the flow channels.

The transient heat-transfer situation considered here has been treated by another method in [3] and [4]. However, in these references only the thermal entrance region is examined and the results do not extend far down the passage. The present method yields results for the entire length of the channel, but in the series-expansion method which is employed, many terms are required to calculate results for the region very close to the tube entry. Thus, by joining the present results to those of [3] and [4], information is obtained for all positions in the flow passage.

Two methods for performing the analysis are given here; one method is used in the calculations for the circular tube while the other is used for the parallel plate configuration. As will be shown in the analysis these two methods differ in the way certain required functions are computed. For the circular tube the computation involves the numerical integration of an ordinary differential equation, while for the parallel-plate channel the functions are obtained by a series expansion in terms of more simple functions. A method somewhat similar to the second approach has been briefly outlined in [5]. The method given here is not an exact solution of the governing partial differential equation, but involves an approximation at one step in the analysis. The validity of this approximation is tested by comparison with exact results available for part of the solution and good agreement is obtained. For arbitrary time variations in wall temperature results are obtained by generalizing the transient corresponding to a unit step change in wall temperature.

The analysis thus proceeds in the following order: The circular tube is analyzed for a step in wall temperature, and the results are then generalized for arbitrary time variations. Then the parallel-plate configuration is treated by a slightly different method. Results of transient heat-flux variations and times required to reach steady state are given graphically and compared with previous work.

Step-Change in Wall Temperature for Flow in a Circular Tube

This portion of the analysis is concerned with fully developed laminar flow through a circular tube as shown in Fig. 1. The tube and fluid are assumed to be initially isothermal at temperature t_0. Then the wall is given an instantaneous step in temperature to a new value t_w and maintained at t_w for all time thereafter.

The energy equation for incompressible flow in a tube can be written as

$$\frac{\partial t}{\partial \theta} + u\frac{\partial t}{\partial x} = \alpha\frac{1}{r}\frac{\partial}{\partial r}\left(r\frac{\partial t}{\partial r}\right) \tag{1}$$

To obtain the equation in this form viscous dissipation and axial heat conduction are neglected compared with heat conduction in the radial direction. It is convenient to rewrite this equation in terms of dimensionless variables defined as,

$$\Theta = \frac{\theta\nu}{r_0^2\mathrm{Pr}};\quad X = \frac{x/r_0}{\mathrm{Re\ Pr}};\quad R = \frac{r}{r_0};\quad T = \frac{t - t_0}{t_w - t_0}$$

Θ, X, and R are, respectively, the dimensionless time, distance along the tube, and radial distance, and are the three independent variables of the problem. The dimensionless temperature T is defined so that at the entrance to the heated section the value of T is zero while at the tube wall T becomes unity. Since the flow is fully developed the velocity distribution has the parabolic form,

$$\frac{u}{\bar{u}} = 2\left[1 - \left(\frac{r}{r_0}\right)^2\right] \tag{2}$$

Substituting these quantities into Equation (1) results in the following dimensionless equation,

$$\frac{\partial T}{\partial \Theta} + (1 - R^2)\frac{\partial T}{\partial X} = \frac{1}{R}\frac{\partial}{\partial R}\left(R\frac{\partial T}{\partial R}\right) \tag{3}$$

This must be solved subject to the following boundary conditions:

$$\left.\begin{aligned} &T = 0 \text{ at } X = 0 \text{ for all } R \text{ and } \Theta, && \text{entrance condition}\\ &T = 0 \text{ at } \Theta = 0, \text{ for all } R \text{ and } X, && \text{initial condition}\\ &\frac{\partial T}{\partial R} = 0 \text{ at } R = 0, && \text{symmetry}\\ &T = 1 \text{ at } R = 1 \text{ for all } X \text{ and for } \Theta > 0, && \text{specified wall temperature} \end{aligned}\right\} \tag{3a}$$

To obtain a solution we first consider the results for the steady-state heat-transfer condition.

Steady-State Solution. At steady state there are of course no variations with time and hence Equation (3) reduces to

$$(1 - R^2)\frac{\partial T_s}{\partial X} = \frac{1}{R}\frac{\partial}{\partial R}\left(R\frac{\partial T_s}{\partial R}\right) \tag{4}$$

The steady-state solution corresponding to the boundary conditions (3a) is for the situation of fluid at uniform temperature entering a pipe maintained at a different constant wall temperature. This problem was treated by Graetz in 1885,[3] and for convenience will be reviewed briefly as the results will be needed later in the analysis.

A product solution is employed of the form

$$T_s = 1 - \chi(X)\varphi(R) \tag{5}$$

When this is inserted into Equation (4) it is found that

$$\chi = e^{-\beta^2 X} \tag{6}$$

where $-\beta^2$ is the separation constant arising in the product solution. The equation for the function φ is

$$\frac{d^2\varphi}{dR^2} + \frac{1}{R}\frac{d\varphi}{dR} + \varphi\beta^2(1 - R^2) = 0 \tag{7}$$

with the boundary conditions

$$\left.\begin{aligned} &\frac{d\varphi}{dR} = 0 \quad \text{at} \quad R = 0\\ &\varphi = 0 \quad \text{at} \quad R = 1 \end{aligned}\right\} \tag{7a}$$

[1] For the parallel-plate channel both walls are at the same temperature.

[2] Numbers in brackets designate References at end of paper.

[3] Reference [6], p. 451.

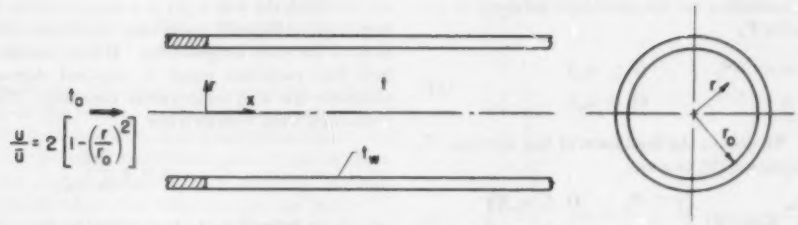

Fig. 1 Co-ordinate system for circular-tube geometry

Equations (7) and (7a) form an eigenvalue problem of the Sturm-Liouville type. Solutions are possible only for a discrete, though infinite, set of β-values. Hence the solution for T_s can be written as

$$T_s = 1 - \sum_{n=0}^{\infty} C_n \varphi_n(R) e^{-\beta_n^2 X} \tag{8}$$

where β_n^2 and φ_n are the eigenvalues and corresponding eigenfunctions of Equations (7) and (7a).

The coefficients C_n are evaluated from the boundary condition that $T_s = 0$ at the tube entrance ($X = 0$). Applying this condition to Equation (8), we find that the C_n must satisfy,

$$0 = 1 - \sum_{n=0}^{\infty} C_n \varphi_n \tag{8a}$$

From the properties of the Sturm-Liouville system it follows immediately that

$$C_n = \frac{\int_0^1 (R - R^3)\varphi_n dR}{\int_0^1 (R - R^3)\varphi_n^2 dR} \tag{8b}$$

The first five eigenvalues of Equation (7) and values of C_n are available to very good accuracy in reference [7] and asymptotic results for higher values of β_n^2 and C_n are given in reference [8].

This completes the steady-state solution and we now turn to the transient problem.

Transient Solution. To form a transient solution, we try a series expansion about the steady-state condition. With this type of formulation the transient solution will automatically converge, at large times, to exactly the steady-state result. Thus we try a transient solution of the same general form as the steady-state equation (8),

$$T = 1 - \sum_{n=0}^{\infty} C_n F_n(X, \Theta)\varphi_n(R) \tag{9}$$

For large times the function F_n should, by comparison with Equation (8), converge to

$$F_n = e^{-\beta_n^2 X} \tag{10}$$

The approximation which is now made is that the transient solution is only required to satisfy an integrated form of the energy equation, and will only exactly satisfy the equation in differential form for the limit of very large time. Multiplying Equation (3) by R and integrating from 0 to 1 gives the integrated form,

$$\int_0^1 R \frac{\partial T}{\partial \Theta} dR + \int_0^1 R(1 - R^2) \frac{\partial T}{\partial X} dR = \left(\frac{\partial T}{\partial R}\right)_{R=1} \tag{11}$$

The trial solution, Equation (9), is then substituted into Equation (11) with the result that each F_n must satisfy the relation

$$\frac{\partial F_n}{\partial \Theta} \int_0^1 R\varphi_n dR + \frac{\partial F_n}{\partial X} \int_0^1 (R - R^3)\varphi_n dR - F_n \left(\frac{\partial \varphi_n}{\partial R}\right)_{R=1} = 0 \tag{12}$$

This type of partial differential equation can be treated by using the method of characteristics. In this method the solution is obtained by considering the following auxiliary ordinary differential equations,[4]

$$\frac{d\Theta}{\int_0^1 R\varphi_n dR} = \frac{dX}{\int_0^1 (R - R^3)\varphi_n dR} = \frac{dF_n}{F_n \left.\frac{\partial \varphi_n}{\partial R}\right|_{R=1}} \tag{13}$$

Equating the second and third terms yields a solution for F_n as,

$$F_n = \exp\left\{ - \frac{-\partial\varphi_n/\partial R|_{R=1}}{\int_0^1 (R - R^3)\varphi_n dR} X \right\} \tag{14a}$$

To simplify this, the steady-state Equation (7) is multiplied by R and integrated from $R = 0$ to $R = 1$, with the result

$$\beta_n^2 = \frac{-\partial\varphi_n/\partial R|_{R=1}}{\int_0^1 (R - R^3)\varphi_n dR}$$

Comparing this with the exponent in Equation (14a) we find that

$$F_n = e^{-\beta_n^2 X} \tag{14b}$$

which is the desired form for steady state as given by Equation (10). In a similar fashion the first and third terms of Equation (13) are equated which gives the solution

$$F_n = \exp\left\{ \frac{-\partial\varphi_n/\partial R|_{R=1}}{\int_0^1 R\varphi_n dR} \Theta \right\} \tag{15}$$

Thus we have obtained two results, one being the steady-state solution, Equation (14b), and the other, Equation (15), a solution which is dependent on time only. The latter will be called the "initial transient" solution. The method of characteristics indicates that these two results can be joined along a characteristic line which passes through the origin of the $X - \Theta$ plane. This line is obtained by integrating the equation formed by the first and second terms of Equation (13) subject to the condition that $X = 0$ when $\Theta = 0$. This yields

$$\Theta = \left[\frac{\int_0^1 R\varphi_n dR}{\int_0^1 (R - R^3)\varphi_n dR} \right] X \equiv a_n X \tag{16}$$

where the ratio of the two integrals has been denoted by a_n.

[4] Reference [9], p. 368.

Using an abbreviated notation for the constants involved in the exponentials we have for F_n

$$F_n = e^{-\gamma_n \Theta}, \qquad \Theta \leqslant a_n X$$
$$F_n = e^{-\beta_n^2 X}, \qquad \Theta \geqslant a_n X \tag{17}$$

where $a_n = \beta_n^2/\gamma_n$. To obtain the final form of the solution, F_n is substituted into Equation (9) to give

$$T = 1 - \sum_{n=0}^{\infty} C_n \varphi_n(R) \begin{Bmatrix} e^{-\gamma_n \Theta}, & \Theta \leqslant a_n X \\ e^{-\beta_n^2 X}, & \Theta \geqslant a_n X \end{Bmatrix} \tag{18}$$

Now it is necessary to consider the boundary conditions as given by Equation (3*a*). At $X = 0$, for any finite Θ, the condition $\Theta > a_n X$ in Equation (18) is fulfilled, and we have (since $T = 0$ at $X = 0$)

$$0 = 1 - \sum_{n=0}^{\infty} C_n \varphi_n$$

This condition has already been satisfied according to Equation (8*a*). For $\Theta = 0$, we have for any finite X the condition $\Theta < a_n X$ and Equation (18) gives (since $T = 0$ at $\Theta = 0$)

$$0 = 1 - \sum_{n=0}^{\infty} C_n \varphi_n$$

which is again the same condition that has been satisfied already by proper evaluation of the C_n. The first two boundary conditions of Equations (3*a*) are thus satisfied by using the same C_n obtained in the steady-state solution. The last two boundary conditions are identically satisfied as they were used in determining the φ_n. Hence the solution satisfies all of the required boundary conditions, converges exactly to the steady-state condition for large times, and is approximate to the extent that it satisfies an integrated form of the energy equation. The accuracy of this approximation will be discussed a little later.

Numerical Solution. In order to compute heat-transfer quantities from the temperature distribution of Equation (18) it is necessary to know values of C_n, φ_n, γ_n, β_n^2, and a_n. As mentioned before, some of these quantities are already available in the literature, but the values of φ_n were generally not tabulated in sufficient detail so that the integrations necessary to determine γ_n could be performed. To obtain the desired numerical information, Equation (7) and the required integrals were programmed for numerical computation on an IBM 653 electronic digital computer. A forward integration scheme (Runge-Kutta) was employed, and quantities were evaluated for the first seven eigenvalues. These are listed in Table 1 along with the derivative of the eigenfunction at the wall which will be needed for the calculations in the next section. Space limitations preclude a presentation of the φ_n-values but they are available as IBM listings.

Wall Heat Flux. It is recalled that the transient heating process which yields the temperature distribution of Equation (18) is one in which the wall is given a step-function change in temperature from an initially isothermal condition with both the wall and fluid at the same temperature. It is of interest to look at the wall heat-flux variation which is required during the transient to maintain the wall temperature constant. This heat flux can be evaluated from Fourier's law

$$q = k \left.\frac{\partial t}{\partial r}\right|_{r=r_0} \tag{19}$$

where q is defined as the heat added at the wall. Applying this to Equation (18) gives the result for the wall heat flux as a function of position along the tube and time

$$\frac{qr_0}{k(t_w - t_0)} = -\sum_{n=0}^{\infty} C_n \left.\frac{d\varphi_n}{dR}\right|_{R=1} \begin{Bmatrix} e^{-\gamma_n \Theta}, & \Theta \leq a_n X \\ e^{-\beta_n^2 X}, & \Theta \geq a_n X \end{Bmatrix} \tag{20}$$

Before examining this expression in detail, the portion of it which forms the initial transient solution will be considered as it will indicate to some extent the accuracy of the integral approximation used in the analysis.

To understand the initial transient process better, consider the fluid which is at the entrance of the heated section at the time the step in wall temperature occurs. After a period of time has elapsed, this fluid will have traveled a certain distance down the tube. Beyond this distance there has not been any penetration, during the heating process, of fluid which was originally outside the tube, and hence the heat-flow process in this region has not been affected by the fact that the tube has an entrance. The behavior in this region is then that of a tube of infinite length in both directions, and for the case of uniform wall temperature there are no variations of heat-transfer quantities with distance X. With no X variation the convective term in the energy equation (1) is identically zero and a pure transient heat-conduction process takes place. The heat-flux variation during this initial transient is obtained from Equation (20) by considering the terms which vary with time only; that is, we observe the heat-transfer process at sufficiently large X so that Θ will always be less than $a_n X$. The initial transient solution is then

Table 1 Coefficients for flow in circular tubes

n	β_n^2	γ_n	C_n	$d\varphi_n/dR\|_{R=1}$	a_n
0	7.31358	5.1540	1.4764	-1.0145	1.4190
1	44.6095	16.262	-.80612	1.3492	2.7432
2	113.921	29.918	.58876	-1.5725	3.8078
3	215.241	45.392	-.47585	1.7460	4.7418
4	348.564	62.327	.40502	-1.8909	5.5925
5	513.78	80.324	-.35542	2.0145	6.3963
6	711.11	99.592	.31892	-2.1265	7.1403

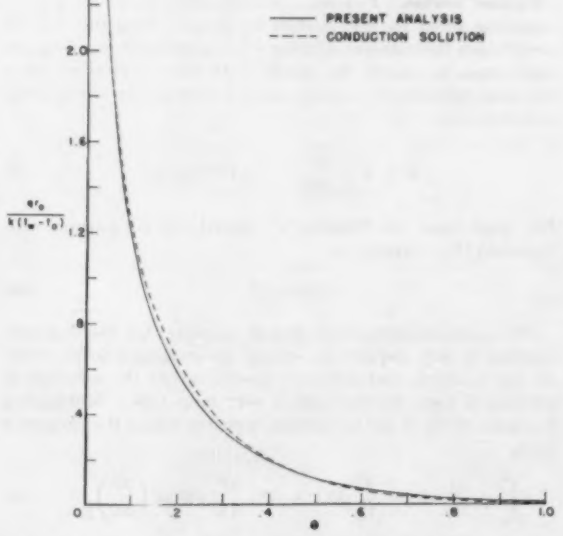

Fig. 2 Comparison of initial transient results in round tube with conduction transient

$$\frac{qr_0}{k(t_w - t_0)} = -\sum_{n=0}^{\infty} C_n \left.\frac{d\varphi_n}{dR}\right|_{R=1} e^{-\gamma_n \Theta} \qquad (21)$$

This expression provides the opportunity for evaluating, to some extent, the accuracy of the present method, since a direct comparison can be made with a known heat-conduction transient. The exact solution for the initial transient is that resulting from suddenly changing the surface temperature of an infinitely long solid cylinder. The surface heat-flux variation for this case is[5]

$$\frac{qr_0}{k(t_w - t_0)} = 2\sum_{n=0}^{\infty} e^{-\epsilon_n^2 \Theta} \qquad (22)$$

where ϵ_n are the zeros of the Bessel function J_0. Equation (21) has been evaluated for a seven-term approximation and is compared with Equation (22) in Fig. 2. The agreement is generally quite good, so the present solution not only gives good results near steady state as it is constrained to do, but is also well behaved in the initial transient region.

Returning now to Equation (20), it is noted that the nth term is a negative exponential in time until Θ becomes equal to $a_n X$. For larger Θ-values the term is a constant which depends only on the value of X being considered. Thus, for the seven-term approximation which has been carried out here, a graphical plot of the wall heat flux is found as the sum of seven different curves each of which is a negative exponential up to a certain break point and then becomes a constant. This is shown schematically in Fig. 3 which illustrates, in graphical form, the way in which the transient heat flux is determined at a given location along the tube. Equation (20) has been evaluated for several different values of X and results are shown in Fig. 4. The figure illustrates the transient process for several axial locations in the heated section.

Steady-State Times. A quantity of practical importance is the

[5] Reference [6], p. 262.

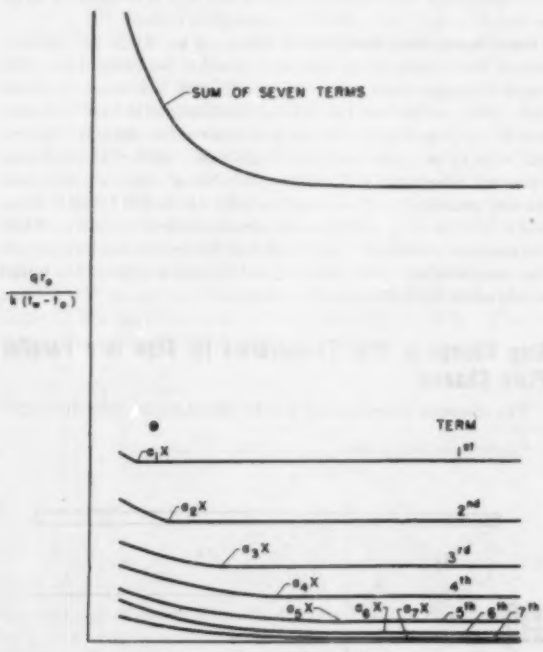

Fig. 3 Schematic representation of wall heat-flux computation following a step change in wall temperature

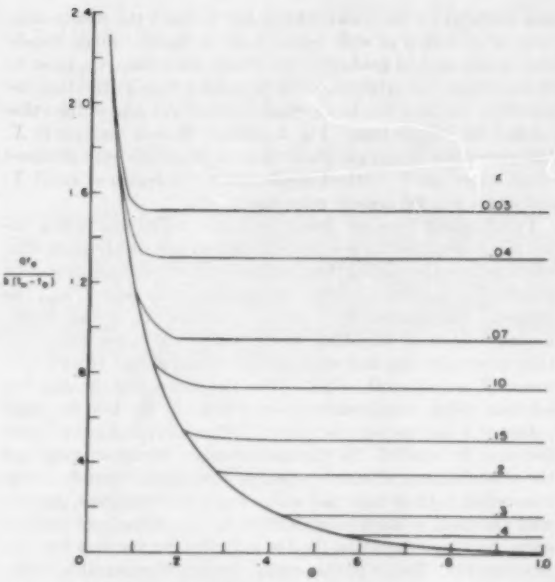

Fig. 4 Transient variation in wall heat flux following a step change in wall temperature for flow in a circular tube

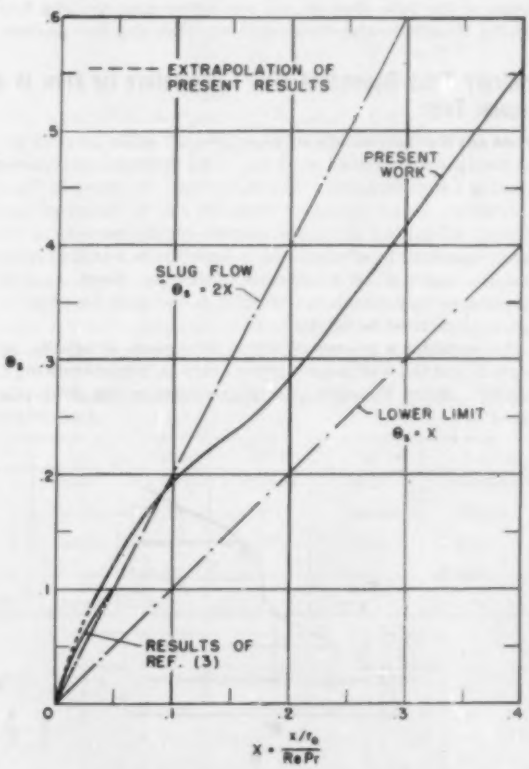

Fig. 5 Time to reach steady state after a step change in wall temperature for flow in a circular tube

time required for the wall heat transfer to reach the steady-state value after a step in wall temperature is made. Since steady state is approached gradually, the steady-state time, Θ_s, must be chosen somewhat arbitrarily. It is defined here as the time required for the heat flux to approach within 5 per cent of the value reached for infinite time. Fig. 5 presents Θ_s as a function of X. Also shown are the steady-state times of [3] which were obtained by an approximate method applicable in the region of small X, and which join the present curve fairly well.

Two limiting lines are drawn in Fig. 5. The line falling below the present results is a lower bound on the steady-state time which is found by saying that the heat-transfer process cannot be stabilized at a certain location until a time of at least x/u_{max} has elapsed. The relation $\theta_s = x/u_{max}$ is equivalent, in the dimensionless system of variables, to $\Theta_s = X$. The upper line is obtained from the slug flow solution [10], which gives a steady-state time of $\theta_s = x/\bar{u}$, or $\Theta_s = 2X$. This line shows that the slug flow solution yields steady-state times which are too low for small values of X and too high for large X. Physically this is due to the fact that for small X the thermal boundary layers are thin, and the establishment of steady state in this region depends on the convection process near the wall. Since the velocities near the wall are small, it takes longer for the fluid to move from the tube entry to a given location than is indicated by the slug flow approximation. Hence in this region the slug flow solution underestimates the steady-state time. For large X the establishment of steady state is evidently more dependent on the velocities farther away from the wall. This is because during the initial transient period, heat has been able to penetrate all the way across the tube and the fluid temperature near the wall has already been brought close to the wall temperature. Since the velocities in the central portion of the tube cross section are higher than the slug flow velocity, the steady-state times are lower than slug flow predicts.

Arbitrary Time-Dependent Wall Temperature for Flow in a Circular Tube

Fluid and Wall Both Initially at Temperature t_0. In the previous section results were obtained which described the transient behavior following a step change in wall temperature. As shown in Fig. 6 an arbitrary wall-temperature variation can be visualized as a series of differential steps, and because of the linearity of the energy equation the effects of these steps can be added to determine the response for an arbitrary variation. Since the wall-temperature variation is specified, it is the wall heat-flux response which must be determined.

First consider a process in which the system is initially isothermal, and the wall is then given a step in temperature dt_w at time Θ^*. From Equation (20) the response to this differential step is

$$dq = -\frac{k}{r_0}\sum_{n=0}^{\infty} C_n \left.\frac{d\varphi_n}{dR}\right|_{R=1} \begin{cases} e^{-\gamma_n(\Theta-\Theta^*)}, & 0 < (\Theta-\Theta^*) \leq a_n X \\ e^{-\beta_n^2 X}, & (\Theta-\Theta^*) \geq a_n X \end{cases} dt' \quad (23)$$

where $t' = t_w - t_0$. This response is then integrated over the arbitrary wall-temperature variation to obtain the variation in q. For a general discussion of this type of superposition procedure, the reader is referred to [11].[6] The integration of Equation (23) can be put in the form,

$$\frac{qr_0}{k}(\Theta, X) = \sum_{n=0}^{n=N-1} -C_n \left.\frac{d\varphi_n}{dR}\right|_{R=1} \left[e^{-\beta_n^2 X}(t')_{\Theta-a_nX} + \int_{\Theta-a_nX}^{\Theta} -\gamma_n e^{-\gamma_n(\Theta-\Theta^*)}\, t'(\Theta^*)d\Theta^*\right] + \sum_{n=N}^{\infty} \gamma_n C_n \left.\frac{d\varphi_n}{dR}\right|_{R=1} \int_0^{\Theta} e^{-\gamma_n(\Theta-\Theta^*)}\, t'(\Theta^*)d\Theta^* \quad (24)$$

where for a given Θ, the value of N is found from the relation

$$a_{N-1}X < \Theta \leqslant a_N X \quad (24a)$$

and for $N = 0$ we define the first summation as

$$\sum_{n=0}^{-1} \equiv 0,$$

and also let $a_{-1} \equiv 0$. To use this relation we can think in terms of evaluating the heat flux as a function of time at a particular X, say $X = X_i$. For early times, Θ will be less than all of the $a_n X_i$ and we use only the second summation from $n = 0$ to $n = \infty$. As we go to later times more and more terms are evaluated from the first summation. Since the problem, as given here, has only been evaluated for seven terms, when the time is sufficiently large so that $\Theta > a_6 X_i$ only the first summation is used.

Initial Steady-State Heat Transfer With $t_w \neq t_0$. Here we are concerned with computing the heat-transfer behavior when the transient begins from an initial steady-state heat-transfer situation. This can be done by utilizing the results of the previous section in the proper way. In the previous section the transient began with $t_w = t_0$ and we now begin again with this condition. Then we allow the wall temperature to go through any convenient transient (e.g., a step function) which will bring it to t_w, and it is kept at t_w until steady steady-state is reached. Then the specified transient is initiated and the results for this part of the computation yield the desired response from an initial steady-state heat-transfer condition.

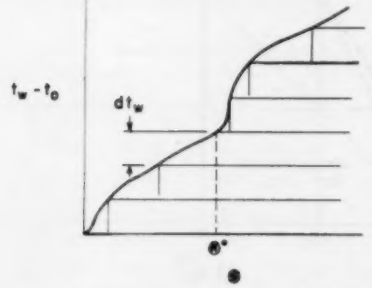

Fig. 6 Representation of arbitrary time-dependent wall temperature

Step Change in Wall Temperature for Flow in a Parallel Plate Channel

The transient problem will now be discussed for fully developed

[6] Reference [11], p. 403.

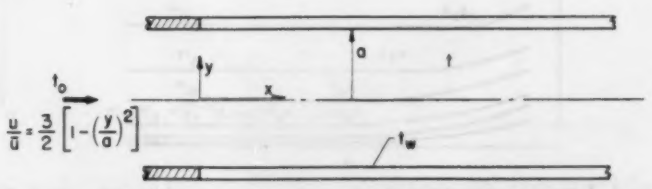

Fig. 7 Parallel-plate co-ordinate system

laminar flow between parallel flat plates as illustrated in Fig. 7. We consider the same step-function transient which was discussed for the circular tube; that is, the system is initially isothermal at temperature t_0 and the wall temperature is then suddenly changed to t_w. The final results are in the same form as those for the circular-tube case. Hence they can be generalized to include arbitrary time variations in wall temperature which yields an expression of the same form as Equation (24). Owing to this similarity only the results for a step change will be given here.

The energy equation analogous to Equation (1) is

$$\frac{\partial t}{\partial \theta} + u\frac{\partial t}{\partial x} = \alpha\frac{\partial^2 t}{\partial y^2} \tag{25}$$

This is rewritten in dimensionless form by defining the following variables:

$$\Theta = \frac{\theta\nu}{a^2\mathrm{Pr}}; \qquad X = \frac{8}{3}\frac{x/a}{\mathrm{Re\ Pr}}; \qquad Y = \frac{y}{a}; \qquad T = \frac{t - t_0}{t_w - t_0}$$

where $\mathrm{Re} = \bar{u}4a/\nu$. Inserting the fully developed velocity distribution,

$$\frac{u}{\bar{u}} = \frac{3}{2}\left[1 - \left(\frac{y}{a}\right)^2\right] \tag{26}$$

into Equation (25) yields the differential equation

$$\frac{\partial T}{\partial \Theta} + (1 - Y^2)\frac{\partial T}{\partial X} = \frac{\partial^2 T}{\partial Y^2} \tag{27}$$

which must be solved subject to the same boundary conditions as given by Equations (3a) with the co-ordinate Y replacing R.

Steady-State Solution. To obtain the transient solution we first consider the steady-state equation,

$$(1 - Y^2)\frac{\partial T_s}{\partial X} = \frac{\partial^2 T_s}{\partial Y^2} \tag{28}$$

For the circular tube the eigenfunctions, $\varphi(R)$, of Equation (7) were determined by numerical integration of the governing differential equation. For the parallel-plate channel another approach will be illustrated which provides an alternate method of attack. To begin this method we look at the slug flow problem corresponding to the situation described by Equation (28). For slug flow the velocity distribution, $1 - Y^2$, is replaced by a constant value. Reference [10] shows that the eigenfunctions for this case are in the form of cosines, $\cos[(2m + 1)\pi Y/2]$, where the m are integers from zero to infinity. It is then proposed to bring in the Y dependence of the velocity distribution by expanding the eigenfunctions in the solution of Equation (28) in terms of the eigenfunctions of the slug flow problem. Thus a solution to Equation (28) is tried in the form

$$T_s = 1 - \sum_{n=0}^{\infty} e^{-\lambda_n^2 X}\left[b_{n0}\cos\frac{\pi Y}{2} + b_{n1}\cos\frac{3\pi Y}{2} + b_{n2}\cos\frac{5\pi Y}{2} + \ldots\right]$$

or

$$T_s = 1 - \sum_{n=0}^{\infty} e^{-\lambda_n^2 X}\left[\sum_{m=0}^{\infty} b_{nm}\cos\frac{(2m+1)\pi Y}{2}\right] \tag{29}$$

For purposes of illustration, the procedure will be discussed here for a five-term approximation, that is, the m and n indexes will vary from 0 to 4.

If Equation (29) is substituted into Equation (28) there is obtained after rearrangement

$$(1 - Y^2)\left[b_{n0}\cos\frac{\pi Y}{2} + b_{n1}\cos\frac{3\pi Y}{2} + \ldots + b_{n4}\cos\frac{9\pi Y}{2}\right] - \left[\left(\frac{\pi}{2\lambda_n}\right)^2 b_{n0}\cos\frac{\pi Y}{2} + \left(\frac{3\pi}{2\lambda_n}\right)^2 b_{n1}\cos\frac{3\pi Y}{2} + \ldots + \left(\frac{9\pi}{2\lambda_n}\right)^2 b_{n4}\cos\frac{9\pi Y}{2}\right] = 0 \tag{30}$$

Equation (30) is then multiplied by $\cos(\pi Y/2)$ and integrated over Y from zero to 1. This results in the first of the following five simultaneous equations. Then Equation (30) is multiplied by $\cos 3\pi Y/2$ and integrated to yield the second equation, and this process is repeated for each of the cosine harmonics. This yields the set of five simultaneous equations for the five-term approximation being considered:

$$\left.\begin{aligned}
&\left(-\frac{\pi^2}{3} - 1 + \frac{\pi^4}{8\lambda_n^2}\right)b_{n0} - {}^3/_4\, b_{n1} + {}^5/_{28}\, b_{n2} - {}^7/_{144}\, b_{n3} + {}^9/_{400}\, b_{n4} = 0\\
&-{}^3/_4\, b_{n0} + \left(-\frac{\pi^2}{3} - {}^1/_9 + \frac{9\pi^4}{8\lambda_n^2}\right)b_{n1} - {}^{15}/_{16}\, b_{n2} + {}^{21}/_{100}\, b_{n3} - {}^1/_{12}\, b_{n4} = 0\\
&{}^5/_{28}\, b_{n0} - {}^{15}/_{16}\, b_{n1} + \left(-\frac{\pi^2}{3} - {}^1/_{25} + \frac{25\pi^4}{8\lambda_n^2}\right)b_{n2} - {}^{35}/_{36}\, b_{n3} + {}^{45}/_{196}\, b_{n4} = 0\\
&-{}^7/_{144}\, b_{n0} + {}^{21}/_{100}\, b_{n1} - {}^{35}/_{36}\, b_{n2} + \left(-\frac{\pi^2}{3} - {}^1/_{49} + \frac{49\pi^4}{8\lambda_n^2}\right)b_{n3} - {}^{63}/_{64}\, b_{n4} = 0\\
&{}^9/_{400}\, b_{n0} - {}^1/_{12}\, b_{n1} + {}^{45}/_{196}\, b_{n2} - {}^{63}/_{64}\, b_{n3} + \left(-\frac{\pi^2}{3} - {}^1/_{81} + \frac{81\pi^4}{8\lambda_n^2}\right)b_{n4} = 0
\end{aligned}\right\} \tag{31}$$

Since these equations are homogeneous, the b_{nm} can only be nontrivial if the matrix of their coefficients is zero, and hence the λ_n^2 are the roots of the coefficient matrix. The λ_n^2 were found by solving the matrix on an IBM 653 electronic digital computer using a double precision routine which carried 16 significant figures. An accuracy of about 12 figures in the λ_n^2-values was

Table 2 Coefficients in five-term approximation for flow between parallel plates

n	b_{n0}	b_{n1}/b_{n0}	b_{n2}/b_{n0}	b_{n3}/b_{n0}	b_{n4}/b_{n0}
0	1.17776	0.0211634	-0.00113896	0.000207037	-0.0000586707
1	.0579815	-5.37195	-.838971	.0230766	-.00930795
2	.0165696	-4.00649	9.45808	3.31526	-1.51483
3	.00706883	-3.59673	7.94700	-12.0113	-7.12402
4	.0136607	-3.32432	6.61879	-11.0745	13.7624

n	λ_n^2	σ_n	τ_n	ξ_n
0	2.82776	2.30858	2.82948	1.22564
1	32.1475	11.9441	32.3656	2.70975
2	93.4792	24.9156	95.2824	3.82421
3	187.388	37.4291	178.074	4.75764
4	414.761	92.5592	608.811	6.57754

found necessary to obtain good values of the b_{nm}. The λ_n^2 are listed in Table 2 and the first four show good agreement with those evaluated by other methods [8] and [12]. The poor agreement of λ_4^2 is due to the fact that only a five-term approximation is being used here.

With the λ_n^2 known, the set of homogeneous Equations (31) cannot be solved to yield all the b_{nm}, but will only yield four coefficients in each equation in terms of the fifth coefficient which remains yet undetermined. Thus, if each equation in the set is divided by its b_{n0} the ratios b_{n1}/b_{n0}, b_{n2}/b_{n0}, and so on, can be determined by solving any four of the resulting five simultaneous equations. The solution as given by Equation (29) is now in the form

$$T_s = 1 - \sum_{n=0}^{4} b_{n0} e^{-\lambda_n^2 X} \left[\cos \frac{\pi Y}{2} + \sum_{m=1}^{4} \frac{b_{nm}}{b_{n0}} \cos \frac{(2m+1)\pi Y}{2} \right] \quad (29a)$$

where the b_{nm}/b_{n0} are known.

To determine the b_{n0} we apply the boundary condition that $T_s = 0$ at $X = 0$. This yields

$$1 = \sum_{n=0}^{4} b_{n0} \left[\cos \frac{\pi Y}{2} + \sum_{m=1}^{4} \frac{b_{nm}}{b_{n0}} \cos \frac{(2m+1)}{2} \pi Y \right] \quad (32)$$

Equation (32) is now multiplied separately by each of the cos $(2m+1)\pi Y/2$ and integrated over Y from zero to 1. This yields, for the five-term approximation, five simultaneous equations for the unknown b_{n0},

$$\sum_{n=0}^{4} b_{n0} = \frac{4}{\pi}$$

$$\left[\sum_{n=0}^{4} \left(\frac{b_{nm}}{b_{n0}} \right) b_{n0} = (-1)^m \frac{4}{(2m+1)\pi} \right]_{m=1,2,3,4} \quad (33)$$

When the b_{n0} have been determined from this set, Equation (29a) provides the complete solution to the steady-state problem. The numerical values of the constants are given in Table 2.

Transient Solution. The steady-state solution as given by Equation (29a) is seen to be of the same form as that obtained for the round pipe, Equation (8), except that the eigenfunctions are given in terms of cosine series expansions rather than by $\varphi_n(r)$ which are obtained by numerical integration of an ordinary differential equation. Since the two results are of the same basic form, the solution of the transient equation follows as before and will only be given in brief outline here.

The energy Equation (27) is integrated to yield,

$$\frac{\partial}{\partial \Theta} \int_0^1 T \, dY + \frac{\partial}{\partial X} \int_0^1 (1 - Y^2) T \, dY = \left. \frac{\partial T}{\partial Y} \right|_{Y=1} \quad (34)$$

Table 3 Coefficients in three-term approximation for flow between parallel plates

n	b_{n0}	b_{n1}/b_{n0}	b_{n2}/b_{n0}
0	1.18025	0.0211847	-0.00114101
1	.0589906	-5.37097	-.842957
2	.0339989	-3.89954	8.99210

n	λ_n^2	σ_n	τ_n	f_n
0	2.82777	2.31357	2.85546	1.22568
1	32.1508	12.1389	32.9332	2.71304
2	104.683	34.7142	144.296	4.15668

A transient solution is then assumed in the form

$$T = 1 - \sum_{n=0}^{4} b_{n0} G_n(X, \Theta) \left[\cos \frac{\pi Y}{2} + \sum_{m=1}^{4} \frac{b_{nm}}{b_{n0}} \cos \frac{(2m+1)\pi Y}{2} \right] \quad (35)$$

and this is inserted into Equation (34). After the integrations are carried out, this yields the following partial differential equation for a five-term approximation,

$$\frac{2}{\pi} \left(1 - {}^1/_3 \frac{b_{n1}}{b_{n0}} + {}^1/_5 \frac{b_{n2}}{b_{n0}} - {}^1/_7 \frac{b_{n3}}{b_{n0}} + {}^1/_9 \frac{b_{n4}}{b_{n0}} \right) \frac{\partial G_n}{\partial \Theta}$$
$$+ \frac{16}{\pi^2} \left(1 - \frac{1}{(3)^3} \frac{b_{n1}}{b_{n0}} + \frac{1}{(5)^3} \frac{b_{n2}}{b_{n0}} - \frac{1}{(7)^3} \frac{b_{n3}}{b_{n0}} + \frac{1}{(9)^3} \frac{b_{n4}}{b_{n0}} \right) \frac{\partial G_n}{\partial X}$$
$$+ \frac{\pi}{2} \left(1 - 3 \frac{b_{n1}}{b_{n0}} + 5 \frac{b_{n2}}{b_{n0}} - 7 \frac{b_{n3}}{b_{n0}} + 9 \frac{b_{n4}}{b_{n0}} \right) G_n = 0$$

This is of the same form as Equation (12) and hence the solution can be written immediately by analogy with the previous solution, Equation (18),

$$T = 1 - \sum_{n=0}^{4} b_{n0} \left[\cos \frac{\pi Y}{2} + \sum_{m=1}^{4} \frac{b_{nm}}{b_{n0}} \cos \frac{(2m+1)\pi Y}{2} \right] \begin{cases} e^{-\sigma_n \Theta}, & \Theta \le f_n X \\ e^{-\tau_n X}, & \Theta \ge f_n X \end{cases} \quad (36)$$

where

$$\sigma_n = \frac{\pi^2}{4} \frac{\left[1 + \sum_{m=1}^{4} (2m+1)(-1)^m \frac{b_{nm}}{b_{n0}} \right]}{\left[1 + \sum_{m=1}^{4} \frac{1}{(2m+1)} (-1)^m \frac{b_{nm}}{b_{n0}} \right]} \quad (36a)$$

$$\tau_n = \frac{\pi^4}{32} \frac{\left[1 + \sum_{m=1}^{4} (2m+1)(-1)^m \frac{b_{nm}}{b_{n0}} \right]}{\left[1 + \sum_{m=1}^{4} \frac{1}{(2m+1)^3} (-1)^m \frac{b_{nm}}{b_{n0}} \right]} \quad (36b)$$

and

$$f_n = \tau_n / \sigma_n$$

Numerical values of σ_n, τ_n, and f_n are given in Table 2 for a five-term approximation. Table 3 gives values for a three-term approximation which, when compared with Table 2, indicates how the solution converges with increasing numbers of terms in the approximation.

Wall Heat Flux. By using Fourier's law the heat transferred at the channel walls is obtained as

$$\frac{qa}{k(t_w - t_0)} = \frac{\pi}{2} \sum_{n=0}^{\infty} b_{n0} \left[1 + \sum_{m=1}^{\infty} \frac{b_{nm}}{b_{n0}} (-1)^m (2m+1) \right] \begin{cases} e^{-\sigma_n \Theta}, & \Theta \le f_n X \\ e^{-\tau_n X}, & \Theta \ge f_n X \end{cases} \quad (37)$$

In the initial transient period this reduces to the purely time-dependent equation,

$$\frac{qa}{k(t_w - t_0)} = \frac{\pi}{2} \sum_{n=0}^{\infty} b_{n0} \left[1 + \sum_{m=1}^{\infty} \frac{b_{nm}}{b_{n0}} (-1)^m (2m+1) \right] e^{-\sigma_n \Theta} \quad (38)$$

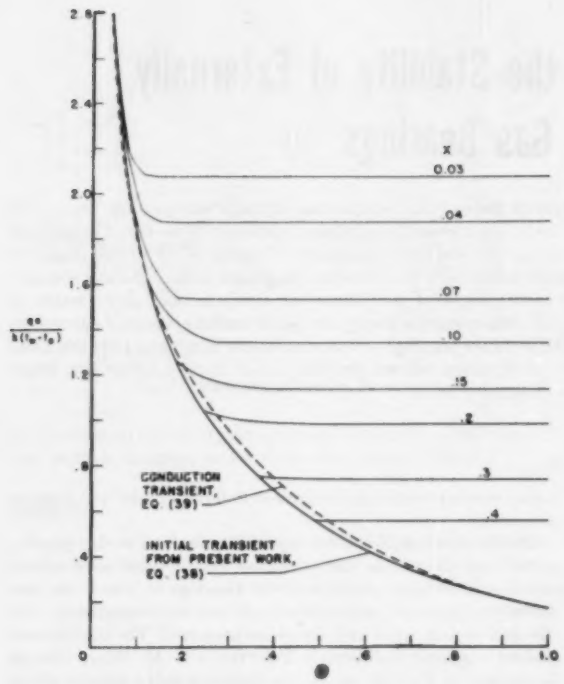

Fig. 8 Transient variation in wall heat flux following a step change in wall temperature for flow between parallel flat plates

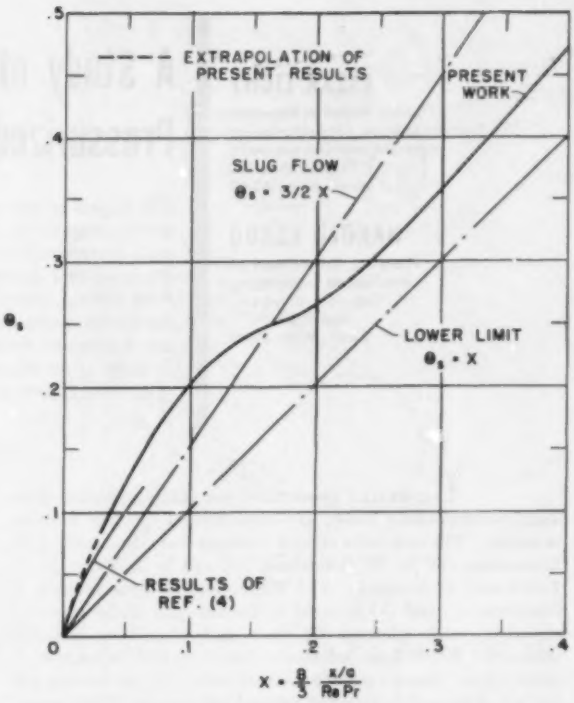

Fig. 9 Time to reach steady state after a step change in wall temperature for flow between parallel flat plates

This can be compared with the pure conduction solution resulting from suddenly changing the temperature at the surfaces of a slab of finite thickness and infinite extent[5]

$$\frac{qa}{k(t_w - t_0)} = 2\sum_{n=0}^{\infty} e^{-(2n+1)^2\frac{\pi^2}{4}\Theta} \tag{39}$$

Curves calculated from Equations (38) and (39) are included in Fig. 8, and good agreement is obtained.

Figs. 8 and 9 show the transient heat flux and steady-state times as a function of location along the channel. These results were obtained from Equation (37) in the same way that the computations were made for the circular-tube case. The lower limiting curve in Fig. 9 is obtained by letting the steady-state time be x/u_{max} which is equivalent to $\Theta_s = X$, while for the slug flow assumption $\theta_s = x/\bar{u}$ or $\Theta_s = (3/2)X$. The curve of steady-state time for small X, as given in [4], is also shown and joins fairly well onto the present results.

References

1 J. A. Clark, V. S. Arpaci, and K. M. Treadwell, "Dynamic Response of Heat Exchangers Having Internal Heat Sources—Part I," TRANS. ASME, vol. 80, 1958, pp. 612–624.

2 V. S. Arpaci and J. A. Clark, "Dynamic Response of Heat Exchangers Having Internal Heat Sources—Part II," TRANS. ASME, vol. 80, 1958, pp. 625–634.

3 E. M. Sparrow and R. Siegel, "Thermal Entrance Region of a Circular Tube Under Transient Heating Conditions," Proceedings of the Third U. S. Congress for Applied Mechanics, ASME, 1958, pp. 817–826.

4 R. Siegel and E. M. Sparrow, "Transient Heat Transfer for Laminar Forced Convection in the Thermal Entrance Region of Flat Ducts," *Journal of Heat Transfer*, TRANS. ASME (Series C), vol. 81, 1959, pp. 29–36.

5 Knox Millsaps and Karl Pohlhausen, "Heat Transfer to Hagen-Poiseuille Flows," *Proceedings*, Conference on Differential Equations, University of Maryland, March, 1955.

6 M. Jakob, "Heat Transfer," vol. 1, John Wiley & Sons, Inc., New York, N. Y., 1949.

7 R. P. Lipkis, discussion of paper by Sellars, Tribus, and Klein, TRANS. ASME, vol. 78, 1956, p. 448.

8 J. R. Sellars, M. Tribus, and J. S. Klein, "Heat Transfer to Laminar Flow in a Round Tube or Flat Conduit—The Graetz Problem Extended," TRANS. ASME, vol. 78, 1956, pp. 441–448.

9 F. B. Hildebrand, "Advanced Calculus for Engineers," Prentice-Hall, Inc., New York, N. Y., 1949.

10 R. Siegel, "Transient Heat Transfer for Laminar Slug Flow in Ducts," JOURNAL OF APPLIED MECHANICS, vol. 26, TRANS. ASME, vol. 81, series E, 1959, pp. 140–142.

11 T. von Kármán and M. A. Biot, "Mathematical Methods in Engineering," McGraw-Hill Book Company, Inc., New York, N. Y., 1940.

12 C. S. Yih and J. E. Cermak, "Laminar Heat Convection in Pipes and Ducts," Report No. 5, Civil Engineering Department, Colorado Agricultural and Mechanical College, September, 1951.

LAZAR LICHT
Senior Research Engineer,
The Franklin Institute, Laboratories for Research and Development,
Philadelphia, Pa.
Assoc. Mem. ASME

HAROLD ELROD
Professor, Department of Mechanical Engineering,
Columbia University,
New York, N. Y.
Assoc. Mem. ASME

A Study of the Stability of Externally Pressurized Gas Bearings[1]

The subject of this paper is the stability of externally pressurized gas bearings. The pertinent equations of motion are linearized and the stability criteria stated in terms of small deviations from the equilibrium operating point. The flow in the bearing clearance is treated on a distributed rather than on a lumped-parameter basis. Results obtained from present analysis when compared with those previously arrived at by means of simplified analyses [1, 3][2] show a marked divergence in the limiting values of parameters which influence the stability of the bearing. These results and divergences are discussed in terms of permissible compression volume, pressure ratios, supply-nozzle size, length of annular clearance, and bearing mass.

EXTERNALLY pressurized gas bearings, unlike those using incompressible fluids, are characterized by their unstable behavior. The dynamics of such bearings were discussed by H. Richardson [1], W. H. Roudebush [2], and by L. Licht, D. D. Fuller, and B. Sternlicht [3]. The approach to the problem in references [1] and [3] is based on linearization of the pertinent equations, while reference [2] offers specific nonlinear computer solutions. In all these references, however, the "squeeze-film" effect which accompanies the relative motion of the bearing surfaces is described in terms of lumped parameters. The manner in which the pressure varies with time along the bearing clearance is assumed in advance and expressed in terms of inlet and ambient pressures.

The distributed-parameter approach presented in this paper is an attempt to examine the validity of such *a priori* assumptions and simplifications, particularly for bearings in which the area corresponding to the clearance is large, or at least comparable with the area exposed to a uniform recess pressure. The discussion is limited to geometries shown in Figs. 1(*a*) and (*b*). The rectangular element of Fig. 1(*a*) can be thought of as unit length of a long, rectangular bearing which can be approximated in practice by the circular thrust plate in Fig. 2(*a*), provided the inner and outer radii are large and do not differ greatly in magnitude. It can be considered also as the "equivalent" slot of a developed journal bearing [1, 5] as illustrated in Fig. 2(*b*). The circular bearing shown schematically in Fig. 1(*b*) is identical with those discussed in references [2] and [3].

Referring to Fig. 1, we assume that one surface is fixed while the other, including the attached mass, m, is free to move in the z-direction only. Gas from a constant-pressure reservoir enters the recess via a nozzle and its *mean* flow in the annulus is taken to be in the x (or r)-direction only. The variation in gap width induces pressure changes which depend on time as well as on the distance along the annulus, but which are assumed to vary uni-

[1] The research underlying this paper was done in part by L. Licht in partial fulfillment of requirements for the degree of Doctor of Engineering Science at Columbia University.

[2] Numbers in brackets designate References at end of paper.

For presentation at the Summer Conference of the Applied Mechanics Division, University Park, Pa., June 20–22, 1960, of THE AMERICAN SOCIETY OF MECHANICAL ENGINEERS.

Discussion of this paper should be addressed to the Secretary, ASME, 29 West 39th Street, New York, N. Y., and will be accepted until July 22, 1960, for publication at a later date. Discussion received after the closing date will be returned.

NOTE: Statements and opinions advanced in papers are to be understood as individual expressions of their authors and not those of the Society. Manuscript received by ASME Applied Mechanics Division, April 29, 1959. Paper No. 60—APM-5.

Nomenclature

Linear Dimensions

$2X_r$ = width of recess, in.
$2X$ = width of bearing, in.
$2R_r$ = recess diameter, in.
$2R$ = bearing diameter, in.
H = width of annulus, in.
$h = H - H_0$ = deviation from equilibrium value H_0, in.
d = nozzle diameter, in.
δ = depth of recess, in.
x = co-ordinate in Cartesian system, in.
r = co-ordinate in cylindrical system, in.

Pressures

P = pressure, psia
$p_r = P_r - P_{r0}$ = deviation of recess pressure from equilibrium value P_{r0}, psi
$p = P - P_0$ = deviation of pressure in annulus from equilibrium value P_0, psi

Other Quantities

L = bearing load, lb.
m = mass of bearing, lb-sec²/in.
M = gas mass content of bearing, lb-sec²/in.
W_1 = rate of gas flow into recess, lb-sec/in.
W_2 = rate of gas flow out of recess lb-sec/in.
$W_0 = (W_1)_0 = (W_2)_0$ = rate of gas-flow equilibrium, lb-sec/in.
ρ = gas density lb-sec²/in.⁴
t = time, sec
μ = viscosity of gas, lb-sec/in.²
T_0 = gas temperature, equilibrium, deg F abs
R = gas constant, in²/sec²-deg F abs
γ = ratio of specific heats
s = complex variable, 1/sec
ω = imaginary part of complex variables, 1/sec; also circular frequency rad/sec

Subscripts

at = atmospheric or ambient
c = critical
o = equilibrium
r = recess
s = supply
$(\cdot)$ = denotes differentiation with respect to time
$(')$ = denotes differentiation with respect to any other (mainly space) independent variable

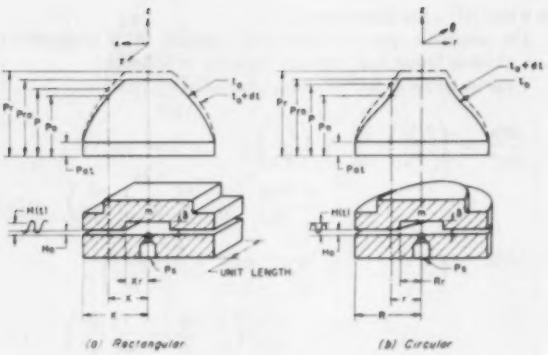

Fig. 1 Schematic of bearing geometry

formly over the recess region, provided the depth of the recess is large enough in comparison with the magnitude of the slot.

Analysis

In what follows, basic equations are simultaneously developed for the two configurations shown in Figs. 1(*a*) and (*b*). Equations applicable to both geometries are denoted with plain numbers. Those denoted by the letter *a* refer to the rectangular geometry, while those denoted by the letter *b* refer to the circular geometry. The equation representing the conservation of mass for the recess region, Fig. 1, is

$$\frac{dM_r}{dt} = W_1 - W_2 \tag{1}$$

in which

$$\begin{cases} M_r = 2X_r(\delta + H)\rho_r & (2a) \\ M_r = \pi R_r^2(\delta + H)\rho_r & (2b) \end{cases}$$

$$\begin{cases} W_2 = -\dfrac{H^3}{6\mu}\left(\rho\,\dfrac{\partial P}{\partial x}\right)_{X_r} & (3a) \\ W_2 = -\dfrac{\pi H^3}{6\mu}\left(r\rho\,\dfrac{\partial P}{\partial r}\right)_{R_r} & (3b) \end{cases}$$

$$W_1 = 2\left(\frac{\pi d^2}{4}\right)\left[\frac{\gamma}{RT_0}\left(\frac{2}{\gamma+1}\right)^{\frac{\gamma+1}{\gamma-1}}(P_s P_r - P_r^2)\right]^{1/2} \tag{4}[3]$$

The pressure-density relationship in the recess region can be described adequately by the equation:

$$\left(\frac{\rho_r}{\rho_{ro}}\right)^{\gamma} = \frac{P_r}{P_{ro}} \tag{5}$$

but the proximity of the metallic surfaces suggests an isothermal [4] rather than an adiabatic change in the annular region; e.g.,

$$p = \frac{p}{RT_0} \tag{6}$$

The bearing and attached mass are restrained to move in the axial direction only. Hence in the absence of external damping,[4] the equation of motion is

[3] The flow through the supply nozzle can be approximated closely by a quadrant of an ellipse whenever P_r/P_s is considerably above the critical-pressure ratio. This is Fliegner's approximation, and is convenient for computational purposes.

[4] The inclusion of a velocity proportional term in the equation of motion would adequately approximate the effect of external damping without introducing additional difficulties into the analysis.

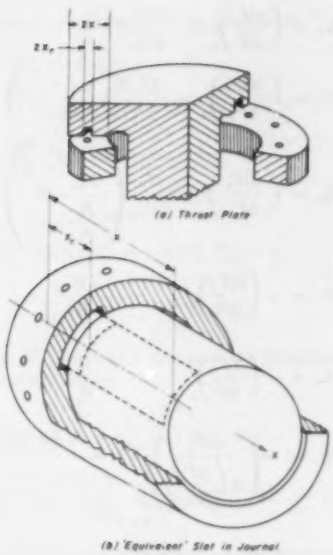

Fig. 2

$$\begin{cases} m\,\dfrac{d^2H}{dt^2} = 2X_r(P_r - P_{ro}) + 2\displaystyle\int_{X_r}^{X}(P - P_0)dx + F(t) & (7a) \\ m\,\dfrac{d^2H}{dt^2} = \pi R_r^2(P_r - P_{ro}) + 2\pi\displaystyle\int_{R_r}^{R}(P - P_0)rdr + F(t) & (7b) \end{cases}$$

in which

$$P_r = P_r(t); \quad P = \begin{cases} P(x, t) \\ P(r, t) \end{cases}$$

and $F(t)$ is the excitation function.

For the annular region a simplified version of the Navier Stokes' equation, as applicable to predominantly viscous, laminar and isothermal flow, is combined with the continuity equation, resulting in the following:

$$\begin{cases} \dfrac{\partial}{\partial x}\left(P\,\dfrac{\partial P}{\partial x}\right) = \dfrac{12\mu}{H^3}\,\dfrac{\partial}{\partial t}\,(PH) & (8a) \\ \dfrac{1}{r}\,\dfrac{\partial}{\partial r}\left(rP\,\dfrac{\partial P}{\partial r}\right) = \dfrac{12\mu}{H^3}\,\dfrac{\partial}{\partial t}\,(PH) & (8b) \end{cases}$$

In the next step the perturbation quantities

$$\begin{aligned} P - P_0 &= p \\ P_r - P_{ro} &= p_r \\ H - H_0 &= h \end{aligned} \tag{9}$$

and their derivatives are introduced. Neglecting their squares and cross products as quantities of higher order, we obtain instead of equations (1), (7), and (8) a set of corresponding expressions. Equation (1) reduces to

$$\begin{cases} K_1\,\dfrac{dh}{dt} - K_4 h = (K_2 + K_5)p_r + K_6\,\dfrac{\partial p_r}{\partial x} - K_2\,\dfrac{\partial p_r}{\partial t} & (10a) \\ C_1\,\dfrac{dh}{dt} - C_4 h = (C_2 + C_5)p_r + C_6\,\dfrac{\partial p_r}{\partial r} - C_2\,\dfrac{\partial p_r}{\partial t} & (10b) \end{cases}$$

in which the coefficients K and C represent the quantities listed in the following:

$$
\left.
\begin{aligned}
K_1 &= \left(\frac{\partial M_r}{\partial H}\right)_0 = \frac{2X_rP_{ro}}{RT_0} \\
K_2 &= \left(\frac{\partial M_r}{\partial P_r}\right)_0 = \frac{2X_rH_0}{\gamma RT_0}\left(\frac{\delta}{H_0}+1\right) \\
K_3 &= \left(\frac{\partial W_1}{\partial P_r}\right)_0 = \frac{W_0}{2P_{ro}}\left(\frac{\dfrac{P_s}{P_{ro}}-2}{\dfrac{P_s}{P_{ro}}-1}\right) \\
K_4 &= -\left(\frac{\partial W_2}{\partial H}\right)_{\substack{0\\ x=X_r}} = -\frac{3W_0}{H_0} \\
K_5 &= -\left(\frac{\partial W_2}{\partial P}\right)_{\substack{0\\ x=X_r}} = -\frac{W_0}{P_{ro}} \\
K_6 &= -\left(\frac{\partial W_2}{\partial\left(\dfrac{\partial P}{\partial x}\right)}\right)_{\substack{0\\ x=X_r}} = -\frac{2P_{ro}W_0}{A_0}
\end{aligned}
\right\} \tag{11a}
$$

$$
\left.
\begin{aligned}
C_1 &= \left(\frac{\partial M_r}{\partial H}\right)_0 = \frac{\pi R_r^2P_{ro}}{RT_0} \\
C_2 &= \left(\frac{\partial M_r}{\partial P_r}\right)_0 = \frac{\pi R_r^2H_0}{\gamma RT_0}\left(\frac{\delta}{H_0}+1\right) \\
C_3 &= \left(\frac{\partial W_1}{\partial P_r}\right)_0 = \frac{W_0}{2P_{ro}}\left(\frac{\dfrac{P_s}{P_{ro}}-2}{\dfrac{P_s}{P_{ro}}-1}\right) \\
C_4 &= -\left(\frac{\partial W_2}{\partial H}\right)_{\substack{0\\ r=R_r}} = -\frac{3W_0}{H_0} \\
C_5 &= -\left(\frac{\partial W_2}{\partial P}\right)_{\substack{0\\ r=R_r}} = -\frac{W_0}{P_{ro}} \\
C_6 &= -\left[\frac{\partial W_2}{\partial\left(\dfrac{\partial P}{\partial r}\right)}\right]_{\substack{0\\ r=R_r}} = -\frac{2R_rP_{ro}W_0}{B_0}
\end{aligned}
\right\} \tag{11b}
$$

in which

$$P_0(x) = [P_{ro}^2 + A_0(x - X_r)]^{1/2}$$

$$P_0(r) = \left(P_{ro}^2 + B_0 \log_e \frac{r}{R_r}\right)^{1/2}$$

$$A_0 = -\frac{P_{ro}^2 - P_{at}^2}{X - X_r} \qquad B_0 = -\frac{P_{ro}^2 - P_{at}^2}{\log_e \dfrac{R}{R_r}}$$

The subscripts 0 and r refer to the equilibrium point and the recess boundary, respectively.

Thus $(\ )_{\substack{0\\ x=X_r}}$ signifies that the partial derivative is evaluated at the equilibrium point and at the edge of the recess. From equation (7) we obtain:

$$m\frac{d^2h}{dt^2} = 2X_rp_r + 2\int_{X_r}^{X} p\,dx + f(t) \tag{12a}$$

$$m\frac{d^2h}{dt^2} = \pi R_r^2p_r + 2\pi\int_{R_r}^{R} pr\,dr + f(t) \tag{12b}$$

in which $f(t)$ is the disturbance.

The nonlinear, partial differential equation (8) is replaced by one which is linear, but contains variable coefficients.

Thus in terms of perturbation quantities we have:

$$\frac{\partial^2p}{\partial x^2} + \left(\frac{2P_0'}{P_0}\right)\frac{\partial p}{\partial x} + \left(\frac{P_0''}{P_0}\right)p = \frac{12\mu}{H_0^2}\left(\frac{1}{P_0}\frac{\partial p}{\partial t} + \frac{1}{H_0}\frac{dh}{dt}\right) \tag{13a}$$

$$\frac{\partial^2p}{\partial r^2} + \left(\frac{2P_0'}{P_0} + \frac{1}{r}\right)\frac{\partial p}{\partial r} + \left(\frac{P_0''}{P_0} + \frac{1}{r}\frac{P_0'}{P_0}\right)p = \frac{12\mu}{H_0^2}\left(\frac{1}{P_0}\frac{\partial p}{\partial t} + \frac{1}{H_0}\frac{dh}{dt}\right) \tag{13b}$$

Solutions of equation (13) must satisfy equations (10) and (12) as well as the boundary condition

$$p(X, t) = 0 \tag{14a}$$

$$p(R, t) = 0 \tag{14b}$$

The first space derivative in equation (13) can be eliminated by means of the following substitution:

$$p = \frac{v}{P_0} = \frac{v}{z^{1/2}} \tag{15a}$$

$$p = \frac{v}{r^{1/2}P_0} \tag{15b}$$

Introducing the new variable v into equations (10), (12), and (13) we take the Laplace transform under the assumption of initial rest conditions.

Then with

$$\mathfrak{L}_t(v) \equiv \bar{V} \equiv \int_0^\infty ve^{-st}dt$$

$$\mathfrak{L}_t(h) \equiv \bar{h} \equiv \int_0^\infty he^{-st}dt$$

$$\mathfrak{L}_t(f) \equiv \bar{f} \equiv \int_0^\infty fe^{-st}dt$$

equation (10) transforms to:

$$(sK_1 - K_4)\frac{\bar{h}}{H_0} + (sK_2 - K_3)\frac{(\bar{V})_{P_{ro}^2}}{H_0P_{ro}} - \frac{2P_{ro}}{H_0}K_5\left(\frac{\partial\bar{V}}{\partial z}\right)_{P_{ro}^2} = 0 \tag{16a}$$

$$(sC_1 - C_4)\frac{\bar{h}}{H_0} + \left(sC_2 - C_3 + C_5\frac{P_{ro}^2}{B_0}\right)\frac{(\bar{V})_{R_r}}{H_0R_r^{1/2}P_{ro}} - \frac{2R_r^{1/2}P_{ro}}{B_0H_0}C_5\left(\frac{\partial\bar{V}}{\partial r}\right)_{R_r} = 0 \tag{16b}$$

in which the coefficients K_6 and C_6 have been replaced by means of the identity

$$K_6 = \frac{2P_{ro}^2}{A_0}K_5 \tag{17a}$$

$$C_6 = \frac{2R_rP_{ro}^2}{B_0}C_5 \tag{17b}$$

Equation (12) transforms to:

$$\begin{cases} ms^2 \dfrac{\bar{h}}{H_0} - \dfrac{2X_r}{H_0 P_{ro}} (\bar{V})_{P_{ro}^2} \\ \qquad + \dfrac{2(X - X_r)}{H_0(P_{ro}^2 - P_{at}^2)} \displaystyle\int_{P_{ro}^2}^{P_{at}^2} \frac{\bar{V}}{z^{1/2}}\, dz = \bar{f}(s) \end{cases} \quad (18a)$$

$$ms^2 \frac{\bar{h}}{H_0} - \frac{\pi R_r^{3/2} (\bar{V})_{R_r}}{H_0 P_{ro}} - \frac{2\pi}{H_0} \int_{R_r}^{R} \frac{\bar{V} r^{1/2}}{P_0}\, dr = f(s) \quad (18b)$$

Equation (13) transforms to:

$$\begin{cases} \bar{V}'' - \dfrac{\epsilon s}{z^{1/2}} V = \epsilon s z^{1/2} \dfrac{\bar{h}}{H_0} \end{cases} \quad (19a)$$

$$\begin{cases} \bar{V}'' + \left(\dfrac{1}{4r^2} - \dfrac{\eta s}{P_0} \right) \bar{V} = \eta s r^{1/2} P_0 \dfrac{\bar{h}}{H_0} \end{cases} \quad (19b)$$

in which

$$\begin{cases} \epsilon = \dfrac{12\mu}{H_0^3 A_0^3} = \dfrac{12\mu}{H_0^3} \left(\dfrac{X - X_r}{P_{ro}^2 - P_{at}^2} \right)^2 \end{cases} \quad (20a)$$

$$\begin{cases} \eta = \dfrac{12\mu}{H_0^3} \end{cases} \quad (20b)$$

Finally, the boundary condition (14) transforms to

$$\begin{cases} \bar{V}(P_{at}^2, s) = 0 \end{cases} \quad (21a)$$

$$\begin{cases} \bar{V}(R_r, s) = 0 \end{cases} \quad (21b)$$

Furthermore, by integrating equation (19) between the appropriate limits, we can replace the integral in equation (18). For this purpose we have

$$\begin{cases} \displaystyle\int_{P_{ro}^2}^{P_{at}^2} \frac{\bar{V}}{z^{1/2}}\, dz = {}^2/_3 (P_{ro}^2 - P_{at}^2) \frac{\bar{h}}{H_0} \\ \qquad - \dfrac{1}{\epsilon s} \left[\left(\dfrac{\partial \bar{V}}{\partial z} \right)_{P_{ro}^2} - \left(\dfrac{\partial \bar{V}}{\partial z} \right)_{P_{at}^2} \right] \end{cases} \quad (22a)$$

$$\begin{cases} \displaystyle\int_{R_r}^{R} \frac{\bar{V} r^{1/2}}{P_0}\, dr = -g \frac{\bar{h}}{H_0} \\ \qquad - \dfrac{1}{\eta s} \left[R_r^{1/2} \left(\dfrac{\partial \bar{V}}{\partial r} \right)_{R_r} - R^{1/2} \left(\dfrac{\partial \bar{V}}{\partial r} \right)_{R} - \dfrac{(\bar{V})_{R_r}}{2R_r} \right] \end{cases} \quad (22b)$$

in which

$$g = \int_{R_r}^{R} P_0(r) r\, dr \quad (23)$$

The foregoing integral is expressed explicitly in Appendix 1.

A particular solution of equation (19) is:

$$\begin{cases} \bar{V}_P = -\dfrac{\bar{h}}{H_0} z \end{cases} \quad (24a)$$

$$\begin{cases} \bar{V}_P = -\dfrac{\bar{h}}{H_0} r^{1/2} P_0^2(r) \end{cases} \quad (24b)$$

If y_I and y_{II} are two independent solutions which satisfy the homogeneous part of the differential equation (19), then

$$\begin{cases} Q(z, \zeta) = \dfrac{y_I(z) y_{II}(\zeta) - y_I(\zeta) y_{II}(z)}{y_I(P_{ro}^2) y_{II}(P_{at}^2) - y_I(P_{at}^2) y_{II}(P_{ro}^2)} \end{cases} \quad (25a)$$

$$\begin{cases} Q(r, \rho) = \dfrac{y_I(r) y_{II}(\rho) - y_I(\rho) y_{II}(r)}{y_I(R_r) y_{II}(R) - y_I(R) y_{II}(R_r)} \end{cases} \quad (25b)$$

are also solutions having the following properties:

$$\begin{cases} Q(z, z) = 0 \\ Q(P_{ro}^2, P_{at}^2) = -Q(P_{at}^2, P_{ro}^2) = 1 \\ \dfrac{\partial Q}{\partial \zeta}(z, z) = \text{constant}^* \end{cases} \quad (26a)$$

$$\begin{cases} Q(r, r) = 0 \\ Q(R_r, R) = -Q(R, R_r) = 1 \\ \dfrac{\partial Q}{\partial \rho}(r, r) = \text{const}^* \end{cases} \quad (26b)$$

The solution of (19) which satisfies the boundary condition (21) can then be written as:

$$\begin{cases} \bar{V} = \bar{A} Q(P_{at}^2, z) + \dfrac{\bar{h}}{H_0} [P_{at}^2 Q(P_{ro}^2, z) - z] \end{cases} \quad (27a)$$

$$\begin{cases} \bar{V} = \bar{A} Q(R, r) + \dfrac{\bar{h}}{H_0} [R^{1/2} P_{at}^2 Q(R_r, r) - r^{1/2} P_0^2(r)] \end{cases} \quad (27b)$$

in which $\bar{A}(s)$ and $\bar{h}(s)$ are determined from equations (16) and (18).

Using equation (22) and substituting into equation (16) the boundary values of $\bar{V}$ and its derivatives obtained by differentiation of equation (27), we have at our disposal two simultaneous equations for the determination of $\bar{A}(s)$ and $\bar{h}(s)$. The "two by two" determinant formed from the coefficients of the homogeneous parts of these equations is then set equal to zero. The location in the complex plane of roots of this characteristic equation determines the stability of the bearing. The characteristic determinant referred to in the foregoing is as follows:

$$\begin{vmatrix} \dfrac{mH_0\epsilon}{2X_r} \left(\dfrac{P_{ro}^2 - P_{at}^2}{\dfrac{X}{X_r} - 1} \right) s^2 + {}^2/_3 (P_{ro}^2 - P_{at}^2) \epsilon s \\ \qquad + \left[P_{ro}^2 \dfrac{\partial Q}{\partial \zeta}(P_{at}^2, P_{ro}^2) + P_{at}^2 \dfrac{\partial Q}{\partial \zeta}(P_{ro}^2, P_{at}^2) \right. \\ \qquad \left. - (P_{ro}^2 + P_{at}^2) \dfrac{\partial Q}{\partial \zeta}(z, z) \right] \\ \dfrac{K_1}{2K_3} \dfrac{H_0}{P_{ro}} s - \dfrac{K_4}{2K_3} \dfrac{H_0}{P_{ro}} \\ \qquad + \left[P_{ro}^2 \dfrac{\partial Q}{\partial \zeta}(P_{at}^2, P_{ro}^2) - P_{at}^2 \dfrac{\partial Q}{\partial \zeta}(z, z) + 1 \right] \end{vmatrix}$$

$$\frac{-P_{ro} \left(\dfrac{P_{ro}^2 - P_{at}^2}{\dfrac{X}{X_r} - 1} \right) \epsilon s + \left[P_{ro}^2 \dfrac{\partial Q}{\partial \zeta}(P_{at}^2, P_{ro}^2) - P_{ro}^2 \dfrac{\partial Q}{\partial \zeta}(z, z) \right]}{\dfrac{K_2}{2K_3} s - \dfrac{K_2}{2K_3} + \left[P_{ro}^2 \dfrac{\partial Q}{\partial \zeta}(P_{at}^2, P_{ro}^2) \right]} = 0 \quad (28a)$$

* The Wronskian of second-order differential equations having the form $y'' + f(x)y = 0$ is a constant.

$$\left\| \begin{array}{l} \dfrac{mH_0\eta}{2\pi P_{at}^2}\, s^2 + \dfrac{\eta g s}{P_{at}^2} \\ \qquad - \left\{ R\,\dfrac{\partial Q}{\partial \rho}\,(R_r, R) + \left(\dfrac{P_{ro}}{P_{at}}\right)^2 R_r\,\dfrac{\partial Q}{\partial \rho}\,(R, R_r) \right. \\ \qquad\quad - \left[\left(\dfrac{P_{ro}}{P_{at}}\right)^2 + 1\right] R_r^{1/2} R^{1/2}\,\dfrac{\partial Q}{\partial \rho}\,(r, r) \\ \qquad\quad \left. + \dfrac{1}{2}\left[\left(\dfrac{P_{ro}}{P_{at}}\right)^2 - 1\right]\right\} \end{array} \right.$$

$$\left. \begin{array}{l} - \dfrac{C_1}{2C_5}\left(\dfrac{H_0}{P_{ro}}\right) \dfrac{\left(\dfrac{P_{ro}}{P_{at}}\right)^2 - 1}{\log \dfrac{R}{R_r}}\, s + \dfrac{C_4}{2C_5}\left(\dfrac{H_0}{P_{ro}}\right) \dfrac{\left(\dfrac{P_{ro}}{P_{at}}\right)^2 - 1}{\log \dfrac{R}{R_r}} \\ \qquad + \left\{ \left(\dfrac{P_{ro}}{P_{at}}\right)^2 R_r\,\dfrac{\partial Q}{\partial \rho}\,(R, R_r) - R_r^{1/2} R^{1/2}\,\dfrac{\partial Q}{\partial \rho}\,(r, r) \right. \\ \qquad\quad \left. + \dfrac{1}{2}\left(\dfrac{P_{ro}}{P_{at}}\right)^2 - \dfrac{\left(\dfrac{P_{ro}}{P_{at}}\right)^2 - 1}{\log \dfrac{R}{R_r}} \right\} \end{array} \right\|$$

$$\left. \begin{array}{l} \dfrac{P_{ro} R_r^2 \eta}{2P_{at}^2}\, s + \left\{ \left(\dfrac{P_{ro}}{P_{at}}\right)^2 R_r\,\dfrac{\partial Q}{\partial \rho}\,(R, R_r) \right. \\ \qquad \left. - \left(\dfrac{P_{ro}}{P_{at}}\right)^2 R_r^{1/2} R^{1/2}\,\dfrac{\partial Q}{\partial \rho}\,(r, r) + \dfrac{1}{2}\left(\dfrac{P_{ro}}{P_{at}}\right)^2 \right\} \\ \dfrac{C_2}{2C_5}\dfrac{\left(\dfrac{P_{ro}}{P_{at}}\right)^2 - 1}{\log \dfrac{R}{R_r}}\, s - \dfrac{C_3}{2C_5}\dfrac{\left(\dfrac{P_{ro}}{P_{at}}\right)^2 - 1}{\log \dfrac{R}{R_r}} \\ \qquad - \left\{ \left(\dfrac{P_{ro}}{P_{at}}\right)^2 R_r\,\dfrac{\partial Q}{\partial \rho}\,(R, R_r) + \dfrac{1}{2}\left(\dfrac{P_{ro}}{P_{at}}\right)^2 \right\} \end{array} \right\| = 0 \qquad (28b)$$

Further progress in the analysis depends on a knowledge of the solutions y_I and y_{II} of the homogeneous part of equation (19). Even with such knowledge the location of roots in the complex plane of the characteristic equation (28) might be very involved. Our interest lies in assessing the limiting values of certain bearing parameters which influence stability. Within limits of applicability of our equations, we are guided in the expected range of their magnitudes by results obtained by means of a simplified analysis which we have summarized in Appendix 2. Different approaches were employed for the rectangular and circular geometries and these are described in what follows.

Rectangular Geometry

The homogeneous part of equation (19a) is

$$y'' - \epsilon s z^{1/2} y = 0 \qquad (29a)$$

Two independent solutions,[6] which involve Bessel functions of order $\pm 2/3$, can be written as

$$\underset{\text{II}}{y_{\text{I}}} = z^{1/2} J_{\pm 2/3}\left(\tfrac{4}{5} z^{5/4} i \sqrt{\epsilon s}\right) \qquad (30a)$$

in which $+2/3$ corresponds to I and $-2/3$ to II.

[6] "Differentialgleichungen, Lösungsmethoden und Lösungen," by E. Kamke, third ed., Chelsea Publ. Co., 1948, eq. (2), 162(10), p. 440.

The series representing the Bessel function $J_\nu(2i\lambda^{1/2})$ can be written as:

$$J_\nu(2i\lambda^{1/2}) = (i\lambda^{1/2})^\nu \left[\frac{1}{\Gamma(\nu+1)} + \frac{\lambda}{1!\Gamma(\nu+2)} + \frac{\lambda^2}{2!\Gamma(\nu+3)} + \cdots \right] \qquad (31a)$$

With

$$\nu = \pm 2/3 \text{ and } 2i\lambda^{1/2} = \tfrac{4}{5} z^{5/4} i \epsilon s$$

the first four terms of the expansion of y_I and y_{II} become

$$y_I = \frac{\left(\frac{2}{5} i \sqrt{\epsilon s}\right)^{2/3}}{\Gamma(\frac{2}{3})} \left[\tfrac{3}{5} z + \tfrac{2}{55} z^{3/2} (\epsilon s) + \tfrac{1}{880} z^{3/4} (\epsilon s)^2 + \tfrac{2}{14080} z^{11/2} (\epsilon s)^3 \right] \qquad (32a)$$

$$y_{II} = \frac{\left(\frac{2}{5} i \sqrt{\epsilon s}\right)^{-2/3}}{\Gamma(\frac{1}{3})} \left[1 + \tfrac{4}{15} z^{5/2} (\epsilon s) + \tfrac{2}{55} z^{5/2} (\epsilon s)^2 + \tfrac{8}{1672} z^{7/2} (\epsilon s)^3 \right] \qquad (33a)$$

These truncated series are then substituted into the expression $Q(z, \zeta)$ in (25a) and the derivative $(\partial Q/\partial \zeta)(z, \zeta)$ evaluated with z and ζ assuming the boundary values of P_{ro}^2 and P_{at}^2 in the order indicated in the components of the characteristic determinant (28a). In forming the expressions for the afore-mentioned derivatives of Q, we retain in all subsequent multiplications, divisions, and so on, terms of order s^3 and lower. The assumption that higher powers in s may be neglected, because of the relative smallness of their coefficients, is justified *post factum* by noting the magnitude of the complex-conjugate roots $s = \pm i\omega$ of the characteristic cubic to which the determinant (28a) is thus reduced. The coefficients of this cubic and those obtained by means of the simplified analysis in Appendix 2 are not the same. The effect of this difference in results is best illustrated by reference to Fig. 3.

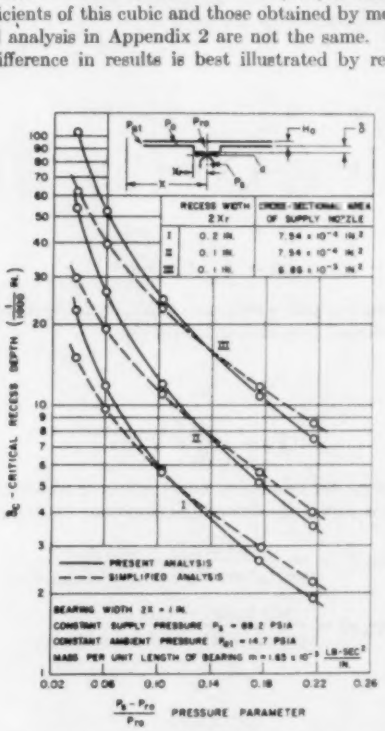
RECESS WIDTH 2Xr
CROSS-SECTIONAL AREA OF SUPPLY NOZZLE
I 0.2 IN. 7.54 x 10⁻⁴ IN.²
II 0.1 IN. 7.54 x 10⁻⁴ IN.²
III 0.1 IN. 5.65 x 10⁻⁴ IN.²
PRESENT ANALYSIS
SIMPLIFIED ANALYSIS
BEARING WIDTH 2X = 1 IN.
CONSTANT SUPPLY PRESSURE Ps = 88.2 PSIA
CONSTANT AMBIENT PRESSURE Pat = 14.7 PSIA
MASS PER UNIT LENGTH OF BEARING m = 1.65 x 10⁻³ LB-SEC²/IN.
Hc - CRITICAL RECESS DEPTH (1/1000 IN.)
(Ps - Pro)/Pro PRESSURE PARAMETER

Fig. 3 Critical recess depth versus pressure parameter

Circular Geometry

In this case, computer solutions for a set of discrete values of $s = i\omega$ on the axis of the imaginaries were obtained. The probable range of values for ω was dictated by predictions based on the simplified analysis and by taking into account the difference in the results of the two analyses for the rectangular case. Stability was assessed from physical conditions rather than proved.

If we write

$$\xi = \frac{r}{R_r}; \quad \alpha = \frac{12\mu\omega R_r^2}{P_{ro}H_0^2}; \quad s = i\omega; \quad \beta = \frac{1 - \left(\frac{P_{at}}{P_{ro}}\right)^2}{\log \frac{R}{R_r}}$$

then the homogeneous part of equation (19b) becomes

$$y'' + \left[\frac{1}{4\xi^2} - \frac{i\alpha}{(1 - \beta \log \xi)^{1/3}}\right] y = 0 \tag{34b}$$

the solutions of which

$$y_{\substack{I \\ II}} = \phi_{\substack{I \\ II}}(\xi) + i\psi_{\substack{I \\ II}}(\xi) \tag{35b}$$

satisfy the conveniently chosen boundary conditions

$$\begin{aligned} y_I(1) &= 1; \quad y_I'(1) = 0 \\ y_{II}(1) &= 0; \quad y_{II}'(1) = 1 \end{aligned} \tag{36b}$$

The set of equations corresponding to (34b) is

$$\begin{aligned} \phi'' + \frac{\phi}{4\xi^2} &= -\frac{\alpha\psi}{(1 - \beta \log \xi)^{1/3}} \\ \psi'' + \frac{\psi}{4\xi^2} &= \frac{\alpha\phi}{(1 - \beta \log \xi)^{1/3}} \end{aligned} \tag{37b}$$

and the boundary conditions (36b) become

$$\begin{aligned} \phi_I(1) &= 1; \quad \phi_I'(1) = 0 \\ \phi_{II}(1) &= 0; \quad \phi_{II}'(1) = 1 \\ \psi_I(1) &= \psi_I'(1) = \psi_{II}(1) = \psi_{II}'(1) = 0 \end{aligned} \tag{38b}$$

Solutions of equations (37b), satisfying the conditions (38b) were obtained for a fixed value of β and a set of values of the parameter

$$\alpha = \frac{12\mu\omega R_r^2}{P_{ro}H_0^2}$$

by means of a digital computer. Those shown graphically in Fig. 4 corresponds to the value of $\alpha = 0.093$.

We are now in a position to express numerically the derivatives

$$\begin{aligned} \frac{\partial Q}{\partial \rho}(R, R_r) &= \frac{\phi_I(R) + i\psi_I(R)}{\phi_{II}(R) + i\psi_{II}(R)} \\ \frac{\partial Q}{\partial \rho}(R_r, R) &= \frac{\phi_{II}'(R) + i\psi_{II}'(R)}{\phi_{II}(R) + i\psi_{II}(R)} \\ \frac{\partial Q}{\partial \rho}(r, r) &= \frac{1}{\phi_{II}(R) + i\psi_{II}(R)} \end{aligned} \tag{39b}$$

for discrete values of α.

All other quantities in equation (28b) can then be expressed in terms of the ratio ω/α and one variable bearing parameter; the recess depth δ, for example. This reduces the characteristic determinant (28b) to the form

$$\left[\delta - g_1\left(\frac{\omega}{\alpha}\right)\right] + ib\left[\delta - g_2\left(\frac{\omega}{\alpha}\right)\right] = 0 \tag{40b}$$

in which g_1 and g_2 depend on the ratio ω/α, and b is a numerical constant. The critical recess depth δ_c can then be determined from the condition

$$\delta = g_1\left(\frac{\omega}{\alpha}\right) = g_2\left(\frac{\omega}{\alpha}\right) = \delta_c \tag{41b}$$

In the numerical calculations of δ_c for any fixed value of

$$\alpha = \frac{12\mu\omega R_r^2}{P_{ro}H_0^2}$$

the ratio ω/H_0^2 is allowed to vary until the values of δ in the real and imaginary part of (40b) coincide.

The experimental counterpart of this procedure is to set the gap width H_0 by changing the supply pressure P_s while keeping the recess pressure P_{ro} constant. The recess depth δ is then increased up to the critical value δ_c on the threshold of instability. The determination of the critical recess depth δ_c from equation (40b) is illustrated in Fig. 6. In Fig. 5 the results of the present analysis are shown and compared with those based on the assumptions of the lumped-parameter theory.

The Effect of Bearing Parameters on Stability. The most important factor influencing the stability of externally pressurized bearings is the interaction of the total gas-storage capacitance with the flow-regulating characteristics of a fixed supply restrictor and a variable annulus. The ratio L/mg, where L is the load and m the mass of the bearing, also influences stability. Deeper pockets can generally only be tolerated for very moderate pressure drops across the supply nozzle. The limiting depth increases with the nozzle diameter and decreases with the length of the annulus, as well as with the mass of the bearing. These trends are illustrated in Figs. 3 and 5.

The advantage of recessed pockets, channels, or grooves is that they increase the load capacity and static stiffness. The recess perimeter also provides a larger area of admission into the annulus, thereby reducing entrance velocities and preventing shocks. These advantages, however, must be weighed very carefully in the light of requirements dictated by stability conditions.

The Influence of Bearing Mass. The smaller the mass of a bearing, the greater its rate of response to external disturbances tends to become. When the response rate is large, the gas in each volume element becomes partly "trapped" rather than "squeezed out."

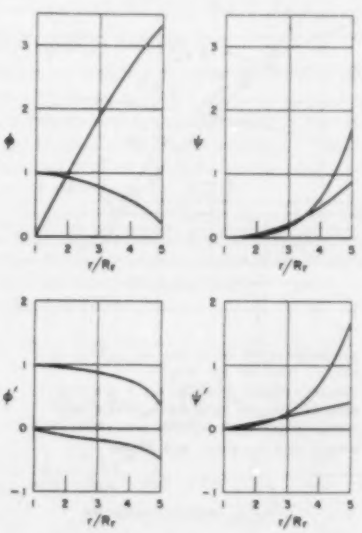

Fig. 4 Computer solutions of Equation (37b)

This, in turn, causes the film stiffness in the annulus to increase and permit greater compliance of a deeper recess without compromising stability. The influence of varying the mass is best illustrated in Fig. 5, since the foregoing effect is more pronounced in the case of the circular bearing, which has a relatively large annular region.

When the mass is large, the dynamic changes in pressure profile approach the quasi-static condition, and the foregoing effects are reversed. These two cases are illustrated diagrammatically in Fig. 7 for the conditions of a heavily (*a*) and lightly (*b*) loaded bearing.

Comparison of Present and Simplified Theories. Though perhaps deficient from the quantitative point of view, the simplified analysis [3] (Appendix 2) gives explicit relationships between parameters which affect the stability of the bearing. The inequality (53) (Appendix 2), for example, can be written as follows:

$$\frac{\left(\frac{\partial M}{\partial H}\right)_0}{\left(\frac{\partial M}{\partial P_r}\right)_0} > \frac{\frac{\partial}{\partial H}(W_2 - W_1)_0}{\frac{\partial}{\partial P_r}(W_2 - W_1)_0} \tag{42}$$

in which, for a given bearing geometry,

$$M = f(T_0, P_{a0}, P_{r0}, P_r, H)$$

$$(W_2 - W_1) = g(T_0, P_{a0}, P_s, P_r, H)$$

It follows that the stability condition also can be written as

$$-\left[\frac{dP_r}{dH}\right]_{M=M_0} > -\left[\frac{dP_r}{dH}\right]_{W_r=W_r=W_0} \tag{43}$$

The physical interpretation of the above inequality is as follows. The left side of inequality (43) represents a change in recess pressure caused by a rapid change in gap width, each volume element acting as a closed cylinder in which the gas becomes trapped. The right side of inequality (43) represents a change in pressure caused by slow, quasi-static displacement, the annulus having a flow-regulating, rather than gas-trapping effect.

Comparison of results in Fig. 3 and Fig. 5 shows that for small pressure drops across the supply nozzle the simplified theory gives values of δ_c which are too conservative. The agreement is considerably better when the pressure difference becomes larger. The simplified analysis is based on *a priori* assumptions of quasi-static changes in pressure and gas content, and these account for the discrepancies between results of present and simplified analyses. That the latter analysis does not properly account for the effect of mass on frequency, inasmuch as it applies quasi-static concepts to dynamic conditions, Fig. 7, becomes apparent when the inequality (53) (Appendix 2) is written in its original form:

$$\left(\frac{\lambda_2 + \lambda_3}{\lambda_2}\right)\left(\frac{A_s}{m}\,\frac{\lambda_1}{\lambda_3}\right) > \left(\frac{A_s}{m}\,\frac{\lambda_4}{\lambda_2}\right) \tag{44}$$

Since the quantity, m, cancels in the denominator on both sides of the inequality, a shortcoming of the simplified analysis is that it makes the stability condition independent of the bearing mass.

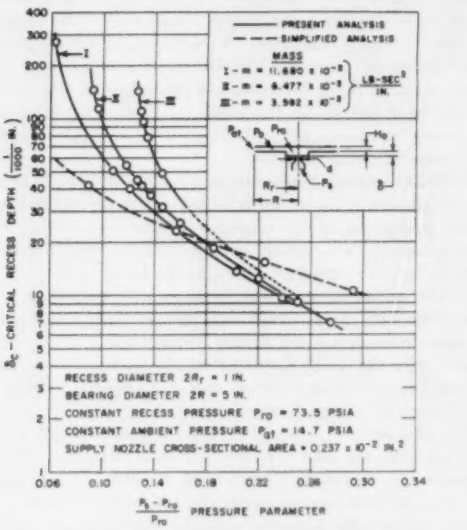
PRESENT ANALYSIS
SIMPLIFIED ANALYSIS
MASS
RECESS DIAMETER 2R_r = 1 IN.
BEARING DIAMETER 2R = 5 IN.
CONSTANT RECESS PRESSURE P_r0 = 73.5 PSIA
CONSTANT AMBIENT PRESSURE P_a1 = 14.7 PSIA
SUPPLY NOZZLE CROSS-SECTIONAL AREA = 0.237 x 10^-2 IN.^2
PRESSURE PARAMETER

Fig. 5 Critical recess depth versus pressure parameter

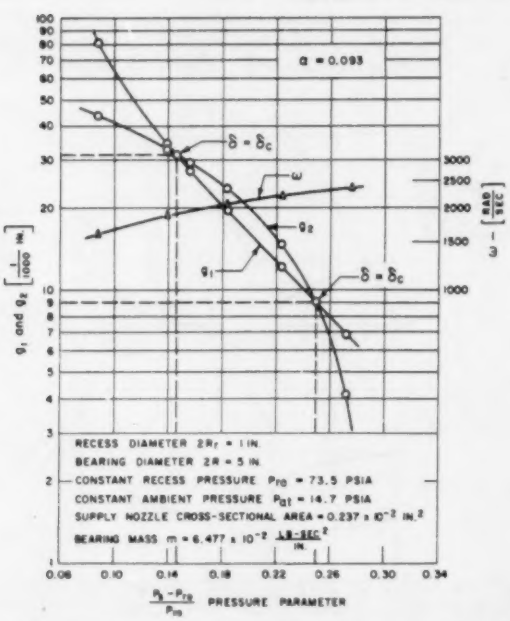
α = 0.093
δ = δc
ω
q2
q1
RECESS DIAMETER 2R_r = 1 IN.
BEARING DIAMETER 2R = 5 IN.
CONSTANT RECESS PRESSURE P_r0 = 73.5 PSIA
CONSTANT AMBIENT PRESSURE P_a1 = 14.7 PSIA
SUPPLY NOZZLE CROSS-SECTIONAL AREA = 0.237 x 10^-2 IN.^2
BEARING MASS m = 6.477 x 10^-2
PRESSURE PARAMETER

Fig. 6 Determination of the critical recess depth form Equation (40b)

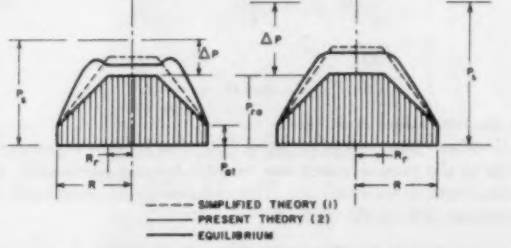

Fig. 7 Schematic of pressure profiles under dynamic conditions with reference to present and simplified analyses and predicted values of δ_c

Summary and Conclusions

An analysis was made which treats the flow within the gas film in a thrust bearing on a continuous, rather than "lumped," basis. It shows that within the limitation imposed upon the design of the bearing by other considerations, the following parameters or combinations of parameters should be minimized or maximized in order to insure stability:

Minimized	Maximized
1 Depth of pockets	1 Supply nozzle diameter
2 Difference between supply and recess pressures	2 Length of annulus
3 Effective mass of bearing	3 Area ratio of annular and pocket regions

One may also conclude from results of earlier, simplified analyses [1, 2, 3] which show good qualitative agreement with the present one, that high gas temperatures and adiabatic conditions favor stability.

Acknowledgments

This paper is based on the work performed under contract and administered by the Office of Naval Research and supported jointly by the Department of Defense, Atomic Energy Commission, and the Maritime Administration.

The authors are indebted to Miss S. Goff, Mr. S. Malanoski, and Mr. C. Stevenson for their help in performing the laborious calculations, as well as to Mr. L. McGinn and Mr. W. Reugner who programmed the digital computer.

They also wish to thank Capt. W. T. Sawyer, Office of Naval Research, and Prof. D. D. Fuller, The Franklin Institute, for the interest displayed in and support given to this phase of the project.

References

1 H. Richardson, "Static and Dynamic Characteristics of Compensated Gas Bearings," TRANS. ASME, vol. 80, 1958, pp. 1503–1509.

2 W. H. Roudebush, "An Analysis of the Effect of Several Parameters on the Stability of an Air-Lubricated, Hydrostatic Thrust Bearing," NACA TN 4095, October, 1957.

3 L. Licht, D. D. Fuller, and B. Sternlicht, "Self-Excited Vibrations of an Air-Lubricated Thrust Bearing," TRANS. ASME, vol. 80, 1958, pp. 411–414.

4 Geoffrey Taylor and P. G. Saffman, "Effects of Compressibility at Low Reynolds Numbers," *Journal of the Aeronautical Sciences*, vol. 24, 1957, pp. 553–562.

5 G. L. Shires, "On a Type of Air-Lubricated Journal Bearing," National Gas Turbine Establishment (British), Report No. R 61, November, 1949.

6 E. B. Sciulli, "A Bibliography on Gas Lubricated Bearings," Interim Report I-A2049-1, Office of Naval Research, Contract Nonr-2342(00), Task NR 097-343.

APPENDIX 1

The weighted pressure integral

$$\mathcal{J} = \int_{R_r}^{R} P_0(r) r \, dr$$

with

$$P_0(r) = \left(P_{ro}^2 - \frac{P_{ro}^2 - P_{at}^2}{\log \frac{R}{R_r}} \log \frac{r}{R_r} \right)^{1/2}$$

let

$$\frac{P_{ro}^2 - P_{at}^2}{\log \frac{R}{R_r}} \frac{\xi^2}{2} = P_0^2 = P_{ro}^2 - \frac{P_{ro}^2 - P_{at}^2}{\log \frac{R}{R_r}} \log \frac{r}{R_r}$$

then

$$r = R_r \left(\frac{R}{R_r} \right)^{\frac{P_{ro}^2}{P_{ro}^2 - P_{at}^2}} e^{-\frac{\xi^2}{2}}$$

$$dr = -R_r \left(\frac{R}{R_r} \right)^{\frac{P_{ro}^2}{P_{ro}^2 - P_{at}^2}} \xi e^{-\frac{\xi^2}{2}} d\xi$$

$$P_0 = \left(\frac{P_{ro}^2 - P_{at}^2}{2 \log \frac{R}{R_r}} \right)^{1/2} \xi$$

Substituting into the integral we have:

$$\mathcal{J} = -R_r^2 \left(\frac{R}{R_r} \right)^{\frac{2P_{ro}^2}{P_{ro}^2 - P_{at}^2}} \left(\frac{P_{ro}^2 - P_{at}^2}{2 \log \frac{R}{R_r}} \right)^{1/2} \int_{\xi_{R_r}}^{\xi_R} \xi^2 e^{-\xi^2} d\xi \tag{45}$$

Integrating and introducing the factor $2/\pi$, we have

$$\mathcal{J} = \frac{\sqrt{\pi}}{4} R_r^2 \left(\frac{R}{R_r} \right)^{\frac{2P_{ro}^2}{P_{ro}^2 - P_{at}^2}} \left(\frac{P_{ro}^2 - P_{at}^2}{2 \log \frac{R}{R_r}} \right)^{1/2} \left[\frac{2}{\sqrt{\pi}} \xi e^{-\xi^2} - \frac{2}{\sqrt{\pi}} \int e^{-\xi^2} d\xi \right]_{\xi_{R_r}}^{\xi_R} \tag{46}$$

in which the limits ξ_R and ξ_{R_r} are:

$$\xi_R = \left(\frac{2P_{at}^2 \log \frac{R}{R_r}}{P_{ro}^2 - P_{at}^2} \right)^{1/2} \qquad \xi_{R_r} = \left(\frac{2P_{ro}^2 \log \frac{R}{R_r}}{P_{ro}^2 - P_{at}^2} \right)^{1/2} \tag{47}$$

The values of the probability integral

$$\frac{2}{\sqrt{\pi}} \int_0^{\xi} e^{-x^2} dx$$

are listed in standard mathematical tables.

APPENDIX 2

A Simplified Stability Analysis

In the simplified stability analysis [3] the flow in the annulus is treated on a lumped-parameter basis and the pressure distribution under conditions of dynamic loading is assumed to be the same as if the bearing were loaded statically. In the case of the circular bearing a further simplification is made in assuming a linear pressure profile along the annulus.

The perturbation equations which correspond to (10), (12), and (13) of the more exact analysis presented in this paper can then be expressed in terms of variation in the annular width (h) and of the pressure at the recess boundary (p_r).

To this effect we have:

$$\lambda_1 \dot{h} + \lambda_2 \dot{p}_r = -\lambda_0 h - (\lambda_3 + \lambda_4) p_r \tag{48}$$

$$m\ddot{h} = A_r p_r + \iint_{A_a} p dA = A_a p_r \tag{49}$$

in which

A_r = area over recess

A_a = area over annulus

A_e = "equivalent" area

the explicit expression for A_e being:

$$A_e = 2X_r\left[1 + {}^2/_3\left(\frac{X}{X_r} - 1\right)\frac{\left(\frac{P_{ro}}{P_{at}}\right)^2 + 2\left(\frac{P_{at}}{P_{ro}}\right) - 3}{\left(\frac{P_{ro}}{P_{at}} - \frac{P_{at}}{P_{ro}}\right)^2}\right] \tag{50a}$$

$$A_e = {}^1/_3\pi R_r^2\left[\left(\frac{R}{R_r}\right)^2 + \left(\frac{R}{R_r}\right) + 1\right] \tag{50b}$$

while the coefficients λ, denoted with α for the rectangular and with β for the circular geometry are as follows:

$$\alpha_1 = \left(\frac{\partial M}{\partial H}\right)_0 = \frac{2X_rP_{ro}}{RT_0}\left\{1 + {}^2/_3\left(\frac{X}{X_r} - 1\right)\left(\frac{P_{ro}}{P_{at}}\right)\frac{1 - \left(\frac{P_{at}}{P_{ro}}\right)^2}{\left(\frac{P_{ro}}{P_{at}} - \frac{P_{at}}{P_{ro}}\right)}\right\}$$

$$\alpha_2 = \left(\frac{\partial M}{\partial P_r}\right)_0 = \frac{2X_rH_0}{\gamma RT_0}\left\{\left(\frac{\delta}{H_0} + 1\right) + {}^2/_3\gamma\left(\frac{X}{X_r} - 1\right)\frac{\left(\frac{P_{ro}}{P_{at}}\right)^2 + 2\left(\frac{P_{at}}{P_{ro}}\right) - 3}{\left(\frac{P_{ro}}{P_{at}} - \frac{P_{at}}{P_{ro}}\right)^2}\right\} \tag{51a}$$

$$\alpha_3 = -\left(\frac{\partial W_1}{\partial P_r}\right)_0 = \frac{W_0}{2P_{ro}}\left(\frac{2 - \frac{P_s}{P_{ro}}}{\frac{P_s}{P_{ro}} - 1}\right)$$

$$\alpha_4 = \left(\frac{\partial W_2}{\partial H}\right)_0 = \frac{3W_0}{H_0}$$

$$\alpha_5 = \left(\frac{\partial W_2}{\partial P_r}\right)_0 = \frac{2P_{ro}W_0}{P_{ro}^2 - P_{at}^2}$$

$$\beta_1 = \left(\frac{\partial M}{\partial H}\right)_0 = \frac{\pi R_r^2P_{ro}}{RT_0}\left\{1 + \left(\frac{P_{at}}{P_{ro}}\right)\left[\left(\frac{R}{R_r}\right)^2 - 1\right] + \left(1 - \frac{P_{at}}{P_{ro}}\right)\frac{\left(\frac{R}{R_r}\right)^3 - 3\left(\frac{R}{R_r}\right) + 2}{3\left(\frac{R}{R_r} - 1\right)}\right\}$$

$$\beta_2 = \left(\frac{\partial M}{\partial P_r}\right)_0 = \frac{\pi R_r^2H_0}{\gamma RT_0}\left\{\left(\frac{\delta}{H_0} + 1\right) + \gamma\frac{\left(\frac{R}{R_r}\right)^3 - 3\left(\frac{R}{R_r}\right) + 2}{3\left(\frac{R}{R_r} - 1\right)}\right\} \tag{51b}$$

$$\beta_3 = -\left(\frac{\partial W_1}{\partial P_r}\right)_0 = \frac{W_0}{2P_{ro}}\left(\frac{2 - \frac{P_s}{P_{ro}}}{\frac{P_s}{P_{ro}} - 1}\right)$$

$$\beta_4 = \left(\frac{\partial W_2}{\partial H}\right)_0 = \frac{3W_0}{H_0}$$

$$\beta_5 = \left(\frac{\partial W_2}{\partial P_r}\right)_0 = \frac{2P_{ro}W_0}{P_{ro}^2 - P_{at}^2}$$

Combining equations (48) and (50) we obtain:

$$\ddot{h} + \left(\frac{\lambda_3 + \lambda_5}{\lambda_2}\right)\dot{h} + \left(\frac{A_e}{m}\frac{\lambda_1}{\lambda_2}\right)h + \left(\frac{A_e}{m}\frac{\lambda_4}{\lambda_2}\right)h = 0 \tag{52}$$

Stability conditions require the coefficients of equation (52) to be positive, and in addition that the following inequality be satisfied:

$$\frac{\lambda_1}{\lambda_2} > \frac{\lambda_4}{\lambda_3 + \lambda_5} \tag{53}$$

The critical recess depth indicated with broken lines in Figs 3 and 6 was calculated from the foregoing inequality.

It is to be noted that the coefficients λ correspond to similar quantities in the more exact analysis, but that there is no one-to-one correspondence, except for λ_2 and λ_4.

On the Theoretical Analysis of a Dynamic Thermocouple: 2—The Continuous Area Interface[1]

W. F. HUGHES

E. W. GAYLORD

Assistant Professors,
Department of Mechanical Engineering,
Carnegie Institute of Technology,
Pittsburgh, Pa.
Assoc. Mem. ASME

The dynamic thermocouple formed by the moving junctions of two dissimilar metals is analyzed for the case of two semi-infinite bodies of dissimilar metals having continuous contact and nonuniform temperature distribution over a circular area. A procedure is given for determining the potential measured by the thermocouple leads placed in the two respective bodies at an infinite distance away from the contact area in terms of the Seebeck emf corresponding to the contact-area temperature distribution. This thermocouple potential at infinity is solved completely for a circular contact area, and numerical examples are given for the case of radial symmetry. It is found that the potential at infinity is not in general equal to the area average Seebeck emf. Instead, it is shown that the potential at infinity is equal to the average Seebeck emf weighted by the area divided by its distance from the perimeter of the circle. This result together with comparison with the results of a previous paper leads to the conclusion that the temperature near the perimeter of a contact area has a greater influence on the thermocouple emf than the temperature in the interior of the contact area.

THE dynamic thermocouple utilizes the interface between two dissimilar metals in relative motion as one junction of a thermocouple. The emf generated by this arrangement is used to estimate the interface temperature between the two rubbing metals.

Two examples of the dynamic thermocouple as a research tool may be cited. One application is its use in studying the frictional heating of two dissimilar metallic surfaces sliding over each other with relatively low normal pressures between the two sliding surfaces. Only a small portion of the apparent contact area is true contact area formed by asperities on the rubbing surfaces. The dynamic thermocouple has been used to estimate the temperature of these asperities [1].[2] Another example involves the problem of finding the temperature between the tool and tool-chip in metal cutting. Analytical results for this problem have been presented by various investigators [2–5], and the dynamic-thermocouple technique has been used in some cases to verify these results experimentally [2, 3]. Here the interface pressures are very high and true contact is assumed to be continuous over the entire interface between tool and tool chip.

In these applications of the dynamic thermocouple the question of what is the relationship between the thermocouple emf and the interface temperature has to be considered. To establish any relationship at all between the thermocouple emf and the interface temperature, it has to be shown that the thermocouple emf depends only on the thermoelectric effects, that is, only on the Seebeck emf due to the interface temperatures, and not on any extraneous emf produced by physical changes in the metal, and so on. There is some evidence that any emf resulting from nonthermoelectric effects has a time average value of zero [6]. Then, assuming that the thermocouple emf depends only on interface temperature, the problem is to show how the thermocouple can be correlated with the temperature. In the tool-chip problem it has commonly been assumed that the thermocouple emf corresponds to the contact-area average Seebeck emf. In a previous paper [7] the authors presented an analysis of randomly distributed small circular contact areas between semi-infinite bodies, a model which represents frictional rubbing. The results indicate that the measured emf may not necessarily be equal to the area average Seebeck emf.

The following analysis deals with the thermocouple emf produced by a nonuniform Seebeck emf distribution between two semi-infinite bodies of dissimilar metals having a continuous contact area of circular shape. The continuous contact area could represent physically the continuous contact between a tool

[1] This work was done in part by one of the authors (Hughes) while a National Science Postdoctoral Fellow at the Cavendish Laboratory of the University of Cambridge, England.

[2] Numbers in brackets designate References at end of paper.

For presentation at the Summer Conference of the Applied Mechanics Division, University Park, Pa., June 20–22, 1950, of THE AMERICAN SOCIETY OF MECHANICAL ENGINEERS.

Discussion of this paper should be addressed to the Secretary, ASME, 29 West 39th Street, New York, N. Y., and will be accepted until July 22, 1960, for publication at a later date. Discussion received after the closing date will be returned.

NOTE: Statements and opinions advanced in papers are to be understood as individual expressions of their authors and not those of the Society. Manuscript received by ASME Applied Mechanics Division, April 3, 1959. Paper No. 60—APM-19.

Nomenclature

E = Seebeck emf
P_∞ = potential measured by the potentiometer
σ = current source density function
$V = E - P_\infty$
r = co-ordinate of current source on contact surface
r' = co-ordinate of V measured on contact surface
$\mathbf{R}$ = co-ordinate of V measured in solid
$\bar{E}$ = average value of E over contact surface
a = radius of circular contact surface
p = perimeter of surface of interface

and tool chip, and the results give an indication of how the mean interface temperature is related to the emf read on the potentiometer of a dynamic thermocouple of which the interface is one junction.

Analysis

We consider as a model a large body of metal A rubbing over a large body of metal B. A co-ordinate system (x, y, z) is attached to the interface surface of body A which moves in the x-direction as shown in Fig. 1. It is assumed that the rubbing itself does not generate appreciable voltage so that the potential is the same as it would be in the static situation with the same temperature and contact situation. Assume that the electrical time constants are effectively zero so that the system is electrically in steady state.

Physically the interface between the two metals may be considered, instantaneously, to consist of a great number of small contact areas which in the limit become effectively a continuous contact area with a continuous temperature distribution. The thermocouple lead contact points a and b are located a great distance away from the interface (compared to the size of the interface) so that we assume both bodies to be semi-infinite solids with the potentials at a and b essentially the values at infinity. The problem then is to determine the value of the potential P at infinity, which is what is measured by the potentiometer, and to compare it with the average value of the Seebeck emf, $\bar{E}$, on the interface surface.

In their previous paper [7], it was shown by the authors that if thermocouple leads a and b are symmetrically placed with respect to each other in semi-infinite bodies A and B, and potential P is defined as the potential indicated by the potentiometer shown in Fig. 1, then for any location of the leads (x, y, z), the potential as defined before satisfies the Laplace equation

$$\nabla^2 P = 0 \tag{1}$$

On the interface surface

$$P = E(x, y) \tag{2}$$

where $E(x, y)$ is the Seebeck emf corresponding to the local interface temperature. On the other free surfaces, $\partial P/\partial n = 0$ where n is the normal direction to the surface. Besides symmetrical placing of the thermocouple leads, another assumption necessary to the derivation of the foregoing relationships is that the resistivity is uniform though not necessarily the same in bodies A and B.

With $E(x, y)$ given then, we wish to find P_∞; i.e., P at very large distances away from the interface, which is the value measured by the potentiometer.

We define a new function V such that:

$$V = P - P_\infty \tag{3}$$

and on the interface surface then

$$V(x, y) = E(x, y) - P_\infty \tag{4}$$

and

$$\nabla^2 V = \nabla^2 P = 0 \tag{5}$$

with $\partial V/\partial n = 0$ on the free surfaces. Hence if $E(x, y)$ is given, and $V(x, y)$ determined, then P_∞ is prescribed by equation (4).

A solution of the potential problem for V can be represented as an integral over the interface surface S. Referring to Fig. 2,

$$V(\mathbf{R}) = \int_S \frac{\sigma(\mathbf{r})dA}{|\mathbf{R} - \mathbf{r}|} \tag{6}$$

where V is measured at $\mathbf{R}$, and $\sigma(\mathbf{r})$ is the current density distribution which gives the proper $E(x, y)$ on S. When the potentiometer is balanced, the current must be conserved, and we get the relationship

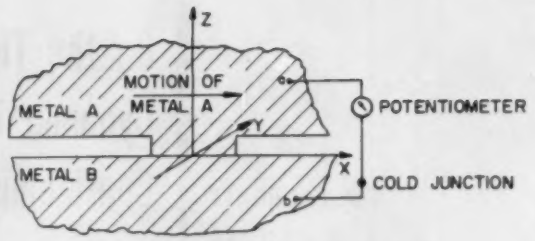

Fig. 1 Schematic of dynamic thermocouple

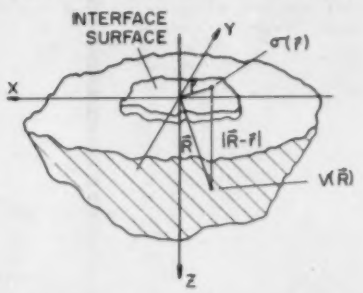

Fig. 2 Current source over interface showing potential $V(\bar{R})$ at an interior point. (In the text $\bar{R}$, $\bar{r}$ are replaced by R, r.)

$$\int_S \sigma(\mathbf{r})dA = 0 \tag{7}$$

On the surface S we also have

$$V(\mathbf{r}') = E(\mathbf{r}') - P_\infty = \int_S \frac{\sigma(\mathbf{r})dA}{|\mathbf{r}' - \mathbf{r}|} \tag{8}$$

where $\mathbf{r}'$ is the co-ordinate of the point on S where E is measured, and $\mathbf{r}$ is the co-ordinate of the current density which is integrated over the surface. If $E(\mathbf{r}')$ is given, then equations (7) and (8) are sufficient to allow P_∞ to be determined.

The integral transform of equation (8) can be written

$$\sigma(\mathbf{r}) = T[V(\mathbf{r}')] \tag{9}$$

where T is an integral operator determined by the transform. Then

$$\sigma(\mathbf{r}) = T[E(\mathbf{r}') - P_\infty] \tag{10}$$

Applying condition (7),

$$\int_S \sigma(\mathbf{r})dA = \int_S T[E(\mathbf{r}') - P_\infty]dA = 0 \tag{11}$$

The right-hand side of this equation specifies the method of finding P_∞, if $E(\mathbf{r}')$, i.e., the Seebeck emf, is known over the surface S. P_∞ can then be compared to $\bar{E}$, the average Seebeck emf which is

$$\bar{E} = \frac{\int_S E(\mathbf{r}')dA}{\int_S dA} \tag{12}$$

The problem now is to find the transform T for any specific situation.

Determining the Integral Transform for a Circular Interface

If we write $V(\mathbf{r}')$ for a disk of radius a as (referring to Fig. 3)

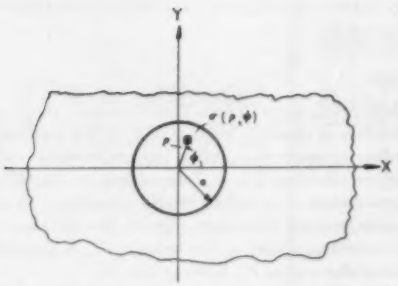

Fig. 3 Current source on a circular interface

$$V(\rho,\varphi) = \sum_n f_n(\rho)\cos n(\varphi+\alpha) \tag{13}$$

for $0 < \rho < a$, and α is a constant phase angle, we can find T. If V is radially symmetrical, only one harmonic (with $n = 0$) need be considered. For more complicated shapes the complete series must be used. The transform for a single harmonic, n, can be found and the result applied to the other terms [8]. Consider the nth harmonic and define a function $S_n(\rho)$:

$$S_n(t') = \frac{1}{2\pi t'^{2n}}\frac{d}{dt'}\int_0^{t'}\frac{t^{n+1}f_n(t)}{(t'^2-t^2)^{1/2}}\,dt \tag{14}$$

Then, as shown in reference [8], σ is given by

$$\sigma_n(\rho,\varphi) = -\frac{2}{\pi}\rho^{n-1}\frac{d}{d\rho}\int_\rho^a \frac{t'S_n(t')}{(t'^2-\rho^2)^{1/2}}\,dt'\cos n(\varphi+\alpha) \tag{15}$$

This then completely defines the operator T. If we wish to consider the φ dependence, we add the suitable harmonics, otherwise take $n = 0$ and use only the ρ-variation. In general then

$$\sigma(\rho,\varphi) = -\sum_{n=0}^{\infty}\frac{2}{\pi}\rho^{n-1}\frac{d}{d\rho}\int_\rho^a\frac{t'S_n(t')}{(t'^2-\rho^2)^{1/2}}\,dt'\cos n(\varphi+\alpha) \tag{16}$$

Now using equations (16) and (11), we have

$$\int_S \sigma(\rho,\varphi)dA = -\int_0^{2\pi}\int_0^a\left\{\sum_{n=0}^{\infty}\frac{2}{\pi}\rho^{n-1}\frac{d}{d\rho}\int_\rho^a\frac{t'S_n(t')}{(t'^2-\rho^2)^{1/2}}\,dt'\cos n(\varphi+\alpha)\right\}\rho\,d\varphi\,d\rho \tag{17}$$

In equation (14) f_n can be replaced by the following:

$$f_0 = (g_0 - P_\infty)$$
$$f_{n\neq 0} = g_n \tag{18}$$

where the function g_n is defined by

$$E(\rho,\varphi) = \sum_{n=0}^{\infty} g_n\cos n(\varphi+\alpha) \tag{19}$$

Equation (17) together with (18) and (19) will lead to one equation for P_∞.

Determining P_∞ for Case of Radially Symmetric Temperatures

The problem can be simplified considerably if the emf, E, is only a function of ρ. Then, $V(\rho) = E(\rho) - P_\infty = f(\rho)$ and $n = 0$. Equation (15), for $n = 0$ becomes

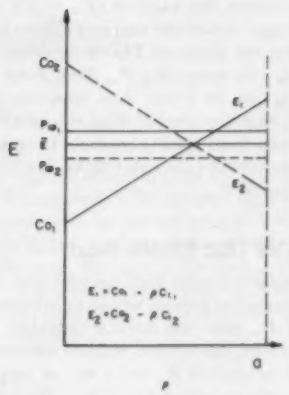

Fig. 4 Example of relationship between potentials on a circular interface for curves of the same $\bar{\varepsilon}$

$$\sigma = -\frac{2}{\pi}\rho^{-1}\frac{d}{d\rho}\int_\rho^a t'\frac{1}{2\pi}\frac{\left\{\dfrac{d}{dt'}\displaystyle\int_0^{t'}\frac{t[E(t)-P_\infty]}{(t'^2-t^2)^{1/2}}\,dt\right\}}{(t'^2-\rho^2)^{1/2}}\,dt' \tag{20}$$

Integrating $\sigma(\rho)$ over the surface we obtain

$$\int_0^a \sigma(\rho, P_\infty)2\pi\rho\,d\rho = 0 \tag{21}$$

which is an algebraic equation for P_∞. Evaluating this expression we obtain finally

$$\int_0^a\frac{t[E(t)-P_\infty]}{(a^2-t^2)^{1/2}}\,dt = 0 \tag{22}$$

Hence if $E(\rho)$ is known, P_∞ can be found simply from (22).

In practice, if the shape of $E(\rho)$ is known roughly from theoretical calculations, then $(P_\infty - \bar{E})$ can be calculated in terms of one parameter, say $\bar{E}$, and then using the measured value of P_∞, $\bar{E}$ and the level of the shape determined. Fig. 4 shows how these quantities are related for a sample $E(\rho)$-curve.

Numerical Examples of a Radially Symmetrical Distribution

If we assume $E(\rho)$ is given approximately by a power series in ρ, we can work out some informative examples. Let

$$E(\rho) = c_0 + c_1\rho + \ldots + c_N\rho^N \tag{23}$$

For this $E(\rho)$ distribution we can find $\bar{E}$ and P_∞. For $N = 5$, we have

$$P_\infty = c_0 + \frac{\pi}{4}ac_1 + {}^3/_8a^2c_2 + {}^3/_{16}\pi a^3c_3 + {}^5/_{16}a^4c_4 + \frac{30}{192}\pi a^5c_5 \tag{24}$$

and

$$\bar{E} = c_0 + {}^2/_3ac_1 + {}^1/_2a^2c_2 + {}^2/_5a^3c_3 + {}^1/_3a^4c_4 + {}^2/_7a^5c_5 \tag{25}$$

For a set of coefficients c_i then the values of $\bar{E}$ and P_∞ can be determined. If all c_i are zero except c_0 and c_1, we see that

$$P_\infty - \bar{E} = c_1a(\pi/4 - {}^2/_3) = 0.1187c_1a \tag{26}$$

Depending on the sign of c_1 then, P_∞ can be greater or less than $\bar{E}$ by about 17.7 per cent. For certain distributions then the difference between P_∞ and $\bar{E}$ may be significant. Fig. 4 shows the relationship between $\bar{E}$ and P_∞ for curves of c_1 both negative and positive with the same value of $\bar{E}$.

In practice, of course, the value of $(P_\infty - \bar{E})$ could be determined only if a rough idea of the shape of $E(\rho)$ is known. In this example, assuming the shape of $E(\rho)$ is equivalent to assuming all the c_i except c_0. By measuring P_∞ then, $\bar{E}$ can be found from equation (26); c_0 can be found then from the expression for $\bar{E}$, equation (25), and the level of $E(\rho)$ established. Of course, any other functional form for $E(\rho,\varphi)$ could be used and the level left as the undetermined parameter to be established from the experimental value of P_∞.

Extension to Other Than Circular Areas

The analysis so far indicates that, per unit area, the potential at the edge of the circle has greater weight or influence in determining the value of P_∞ than the interior potential. The previous paper [5] on random distributed sources showed that the P_∞ due to a set of potentials E_j on a set of corresponding circular areas A_i' was weighted by $\sqrt{A_j}$. The same idea seems valid here. The outer area is more influential than the inner area and the results seem compatible since the perimeter of a circle is proportional to $\sqrt{A}$ and is an indication of the proportion of area along the perimeter of S to the total area of S.

Now, we can calculate a weighting factor for the potential depending on its distance from the area centroid of current sources. The weighting factor can be calculated exactly for the circle and we assume that the result will give at least a rough idea of the behavior for a square or rectangle. Define W as

$$P_\infty = \int_S WE(\rho)dA \tag{27}$$

For a circle, from equation (22)

$$\int_0^a \frac{\rho E(\rho)d\rho}{(a^2 - \rho^2)^{1/2}} = P_\infty \int_0^a \frac{\rho}{(a^2 - \rho^{2\prime})^{1/2}}\, d\rho \tag{28}$$

Comparing (27) and (28) we find

$$W = \frac{1}{2\pi a(a^2 - \rho^2)^{1/2}} \tag{29}$$

or

$$W = \frac{1}{p(a^2 - \rho^2)^{1/2}} \tag{30}$$

where p is the perimeter of the surface S and $(a - \rho)$ is the distance in from the perimeter toward the centroid. Equation (30) holds exactly for a circle, but we might expect it to give an approximation to P_∞ for other regular surfaces such as a square. P_∞ is then

$$P_\infty = \int_S \frac{E(\rho)}{p(a^2 - \rho^2)^{1/2}}\, dA \tag{31}$$

which may have to be evaluated numerically for shapes other than a circle.

Conclusions

The value of voltage read on a potentiometer, P_∞, may be significantly different than the average surface Seebeck emf and the corresponding temperatures differ proportionately. The value of P_∞ may be above or below $\bar{E}$ depending on the shape of the temperature distribution on the interface surface. In general, if the temperature near the outer edge of the interface is higher than the inner temperatures, the value of P_∞ is greater than $\bar{E}$, and for lower edge values P_∞ is lower than $\bar{E}$.

In practice $E(\rho)$, which is proportional to the temperature, must be known approximately as to shape before the experimental data can be used to calculate $\bar{E}$. If this shape is known approximately from other theoretical considerations [1–5], a measurement of P_∞ suffices to determine the average value $\bar{E}$ and consequently the level of the shape of $E(\rho)$.

An exact solution has been given for the circular interface problem and an approximate estimation scheme for other shapes. For any shape in general, a more exact result can be obtained by numerical integration of the basic equations. In such instances a distribution of current $\sigma(\mathbf{r})$ is picked such that the two conditions are satisfied: (*a*) $V(\mathbf{r})$ is the same shape as $E(\mathbf{r})$ and (*b*) the level of $V(\mathbf{r})$ is such that the conservation equation (7) is satisfied. These two conditions determine $\sigma(\mathbf{r})$ uniquely and allow P_∞ to be determined, since $P_\infty = V(r) - \bar{E}$. The calculation of $\sigma(\mathbf{r})$ can be formidable since it involves a double iteration. For most applications the method outlined in this paper should be adequate to estimate P_∞ even for noncircular interfaces.

References

1 F. P. Bowden and D. Tabor, "The Friction and Lubrication of Solids," Oxford University Press, New York, N. Y., 1950.

2 B. T. Chao and K. J. Trigger, "Temperature Distribution at the Tool-Chip Interface in Metal Cutting," TRANS. ASME, vol. 77, 1955, pp. 1107–1121.

3 B. T. Chao and K. J. Trigger, "Temperature Distribution at Tool-Chip and Tool-Work Interface in Metal Cutting," TRANS. ASME, vol. 80, 1958, pp. 311–320.

4 F. F. Ling, "A Quasi-Iterative Method for Computing Interface Temperature Distributions," U. S. Air Force Office of Scientific Research Contract No. AF 49(638)-67, Technical Note No. 3, Research Project No. 19751, October, 1958.

5 E. G. Loewen and M. C. Shaw, "On the Analysis of Cutting-Tool-Temperatures," TRANS. ASME, vol. 76, 1954, pp. 217–231.

6 E. W. Gaylord, "Research and Development on Investigations of Galling and Friction Characteristics of Metallic Materials and Surface Treated Materials," Technical Report to Watertown Arsenal Contract No. DA-36-061-ORD-460, WAL Report No. 401/65-38, July, 1956.

7 E. W. Gaylord, W. F. Hughes, F. C. Appl, and F. F. Ling, "On the Theoretical Analysis of a Dynamic Thermocouple," TRANS. ASME, vol. 80, 1958, pp. 307–310.

8 E. T. Copson, "On the Problem of the Electrified Disk," *Proceedings of The Edinburgh Mathematical Society*, vol. 8, 1947–1950, pp 14–19.

Normal Modes of Nonlinear Dual-Mode Systems

R. M. ROSENBERG
Professor of Engineering Mechanics, Mechanical Engineering: Mechanics and Design, University of California, Berkeley, Calif.

A system consisting of two unequal masses, interconnected by a coupling spring, and each connected to an anchor spring, is examined. The springs may all be unequal and nonlinear, but each resists being compressed to the same degree as being stretched. The concept of normal modes is rigorously defined, and methods of finding them are given. A knowledge of these modes reduces the coupled system to two uncoupled ones which can always be integrated in quadrature. There exists an infinity of systems, of which the linear is one, which can be integrated in closed form. This approach yields, even for the linear system, new results of great simplicity.

In an earlier paper [1][1] the "natural modes" of a nonlinear two-degree-of-freedom system have been examined, as well as the stability of these modes. That system was a special case of the one illustrated in Fig. 1, consisting of two masses m_1 and m_2 connected to the two anchor springs S_1 and S_3 and the coupling spring S_2. The forces with which the springs resist being deflected are odd polynomials in the deflections. The case treated earlier is that of a special symmetric system in which the two masses and the two anchor springs are identical, and all spring forces are odd cubic polynomials. For that system, it could be shown without difficulty that two vibration modes exist which have in common that the magnitudes of the displacements of the two masses are equal at every instant. In one of these modes the masses move in phase, in the other they move out of phase, with respect to each other. This fact was used to reduce the coupled equations of motion of the two-degree-of-freedom system to two uncoupled equations, each in a single degree of freedom. The two vibration modes were called "normal modes" because the equivalent phenomenon in the linear system *is* vibration in normal modes. However, the earlier paper left unanswered the interesting question of just what constitutes a normal mode in a multi-degree-of-freedom nonlinear system.

In this paper we deal with a much more general system than in the earlier investigation. We admit unequal masses and unequal anchor springs, and we do not prescribe the degree of the "spring polynomials." We do require, however, that they be odd polynomials of the spring deflections.

The principal results of this investigation are:

1 The term "normal mode" is defined rigorously for linear or nonlinear systems. This definition permits a determination of the normal modes independent of the natural frequencies; the natural frequencies may be found afterwards in terms of the normal modes. This procedure is the reverse of the usual one where normal modes are defined in terms of the natural frequencies. The procedure suggested here yields, even for the linear problem, some results of great simplicity which appear to have escaped discovery until now.

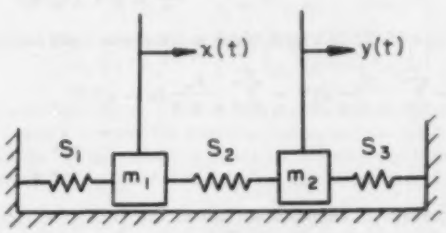

Fig. 1

2 It is shown that a knowledge of the normal modes reduces the (linear or nonlinear) two-degree-of-freedom problem to two systems each in only a single degree of freedom. The problem of finding the frequency-amplitude relations of these is straightforward and can always be reduced to a quadrature.

3 Among systems of the type shown in Fig. 1 there exists an infinite class which can be discussed with particularly great simplicity, and where the results can be given in terms of tabulated functions. Each of its members is associated with a positive odd integer k, and when $k = 1$, the linear case emerges. Thus the linear system becomes simply a special case of an entire set whose frequency-amplitude relation can be given in closed form.

The Equations of Motion

The equations of motion of the system illustrated in Fig. 1 are

$$\left.\begin{aligned} m_1\ddot{x} &= -\sum_{n}^{r} a_n x^n - \sum_{n}^{s} A_n (x-y)^n \\ m_2\ddot{y} &= -\sum_{n}^{t} b_n y^n + \sum_{n}^{s} A_n (x-y)^n \end{aligned}\right\} (n = 1, 3, \ldots) \quad (1)$$

where we assume for the order of the summation limits $r \leq s \leq t$ (although any other order could have been prescribed just as well) and, for the present, the a_n, b_n, A_n are taken to be positive.

The equations

$$\xi = \sqrt{m_1}\, x; \qquad \eta = \sqrt{m_2}\, y \quad (2)$$

transform (1) into

[1] Numbers in brackets designate References at end of paper.

Contributed by the Applied Mechanics Division and presented at the Annual Meeting, Atlantic City, N. J., November 29–December 4, 1959, of The American Society of Mechanical Engineers.

Discussion of this paper should be addressed to the Secretary, ASME, 29 West 39th Street, New York, N. Y., and will be accepted until July 10, 1960, for publication at a later date. Discussion received after the closing date will be returned

Note: Statements and opinions advanced in papers are to be understood as individual expressions of their authors and not those of the Society. Manuscript received by ASME Applied Mechanics Division, February 27, 1959. Paper No 59—A-93.

$$\ddot{\xi} = -\sum_n^r \frac{a_n}{\sqrt{m_1}}\left(\frac{\xi}{\sqrt{m_1}}\right)^n - \sum_n^s \frac{A_n}{\sqrt{m_1}}\left(\frac{\xi}{\sqrt{m_1}} - \frac{\eta}{\sqrt{m_2}}\right)^n$$
$$\ddot{\eta} = -\sum_n^t \frac{b_n}{\sqrt{m_2}}\left(\frac{\eta}{\sqrt{m_2}}\right)^n + \sum_n^s \frac{A_n}{\sqrt{m_2}}\left(\frac{\xi}{\sqrt{m_1}} - \frac{\eta}{\sqrt{m_2}}\right)^n \quad (3)$$

and most of the future development is based on the equations of motion in the form (3).

Inasmuch as the set (1) or (3) defines a conservative system, the right-hand sides must be derivable from a potential function, and one finds without difficulty

$$U = -\sum_n^r \frac{a_n}{n+1}\left(\frac{\xi}{\sqrt{m_1}}\right)^{n+1} - \sum_n^s \frac{A_n}{n+1}\left(\frac{\xi}{\sqrt{m_1}} - \frac{\eta}{\sqrt{m_2}}\right)^{n+1} - \sum_n^t \frac{b_n}{n+1}\left(\frac{\eta}{\sqrt{m_2}}\right)^{n+1} \quad (4)$$

or, in view of (2), in a form which is sometimes more convenient,

$$U = -\sum_n^r \frac{a_n}{n+1}x^{n+1} - \sum_n^s \frac{A_n}{n+1}(x-y)^{n+1} - \sum_n^t \frac{b_n}{n+1}y^{n+1}$$

The function U defines a surface in the $\xi\eta U$-space called the "potential energy surface." This surface has the property of being symmetric with respect to the U-axis, that is,

$$U(\xi, \eta) = U(-\xi, -\eta)$$

This is a direct consequence of the fact that the spring forces are odd polynomials in the spring deflections.

The kinetic energy is seen from (3) to be

$$T = \tfrac{1}{2}(\dot{\xi}^2 + \dot{\eta}^2) \quad (5)$$

and, being conservative, a first integral of the equations of motion is

$$T - U = U_0$$

with T and U defined as previously. The constant U_0 is the total energy of the system, and $0 \leq -U \leq U_0$ since T is positive. The potential energy is $V = -U$.

The Normal Modes

The concept of normal modes is well defined only in the case of the linear system. In that system, normal modes are identified with a fundamental set of solutions, and these have the important property that all solutions are linear combinations of the fundamental set. Expressed differently, all modes of motion are linear combinations of the normal modes. Even if one should be able to define "normal modes" in the nonlinear system, these latter can not possess the same property because the superposition theorem fails in the nonlinear case. Nevertheless, it is an intuitively appealing idea that the nonlinear system has natural frequencies, and that the modes of vibration in which the natural frequencies occur are the counterparts of the normal modes of the linear system.

Aside from the mathematical property of superposition, the normal modes have another property of great technical importance. When the system, linear or not, is subjected to an oscillatory force, resonance occurs when the frequency of that force lies close to the natural frequencies and, in the neighborhood of resonance, the system vibrates essentially in normal modes Since the motive of the engineer in his investigations of vibrations is almost invariably either to produce or to prevent vibrations of large amplitude, the meaning of the term normal modes is of considerable interest even when the superposition property of these modes no longer exists.

In the linear system the normal modes are given through the eigenvalues, and the latter are the roots of the characteristic equation. If these roots are distinct, one distinct eigenvector is attached uniquely to each eigenvalue; i.e., the former are defined by means of the latter. In fact, finding the normal modes is always preceded by finding the eigenvalues. For instance, the linear problem has the equations of motion

$$m_1\ddot{x} = -a_1x - A_1(x - y)$$
$$m_2\ddot{y} = -b_1y + A_1(x - y)$$

and the normal modes are given by [2]

$$\tan\theta = \frac{Y_0}{X_0} = \frac{-m_1\omega_{1,2}^2 + a_1 + A_1}{A_1} \quad (6)$$

where $\omega_{1,2}^2 = -\lambda_{1,2}^2$ are the roots of

$$\lambda^4 + \left(\frac{a_1 + A_1}{m_1} + \frac{b_1 + A_1}{m_2}\right)\lambda^2 + \frac{a_1b_1 + a_1A_1 + b_1A_1}{m_1m_2} = 0 \quad (7)$$

and the constants X_0 and Y_0 are defined through the solutions

$$x(t) = X_0e^{\lambda t}; \quad y(t) = Y_0e^{\lambda t} \quad (8)$$

of the equations of motion.

Another way of regarding normal modes in the linear system is to state that they are given by constants c_i (if they exist) such that normal solutions of the equations of motion satisfy the condition

$$y(t)/x(t) \equiv c_i \quad (9)$$

Such solutions evidently have the property that, if there exists a $t = t_0$ such that $y(t_0) = 0$, then necessarily $x(t_0) = 0$ as well. In other words, normal modes of the linear two-degree-of-freedom system are oscillations of such a nature that both masses pass through their equilibrium positions at the same instant.

The normal modes of the linear system have a further property connected with the manner in which the system is set into motion. Suppose we seek initial amplitudes $x(0) = X_0$, $y(0) = Y_0$ such that the system will vibrate in normal modes when the initial velocities $\dot{x}(0) = \dot{y}(0) = 0$. In that case, the initial potential energy of the system is also the total energy, and that energy is defined by an equation

$$-U(\bar{x}, \bar{y}) = U_0 \quad (10)$$

where $(\bar{x}, \bar{y})$ are points on the ellipse $-U = U_0$. In the linear case considered here, (10) is an ellipse in the xy-plane as one may readily ascertain from the form of the unnumbered equation below (4). The slope of that ellipse is given everywhere by

$$d\bar{y}/d\bar{x} = -U_x/U_y \quad (11)$$

where the subscripts denote partial derivatives. While the initial value of $dy/dx = \dot{y}(0)/\dot{x}(0)$ is indeterminate in view of the value of the initial velocities, one can readily evaluate it from the equations of motion written in the form

$$d\dot{x}/dt = U_x; \quad d\dot{y}/dt = U_y$$

and one finds

$$\dot{y}(0)/\dot{x}(0) = \bar{y}(0)/\bar{x}(0) = U_y/U_x \quad (12)$$

A comparison between (11) and (12) shows that the lines $y(t) = c_ix(t)$ must intersect the line $U_0 + U = 0$ orthogonally.

Once these properties are established we are in a position to define normal modes in the nonlinear system.

A normal mode of the system

$$\ddot{\xi} = U_\xi; \quad \ddot{\eta} = U_\eta \tag{13}$$

where U is given by (4), is a function

$$\eta = \eta(\xi) \tag{14}$$

which is satisfied for all t by periodic solutions $\xi = \xi(t) = \xi(t + T)$; $\eta = \eta(t) = \eta(t + T)$ of (13), where $\eta(\xi)$ is a single-valued function of ξ in the closed domain $-U(\xi, \eta) = U_0$ of the $\xi\eta$-plane which satisfies the boundary condition $\eta(0) = 0$ and which intersects the line $-U(\xi, \eta) = U_0$ orthogonally. The relation (14) was called the "modal relation" in the earlier paper, and this terminology will be retained here.

Clearly, if the modal relations can be found without the necessity of finding first the natural frequencies of the system, the solutions of (13) involve merely those of the uncoupled equations

$$\ddot{\xi} = U_\xi(\xi, \eta(\xi)); \quad \ddot{\eta} = U_\eta(\xi(\eta), \eta)$$

Darboux [3] has pointed out that the dynamical problem defined by (13) is completely equivalent to that of finding the geodesics in the surface whose metric is given by

$$d\sigma^2 = (U_0 + U')(d\xi^2 + d\eta^2) \tag{15}$$

and that this is merely the differential form of the principle of least action. The differential equation of the geodesics in question is the Euler equation of

$$\delta \int_{t_1}^{t_2} (U_0 + U)^{1/2} (1 + \eta'^2)^{1/2} d\xi = 0 \tag{16}$$

and that equation is found to be

$$2(U_0 + U)\eta'' + (1 + \eta'^2)(\eta' U_\xi - U_\eta) = 0 \tag{17}$$

This equation can also be found by elementary means [4]. Solutions which satisfy (17) are solutions of the dynamical system. Those among the solutions of (17) which satisfy (14) as well are normal modes or modal relations.

In view of the fact that $U(\xi, \eta)$ is symmetric, and that U_ξ and U_η are odd in ξ and η, one can easily ascertain by substitution into (17) that the solutions of that equation are odd. Thus all solutions including the modal relations have the property that $\eta(-\xi) = -\eta(\xi)$.

Inasmuch as U and its derivatives are, in general, highly nonlinear functions of ξ and η, one can not integrate (17) in the general case. There exist, however, important special cases for which the modal relations are straight lines; i.e., where these relations are of the form $\eta = c_1\xi$. Since these solutions imply $\eta'' \equiv 0$, one sees from (17) that they must satisfy

$$\eta' = U_\eta/U_\xi \tag{18}$$

But these lines intersect the lines of constant potential energy H

$$-U(\xi, \eta) = H \leq U_0$$

orthogonally as will be seen when one differentiates this last equation. It turns out, therefore, that every straight line which intersects all lines of constant potential energy orthogonally is a modal relation since it satisfies (17) as well as our definition of normal modes.

The Straight Modal Relations

We show here that there exist two types of problems for which the modal relations are straight lines. One type consists of an infinite class called the "homogeneous case of degree k" and when $k = 1$ the linear case arises. The other is called the "symmetric case."

In order to derive this result we make use of the easily proved theorem that the straight line between the origin of the $\xi\eta$-plane and that point (ξ_0, η_0) on a continuously differentiable curve $U(\xi, \eta) + U_0 = 0$ which is farthest from, or nearest to (0, 0) intersects the curve $U + U_0 = 0$ orthogonally.

We shall consider the family of equipotential lines

$$-U(\xi, \eta) = H = \text{const}$$

$$U_0 \geq H > 0$$

and we desire to find the locus of those points on these curves which are farthest from, or nearest to, the origin of the $\xi\eta$-plane. In view of the foregoing theorem, if the locus of these points is a straight line, it is a modal relation because it satisfies (17), passes through the origin of the $\xi\eta$-plane, and it intersects the equipotential line $U + U_0 = 0$ orthogonally.

We shall single out among (3) a class called the "homogeneous case of degree k" whose equations of motion are

$$\left.\begin{aligned} \ddot{\xi} &= -\frac{a_k}{\sqrt{m_1}}\left(\frac{\xi}{\sqrt{m_1}}\right)^k - \frac{A_k}{\sqrt{m_1}}\left(\frac{\xi}{\sqrt{m_1}} - \frac{\eta}{\sqrt{m_2}}\right)^k \\ \ddot{\eta} &= -\frac{b_k}{\sqrt{m_2}}\left(\frac{\eta}{\sqrt{m_2}}\right)^k + \frac{A_k}{\sqrt{m_2}}\left(\frac{\xi}{\sqrt{m_1}} - \frac{\eta}{\sqrt{m_2}}\right)^k \end{aligned}\right\} \tag{19}$$

where k is an odd integer. This system is called the homogeneous case of degree k because the restoring forces, i.e., the right-hand sides of (19), are homogeneous functions in ξ and η of degree k.

The equipotential lines of this system are, in view of (2)[2]

$$\frac{a_k}{k+1}x^{k+1} + \frac{b_k}{k+1}y^{k+1} + \frac{A_k}{k+1}(x - y)^{k+1} = H \leq U_0 \tag{20}$$

This equation defines a family of curves with H as a parameter. The locus of the points of maximum and minimum distance from the origin of the xy-plane is most easily found by transforming (20) into polar co-ordinates through

$$x = r\cos\theta; \qquad y = r\sin\theta$$

resulting in an equation

$$R(r, \theta) = H \tag{21}$$

If one puts $dr/d\theta = -R_\theta/R_r = 0$, the vanishing of this derivative (which defines the locus in question) implies $R_\theta = 0$. That locus will be a straight line if, and only if

$$R_\theta = \Theta_1(\theta) \cdot \Theta_2(r, \theta) \tag{22}$$

For (20), it turns out that

$$R_\theta = r^{k+1}[-a_k\cos^k\theta\sin\theta + b_k\cos\theta\sin^k\theta - A_k(\cos\theta - \sin\theta)^k(\cos\theta + \sin\theta)]$$

It follows that, in the homogeneous case of degree k, R_θ has the required form, and the modal relation is a straight line which makes an angle θ with the x-axis. This modal relation is found from the vanishing of the quantity in the square brackets in the foregoing equation. That result can be put into the convenient form

$$\tan 2\theta = \frac{2A_k(1 - \sin 2\theta)^{\frac{k-1}{2}}}{b_k[1/2(1 - \cos 2\theta)]^{\frac{k-1}{2}} - a_k[1/2(1 + \cos 2\theta)]^{\frac{k-1}{2}}}; \quad (b_k \neq a_k) \tag{23}$$

[2] This form is useful only when $m_1 = m_2$ because the transformations (2) are not "angle-preserving." However, similar results as those given here can easily be derived also when $m_1 \neq m_2$, and the general conclusions remain the same. In particular, the modal relations remain straight.

In order to discuss the roots of (23), it is convenient to write that equation in the form

$$f(2\theta) = g(2\theta)$$

$$\left.\begin{aligned} &\text{where } f(2\theta) = {}^1/_2\alpha_k \tan 2\theta, \\ &g(2\theta) = \frac{(1 - \sin 2\theta)^{\frac{k-1}{2}}}{\gamma_k[{}^1/_2(1 - \cos 2\theta)]^{\frac{k-1}{2}} - [{}^1/_2(1 + \cos 2\theta)]^{\frac{k-1}{2}}}, \end{aligned}\right\} \quad (24)$$

$$\alpha_k = \frac{a_k}{A_k}, \qquad \gamma_k = \frac{b_k}{a_k}$$

and the problem consists in determining the number, and bounds on the location, of the intersections of $f(2\theta)$ and $g(2\theta)$ in $0 \leq 2\theta \leq 2\pi$. In this discussion we may restrict γ_k with little loss of generality to the interval $0 \leq \gamma_k \leq 1$. The lower bound on γ_k is implicit in the physics of the problem since we cannot admit simultaneously $a_k = 0$ *and* $b_k = 0$. If we did, we should be discussing a system with no anchor springs and this would eliminate one degree of freedom. If one anchor spring is absent, as in the configuration of the dynamic-vibration absorber, we shall say that $b_k = 0$; $a_k \neq 0$. We need not examine the problem for $\gamma_k > 1$ because that range implies $b_k > a_k$. But, when $b_k > a_k$, one may simply turn the system end for end without making a similar exchange in the nomenclature for the anchor springs; this will again restore the condition $\gamma_k \leq 1$. The only loss of generality implied by the restrictions on γ_k is that we do not admit a negative ratio for the coefficients of the anchor springs; in other words, a system in which one anchor spring is restoring while the other is exciting is not admitted. This restriction is consistent with the earlier statement that all spring coefficients are positive.

The function $g(2\theta)$ has the following properties: It has a single zero at $2\theta = \pi/2$, and at that point, the slope vanishes as well. It has a pair of poles at $2\theta = \pi - \varphi$ and $2\theta = \pi + \varphi$, and $0 < \varphi < \pi/4$. It is positive between the poles and negative elsewhere in $0 \leq 2\theta \leq 2\pi$ (except, of course, at the zero where it is merely nonpositive). Another interesting property is that the poles of $g(2\theta)$ tend to $\pi/2$ and $3\pi/2$ as $k \to \infty$. The function $g(2\theta)$ is shown in Fig. 2 by the heavy line, and $f(2\theta)$ by the broken line. Their intersection furnishes the roots $2\theta_1^*$ and $2\theta_2^*$ of (23).

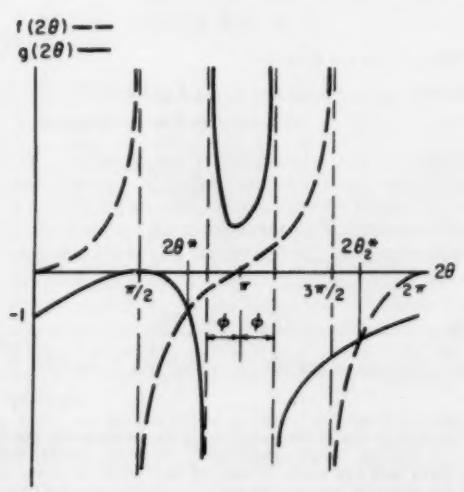

Fig. 2

In view of the character of $f2(\theta)$ and $g(2\theta)$, and the restrictions on γ_k we may conclude that (23) has two and only two roots θ_1^* and θ_2^* in one period of $f(2\theta)$ and $g(2\theta)$; these roots lie in the intervals $\pi/4 < \theta_1^* < \pi/2$ and $3\pi/4 < \theta_2^* < \pi$ for finite k. To each root there belongs one modal relation $\eta = c_{1,2}\xi$ where $c_{1,2} = c(\theta_{1,2}^*) = \tan \theta_{1,2}^*$. The constant $c_1 > 0$ and defines an in-phase mode; $c_2 < 0$, and defines an out-of-phase mode. As $k \to \infty$, $c_1 \to 1$ and $c_2 \to -1$. In other words, for sufficiently large k, the modal relations approach those of a symmetric system. For $k \to 1$, the modal relations approach those of the linear system and, when $k = 1$,

$$\left.\begin{aligned} &\tan 2\theta^* = \frac{2A_1}{b_1 - a_1}, \quad (b_1 \neq a_1) \\ &\theta_{1,2}^* = \pm\pi/4, \qquad (b_1 = a_1) \end{aligned}\right\} \quad (25)$$

A comparison between this result on the one hand and (6) and (7) on the other shows how much simpler (25) is than the relation usually encountered.[3] It appears that the great simplicity of the modal relations for the linear case, when expressed in terms of the double angle has been overlooked heretofore.

In the two limiting cases $k = \infty$ and $k = 1$, the modal lines intersect each other orthogonally. It can be shown easily that they do not have this property when $k > 1$ is a positive, finite, odd integer, but the departure from orthogonal intersection is then small.

Substitution of the modal relations (24) in the equations of motion reduces the latter to equations of the form

$$\ddot{u} + M_{1,2}u^k = 0; \; M_{1,2} = M(c_{1,2}) = \text{const}$$

and these can be integrated to yield the frequency-amplitude relations in terms of gamma functions. Thus the procedure here is to attach one eigenvalue-relation to each normal mode. Furthermore, it is seen that all homogeneous cases of degree k can be solved exactly in closed form.

A second important case in which the modal relations are straight lines is a generalization of a system treated earlier [1]. This is the symmetric case which arises when $a_n = b_n$ for all n, and $m_1 = m_2$. For that case, the equipotential lines are given by

$$\sum_n^r \frac{a_n}{n+1}(x^{n+1} + y^{n+1}) + \sum_n^s \frac{A_n}{n+1}(x - y)^{n+1} = H \leq U_0 \quad (26)$$

Transformation to polar co-ordinates, and proceeding as before, shows that the function R_θ now becomes

$$R_\theta = \sum_n^r a_n r^{n+1}(\sin^n\theta\cos\theta - \sin\theta\cos^n\theta) - \sum_n^s A_n r^{n+1}(\cos\theta - \sin\theta)^n(\cos\theta + \sin\theta)$$

This equation can be cast into the form

$$R_\theta = -\cos 2\theta\left\{\sin 2\theta \sum_n^r \sum_m C_{m+1} a_n r^{n+1}({}^1/_2)^{\frac{n-1}{2}} \cos^{n-1}\theta - \sum_n^s A_n r^{n+1}(\cos\theta - \sin\theta)^{n-1}\right\} \quad (27)$$

where the C_{m+1} are binomial coefficients. Since (27) is also of the form (22), the modal relations are again straight lines defined through (27) by $\theta = \pm\pi/4$ or $\eta = \xi$; $\eta = -\xi$. We conclude that the normal modes of symmetric systems are such that the

[3] It can be shown, of course, that (6) and (7) can be combined to give the same result as (25).

absolute values of the displacements of the two masses are equal at all times, and the masses move either in-phase or out-of-phase.

When the modal relations of symmetric systems are substituted in the equations of motion of these systems, the latter become

$$\ddot{x} = -\sum_{n}^{r} a_n x^n$$

$$\ddot{x} = -\sum_{n}^{r} (a_n + 2^n A_n) x^n - \sum_{n=r+2}^{s} 2^n A_n x^n$$

The resulting frequency-amplitude relations can always be found by a single quadrature. When $r = s = 3$, they become complete elliptic integrals of the first kind.

The Curved Modal Relations

While there are technically important cases in which the modal relations are straight, they are, in general, curves which must satisfy (17) and the boundary conditions stated in connection with the definition of a normal mode. But, (17) cannot, in general, be integrated except by numerical methods. Even when modern computing equipment is used to integrate (17), the process may be expected to be tedious because the boundary conditions are mixed. However, an insight into the general nature of the curved modal relations may be gained simply by the iteration

$$\eta_{i+1}' = -\frac{(1 + \eta_i'^2)[\eta_i' U_\xi(\xi, \eta_i) - U_\eta(\xi, \eta_i)]}{2[U_0 + U(\xi, \eta_i)]} \tag{28}$$

if one is satisfied with a single iteration and if one adopts a straight-line modal relation as the zero'th estimate. Not only is the convergence of the iteration assured in all cases where U has the general form of (4), but it may be expected that a single iteration gives very satisfactory results whenever the case under consideration lies in the neighborhood of either a homogeneous, or a symmetric case.

In particular, the generalization of the Duffing problem to two degrees of freedom is such a case because that problem deals with spring forces in which the coefficients of the linear terms are large compared to those of the cubic terms, and all terms of degree higher than third order are absent. Thus it lies in the neighborhood of the homogeneous case of degree 1. Since the Duffing problem in a single degree of freedom has been the basis of many investigations, one should think that its extension to two degrees of freedom forms an interesting field of inquiry. Moreover, we can discuss by the same methods the system in which the cubic "spring terms" are large compared to the linear ones, and all others are absent. This permits analysis of two limiting cases of the general system in which all spring forces are general odd, cubic polynomials of the spring deflections.

Since the equations of motion are of degree t, adoption of a straight line for the zero'th estimate of the modal relation yields, in place of (28)

$$\eta_1' = \frac{f(\xi)}{F(\xi)} = \sum_{m=1,2,\ldots}^{\frac{t+1}{2}} \gamma_m \left[\frac{1}{\xi - \delta_m} + \frac{1}{\xi + \delta_m}\right] \tag{29}$$

where $f(\xi)$ is an odd polynomial of degree t, $F(\xi)$ is an even polynomial of degree $t + 1$, δ_m are the zeroes of $F(\xi)$, and

$$\gamma_m = \frac{f(\delta_m)}{F'(\delta_m)}$$

It should be observed that, since $F(\xi)$ is an even function, the negatives of the roots of $F(\xi) = 0$ are also roots. We are assuming here that the roots are distinct. Multiple zeros of $F(\xi)$ may occur because of a particular combination of values of the coefficients a_n, b_n, A_n in U. However, no constraints exist which would produce multiple zeros. In any event, if multiple zeros of $F(\xi)$ do occur, a result similar to that given in the following can be derived for that case also. It will be observed that there are only $(t + 1)/2$ terms in the summation of (29), instead of the expected $t + 1$. This is a result of the fact that $f(\xi)$ and $F'(\xi)$ are both odd, so that $f(-\delta_m)/F'(-\delta_m) = f(\delta_m)/F'(\delta_m)$.

If one integrates (29) and satisfies the boundary conditions one finds

$$\eta_1 = (C - t - 1)\xi + \sum_{m=1,2,\ldots}^{\frac{t+1}{2}} \log\left[\frac{(\xi^2 - \delta_m^2)^{t+\delta_m}}{(\xi - \delta_m)^{2\delta_m}}\right]^{\gamma_m} \tag{30}$$

where C is a constant of integration that must be determined from the second boundary condition.

It is interesting to note that the curved modal relation consists of a straight line plus a sum of logarithmic terms. These latter are evidently corrections on the initial assumption of straightness of the modal lines. However, one sees from (30) that there emerges also a correction on the slope of the zero'th estimate of the modal line; this is evident from the presence of C in the linear term; it is required so that the modal line will intersect the curve $U + U_0 = 0$ orthogonally.

Maximum-Minimum Properties

It is well known [5] that the characteristic values of linear problems possess maximum-minimum properties; therefore the method of finding them can be reduced to a maximum-minimum problem. Here we would like to show that, the modal relations arising from linear or nonlinear eigenvalue problems, also have such properties.

To deduce the desired properties we examine the geodesics in the space whose metric is given by

$$d\sigma^2 = (U_0 + U)(d\xi^2 + d\eta^2) \tag{31}$$

where U is defined in (4), and we remember that these geodesics are solutions to the dynamical problem. This space lies in the $\xi\eta$-plane, and on it we map the lines of constant potential energy H in the interval $0 \leq H \leq U_0$. If the a_n, b_n, $A_n > 0$, the lines of constant energy are nonintersecting concentric closed curves, and the $\xi\eta$-plane appears somewhat as shown in Fig. 3.

We now choose on the line $-U = U_0$ a point (ξ, η) denoted by (ξ, η, U_0) and we consider the geodesic connecting this point with the origin (0, 0, 0) of the $\xi\eta$-plane. This geodesic is by definition the shortest distance between the points in question. *Then, the modal relations are the shortest and the longest of these lines of minimum length as the point (ξ, η, U_0) moves once completely around the oval $-U = U_0$.* In this way the modal rela-

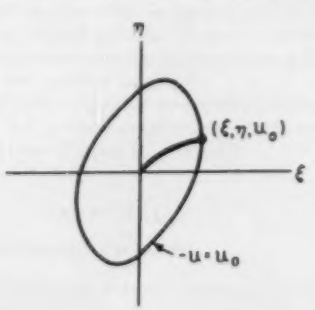

Fig. 3

tions are defined in terms of a minimum-maximum, and of a minimum-minimum problem. In the variational problem just considered, one end point moves on a prescribed curve. The solution, therefore, leads to a transversality condition which states [6] that the geodesic must intersect the line $-U = U_0$ orthogonally. But, this is precisely the condition which normal modes must satisfy; this completes the demonstration.

Acknowledgments

The author has discussed the subject matter of this paper on several occasions with his colleagues, Profs. George Leitmann and René de Vogelaere, and has received from them valuable suggestions. He also wishes to acknowledge gratefully financial aid from the National Science Foundation which has supported a portion of this investigation.

References

1 R. M. Rosenberg and C. P. Atkinson, "On the Natural Modes and Their Stability in Nonlinear Two-Degree-of-Freedom Systems," JOURNAL OF APPLIED MECHANICS, vol. 26, TRANS. ASME, vol. 81, 1959, series E, pp. 377–385.

2 J. P. Den Hartog, "Mechanical Vibrations," McGraw-Hill Book Company, Inc., New York, N. Y., third edition, 1947, pp. 104–105.

3 G. Darboux, "Leçons sur la Théorie Générale des Surfaces," Gauthier-Villars et Fils, vol. 2, 1889, p. 453.

4 H. Kauderer, "Nichtlineare Mechanik," Springer, 1959, p. 599.

5 R. Courant and D. Hilbert, "Methoden der Mathematischen Physik," Springer, vol. 1, 1931, pp. 26–29.

6 O. Bolza, "Vorlesunger ueber Variationsrechnung," Koehler and Amelang, 1909, reprinted 1949, pp. 553–691.

T. K. CAUGHEY
Associate Professor of Applied Mechanics, Division of Engineering, California Institute of Technology, Pasadena, Calif.

Classical Normal Modes in Damped Linear Dynamic Systems

An analysis of the conditions under which a damped linear system possesses classical normal modes is presented. It is shown that a necessary and sufficient condition for the existence of classical normal modes is that the damping matrix be diagonalized by the same transformation that uncouples the undamped systems. Sufficient though not necessary conditions on the damping matrix are developed, and it is shown that Rayleigh's solution is a special case of the present theory.

It is well known that undamped linear dynamic systems possess normal modes, and that in each normal mode the various parts of the system vibrate in the same phase. In damped systems, however, this property is generally violated and classical normal modes do not exist; in such cases the more general treatment of K. A. Foss[1] is required. Rayleigh[2] showed that if the damping matrix is a linear combination of the stiffness and inertia matrices, the damped system will have classical normal modes. The purpose of this paper is to determine the general conditions under which a damped dynamic system possesses classical normal modes. It will be shown that a necessary and sufficient condition that a damped dynamic system possess classical normal modes is that the damping matrix be diagonalized by the same transformation which uncouples the undamped system.

Theory

The equations of motion of an N-degree-of-freedom linear dynamic system with lumped parameters may be written in matrix notation as:

$$[m]\{\ddot{g}\} + [c]\{\dot{g}\} + [k]\{g\} = \{f(t)\} \tag{1}$$

For passive systems the $N \times N$ matrices $[m]$, $[c]$, and $[k]$ are symmetric and positive definite.

Consider the homogeneous problem obtained by setting $\{f(t)\} = 0$ in (1); i.e.,

$$[m]\{\ddot{g}\} + [c]\{\dot{g}\} + [k]\{g\} = 0 \tag{2}$$

Since $[m]$ is a symmetric matrix, it is always possible to find a transformation which will remove the inertia coupling terms. Let

$$\{g\} = [\theta]\{x\} \tag{3}$$

be the transformation which diagonalizes $[m]$, i.e., the transformation for which $[\theta]^T [m] [\theta]$ is diagonal. Substitute (3) into (2) and premultiply by $[\theta]^T$

$$[\theta]^T[m][\theta]\{\ddot{x}\} + [\theta]^T[c][\theta]\{\dot{x}\} + [\theta]^T[k][\theta]\{x\} = 0 \tag{4}$$

$$\text{Define} \begin{cases} [\theta]^T[m][\theta] = [\overline{m}] \text{ a diagonal matrix} \\ [\theta]^T[c][\theta] = [\overline{c}] \\ [\theta]^T[k]\ [\theta] = [\overline{k}] \end{cases} \tag{5}$$

It will be observed that since $[m]$, $[c]$, and $[k]$ are symmetric and positive definite, $[\overline{m}]$, $[\overline{c}]$, and $[\overline{k}]$ will also be symmetric and positive definite. In particular $[\overline{m}]$ is diagonal, hence $[\overline{m}]$ will have only positive diagonal elements.

Equation (4) may now be written:

$$[\overline{m}]\{\ddot{x}\} + [\overline{c}]\{\dot{x}\} + [\overline{k}]\{x\} = 0 \tag{6}$$

It is convenient for the analysis which follows to introduce a second transformation such that the inertia matrix will be an identity matrix.

Let

$$[n]\{x\} = \{p\} \tag{7}$$

where

$$[n] = [\sqrt{\overline{m}}] \text{ a diagonal matrix} \tag{8}$$

Substitute (7) into (6) and premultiply by $[n]^{-1}$. Thus

$$[I]\{\ddot{p}\} + [n]^{-1}[\overline{c}][n]^{-1}\{\dot{p}\} + [n]^{-1}[\overline{k}][n]^{-1}\{p\} = 0 \tag{9}$$

which may be written

$$[I]\{\ddot{p}\} + [A]\{\dot{p}\} + [B]\{p\} = 0 \tag{10}$$

where

$$\begin{cases} [I] \text{ is the identity matrix} \\ [A] = [n]^{-1}\,[\overline{c}][n]^{-1} \\ [B] = [n]^{-1}[\overline{k}][n]^{-1} \end{cases} \tag{11}$$

Equation (10) will be referred to as the standard or canonical form of the damped coupled system. It should be noted that since $[\overline{c}]$ and $[\overline{k}]$ are symmetric and positive definite, $[A]$ and $[B]$ are also symmetric and positive definite.

Since $[A]$ and $[B]$ are symmetric and positive definite, it is always possible to find a transformation which will simultaneously diagonalize $[A]$ and $[B]$ (see Hildebrand[3]).

Let

$$\{p\} = [\Phi]\{\xi\} \tag{12}$$

be the required transformation, for which

[1] K. A. Foss, "Co-Ordinates Which Uncouple the Equations of Motion of Damped Linear Systems," Technical Report 25-30, Massachusetts Institute of Technology, March, 1956.

[2] Lord Rayleigh, "Theory of Sound," vol. 1, Dover Publications, New York, N. Y. 1945. Rayleigh did not use matrix algebra; however, his results are equivalent to those stated.

[3] F. B. Hildebrand, "Methods of Applied Mathematics," Prentice-Hall, Inc., New York, N. Y., 1952.

Contributed by the Applied Mechanics Division and presented at the Annual Meeting, Atlantic City, N. J., November 29–December 4, 1959 of THE AMERICAN SOCIETY OF MECHANICAL ENGINEERS.

Discussion of this paper should be addressed to the Secretary, ASME, 29 West 39th Street, New York, N. Y., and will be accepted until July 10, 1960, for publication at a later date. Discussion received after the closing date will be returned.

NOTE: Statements and opinions advanced in papers are to be understood as individual expressions of their authors and not those of the Society. Manuscript received by ASME Applied Mechanics Division, April 13, 1959. Paper No. 59—A-62.

$$[\Phi]^T[A][\Phi] = [a] \text{ a diagonal matrix} \tag{13}$$

$$[\Phi]^T[B][\Phi] = [b] \text{ a diagonal matrix} \tag{14}$$

Substitute (12) into (10) and premultiply by $[\Phi]^T$, thus

$$[\Phi]^T[\Phi]\{\ddot{\xi}\} + [a]\{\xi\} + [b]\{\xi\} = 0 \tag{15}$$

where $[a]$ and $[b]$ are defined in the foregoing.

Equation (15) will be uncoupled if, and only if, $[\Phi]^T[\Phi]$ is a diagonal matrix. If $[\Phi]$ is a normalized matrix, this requirement becomes

$$[\Phi]^T[\Phi] = [I] \tag{16}$$

Hence the transformation (12) which simultaneously diagonalizes $[A]$ and $[B]$ must be an orthogonal transformation; this places restrictions on the forms that $[A]$ and $[B]$ may take.

It is interesting to note that the required orthogonal transformation is exactly the same as that required to uncouple the undamped system obtained by setting $[A]$ equal to zero in (10). It therefore follows that, if a damped system possess classical normal modes, these modes are identical with the normal modes for undamped system.

Returning to equation (1), it may be shown as a consequence of the foregoing comments that a necessary and sufficient condition for equation (1) to possess classical normal modes is that the damping matrix $[c]$ be diagonalized by the same transformation which uncouples the undamped system, obtained by setting $[c]$ equal to zero in (1). This may be illustrated in the following way:

Let

$$\{\varrho\} = [\Psi]\{\eta\} \tag{17}$$

be the transformation which uncouples the undamped system. Substitute (17) into (1) and premultiply by $[\Psi]^T$. Then equation (1) becomes

$$[M]\{\ddot{\eta}\} + [\Psi]^T[c][\Psi]\{\dot{\eta}\} + [K]\{\eta\} = 0 \tag{18}$$

where, by definition of $[\Psi]$

$$\begin{aligned} [M] &= [\Psi]^T[m][\Psi] \text{ a diagonal matrix} \\ [K] &= [\Psi]^T[k][\Psi] \text{ a diagonal matrix} \end{aligned} \tag{19}$$

(*a*) Equation (18) will be uncoupled if, and only if, $[\Psi]^T[c][\Psi]$ is diagonal.

(*b*) If $[\Psi]^T[c][\Psi]$ is diagonal, the system will have classical normal modes which are identical with those for the undamped system.

Relationship Between [A] and [B] for Classical Normal Modes

It will now be shown that a sufficient, though not necessary, condition that (10) possess classical normal modes is that $[A]$ may be expressed in the following way:

$$[A] = \sum_{n=1}^{\infty} \sum_{l=0}^{N-1} a_{nl}[B]_1^{l/n} \tag{20}$$

where N is the order of the square matrix $[B]$.

Proof. Let

$$[a] = [b]^l \text{ a diagonal matrix} \tag{21}$$

From (13) and (16),

$$[A] = [\Phi][a][\Phi]^{-1} \tag{22}$$

Using (21),

$$[A] = [\Phi][b]^l[\Phi]^{-1} \tag{23}$$

$$= [\Phi][b][\Phi]^{-1} \ldots\ldots\ldots [\Phi][b][\Phi]^{-1} \tag{24}$$

$$= ([\Phi][b][\Phi]^{-1})^l \tag{25}$$

From (14) and (16),

$$[B] = [\Phi][b][\Phi]^{-1} \tag{26}$$

$$\therefore [A] = [B]^l \tag{27}$$

The Cayley-Hamilton theorem states that every matrix satisfies its own characteristic equation, hence any power of a matrix can be expressed in terms of the $(N\text{-}j)$th powers of that matrix, where $j = 1, 2 \ldots N$, hence l in (21) need only take on the values 0, 1, 2 . . N-1.

From the foregoing it will be seen that if $[A]$ is expressed as a polynomial in $[B]$, $[A]$ will automatically be diagonalized by the transformation which uncouples the undamped system.

Consider now

$$[a] = [b^{l/n}] \text{ a diagonal matrix} \tag{28}$$

Then

$$[A] = [\Phi][b^{l/n}][\Phi]^{-1} \tag{29}$$

Raise both sides of (29) to the power n. Thus

$$[A]^n = ([\Phi][b^{l/n}][\Phi]^{-1})^n \tag{30}$$

$$= [\Phi][b^{l/n}][\Phi]^{-1} \ldots\ldots [\Phi][b^{l/n}][\Phi]^{-1} \tag{31}$$

n-fold

$$= [\Phi][b^{l/n}]^n[\Phi]^{-1} \tag{32}$$

$$= [\Phi][b]^l[\Phi]^{-1}$$

Using (21) and (27),

$$[A]^n = [B]^l \tag{33}$$

$$[A] = [B]_1^{l/n} \tag{34}$$

The subscript denotes that (34) applies to one particular root of $[B]$.

As before, l need only take on the values 1, 2 . . . N-1.

Since $[a]$ of (28) is diagonal, equations (15) are uncoupled, hence the system described by (10) will possess classical normal modes. This result is valid for all $[a]$ of the form $[b^{l/n}]$, and hence is true also of a linear combination of such terms.

Hence if

$$[A] = \sum_{n=1}^{\infty} \sum_{l=0}^{N-1} a_{ln}[B]_1^{l/n} \tag{35}$$

the dynamic system of equations (10) possesses classical normal modes. In particular, it should be noted that if the terms $n = 1$, $l = 0$, $l = 1$ are taken in (35), Rayleigh's result is obtained.

It should be noted in passing that (35) does not form a complete set of functions, since it is well known that many damped dynamic systems do not possess classical normal modes.

Numerical Example

To illustrate the foregoing results, consider the following simple problem:

$$[m]\{\ddot{\varrho}\} + [c]\{\dot{\varrho}\} + [k]\{\varrho\} = 0 \tag{36}$$

$$\text{where} \quad [m] = \begin{bmatrix} 1 & 0 & 0 \\ 0 & 1 & 0 \\ 0 & 0 & 1 \end{bmatrix}$$

$$[c] = 2\zeta \begin{bmatrix} 1.3608 & -0.3836 & -0.0532 \\ -0.3836 & 1.3608 & -0.3836 \\ -0.0532 & -0.3836 & 1.3608 \end{bmatrix} \qquad (37)$$

$$[k] = \begin{bmatrix} 2 & -1 & 0 \\ -1 & 2 & -1 \\ 0 & -1 & 2 \end{bmatrix}$$

It should be noted that $[c]$ has been so chosen that:

$$\begin{bmatrix} 1.3608 & -0.3836 & -0.0532 \\ -0.3836 & 1.3608 & -0.3836 \\ -0.0532 & -0.3836 & 1.3608 \end{bmatrix}^2 = \begin{bmatrix} 2 & -1 & 0 \\ -1 & 2 & -1 \\ 0 & -1 & 2 \end{bmatrix} \qquad (38)$$

Thus the damping matrix is of the form given in (35) with $l = 1$, $n = 2$, hence the system will have classical normal modes.

Consider the undamped problem obtained by setting ζ equal to zero in (36). The eigenvalues and modal vectors are easily obtained for this problem, they are:

$$w_1 = 0.765, \qquad w_2 = 1.414, \qquad w_3 = 1.850$$

$$\{\phi^1\} = \begin{Bmatrix} 0.5 \\ 0.707 \\ 0.5 \end{Bmatrix}, \quad \{\phi^2\} = \begin{Bmatrix} 0.707 \\ 0.0 \\ -0.707 \end{Bmatrix}, \quad \{\phi^3\} = \begin{Bmatrix} 0.5 \\ -0.707 \\ 0.5 \end{Bmatrix} \qquad (39)$$

The transformation which uncouples the undamped system is:

$$\{g\} = \begin{bmatrix} 0.5 & 0.707 & 0.5 \\ 0.707 & 0.0 & -0.707 \\ 0.5 & -0.707 & 0.5 \end{bmatrix} \{\xi\} \qquad (40)$$

Substituting (40) into (35) and premultiplying by $[\phi]^T$ gives

$$[I]\{\ddot{\xi}\} + 2\zeta[\phi]^T[c][\phi]\{\dot{\xi}\} + [\phi]^T[k][\phi]\{\xi\} = 0 \qquad (41)$$

Carrying out the numerical computations just indicated, give:

$$[I]\{\ddot{\xi}\} + 2\zeta \begin{bmatrix} 0.765 & 0 & 0 \\ 0 & 1.414 & 0 \\ 0 & 0 & 1.850 \end{bmatrix} \{\dot{\xi}\} + \begin{bmatrix} (0.765)^2 & 0 & 0 \\ 0 & (1.414)^2 & 0 \\ 0 & 0 & (1.850)^2 \end{bmatrix} \{\xi\} = 0 \qquad (42)$$

Which is of the form:

$$\ddot{\xi}_j + 2\zeta\omega_j\dot{\xi}_j + \omega_j^2\xi_j = 0 \quad j = 1, 2, 3 \qquad (43)$$

It is interesting to note that the system of equation (35) has a constant percentage of critical damping in all three modes, a situation which is similar to a system with linear hysteresis damping.

Acknowledgment

The author wishes to thank Dr. J. K. Knowles for his interest in this problem and for his helpful suggestions.

The Vibration Response of a Linear Undamped System Resting on a Nonlinear Spring

P. R. PASLAY[1]
M. E. GURTIN[2]
General Engineering Laboratory
General Electric Company,
Schenectady, N. Y.
Assoc. Mems. ASME

The steady-state, undamped-displacement-amplitude response of a linear system on a single nonlinear spring due to a force excitation which varies sinusoidally with time is investigated. The force-displacement relation of the spring is

$$F = k(x + \epsilon x^3) \tag{1}$$

The Fourier component of the displacement-amplitude response of the system at the forcing frequency and its third harmonic are considered.

Analysis

THE steady-state displacement response of a linear undamped system to a force system whose components vary sinusoidally with time is expressible in the form

$$x_i = \sum_j M_{ij}(\omega_j) F_j \sin(\omega_j t + \beta_j) \tag{2}$$

where

x_i = displacement at i
$M_{ij}(\omega_j)$ = displacement mobility (i.e., displacement amplitude at i due to a force of unit amplitude at j varying sinusoidally with time at frequency ω_j)
F_j = amplitude of external sinusoidally varying force at j
β_j = phase angle in time of force at j
t = time

If a nonlinear spring, having the characteristics prescribed by (1) is connected between ground, i.e., a fixed point in space, and a point on the system, Fig. 1, the force resulting at the point of connection to the system will contain odd multiples of the frequency of the external force. For the system shown in Fig. 1 the displacement response at point 2 due to a single external force acting at point 1 becomes[3]

$$x_2 = F_1 M_{21}(\omega) \sin \omega t + \sum_{\substack{n=1 \\ \text{odd}}}^{\infty} M_{20}(n\omega) F_{0_n} \sin n\omega t \tag{3}$$

and the displacement response at point 0 becomes

$$x_0 = F_1 M_{01}(\omega) \sin \omega t + \sum_{\substack{n=1 \\ \text{odd}}}^{\infty} M_{00}(n\omega) F_{0_n} \sin n\omega t \tag{4}$$

Since

$$x_0 = \sum_{\substack{n=1 \\ \text{odd}}}^{\infty} x_{0_n} \sin n\omega t \tag{5}$$

the force across the spring becomes

$$-F_0 = -\sum_{\substack{n=1 \\ \text{odd}}}^{\infty} F_{0_n} \sin n\omega t = k \left\{ \sum_{\substack{n=1 \\ \text{odd}}}^{\infty} x_{0_n} \sin n\omega t + \epsilon \left(\sum_{\substack{n=1 \\ \text{odd}}}^{\infty} x_{0_n} \sin n\omega t \right)^3 \right\} \tag{6}$$

If only the first two terms of the summation in (5) and consequently the first two terms of the summations in (4) and (6) are retained, the following procedure determines the solution corresponding to this approximation:

1 The cubed term in (6) is expanded in its Fourier series and only the sin ωt and sin $3\omega t$ terms are retained.

2 The coefficients of sin ωt and sin $3\omega t$ in (6) are required to vanish separately thereby yielding two equations for F_{0_1} and F_{0_3} explicitly in terms of x_{0_1} and x_{0_3}.

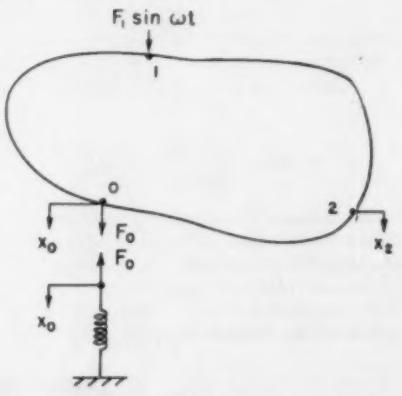

Fig. 1 Combination of a linear undamped system and a nonlinear spring
Point 0 is point of attachment of nonlinear spring
Point 1 is point at which external force acts
Point 2 is point at which displacement response is to be determined
Spring force-deflection characteristic
$-F_0 = k(x_0 + \epsilon x_0^3)$

---

[1] Currently at Rice Institute, Houston, Texas.
[2] Currently at Brown University, Providence, R. I.
[3] The following notation system is used in the analysis: A subscript denotes a physical point on the system. A sub-subscript denotes a Fourier component.

For presentation at the Summer Conference of the Applied Mechanics Division, University Park, Pa., June 20–22, 1960, of THE AMERICAN SOCIETY OF MECHANICAL ENGINEERS.
Discussion of this paper should be addressed to the Secretary, ASME, 29 West 39th Street, New York, N. Y., and will be accepted until July 22, 1960, for publication at a later date. Discussion received after the closing will be returned.
NOTE: Statements and opinions advanced in papers are to be understood as individual expressions of their authors and not those of the Society. Manuscript received by ASME Applied Mechanics Division, April 23, 1959. Paper No. 60-APM-6.

3 The equations resulting from step (2) and (5) are substituted into (4) to eliminate F_{0_1} and F_{0_3}. Finally, the coefficients of sin ωt and sin $3\omega t$ are equated separately to zero to yield

$$x_{0_1} = F_1 M_{11}(\omega) - M_{11}(\omega)\{kx_{0_1} + \epsilon k(\tfrac{3}{4}x_{0_1}^3 - \tfrac{3}{4}x_{0_1}^2 x_{0_3} + \tfrac{3}{2}x_{0_1}x_{0_3}^2)\} \quad (7)$$

$$x_{0_3} = -M_{33}(3\omega)\{kx_{0_3} + \epsilon k(-\tfrac{1}{4}x_{0_1}^3 + \tfrac{3}{2}x_{0_1}^2 x_{0_3} + \tfrac{3}{4}x_{0_3}^3)\} \quad (8)$$

If the solution is restricted to cases where x_{0_3} is small in comparison to x_{0_1} there results

$$x_{0_1} = F_1 M_{11}(\omega) - M_{11}(\omega)k\{x_{0_1} + \tfrac{3}{4}\epsilon x_{0_1}^3\} \quad (9)$$

$$x_{0_3} = -kM_{33}(3\omega)\left\{x_{0_3} - \frac{\epsilon}{4}x_{0_1}^3\right\} \quad (10)$$

Clearly, for the free-vibration solution F_1 should be set to zero and the equations for the free-vibration amplitude-frequency dependence become

$$x_{0_1} = \mathrm{Re}\left[\left\{\frac{4}{3\epsilon}\left(1 + \frac{1}{kM_{33}(\omega)}\right)\right\}^{1/2}\right] \quad (11)$$

$$x_{0_3} = \frac{\epsilon x_{0_1}^3}{4\left[1 + \dfrac{1}{kM_{33}(3\omega)}\right]} \quad (12)$$

Sample Calculation

To illustrate the results of the analysis, consider a uniform free-free beam attached to a nonlinear spring at its mid-point and driven laterally by a force varying sinusoidally with time at its mid-point. In the calculations presented here the first four symmetric modes are used to represent the beam. For this case[4]

$$kM_{33}(\omega) = -\frac{1}{\alpha^2\left(\dfrac{\omega}{\omega^1}\right)^2} + \sum_{r=1}^{3}\frac{(\varphi_0^r)^2}{\alpha^2(c^r)^2\left[1 - \left(\dfrac{\omega}{\omega^1}\right)^2\dfrac{1}{(c^r)^2}\right]} \quad (13)$$

where superscripts refer to mode numbers of the linear system and

ω^r = rth natural frequency of linear system
φ_0^r = amplitude of rth normal mode at beam center
m = mass of beam
$c^r = \dfrac{\omega^r}{\omega^1}$
$\alpha^2 = \dfrac{(\omega^1)^2}{k/m}$

For the first three nonrigid-body symmetric modes, Table 1[4] gives the values of the constants.

Table 1 Values of constants

r	$(c^r)^2$	φ_0^r
1	1.0	1.2157
2	29.20	1.4224
3	178.07	1.4139

Calculations were performed for $F_1/k = 1$ in. and $F_1/k = 10$ in. for cases where $\epsilon = 0.05$ in.$^{-2}$ and $\epsilon = 0.1$ in.$^{-2}$ and $\alpha^2 = 10$.

[4] T. von Karman and M. A. Biot, "Mathematical Methods in Engineering," McGraw-Hill Book Company, Inc., New York, N. Y., 1940.

[5] D. Young and R. P. Felgar, "Tables of Characteristic Functions Representing Normal Modes of Vibration of a Beam," University of Texas Publication, No. 4913, 1949.

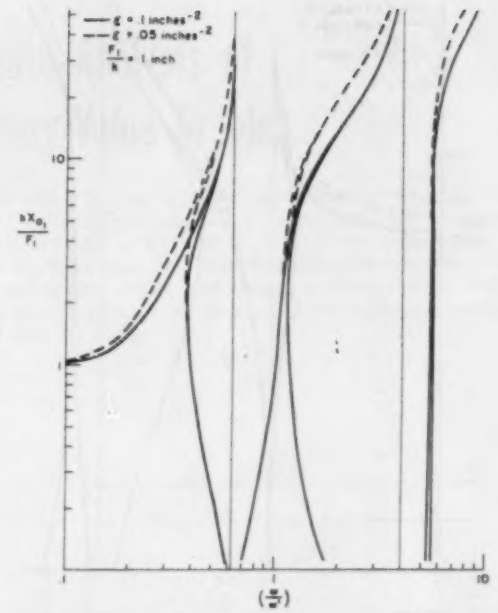

Fig. 2 Absolute value of dimensionless first-harmonic response (kx_{0_1}/F_1) as a function of ratio of exciting frequency to first free-free beam frequency (ω/ω^1) for cases where dimensionless spring characteristic $[\alpha^2 = (\omega^1)^2/(k/m)]$ is 10, characteristic force (F_1/k) is 1 in., with nonlinearity factor (ϵ) as parameter

Discussion

Figs. 2 through 4 show the results of the sample calculations. It is evident from the first-harmonic response shown in Figs. 2 and 3 that for $\epsilon > 0$ the displacement amplitude begins to increase in a manner similar to the case associated with the linear system resting on a linear spring with spring constant k, and approaches asymptotically the natural frequency corresponding to the linear system supported by an infinitely rigid spring. The behavior for $\epsilon < 0$ approaches asymptotically the corresponding resonance of a free-free beam.

Fig. 4 shows the third-harmonic solution for the case of $F_1/k = 10$ in. and $\epsilon = 0.1$ in.$^{-2}$. The corresponding curves for $F_1/k = 1$ in. are not shown since all of the salient points can be demonstrated with Fig. 4. Clearly, when $F_1/k = 1$ in., the fraction of third harmonic appearing in the solution is smaller than the case shown here.

The frequencies at which peaks 1 and 2 occur are one third the values of the first two natural frequencies associated with the linear system resting on a linear spring with spring constant k. This behavior results from excitation from the third harmonic of the force in the nonlinear spring.

When the displacement amplitude of the first harmonic approaches asymptotically the natural frequency corresponding to the linear system supported by a rigid center support, the third harmonic of the force in the nonlinear spring approaches infinity which leads to infinite third-harmonic amplitude. This phenomenon accounts for peak 3. Peaks 4 and 5 both occur at a frequency equal to one third of the third natural frequency associated with the linear system resting on a linear spring with spring constant k. It may be seen from Fig. 3 that the force excitation for peaks 4 and 5 is triple-valued thus leading to three response curves for the third harmonic, the lowest response being too small to appear in Fig. 4.

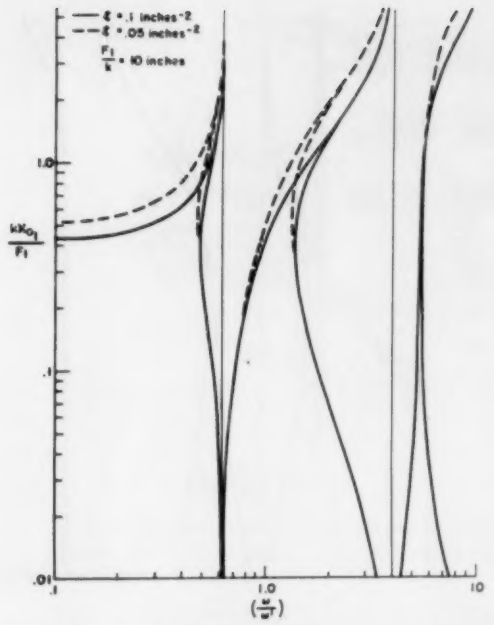

Fig. 3 Absolute value of dimensionless first-harmonic response (kx_{0_1}/F_1) as a function of ratio of exciting frequency to first free-free beam frequency (ω/ω^1) for cases where dimensionless spring characteristic $[\alpha^2 = (\omega^1)^2/(k/m)]$ is 10, characteristic force (F_1/k) is 10 in., with nonlinearity factor (ϵ) as a parameter

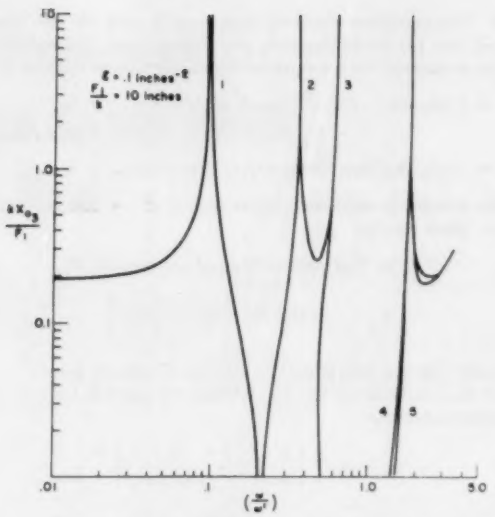

Fig. 4 Absolute value of dimensionless third-harmonic response (kx_{0_3}/F_1) as a function of ratio of exciting frequency to first free-free beam frequency (ω/ω^1) for case where dimensionless spring characteristic $[\alpha^2 = (\omega^1)^2/(k/m)]$ is 10, characteristic force (F_1/k) is 1 in., with a nonlinearity factor (ϵ) equal to 0.1 in.$^{-2}$

The reader should note the two different types of third-harmonic "resonances":

1 A linear system resonance excited by a finite third harmonic of the force in the spring (peaks 1, 2, 4, and 5).

2 The response due to an infinite third-harmonic force in the spring due to an infinite first-harmonic force in the spring (peak 3).

Among other restrictions on the solution, the third-harmonic response must be much less than the first-harmonic response at a given frequency. Cases where this restriction is not satisfied can be found by comparing Figs. 3 and 4. Peaks in Fig. 4 associated with the first case mentioned violate this restriction. This leads to regions in the neighborhood of peaks 1, 2, 4, and 5 where the solution is not valid.

H. D. CONWAY[1]
Julius F. Stone Visiting Professor,
Department of Engineering Mechanics,
The Ohio State University,
Columbus, Ohio

The Approximate Analysis of Certain Boundary-Value Problems

A simple method is given which is suitable for the approximate analysis of certain boundary-value problems, including, for example, the small deflections of clamped plates and the torsion of prismatic bars. The analysis is particularly simple and lends itself well to the use of the digital computer. The method is applied here to four problems, the uniformly loaded, clamped square, and equilateral-triangle plates, and the torsion of bars of square and hexagonal cross section. The results agree well with the exact solutions, where these are known.

When analyzing certain boundary-value problems, such as the bending of plates with clamped edges and the torsion of prismatic bars, to obtain an exact solution is the exception rather than the rule. In cases where the exact solution is unknown, and particularly if the boundary in the problem is a regular polygon, the following method yields good results with a small amount of arithmetic.

Although it is illustrated here by problems of clamped plates and the torsion of prismatic bars, it has much wider application and, for example, has been applied successfully to the torsion of shafts of circular cross sections but varying diameter, certain fluid-flow problems, buckling and vibration of plates, and so on.

Analysis

The method will first be illustrated in relation to small deflection-plate problems. When treating problems in the bending of circular plates involving the differential equation

$$\nabla^4\omega = q/D \tag{1}$$

it is naturally convenient to use the well-known solution in polar co-ordinates

$$\omega = R_0 + \sum_{m=1}^{\infty} R_m \cos m\theta + \sum_{m=1}^{\infty} R_m' \sin m\theta + \omega_0 \tag{2}$$

where ω_0 is a particular solution for the loading and

$$\begin{aligned} m = 0,\ & R_0 = A_0 + B_0 r^2 + C_0 \log r + D_0 r^2 \log r \\ m = 1,\ & R_1 = A_1 r + B_1 r^3 + C_1 r^{-1} + D_1 r \log r \\ m > 1,\ & R_m = A_m r^m + B_m r^{-m} + C_m r^{m+2} + D_m r^{-m+2} \end{aligned} \tag{3}$$

It will now be shown that it is convenient to use this equation for the solution of plates with other boundaries. For a first example, the problem of the uniformly loaded, clamped square plate is chosen, because this has been the subject of a large number of investigations and because it is very convenient for illustrative purposes.

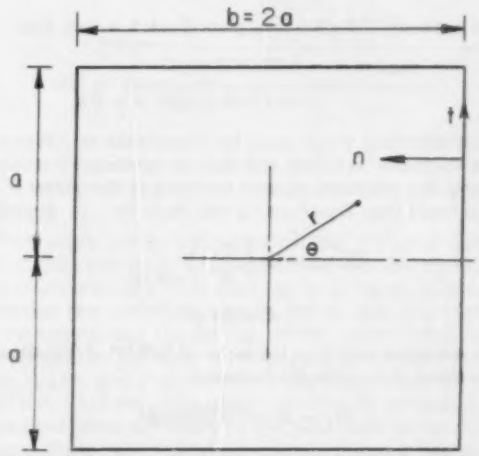

Fig. 1 Co-ordinate system for square

Fig. 1 shows the plate of side $2a$ and the co-ordinate system. Having due regard for the symmetry of the problem, Equation (2) is used, with appropriate terms omitted for a solid plate, to write with a slight change of notation

$$\omega = \frac{qr^4}{64D} + A + Br^2 + (Cr^4 + Dr^6)\cos 4\theta + (Er^8 + Fr^{10})\cos 8\theta + \dots \tag{4}$$

All terms higher than the foregoing will be omitted, and the problem is then to find A, B, C, D, E, and F. This is done by assuming conditions of zero deflection and radial slope at the centers, quarter points, and ends of the sides; namely,

$$\begin{aligned} \omega = \frac{\partial\omega}{\partial r} = 0 \quad & \text{at} \quad r = a,\ \theta = 0 \\ & r = \sqrt{5}\,a/2,\ \tan\theta = 1/2 \\ & r = \sqrt{2}\,a,\ \theta = \pi/4 \end{aligned} \tag{5}$$

Before proceeding, it is desirable to examine the possible accuracy of the foregoing solution. At the centers of the sides, the deflection and the radial slope will be zero, as will also be the tangential slope. At the corners, the deflection will be zero, as will

[1] On leave from Department of Mechanics, Cornell University, Ithaca, N. Y.

Contributed by the Applied Mechanics Division and presented at the Annual Meeting, Atlantic City, N. J., November 29–December 4, 1959, of The American Society of Mechanical Engineers.

Discussion of this paper should be addressed to the Secretary, ASME, 29 West 39th Street, New York, N. Y., and will be accepted until July 10, 1960, for publication at a later date. Discussion received after the closing date will be returned.

Note: Statements and opinions advanced in papers are to be understood as individual expressions of their authors and not those of the Society. Manuscript received by ASME Applied Mechanics Division, December 9, 1958. Paper No. 59—A-80.

also be the slope in the directions of the sides. At the quarter points, the deflection is zero but the normal and tangential slopes will not be zero. However, it is apparent that they will not differ much from zero, and we can at least expect a reasonably accurate solution. If this is not sufficiently accurate, more terms can be taken in Equation (4). It might be thought desirable to make $\partial\omega/\partial n$ zero at the quarter points rather than $\partial\omega/\partial r$, and the effect of this on the present results has been investigated. It was found to be negligible. Both could have been made zero by the addition of another term.

Solving the six equations derived from the foregoing boundary conditions, it is found that

$$A = 1.295846P;\ B = -2.256170\ P/a^2;\quad C = -0.360325P/a^4$$
$$D = 0.307846\ P/a^6;\ E = 0.010735\ P/a^8;\quad F = 0.002069P/a^{10} \tag{6}$$

where $P = qa^4/64D$

The maximum deflection for a plate of side $b = 2a$ is then

$$\omega_{max} = A = 0.0012655\ qb^4/D = 0.013819\ qb^4/Eh^3,\ \nu = 0.3 \tag{7}$$

The corresponding factor given by Timoshenko in "Theory of Plates and Shells" is 0.0138, and thus the agreement is excellent. Similarly, the maximum moment occurring at the centers of the sides is found from Equations (4) and (6) to be

$$M_{x\,max} = D\left(\frac{\partial^2\omega}{\partial r^2}\right)_{r=b/2,\ \theta=0} = 0.05151\ qb^2 \tag{8}$$

which compares well with the factor of 0.0513[1] of Timoshenko. At the center of the plate, the moment is

$$M_x = M_y = 0.02291\ qb^2 \tag{9}$$

Timoshenko does not compute this value, but again the result agrees excellently with the value $0.023qb^2$ found by Hencky.[2]

Before leaving this problem, a partial check on the accuracy of the solution may be found by computing the normal ($\partial\omega/\partial n$) and tangential ($\partial\omega/\partial t$) slopes at the quarter points. These are easily obtained by resolution from the value of $\partial\omega/\partial\theta$; $\partial\omega/\partial r$ is, of course, zero at these points. It is found that these slopes are

$$\frac{\partial\omega}{\partial n} = 0.000005486\ qb^3/D$$
$$\frac{\partial\omega}{\partial t} = 0.000010972\ qb^3/D \tag{10}$$

While these are not necessarily the maximum values, they are close to them and are certainly very small.

In view of the success of the method with the square plate, the next example chosen was the uniformly loaded, equilateral-triangle plate shown in Fig. 2. Again having regard for symmetry, the deflection is here written as

$$\omega = \frac{qr^4}{64D} + A + Br^2 + (Cr^3 + Dr^6)\cos 3\theta + (Er^9 + Fr^{12})\cos 6\theta \tag{11}$$

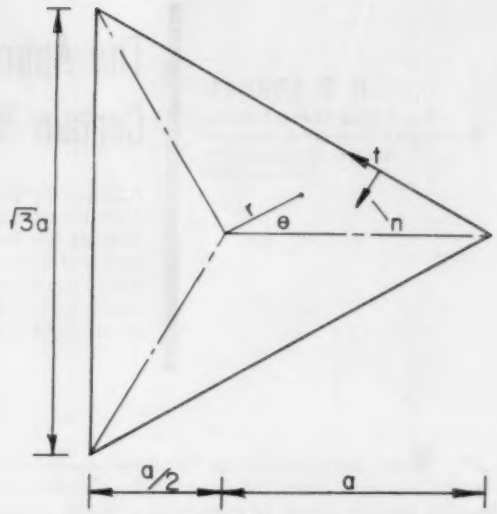

Fig. 2 Co-ordinate system for equilateral triangle

higher terms again being neglected. The boundary conditions chosen are again that the deflection and radial slope shall be zero at the center, quarter points, and corners. The boundary conditions at the corners and centers of the sides are then satisfied exactly.

Solving the six equations resulting from the foregoing boundary conditions,

$$A = 0.095918P;\ B = -0.601443\ P/a^2;\quad C = 0.351443\ P/a^3$$
$$D = -1.066912\ P/a^4;\ E = 0.142419\ P/a^5;\quad F = 0.078576\ P/a^6 \tag{12}$$

where $P = qa^4/64D$.

The maximum deflection is then

$$\omega_{max} = A = 0.0014987\ qa^4/D = 0.016366\ qa^4/Eh^3,\ \nu = 0.3 \tag{13}$$

and the moment at the center of the sides is

$$M = D\left(\frac{\partial^2\omega}{\partial r^2}\right)_{r=a/2,\ \theta=\pi/3} = 0.058529\ qa^2 \tag{14}$$

These results are apparently new. Finally, as a partial check on the accuracy of the results, the values of the normal ($\partial\omega/\partial n$) and tangential ($\partial\omega/\partial t$) slopes are calculated at the quarter points. These are found to be

$$\frac{\partial\omega}{\partial n} = 0.00006308\ qa^3/D$$
$$\frac{\partial\omega}{\partial t} = 0.00005463\ qa^3/D \tag{15}$$

and are again seen to be negligibly small.

The method will now be applied to torsion problems, these being somewhat less laborious than plate problems because there is only one boundary condition for each point on the boundary instead of two. The section chosen for test is the square rather than the equilateral triangle since the exact torsion function for the latter problem is expressible in polar co-ordinates, Fig. 2, as

[1] The factor using a 10 × 10 solution in the present method was 0.051336.

[2] H. Hencky, "Der Spannungszustand in rechteckigen Platten," Munich, Germany, 1913.

$$\phi = \frac{G\alpha}{6a}(a^3 - 3ar^2 + 2r^3\cos 3\theta) \tag{16}$$

For the square shaft shown in Fig. 1, the torsion function satisfying $\nabla^2\phi = -2G\alpha$ is taken as

$$\phi = A + Br^4\cos 4\theta + Cr^8\cos 8\theta + \ldots - \frac{G\alpha r^2}{2} \tag{17}$$

Ignoring terms other than the foregoing and solving the three equations necessary to make ϕ zero at the centers, quarter points, and corners,

$$A = 0.589825\ G\alpha a^2;\ B = -0.092369\ G\alpha/a^4;$$
$$C = 0.0025437\ G\alpha/a^8 \tag{18}$$

The maximum stress occurs at the centers of the sides and is given by

$$\tau_{max} = \left(\frac{\partial\phi}{\partial r}\right)_{r=a,\,\theta=0} = -0.67456G\alpha(2a) \tag{19}$$

in excellent agreement with the value of $-0.675G\alpha(2a)$ quoted in Timoshenko and Goodier, "Theory of Elasticity." This degree of accuracy is perhaps not really surprising, since the stress is at a point on the boundary where ϕ is made zero and where $\partial\phi/\partial t$ is also zero from symmetry.

The torque T is given by the integral

$$T = 2\int\int \phi r d\theta dr \tag{20}$$

taken over the cross section, and fortunately the integration presents no difficulty. The torque is

$$T = 0.14084\ G\alpha(2a)^4 \tag{21}$$

the factor in which is about 0.2 per cent greater than the true factor of 0.1406.

The last example is that of the torsion of the regular hexagon shown in Fig. 3. The torsion function is here written as

$$\phi = A + Br^6\cos 6\theta + Cr^{12}\cos 12\theta + \ldots - \frac{G\alpha r^2}{2} \tag{22}$$

Ignoring other terms and finding A, B, C for the centers, quarter points, and corners

$$A = 0.540858\ G\alpha a^2;\ B = -0.044483\ G\alpha/a^4;$$
$$C = 0.003625\ G\alpha/a^{10} \tag{23}$$

The maximum shear stress is then

$$\tau_{max} = \left(\frac{\partial\phi}{\partial r}\right)_{r=a,\,\theta=0} = -1.22340\ G\alpha a \tag{24}$$

This result is apparently new and, remembering the stress value obtained for the square, is probably quite accurate.[4] The torque found in the usual way from Equation (20) is then given by

$$T = -1.04080\ G\alpha H^4 \tag{25}$$

where $H = 2a/\sqrt{3}$ is the side of the hexagon. This factor differs less than 0.5 per cent from the more accurate factor of -1.0359, given by Pólya and Szegö.[5]

[4] The factor is -1.22581 according to C. Weber, "Die Lehre von der Drehungsfestigkeit," Berlin, 1921. See also, S. Timoshenko, "Strength of Materials," part 2, D. Van Nostrand Company, New York, N. Y., 1941, p. 266.

[5] G. Pólya and G. Szegö, "Isoperimetric Inequalities in Mathematical Physics," Annals of Mathematical Studies, Princeton University Press, Princeton, N. J., 1951.

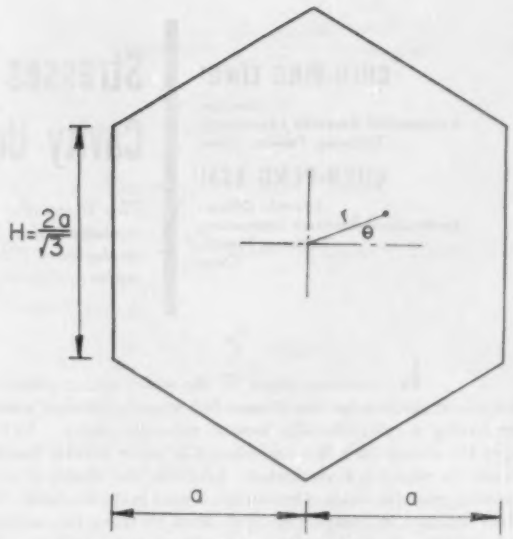

Fig. 3 Co-ordinate system for regular hexagon

Summary

The method is very convenient to use, and gives accurate results, with little labor, for clamped-plate and torsion problems, particularly when the latter have regular polygonal boundaries. It appears that plate-boundary conditions other than clamped can be treated, and the method applied to other boundaries. It is natural that the labor increases when advantage cannot be taken of symmetry, but the use of the digital computer minimizes this. The use of the latter is particularly convenient, and it can incorporate the finding of the polar radii for the various values of the co-ordinate angle given the boundary or boundaries.

The method is not confined to the two problems cited, but can be extended to many others. It has, for example, been applied successfully to the finding of the torsional rigidity of circular cross-section rods of periodically varying diameter. In this case, the torsion function is a series of products of trigonometrical and modified Bessel functions but, other than this, the method is the same. Other examples of its use consist of fluid-flow problems, buckling and vibration of plates, plane-stress and strain[6] problems, and so on. Some of these will be given in later papers.

NOTE ADDED IN PROOF: The author's attention has been drawn to the following investigation along the same lines (J. Barta, "Über die näherungsweise Lösung einiger Zweidimensionaler Elastizitätsaufgaben," *ZAMM*, vol. 17, 1937, p. 184). However, the idea of meeting conditions at discrete points as a rather general method for solving certain boundary-value problems does not seem to have been appreciated there. The wider viewpoint together with the advent in recent years of the electronic digital computer makes the method very attractive.

[6] H. T. Johnson, "Stress Distribution in a Uniformly Rotating Equilateral Triangle Shaft," JOURNAL OF APPLIED MECHANICS, vol. 22, TRANS. ASME, vol. 77, 1955, p. 255.

CHIH-BING LING[1]
Director,
Aeronautical Research Laboratory,
Taichung, Taiwan, China

CHEN-PENG TSAI
Scientific Officer,
Aeronautical Research Laboratory,
Taichung, Taiwan,
China

Stresses in a Slab Having a Spherical Cavity Under Circular Bending

This is one of a series of investigations on the effect of a spherical cavity in a solid of revolution when the solid is acted on by a given stress system symmetrical to the axis of revolution. Three problems of this nature have been investigated previously by the senior author in a succession of papers [1, 2, 3].[2]

In a previous paper [3] the senior author presented an analytic solution for the stresses in a stretched slab of infinite size having a symmetrically located spherical cavity. In this paper the stresses in a like slab when it is under circular bending around its edge are investigated. Likewise, the theory of symmetrical strain for solids of revolution is used in the analysis. The stress function in question is constructed by using two series of periodic biharmonic functions and a biharmonic integral. The series of biharmonic functions have been defined in the previous paper. However, unlike the previous solution for a stretched slab, here the stress function is necessarily even with respect to the mid-plane of the slab by symmetry.

The solution is illustrated by numerical examples for two radii of the cavity. In particular, the maximum stresses in the slab are computed to show the effect of the cavity on the stresses in the slab.

Method of Solution

Consider an infinite slab of thickness $2a$ having a spherical cavity of radius λa located symmetrically between the surfaces of the slab. Denote as usual the cylindrical and spherical coordinates by (r, θ, z) and (ρ, ϕ, θ), respectively,

where

$$z = \rho \cos \phi, \qquad r = \rho \sin \phi \tag{1}$$

Let the origin be situated at the center of the cavity and the z-axis normal to the surfaces of the slab. For convenience, the coordinates z, r and ρ are taken as dimensionless quantities referring to the length a or one half of the thickness of the slab.

Suppose that the required stress function χ is composed of two parts as follows:

$$\chi = \chi_0 + \chi_1 \tag{2}$$

The basic stress function χ_0 gives the stresses in the slab in the absence of the cavity. When the slab is acted on by a circular bending moment of $-M$ per unit length around the edge, it takes the form

$$\chi_0 = \frac{Ma}{64(1+\nu)} \{8(2-\nu)z^4 - 24(1-\nu)r^2z^2 - 3\nu r^4\} \tag{3}$$

where ν is Poisson's ratio. The auxiliary stress function χ_1 is here constructed by using the following functions even in z:

$$\chi_1 = Ma \sum_{s=0}^{\infty} (A_{2s}U_{2s+1} + B_{2s}V_{2s+1}) + Ma \int_0^{\infty} \{\psi_1(k) \cosh kz + \psi_2(k) z \sinh kz\} J_0(kr)dk \tag{4}$$

where A_{2s} and B_{2s} are coefficients of superposition and ψ_n are arbitrary functions. J_n is Bessel function of the first kind of order n. U_s and V_s are periodic biharmonic functions defined as follows. For $s \geqslant 1$,

$$U_s = \frac{(-1)^s}{(s-1)!} \frac{\partial^s U_0}{\partial z^s}, \qquad V_s = (-1)^s \frac{2s+1}{(s+1)!} \frac{\partial^s V_0}{\partial z^s} \tag{5}$$

where

$$U_0 = -\frac{1}{2} \log \left\{ \frac{1+\mu}{1-\mu} \prod_{p=1}^{\infty} \frac{(1+\mu_p)(1+\mu_{-p})}{(1-\mu_p)(1-\mu_{-p})} \exp\left(-\frac{2z}{p}\right) \right\} \tag{6}$$

$$V_0 = \mu + \sum_{p=1}^{\infty} (\mu_p + \mu_{-p})$$

in which

$$\mu = \cos \phi = \frac{z}{\rho}, \qquad \mu_p = \frac{z - 2p}{(\rho^2 - 4p\rho\mu + 4p^2)^{1/2}} \tag{7}$$

The reader may consult the senior author's previous paper [3] for the properties of these functions.

The foregoing auxiliary stress function gives the following normal and tangential stresses on the surfaces $z = \pm 1$:

$$\sigma_z = \frac{1}{a^2}\left[\frac{\partial}{\partial z}\left\{(2-\nu)\nabla^2 - \frac{\partial^2}{\partial z^2}\right\}\chi_1\right]_{z=\pm 1} = \mp \frac{M}{a^2} \int_0^{\infty} k^3 [\psi_1(k)k \sinh k + \psi_2(k) \{k \cosh k - (1-2\nu) \sinh k\}] J_0(kr)dk \tag{8}$$

$$\tau_{rz} = \frac{1}{a^2}\left[\frac{\partial}{\partial r}\left\{(1-\nu)\nabla^2 - \frac{\partial^2}{\partial z^2}\right\}\chi_1\right]_{z=\pm 1} = -\frac{M}{a^2} \sum_{s=0}^{\infty} \Big[\{(2s+1)(2s+2)A_{2s}$$

[1] Concurrently, Acting Director, Institute of Mathematics, Academia Sinica, Taipei, Taiwan, China.

[2] Numbers in brackets designate References at end of paper.

Contributed by the Applied Mechanics Division and presented at the Annual Meeting, Atlantic City, N. J., November 29–December 4, 1959, of The American Society of Mechanical Engineers.

Discussion of this paper should be addressed to the Secretary, ASME, 29 West 39th Street, New York, N. Y., and will be accepted until July 10, 1960, for publication at a later date. Discussion received after the closing date will be returned.

Note: Statements and opinions advanced in papers are to be understood as individual expressions of their authors and not those of the Society. Manuscript received by ASME Applied Mechanics Division, April 8, 1959. Paper No. 59—A-64.

$$+ 2(1-\nu)(4s+3)B_{2s}\Big\}\frac{\partial U_{2s+2}}{\partial r}$$
$$+\frac{(2s+3)(2s+4)(4s+3)B_{2s}}{4s+7}\frac{\partial V_{2s+2}}{\partial r}\Big]_{z=\pm 1}$$
$$+\frac{M}{a^2}\int_0^\infty k^3\{\psi_1(k)k\cosh k+\psi_2(k)(k\sinh k + 2\nu\cosh k)\}J_1(kr)dk \quad (9)$$

where ∇^2 stands for the Laplace operator.

The former vanishes identically for any value of r provided that

$$\psi_1(k)k\sinh k+\psi_2(k)\{k\cosh k-(1-2\nu)\sinh k\}=0 \quad (10)$$

Again, the latter vanishes identically for any value of r provided that by Hankel transform of order unity the following relation is satisfied:

$$\psi_1(k)k\cosh k+\psi_2(k)(k\sinh k+2\nu\cosh k)$$
$$=\frac{1}{k}\sum_{s=0}^{\infty}\int_0^\infty\Big[\{(2s+1)(2s+2)A_{2s}$$
$$+2(1-\nu)(4s+3)B_{2s}\}\frac{\partial U_{2s+2}}{\partial r}$$
$$+\frac{(2s+3)(2s+4)(4s+3)}{4s+7}\frac{\partial V_{2s+2}}{\partial r}\Big]_{z=\pm 1}rJ_1(kr)dr \quad (11)$$

Now, by integrating by parts and then using the relations (28) in the previous paper [3], we find

$$\int_0^\infty\left[\frac{\partial U_{2s+2}}{\partial r}\right]_{z=\pm 1}rJ_1(kr)dr=-k\int_0^\infty[U_{2s+2}]_{z=\pm 1}rJ_0(kr)dr$$
$$=-\frac{k^{2s+2}}{(2s+2)!\sinh k},$$
$$\int_0^\infty\left[\frac{\partial V_{2s+2}}{\partial r}\right]_{z=\pm 1}rJ_1(kr)dr=-k\int_0^\infty[V_{2s+2}]_{z=\pm 1}rJ_0(kr)dr$$
$$=-\frac{(4s+7)k^{2s+2}}{(2s+4)!\sinh k}(k\coth k-2s-3) \quad (12)$$

Consequently, we have for zero traction on the surfaces,

$$\psi_1(k)=(1-2\nu-k\coth k)\psi_2(k)/k$$
$$\psi_2(k)=-\frac{2}{\sinh 2k-2k}\sum_{s=0}^{\infty}k^{2s+1}\times$$
$$\left\{\frac{A_{2s}}{(2s)!}+\frac{(4s+3)B_{2s}}{(2s+2)!}(k\coth k-2s-1-2\nu)\right\} \quad (13)$$

However, since A_{2s} and B_{2s} are independent of k, the integral in Equation (4) with the values of ψ_1 and ψ_2 given previously becomes divergent at the lower limit, for the integrand of the integral becomes of the order $0(k^{-3})$ as k tends to zero. Nevertheless, the divergence can be removed by subtracting some suitable terms of the same order from the integrand so that the resulting integrand vanishes as k tends to zero and the new integral is now convergent. Such a modification is permissible for it does not affect the stresses in the slab as well as the convergence at the upper limit.

To expand the stress function in spherical co-ordinates, the following relations are useful:

$$J_0(kr)\cosh kz=\sum_{n=0}^{\infty}\frac{(k\rho)^{2n}}{(2n)!}P_{2n}(\mu),$$
$$J_0(kr)\sinh kz=\sum_{n=0}^{\infty}\frac{(k\rho)^{2n+1}}{(2n+1)!}P_{2n+1}(\mu) \quad (14)$$
$$U_{2s+1}=\frac{P_{2s}(\mu)}{\rho^{2s+1}}+\sum_{n=0}^{\infty}{}^{2n}\alpha_{2s+1}\rho^{2n}P_{2n}(\mu),$$
$$V_{2s+1}=\frac{1}{\rho^{2s+1}}\{P_{2s+2}(\mu)-P_{2s}(\mu)\}$$
$$-\sum_{n=1}^{\infty}{}^{2n}\beta_{2s+1}\rho^{2n}\{P_{2n-2}(\mu)-P_{2n}(\mu)\} \quad (15)$$

and in particular,

$$U_1=\frac{1}{\rho}+\sum_{n=1}^{\infty}{}^{2n}\alpha_1\rho^{2n}P_{2n}(\mu)$$

where P_n is the Legendre function of the first kind of order n and

$${}^nG_s=\binom{n+s-1}{s-1}\frac{\omega_{n+s}}{2^{n+s-1}},$$
$${}^n\beta_s=\frac{2s+1}{2n-1}\binom{n+s-1}{s+1}\frac{\omega_{n+s}}{2^{n+s-1}} \quad (16)$$

in which

$$\omega_n=1+\frac{1}{2^n}+\frac{1}{3^n}+\frac{1}{4^n}+\ldots \quad (17)$$

The resulting expansion, apart from some trivial terms, is thus as follows:

$$\chi=\chi_0+\chi_1$$
$$=\frac{Ma\rho^4}{56(1+\nu)}\{6P_3(\mu)+(8-7\nu)P_1(\mu)\}+\frac{Ma(A_0-B_0)}{\rho}$$
$$+Ma\sum_{n=1}^{\infty}\Big\{\frac{A_{2n}-B_{2n}+B_{2n-2}\rho^2}{\rho^{2n+1}}$$
$$+(C_{2n}+D_{2n+2}\rho^2)\rho^{2n}\Big\}P_{2n}(\mu) \quad (18)$$

where, for $n\geqslant 2$,

$$C_{2n}=\sum_{s=0}^{\infty}({}^{2n}\alpha_{2s+1}A_{2s}+{}^{2n}\beta_{2s+1}B_{2s})$$
$$+\frac{1}{(2n-1)!}\int_0^\infty\left\{\frac{k\psi_1(k)}{2n}+\frac{2n\psi_2(k)}{4n-1}\right\}k^{2n-1}dk \quad (19)$$
$$D_{2n}=-\sum_{s=0}^{\infty}{}^{2n}\beta_{2s+1}B_{2s}+\frac{1}{(4n-1)(2n-2)!}\int_0^\infty\psi_2(k)k^{2n-1}dk$$

Note that here the coefficient C_2 is not defined. It is immaterial, for it is the coefficient of the trivial term $\rho^2P_2(\mu)$.

Consequently, the following normal and tangential stresses in spherical co-ordinates are derived:

$$\sigma_\rho=\frac{1}{a^3}\left\{(2-\nu)\mu\frac{\partial}{\partial\rho}+\frac{\nu(1-\mu^2)}{\rho}\frac{\partial}{\partial\mu}\right\}\nabla^2\chi$$
$$-\frac{1}{a^3}\frac{\partial^3}{\partial\rho^3}\left(\mu\frac{\partial}{\partial\rho}+\frac{1-\mu^2}{\rho}\frac{\partial}{\partial\mu}\right)\chi$$
$$=\frac{3M\rho}{5a^2}\{P_1(\mu)-P_3(\mu)\}+\frac{M}{a^2}\sum_{n=0}^{\infty}(2n+2)\times$$
$$\left\{\frac{(2n+1)(2n+3)(A_{2n}-B_{2n})}{\rho^{2n+4}}\right.$$

$$+\frac{4(2n+3)(3n-4n\nu+2-3\nu)B_{2n}}{(4n+5)\rho^{2n+4}}$$

$$-\frac{2(4n+7)(2n^2+n-1-\nu)D_{2n+4}\rho^{2n+1}}{4n+5}\Bigg\}P_{2n+1}(\mu)$$

$$+\frac{M}{a^3}\sum_{n=1}^{\infty}(2n+1)\Bigg\{\frac{2(4n-1)(2n^2+5n+2-\nu)B_{2n-2}}{(4n+1)\rho^{2n+2}}$$

$$-2n(2n+2)C_{2n+2}\rho^{2n-1}$$

$$+\frac{4n(6n-8n\nu+5-6\nu)D_{2n+2}\rho^{2n-1}}{4n+1}\Bigg\}P_{2n+1}(\mu) \quad (20)$$

$$\tau_{\rho\phi}=\frac{(1-\mu^2)^{1/2}}{a^3}\Bigg\{-(1-\nu)\left(\frac{\partial}{\partial\rho}+\frac{\mu}{\rho}\frac{\partial}{\partial\mu}\right)\nabla^2\chi$$

$$+\frac{\partial}{\partial\rho}\left(\frac{1}{\rho}\frac{\partial}{\partial\mu}\right)\left(\mu\frac{\partial}{\partial\rho}+\frac{1-\mu^2}{\rho}\frac{\partial}{\partial\mu}\right)\chi\Bigg\}$$

$$=\frac{M\rho(1-\mu^2)^{1/2}}{10a^3}\{3P_1'(\mu)+2P_3'(\mu)\}$$

$$+\frac{M(1-\mu^2)^{1/2}}{a^3}\sum_{n=0}^{\infty}\Bigg\{\frac{(2n+1)(2n+3)(A_{2n}-B_{2n})}{\rho^{2n+4}}$$

$$+\frac{4(2n+3)(3n-4n\nu+2-3\nu)B_{2n}}{(4n+5)\rho^{2n+4}}$$

$$+\frac{2(4n+7)(2n^2+4n+1+\nu)D_{2n+2}\rho^{2n+1}}{4n+5}\Bigg\}P'_{2n+1}(\mu)$$

$$+\frac{M(1-\mu^2)^{1/2}}{a^3}\sum_{n=1}^{\infty}\Bigg\{\frac{(4n-1)(4n^2+4n-1+2\nu)B_{2n-2}}{(4n+1)\rho^{2n+2}}$$

$$+2n(2n+2)C_{2n+2}\rho^{2n-1}$$

$$-\frac{4n(6n-8n\nu+5-6\nu)D_{2n+2}\rho^{2n-1}}{4n+1}\Bigg\}P'_{2n+1}(\mu) \quad (21)$$

These stresses vanish identically on the surface of the cavity provided that, when $\rho=\lambda$, the coefficient of each Legendre function or its derivative vanishes separately. A system of linear equations is thus obtained. The system of equations may be replaced by the following system:

$$A_{2n}'=-\frac{3}{10}\delta_{0,n}-\frac{15}{2(13-7\nu)}\delta_{1,n}$$

$$-2n(2n+1)(2n+3)(4n+1)C_{2n+2}'$$

$$-(4n+3)(4n^4+12n^3+11n^2+3n+1-\nu^2)D_{2n+4}' \quad (n\geqslant 0)$$

$$B_{2n-2}'=\frac{7}{10(13-7\nu)}\delta_{1,n}+2n(4n+3)C_{2n+2}'$$

$$+n(n+1)(4n+5)D_{2n+4}' \ (n\geqslant 1) \quad (22)$$

where $\delta_{m,n}=1$ or 0, according as $m=n$ or $m\neq n$, and

$$A_{2n}'=\frac{(2n+1)(2n+3)(A_{2n}-B_{2n})}{\lambda^{2n+5}}$$

$$+\frac{4(2n+3)(3n-4n\nu+2-3\nu)B_{2n}}{(4n+5)\lambda^{2n+5}}$$

$$B_{2n}'=\frac{(4n+3)B_{2n}}{(4n+5)\lambda^{2n+5}}$$

$$C_{2n+2}'=\frac{(n+1)\lambda^{2n-2}C_{2n+2}}{4n^2+6n-4n\nu+3-3\nu}$$

$$-\frac{(6n-8n\nu+5-6\nu)\lambda^{2n-2}D_{2n+2}}{(4n+1)(4n^2+6n-4n\nu+3-3\nu)}$$

$$D_{2n+4}'=\frac{2(4n+7)\lambda^{2n}D_{2n+4}}{(4n+5)(4n^2+6n-4n\nu+3-3\nu)} \quad (23)$$

By Equations (23), (19), and (13), C_{2n}' and D_{2n}' may be expressed in terms of A_{2n}' and B_{2n}' as follows: For $n\geqslant 2$,

$$C_{2n}'=\sum_{s=0}^{\infty}({}^{2n}\gamma_{2s}A_{2s}'+{}^{2n}\epsilon_{2s}B_{2s}')\lambda^{2n+2s+1}$$

$$D_{2n}'=\sum_{s=0}^{\infty}({}^{2n}\delta_{2s}A_{2s}'+{}^{2n}\sigma_{2s}B_{2s}')\lambda^{2n+2s+1} \quad (24)$$

where

$${}^{2n}\delta_{2s}=-\binom{2n+2s}{2s+1}\times$$

$$\frac{(2n-1)I_{2n+2s}^{*}}{(2s+3)(4n-3)(4n^2-10n-4n\nu+7+5\nu)2^{2n+2s-3}}$$

$${}^{2n}\gamma_{2s}=-\binom{2n+2s}{2s+1}\times$$

$$\frac{1}{(2s+3)(4n^2-2n-4n\nu+1+\nu)2^{2n+2s+1}}\times$$

$$\Bigg\{\frac{2(4n^2-4n-1+2\nu)}{4n-3}I_{2n+2s}^{*}-\omega_{2n+2s+1}$$

$$-(2n+2s+1)I_{2n+2s+1}^{*}\Bigg\}$$

$${}^{2n}\sigma_{2s}=\binom{2n+2s}{2s+2}\times$$

$$\frac{4s+5}{(4n-3)(4n^2-10n-4n\nu+7+5\nu)2^{2n+2s-1}}\times$$

$$\Bigg\{\frac{2(4s^2+12s+7+2\nu)}{4s+5}I_{2n+2s}^{*}-\omega_{2n+2s+1}$$

$$-(2n+2s+1)I_{2n+2s+1}^{*}\Bigg\}$$

$${}^{2n}\epsilon_{2s}=\binom{2n+2s}{2s+2}\frac{4s+5}{(2n-1)(4n^2-2n-4n\nu+1+\nu)2^{2n+2s}}$$

$$\times\Bigg\{\frac{(4s^2+12s+7+2\nu)(4n^2-4n-1+2\nu)}{(4s+5)(4n-3)}I_{2n+2s}^{*}$$

$$+\left(\frac{(s+1)(2s-1+4\nu)}{4s+5}+\frac{(2n-1)(n+1-2\nu)}{4n-3}\right)\omega_{2n+2s+1}$$

$$-\left(\frac{4s^2+12s+7+2\nu}{4s+5}+\frac{4n^2-4n-1+2\nu}{4n-3}\right)\times$$

$$\frac{2n+2s+1}{2}I_{2n+2s+1}^{*}+\frac{(2n+2s+1)(2n+2s+2)}{4}K_{2n+2s+2}^{*}\Bigg\} \quad (25)$$

The coefficient ω_n is defined by (17), while the remaining coefficients defined by

$$I_n^* = \frac{2^n}{n!}\int_0^\infty \frac{k^n dk}{\sinh 2k - 2k},$$

$$L_n^* = \frac{2^n}{n!}\int_0^\infty \frac{k^n \coth k\, dk}{\sinh 2k - 2k}, \tag{26}$$

$$K_n^* = \frac{2^n}{n!}\int_0^\infty \frac{k \coth^2 k\, dk}{\sinh 2k - 2k}$$

each of which tends asymptotically to unity as n tends to infinity.

To solve the system of linear equations in (22) by method of successive approximations, we write, for $n \geqslant 0$,

$$A_{2n}' = \sum_{p=0}^{\infty} A_{2n}'^{(p)} \qquad B_{2n}' = \sum_{p=0}^{\infty} B_{2n}'^{(p)} \tag{27}$$

where
$$A_{2n}'^{(0)} = -\frac{3}{10}\delta_{0,n} - \frac{15}{2(13-7\nu)}\delta_{1,n}$$
$$B_{2n}'^{(0)} = \frac{7}{10(13-7\nu)}\delta_{0,n} \tag{28}$$

and for $p \geqslant 1$,

$$A_{2n}'^{(p)} = -2n(2n+1)(2n+3)(4n+1)C_{2n+2}'^{(p-1)} - (4n+3) \times (4n^4 + 12n^3 + 11n^2 + 3n + 1 - \nu^2)D_{2n+4}'^{(p-1)}, \quad (n \geqslant 0)$$
$$B_{2n-2}'^{(p)} = 2n(4n+3)C_{2n+2}'^{(p-1)} + n(n+1)(4n+5)D_{2n+4}'^{(p-1)} \quad (n \geqslant 1) \tag{29}$$

in which $C_{2n}'^{(p-1)}$ and $D_{2n}'^{(p-1)}$ are computed from $A_{2n}'^{(p-1)}$ and $B_{2n}'^{(p-1)}$ by using Equations (24).

The foregoing method of successive approximations is valid as long as the series in (27) are both convergent. From physical considerations alone, it seems likely that there will be convergence if λ is less than unity. The range of convergence may be ascertained by using the method used by Howland [4] and Knight [5]. However, for the sake of brevity, no details will be given here.

Numerical Examples

Numerical examples will be given for the cases $\lambda = 1/4$ and $\lambda = 1/2$, respectively. Table 1 shows the values of the coefficients ω_{2n+1}, L_{2n+1}^*, I_{2n}^*, and K_{2n}^*. The first coefficient has been tabulated by Glaisher [6] and the subsequent two by Nelson and the senior author [7, 8]. The last one may be evaluated by splitting the integrand into the following and then integrating from zero to infinity:

$$\frac{k^n \coth^2 k}{\sinh 2k - 2k} = \frac{k^n}{\sinh 2k - 2k} + \frac{k^{n-1}\coth k}{\sinh 2k - 2k} - \frac{k^{n-1}}{2\sinh^2 k} \tag{30}$$

This leads to

$$K_n^* = I_n^* + \frac{2}{n}(L_{n-1}^* - \omega_{n-1}) \tag{31}$$

Table 2 shows the values of the coefficients in Equations (25) corresponding to $\nu = 1/4$. The coefficients A_{2n}', B_{2n}', C_{2n}', and D_{2n}' found by the method of successive approximations are shown in Table 3 for the cases $\lambda = 1/4$ and $\lambda = 1/2$. They are readily converted to A_{2n}, B_{2n}, C_{2n}, and D_{2n} by Equations (23).

It is easy to see that here the maximum stresses occur on the surfaces of the slab at the zenith points and also at the poles of the cavity. Now, at any point in the slab we have in general

$$\sigma_\rho + \sigma_\phi + \sigma_\theta = \sigma_r + \sigma_\theta + \sigma_z = \frac{1+\nu}{a^2}\frac{\partial}{\partial z}\nabla^2\chi \tag{32}$$

Since at the poles,

$$\sigma_\rho = 0, \qquad \sigma_\phi = \sigma_\theta, \qquad P_{2n+1}(\pm 1) = \pm 1 \tag{33}$$

we find

$$\max \sigma_\phi = \frac{1+\nu}{2a^2}\left[\frac{\partial}{\partial z}\nabla^2\chi\right]_{(\rho,z)=(\lambda,\pm 1)} = \pm\frac{M\lambda}{a^2}\left[\frac{3}{2} + (1+\nu)\sum_{n=0}^{\infty}(4n+3)\times \{(2n+3)B_{2n}\lambda^{-2n-4} + 2nD_{2n+2}\lambda^{2n-2}\}\right] \tag{34}$$

Again, since at the zeniths,

$$\sigma_\rho = 0, \qquad \sigma_r = \sigma_\theta, \qquad J_0(0) = 1, \tag{35}$$

we find

$$\max \sigma_r = \frac{1+\nu}{2a^2}\left[\frac{\partial}{\partial z}\nabla^2\chi\right]_{(r,z)=(0,\pm 1)} = \pm\frac{M}{a^2}\left\{\frac{3}{2} + (1+\nu)\int_0^\infty k^3\psi_3(k)\sinh k\, dk\right\} = \pm\frac{M}{a^2}\left[\frac{3}{2} - 2(1+\nu)\sum_{s=0}^{\infty}(2s+3)\times \{(2s+1)(2s+2)G_{2s+3}^* A_{2s} - (4s+3)(2s+1 + 2\nu)G_{2s+2}^* B_{2s} + (2s+4)(4s+3)H_{2s+4}^* B_{2s}\}\right] \tag{36}$$

where

$$G_n^* = \frac{1}{n!}\int_0^\infty \frac{k^n \sinh k\, dk}{\sinh 2k - 2k}$$
$$H_n^* = \frac{1}{n!}\int_0^\infty \frac{k^n \cosh k\, dk}{\sinh 2k - 2k} \tag{37}$$

the values of which have been tabulated by the senior author [8]. They are reproduced in Table 1.

The following numerical results are obtained:

	λ	0	1/4	1/2
At pole:	$M^{-1}a^2\lvert\max \sigma_\phi\rvert$	0,	0.667,	1.370
At zenith:	$M^{-1}a^2\lvert\max \sigma_r\rvert$	1.500,	1.496,	1.411

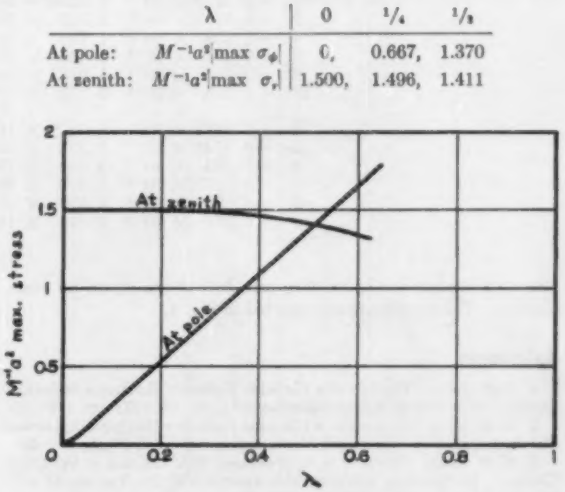

Fig. 1 Maximum stress versus radius of cavity

Table 1 The coefficients

n	ω_{2n+1}	L_{2n+1}^*	G_{2n+1}^*	I_{2n}^*	K_{2n}^*	H_{2n}^*
1	1.202057	...	1.105226	...	...	...
2	1.036928	1.240001	1.012123	1.353294	...	1.051213
3	1.008349	1.050822	1.001611	1.076730	1.144421	1.005564
4	1.002008	1.013199	1.000216	1.020538	1.031156	1.000703
5	1.000494	1.003615	1.000029	1.005785	1.008023	1.000091
6	1.000123	1.001003	1.000004	1.001645	1.002165	1.000012
7	1.000031	1.000278	1.000000	1.000466	1.000592	1.000001
8	1.000008	1.000077		1.000131	1.000162	1.000000
9	1.000002	1.000021		1.000036	1.000044	
10	1.000000	1.000006		1.000010	1.000012	
11		1.000002		1.000003	1.000004	
12		1.000000		1.000001	1.000001	
13				1.000000	1.000000	

Table 2 The coefficients, for $\nu = 1/4$

Coeff.	$2s$	$2n = 2$	$2n = 4$	$2n = 6$	$2n = 8$	$2n = 10$	$2n = 12$
${}^{2n}\gamma_{2s}$	0	...	1.1767×10^{-2}	1.5161×10^{-3}	2.6047×10^{-4}	4.9691×10^{-5}	1.0028×10^{-5}
	2	9.5447×10^{-3}	1.4261×10^{-3}	3.7101×10^{-3}	1.0322×10^{-3}	2.8925×10^{-4}	8.0626×10^{-5}
	4	2.8098×10^{-3}	9.8044×10^{-3}	4.2236×10^{-3}	1.7361×10^{-3}	6.7263×10^{-4}	2.4763×10^{-4}
	6	8.5967×10^{-3}	5.2216×10^{-3}	3.3395×10^{-3}	1.8998×10^{-3}	9.7227×10^{-4}	4.5682×10^{-4}
	8	2.5738×10^{-3}	2.3889×10^{-3}	2.1194×10^{-3}	1.5933×10^{-3}	1.0407×10^{-3}	6.0759×10^{-4}
	10	7.5194×10^{-4}	9.8763×10^{-4}	1.1595×10^{-3}	1.1129×10^{-3}	9.0337×10^{-4}	6.4149×10^{-4}
${}^{2n}\delta_{2s}$	0	...	-1.2029×10^{-1}	-6.6465×10^{-3}	-8.1050×10^{-4}	-1.3020×10^{-4}	-2.3762×10^{-5}
	2	-2.1653×10^{-1}	-7.1782×10^{-2}	-8.8195×10^{-3}	-1.7973×10^{-3}	-4.2790×10^{-4}	-1.0799×10^{-4}
	4	-4.6146×10^{-2}	-3.4018×10^{-2}	-6.9896×10^{-3}	-2.1095×10^{-3}	-6.9452×10^{-4}	-2.3133×10^{-4}
	6	-1.1339×10^{-2}	-1.3969×10^{-2}	-4.2508×10^{-3}	-1.7753×10^{-3}	-7.7143×10^{-4}	-3.2769×10^{-4}
	8	-2.8573×10^{-3}	-5.2169×10^{-3}	-2.1953×10^{-3}	-1.2101×10^{-3}	-6.7055×10^{-4}	-3.5375×10^{-4}
	10	-7.2234×10^{-4}	-1.8238×10^{-3}	-1.0129×10^{-3}	-7.1201×10^{-4}	-4.9001×10^{-4}	-3.1429×10^{-4}
${}^{2n}\epsilon_{2s}$	0	...	2.1575×10^{-1}	4.5580×10^{-2}	1.0568×10^{-2}	2.5324×10^{-3}	6.1569×10^{-4}
	2	5.7204×10^{-1}	3.4337×10^{-1}	1.4325×10^{-1}	5.4241×10^{-2}	1.9192×10^{-2}	6.4602×10^{-3}
	4	2.9908×10^{-1}	3.0348×10^{-1}	2.0676×10^{-1}	1.1564×10^{-1}	5.6618×10^{-2}	2.5186×10^{-2}
	6	1.2306×10^{-1}	1.9804×10^{-1}	1.9923×10^{-1}	1.5419×10^{-1}	9.9748×10^{-2}	5.6646×10^{-2}
	8	4.5257×10^{-2}	1.0725×10^{-1}	1.4938×10^{-1}	1.5278×10^{-1}	1.2618×10^{-1}	8.9060×10^{-2}
	10	1.5548×10^{-2}	5.1211×10^{-2}	9.4343×10^{-2}	1.2321×10^{-1}	1.2648×10^{-1}	1.0860×10^{-1}
${}^{2n}\sigma_{2s}$	0	...	-1.0590	-1.1884×10^{-1}	-2.1024×10^{-2}	-4.3802×10^{-3}	-9.7932×10^{-4}
	2	-1.5276×10^{-1}	-1.0279	-2.3291×10^{-1}	-6.8228×10^{-2}	-2.1104×10^{-2}	-6.5450×10^{-3}
	4	-1.6110×10^{-1}	-6.7315×10^{-1}	-2.4700×10^{-1}	-1.0690×10^{-1}	-4.5763×10^{-2}	-1.8755×10^{-2}
	6	-6.1175×10^{-2}	-3.4972×10^{-1}	-1.8849×10^{-1}	-1.1279×10^{-1}	-6.3780×10^{-2}	-3.3362×10^{-2}
	8	-1.9473×10^{-2}	-1.5722×10^{-1}	-1.1704×10^{-1}	-9.2495×10^{-2}	-6.6751×10^{-2}	-4.3387×10^{-2}
	10	-5.7727×10^{-3}	-6.4132×10^{-2}	-6.3079×10^{-2}	-6.3632×10^{-2}	-5.7065×10^{-2}	-4.5113×10^{-2}

Table 3 The coefficients, for $\nu = 1/4$

λ	$2n$	A_{2n}'	B_{2n}'	C_{2n+2}'	D_{2n+2}'
$1/4$	0	-2.9993×10^{-1}	6.2344×10^{-2}	-6.2258×10^{-3}	1.4124×10^{-4}
	2	-6.6797×10^{-1}	5.715×10^{-6}	9.108×10^{-6}	-2.632×10^{-6}
	4	-1.633×10^{-4}	1.741×10^{-7}	1.366×10^{-7}	-3.081×10^{-7}
	6	-9.494×10^{-6}	4.435×10^{-9}	2.051×10^{-9}	-3.787×10^{-9}
	8	-3.925×10^{-7}	1.016×10^{-10}	3.121×10^{-11}	-5.154×10^{-11}
	10	-1.326×10^{-8}	2.172×10^{-12}	4.770×10^{-13}	-7.364×10^{-13}
$1/2$	0	-2.9818×10^{-1}	6.5169×10^{-2}	-2.0741×10^{-2}	4.7222×10^{-3}
	2	-6.9745×10^{-1}	5.233×10^{-4}	2.532×10^{-4}	-6.480×10^{-4}
	4	-1.485×10^{-2}	5.944×10^{-5}	1.474×10^{-6}	-3.320×10^{-6}
	6	-3.227×10^{-3}	5.579×10^{-6}	8.534×10^{-7}	-1.606×10^{-6}
	8	-4.922×10^{-4}	4.670×10^{-7}	4.973×10^{-8}	-8.509×10^{-8}
	10	-6.077×10^{-5}	3.614×10^{-8}	2.901×10^{-9}	-4.712×10^{-9}

where the values in the limiting case $\lambda = 0$ are shown for comparison. The results are also plotted in Fig. 1.

References

1 C-B. Ling, "Torsion of a Circular Cylinder Having a Spherical Cavity," *Quarterly of Applied Mathematics*, vol. 10, 1952, pp. 149–156.

2 C-B. Ling, "Stresses in a Circular Cylinder Having a Spherical Cavity," *Quarterly of Applied Mathematics*, vol. 13, 1956, pp. 381–391.

3 C-B. Ling, "Stresses in a Stretched Slab Having a Spherical Cavity," JOURNAL OF APPLIED MECHANICS, vol. 26, TRANS. ASME, vol. 81, series E, June, 1959, pp. 235–240.

4 R. C. J. Howland, "Stresses in a Plate Containing an Infinite Row of Holes," *Proceedings of Royal Society*, London, series A, vol. 148, 1935, pp. 471–491.

5 R. C. Knight, "On the Stresses in a Perforated Strip," *Quarterly Journal of Mathematics*, Oxford series, vol. 5, 1934, pp. 255–268.

6 J. W. L. Glaisher, "Tables of $1 \pm 2^{-n} + 3^{-n} \pm 4^{-n} +$ etc., and $1 + 3^{-n} + 5^{-n} + 7^{-n} +$ etc., to 32 Places of Decimals," *Quarterly Journal of Mathematics*, vol. 45, 1914, pp. 141–158.

7 C-B. Ling and C. W. Nelson, "On Evaluation of Howland's Integrals," *Annals of Academia Sinica*, part 2, 1956, pp. 45–56, Taiwan, China.

8 C-B. Ling, "Tables of Values of 16 Integrals of Algebraic-Hyperbolic Type," *Mathematical Tables and Other Aids to Computation*, vol. 11, 1957, pp. 160–166.

Elastic Equilibrium of a Plate With a Reinforced Elliptical Hole[1]

EUGENE LEVIN
Mathematician,
Aero-Astronautics Department,
The Rand Corporation,
Santa Monica, Calif.
Assoc. Mem. ASME

An infinite thin plate with an elliptical hole reinforced by a confocal elliptical ring is subjected to loads in the plane. A solution to the generalized plane-stress problem is obtained using the complex variable techniques of Muskhelishvili. The result is presented in a form well suited to evaluation by digital computers. Specialization to a circular hole with a negligibly thin reinforcement is shown to be in agreement with results obtained by other authors.

1 Introduction

In a recent paper, Radok [1][2] presented a two-dimensional solution for the elastic equilibrium of an infinite thin plate with a compactly reinforced hole. Radok's work utilized the general techniques developed by Muskhelishvili [2] for the solution of two-dimensional elastostatic problems and represented a concise, direct method applicable to any hole which could be mapped onto the unit circle by a rational transformation. The solution for the circle itself was exhibited explicitly while the ellipse was left as a future problem of particular interest. As in earlier attacks on this problem [3–7], the reinforcement was treated as a thin curved beam. The present paper constitutes a generalization to reinforcements of arbitrary width and presents in detail the solution for the reinforced elliptical hole.[3]

The elastic material is assumed to be homogeneous and isotropic; however, in general, the material of the plate may differ from that of the reinforcement. A generalized plane-stress problem is formulated in terms of the mean values of the stresses and displacements over the thickness of the body. This problem is then attacked by the general methods of Muskhelishvili. In Section 3, the solution for the elliptical hole with a confocal elliptical reinforcement is obtained in terms of two constants. Although these constants are not determined explicitly, they can be approximated to any desired accuracy for a given case. The specialization of the ellipse to the circle is presented in Section 4, where a solution for the general case is exhibited. Radok's results may be obtained as a limiting case of the general solution by allowing the width of the reinforcement to approach zero.

2 Formulation

Consider the reinforced plate shown in Fig. 1. It is assumed that the applied loads act parallel to the middle plane, are distributed symmetrically with respect to this plane, and that the body forces are zero.

Let τ_{ij} and u_i denote the three-dimensional components of the stress tensor and displacement vector. Define their mean values by

$$\left.\begin{aligned} S_{ij}(x_1, x_2) &= \frac{1}{2H}\int_{-H}^{H} \tau_{ij}(x_1, x_2, x_3)dx_3 \\ V_i(x_1, x_2) &= \frac{1}{2H}\int_{-H}^{H} u_i(x_1, x_2, x_3)dx_3 \end{aligned}\right\} \text{ in Region I}$$

$$\left.\begin{aligned} T_{ij}(x_1, x_2) &= \frac{1}{2h}\int_{-h}^{h} \tau_{ij}(x_1, x_2, x_3)dx_3 \\ U_i(x_1, x_2) &= \frac{1}{2h}\int_{-h}^{h} u_i(x_1, x_2, x_3)dx_3 \end{aligned}\right\} \text{ in Region II}$$

From symmetry $V_3 = U_3 = T_{13} = T_{23} = S_{13} = S_{23} = 0$.

Since no forces act on the face of the plate, $\tau_{13} = \tau_{23} = \tau_{33} = 0$ on $x_3 = \pm h$. Then the equilibrium equation,

$$\frac{\partial \tau_{11}}{\partial x_1} + \frac{\partial \tau_{21}}{\partial x_2} + \frac{\partial \tau_{31}}{\partial x_3} = 0,$$

implies that $\partial \tau_{31}/\partial x_3 = 0$ on $x_3 = \pm h$. The classic assumption of the theory of generalized plane stress as developed by Filon [8] is that $\tau_{31} \equiv 0$ throughout. Expanding τ_{31} in a Taylor's series

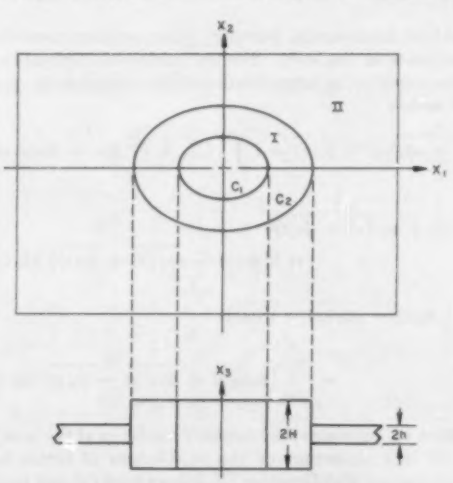

Fig. 1 Reinforced elliptical hole

[1] The results presented in this paper are based on Part 1 of a thesis submitted by the author to the University of California at Los Angeles in partial fulfillment of the requirements for the degree of Doctor of Philosophy, 1955.

[2] Numbers in brackets designate References at end of paper.

[3] The reviewer has indicated that related material is contained in a Russian book by G. N. Savin, "Concentration of Stresses Around Openings," Moscow, 1951.

Contributed by the Applied Mechanics Division and presented at the Annual Meeting, Atlantic City, N. J., November 29–December 4, 1959, of The American Society of Mechanical Engineers.

Discussion of this paper should be addressed to the Secretary, ASME, 29 West 39th Street, New York, N. Y., and will be accepted until July 10, 1960, for publication at a later date. Discussion received after the closing date will be returned.

Note: Statements and opinions advanced in papers are to be understood as individual expressions of their authors and not those of the Society. Manuscript received by ASME Applied Mechanics Division, March 2, 1959. Paper No. 59—A-45.

about $x_3 = h$ shows that $\tau_{33} = 0(h^2)$ and $T_{33} = 0(h^2)$. To within the same degree of approximation,

$$U_\alpha(x_1, x_2) = u_\alpha(x_1, x_2, 0) + 0(h^2), \ \alpha = 1,2 \tag{1}$$

This follows from an expansion of u in a Taylor's series about $x_3 = 0$. The principal assumption now invoked in formulating a two-dimensional problem is that both the region of the plate and the region of the reinforcement may reasonably be taken to be in a state of generalized plane stress. Some information on the deviation of plane solutions from three-dimensional solutions may be found in Michell [9] and in the more recent work of Sadowsky and Sternberg [10]; however, the final determination of the range of applicability of the results obtained here under the generalized plane-stress assumption must await suitable experiments.

From the work of Muskhelishvili, the mean stresses and mean displacements in each region can be represented in terms of two functions of a complex variable. Thus

$$\begin{aligned} S_{11} + S_{22} &= 2[\phi_1'(z) + \overline{\phi_1'(z)}], \\ S_{22} - S_{11} + 2iS_{12} &= 2[\bar{z}\phi_1''(z) + \psi_1'(z)], \\ 2\mu_1(V_1 + iV_2) &= k_1\phi_1(z) - z\overline{\phi_1'(z)} - \overline{\psi_1(z)}, \end{aligned} \tag{2}$$

where

$$z = x_1 + ix_2$$

μ_1 = $E_1/2(1 + \nu_1)$
k_1 = $(3 - \nu_1)/(1 + \nu_1)$
E_1 = Young's modulus in Region I
ν_1 = Poisson's ratio in Region I
$'$ denotes differentiation
— denotes the complex conjugate value.

A similar representation holds for T_{ij} and U_i in Region II in terms of the complex functions ϕ_2 and ψ_2 with the material constants appropriate to the region. The boundary conditions may be expressed in the form

$$\phi(z) + z\overline{\phi'(z)} + \overline{\psi(z)} = i\int^s (X_n + iY_n)ds + \text{const} \tag{3}$$

on each contour, where (X_n, Y_n) is the (mean)stress vector acting on an element of the contour with exterior normal n. The contour is described in the positive sense with the arc length denoted by s.

The first fundamental boundary-value problem prescribes the applied loads on the body. For the reinforced elliptical hole, the solution requires the determination of four functions $\phi_1, \psi_1, \phi_2, \psi_2$ which satisfy

$$\phi_1(z) + z\overline{\phi_1'(z)} + \overline{\psi_1(z)} = i\int^s (X_n + iY_n)ds + \text{const on } C_1, \tag{4}$$

$$H\{\phi_1(z) + z\overline{\phi'(z)} + \overline{\psi_1(z)}\} = k\{\phi_2(z) + z\overline{\phi_2'(z)} + \overline{\psi_2(z)}\} \text{ on } C_2, \tag{5}$$

$$\frac{1}{\mu_1}\{k_1\phi_1(z) - z\overline{\phi_1'(z)} - \overline{\psi_1(z)}\} = \frac{1}{\mu_2}\{k_2\phi_2(z) - z\overline{\phi_2'(z)} - \overline{\psi_2(z)}\} \text{ on } C_2 \tag{6}$$

Equation (4) expresses the boundary condition at the hole, Equation (5) is a statement of the equilibrium of forces between the two regions, and Equation (6) follows from (1) and the known continuity of the three-dimensional displacements.

For an infinite simply connected domain (Region II) the functions ϕ_2, ψ_2 have the structure

$$\begin{aligned} \phi_2(z) &= -\frac{X_1 + iX_2}{2\pi(1 + k_2)}\log z + \Gamma z + \phi_{20}(z), \\ \psi_2(z) &= \frac{k_2(X_1 - iX_2)}{2\pi(1 + k_2)}\log z + \Gamma^* z + \psi_{20}(z), \end{aligned} \tag{7}$$

where

$$\begin{aligned} R_e[2\Gamma - \Gamma^*] &= T_{11}(\infty), \\ R_e[2\Gamma + \Gamma^*] &= T_{22}(\infty), \\ I_m[\Gamma^*] &= T_{12}(\infty), \end{aligned}$$

(X_1, X_2) is the resultant mean force vector acting on the hole, ϕ_{20}, ψ_{20} are holomorphic functions.

The $I_m[\Gamma]$ represents a rotation which does not affect the state of stress, hence Γ may be taken real. The stresses are assumed to be bounded at infinity so that Γ and Γ^* are finite. For a finite doubly connected domain (Region I) the functions ϕ_1 and ψ_1 have the structure indicated by (7) with $\Gamma = \Gamma^* = 0$ and ϕ_{10}, ψ_{10} holomorphic in the ring.

There is a certain degree of arbitrariness in the functions ϕ_{20}, ψ_{20}. From (2) it is seen that ψ_{20} may be replaced by $\psi_{20} + (\alpha_1 + i\alpha_2)$ and ϕ_{20} by $\phi_{20} + (\beta_1 + i\beta_2) + i\gamma z$ without altering the state of stress. The choice of $(\alpha_1 + i\alpha_2)$ will always be taken so that the arbitrary constant in Equation (4) becomes zero. The selection of the remaining constants will be postponed. Indeed, for the reinforcement problem, the choice is not completely free in both regions due to Equation (6) relating the displacements.

The basic reinforcement problem may now be stated as the search for four functions $\phi_1, \psi_1, \phi_2, \psi_2$, which have the structure (7) and which satisfy Equations (4), (5), and (6). In addition, Γ and Γ^* in ϕ_2, ψ_2 must satisfy the prescribed loading conditions at infinity.

3 Reinforced Elliptical Hole

The function

$$z = \omega(\zeta) = A\left(\zeta + \frac{c}{\zeta}\right)$$

represents the conformal map of the confocal elliptical boundaries in the z-plane onto concentric circular boundaries in the ζ-plane. In the ζ-plane the concentric circles γ_1 and γ_2 with radii $R_1 = R < 1$ and $R_2 = 1$ correspond, respectively, to the ellipses C_1 and C_2 in the z-plane. With $\sqrt{c} \leq R < 1$ the region exterior to C_1 corresponds to the region exterior to γ_2 and the positive sense of orientation along the contours is preserved. The purpose of the transformation to a plane where the principal contours are given by concentric circles is to utilize power-series expressions for the unknown functions.

The unknown functions are represented in the image region by

$$\Phi(\zeta) \equiv \phi[\omega(\zeta)], \qquad \Psi(\zeta) = \psi[\omega(\zeta)]$$

and the computation of the components of stress and displacement can be performed directly in terms of $\zeta = \rho\sigma = \rho e^{i\theta}$.

$$S_{\rho\rho} + S_{\theta\theta} = 2\left[\frac{\Phi_1'(\zeta)}{\omega'(\zeta)} + \overline{\frac{\Phi_1'(\zeta)}{\omega'(\zeta)}}\right], \tag{8a}$$

$$S_{\theta\theta} - S_{\rho\rho} + 2iS_{\rho\theta} = \frac{2\zeta^2}{\rho^2\overline{\omega'(\zeta)}}\left\{\overline{\omega(\zeta)}\,\frac{d}{d\zeta}\left[\frac{\Phi_1'(\zeta)}{\omega'(\zeta)}\right] + \Psi_1'(\zeta)\right\}, \tag{8b}$$

$$2\mu_1 |\omega'(\zeta)|(V_\rho + iV_\theta) = \frac{\bar{\zeta}}{\rho}\overline{\omega'(\zeta)}\left[k_1\Phi_1(\zeta) - \frac{\omega(\zeta)\overline{\Phi_1'(\zeta)}}{\omega'(\zeta)} - \overline{\Psi_1(\zeta)}\right] \quad (8c)$$

A similar representation holds for the stresses and displacements in the image of Region II. Hence it is sufficient to determine the functions $\Phi_1(\zeta)$, $\Psi_1(\zeta)$, $\Phi_2(\zeta)$, $\Psi_2(\zeta)$ in the image region.

In order to simplify the boundary conditions, it is convenient to utilize the known solution for the unreinforced plate with an elliptical hole. Let $\phi = A(\zeta)$, $\psi = B(\zeta)$ represent the functions in the *image* region which solve the problem of the unreinforced plate with an elliptical hole.

Take

$$\Phi_1(\zeta) = A_1(\zeta) + F_1(\zeta), \qquad \Psi_1(\zeta) = B_1(\zeta) + G_1(\zeta),$$

$$\Phi_2(\zeta) = A_2(\zeta) + F_2(\zeta), \qquad \Psi_2(\zeta) = B_2(\zeta) + G_2(\zeta),$$

where A_1, B_1 and A_2, B_2 differ from A, B only in the constants appropriate to the region. The conditions imposed by (4), (5), and (6) now become

$$\overline{F_1(\zeta)} + \frac{\overline{\omega(\zeta)}F_1'(\zeta)}{\omega'(\zeta)} + G_1(\zeta) = 0, \quad \text{on} \quad \zeta = R\sigma = Re^{i\theta}, \quad (9)$$

$$s\left\{\overline{F_1(\zeta)} + \frac{\overline{\omega(\zeta)}F_1'(\zeta)}{\omega'(\zeta)} + G_1(\zeta)\right\} = \overline{F_2(\zeta)} + \frac{\overline{\omega(\zeta)}F_2'(\zeta)}{\omega'(\zeta)} + G_2(\zeta) + \sum_{-\infty}^{\infty} C_n\sigma^n, \quad \text{on} \quad \zeta = \sigma, \quad (10)$$

$$t\left\{k_1\overline{F_1(\zeta)} - \frac{\overline{\omega(\zeta)}F_1'(\zeta)}{\omega'(\zeta)} - G_1(\zeta)\right\} = k_2\overline{F_2(\zeta)} - \frac{\overline{\omega(\zeta)}F_2'(\zeta)}{\omega'(\zeta)} - G_2(\zeta) + \sum_{-\infty}^{\infty} D_n\sigma^n, \quad \text{on} \quad \zeta = \sigma, \quad (11)$$

where

$$s = H/h,$$

$$t = \mu_2/\mu_1$$

$$\sum_{-\infty}^{\infty} C_n\sigma^n = \overline{A_2(\zeta)} + \frac{\overline{\omega(\zeta)}A_2'(\zeta)}{\omega'(\zeta)} + B_2(\zeta) - s\left\{\overline{A_1(\zeta)} + \frac{\overline{\omega(\zeta)}A_1'(\zeta)}{\omega'(\zeta)} + B_1(\zeta)\right\}, \quad \text{on} \quad \zeta = \sigma,$$

$$\sum_{-\infty}^{\infty} D_n\sigma^n = k_2\overline{A_2(\zeta)} - \frac{\overline{\omega(\zeta)}A_2'(\zeta)}{\omega'(\zeta)} - B_2(\zeta) - t\left\{k_1\overline{A_1(\zeta)} - \frac{\overline{\omega(\zeta)}A_1'(\zeta)}{\omega'(\zeta)} - B_1(\zeta)\right\}, \quad \text{on} \quad \zeta = \sigma$$

The unknown functions F_1 and G_1 are regular in the ring and the functions F_2 and G_2 are regular in the exterior of γ_2. Hence there is a convenient power-series representation:

$$F_1(\zeta) = F_{11}(\zeta) + F_{12}(\zeta) = a_0 + \sum_1^{\infty} a_n\zeta^n + \sum_1^{\infty} a_{-n}\zeta^{-n},$$

$$F_2(\zeta) = \sum_0^{\infty} \alpha_{-n}\zeta^{-n}$$

and, without loss of generality,

$$G_1(\zeta) = -\frac{\zeta(R^4 + c\zeta^2)F_1'(\zeta)}{R^2(\zeta^2 - c)} + \sum_{-\infty}^{\infty} b_n\zeta^n,$$

$$G_2(\zeta) = -\frac{\zeta(1 + c\zeta^2)F_2'(\zeta)}{(\zeta^2 - c)} + \sum_0^{\infty} \beta_{-n}\zeta^{-n}$$

The constant a_0 is arbitrary and does not affect the state of stress. It will be chosen equal to zero.

From Equation (9)

$$\sum_{-\infty}^{\infty} \bar{a}_n R^n\sigma^{-n} + \sum_{-\infty}^{\infty} b_n R^n\sigma^n = 0$$

Hence

$$b_n = -\bar{a}_{-n}R^{-2n} \quad (12)$$

From (10) and (11)

$$st(1 + k_1)\sum_{-\infty}^{\infty} \bar{a}\sigma^{-n} = (t + sk_2)\sum_0^{\infty} \bar{a}_{-n}\sigma^n + (t - s)\sum_0^{\infty} \beta_{-n}\sigma^{-n} + \sum_{-\infty}^{\infty} (tC_n + sD_n)\sigma^n$$

Hence

$$(t + sk_2)\bar{\alpha}_0 + (t - s)\beta_0 = -[tC_0 + D_0], \quad (13)$$

$$(t - s)\beta_{-n} = st(1 + k_1)\bar{a}_n - [tC_{-n} + sD_{-n}], \qquad n = 1, 2, \ldots \quad (14)$$

$$(t + sk_2)\bar{\alpha}_{-n} = st(1 + k_1)\bar{a}_{-n} - [tC_n + sD_n], \qquad n = 1, 2, \ldots \quad (15)$$

From (12), (13), (14), and (15) all the unknown coefficients can be determined in terms of $\{a_n\}$ and β_0. The basic equations (9), (10), (11) provide one remaining independent relation, say (10). Unfortunately, the direct substitution of the power-series expansions into (10) together with an attempt to equate coefficients of like powers of σ leads to an infinite system of simultaneous linear equations which does not seem to be tractable. Instead of this approach, a method suggested by the work of Sheremetyeff on the elliptical ring [11] will be employed. The technique yields a solution for all the unknown coefficients in terms of two constants, $F_{11}'(\sqrt{c})$ and $F_{11}'(-\sqrt{c})$. These constants can then be approximated to any desired degree of accuracy.

Multiply (10) by

$$\frac{1}{2\pi i}\frac{d\sigma}{\sigma - \zeta}$$

and integrate around γ_2 with $|\zeta| < 1$ and then $|\zeta| > 1$ to obtain

$$s\sum_1^{\infty} \bar{a}_{-n}\zeta^n + \frac{s(1 - R^2)}{R^2}\frac{\zeta(R^2 - c\zeta^2)}{(\zeta^2 - c)}\sum_1^{\infty} na_n\zeta^{n-1} + s\sum_0^{\infty} b_n\zeta^n - \frac{s(1 - R^2)(R^2 - c^2)}{2R^2}\left[\frac{F_{11}'(\sqrt{c})}{\zeta - \sqrt{c}} + \frac{F_{11}'(-\sqrt{c})}{\zeta + \sqrt{c}}\right] = \sum_0^{\infty} \bar{a}_{-n}\zeta^n + \beta_0 + \sum_0^{\infty} C_n\zeta^n, \quad (16)$$

$$s\sum_1^{\infty} \bar{a}_n\zeta^{-n} - \frac{s(1 - R^2)}{R^2}\frac{\zeta(R^2 - c\zeta^2)}{(\zeta^2 - c)}\sum_1^{\infty} na_{-n}\zeta^{-n-1} + s\sum_1^{\infty} b_{-n}\zeta^{-n} + \frac{s(1 - R^2)(R^2 - c^2)}{2R^2}\left[\frac{F_{11}'(\sqrt{c})}{\zeta - \sqrt{c}} + \frac{F_{11}'(-\sqrt{c})}{\zeta + c}\right] = \sum_1^{\infty} \beta_{-n}\zeta^{-n} + \sum_1^{\infty} C_{-n}\zeta^{-n} \quad (17)$$

Using (12), (13), (14), and (15) to eliminate b_n, β_{-n} and α_{-n}, and comparing the coefficients of like powers of ζ in (16) and in (17) leads to the relations

$$\left(\frac{1+k_2}{k_2 s+t}\right)\beta_0 = -\frac{L}{\sqrt{c}} - \frac{k_2 C_0 - D_0}{k_2 s+t}, \tag{18a}$$

$$-c\bar{a}_{-1}A_1 + (R^2-1)a_1 = M + \frac{c[k_2 C_1 - D_1]}{k_2 s+t}, \tag{18b}$$

$$-c\bar{a}_{-2}A_2 + 2(R^2-1)a_2 = +\frac{L}{\sqrt{c}} + \frac{c[k_2 C_2 - D_2]}{k_2 s+t}, \tag{18c}$$

$$\bar{a}_{-n}A_n - c\bar{a}_{-n-2}A_{n+2} - \frac{R^2-1}{R^2}\,cna_n + (R^2-1)(n+2)a_{n+2} = \frac{c[k_2 C_{n+2} - D_{n+2}] - [k_2 C_n - D_n]}{k_2 s+t} \quad \text{for } n = 1, 2, \ldots, \tag{18d}$$

$$\bar{a}_1 B_1 + c\left(\frac{R^2-1}{R^2}\right)a_{-1} = -M - \frac{[C_{-1} + D_{-1}]}{s-t}, \tag{18e}$$

$$\bar{a}_2 B_2 + 2c\left(\frac{R^2-1}{R^2}\right)a_{-2} = -\sqrt{c}L - \frac{[C_{-2} + D_{-2}]}{s-t}, \tag{18f}$$

$$\bar{a}_{n+2}B_{n+2} - c\bar{a}_n B_n + c\left(\frac{R^2-1}{R^2}\right)(n+2)a_{-n-2} - n(R^2-1)a_{-n} = \frac{c[C_{-n} + D_{-n}] - [C_{-n-2} + D_{-n-2}]}{s-t} \quad \text{for } n = 1, 2, \ldots, \tag{18g}$$

where

$$A_n = \left(R^{-2n} - \frac{k_2 s - tk_1}{k_2 s+t}\right),$$

$$B_n = \left(R^{2n} - \frac{s+tk_1}{s-t}\right),$$

$$L = \frac{(R^2-c^2)(R^2-1)}{2R^2}\,[F_{II}'(\sqrt{c}) - F_{II}'(-\sqrt{c})],$$

$$M = \frac{(R^2-c^2)(R^2-1)}{2R^2}\,[F_{II}'(\sqrt{c}) + F_{II}'(-\sqrt{c})]$$

This system of equations can be solved in terms of known quantities and the unknown constants $F_{II}'(\sqrt{c})$ and $F_{II}'(-\sqrt{c})$. The function

$$F_{II}'(\zeta) = \sum_1^\infty n a_n \zeta^{n-1}$$

is regular in the interior of γ_2 and hence the convergent power series can be truncated to yield the approximate function

$$F_{II}'(\zeta) \simeq \sum_1^N n a_n \zeta^{n-1}$$

This relation permits the unknown constants to be determined to any desired accuracy. A reasonable technique is to obtain a rough estimate for $F_{II}'(\sqrt{c})$ and $F_{II}'(-\sqrt{c})$ from a low-order truncation. These values are then used to compute a_n for $n = 1, \ldots, N$. This yields improved values for $F_{II}'(\sqrt{c})$ and $F_{II}'(-\sqrt{c})$ and the process may be iterated until the desired accuracy is attained. Experience with a number of sample problems seems to indicate that the method converges quite rapidly and the iteration technique is very well-suited to stored-program computers.

It should be noted that a related problem of considerable technological importance, the problem of the reinforced slit, is contained in this solution for the reinforced elliptical hole. By taking $c = R^2$ the ellipse C_1 becomes degenerate and the circle $\zeta = R\sigma$ in the ζ-plane corresponds to a slit in the z-plane;

$$z = \omega(\zeta) = A\left(\zeta + \frac{c}{\zeta}\right) \to AR\left(\sigma + \frac{1}{\sigma}\right) = 2AR\cos\theta$$

Hence $x = 2AR\cos\theta$, $y = 0$, and the ellipse becomes the slit of length $4AR$ directed along the x-axis.

4 Reinforced Circular Hole

In the case of a reinforced circular hole $c = 0$ and the system of Equations (18) can be solved explicitly:

$$\frac{1+k_2}{k_2 s+t}\,\beta_0 = -2a_2(R^2-1) - \frac{k_2 C_0 - D_0}{k_2 s+t}, \tag{19a}$$

$$a_1 = \bar{a}_1 = -\frac{[C_{-1} + D_{-1}]}{(s-t)(B_1 + R^2 - 1)}, \tag{19b}$$

$$a_2 = -\frac{[\bar{C}_{-2} + \bar{D}_{-2}]}{B_2(s-t)}, \tag{19c}$$

$$a_{n+2} = -\frac{n(R^2-1)(s-t)[k_2 C_n - D_n] + (k_2 s+t)A_n[\bar{C}_{-n-2} + \bar{D}_{-n-2}]}{[n(n+2)(R^2-1)^2 + A_n B_{n+2}](k_2 s+t)(s-t)}, \quad n = 1, 2, \ldots, \tag{19d}$$

$$a_{-n} = \frac{(n+2)(R^2-1)(k_2 s+t)[C_{-n-2} + D_{-n-2}] - (s-t)B_{n+2}[k_2\bar{C}_n - \bar{D}_n]}{[n(n+2)(R^2-1)^2 + A_n B_{n+2}](k_2 s+t)(s-t)}, \quad n = 1, 2, \ldots \tag{19e}$$

It may be observed from the definition of B_n that the denominators of (19) are nonzero when $s = t$. Since the equations are homogeneous in (C_n, D_n) it can be verified that the solution reduces to the known result for the homogeneous unreinforced plate with a hole when $t = 1$, $k_1 = k_2$, and $s = 1$.

If no external loads are applied at the hole,

$$A(\zeta) = A\left\{\Gamma\zeta - \frac{R^2\overline{\Gamma^*}}{\zeta}\right\},$$

$$B(\zeta) = A\left[\Gamma^*\zeta - \frac{2R^2\Gamma}{\zeta} - \frac{R^4\overline{\Gamma^*}}{\zeta^2}\right]$$

Then

$$\sum_{-\infty}^{\infty} C_n\sigma^n = (1-s)(1-R^2)A\left[\Gamma^*\sigma + \frac{2\Gamma}{\sigma} + \frac{R^2\overline{\Gamma^*}}{\sigma^2}\right],$$

$$\sum_{-\infty}^{\infty} D_n\sigma^n = -\Gamma^* A\sigma[(1-t) + (k_2 - tk_1)] - \frac{\Gamma A}{\sigma}[(1-t)(1-2R^2) - (k_2 - tk_1)] - \frac{\overline{\Gamma^* A}}{\sigma^2}R^2(1-t)(1-R^2),$$

and

$$\left.\begin{aligned}
\Phi_1(\zeta) &= A(\zeta) + \frac{a_{-1}}{\zeta} + a_1\zeta + a_3\zeta^3, \\
\Psi_1(\zeta) &= B(\zeta) - \zeta\left[\frac{\bar{a}_{-1}}{R^2} + 3R^2a_3\right] - \frac{2}{\zeta}\,[a_1R^2] \\
&\quad + \frac{R^2}{\zeta^3}\,[a_{-1} - R^4\bar{a}_3], \\
\Phi_2(\zeta) &= A(\zeta) + \frac{\alpha_{-1}}{\zeta}, \\
\Psi_2(\zeta) &= B(\zeta) + \frac{\alpha_{-1}}{\zeta^3} + \frac{\beta_{-1}}{\zeta} + \frac{\beta_{-3}}{\zeta^3}
\end{aligned}\right\} \qquad (20)$$

When the plate and reinforcement are made of the same material, $k_1 = k_2 = k$, and $t = 1$. In this case the principal coefficients in the foregoing become

$$a_1 = \frac{-2\Gamma A(s-1)(1-R^2)}{(k+1) + 2(s-1)(1-R^2)},$$

$$a_{-1} = \frac{\overline{\Gamma^*}A\{3(1-R^2)^2(s-1)R^2(ks+1) + k(s-1)(1-R^2)[R^4(s-1) - (s+k)]\}}{3(1-R^2)^2(s-1)(ks+1) + [R^{-2}(ks+1) - k(s-1)][R^4(s-1) - (s+k)]},$$

$$a_3 = \frac{\Gamma^*A(s-1)(1-R^2)(k+1)}{3(1-R^2)^2(s-1)(ks+1) + [R^{-2}(ks+1) - k(s-1)][R^4(s-1) - (s+k)]}$$

The special case just described where the hole is free of external loads and the plate and reinforcement are made of the same material corresponds to the most common experimental test arrangement. It is of some interest to investigate the theoretical behavior of the maximum mean stress in the plate and in the reinforcement. The loading states of unit uniform uniaxial tension, equal biaxial tension, and pure shear may be characterized [see Equation (7)] by

$$\Gamma = \frac{\gamma+1}{4}, \quad \Gamma^* = \frac{\gamma-1}{2},$$

where $\gamma = 0, 1, -1$, respectively, for the three loading cases. To study the effect of varying the height-to-width ratio of the reinforcement cross section, consider a sequence of doubler-type reinforcements of constant volume equal to the volume of the material removed by the hole. Then,

$$2h\pi R^2 = \pi(2H - 2h) - \pi R^2(2H - 2h),$$

or

$$R^2 = \left(\frac{s-1}{s}\right)$$

where $s = H/h$. The maximum mean stress in the reinforcement is given by $S_{\theta\theta}$ at $\rho = R$. Except for the case of biaxial tension, the maximum mean stress in the plate is different from $T_{\theta\theta}$. It does, however, occur at $\rho = 1$ and can be easily computed. The principal stresses in a two-dimensional problem are given by

$$\tau = \frac{(\tau_{11} + \tau_{22})}{2} \pm \left[\left(\frac{\tau_{22} - \tau_{11}}{2}\right)^2 + (\tau_{12})^2\right]^{1/2}$$

This may be conveniently represented by

$$\tau = (\phi'(z) + \overline{\phi'(z)}) \pm |z\phi''(z) + \psi'(z)|$$

For definiteness, Poisson's ratio was chosen to be $\nu = 1/3$ and the mapping constant A was taken to be unity. The values of the maximum mean stress for the three loading states are presented in Fig. 2 as a function of the ratio $s = H/h$. The values of $S_{\max}$ at $s = 1$ agree with the well-known solution of Kirsch for the unreinforced plate. It also may be noted that the maximum mean stress in the reinforcement decreases with s. This is in agreement with the results of Levy, McPherson, and Smith [12] who found that the "best" reinforcement was one which concentrated most of the material close to the edge of the hole.

For the case of very narrow reinforcements of the same material as the plate, a simple approximation to Equations (20) may be obtained. Let α' denote the reduced cross-sectional area of the reinforcement,

$$\alpha' \equiv \frac{2H(1-R)}{2hR} = \frac{s(1-R)}{R}$$

A "narrow" reinforcement is obtained by holding α' fixed and allowing R to approach unity. For this purpose replace s in Equations (20) by $\alpha'R/(1-R)$ and compute the limit as $R \to 1$:

$$a_1 = -\frac{4\Gamma A\alpha'}{4\alpha' + (1+k)},$$

$$a_{-1} = \frac{2\overline{\Gamma^*}Ak\alpha'}{2k\alpha' + 6\alpha' + (1+k)},$$

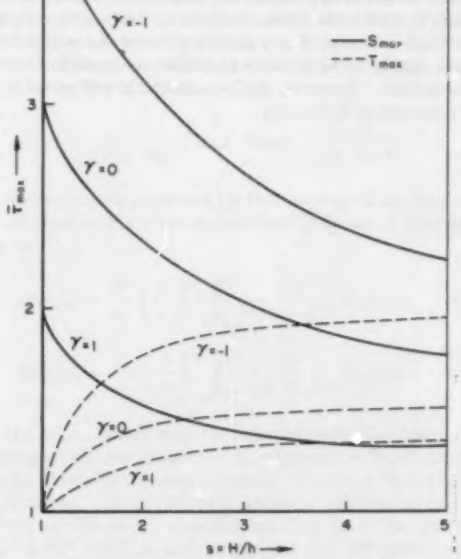

Fig. 2 Maximum mean stress

$$a_2 = -\frac{2\Gamma^* A\alpha'}{2k\alpha' + 6\alpha' + (1+k)}$$

The solution for the plate (Region II) becomes

$$\frac{\Phi_2(\zeta)}{A} = \Gamma\zeta - \frac{\overline{\Gamma^*}}{\zeta}\frac{1+\alpha'+\alpha'\nu}{1+3\alpha'+\alpha'\nu},$$

$$\frac{\Psi_2(\zeta)}{A} = \Gamma^*\zeta - \frac{2\Gamma}{\zeta}\frac{1-\alpha'+\alpha'\nu}{1+\alpha'+\alpha'\nu} - \frac{\overline{\Gamma^*}}{\zeta^3}\frac{1-\alpha'+\alpha'\nu}{1+3\alpha'+\alpha'\nu},$$

or in the original plane

$$\phi(z) = \Gamma z - \frac{\overline{\Gamma^*}A^2}{z}\frac{1+\alpha'+\alpha'\nu}{1+3\alpha'+\alpha'\nu},$$

$$\psi(z) = \Gamma^* z - \frac{2\Gamma A^2}{z}\frac{1-\alpha'+\alpha'\nu}{1+\alpha'+\alpha'\nu} - \frac{\Gamma^* A^4}{z^3}\frac{1-\alpha'+\alpha'\nu}{1+3\alpha'+\alpha'\nu}$$

This approximate solution was originally obtained by Radok [1] whose investigations were concerned with negligibly thin reinforcing rings. Radok's results are in good agreement with the experimental results of Reissner and Morduchow [6] in which the value of R was approximately 0.92. Application of the present results to such narrow reinforcements differs very little from the results obtained by the Radok approximation. For smaller values of R, the predicted results differ considerably.

5 Summary

Equations (18) represent a generalized plane-stress solution to the first boundary-value problem for a plate with a reinforced elliptical hole. The treatment has been carried out in full generality to include arbitrary loading at the hole and at infinity, to allow for arbitrary dimensions of the reinforcement cross section and for different values of the material constants of the plate and reinforcement. The presence of concentrated forces or concentrated moments acting on the boundary of the hole does not introduce any difficulties since the effect may be absorbed into the solution for the unreinforced plate. The second boundary-value problem, in which the displacements are prescribed on the contours, can be solved in a completely analogous fashion. It is only necessary to replace the stress condition at the hole by a condition on the displacements. For a general value of the eccentricity, it does not appear to be possible to exhibit an explicit solution to Equations (18). However, the formulation is well suited to solution by numerical techniques.

For a circular hole, an explicit solution is exhibited in Equations (19). This solution retains generality as to loading and materials. The specialization of this solution to a "narrow" reinforcement is shown to agree with the results of Radok and hence with the experiments of Reissner and Morduchow. This agreement with Radok provides new insight into the meaning of a "compact" reinforcement. This was taken by Radok and others to be a curved beam without bending stiffness. It now appears as a limiting case of the generalized plane-stress solution. Of considerable interest would be a series of experiments with smaller values of R in order to ascertain the range of application of the narrow reinforcement approximation. Experiments using face-plate reinforcements of different materials and various cross-section dimensions would provide an indication of the validity of the generalized plane-stress assumption.

References

1 J. R. M. Radok, "Problems of Plane Elasticity for Reinforced Boundaries," JOURNAL OF APPLIED MECHANICS, vol. 22, TRANS. ASME, vol. 77, 1955, pp. 249–254.

2 N. I. Muskhelishvili, "Some Basic Problems of the Mathematical Theory of Elasticity," N. V. P. Noordhoff Publishing Company, Groningen, Holland, 1953.

3 S. Timoshenko, "On Stresses in a Plate With a Circular Hole," *Journal of The Franklin Institute*, vol. 197, 1924, pp. 505–516.

4 G. Gurney, "An Analysis of the Stresses in a Flat Plate With a Reinforced Circular Hole Under Edge Forces," British Report 1834, 1938.

5 L. Beskin, "Strengthening of Circular Holes in Plates Under Edge Loads," JOURNAL OF APPLIED MECHANICS, vol. 11, TRANS. ASME, vol. 66, 1944, pp. 140–148.

6 H. Reissner and M. Morduchow, "Reinforced Circular Cutouts in Plane Sheets," NACA TN 1852, 1949.

7 G. H. Mansfield, "Neutral Holes in Plane Sheets—Reinforced Holes Which are Elastically Equivalent to the Uncut Sheet," *Quarterly Journal of Mechanics and Applied Mathematics*, vol. 6, 1953, pp. 370–378.

8 L. N. G. Filon, "On an Approximative Solution for the Bending of a Beam of Rectangular Cross Section Under any System of Load," *Philosophical Transactions of The Royal Society*, vol. 201, 1903, pp. 65–155.

9 J. H. Michell, "On the Inversion of Plane Stress," *Proceedings of the London Mathematical Society*, vol. 34, 1901, pp. 134–142.

10 E. Sternberg and M. A. Sadowsky, "Three-Dimensional Solution for the Stress Concentrations Around a Circular Hole in a Plate of Arbitrary Thickness," JOURNAL OF APPLIED MECHANICS, vol. 16, TRANS. ASME, vol. 71, 1949, pp. 27–38.

11 M. P. Sheremetyeff, "Elastic Equilibrium of Elliptical Ring," *Prikladnaia Matematika i Mekhanika*, vol. 17, 1953, pp. 107–113.

12 S. Levy, A. E. McPherson, and F. C. Smith, "Reinforcement of a Small Circular Hole in a Plane Sheet Under Tension," JOURNAL OF APPLIED MECHANICS, vol. 15, TRANS. ASME, vol. 70, 1948, pp. 160–168.

A Method of Solution for the Elastic Quarter-Plane[1]

M. HETÉNYI
Walter P. Murphy Professor of Engineering Science, The Technological Institute, Northwestern University, Evanston, Ill.
Mem. ASME

It is shown in this paper that for given loads on the elastic quarter-plane the prescribed boundary conditions can be fulfilled by repeated superposition of known solutions for the elastic half-plane. This leads to a sequence of infinite integrals of a simple recursion pattern. The solution is exact, since the sequence may be continued to obtain any required accuracy. Solutions are derived in this manner for three types of boundary loads: (a) concentrated normal force, (b) concentrated tangential force, and (c) partially distributed uniform loading.

Concentrated Force Normal to Boundary

Let us consider an infinite elastic half-plane, subjected at its boundary to two equal concentrated normal forces, Fig. 1. The Cartesian stress components at any point in this half-plane ($x > 0$) are defined by the well-known solution of Flamant[2] as:

$$\sigma_x = -\frac{2P}{\pi}\left\{\frac{\xi^2}{[\xi^2+(\eta+a)^2]^2}+\frac{\xi^2}{[\xi^2+(\eta-a)^2]^2}\right\} \quad (1a)$$

$$\sigma_y = -\frac{2P}{\pi}\left\{\frac{\xi(\eta+a)^2}{[\xi^2+(\eta+a)^2]^2}+\frac{\xi(\eta-a)^2}{[\xi^2+(\eta-a)^2]^2}\right\} \quad (1b)$$

$$\tau_{xy} = -\frac{2P}{\pi}\left\{\frac{\xi^2(\eta+a)}{[\xi^2+(\eta+a)^2]^2}+\frac{\xi^2(\eta-a)}{[\xi^2+(\eta-a)^2]^2}\right\} \quad (1c)$$

Introducing dimensionless co-ordinates, $x = \xi/a$ and $y = \eta/a$, on the axis of symmetry ($y = 0$) we will have

$$[\sigma_x]_{y=0} = -\frac{4P}{\pi a}\frac{x^3}{(1+x^2)^2} \quad (2a)$$

$$[\sigma_y]_{x=0} = -\frac{4P}{\pi a}\frac{x}{(1+x^2)^2} \quad (2b)$$

$$[\tau_{xy}]_{y=0} = 0 \quad (2c)$$

Now, if we succeed in removing the above $[\sigma_y]_{y=0}$ distributed normal load from the 0,x-boundary, the result will evidently be the solution for the quarter-plane (x, 0, y) loaded only by a concentrated normal force P at an arbitrary a-distance from the vertex.

The removal of this boundary load will be accomplished in successive steps. First, we will take a half-plane ($y > 0$) loaded along its boundary, the x-axis, by a distributed normal tensile load that is the reverse of the foregoing $[\sigma_y]_{y=0}$ loading, and is symmetrical with respect to the y-axis, as shown in Fig. 2.

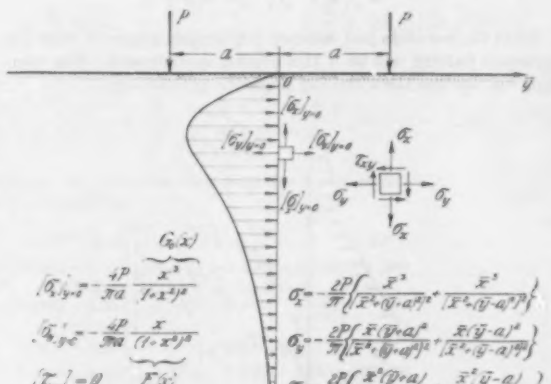

Fig. 1 Initial loading condition used in deriving solution for the quarter-plane subjected to a single concentrated normal force

In introducing the notations

$$F_0(x) = \frac{x}{(1+x^2)^2}, \quad \text{and} \quad G_0(x) = \frac{x^3}{(1+x^2)^2},$$

the stress components produced by this loading along the y-axis of the half-plane in Fig. 2 can be written, by means of Flamant's solution, as

$$[\sigma_x]_{x=0} = \frac{P}{a}\left(\frac{4}{\pi}\right)^2\int_0^\infty \frac{x^2y}{(x^2+y^2)^2}F_0(x)dx, \quad (3a)$$

$$[\sigma_y]_{x=0} = \frac{P}{a}\left(\frac{4}{\pi}\right)^2\int_0^\infty \frac{y^2}{(x^2+y^2)^2}F_0(x)dx \quad (3b)$$

Here the $[\sigma_x]_{x=0}$-stress may be regarded as a distributed normal loading on the half-plane $x > 0$, which needs to be removed in order to obtain the desired solution. Denoting the integrals in Equations (3a) and (3b) by $F_1(y)$ and $G_1(y)$, through a repeated application of Flamant's formula we find that the reversed boundary load, $-[\sigma_x]_{x=0}$, will produce in this half-plane, along its axis of symmetry, Fig. 3, the stress components

---

[1] This paper was prepared during the academic year 1958–1959, while the author was Visiting Professor of Mechanics and member of the Mathematics Research Center, U. S. Army, at the University of Wisconsin, Madison, Wis.

[2] S. Timoshenko and J. N. Goodier, "Theory of Elasticity," McGraw-Hill Book Company, Inc., New York, N. Y., second edition, 1951, p. 85 ff.

Contributed by the Applied Mechanics Division and presented at the Annual Meeting, Atlantic City, N. J., November 29–December 4, 1959, of The American Society of Mechanical Engineers.

Discussion of this paper should be addressed to the Secretary, ASME, 29 West 39th Street, New York, N. Y., and will be accepted until July 10, 1960, for publication at a later date. Discussion received after the closing date will be returned.

Note: Statements and opinions advanced in papers are to be understood as individual expressions of their authors and not those of the Society. Manuscript received by ASME Applied Mechanics Division, April 21, 1959. Paper No. 59—A-92.

$$[\sigma_x]_{y=0} = -\frac{P}{a}\left(\frac{4}{\pi}\right)^3 \int_0^\infty \frac{x^3}{(x^2+y^2)^2} F_1(y)dy, \qquad (4a)$$

$$[\sigma_y]_{y=0} = -\frac{P}{a}\left(\frac{4}{\pi}\right)^3 \int_0^\infty \frac{xy^2}{(x^2+y^2)^2} F_1(y)dy \qquad (4b)$$

In the next step we take again the $y > 0$ half-plane, Fig. 4, subjected along its boundary to a symmetrically distributed loading that is the reverse of the $[\sigma_y]_{y=0}$ normal stress obtained in Equation (4b): Denoting the two integrals in Equations (4a) and (4b) by $G_2(x)$ and $F_2(x)$, respectively, the stress components along the y-axis of symmetry can be written now as

$$[\sigma_x]_{x=0} = \frac{P}{a}\left(\frac{4}{\pi}\right)^4 \int_0^\infty \frac{x^2 y}{(x^2+y^2)^2} F_2(x)dx, \qquad (5a)$$

$$[\sigma_y]_{x=0} = \frac{P}{a}\left(\frac{4}{\pi}\right)^4 \int_0^\infty \frac{y^3}{(x^2+y^2)^2} F_2(x)dx \qquad (5b)$$

From the few steps just outlined it is already apparent what the recursion pattern will be if this process is continued. The solution will involve the following sequence of functions:

$$\left.\begin{aligned}
F_0(x) &= \frac{x}{(1+x^2)^2}, \quad G_0(x) = \frac{x^2}{(1+x^2)^2}, \\
F_1(y) &= \int_0^\infty \frac{x^2 y}{(x^2+y^2)^2} F_0(x)dx, \\
G_1(y) &= \int_0^\infty \frac{y^3}{(x^2+y^2)^2} F_0(x)dx, \\
F_2(x) &= \int_0^\infty \frac{xy^2}{(x^2+y^2)^2} F_1(y)dy, \\
G_2(x) &= \int_0^\infty \frac{x^3}{(x^2+y^2)^2} F_1(y)dy, \\
F_3(y) &= \int_0^\infty \frac{x^2 y}{(x^2+y^2)^2} F_2(x)dx, \\
G_3(y) &= \int_0^\infty \frac{y^3}{(x^2+y^2)^2} F_2(x)dx, \\
F_4(x) &= \int_0^\infty \frac{xy^2}{(x^2+y^2)^2} F_3(y)dy, \\
G_4(x) &= \int_0^\infty \frac{x^3}{(x^2+y^2)^2} F_3(y)dy,
\end{aligned}\right\} \qquad (6)$$

and so on.

As $n \to \infty$, $F_n \to 0$ and $G_n \to 0$.

The convergence of this procedure, and the proof of the statement in the foregoing last line, is given in the Appendix, together with a discussion of some pertinent properties of the F-functions.

Ultimately the solution is obtained in terms of two half-planes, one of which ($y > 0$) is subjected distributed normal boundary load

$$\frac{a}{P}[\sigma_y]_{y=0} = \frac{4}{\pi} \sum_{n=0,2,4\ldots} \left(\frac{4}{\pi}\right)^n F_n(x), \qquad (7a)$$

and the other half-plane ($x > 0$) is loaded by

$$\frac{a}{P}[\sigma_x]_{x=0} = -\frac{4}{\pi} \sum_{n=1,3,5,\ldots} \left(\frac{4}{\pi}\right)^n F_n(y) \qquad (7b)$$

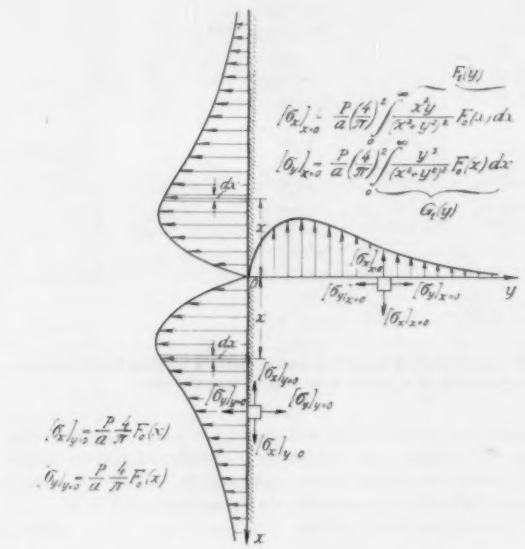

Fig. 2 First reversal of boundary load on the half-plane $y > 0$

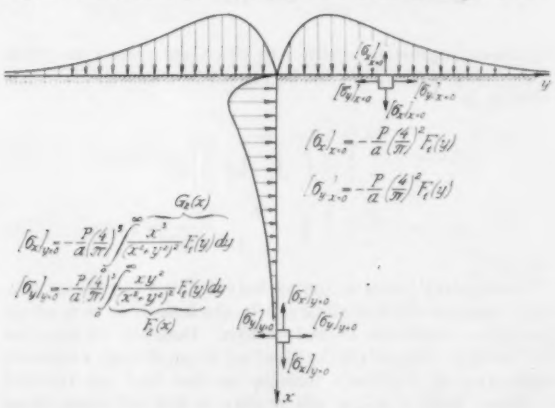

Fig. 3 First reversal of boundary load on the half-plane $x > 0$

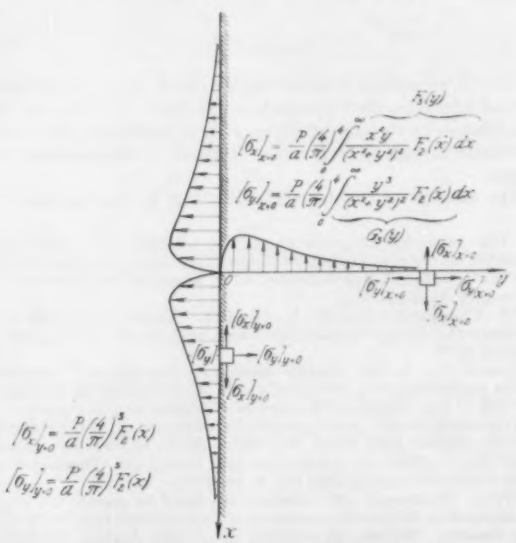

Fig. 4 Second reversal of boundary load on the half-plane $y > 0$

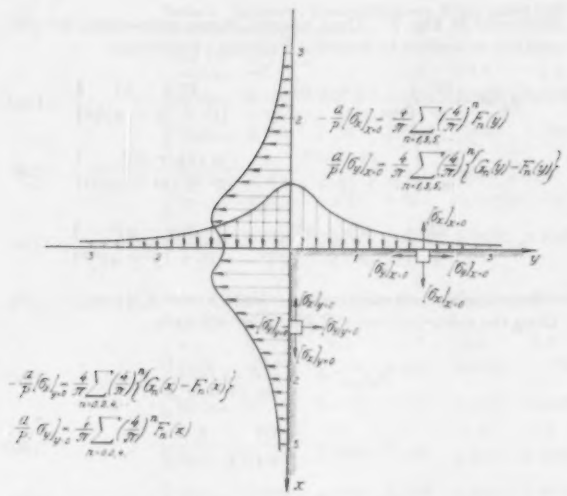

Fig. 5 Distribution of boundary loads on the two overlapping half-planes, in the solution for the quarter-plane under a concentrated normal force

$$F_{n+1}(y) = \int_0^\infty \frac{x^2 y}{(x^2 + y^2)^2} F_n(x)dx,$$

we find that successive terms on the left side of Equation (9a) will cancel out in pairs. The same argument also holds for Equation (9b), once we remove F_0 which occurs on the left side of this equation as well as the right side. From another point of view, these F-functions may be regarded as solutions of the simultaneous integral equations in Equations (9a) and (9b). Or, the procedure may be looked upon as an analytically performed "systematic relaxation of constraints," since at each reversal of the loading on one of the boundaries the other boundary is temporarily restrained against normal displacements by the condition of symmetry.

The boundary stresses, $[\sigma_x]_{y=0}$ and $[\sigma_y]_{x=0}$, in the resulting quarter-plane, due to a concentrated P-force at an a-distance from the vertex, are obtained in a similar manner as

$$-\frac{a}{P}[\sigma_x]_{y=0} = \frac{4}{\pi} \sum_{n=0,\,2,\,4,\,\ldots} \left(\frac{4}{\pi}\right)^n \{G_n(x) - F_n(x)\}, \tag{10a}$$

$$\frac{a}{P}[\sigma_y]_{x=0} = \frac{4}{\pi} \sum_{n=1,\,3,\,5,\,\ldots} \left(\frac{4}{\pi}\right)^n \{G_n(y) - F_n(y)\} \tag{10b}$$

Table 1 Boundary loads on the two overlapping half-planes, Fig. 5, used in the solution for a concentrated normal force on the quarter-plane

$\log_e x$ or $\log_e y$	−5.0	−3.0	−2.0	−1.4	−1.0	−0.8	−0.6	−0.4	−0.2	0	0.2
$\frac{a}{P}[\sigma_x]_{y=0}$	−0.5000	−0.4999	−0.4804	−0.4353	−0.3820	−0.3483	−0.3110	−0.2713	−0.2309	−0.1915	−0.1548
$\frac{a}{P}[\sigma_y]_{x=0}$	0.5000	0.5010	0.5193	0.5586	0.5885	0.5939	0.5840	0.5524	0.4962	0.4194	0.3326
$\log_e x$, or $\log_e y$	0.4	0.6	0.8	1.0	1.2	1.4	1.6	1.8	2.0	3.0	4.0
$\frac{a}{P}[\sigma_x]_{y=0}$	−0.1219	−0.0937	−0.0703	−0.0517	−0.0373	−0.0265	−0.0185	−0.0128	−0.0088	−0.0012	−0.0002
$\frac{a}{P}[\sigma_y]_{x=0}$	0.2482	0.1759	0.1199	0.0796	0.0522	0.0340	0.0221	0.0145	0.0095	0.0012	0.0002

By overlapping these two half-planes in a manner shown in Fig. 5, we obtain for the resulting quarter-plane (x, 0, y) the required solution.

As was stated at the beginning, the required boundary conditions for this quarter-plane are

$$[\sigma_x]_{x=0} = 0 \tag{8a}$$

and

$$[\sigma_y]_{x=0} = \frac{4P}{\pi a} F_0(x) \tag{8b}$$

By means of the F-functions, these two boundary conditions can be written in the form:

$$\int_0^\infty \left\{\frac{P}{a}\frac{4}{\pi} \sum_{n=0,\,2,\,4,\,\ldots}^{\infty} \left(\frac{4}{\pi}\right)^n F_n(x)\right\} \frac{4}{\pi} \frac{x^2 y}{(x^2 + y^2)^2} dx - \frac{P}{a}\frac{4}{\pi} \sum_{n=1,\,3,\,5,\,\ldots}^{\infty} \left(\frac{4}{\pi}\right)^n F_n(y) = 0, \tag{9a}$$

$$-\int_0^\infty \left\{\frac{P}{a}\frac{4}{\pi} \sum_{n=1,\,3,\,5,\,\ldots}^{\infty} \left(\frac{4}{\pi}\right)^n F_n(y)\right\} \frac{4}{\pi} \frac{xy^2}{(x^2 + y^2)^2} dy + \frac{P}{a}\frac{4}{\pi} \sum_{n=0,\,2,\,4,\,\ldots}^{\infty} \left(\frac{4}{\pi}\right)^n F_n(x) = \frac{4P}{\pi a} F_0(x) \tag{9b}$$

The fact that these boundary conditions are satisfied becomes obvious by a simple inspection of the sequence of the F-functions given in Equations (6). Since

The numerical evaluation of this solution was made on an IBM-650 electronic digital computer, carrying the calculation up to $n = 20$ terms, which provided in the resulting stress components an accuracy of at least 4 correct decimals. Characteristic values of the boundary-load ordinates for the two half-planes are given in Table 1, in the original logarithmic scale in which the calculation was performed. It is to be noted that these loading functions are discontinuous at the origin. While $[\sigma_x]_{x=0} \to [\sigma_y]_{y=0} \to 1/2$ as x or $y \to 0$, at $x = y = 0$ we have $[\sigma_x]_{x=0} = [\sigma_y]_{y=0} = 0$. This follows from the fact that $F_0(x)$ was zero at $x = 0$ and the stress remained zero at the vertex at each reversal of the loading.

The boundary-stress values are given, in a linear scale, in Table 2 and graphically represented in Fig. 6. These values are essentially the same, though more accurate, than the ones derived by W. M. Shepherd[3] through a different approach. For points sufficiently removed from the point of application of the P-load (for instance, for $x \geq 5$ and $y \geq 5$) the stress components approach asymptotically the values

$$[\sigma_x]_{y=0} = -\frac{P}{a}\left\{\frac{4\pi}{\pi^2 - 4}\frac{1}{x} - \frac{2}{x^2}\right\}, \tag{11a}$$

$$[\sigma_y]_{x=0} = \frac{P}{a}\left\{\frac{8}{\pi^2 - 4}\frac{1}{y} - \frac{2}{y^2}\right\}, \tag{11b}$$

These are the results of a replacement of the original P-load, acting at an a distance from the vertex, by its statically equivalent

[3] W. M. Shepherd, "Stress Systems in an Infinite Sector," *Proceedings of the Royal Society*, London, England, series A, vol. 148, 1935, pp. 284–303.

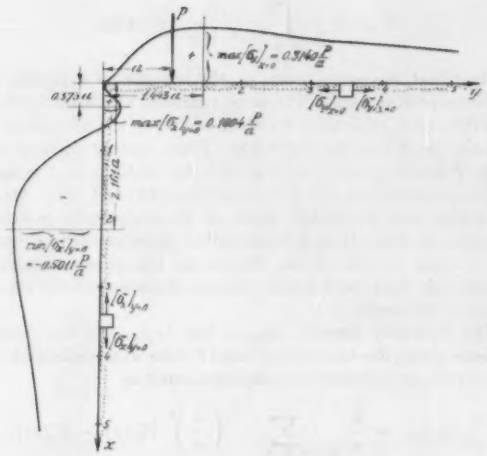

Fig. 6 Boundary stresses in the quarter-plane loaded by a concentrated normal force

Table 2 Boundary stresses in the quarter-plane, loaded by a concentrated normal force P, at an a-distance from the vertex, Fig. 6

x or y	0	0.1	0.2	0.3	0.4	0.5	0.6	0.7	0.8	0.9	1.0
$\frac{a}{P}[\sigma_x]_{y=0}$	0	0.0148	0.0584	0.0924	0.0993	0.0767	0.0303	−0.0312	−0.0994	−0.1677	−0.2315
$\frac{a}{P}[\sigma_y]_{x=0}$	0	0.0139	0.0618	0.1143	0.1612	0.2002	0.2314	0.2557	0.2743	0.2882	0.2983
x or y	1.2	1.4	1.6	1.8	2.0	2.5	3.0	3.5	4.0	4.5	5.0
$\frac{a}{P}[\sigma_x]_{y=0}$	−0.3376	−0.4122	−0.4595	−0.4863	−0.4986	−0.4932	−0.4656	−0.4326	−0.4002	−0.3704	−0.3437
$\frac{a}{P}[\sigma_y]_{x=0}$	0.3100	0.3139	0.3128	0.3086	0.3025	0.2835	0.2633	0.2441	0.2267	0.2111	0.1972

loading at the vertex, consisting of a P-force and a clock-wise Pa-couple.

Stress components for points within the boundaries of the quarter-plane can be calculated in a similar manner from the boundary loadings given for the two half-planes in Table 1, and adding these values to the original stress components defined by Equations (1a, b, c).

Concentrated Force Tangential to Boundary

In deriving the solution for the quarter-plane under a single concentrated tangential force at the boundary, we will start with a corresponding symmetrical loading case on the half-plane, as

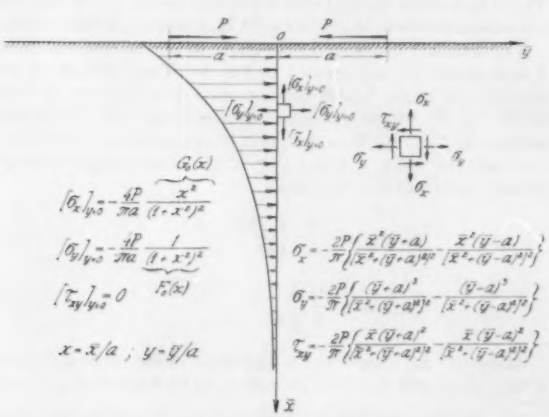

Fig. 7 Initial loading condition used in deriving solution for the quarter-plane subjected to a single concentrated tangential force

illustrated in Fig. 7. The Cartesian stress components for this case can be written by means of Flamant's solution as

$$\sigma_x = -\frac{2P}{\pi}\left\{\frac{\bar{x}^2(\bar{y}+a)}{[\bar{x}^2+(\bar{y}+a)^2]^2} - \frac{\bar{x}^2(\bar{y}-a)}{[\bar{x}^2+(\bar{y}-a)^2]^2}\right\} \quad (12a)$$

$$\sigma_y = -\frac{2P}{\pi}\left\{\frac{(\bar{y}+a)^3}{[\bar{x}^2+(\bar{y}+a)^2]^2} - \frac{(\bar{y}-a)^3}{[\bar{x}^2+(\bar{y}-a)^2]^2}\right\} \quad (12b)$$

$$\tau_{xy} = -\frac{2P}{\pi}\left\{\frac{\bar{x}(\bar{y}+a)^2}{[\bar{x}^2+(\bar{y}+a)^2]^2} - \frac{\bar{x}(\bar{y}-a)^2}{[\bar{x}^2+(\bar{y}-a)^2]^2}\right\} \quad (12c)$$

Introducing dimensionless co-ordinates, $x = \bar{x}/a$ and $y = \bar{y}/a$, along the axis of symmetry ($y = 0$) we will have

$$[\sigma_x]_{y=0} = -\frac{4P}{\pi a}\frac{x^2}{(1+x^2)^2} \quad (13a)$$

$$[\sigma_y]_{y=0} = -\frac{4P}{\pi a}\frac{1}{(1+x^2)^2} \quad (13b)$$

$$[\tau_{xy}]_{y=0} = 0 \quad (13c)$$

As in the preceding case, the derivation of the solution will again consist in removing the distributed normal load, $[\sigma_y]_{y=0}$, from the 0, x-boundary of the quarter-plane. The sequence of F and G-functions used for this purpose will be generated according to the same scheme as before, shown by Equations (6), with the only exception that for the initial step we will have now

$$F_0(x) = \frac{1}{(1+x^2)^2} \quad \text{and} \quad G_0(x) = \frac{x^2}{(1+x^2)^2} \quad (14)$$

The solution for the quarter-plane under a distributed tensile load, of the magnitude defined by Equation (13b), will be represented in a similar manner by two overlapping half-planes, loaded on their respective boundaries by normal loads according to Equations (7a) and (7b). These distributed normal loads were evaluated numerically, using 20 terms of the corresponding series of F-functions, and the results are given in Table 3. The boundary stresses in the resulting quarter-plane will be defined by the same formulas as before, Equations (10a) and (10b), the only difference being that along the y-axis we will have to add now the boundary stress resulting from the basic loading condition represented in Fig. 7. This, according to Equation (12b), is of the magnitude

$$[\sigma_y^*]_{x=0} = -\frac{2P}{\pi a}\left\{\frac{1}{1+y} + \frac{1}{1-y}\right\} \quad (15)$$

In the preceding case no correction of this kind was needed, since concentrated normal forces produce no boundary stresses in the half-plane.

The final values of the boundary stresses for the quarter-plane loaded by a single concentrated P-force, tangential to the boundary and at an a-distance from the corner of the quadrant, are given in Table 4 and plotted in Fig. 8.

Table 3 Boundary loads on the two overlapping half-planes, used in the solution for a concentrated tangential force on the quarter-plane

$\log_e x$ or $\log_e y$	−5.0	−3.0	−2.0	−1.4	−1.0	−0.8	−0.6	−0.4	−0.2	0	0.2
$\frac{a}{P}[\sigma_x]_{x=0}$	−2.5662	−2.0508	−1.3860	−0.9806	−0.7230	−0.6036	−0.4935	−0.3946	−0.3082	−0.2352	−0.1753
$\frac{a}{P}[\sigma_y]_{y=0}$	3.8394	2.7011	2.0818	1.6904	1.3845	1.2090	1.0187	0.8201	0.6254	0.4500	0.3061
$\log_e x$ or $\log_e y$	0.4	0.6	0.8	1.0	1.2	1.4	1.6	1.8	2.0	3.0	4.0
$\frac{a}{P}[\sigma_x]_{x=0}$	−0.1279	−0.0914	−0.0641	−0.0443	−0.0302	−0.0204	−0.0137	−0.0092	−0.0061	−0.0008	−0.0001
$\frac{a}{P}[\sigma_y]_{y=0}$	0.1988	0.1252	0.0778	0.0485	0.0307	0.0197	0.0129	0.0085	0.0057	0.0008	0.0001

Table 4 Boundary stresses in the quarter-plane, loaded by a concentrated tangential force P, at an a-distance from the vertex, Fig. 8

x or y	0	0.1	0.2	0.3	0.4	0.5	0.6	0.7	0.8	0.9	1.0
$\frac{a}{P}[\sigma_x]_{y=0}$	0	0.0181	−0.0005	−0.0728	−0.1796	−0.2986	−0.4122	−0.5098	−0.5871	−0.6435	−0.6814
$\frac{a}{P}[\sigma_y]_{x=0}$	0	0.0171	0.0022	−0.0716	−0.2080	−0.4214	−0.7514	−1.2999	−2.3828	−5.5896	$\mp\infty$
x or y	1.2	1.4	1.6	1.8	2.0	2.5	3.0	3.5	4.0	4.5	5.0
$\frac{a}{P}[\sigma_x]_{y=0}$	−0.7133	−0.7070	−0.6805	−0.6450	−0.6068	−0.5164	−0.4425	−0.3845	−0.3388	−0.3022	−0.2725
$\frac{a}{P}[\sigma_y]_{x=0}$	3.8860	2.2479	1.6745	1.2438	1.1757	0.8895	0.7258	0.6163	0.5369	0.4761	0.4281

At points sufficiently removed from the point of application of the above force (for $x \geq 5$ and $y \geq 5$, for instance), the boundary stresses will approach asymptotically the values

$$[\sigma_x]_{y=0} = -\frac{P}{x}\frac{8}{\pi^2 - 4} \tag{16a}$$

and

$$[\sigma_y]_{x=0} = \frac{P}{y}\frac{4\pi}{\pi^2 - 4}, \tag{16b}$$

which are the results of a replacement of the original loading by a statically equivalent force at the vertex.

Partially Distributed Uniform Loadings

Here we will first consider the case when the loaded region on the boundary extends from $y = 1$ to $y = 2$. A satisfactory numerical answer to this problem may be derived in replacing small sections of this distributed load by equivalent concentrated forces, and using the results obtained for the first loading case in this paper. However, it is believed that the results will have a greater degree of accuracy if we proceed in the same manner as in the previous solutions, that is, by canceling the unwanted boundary loads in successive stages.

We begin with the corresponding symmetrical load on the half-plane, as shown in Fig. 9. The Cartesian stress components along the x-axis of symmetry will be now

$$[\sigma_x]_{y=0} = -\frac{4q}{\pi} G_0(x), \tag{17a}$$

$$[\sigma_y]_{y=0} = -\frac{4q}{\pi} F_0(x), \tag{17b}$$

where

$$F_0(x) = \tfrac{1}{2}\left\{\tan^{-1}\frac{2}{x} - \tan^{-1}\frac{1}{x} - \frac{2x}{4 + x^2} + \frac{x}{1 + x^2}\right\},$$

and

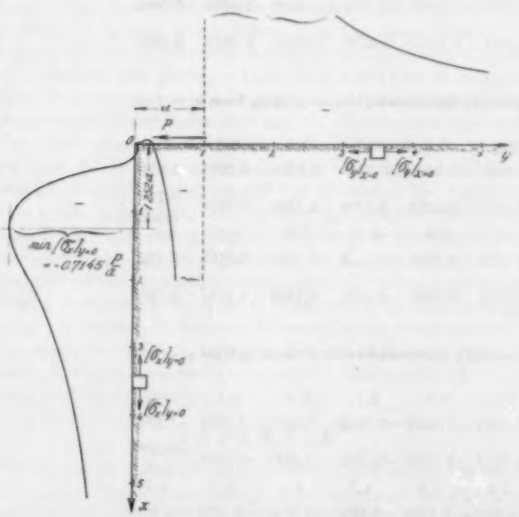

Fig. 8 Boundary stresses in the quarter-plane loaded by a concentrated tangential force

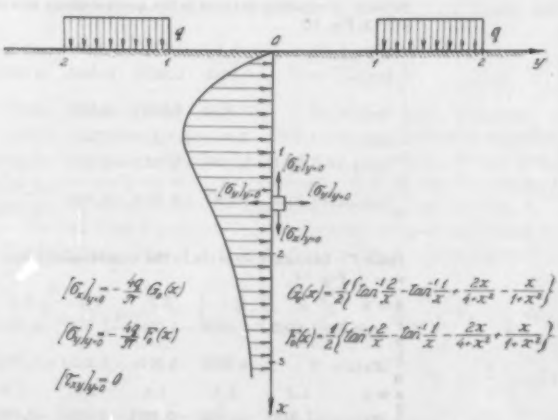

Fig. 9 Initial loading condition used in deriving solution for the quarter-plane subjected to partially distributed uniform loading

$$G_0(x) = {}^1/_2\left\{\tan^{-1}\frac{2}{x} - \tan^{-1}\frac{1}{x} + \frac{2x}{4+x^2} - \frac{x}{1+x^2}\right\}$$

Using these F_0 and G_0-functions as bases in the recursion scheme, given by Equations (6), the equivalent boundary loads and boundary stresses will be obtained in the same form as stated previously by Equations (7*a*, *b*) and (10*a*, *b*), respectively. The corresponding boundary-load ordinates for the two overlapping half-planes are given in Table 5. The final boundary stresses are obtained by adding to the stresses produced by these combined loadings, between $y = 1$ and $y = 2$, a compressive stress of the same intensity as that of the applied load, in accordance with the equivalent solution for the half-plane. The resulting boundary-stress values are listed in Table 6, and graphically represented in Fig. 10.

It can be shown that from the results obtained for the foregoing specific loading condition, one can derive by superposition a solution for partially distributed loads extending between any two arbitrarily chosen points on the boundary of the quarter-plane. As an example, we give here the solution for the case when the uniformly distributed load extends from $y = 0$ to $y = 1$, Table 7 and Fig. 11. The steps taken in the derivation of these results are indicated in the insert in Fig. 11. It is seen that every element involves a partially distributed loading, the length of which is the same as the distance of its beginning from the corner. It is interesting to note that, while in a half-plane a partially distributed loading produces no tensile stress along the boundary, the same load on the quarter-plane, as shown in Fig. 11, produces tensile stresses whose maximum value is more than 2/3 of that of the applied compression.

A solution for a similar case, when the partially distributed load is applied symmetrically on both sides of the quarter-plane,

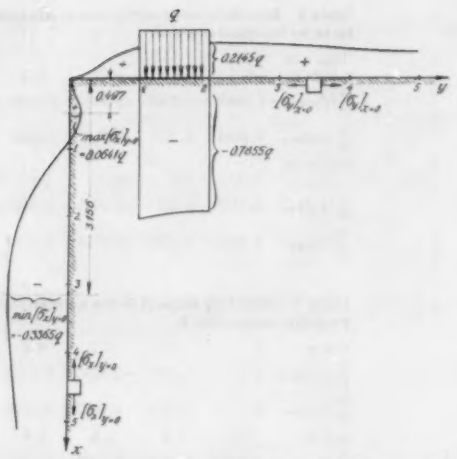

Fig. 10 Boundary stresses in the quarter-plane due to a partially distributed uniform loading from $y = 1$ to $y = 2$

was given previously by C. J. Tranter[4] by means of the Mellin transform, without any numerical evaluation of the results.

Conclusions

It is to be noted that each of the loading cases analyzed in the paper involves only one parameter, representing the distance of the load from the corner. These results are, therefore, basic

[4] C. J. Tranter, "The Use of the Mellin Transform in Finding the Stress Distribution in an Infinite Wedge," *The Quarterly Journal of Mechanics and Applied Mathematics*, vol. 1, 1948, pp. 125–130.

Table 5 Boundary loads on the two overlapping half-planes, used in the solution for a partially distributed loading on the quarter-plane, from $y = 1$ to $y = 2$

$\log_e x$ or $\log_e y$	−5.0	−3.0	−2.0	−1.4	−1.0	−0.8	−0.6	−0.4	−0.2	0	0.2
$\frac{1}{q}[\sigma_x]_{x=0}$	−0.3462	−0.3470	−0.3405	−0.3215	−0.2959	−0.2782	−0.2574	−0.2336	−0.2077	−0.1805	−0.1513
$\frac{1}{q}[\sigma_y]_{y=0}$	0.3462	0.3459	0.3525	0.3703	0.3901	0.3999	0.4061	0.4051	0.3927	0.3659	0.3246
$\log_e x$ or $\log_e y$	0.4	0.6	0.8	1.0	1.2	1.4	1.6	1.8	2.0	3.0	4.0
$\frac{1}{q}[\sigma_x]_{x=0}$	−0.1268	−0.1023	−0.0806	−0.0620	−0.0466	−0.0343	−0.0248	−0.0176	−0.0124	−0.0018	−0.0003
$\frac{1}{q}[\sigma_y]_{y=0}$	0.2726	0.2162	0.1623	0.1160	0.0798	0.0534	0.0352	0.0230	0.0150	0.0019	0.0003

Table 6 Boundary stresses in the quarter-plane due to a partially distributed uniform loading from $y = 1$ to $y = 2$, Fig. 10

x or y	0	0.1	0.2	0.3	0.4	0.5	0.6	0.7	0.8	0.9	1.0
$\frac{1}{q}[\sigma_x]_{y=0}$	0	0.0043	0.0233	0.0443	0.0591	0.0641	0.0587	0.0440	0.0220	−0.0049	−0.0349
$\frac{1}{q}[\sigma_y]_{x=0}$	0	0.0039	0.0237	0.0491	0.0747	0.0983	0.1193	0.1374	0.1528	0.1657	0.1765 −0.8235
x or y	1.2	1.4	1.6	1.8	2.0	2.5	3.0	3.5	4.0	4.5	5.0
$\frac{1}{q}[\sigma_x]_{y=0}$	−0.0971	−0.1553	−0.2051	−0.2453	−0.2763	−0.3213	−0.3358	−0.3339	−0.3239	−0.3104	−0.2956
$\frac{1}{q}[\sigma_y]_{x=0}$	−0.8073	−0.7967	−0.7903	−0.7868	−0.7855 0.2145	0.2117	0.2045	0.1955	0.1860	0.1767	0.1678

Table 7 Boundary stresses in the quarter-plane due to a partially distributed uniform loading from $y = 0$ to $y = 1$, Fig. 11

x or y	0	0.1	0.2	0.3	0.4	0.5	0.6	0.7	0.8	0.9	1.0
$\frac{1}{q}[\sigma_x]_{y=0}$	−1.0000	−1.0028	−1.0261	−1.0567	−1.0852	−1.1053	−1.1154	−1.1156	−1.1072	−1.1915	−1.0704
$\frac{1}{q}[\sigma_y]_{x=0}$	0	−0.0037	−0.0274	−0.0623	−0.1020	−0.1422	−0.1815	−0.2191	−0.2548	−0.2878	−0.3187 0.6813
x or y	1.2	1.4	1.6	1.8	2.0	2.4	2.8	3.2	3.6	4.0	4.8
$\frac{1}{q}[\sigma_x]_{y=0}$	−1.0183	−0.9602	−0.9021	−0.8462	−0.7941	−0.7029	−0.6276	−0.5657	−0.5138	−0.4702	−0.4014
$\frac{1}{q}[\sigma_y]_{x=0}$	0.6258	0.5776	0.5355	0.4990	0.4668	0.4130	0.3699	0.3345	0.3054	0.2808	0.2418

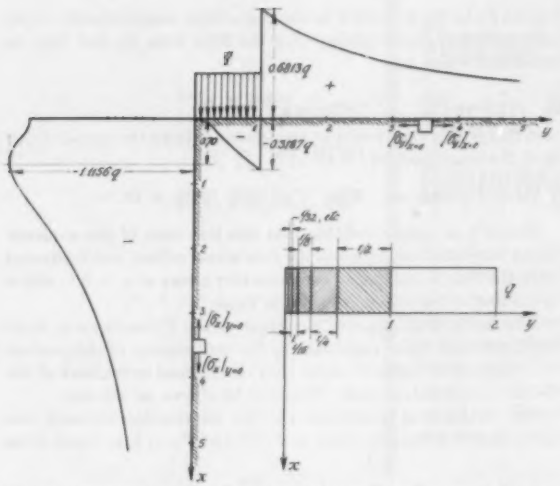

Fig. 11 Boundary stresses in the quarter-plane due to a partially distributed uniform loading from $y = 0$ to $y = 1$

solutions which can be easily combined or superimposed to derive answers to a large variety of problems. This approach is not limite to boundary loadings. Starting, for instance, with the solutions of E. Melan[6] for the elastic half-plane loaded by concentrated forces in its interior, the unwanted boundary loadings can be eliminated in an identical manner, to produce equivalent solutions for the quarter-plane.

The procedure presented here can also be used in the analysis of infinite wedges of any angle of opening, as long as the angle is less than π, or to derive solutions for cognate three-dimensional problems, such as the quarter-space under an arbitrarily placed loading. The amount of computational work required in such cases would be, of course, much more extensive.

It may be well to comment here on the possibility of checking the foregoing results by experimental means. It seems that the first loading case, that of a concentrated normal force at some distance from the corner, should be easy to reproduce in a photoelastic test. However, on further consideration we find that there are some basic difficulties in this regard. From the analytical results it is seen, for instance, that the magnitude of the stresses does not decrease very rapidly from the point of application of the load and, therefore, there always will be a considerable difference between the infinite plate considered here and any finite plate, no matter how wide it may be. Taking, as an example, a finite plate whose width is 20 times the distance of the applied load from the corner, we find that the boundary stress disregarded in this case would be still 1/5 of that of the maximum tensile stress in the plate. We also find that in a test the normality of the load to the boundary would have to be ascertained with an unusually high degree of precision. In comparing the analytical results for the normal and the tangential concentrated forces, it is seen that even 1-deg angle of deviation of the load from the normal will cause a 10 per cent difference in the boundary-stress value at a point as far as twice the distance of the load from the corner. For points nearer to the load the difference would be, of course, very much greater.

APPENDIX

The convergence and accuracy of the method used in the paper will be demonstrated here by means of the first example, that of a concentrated normal force on the boundary.

If we take the expression for σ_y in Equation (1*b*) and integrate it with respect to x between the limits of 0 and ∞, we find that

$$\int_0^\infty \sigma_y dx = -\frac{2P}{\pi}\int_0^\infty \left\{\frac{x(y+a)^2}{[x^2+(y+a)^2]^2} + \frac{x(y-a)^2}{[x^2+(y-a)^2]^2}\right\} dx = -\frac{2P}{\pi}$$

The result, which is the total horizontal force resultant or total lateral thrust acting on a vertical section of the elastic half-plane, is seen to be independent of the position (a) of the normal load on the boundary, or of the location (y) where the vertical section is taken. Since any normal loading on the boundary may be regarded as consisting of concentrated-load elements, it can be stated in general that in an elastic half-plane:

$$\text{Total lateral thrust} = \frac{1}{\pi} \times (\text{total normal load on boundary}) \quad (a)$$

This relationship will be used now to derive the area of any of the F-functions used in the solution. First we have, from Equation (2*b*),

$$\int_0^\infty [\sigma_y]_{y=0}\, dx = -\frac{4P}{\pi a}\int_0^\infty \frac{x}{(1+x^2)^2}\, dx = -\frac{4P}{\pi a}\int_0^\infty F_0(x)dx = -\frac{2P}{\pi a},$$

which gives

$$\int_0^\infty F_0(x)dx = \frac{1}{2}$$

Taking now the first step in our sequence of boundary-load reversals, we find that in Fig. 2 the total normal load on the boundary of the $y > 0$ half-plane is twice the area of $F_0(x)$ multiplied by $4P/\pi a$. Therefore from Equation (3*a*) we get

$$\int_0^\infty [\sigma_x]_{x=0}dy = \frac{P}{a}\left(\frac{4}{\pi}\right)^2\int_0^\infty F_1(y)dy = \frac{1}{\pi}\,\frac{4P}{\pi a},$$

or

$$\int_0^\infty F_1(y)dy = \frac{1}{4}$$

A continuation of this process leads to the general formula that

$$\text{Area of } F_n = \frac{1}{2^{n+1}} \quad (b)$$

The areas of the successive F-functions form, therefore, a simple geometric progression. This makes it possible to establish explicit formulas for the limits of the magnitude of the total boundary loads on the two overlapping half-planes, by means of which the solution for the quarter-plane was derived, Fig. 5.

We find from Equation (7*a*), for the total normal load acting on the boundary (from $x = 0$ to $x = \infty$) of the $y > 0$ half-plane:

$$\frac{a}{P}\int_0^\infty [\sigma_y]_{y=0}dx = \int_0^\infty \left\{\frac{4}{\pi}\sum_{n=0,\,2,\,4,\,\ldots}^{\infty}\left(\frac{4}{\pi}\right)^n F_n(x)\right\} dx = \frac{2\pi}{\pi^2-4} \quad (c)$$

Similarly we get, from Equation (7*b*), for the total boundary load on the $x > 0$ half-plane, from $y = 0$ for $y = \infty$, the value

[6] E. Melan, "Der Spannungszustand der durch eine Einzelkraft im Innern beanspruchten Halbscheibe," *Zeitschrift für angewandte Mathematik und Mechanik*, vol. 12, 1932, pp. 343–346; vol. 20, 1940, p. 368.

$$-\frac{a}{P}\int_0^\infty [\sigma_x]_{x=0}dy = \int_0^\infty \left\{\frac{4}{\pi}\sum_{n=1,3,5,\ldots}^{\infty}\left(\frac{4}{\pi}\right)^n F_n(y)\right\} dy$$

$$= \frac{4}{\pi^2 - 4} \quad (d)$$

Applying here again the relationship from Equation (a) to the combination of the loads defined by the last two equations, we find that

$$\frac{P}{a}\,\frac{2\pi}{\pi^2-4} - 2\,\frac{1}{\pi}\,\frac{P}{a}\,\frac{4}{\pi^2-4} = \frac{2P}{\pi a}$$

This means that the total lateral thrust on any vertical section (y = const) of the quarter-plane subjected to a concentrated normal force, Fig. 6, will be equal to zero, thus fulfilling the condition that there cannot be a horizontal force resultant in this case.

The limit values for the boundary loads in Equations (c) and (d) were obtained for the case when $n \to \infty$. In the same manner, however, we can derive corresponding values for the finite, n = 20, sum of the F_n-functions used in the numerical evaluation of the solutions. Thus we get

$$\int_0^\infty \left\{\frac{4}{\pi}\sum_{n=0,2,4,\ldots}^{n=20}\left(\frac{4}{\pi}\right)^n F_n(x)\right\} dx$$

$$= \frac{2}{\pi^2-4}\left\{1 - \left(\frac{2}{\pi}\right)^{22}\right\} \quad (e)$$

and

$$\int_0^\infty \left\{\frac{4}{\pi}\sum_{n=1,3,5,\ldots}^{n=19}\left(\frac{4}{\pi}\right)^n F_n(y)\right\} dy$$

$$= \frac{4}{\pi^2-4}\left\{1 - \left(\frac{2}{\pi}\right)^{20}\right\} \quad (f)$$

The difference, represented by the powers of $2/\pi$ on the right side of these equations, is found to be in each case about one hundredth of one per cent of the load. Hence the degree of approximation afforded by 20 terms is found to be extremely high. Furthermore, it is interesting to note that the contribution of the higher F_n-terms is limited to the immediate neighborhood of the corner of the quarter-plane. For the 20th term we find that its maximum value is

$$[F_{20}]_{max} = 455\,6 \times 10^{-6},$$

and this peak value occurs at an x-distance from the corner which is of the magnitude of

$$\log_e x = -20.4, \qquad \text{or } x = 1.382 \times 10^{-9}$$

Hence it is understandable that this last term of the sequence had a very small influence on the final stress values, and it affected only the fourth decimal in the boundary stress at $x = 0.1$, which is the first of the ordinates listed in Table 2.

The rapid diminution of the areas of the F-functions is, however, only one of the requisites for the convergence of the process. In addition, we have to prove that the successive maxima of the F-functions are bounded. This can be shown as follows:

On the basis of Equations (6) the relationship between two successive F-functions, such as $F_n(x)$ and $F_{n+1}(y)$, is found to be

$$F_{n+1}(y) = \int_0^\infty \frac{x^2 y}{(x^2+y^2)^2} F_n(x)dx$$

Replacing now $F_n(x)$ by its maximum ordinate $[F_n(x)]_{max}$, we can write that

$$[F_{n+1}(y)]_{max} < [F_n(x)]_{max}\int_0^\infty \frac{x^2 y}{(x^2+y^2)}\,dx$$

Since the value of the integral on the right side of the foregoing equation is $\pi/4$, we find that

$$[F_{n+1}]_{max} < \frac{\pi}{4}\,[F_n]_{max}$$

This last result, in conjunction with that in Equation (b), provides a complete proof of the convergence of the process.

Though the foregoing proof was established by using the first loading case as an example, the arguments employed here are valid, of course, in the other loading conditions for which solutions have been obtained in the paper.

H. G. LANDAU[1]
J. H. WEINER[2]
E. E. ZWICKY, JR.[3]

Thermal Stress in a Viscoelastic-Plastic Plate With Temperature-Dependent Yield Stress

Equations are given for the determination of transient and residual stresses in plates subject to transient temperature distributions, based on the assumption of a viscoelastic, perfectly plastic material obeying a von Mises temperature-dependent yield condition. A numerical procedure for integrating the equations is developed and applied to the case of a symmetrically cooled plate. It is found that, for steel, viscoelasticity has little effect on the residual stress distribution, but the temperature dependence of yield stress is important. The types of residual stress distribution after cooling are similar to those for an elastic-plastic material with constant yield stress, and for this case the residual stress is given approximately by formulas developed earlier for a slowly varying heat input.

1 Introduction

In the heat-treatment of metals, the transient temperature distribution will frequently result in the development of transient stresses large enough to cause plastic flow during the process, and there will then be residual stresses in the body after completion of the treatment. At the same time viscoelastic effects will occur which may affect the magnitude of these residual stresses. In this paper a thermal stress analysis of a plate is given in which these two types of inelastic behavior are included. The plasticity theory employed uses the temperature-dependent von Mises yield condition for perfectly plastic solids. The viscous effects are expressed by a Maxwell type relation, and residual stress calculations made with a viscosity coefficient which is a function of temperature, but more general, nonlinear viscous behavior can be included. The other mechanical and thermal properties of the material are assumed to be temperature independent.

Thermal stress analyses for an elastic, perfectly plastic free plate have been given [1],[4] [2], [3] using a material model with temperature-independent yield condition. Special temperature distributions were considered in [1] and [3], while [2] considered a temperature varying arbitrarily in the direction normal to the face of the plate and in time. The present paper is an extension of the results of [2] using a material model, which, although still an idealization, is closer to representing the behavior of metal at high temperature and stress levels.

The stress-strain relations are formulated in Section 2 and applied in Section 3 to the problem of a plate with a symmetrical temperature distribution varying with time and the thickness coordinate. Equations are obtained for the time rate of change of stress in terms of the existing stress state, and the rate of change of temperature.

Analytical integration of the stress-rate equations does not seem possible, and a numerical method is outlined in Section 4. Calculations of residual stress distribution were made for the case of a plate cooled from an initially uniform temperature, and some typical results and conclusions are presented in Section 5.

2 Stress-Strain Relations

Since, under hydrostatic stress, materials behave almost perfectly elastically, it is convenient to decompose the stress and strain tensors, σ_{ij} and ϵ_{ij}, into their mean portions $(1/3)\sigma_{kk}$ and $(1/3)\epsilon_{kk}$, and deviatoric portions, s_{ij} and e_{ij}.

Then the mean strain rate is given by

$$^1/_3\dot{\epsilon}_{kk} = \frac{1-2\nu}{3E}\,\dot{\sigma}_{kk} + \alpha\dot{T} \tag{1}$$

where the superposed dot is used for differentiation with respect to time, ν is Poisson's ratio, E is Young's modulus, α is the coefficient of linear thermal expansion, and T is temperature.

The deviatoric strain rate may be taken [4] as the sum of three parts, elastic, viscous, and plastic:

$$\dot{e}_{ij} = \dot{e}_{ij}{}^E + \dot{e}_{ij}{}^V + \dot{e}_{ij}{}^P \tag{2}$$

The elastic strain rate is given by the usual relation

$$\dot{e}_{ij}{}^E = \frac{1}{2G}\,\dot{s}_{ij} \tag{3}$$

where $G = E/2(1+\nu)$ is the elastic shear modulus.

For the viscous strain rate, we use the relations of the same form as that for the Maxwell body of viscoelasticity[5] theory,

[1] Research Associate in Mechanical Engineering; Mathematician, Heat and Mass Flow Analyzer Laboratory, Columbia University, New York, N. Y.

[2] Associate Professor in Mechanical Engineering; Consultant, Heat and Mass Flow Analyzer Laboratory, Columbia University, New York, N. Y. Mem. ASME.

[3] Supervisor, Stress Analysis Engineering, Large Steam Turbine-Generator Department, General Electric Company, Schenectady, N. Y. Mem. ASME.

[4] Numbers in brackets designate References at end of paper.

Contributed by the Applied Mechanics Division and presented at the Annual Meeting, Atlantic City, N. J., November 29–December 4, 1959, of The American Society of Mechanical Engineers.

Discussion of this paper should be addressed to the Secretary, ASME, 29 West 39th Street, New York, N. Y., and will be accepted until July 10, 1960, for publication at a later date. Discussion received after the closing date will be returned.

Note: Statements and opinions advanced in papers are to be understood as individual expressions of their authors and not those of the Society. Manuscript received by ASME Applied Mechanics Division, March 9, 1959. Paper No. 59—A-33.

[5] The term viscoelasticity is used to refer to processes which are essentially time dependent, such as creep and stress relaxation. Plasticity is reserved for time-independent material behavior, in accordance with the usual terminology in theoretical formulations of the subject, despite the use of terms such as strain rate. It will be seen that time enters homogeneously in the plastic stress-strain relations.

that is

$$\dot{e}_{ij}{}^{V} = \frac{1}{2\eta}\, \dot{s}_{ij} \tag{4}$$

where η is the coefficient of viscosity. In using this relation, η need not be restricted to be a constant or function of temperature alone, but can be a more general function depending also on stress. Then Equation (4) can be used to represent a wide range of viscoelastic behavior.

In the calculations to be described, only the temperature dependence of η is included using the relation [5]:

$$\eta = c_0 e^{\frac{c_1}{T+460}} \tag{5}$$

where T is in degrees F.

The plastic stress-strain relations used here are given by the temperature dependent von Mises yield condition for the perfectly plastic solid and the associated flow rules. These relations can be obtained as a special case of the possible plasticity laws satisfying the general requirements for a plastic flow theory; that is, strain rate independent of the time scale, the condition of irreversibility, and for an isothermal work-hardening solid, the condition of stability. Starting with the assumption that there is a function, $f(s_{ij}, e_{ij}{}^{P}, T)$, the yield condition, such that plastic flow occurs only during a period when $f = 0$, and assuming a very general form for the flow rate in accordance with the foregoing requirements, it can be shown that the yield condition must satisfy certain limitations and that the flow rules are then determined by the yield condition. Detailed discussion of these general considerations has been given by Prager [6, 7].

The particular form of the yield condition used here is

$$f(s_{ij}, T) = {}^{1}/_{2} s_{ij} s_{ij} - k^2(T) = J_2 - k^2(T) \tag{6}$$

where J_2 is the second invariant of the deviatoric stress tensor and $k(T)$ is the yield stress in simple shear at temperature T.

The flow rules associated with this yield condition are

$$\dot{e}_{ij}{}^{P} = 0, \quad \text{if } f < 0, \text{ or if } f = 0, \ \dot{f} < 0$$

$$\dot{e}_{ij}{}^{P} = \mu s_{ij}, \quad \text{if } f = 0, \ \dot{f} = 0, \ \mu = \frac{s_{ij}\dot{e}_{ij}{}^{P}}{2k^2(T)} \geq 0 \tag{7}$$

where

$$= s_{ij}\dot{s}_{ij} - 2k\dot{k}, \qquad \dot{k} = \frac{dk}{dT}\, T \tag{8}$$

The requirement that μ be non-negative results from the condition of irreversibility, and can also be seen from the fact that μ is proportional to and has the same sign as $s_{ij}\dot{e}_{ij}{}^{P}$, the power expended per unit volume in plastic distortion, which must be non-negative.

Also it is to be noted that although the equations for the viscoelastic strain rate, Equation (4), and for the plastic strain rate, the second of Equations (7), are of similar appearance, they describe different types of behavior. In Equation (4), η is a material property whose numerical value would be changed by a change in time scale, so that the result of using this viscoelastic relation depends on the time scale. On the other hand, it can be seen from the value of μ in Equation (7) that the plastic strain rate is independent of the time scale.

For thermal stress calculations, the flow rules, Equations (7), are not convenient to use because the distinction between the two equations when $f = 0$ depends on the unknown stress rates, $\dot{s}_{ij}$. The rules can be put in a more suitable, equivalent form by using the requirement of positive plastic power.

From Equations (2) and (3)

$$\frac{1}{2G}\, \dot{s}_{ij} = \dot{e}_{ij} - \dot{e}_{ij}{}^{V} - \dot{e}_{ij}{}^{P} \tag{9}$$

We introduce a stress rate $\dot{s}_{ij}{}^{V}$ defined by

$$\frac{1}{2G}\, \dot{s}_{ij}{}^{V} = \dot{e}_{ij} - \dot{e}_{ij}{}^{V} \tag{10}$$

so that $\dot{s}_{ij}{}^{V}$ is the actual stress rate in a viscoelastic region and is a ficticious stress rate in a plastic region. Then the plastic power, which is proportional to μ, is

$$s_{ij}\dot{e}_{ij}{}^{P} = s_{ij}(\dot{e}_{ij} - \dot{e}_{ij}{}^{E} - \dot{e}_{ij}{}^{V}) = \frac{s_{ij}\dot{s}_{ij}{}^{V} - s_{ij}\dot{s}_{ij}}{2G} \tag{11}$$

Now if at a given instant

$$f = {}^{1}/_{2} s_{ij}s_{ij} - k^2(T) = 0 \tag{12}$$

then the stress rates must satisfy one of the two equations

$$\dot{f} = s_{ij}\dot{s}_{ij} - 2k\dot{k} < 0 \tag{13}$$

or

$$\dot{f} = s_{ij}\dot{s}_{ij} - 2k\dot{k} = 0 \tag{14}$$

The second condition, Equation (14), is permissible only if the requirement of non-negative plastic power ($\mu \geq 0$) is also satisfied. In this case we see from Equation (11) that

$$s_{ij}\dot{s}_{ij}{}^{V} - 2k\dot{k} \geq 0 \tag{15}$$

If on the other hand,

$$s_{ij}\dot{s}_{ij}{}^{V} - 2k\dot{k} < 0 \tag{16}$$

then μ would be negative if Equation (14) holds, so that the alternative, Equation (13), must hold. In this case it is seen that Equations (16) and (13) are equivalent since now $\dot{s}_{ij}{}^{V} = \dot{s}_{ij}$. The flow rules may then be restated in the form:

$$\dot{e}_{ij}{}^{P} = 0, \quad \text{if } f < 0, \text{ or if } f = 0, \ s_{ij}\dot{s}_{ij}{}^{V} - 2k\dot{k} < 0 \tag{17}$$

$$\dot{e}_{ij}{}^{P} = \mu s_{ij}, \quad \text{if } f = 0, \ s_{ij}\dot{s}_{ij}{}^{V} - 2k\dot{k} \geq 0 \tag{18}$$

These equations are more suitable for thermal stress problems since the criterion for choice between them depends not on the unknown stress rates but on the strain rates through the fictitious stress rates, $\dot{s}_{ij}{}^{V}$. The strain rates are generally continuous functions of time, while the stress components have discontinuous time derivatives at a point when the material behavior changes from viscoelastic to plastic in loading or the reverse in unloading. The continuity of the criterion is important for numerical computations, since it permits the value of the criterion within a small time interval to be estimated from its value at the start of the interval.

3 Stress Equation for a Free Plate

The equations of Section 2 are now applied to the thermal stress analysis of a free plate of thickness $2h$ and arbitrary shape. Rectangular Cartesian co-ordinate axes, x, y, z are used with the origin in the central plane of the plate, and the x-axis perpendicular to its faces. The faces $x = \pm h$ are free of traction, while the tractions on the edges have zero resultant and zero moment. The temperature distribution in the plate is assumed to be of the form $T(x, t)$ and the plate is initially free of stress. Attention is confined to that portion of the plate at a sufficient distance from its edges so that all quantities may be considered functions of x and t only.

Equations will be derived for the time rates of change of the stress components at a generic instant of time t. These equations will express these quantities in terms of the state of stress at time t and the rate of change of the prescribed temperature distribution at that time. The rates of change of the stress components can then be integrated forward to obtain the stress distribution for all times.

It is convenient to introduce first a function $g(x, t)$ which is zero in the plastic state and equal to one elsewhere; i.e.,

$$g(x, t) = 1, \quad \text{if} \quad f < 0, \quad \text{or if} \quad f = 0, \quad s_{ij}\dot{s}_{ij}{}^{V} - 2k\dot{k} < 0$$

$$g(x, t) = 0, \quad \text{if} \quad f = 0, \qquad s_{ij}\dot{s}_{ij}{}^{V} - 2k\dot{k} \geq 0 \tag{19}$$

Then the stress-strain relations, Equations (1), (2), (3), (4), (17), and (18) can be combined into the single relation

$$\dot{\epsilon}_{ij} = \frac{1+\nu}{E}\dot{\sigma}_{ij} - \delta_{ij}\frac{\nu}{E}\dot{\sigma}_{kk} + \left(\frac{1}{2\eta} + (1-g)\mu\right)\left(\sigma_{ij} - \delta_{ij}\frac{\sigma_{kk}}{3}\right) + \delta_{ij}\alpha\dot{T} \tag{20}$$

Under the conditions stated for the plate, we can assume that, as in the thermoelastic case,

$$\sigma_{xx} = \sigma_{xy} = \sigma_{yz} = \sigma_{zx} = 0,$$
$$\sigma_{yy} = \sigma_{zz} = \sigma \tag{21}$$

Also for this state of stress it follows from Equation (20) that the only nonzero strain components are ϵ_{xx} and

$$\epsilon_{yy} = \epsilon_{zz} = \epsilon \tag{22}$$

Then from Equation (20),

$$\dot{\epsilon} = \frac{1-\nu}{E}\dot{\sigma} + \left[\frac{1}{2\eta} + (1-g)\mu\right]\frac{\sigma}{3} + \alpha\dot{T} \tag{23}$$

The only nontrivially satisfied equation of compatibility is in this case

$$\frac{\partial^2\epsilon}{\partial x^2} = 0 \tag{24}$$

so that ϵ is a linear function of x. For simplicity we restrict consideration here to the case where $T(x, t)$ is symmetric in x. Then σ and ϵ are symmetric in x, and Equation (24) gives

$$\epsilon = \epsilon(t) \tag{25}$$

From Equation (23) the stress rate when there is no plastic flow, i.e., $g = 1$, is

$$\dot{\sigma} = \frac{E}{1-\nu}\left(\dot{\epsilon} - \frac{\sigma}{6\eta} - \alpha\dot{T}\right) \quad \text{for} \quad g = 1 \tag{26}$$

For the state of stress given by Equation (21) the yield condition, $(1/2)s_{ij}s_{ij} = k^2(T)$, becomes $(1/3)\sigma^2 = k^2(T)$ or

$$\sigma^2 = Y^2(T) \tag{27}$$

where $Y(T) = \sqrt{3}\,k(T)$ is the yield stress in tension.

It follows that during plastic flow

$$\sigma\dot{\sigma} = Y\dot{Y} \quad \text{for} \quad g = 0 \tag{28}$$

where $\dot{Y} = (dY/dT)\dot{T}$.

During plastic flow, $\sigma = +Y$ or $-Y$, so Equation (28) may be written

$$\dot{\sigma} = (\operatorname{sgn}\sigma)\dot{Y} \quad \text{for} \quad g = 0 \tag{29}$$

where

$\operatorname{sgn}\sigma = +1$ for yielding in tension

$\operatorname{sgn}\sigma = -1$ for yielding in compression

Equations (26) and (29) may then be combined into a single equation for $\dot{\sigma}$ which is valid throughout the plate,

$$\dot{\sigma} = \frac{E}{1-\nu}g\left(\dot{\epsilon} - \frac{\sigma}{6\eta} - \alpha\dot{T}\right) + (1-g)(\operatorname{sgn}\sigma)\dot{Y} \tag{30}$$

The strain rate may now be obtained by using the condition that the stress distribution have zero resultant across the plate thickness; that is

$$\int_0^h \sigma(x, t)dx = 0 \tag{31}$$

so that

$$\int_0^h \dot{\sigma}(x, t)dx = 0 \tag{32}$$

Substituting Equation (30) in (32) gives

$$\dot{\epsilon}(t) = \frac{1}{L_V}\int_0^h \left[g(x, t)\left(\frac{\sigma}{6\eta} + \alpha\dot{T}\right) - (1 - g(x, t))\left(\frac{1-\nu}{E}\right)(\operatorname{sgn}\sigma)\dot{Y}\right]dx \tag{33}$$

where

$$L_V = \int_0^h g(x, t)dx \tag{34}$$

is the half-width of the nonplastic regions of the plate.

With this expression for $\dot{\epsilon}(t)$, Equation (30) gives $\dot{\sigma}(x, t)$ in terms of $\dot{T}(x, t)$, $\sigma(x, t)$, and $g(x, t)$. To complete the solution, we therefore need only to express the criterion for determining $g(x, t)$, Equation (19), in terms of these quantities. For this purpose, we define $\dot{\sigma}_{ij}{}^{V}$ in an analogous way to Equation (10) for $\dot{s}_{ij}{}^{V}$, i.e., it is given in terms of $\dot{\epsilon}_{ij}$, σ_{ij}, and $\dot{T}$ by Equation (20) with $\mu = 0$ for both plastic and nonplastic states. Then

$$\sigma_{ij}\dot{\sigma}_{ij}{}^{V} = (s_{ij} + {}^1/_3\delta_{ij}\sigma_{kk})(\dot{s}_{ij}{}^{V} + {}^1/_3\delta_{ij}\dot{\sigma}_{mm}{}^{V}) = s_{ij}\dot{s}_{ij}{}^{V} + {}^1/_3\sigma_{kk}\dot{\sigma}_{mm} \tag{35}$$

where we use the fact that

$$\dot{\sigma}_{mm}{}^{V} = \dot{\sigma}_{mm} \tag{36}$$

since the relation between the mean stress, mean strain, and temperature is the same in the plastic and nonplastic states.

For the particular stress distribution, Equation (21), considered here, Equation (35) becomes

$$s_{ij}\dot{s}_{ij}{}^{V} = 2\sigma\dot{\sigma}^{V} - {}^4/_3\sigma\dot{\sigma} \tag{37}$$

where $\dot{\sigma}^{V}$ is given by Equation (26) for any value of g; i.e.,

$$\dot{\sigma}^{V} = \frac{E}{1-\nu}\left(\dot{\epsilon} - \frac{\sigma}{6\eta} - \alpha\dot{T}\right) \tag{38}$$

From Equation (19) the quantity used to determine g is then

$$s_{ij}\dot{s}_{ij}{}^{V} - 2k\dot{k} = 2\sigma\dot{\sigma}^{V} - {}^4/_3\sigma\dot{\sigma} - 2k\dot{k} = 2(\sigma\dot{\sigma}^{V} - Y\dot{Y}) \tag{39}$$

since, when the criterion is used

$$\sigma\dot{\sigma} = Y\dot{Y} = 3k\dot{k}$$

The equations for determining the stress distribution can now be summarized as

$$\sigma(x, t) = \int_0^t [g\dot{\sigma}^{V} + (1-g)(\operatorname{sgn}\sigma)\dot{Y}]dt \tag{40}$$

$$\dot{\sigma}^{V}(x, t) = \frac{E}{1-\nu}\left(\dot{\epsilon} - \frac{\sigma}{6\eta} - \alpha\dot{T}\right) \tag{41}$$

$$\dot{\epsilon}(t) = \frac{1}{L_V}\int_0^h \left[g\left(\frac{\sigma}{6\eta} + \alpha\dot{T}\right) - (1-g)\left(\frac{1-\nu}{E}\right)(\operatorname{sgn}\sigma)\dot{Y}\right]dx \tag{42}$$

$$L_V(t) = \int_0^h g(x, t)dx \tag{43}$$

$$g(x, t) = 1, \quad \text{if} \quad \sigma^2 < Y^2 \quad \text{or if} \quad \sigma^2 = Y^2, \quad \sigma\dot{\sigma}^V - Y\dot{Y} < 0$$

$$g(x, t) = 0, \quad \text{if} \quad \sigma^2 = Y^2, \quad \sigma\dot{\sigma}^V - Y\dot{Y} \geq 0 \tag{44}$$

These equations are well suited for digital computation using a step-by-step forward calculation in time with simultaneous determination of g, $\dot{\sigma}^V$, and σ. These has been carried out for the plate-cooling problem with some results reported in the following text. In the later stages of the process the temperature becomes low enough so that viscous flow is negligible, then an integrated form of the equations can be used, provided no further unloading occurs, just as in [2]. These integrated equations can be obtained in the same way as in that case and are:

$$\sigma(x, t) = \sigma(x, t_0) + \frac{E}{1 - \nu}\,[\epsilon(t) - \epsilon(t_0) - \alpha T(x, t) + \alpha T(x, t_0)], \quad \text{for} \quad g(x, t) = 1$$

$$\sigma(x, t) = (\operatorname{sgn}\sigma)Y(T(x, t)), \quad \text{for} \quad g(x, t) = 0 \tag{45}$$

with

$$L_V(t)[\epsilon(t) - \epsilon(t_0)] = \int_0^h \left\{ g(x, t)\left[-\frac{1 - \nu}{E}\,\sigma(x, t_0) + \alpha T(x, t) - \alpha T(x, t_0)\right] - \left(\frac{1 - \nu}{E}\right)(1 - g(x, t))\,(\operatorname{sgn}\sigma)Y(T(x, t))\right\} dx \tag{46}$$

which hold if $1/\eta = 0$ and $g(x, t)$ does not change from 0 to 1 during the period t_0 to t.

4 Numerical Computation

Computations for the symmetrically cooled plate were carried out on the IBM 704 computer for a viscosity of the form of Equation (5) and $Y(T)$ piecewise linear in T. A step-by-step procedure in time was used; that is, the temperature, stress, and location of the plastic regions at time, $t + \Delta t$, are computed from the values at time, t.

The temperature is the solution of the problem:

$$\frac{\partial^2 \bar{T}}{\partial \bar{x}^2} = \frac{\partial \bar{T}}{\partial \bar{t}}, \quad 0 \leq \bar{x} < 1, \quad \bar{t} > 0$$

$$\bar{T}(\bar{x}, 0) = 1$$

$$\frac{\partial \bar{T}}{\partial \bar{x}} = 0 \quad \text{at} \quad \bar{x} = 0, \quad \text{and} \quad \frac{\partial \bar{T}}{\partial \bar{x}} = -\lambda \bar{T} \quad \text{at} \quad \bar{x} = 1$$

where dimensionless variables are used as follows:

$\bar{T} = (T - T_0)/(T_1 - T_0)$, with T_1 = initial temperature and T_0 = ambient temperature,

$$\bar{x} = \frac{x}{h}, \quad \bar{t} = \frac{K}{c\rho h^2}\,t, \quad \lambda = \frac{Hh}{K}$$

where K = thermal conductivity, c = specific heat, ρ = density, H = surface heat-transfer coefficient.

The calculation was carried out for equally spaced values of $\bar{x}$ and of $\bar{t}$,

$$\bar{x} = (i - 1/2)\Delta\bar{x}, \quad i = 1, 2, \ldots, n, \quad n\Delta\bar{x} = 1,$$

$$\bar{t} = j\Delta\bar{t} = j\,\frac{(\Delta\bar{x})^2}{2}, \quad j = 0, 1, \ldots$$

Writing

$$\bar{T}((i - 1/2)\Delta\bar{x}, j\Delta\bar{t}) = \bar{T}_i^0, \quad \bar{T}((i - 1/2)\Delta\bar{x}, (j + 1)\Delta\bar{t}) = \bar{T}_i$$

and similarly for σ, then $\bar{T}$ can be calculated from the explicit finite-difference expressions

$$\bar{T}_1 = 1/2(\bar{T}_1^0 + \bar{T}_2^0)$$

$$\bar{T}_i = 1/2(\bar{T}_{i-1}^0 + \bar{T}_{i+1}^0), \quad i = 2, 3, \ldots, n - 1,$$

$$\bar{T}_n = 1/2\left[\left(\frac{1 + 1/2\,\dfrac{\lambda}{n}}{1 + 3/8\,\dfrac{\lambda}{n}}\right)\bar{T}_{n-1}^0 + \left(\frac{1 - 3/4\,\dfrac{\lambda}{n}}{1 + 3/8\,\dfrac{\lambda}{n}}\right)\bar{T}_n^0\right]$$

The increments of viscoelastic strain, $(\sigma/6\eta)\Delta\bar{t}$ are estimated by using the values of σ at $j\Delta\bar{t}$, i.e. σ_i^0; and similarly the g_i^0 are used to estimate the position of the plastic regions. Then the increment $\Delta\epsilon$ is calculated using the finite-difference equivalents of Equations (42) and (43), and the increments $\Delta\sigma_i^V$ using Equation (41). From Equation (44), $g_i = 0$ if $|\sigma_i^0 + \Delta\sigma_i^V| \geq Y(\bar{T}_i)$ and $g_i = 1$, otherwise. For $g_i = 1$, Equation (40) gives $\sigma_i = \sigma_i^0 + \Delta\sigma_i^V$, and for $g_i = 0$, Equation (44) gives $\sigma_i = (\operatorname{sgn}\sigma_i^0)Y(\bar{T}_i)$.

If none of the g_i have changed, indicating no change in the position of the plastic regions during the time interval $\Delta\bar{t}$, these estimates are accepted and the calculation proceeds to the next time step. If some g_i has changed, indicating unloading or the beginning of plastic loading at some point, then these estimates are not sufficiently accurate and the zero resultant condition, Equation (32) which gave Equation (42), may not be satisfied, even though it was satisfied by the σ_i^0. The necessary correction to $\Delta\epsilon$ to satisfy this condition is determined using the estimated g_i and σ_i. This is used to correct the $\Delta\sigma_i^V$, and the g_i are redetermined. If these second estimates of g_i agree with the first, the corrected values are accepted, otherwise the correction process is repeated. The correction process was found necessary because of the discontinuous rate of change of stress when plastic yielding occurs.

5 Calculated Residual Stress Distributions

Examples of the calculated residual stress in cooled plates are given in Fig. 1. The following values of the parameters were used: K = 34 Btu/ft, hr, ° F; $c\rho$ = 70 Btu/ft³, °F; ν = 0.3; E = 30×10^6 psi; α = 7.5×10^{-6}/°F; H = 34 Btu/ft², hr, °F; h = 1.5 ft.

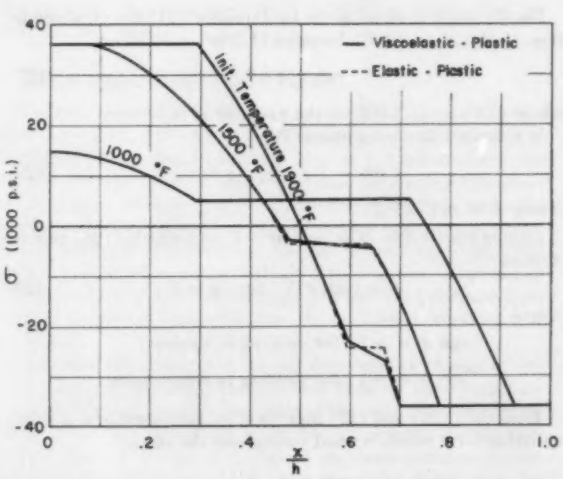

Fig. 1 Calculated residual stress in a cooled steel plate; effect of viscoelasticity

$$\eta = 8300 \exp\left(\frac{18{,}650}{T + 460}\right), \quad \text{lb, hr/in.}^2, \quad T > 500 \text{ F}$$

$$\frac{1}{\eta} = 0, \quad T \leq 500 \text{ F}$$

$$Y = 36{,}000\left(1 - \frac{T - 250}{2000}\right), \text{ psi}, \quad T > 250 \text{ F}$$

$$Y = 36{,}000 \text{ psi}, \quad T \leq 250 \text{ F}$$

These values were chosen as extremes to test the effect of viscoelasticity in steel. The calculations were repeated assuming no viscous flow and it was found that the effect of viscosity on the residual stress was small in this problem. In the elastic-plastic case there is a region of constant residual stress, intermediate between the center and surface, where no plastic yielding took place at any time. Viscosity produces stress relaxation in this region at the higher initial temperature, but hardly affects the location of the plastic regions.

In this problem, when cooling is so rapid as to cause considerable plastic yielding, the plate does not remain at high temperatures long enough for viscous effects to influence the residual-stress distribution. The result would, of course, be different for a heat-treatment in which high temperature was maintained for a longer period.

Fig. 2 shows the effect on residual stress of temperature dependence of yield stress, with no viscous flow. The solid curve was calculated for a 1-in-thick steel plate spray-quenched from 800 to 75 F, with a $Y(T)$ that decreased approximately linearly from 37,300 psi at room temperature to 23,000 psi at 800 F. The dashed curve is the calculated residual stress using a constant room temperature value for Y. The difference is large in the central part of the plate which yielded when at high temperature. Using an average constant value for Y would give an intermediate value at the center but too low a value at the surface, where the residual stress equals the room temperature yield stress.

For values of $Y(T)$ and η in the range found in steel, the growth of the plastic zones in the plate during cooling follows a pattern similar to that in the elastic-plastic case with temperature-independent properties. For this case, the calculations showed that the possible plastic regions and the corresponding types of residual stress distributions are those shown schematically in Fig. 3. The purely elastic case, of course, gives zero residual stress.

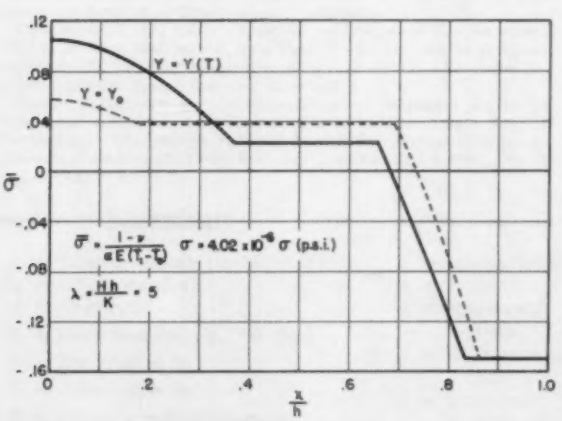

Fig. 2 Calculated residual stress in a cooled steel plate; effect of temperature dependence of yield stress. Y_0 = yield stress at 75 F

These five types of residual stress distribution are similar to those obtained in [1] for a plate whose face is exposed to a slowly varying uniform heat input which first increases and then decreases monotonically with time. The qualitative similarity of the residual stress distribution types might have been anticipated by considering that the temperature during cooling could be approximated roughly by an expression of similar form to that for the temperature caused by the slowly varying heat input. This suggests that the residual stress distribution in the cooling problem could be determined, at least approximately, by using the formulas in [1] which give the residual stress in terms of the parameter

$$q_M = \frac{\alpha E \bar{q}_M h}{4(1 - \nu)YK} \tag{47}$$

where q_M is the maximum heat input. This was found to be possible, if in the cooling problem we put

$$\frac{1}{q_M} = 1.07\left(1 + \frac{2}{\lambda}\right)\bar{Y} \tag{48}$$

where

$$\bar{Y} = \frac{1 - \nu}{\alpha E(T_1 - T_0)}Y \tag{49}$$

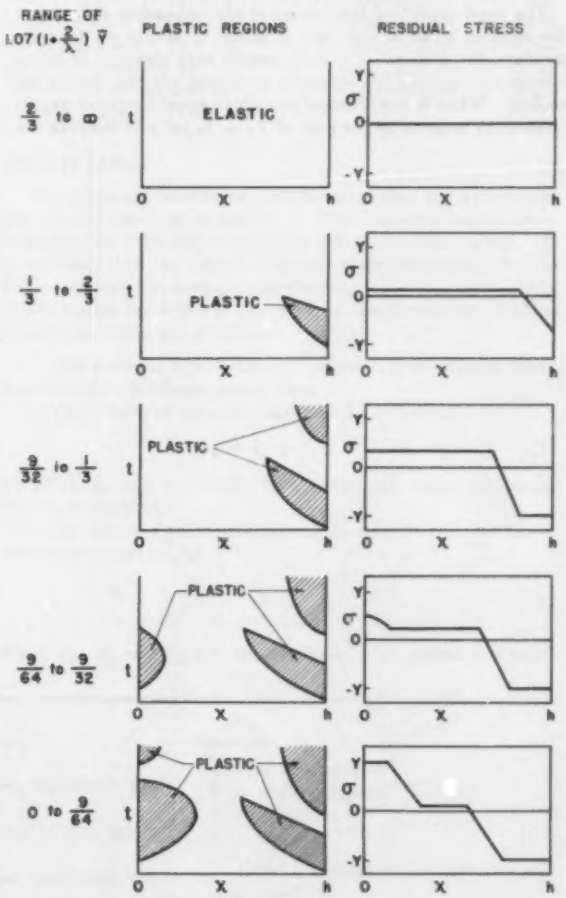

Fig. 3 Types of plastic regions and corresponding residual stress distribution. Cooling of elastic-plastic plate with constant yield stress

The form of the relation in Equation (48) was suggested by an approximation to the temperature during cooling. To obtain the values of the constants, a curve was fitted to the condition for no plastic flow to occur in the cooling problem. This was

$$1.07\left(1+\frac{2}{\lambda}\right)\bar{Y} > {}^2/_3 \tag{50}$$

which when compared to the same condition in the slowly varying heat-input problem

$$\frac{1}{q_M} > {}^2/_3 \tag{51}$$

gives Equation (48).

Calculations of residual stress after cooling were made for several values of the parameters in the range $0.05 \leq \bar{Y} \leq 0.4$, $\lambda \leq 20$ and compared with the values given by the formulas in [1]. It was found that the residual-stress type was given quite accurately, and the residual-stress values (with τ in [1] replaced by $-\sigma/Y$) also agreed, with a maximum error ranging from 5 per cent for small λ to 15 per cent for $\lambda = 20$.

The type of residual-stress distribution indicated by Fig. 3 will also be correct when the temperature dependence of Y is taken into consideration, provided the variation of yield stress with temperature is not too great.

The applicability of the foregoing approximation shows that the residual stress is not very sensitive to details of the temperature distribution. The same results were observed in calculations with surface heat-transfer coefficient varying during the cooling. When λ was changed enough to cause temperature differences as large as 20 per cent of $T_1 - T_0$ (at $x = 0.8h$) in the early stages of cooling, there was almost no effect on residual stress provided the same temperature-time curve was followed during the last half of the process. The residual stress is determined mainly by the extent of plastic yielding which was the same in both cases.

Acknowledgment

This investigation is part of a research program on residual stresses for the Large Steam Turbine-Generator Department of General Electric Company. Financial support of the investigation and permission to publish the results are gratefully acknowledged.

References

1 J. H. Weiner, "An Elastoplastic Thermal-Stress Analysis of a Free Plate," JOURNAL OF APPLIED MECHANICS, vol. 23, TRANS. ASME, vol. 78, 1956, pp. 397–401.

2 H. G. Landau and J. H. Weiner, "Transient and Residual Stresses in Heat Treated Plates," JOURNAL OF APPLIED MECHANICS, vol. 25, TRANS. ASME, vol. 80, 1958, pp. 453–465.

3 H. Yuksel, "Elastic, Plastic Stresses in Free Plate with Periodically Varying Surface Temperatures," JOURNAL OF APPLIED MECHANICS, vol. 25, TRANS. ASME, vol. 80, 1958, pp. 603–606.

4 A. J. Wang and W. Prager, "Thermal and Creep Effects in Work-Hardening Elastic-Plastic Solids," *Journal of the Aeronautical Sciences*, vol. 21, 1954, pp. 343–344, 360.

5 A. M. Freudenthal, "The Inelastic Behavior of Engineering Materials and Structures," John Wiley and Sons, New York, N. Y., 1950.

6 W. Prager, "An Introduction to the Concepts and Principles of Plasticity," special lectures delivered at the Seminar in Applied Mathematics, Boulder, Colo., July 1957.

7 W. Prager, "Non-Isothermal Plastic Deformation," Brown University, Technical Report Nonr 526 (02)/4, November, 1957.

Prediction of Creep Failure Time for Pressure Vessels

F. P. J. RIMROTT[2]
Assistant Professor,
Department of Mechanical Engineering,
University of Toronto,
Toronto, Ontario, Canada.
Mem. ASME

EARL J. MILLS[2]
Principal Mechanical Engineer,
Battelle Memorial Institute,
Columbus, Ohio.
Assoc. Mem. ASME

JOSEPH MARIN
Professor and Head,
Department of Engineering Mechanics,
The Pennsylvania State University,
University Park, Pa.
Mem. ASME

When a pressure vessel is subjected to internal pressure and is made from a material which exhibits creep, the vessel will expand. If the internal pressure is held constant during expansion, the load on the wall will increase. At the same time, the thickness of the wall decreases. The result of these two simultaneous effects is that the expansion of the vessel is continuously accelerated until the wall thickness has decreased and the load increased to such an extent that the strength of the material is no longer sufficient and fracture of the vessel occurs. The time-to-fracture in the case of simple tensile creep was predicted theoretically by Orowan [8][1] and shown by Hoff [1] to be in good agreement with experimental results. The basis of their approach is to use true stress and true strain. The creep-failure time is then defined as the time at which the true strain reaches infinity. The present paper extends the foregoing concept to the problem of combined stresses. The creep-failure time is determined for thin, thick, and very thick-walled cylindrical vessels of circular cross section with closed ends subjected to constant internal pressure. The theory is based upon the usual assumptions for predicting creep deformation under combined stress [4–7]. A power relation is used to express the creep rate versus stress relation in simple tension.

Based upon a large strain theory [2] for a pressure vessel with closed ends under internal pressure, an expression can be obtained relating the significant creep rate to the internal pressure in the vessel and the significant stress.

An internal-pressure versus significant-creep-rate relation can be obtained from a significant-creep-rate versus stress relation, based upon a simple tension-creep relation. In this manner, an expression is obtained which relates the creep rate to the creep strain. This equation can be integrated and results in a relation giving the creep strain as a function of time.

The creep-failure time is now obtained by letting the true creep strain approach infinity. It so happens that the time necessary to reach infinite strain is a finite quantity. The time to reach infinite strain, called creep-failure time, can be used to predict the time of actual fracture, called creep-fracture time. In reality, the vessel will fracture before it has expanded to infinity. However, the expansion of the vessel (accompanied by a reduction of the wall thickness) proceeds very slowly at the beginning and very rapidly toward the end of the life of the vessel. For this reason, the actual fracture time and the time for infinite theoretical strain occur at essentially the same time. This means that the creep-failure time can be used in place of the creep-fracture time for the prediction of fracture of a vessel.

[1] Numbers in brackets designate References at end of paper.

[2] Formerly with Department of Engineering Mechanics, The Pennsylvania State University, University Park, Pa.

For presentation at the Summer Conference of the Applied Mechanics Division, University Park, Pa., June 20–22, 1960, of The American Society of Mechanical Engineers.

Discussion of this paper should be addressed to the Secretary, ASME, 29 West 39th Street, New York, N. Y., and will be accepted until July 22, 1960, for publication at a later date. Discussion received after the closing date will be returned.

Note: Statements and opinions advanced in papers are to be understood as individual expressions of their authors and not those of the Society. Manuscript received by ASME Applied Mechanics Division, December 29, 1958; final draft received July 6, 1959. Paper No. 60—APM-7.

Basis of Theory

This paper assumes times of such values that the influence of the primary creep can be neglected. The creep relation used here expresses the behavior of materials during secondary creep. It is assumed that the relation also expresses adequately the behavior of materials during tertiary creep.

The theory developed in this paper is based upon the usual assumptions, which are as follows:

1 The material is isotropic and homogeneous, and the vessel retains its circular shape during creep.

2 The density of the material remains constant, or

$$\epsilon_\varphi + \epsilon_r + \epsilon_z = 0 \tag{1}$$

where ϵ_φ, ϵ_r, and ϵ_z are the true tangential, radial, and axial strains, respectively.

3 The ratios of principal shear-strain rates to principal shear stresses are constant, or

$$\frac{\dot{\epsilon}_\varphi - \dot{\epsilon}_r}{\sigma_\varphi - \sigma_r} = \frac{\dot{\epsilon}_r - \dot{\epsilon}_z}{\sigma_r - \sigma_z} = \frac{\dot{\epsilon}_z - \dot{\epsilon}_\varphi}{\sigma_z - \sigma_\varphi} = \frac{3}{2K} \tag{2}$$

where σ_φ, σ_r, and σ_z are the true tangential, radial, and axial

Nomenclature

A = creep coefficient, (in.^{2n} lb^{-n} day^{-1})
B_n = a function of n
I = an integral
K = creep modulus, (in.$^{-2}$ lb day)
a = inner radius, in.
b = outer radius, in.
h = $b - a$ = wall thickness, in.
n = creep exponent
p = internal pressure, psi
t = time
ϵ = true strain; also significant true strain
$\dot{\epsilon}$ = $d\epsilon/dt$ = time rate of true strain, (day^{-1})
σ = true stress; also significant true stress, psi
σ' = nominal significant stress, psi

Subscripts

a = at inner radius
b = at outer radius
f = at failure
r = radial
v = for very thick-walled cylinder
z = axial
φ = tangential

stresses, and $\dot{\epsilon}_\varphi$, $\dot{\epsilon}_r$, and $\dot{\epsilon}_z$ the first derivatives with respect to time of the true strains ϵ_φ, ϵ_r, and ϵ_z.

From equation (1) and equations (2) the following strain rate versus stress relations can be obtained:

$$\dot{\epsilon}_\varphi = \frac{1}{K}\left[\sigma_\varphi - {}^1/_2(\sigma_r + \sigma_z)\right]$$

$$\dot{\epsilon}_r = \frac{1}{K}\left[\sigma_r - {}^1/_2(\sigma_z + \sigma_\varphi)\right] \quad (3)$$

$$\dot{\epsilon}_z = \frac{1}{K}\left[\sigma_z - {}^1/_2(\sigma_\varphi + \sigma_r)\right]$$

where K is the modulus of creep. The value of K is $K = \sigma/\dot{\epsilon}$ and can be determined for any state of stress by means of the following assumption:

4 A significant rate of true-strain versus true-stress relation exists, which can be obtained from a simple tension test. That is

$$\dot{\epsilon} = f(\sigma) \quad (4)$$

In this paper, the relation expressed by equation (4) is assumed to be a power relation of the form

$$\dot{\epsilon} = A\sigma^n \quad (5)$$

Assumptions similar to the foregoing also were made by Soderberg [4], Marin [5], Johnson [6], and Nadai [7].

Three equations for creep-failure time, defined as the time required for the true strain to reach infinity, will now be derived. The first is the exact equation for a thick-walled cylinder, the second is based upon the assumption that the cylinder has a very thin wall, and the third is based upon the assumption that the cylinder has a very thick wall.

Failure-Time Equation

Thick-Walled Cylinder (exact equation). The equation which relates the internal pressure to the significant creep rate can be shown to be [2]

$$p = 1/\sqrt{3}\int_{\dot{\epsilon}_b}^{\dot{\epsilon}_a} K d\dot{\epsilon} \quad (6)$$

where

$$\dot{\epsilon}_b = \frac{(a/b)^2 \exp \sqrt{3}\,\epsilon_a}{1 + (a/b)^2(\exp \sqrt{3}\,\epsilon_a - 1)}\,\dot{\epsilon}_a \quad (7)$$

By the power creep rate-stress relation for tension

$$\dot{\epsilon} = A\sigma^n \quad (8)$$

By equation (3) for simple tension, $\dot{\epsilon} = \sigma/K$ and

$$K = \frac{\sigma}{\dot{\epsilon}} = A^{-1/n}\dot{\epsilon}^{1/n-1} \quad (9)$$

Entering K from equation (9) in equation (6), integrating, and using the expression for $\dot{\epsilon}_b$ given by equation (7), the following expression is obtained:

$$\dot{\epsilon}_a = \frac{\sqrt{3}^n A p^n}{n^n}\left\{1 - \left[\frac{(a/b)^2 \exp \sqrt{3}\,\epsilon_a}{1 + (a/b)^2(\exp \sqrt{3}\,\epsilon_a - 1)}\right]^{1/n}\right\}^{-n} \quad (10)$$

Equation (10) expresses the significant creep rate at the bore, as a function of the significant creep strain at the bore. An inspection of equation (10) indicates that for a constant pressure the creep rate increases with increasing strain.

In order to establish the strain as a function of time for a constant internal pressure, equation (10) can be integrated. Then

$$\int_0^{\epsilon_a}\left\{1 - \left[\frac{(a/b)^2 \exp \sqrt{3}\,\epsilon_a}{1 + (a/b)^2(\exp \sqrt{3}\,\epsilon_a - 1)}\right]^{1/n}\right\} d\epsilon_a = \frac{\sqrt{3}^n A p^n}{n^n} t \quad (11)$$

Equation (11) can now be used to define the creep failure-time t_f. Letting $\epsilon_a \to \infty$, and rearranging the resulting equation,

$$t_f = \frac{n^n}{\sqrt{3}^n A p^n} I_\infty \quad (12)$$

where

$$I_\infty = \int_0^\infty \left\{1 - \left[\frac{(a/b)^2 \exp \sqrt{3}\,\epsilon_a}{1 + (a/b)^2(\exp \sqrt{3}\,\epsilon_a - 1)}\right]^{1/n}\right\}^n d\epsilon_a \quad (13)$$

A general solution of integral I is given in the Appendix.

Curves for creep-failure time as defined by equation (12) are

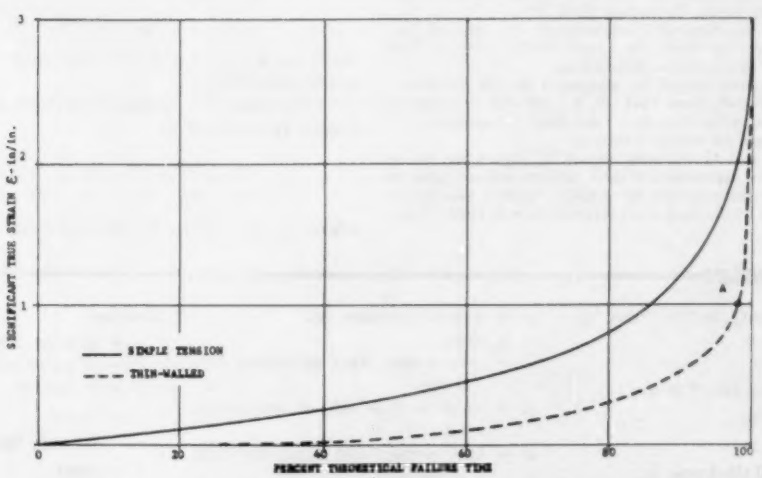

Fig. 1 Strain versus per cent of failure time for $n = 2$, $\sigma' = 1000$ psi

plotted in Figs. 2 to 7 for different values of the creep exponent n.

Thin-Walled Cylinder. Making the assumption that the wall of the vessel is so thin that $\sigma_r = 0$, and that σ, σ_φ, and σ_z are uniformly distributed across the wall, a pressure versus strain-rate relation for the thin-walled cylinder can be obtained. Assuming that the length of the cylinder is constant, the condition of constant density can be expressed by

$$2\pi a h = 2\pi a' h' \qquad (a)$$

where a and a' are the original and the actual radius of the vessel, and h and h' are the original and the actual wall thickness. From equations (6) and (11) of reference [2] it can be shown that

$$a' = a \exp\left[(\sqrt{3}/2)\epsilon\right] \qquad (b)$$

where ϵ is the significant strain.

Placing the expression for a' from equation (b) in equation (a)

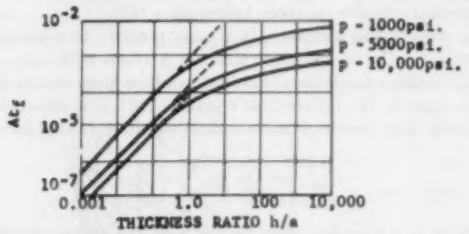

Fig. 2 Failure time versus thickness ratio for $n = 1$

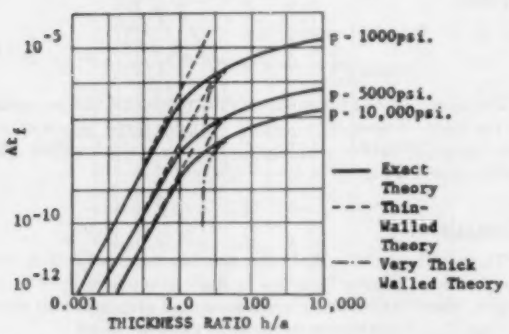

Fig. 3 Failure time versus thickness ratio for $n = 2$

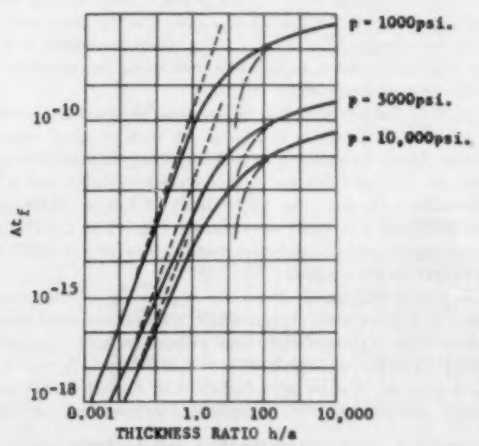

Fig. 4 Failure time versus thickness ratio for $n = 3$

$$h' = \frac{h}{\exp\left[(\sqrt{3}/2)\epsilon\right]} \qquad (c)$$

The stresses in a thin-walled cylinder are given by

$$\sigma_\varphi = \frac{a'}{h'} p, \qquad \sigma_r = 0 \qquad (d)$$

The significant stress for a cylinder (with $\dot{\epsilon}_z = 0$) can be shown to be [2]

$$\sigma = \frac{\sqrt{3}}{2}(\sigma_\varphi - \sigma_r) \qquad (e)$$

Placing σ_φ and σ_r from equations (d) in equation (e) and using a'

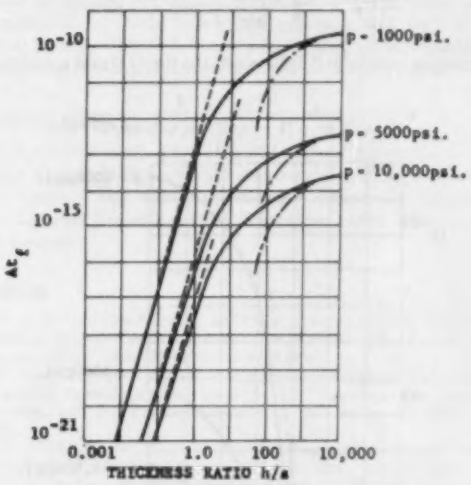

Fig. 5 Failure time versus thickness ratio for $n = 4$

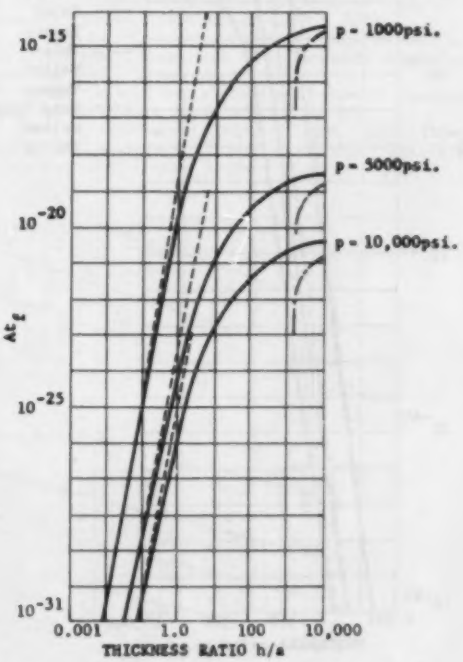

Fig. 6 Failure time versus thickness ratio for $n = 6$

and h' as expressed by equations (b) and (c), gives

$$\sigma = \frac{\sqrt{3}\,a}{2h}\,p \exp \sqrt{3}\,\epsilon \qquad (f)$$

If σ is now expressed by the creep modulus K of equation (9), then

$$p = \frac{2h}{\sqrt{3}\,a} \frac{K\dot{\epsilon}}{\exp \sqrt{3}\,\epsilon} \qquad (14)$$

The creep rate as a function of creep strain for a given pressure is obtained by rearranging equation (14) and using equation (9), then

$$\dot{\epsilon} = A\left(\frac{\sqrt{3}\,ap}{2h}\right)^n \exp \sqrt{3}\,n\epsilon \qquad (15)$$

Integrating equation (15) between the limits 0 and ϵ, and 0 and t,

$$\epsilon = \frac{1}{\sqrt{3}\,n} \ln \frac{1}{[1 - \sqrt{3}\,An(\sqrt{3}\,ap/2h)^n t]} \qquad (16)$$

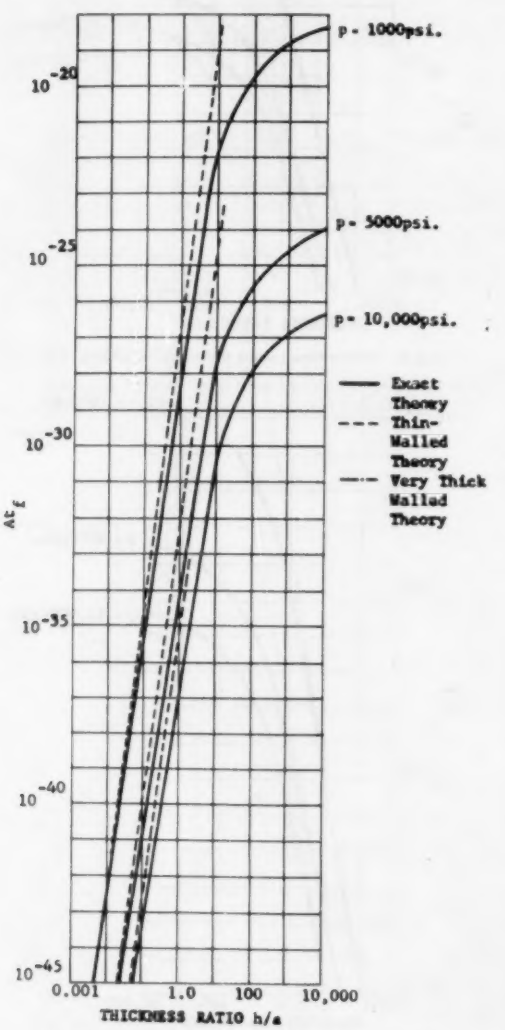

Fig. 7 Failure time versus thickness ratio for $n = 8$

Equation (16) gives the significant strain as a function of time t. It is used in Fig. 1 to illustrate the characteristic expansion of a vessel as a function of time. Fig. 1 shows how slowly creep takes place at the beginning, and how much it is accelerated when the time approaches the failure time. If actual fracture would take place at a significant strain of, say, $\epsilon = 1$, the fracture time would be about 97 per cent of the failure time (point A in Fig. 1). It is found that the larger the value of n, the closer is the foregoing approximation.

Letting $\epsilon \to \infty$ in equation (16), the equation for the creep-failure time for a thin-walled cylinder is obtained; that is,

$$t_f = \frac{1}{\sqrt{3}\,An}\left(\frac{2h}{\sqrt{3}\,ap}\right)^n \qquad (17)$$

As can be seen in Figs. 2 to 7, the curves defining the creep-failure time for a thick-walled cylinder, as given by equation (12), become asymptotic for small values of b/a to the curves for the thin-walled cylinder [as given by equation (17)].

Very Thick-Walled Cylinder. It is also possible to simplify the equation for the creep-failure time for a vessel with very thick walls. Making the assumption that b/a is so large that $a/b = 0$ can be used in the failure-time equation (12), it is shown in the Appendix that the integral defined in equation (13) reduces to

$$(I_\infty)_v = \frac{2n}{\sqrt{3}} \ln \frac{b}{a} - B_n \qquad (18)$$

where B_n is a quantity which varies with the creep exponent n.

The creep-failure time for a very thick-walled cylinder is then given by

$$t_f = \frac{n^n}{\sqrt{3}^n\,Ap^n}(I_\infty)_v \qquad (19)$$

The curve defined by equation (19) represents the asymptote to the curve defined by equation (12), for large values of b/a. The curve for the creep-failure time for very thick-walled cylinders is shown in Figs. 2[2] to 6.

Discussion

The calculation of creep-failure time for the exact and the very thick-walled cylinder formulas is quite complicated. For this reason, creep-failure times are represented graphically as shown in Figs. 2 to 7.

In the graphical presentation of creep-failure time, there are four variables which must be considered. They include the internal pressure p, the wall-thickness ratio b/a, the creep exponent n, and the creep-failure time t_f. The creep coefficient A is also to be considered, but it so happens that A can be combined with t_f in the form of a parameter At_f.

Figs. 2 to 7 show the creep-failure-time parameter At_f plotted versus the wall-thickness ratio h/a. A wide range of values for h/a was chosen in order to include the creep-failure time as predicted by the formulas for a thin-walled cylinder and a very thick-walled cylinder. An upper limit of $h/a = 10{,}000$ and a lower limit of $h/a = 0.001$ were chosen, Figs. 2 to 7. The internal pressure is used as a parameter and curves for $p = 1000$, 5000, and 10,000 psi are drawn.

A separate diagram is drawn for each value of the creep exponent n. Values were chosen which allowed the most accurate determination of creep-failure time without an undue expenditure of effort. The values chosen are $n = 1$, $n = 2$, $n = 3$, $n = 4$, $n = 6$, and $n = 8$. Values of n higher than 8, and higher than 5 for odd integers, present complicated expressions for the in-

[2] For $n = 1$, the curves for the thick-walled cylinder and the very thick-walled cylinder coincide.

tegral I_∞. The accurate numerical determination of these expressions becomes extremely difficult. Figs. 2 to 7 show curves for creep-failure times for thick-walled (exact), thin-walled, and very thick-walled cylinders, determined by means of equations (12) and (13), (17), and (12) and (18). The results are plotted on log-log paper to facilitate the presentation of a wide range of creep-failure times.

Figs. 2 to 7 allow an easy determination of the creep-failure time for vessels of any wall-thickness ratio h/a, if the value of the creep exponent of the material of the vessel is an integer of magnitude $n = 1, 2, 3, 4, 6$, and 8. Curves for pressures of $p = 1000$, 5000, and 10,000 psi are shown; values for other pressures can be obtained by interpolation.

If the creep exponent n is not one of the foregoing integers, Fig. 8 can be used for the determination of creep-failure times. In Fig. 8 the integral I_∞ is plotted against the creep exponent n for values of n from 0 to 12. Since the exact integral, as given by equation (13), was not determined for values of n larger than 8, the values for I_∞ for $n > 8$ were obtained by extrapolation. Various values of wall-thickness ratio h/a are represented as a parameter.

Another possibility is to plot curves of the type shown in Figs. 9

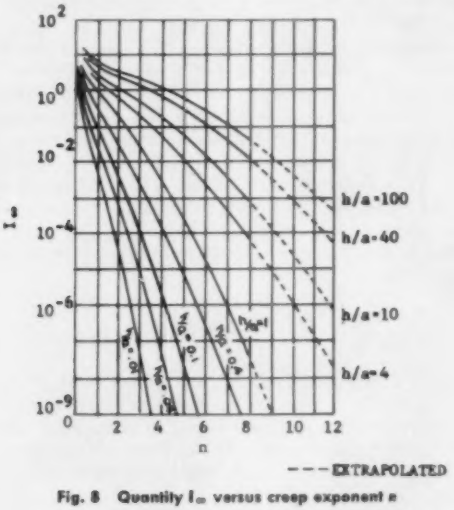

Fig. 8 Quantity I_∞ versus creep exponent n

and 10. In these figures, the creep-failure time is plotted versus the internal pressure with the wall-thickness ratio as a parameter. The slope of the curves is determined by the magnitude of the creep exponent n. Figs. 9 and 10 are similar to the usual stress-to-rupture diagrams.

Conclusion

The creep-failure time for a thick-walled pressure vessel is defined in this paper as the time at which the true creep strain reaches infinity. It was then shown that the creep-failure time defined in this manner can be used to predict the time-to-fracture of a vessel. The mathematical solution of the exact problem is quite complicated. For this reason, the solution is presented in the form of graphs. Simplified formulas for creep-failure time were obtained for both thin-walled cylinders and very thick-walled cylinders. These latter results appear as asymptotes to the curves for the exact solution of the thick-walled cylinder.

Acknowledgments

This work represents part of a Master of Science thesis prepared by Earl J. Mills under the supervision of F. P. J. Rimrott and J. Marin. The work was, in part, financially supported by the Pressure Vessel Research Committee of the Welding Research Council.

References

1 N. J. Hoff, "The Necking and the Rupture of Rods Subjected to Constant Tensile Loads," JOURNAL OF APPLIED MECHANICS, vol. 20, TRANS. ASME, vol. 75, 1953, pp. 105–108.

2 F. P. J. Rimrott, "Creep of Thick-Walled Tubes Under Internal Pressure Considering Large Strains," JOURNAL OF APPLIED MECHANICS, vol. 26, TRANS. ASME, vol. 81, series E, 1959, pp. 271–275.

3 W. Gröbner and N. Hofreiter, "Integraltafel, Erster Teil," Springer-Verlag, Wien und Innsbruck, Germany, vol. 1, 1949.

4 C. R. Soderberg, Discussion on Bailey, "Design Aspects of Creep," TRANS. ASME, vol. 58, 1936, p. A-150.

5 J. Marin, "Design of Members Subjected to Creep at High Temperatures," TRANS. ASME, vol. 58, 1936, p. A-21.

6 A. E. Johnson, "Creep Under Complex Stress Systems at Elevated Temperatures," *Proceedings*, The Institution of Mechanical Engineers, vol. 164, 1951, pp. 432–446.

7 A. Nadai, "On the Creep of Solids at Elevated Temperatures," *Journal of Applied Physics*, vol. 8, 1937, pp. 418–432.

8 E. Orowan, "Mechanical Testing of Solids," in The Principles of Rheological Measurements, British Rheologists' Club, Thomas Nelson and Sons Ltd., London, England, 1949.

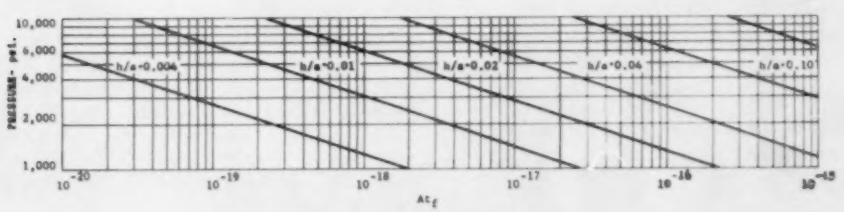

Fig. 9 Pressure versus failure time for $n = 3$

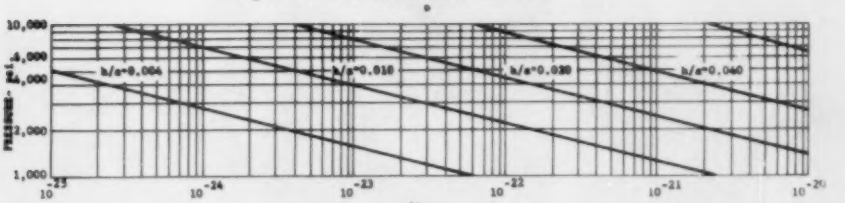

Fig. 10 Pressure versus failure time for $n = 4$

APPENDIX

The integral I_∞ in equation (13) is given by

$$I_\infty = \int_0^\infty \left\{1 - \left[\frac{(a/b)^2 \exp 3\epsilon_a}{1 + (a/b)^2(\exp 3\epsilon_a - 1)}\right]^{1/n}\right\}^n d\epsilon_a \quad (20)$$

For the solution of this integral it is advisable to substitute for the variable ϵ_a by setting

$$x = \left[\frac{(a/b)^2 \exp 3\epsilon_a}{1 + (a/b)^2(\exp 3\epsilon_a - 1)}\right]^{1/n} \quad (21)$$

Placing this new variable in equation (20) gives

$$I = \frac{n}{\sqrt{3}} \int_{(a/b)^{2/n}}^1 \frac{(1-x)^n}{1-x^n} \frac{dx}{x} \quad (22)$$

The integral, as given by equation (22), can be expanded by using the binomial theorem. In order to include the limit 1 appearing in equation (22), the condition that n be an integer must be imposed. Imposing this condition and expanding equation (22) into a binomial expression,

$$I = \frac{n}{\sqrt{3}} \int_{(a/b)^{2/n}}^1 \frac{1}{x^n - 1} \sum_{m=-1}^{n-1} (-1)^m \binom{n}{m+1} x^m \, dx \quad (23)$$

The integral given by equation (23) can be integrated term by term. Each of these terms is of the type

$$I_m = \frac{n}{\sqrt{3}} (-1)^m \binom{n}{m+1} \int_{(a/b)^{2/n}}^1 \frac{x^m}{x^n - 1} \, dx \quad (24)$$

The solution of the integral given by equation (24) is[4]

$$I_m = \frac{n}{\sqrt{3}} (-1)^m \binom{n}{m+1} \left\{\frac{1}{n} \ln (x-1) + \frac{(1-s)(-1)^{m+1}}{n} \ln (x+1) + \frac{2}{n} \sum_{\nu=1}^{\rho-1} \left[R_\nu \cos \frac{2\nu(m+1)\pi}{n} - S_\nu \sin \frac{2\nu(m+1)\pi}{n}\right]\right\}\Bigg|_{(a/b)^{2/n}}^1 \quad (25)$$

with

$$n = 2\rho - s, \qquad s = 0 \text{ or } 1, \qquad n > 2$$
$$m = 0, 1, 2, \ldots, n-1$$

and

$$R_\nu = \tfrac{1}{2} \ln [x^2 - 2x \cos (2\nu\pi/n) + 1] \quad (26)$$

$$S_\nu = \arctan \frac{x - \cos(2\nu\pi/n)}{\sin (2\nu\pi/n)}$$

For the case of $m = -1$ in equation (24), the solution of the integral of equation (24) is[5]

$$I_{-1} = -\frac{1}{\sqrt{3}} \ln \frac{x^n}{x^n - 1}\Bigg|_{(a/b)^{2/n}}^1 \quad (27)$$

Adding the results obtained by applying the solutions of equation (24), as given by equations (25) and (27), as often as necessary, the general solution of the integral of equation (20) can be obtained. Making a few simplifications, its value becomes

$$I_\infty = \frac{1}{\sqrt{3}} \left\{n \ln x - \ln \sum_{\mu=0}^{n-1} x^\mu - (1-s)(2^n - 1) \ln (x+1) + 2 \sum_{m=0}^{n-1} (-1)^m \binom{n}{m+1} \sum_{\nu=1}^{\rho-1} \left[R_\nu \cos \frac{2\nu(m+1)\pi}{n} - S_\nu \sin \frac{2\nu(m+1)\pi}{n}\right]\right\}\Bigg|_{(a/b)^{2/n}}^1 \quad (28)$$

where n is an integer larger than 2, and ρ, s, R_ν, and S_ν are given by equations (26). For $n = 1$ and $n = 2$, the integral of equation (22) becomes very simple and can easily be solved directly.

The numerical value of I_∞, obtained from equation (28), is inserted into equation (12) and the creep-failure time can thus be determined.

If the diameter ratio b/a is so large that the assumption $a/b = 0$ can be made, equation (28) can be reduced considerably. The condition that b/a is very large is valid for "very thick-walled" cylinders. Although such very thick-walled cylinders are hardly ever found in practice, the creep-failure time determined for a very thick-walled cylinder has proved very useful in properly locating the curve for the exact theory. The curve for the creep-failure time for a very thick-walled cylinder is the asymptote to the exact curve for large values of b/a.

Letting $(a/b) \to 0$ in equation (28) leads to an expression of the following form:

$$(I_\infty)_\nu = \frac{2n}{\sqrt{3}} \ln (b/a) - B_n \quad (29)$$

where B_n is a term independent of b/a. Since B_n is, however, a function of n, it must be determined for every value of n separately. The numerical value obtained from equation (29) can then be entered into equation (19) for the determination of the creep-failure time of a very thick-walled pressure vessel.

Since the term B_n is subtracted from the term $2n/\sqrt{3} \ln (b/a)$, it is apparent that the integral $(I_\infty)_\nu$ becomes zero when

$$\frac{2n}{\sqrt{3}} \ln (b/a) = B_n \quad (30)$$

This means that the integral $(I_\infty)_\nu$ will become asymptotic to the value of b/a defined by equation (30), if $(I_\infty)_\nu$ is plotted versus (b/a) on a logarithmic plot. Diagrams of At_f, which is directly proportional to $(I_\infty)_\nu$ versus h/a, which is given by $h/a = b/a - 1$, show the same characteristic if plotted on log-log paper, as can be seen in Figs. 3 to 6.

[4] Reference [3], p. 21.
[5] Ibid., p. 18.

F. P. J. RIMROTT
Assistant Professor,
Department of Mechanical Engineering,
University of Toronto,
Toronto, Ontario, Canada
Mem. ASME

On the Plastic Behavior of Rotating Cylinders

Equations for strain and stress distribution in hollow rotating cylinders are developed. The deformations are considered to be of such magnitude, that the use of finite-strain theory is necessary. It is assumed that the relationship of true stress to true strain can be represented by a power relation. The three possible modes of plastic failure, namely, instability, cleavage, and shear fracture, are also discussed.

For an ideally plastic material without strain-hardening, the stress distribution in solid rotating cylinders has been described by Nadai [1].[1] The addition of a central hole and the consideration of a rigid-plastic material with linear strain-hardening have been discussed by Davis and Connelly [2]. The present paper undertakes to describe the behavior of rotating hollow cylinders by considering finite strains and a power relationship between stress and strain, with the help of which the strain and stress distribution in the wall and the conditions for plastic failure are determined.

In the following analysis, an ideal material will be considered, which behaves according to the following assumptions:

1 The true longitudinal strain ϵ_z is constant with respect to the radius r, or

$$\epsilon_z = k \tag{1}$$

This assumption is valid only for long cylinders.

2 The volume of the material remains constant, or

$$\epsilon_\varphi + \epsilon_r + \epsilon_z = 0 \tag{2}$$

3 The ratios of the principal shearing stresses to the principal shearing strains are equal. That is

$$\frac{\sigma_\varphi - \sigma_r}{\epsilon_\varphi - \epsilon_r} = \frac{\sigma_r - \sigma_z}{\epsilon_r - \epsilon_z} = \frac{\sigma_z - \sigma_\varphi}{\epsilon_z - \epsilon_\varphi} = {}^2/_3 P \tag{3}$$

where P is the modulus of plasticity.

4 The material is isotropic and homogeneous and the cylinder retains its circular shape during deformation.

5 A significant true stress-strain relation exists, and coincides with the true stress-strain relation for simple tension in the plastic range. That is

$$\sigma = f(\epsilon) \tag{4}$$

In the present analysis this stress-strain relationship is assumed to be

$$\sigma = K\epsilon^n \tag{5}$$

where K is the strength coefficient, n is the strain-hardening exponent, σ is the significant true stress, defined by

$$\sigma = \frac{1}{\sqrt{2}} [(\sigma_\varphi - \sigma_r)^2 + (\sigma_r - \sigma_z)^2 + (\sigma_z - \sigma_\varphi)^2]^{1/2} \tag{6}$$

and ϵ is the significant true strain, defined by

$$\epsilon = \frac{\sqrt{2}}{3} [(\epsilon_\varphi - \epsilon_r)^2 + (\epsilon_r - \epsilon_z)^2 + (\epsilon_z - \epsilon_\varphi)^2]^{1/2} \tag{7}$$

Equations (2), (3), (6), and (7) can be combined to give stress-strain relations of the type

$$\epsilon_\varphi = \frac{1}{P}\left[\sigma_\varphi - \frac{1}{2}(\sigma_r + \sigma_z)\right]$$

$$\epsilon_r = \frac{1}{P}\left[\sigma_r - \frac{1}{2}(\sigma_z + \sigma_\varphi)\right] \tag{8}$$

$$\epsilon_z = \frac{1}{P}\left[\sigma_z - \frac{1}{2}(\sigma_\varphi + \sigma_r)\right]$$

where P, the modulus of plasticity, is given by

$$P = \sigma/\epsilon \tag{9}$$

and must be determined for every state of stress.

Strain Distribution

Considering the relations expressed by equations (1) and (2), the expression for the significant strain, given by equation (7) can be reduced to

[1] Numbers in brackets designate References at end of paper.

Contributed by the Applied Mechanics Division and presented at the Annual Meeting, Atlantic City, N. J., November 29–December 4, 1959, of The American Society of Mechanical Engineers.

Discussion of this paper should be addressed to the Secretary, ASME, 29 West 39th Street, New York, N. Y., and will be accepted until July 10, 1960, for publication at a later date. Discussion received after the closing date will be returned.

Note: Statements and opinions advanced in papers are to be understood as individual expressions of their authors and not those of the Society. Manuscript received by ASME Applied Mechanics Division, April 13, 1959. Paper No. 59—A-65.

Nomenclature

B_v = Bernoulli number
F = force, lb
K = strength coefficient, psi
P = modulus of plasticity, psi
a, a' = nominal and actual inner radius, in.
b, b' = outer radius, in.
c = a constant
k = longitudinal strain
n = strain-hardening exponent
r, r' = radius, in.
u = radial deformation, in.
γ = maximum true shearing strain
ϵ = true normal strain; also significant true strain
ρ = mass density, lb sec^2 in.$^{-4}$
σ = true normal stress; also significant true stress, psi
τ = maximum true shearing stress, psi

Subscripts

a = at inner radius
b = at outer radius
h = mean normal (hydrostatic)
r = radial
z = longitudinal
φ = circumferential

$$\epsilon = \frac{2}{\sqrt{3}} [\epsilon_\varphi^2 + k\epsilon_\varphi + k^2]^{1/2} \quad (10)$$

The true circumferential strain ϵ_φ can be shown [3] to be

$$\epsilon_\varphi = \ln \frac{r'}{r} = \ln (1 + u/r) \quad (11)$$

and the true radial strain can be shown [3] to be

$$\epsilon_r = \ln \frac{dr'}{dr} = \ln (1 + du/dr) \quad (12)$$

According to equation (1) this paper assumes the general case of plane strain where the strain in the third direction is constant, but not zero, in the $r - \varphi$ plane. This limits the discussion to long cylinders.

A combination of equations (11) and (12), with elimination of u, gives

$$r \frac{d\epsilon_\varphi}{dr} = \exp(\epsilon_r - \epsilon_\varphi) - 1 \quad (13)$$

From equations (1) and (2),

$$\epsilon_r = -k - \epsilon_\varphi \quad (14)$$

Entering the expression for ϵ_r, as given by equation (14), into equation (13),

$$r \frac{d\epsilon_\varphi}{dr} = \exp(-k - 2\epsilon_\varphi) - 1 \quad (15)$$

Equation (15) can be integrated by separation of variables. Then the true circumferential strain becomes

$$\epsilon_\varphi = {}^1/_2 \ln (e^{-k} + c/r^2) \quad (16)$$

Equation (16), evaluated at $r = a$, is

$$\epsilon_{\varphi a} = {}^1/_2 \ln (e^{-k} + c/a^2) \quad (17)$$

The unknown constant c can now be eliminated by combining equations (16) and (17). Solved for ϵ_φ,

$$\epsilon_\varphi = {}^1/_2 \ln \{[1 - (a/r)^2]e^{-k} + (a/r)^2 \exp 2\epsilon_{\varphi a}\} \quad (18)$$

From equation (10),

$$\epsilon_{\varphi a} = {}^1/_2[-k + \sqrt{3}\, \epsilon_a (1 - k^2/\epsilon_a^2)^{1/2}] \quad (19)$$

Entering the expression for $\epsilon_{\varphi a}$, as given by equation (19), into equation (18), and then inserting the expression for ϵ_φ, as given by equation (18), into equation (10), gives after some simplification

$$\epsilon = \left\langle k^2 + {}^1/_2 \ln^2 \left\{ 1 + \left(\frac{a}{r}\right)^2 \left[\exp \sqrt{3}\, \epsilon_a (1 - k^2/\epsilon_a^2)^{1/2} - 1 \right] \right\} \right\rangle^{1/2} \quad (20)$$

Equation (20) expresses the distribution of the significant true strain ϵ throughout the cylinder wall as a function of the radius r for a given significant strain ϵ_a at $r = a$ and a given longitudinal strain k.

With the distribution of the significant true strain known, the true circumferential strain ϵ_φ can be obtained by rewriting equation (10)

$$\epsilon_\varphi = {}^1/_2[-k + \sqrt{3}\, \epsilon(1 - k^2/\epsilon^2)^{1/2}] \quad (21)$$

With the distribution of ϵ and ϵ_φ known, the true radial strain ϵ_r is obtained from equation (14) as

$$\epsilon_r = -k - \epsilon_\varphi \quad (14)$$

The longitudinal strain ϵ_z is given as

$$\epsilon_z = k \quad (1)$$

The maximum shearing strain γ can also be found. It is

$$\gamma = \epsilon_{max} - \epsilon_{min} \quad (22)$$

where ϵ_{max} is always equal to ϵ_φ, and ϵ_{min} is equal to ϵ_r for an inner portion of the wall and then switches to $\epsilon_{min} = k$ for the outer portion of the wall.

Stress Distribution

It can be shown [4] that the equilibrium equation for a rotating body is

$$(r + u) \frac{d\sigma_r}{d(r + u)} = (\sigma_\varphi - \sigma_r) - \rho\omega^2(r + u)^2 \quad (23)$$

Rearranging equation (23) and observing that from equation (11), $(1 + u/r) = \exp \epsilon_\varphi$, that from equation (12), $(1 + du/dr) = \exp \epsilon_r$, and that from equation (14), $\epsilon_r = -k - \epsilon_\varphi$, it is

$$r \frac{d\sigma_\varphi}{dr} = (\sigma_\varphi - \sigma_r) \exp(-k - 2\epsilon_\varphi) - \rho\omega^2 e^{-k} r^2 \quad (24)$$

By using the relation expressed by equation (21), it becomes possible to write

$$d\sigma_r = (\sigma_\varphi - \sigma_r) \{\exp [-\sqrt{3}\, \epsilon (1 - k^2/\epsilon^2)^{1/2}]\} \frac{dr}{r} - \rho\omega^2 e^{-k} r\, dr \quad (25)$$

From equations (8) and (9),

$$\sigma_z = \sigma \frac{k}{\epsilon} + \frac{1}{2}(\sigma_\varphi + \sigma_r) \quad (26)$$

Substituting the value of σ_z of equation (26) in equation (6), one obtains

$$\sigma_\varphi - \sigma_r = \frac{2}{\sqrt{3}} \sigma (1 - k^2/\epsilon^2)^{1/2} \quad (27)$$

Replacing $(\sigma_\varphi - \sigma_r)$ in equation (25) by the expression of equation (27),

$$d\sigma_r = \frac{2}{\sqrt{3}} \sigma (1 - k^2/\epsilon^2)^{1/2} \{\exp [-\sqrt{3}\, \epsilon (1 - k^2/\epsilon^2)^{1/2}]\} \frac{dr}{r} - \rho\omega^2 e^{-k} r\, dr \quad (28)$$

Equation (20) may be rearranged to

$$r^2 = a^2 \frac{\exp \sqrt{3}\, \epsilon_a (1 - k^2/\epsilon_a^2)^{1/2} - 1}{\exp \sqrt{3}\, \epsilon (1 - k^2/\epsilon^2)^{1/2} - 1} \quad (29)$$

Differentiation of equation (29) with respect to ϵ, and division by $2r^2$, gives

$$\frac{dr}{r} = -\frac{\sqrt{3}}{2}\frac{\exp\sqrt{3}\,\epsilon\,(1-k^2/\epsilon^2)^{1/2}\cdot d\epsilon}{(1-k^2/\epsilon^2)^{1/2}[\exp\sqrt{3}\,\epsilon\,(1-k^2/\epsilon^2)^{1/2}-1]} \quad (30)$$

Inserting the value of dr/r from equation (30) in equation (28),

$$d\sigma_r = -\frac{\sigma d\epsilon}{\exp\sqrt{3}\,\epsilon\,(1-k^2/\epsilon^2)^{1/2}-1} - \rho\omega^2 e^{-k} r\,dr \quad (31)$$

For an n-power stress-strain relation,

$$\sigma = K\epsilon^n \quad (5)$$

Entering of $K\epsilon^n$ in place of σ in equation (31), leads to

$$d\sigma_r = -\frac{K\epsilon^n d\epsilon}{\exp\sqrt{3}\,\epsilon\,(1-k^2/\epsilon^2)^{1/2}-1} - \rho\omega^2 e^{-k} r dr \quad (32)$$

Equation (32) cannot be integrated in closed form; it can, however, be successfully integrated by expansion into series and subsequent integration. The quantity

$$\frac{\sqrt{3}\,\epsilon\,(1-k^2/\epsilon^2)^{1/2}}{\exp\sqrt{3}\,\epsilon\,(1-k^2/\epsilon^2)^{1/2}-1}$$

may, according to reference [5],[2] be expanded into

$$\sum_{\nu=0}^{\infty}\frac{B_\nu}{\nu!}\sqrt{3}^\nu\,\epsilon^\nu(1-k^2/\epsilon^2)^{2/\nu} \quad (33)$$

with $B_0 = 1$, $B_1 = -1/2$, $B_2 = 1/6$, $B_4 = -1/30$, $B_6 = 1/42$, $B_8 = -1/30$, and $B_3 = B_5 = B_7 = 0$. And the quantity

$$(1-k^2/\epsilon^2)^{\nu/2}$$

may, according to reference [5],[2] be expanded to

$$\sum_{\lambda=0}^{\infty}(-1)^\lambda\binom{\nu/2}{\lambda}k^{2\lambda}/\epsilon^{2\lambda} \quad (34)$$

The series (33) is convergent for

$$\epsilon < (k^2 + 1/3\,\pi^2)^{1/2}$$

a condition, which will be found fulfilled for all practical cases. The series (34) is convergent for $\epsilon > k$, a condition, which is always fulfilled, as an inspection of equation (10) will indicate.

Use of series (33) and (34) in equation (32), integration, and consideration of the boundary condition $\sigma_r = 0$ for $r = a$, gives

$$\sigma_r = K\sum_{\nu=0}^{\infty}\frac{B_\nu}{\nu!}\sqrt{3}^{\nu-1}\sum_{\lambda=0}^{\infty}(-1)^\lambda\binom{(\nu-1)/2}{\lambda}\frac{k^{2\lambda}}{\nu-2\lambda+n}$$
$$(\epsilon_a^{\nu-2\lambda+n} - \epsilon^{\nu-2\lambda+n}) - \frac{\rho\omega^2}{2}e^{-k}(r^2-a^2) \quad (35)$$

Equation (35) gives the distribution of the radial stress throughout the wall of the cylinder, provided the distribution of the significant strain ϵ, and the longitudinal strain k and the speed factor $\rho\omega^2/2$ are known.

The distribution of the significant stress is found by means of equation (5),

$$\boxed{\sigma = K\epsilon^n} \quad (5)$$

[2] Reference [5], p. 82.
[2] Ibid., p. 79.

The tangential stress is, from equation (27),

$$\boxed{\sigma_\varphi = \sigma_r + \frac{2}{\sqrt{3}}\sigma(1-k^2/\epsilon^2)^{1/2}} \quad (36)$$

The longitudinal stress can be found from equation (26),

$$\boxed{\sigma_z = \sigma\frac{k}{\epsilon} + 1/2(\sigma_\varphi + \sigma_r)} \quad (26)$$

The maximum shearing stress is defined as

$$\boxed{\tau = 1/2(\sigma_{\max} - \sigma_{\min})} \quad (37)$$

where $\sigma_{\max}$ is found to be always equal to σ_φ, and $\sigma_{\min}$ is equal to σ_r for an inner portion of the wall and equal to σ_z for the outer portion.

The mean normal stress can be found from its definition

$$\boxed{\sigma_h = 1/3(\sigma_\varphi + \sigma_r + \sigma_z)} \quad (38)$$

Equation (35) also can be used to establish a relation between ϵ, k, and $\rho\omega^2/2$. Making use of the condition that $\sigma_r = 0$ at $r = b$,

$$\frac{KR_b}{\sqrt{3}\,n} = \frac{\rho\omega^2}{2}e^{-k}(b^2-a^2) \quad (39)$$

with

$$R_b = \sum_{\nu=0}^{\infty}\frac{B_\nu}{\nu!}\sqrt{3}^\nu\sum_{\lambda=0}^{\infty}(-1)^\lambda\binom{(\nu-1)/2}{\lambda}\frac{nk^{2\lambda}}{\nu-2\lambda+n}$$
$$(\epsilon_a^{\nu-2\lambda+n} - \epsilon_b^{\nu-2\lambda+n}) \quad (40)$$

and, from equation (20),

$$\epsilon_b = \left\langle k^2 + 1/2\ln^2\left\{1+\left(\frac{a}{b}\right)^2\right.\right.$$
$$\left.\left.[\exp\sqrt{3}\,\epsilon\,(1-k^2/\epsilon_a^2)^{1/2}-1]\right\}\right\rangle^{1/2} \quad (41)$$

An inspection of equations (23) and (24) shows, that the right side of equation (39) could also have been obtained in terms of the actual radii $a' = a + u_a$ and $b' = b + u_b$. Then

$$\frac{KR_b}{\sqrt{3}\,n} = \frac{\rho\omega^2}{2}(b'^2 - a'^2) \quad (42)$$

It will be found in numerical work, that the ν-series in equation (40) can be broken off after the term for $\nu = 1$ because of the rapid convergence of this series for all practical cases.

The Longitudinal Force

For a given k, two unknowns ϵ and $\rho\omega^2/2$, must be found. One expression for their determination is equation (42), the other will now be derived from the condition that the force in longitudinal direction must be zero,

$$F_z = 0 \quad (43)$$

The equilibrium equation (23) also may be written

$$d\sigma_r = (\sigma_\varphi - \sigma_r)\frac{dr'}{r'} - \rho\omega^2 r'\,dr' \quad (44)$$

Using the expression for $\sigma_\varphi - \sigma_r$, as given by equation (27), in equation (44) and integrating equation (44),

$$\sigma_r = \int_{a'}^{r'} \frac{2}{\sqrt{3}} \sigma (1 - k^2/\epsilon^2)^{1/2} \frac{dr'}{r'} - \frac{\rho\omega^2}{2} (r'^2 - a'^2) \quad (45)$$

where the limit a' has been chosen to make $\sigma_r = 0$ at $r' = a'$. The radial stress is also $\sigma_r = 0$ at $r' = b'$, hence

$$\int_{a'}^{b'} \frac{2}{\sqrt{3}} \sigma (1 - k^2/\epsilon^2)^{1/2} \frac{dr'}{r'} = \frac{\rho\omega^2}{2} (b'^2 - a'^2) \quad (46)$$

Placing the value for σ_r, as given by equation (45), in equation (27) and rearranging, gives

$$\sigma_\varphi = \int_{a'}^{r'} \frac{2}{\sqrt{3}} \sigma (1 - k^2/\epsilon^2)^{1/2} \frac{dr'}{r'} - \frac{\rho\omega^2}{2} (r'^2 - a'^2) + \frac{1}{\sqrt{3}} \sigma (1 - k^2/\epsilon^2)^{1/2} \quad (47)$$

Inserting the value for σ_φ, as given by equation (47), into equation (26) for the longitudinal stress,

$$\sigma_z = \sigma \left[\frac{k}{\epsilon} + \frac{1}{\sqrt{3}} (1 - k^2/\epsilon^2)^{1/2} \right] + \int_{a'}^{r'} \frac{2}{\sqrt{3}} \sigma (1 - k^2/\epsilon^2)^{1/2} \frac{dr'}{r'} - \frac{\rho\omega^2}{2} (r'^2 - a'^2) \quad (48)$$

The cylinder is not subjected to any force in longitudinal direction, that is

$$F_z = 2\pi \int_{a'}^{b'} \sigma_z r' \, dr' = 0 \quad (49)$$

or

$$\int_{a'}^{b'} \sigma_z r' \, dr' = 0 \quad (50)$$

Using equation (48) for σ_z, equation (50) becomes

$$0 = \int_{a'}^{b'} \sigma \left[\frac{k}{\epsilon} + \frac{1}{\sqrt{3}} (1 - k^2/\epsilon^2)^{1/2} \right] r' \, dr' + \int_{a'}^{b'} r' \int_{a'}^{r'} \frac{2}{\sqrt{3}} \sigma (1 - k^2/\epsilon^2)^{1/2} \frac{dr'}{r'} \, dr' - \frac{\rho\omega^2}{8} [b'^4 - a'^4 - 2a'^2(b'^2 - a'^2)] \quad (51)$$

The double integral in equation (51) may be integrated by parts, giving

$$b'^2 \int_{a'}^{b'} \frac{1}{\sqrt{3}} \sigma (1 - k^2/\epsilon^2)^{1/2} \frac{dr'}{r'} - \int_{a'}^{b'} \frac{1}{\sqrt{3}} \sigma (1 - k^2/\epsilon^2)^{1/2} r' \, dr' \quad (52)$$

which, because of the relation expressed by equation (46), may be written

$$\frac{\rho\omega^2}{4} b'^2 (b'^2 - a'^2) - \int_{a'}^{b'} \frac{1}{\sqrt{3}} \sigma (1 - k^2/\epsilon^2)^{1/2} r' \, dr' \quad (53)$$

Substituting this expression for the double integral back into equation (51), simplifying, and observing that $\sigma = K\epsilon^n$,

$$K k \int_{a'}^{b'} \epsilon^{n-1} r' \, dr' = -1/8 \, \rho\omega^2 (b'^4 - a'^4) \quad (54)$$

It can be shown by use of equations (11), (21), and (29) that

$$r'^2 = a^2 e^{-k} [\exp \sqrt{3}\, \epsilon_a (1 - k^2/\epsilon_a^2)^{1/2} - 1] \frac{\exp \sqrt{3}\, \epsilon (1 - k^2/\epsilon^2)^{1/2}}{\exp \sqrt{3}\, \epsilon (1 - k^2/\epsilon^2)^{1/2} - 1} \quad (55)$$

Consequently is

$$b'^2 = a^2 e^{-k} [\exp \sqrt{3}\, \epsilon_a (1 - k^2/\epsilon_a^2)^{1/2} - 1] \frac{\exp \sqrt{3}\, \epsilon_b (1 - k^2/\epsilon_b^2)^{1/2}}{\exp \sqrt{3}\, \epsilon_b (1 - k^2/\epsilon_b^2)^{1/2} - 1} \quad (56)$$

and

$$a'^2 = a^2 e^{-k} \exp \sqrt{3}\, \epsilon_a (1 - k^2/\epsilon_a^2)^{1/2} \quad (57)$$

Differentiation of equation (55) with respect to ϵ gives

$$r' \, dr' = \frac{\sqrt{3}}{2} a^2 e^{-k} [\exp \sqrt{3}\, \epsilon_a (1 - k^2/\epsilon_a^2)^{1/2} - 1] \frac{1}{(1 - k^2/\epsilon^2)^{1/2}} \frac{1}{\exp \sqrt{3}\, \epsilon (1 - k^2/\epsilon^2)^{1/2} - 1} \frac{1}{\exp [-\sqrt{3}\, \epsilon (1 - k^2/\epsilon^2)^{1/2}] - 1} \, d\epsilon \quad (58)$$

Inserting now $r' \, dr'$ from equation (58), $(\rho\omega^2/2)(b'^2 - a'^2)$ from equation (42), b'^2 from equation (56), and a'^2 from equation (57), into equation (54), and simplifying, gives

$$\boxed{k = -\frac{R_b}{nT} \left[\frac{\exp \sqrt{3}\, \epsilon_a (1 - k^2/\epsilon_a^2)^{1/2}}{\exp \sqrt{3}\, \epsilon_a (1 - k^2/\epsilon_a^2)^{1/2} - 1} + \frac{\exp \sqrt{3}\, \epsilon_b (1 - k^2/\epsilon_b^2)^{1/2}}{\exp \sqrt{3}\, \epsilon_b (1 - k^2/\epsilon_b^2)^{1/2} - 1} \right]} \quad (59)$$

where

$$T = 6 \int_{\epsilon_a}^{\epsilon_b} \frac{\epsilon^{n-1}}{(1 - k^2/\epsilon^2)^{1/2}} \frac{1}{\exp \sqrt{3}\, \epsilon (1 - k^2/\epsilon^2)^{1/2} - 1} \frac{1}{\exp [-\sqrt{3}\, \epsilon (1 - k^2/\epsilon^2)^{1/2}] - 1} \, d\epsilon \quad (60)$$

The expression for T of equation (60) cannot be integrated directly. Using series similar to (33) and (34), T can however be expanded to

$$T = -2 \int_{\epsilon_a}^{\epsilon_b} \sum_{\nu=0}^{\infty} \sum_{\mu=0}^{\infty} (-1)^\mu \frac{B_\nu B_\mu}{\nu! \mu!} \sqrt{3}^{\nu+\mu} \sum_{\lambda=0}^{\infty} (-1)^\lambda \binom{(\nu + \mu - 3)/2}{\lambda} k^{2\lambda} \epsilon^{\nu+\mu-2\lambda+n-3} \, d\epsilon \quad (61)$$

After integration, equation (61) becomes

$$T = 2 \sum_{\nu=0}^{\infty} \sum_{\mu=0}^{\infty} (-1)^\mu \frac{B_\nu B_\mu}{\nu! \mu!} \sqrt{3}^{\nu+\mu} \sum_{\lambda=0}^{\infty} (-1)^\lambda \binom{(\nu + \mu - 3)/2}{\lambda} \frac{k^{2\lambda}}{2 - n - \nu - \mu + 2\lambda} (\epsilon_b^{\nu+\mu-2\lambda+n-2} - \epsilon_a^{\nu+\mu-2\lambda+n-2}) \quad (62)$$

The ν and μ series usually converge so quickly that it is sufficient for practical materials to use terms up to $\nu = 1$ and $\mu = 1$ only. This permits a considerable simplification of the expression for T.

Making this simplification, gives

$$T = 2\sum_{\lambda=0}^{\infty}(-1)^{\lambda}\binom{-3/2}{\lambda}\frac{k^{2\lambda}}{2-n+2\lambda}(\epsilon_b^{n-2-2\lambda}-\epsilon_a^{n-2-2\lambda}) \tag{63}$$

With T as given by equation (62) or by equation (63), R_b as given by equation (40), and ϵ_b as given by equation (41), equation (59) represents the relation which gives k as function of ϵ_a in implicit form. The procedure for the numerical determination of k, ϵ, and $\rho\omega^2/2$ will now be given.

Because of the complexity of the terms involved, it is desirable to begin with an assumed value of k (k will always be a negative quantity). With k fixed, a value for ϵ_a is chosen larger than $|k|$. Then ϵ_b is determined by means of equation (41). With the assumed k and the trial value for ϵ_a and hence ϵ_b, the quantity R_b can be found by use of equation (40). The quantity T also can be determined by means of equation (62) or equation (63). The validity of the trial value for ϵ_a can then be checked by entering all terms into equation (59). If equation (59) is not satisfied, the procedure must be repeated with a new trial value for ϵ_a, and consequently new values for ϵ_b, R_b, and T. The values of ϵ_a, and hence ϵ_b, R_b, and T, for which equation (59) is satisfied, are the correct values corresponding to the assumed value of k.

For other values of k, the corresponding values of ϵ and so on are determined in the same manner. The task is, however, much less formidable, since the fact that the ratios k/ϵ are almost constant, Table 1, can be used to establish the first trial value for ϵ_a.

The speed factor corresponding to an assumed k is found by rearranging equation (39), as

$$\frac{\rho\omega^2}{2} = \frac{KR_b}{\sqrt{3}\,n\,e^{-k}(b^2-a^2)} \tag{64}$$

Strain distributions are determined by employing equations (20), (21), (14), (1), and (22), stress distributions by employing equations (35), (5), (36), (26), (37), and (38). A number of stress and strain distributions have been determined for a cylinder with $b = 4$ in., $a = 1$ in., and made of a material for which $K = 100{,}000$ psi and $n = 0.2$. They are shown in Figs. 1 to 3. The strain in

Table 1

Longitudinal strain, k	Significant strain at $r = a$, ϵ_a	Significant strain at $r = b$, ϵ_b	Ratio, ϵ_a/k	Ratio, ϵ_b/k
−0.01	0.0565	0.01053	−5.65	−1.053
−0.06	0.34	0.06607	−5.75	−1.101

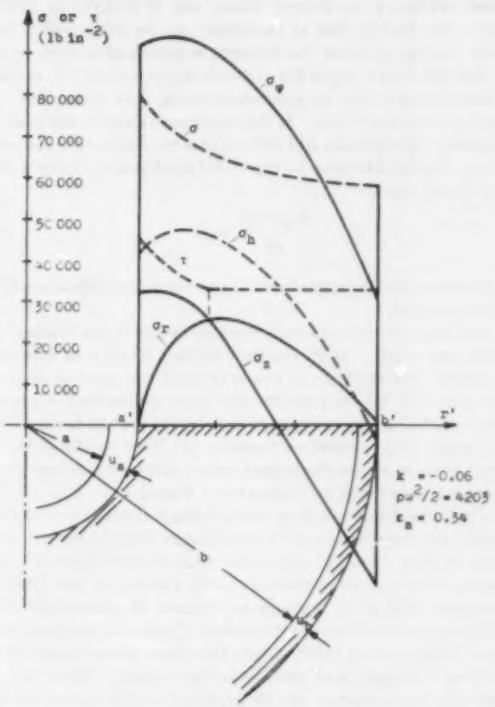

Fig. 2 Plastic stress distribution at a large strain (at instability)

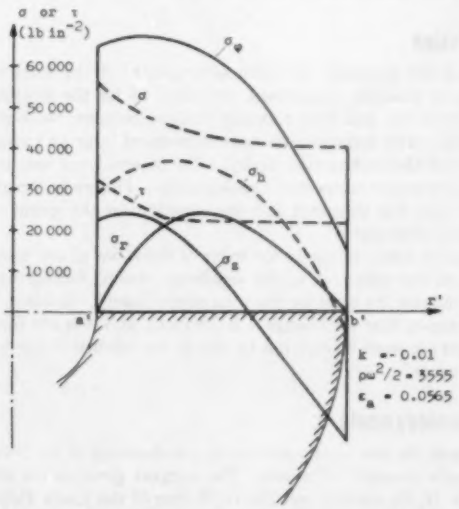

Fig. 1 Plastic stress distribution at a small strain

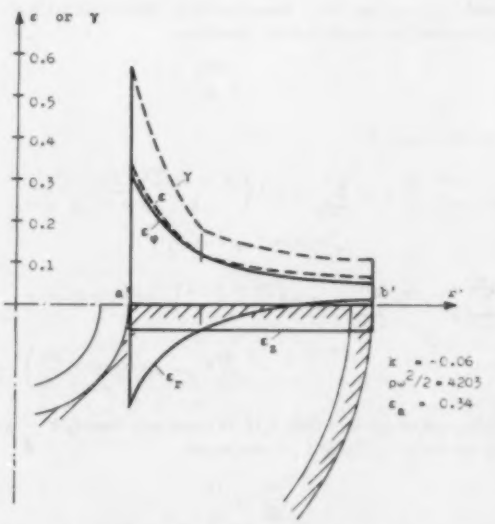

Fig. 3 Plastic strain distribution (at instability)

the longitudinal direction as function of the rotational speed is plotted in Fig. 4 for the same cylinder. In Table 1 the ratios ϵ_a/k and ϵ_b/k are shown for the cylinder at $k = -0.01$ and -0.06 (instability).

Plastic Failure

There are three conditions, which are of interest as plastic failure. The first is that of instability, or, in other words that state of loading at which the material is deformed to such an extent, that the weakening of the material due to contraction exceeds the strengthening due to strain-hardening. At instability the speed reaches a maximum. If this maximum speed is maintained or exceeded, the cylinder will deform at a very high rate and soon fracture. Instability may be expressed mathematically by a condition of the type

$$\frac{d(\rho\omega^2/2)}{dk} = 0 \tag{65}$$

The mathematical determination of the point of instability will be carried out later.

A rotating cylinder also may fracture before it has reached the point of instability. A maximum condition as such as expressed by equation (65) can then no longer be used, but must be replaced by a condition which predicts the type of fracture expected. If the material tends to fracture by cleavage, such fracture will likely begin as a subsurface fracture [2] close to the bore, because it is there where the largest tensile stress, σ_φ, occurs in the wall, as can be seen by an inspection of Figs. 1 or 2.

If a material tends to fail by shear fracture it becomes necessary to study the distribution of the maximum shear stress τ (or the maximum shear strain γ) and of the mean normal stress σ_h. Experiments, such as those carried out by Crossland and Dearden [6], suggest that shear fracture is initiated at points where the absolute maximum shearing stress is the largest at constant mean normal stress, and at points where the mean normal stress is the largest at constant maximum shearing stress. Based on this statement, shear fracture can be expected to commence either at the bore surface or as a subsurface fracture near the bore, as an inspection of Fig. 1 or 2 will indicate. A detailed account of the shear-fracture properties of the material involved will have to be available if more precise predictions are to be made.

Let us now determine mathematically the point of instability defined by equation (65). Equation (64) differentiated with respect to k and set equal to zero, results in

$$R_b = -\frac{dR_b}{dk} \tag{66}$$

From equation (40)

$$\frac{dR_b}{dk} = \sum_{\nu=0}^{\infty} \frac{B_\nu}{\nu!} \sqrt{3}^\nu \sum_{\lambda=0}^{\infty} (-1)^\lambda \binom{(\nu-1)/2}{\lambda} \frac{2\lambda n\, k^{2\lambda-1}}{\nu - 2\lambda + n} (\epsilon_a{}^{\nu-2\lambda+n} - \epsilon_b{}^{\nu-2\lambda+n})$$

$$+ \sum_{\nu=0}^{\infty} \frac{B_\nu}{\nu!} \sqrt{3}^\nu \sum_{\lambda=0}^{\infty} (-1)^\lambda \binom{(\nu-1)/2}{\lambda} n\, k^{2\lambda} \left(\epsilon_a{}^{\nu-2\lambda+n-1} \frac{d\epsilon_a}{dk} - \epsilon_b{}^{\nu-2\lambda+n-1} \frac{d\epsilon_b}{dk}\right) \tag{67}$$

Making use of the fact that $\epsilon_a/k \approx$ const and that $\epsilon_b/k \approx$ const, (see, for instance, Table 1), it can be set

$$\frac{d\epsilon_a}{dk} = \frac{\epsilon_a}{k} \tag{68}$$

and

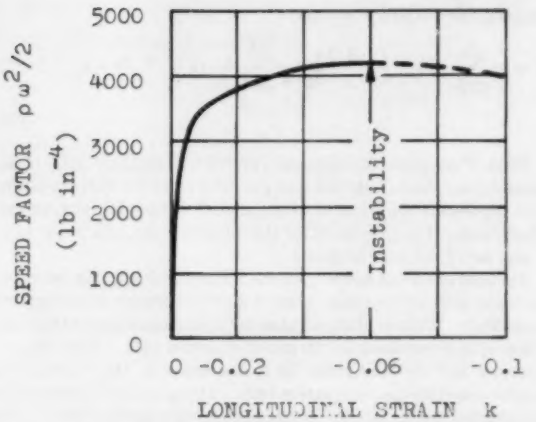

Fig. 4 Longitudinal strain and speed of rotation

$$\frac{d\epsilon_b}{dk} = \frac{\epsilon_b}{k} \tag{69}$$

Insertion of the expressions for $d\epsilon_a/dk$ and $d\epsilon_b/dk$, as given by equations (68) and (69), into equation (66), and use of R_b as defined by equation (64), gives

$$k = -n\left[1 + \frac{1}{R_b} \sum_{\nu=0}^{\infty} \frac{B_\nu \nu}{\nu!} \sqrt{3}^\nu \sum_{\lambda=0}^{\infty} (-1)^\lambda \binom{(\nu-1)/2}{\lambda} \frac{k^{2\lambda}}{\nu - 2\lambda + n} (\epsilon_a{}^{\nu-2\lambda+n} - \epsilon_b{}^{\nu-2\lambda+n})\right] \tag{70}$$

If the ν-series is broken off after the term for $\nu = 1$, equation (70) is simplified to

$$k = -n\left(1 - \frac{\sqrt{3}}{2} \frac{1}{1+n} \frac{\epsilon_a{}^{1+n} - \epsilon_b{}^{1+n}}{R_b}\right) \tag{71}$$

Equation (71) may be used for all practical cases in place of equation (70). The quantities k, ϵ_a, ϵ_b, and R_b must, of course, also fulfill the condition expressed by equation (59). Instability for the cylinder of the example used in this paper occurs at $k = -0.06$, and is marked on the plot in Fig. 4.

Conclusion

Using the generally accepted assumptions of the total strain theory of plasticity, equations were derived for the strains and stresses in the wall of a rotating, hollow, circular, thick-walled cylinder. The deformations were considered large and required the use of the finite-strain theory. The material was assumed to have an n-power stress-strain relationship. Failure in the plastic region also was discussed and the equation for the strain at instability determined.

There is some change in the value of the ratios of one principal strain to the other (or to the significant strain) during loading. This violates the basis for the total strain theory. Table 1, however, shows, that the change is quite small, and it is felt that the changes are small enough not to impair the validity of the derivations made.

Acknowledgments

This study was made possible by a Fellowship of the National Research Council of Canada. The support given to the project by Dr. H. Gaudefroy and Dr. G. Welter of the Ecole Polytechnique, Montreal Canada, is greatly appreciated.

References

1 A. Nadai, "Theory of Flow and Fracture of Solids," vol. 1, second edition, McGraw-Hill Book Company, Inc., New York, N. Y., 1950.

2 E. A. Davis and F. M. Connelly, "Stress Distribution and Plastic Deformation in Rotating Cylinders of Strain-Hardening Material," JOURNAL OF APPLIED MECHANICS, vol. 26, TRANS. ASME, vol. 81, series E, March 1959, pp. 25–30.

3 Joseph Marin and F. P. J. Rimrott, "Design of Thick-Walled Pressure Vessels Based Upon the Plastic Range," Welding Research Council Bulletin 41, New York, N. Y., July, 1958.

4 S. Timoshenko, "Strength of Materials," part 2, third edition, D. Van Nostrand Company, Inc., New York, N. Y., 1956.

5 Hütte, "Des Ingenieurs Taschenbuch," 28th edition, Verlag von Wilhelm Ernst und Sohn, Berlin, Germany, 1955.

6 B. Crossland and W. H. Dearden, "The Plastic Flow and Fracture of a 'Brittle' Material (Grey Cast Iron) with Particular Reference to the Effect of Fluid Pressure," Proceedings of The Institution of Mechanical Engineers, London, England, vol. 172, 1958, pp. 805–820.

R. T. SHIELD
Associate Professor of Applied Mathematics,
Brown University,
Providence, R. I.

On the Optimum Design of Shells[1]

A procedure is developed for obtaining the design of an elastic, perfectly plastic shell or structure which will support prescribed loads and which is the optimum design for a given criterion. The action of body forces is included in the analysis. Some problems in the minimum volume design of a circular cylindrical sandwich shell are solved to illustrate the method, and it is found that only for relatively short shells does the minimum volume design effect an appreciable saving over the membrane design.

THE present paper is a sequel to previous work [1, 2, 3][2] on minimum weight design. The purpose of the work is to supply design procedures for the optimum design of an elastic-plastic shell (or structure) which carries direct stresses or bending stresses or both. The design is sought which supports given loads and which is the optimum design for a given criterion. Here the optimum design is pursued without regard to difficulties and costs that may arise in its manufacture. It is to be expected, therefore, that the optimum design may be too impractical to be of use but it nevertheless will provide a designer with a basis of comparison with any proposed structure.

In the following, a formal design procedure is obtained for the design of a structure which is optimum for a given criterion. A general form is taken for the criterion and it includes minimum volume, minimum weight, and minimum moment of inertia about an axis as special cases. The design procedure is obtained through the use of limit analysis [4] and not by a direct application of the calculus of variations. The use of the limit-analysis theorems greatly simplifies the establishment of the procedure, and in the case of the sandwich shell it is shown that the procedure leads to an absolute minimum rather than to a relative minimum. This is a much stronger result than can be obtained by means of the calculus of variations.

For illustration, some problems are solved for the particular case of the minimum-volume design of a circular cylindrical sandwich shell. The results indicate that only for relatively short shells does the minimum-volume design effect an appreciable saving over either the design with constant thickness or the membrane design.

Statement of the Problem

The exact three-dimensional analysis of the behavior of a thin shell composed of a rigid-plastic material under prescribed loading is usually too difficult to perform or too complex to be of practical use. Useful results can be obtained from an approximate analysis based on a theory formulated in terms of generalized stresses and strain-rates such as the moments and force resultants across sections of the shell and rates of curvature and extension of the middle surface. The theory of limit analysis [4] has been extended by Prager [5] in a general manner to structures characterized by generalized stresses and strain rates. The basic theorems on collapse will be restated here. We remark that the results obtained apply to elastic-plastic materials, but it is convenient here to speak of rigid-plastic structures.

The generalized stresses will be denoted by $Q_1, Q_2, \ldots, Q_N$ or briefly Q_n. The corresponding generalized strain rates $q_1, q_2, \ldots, q_N$ are chosen so that the rate D_A at which energy is dissipated as a result of plastic action is given by

$$D_A = Q_1 q_1 + Q_2 q_2 + \ldots + Q_N q_N, \tag{1}$$

per unit area of the middle surface. Yielding can occur at an element of the shell when the stresses Q_n are such that the point Q_n in a generalized stress space of N-dimensions lies on the yield surface

$$F(Q_n) = K^2, \tag{2}$$

where K is a constant. Shear forces which enter into the equations of equilibrium of the shell have little influence on yielding [6] and are ignored in equations (1, 2). The strain-rate vector with components proportional to q_n is normal to the yield surface (2) at a regular point and at singular points lies in the fan bounded by the normals at adjacent points. For a convex yield surface, the normality condition on the strain rates q_n insures a unique value of the dissipation rate D_A for given strain rates q_n.

The appropriate theorems of limit analysis in terms of the present problem are:

Lower-Bound Theorem. If the applied loads can be carried by an equilibrium distribution of moments and force resultants Q_n in the shell which is at or below yield, the loading is at or below the limit loading.

Upper-Bound Theorem. If the applied loads are such that a deformation of the shell can be found for which the rate at which the applied loads do work is not less than the rate of internal dissipation of energy, the loading is at or above the limit loading.

These theorems can be used to obtain bounds on the load-carrying capacity of a given shell for a given type of loading. Here we assume that the shell has a prescribed middle surface A, and is acted upon by prescribed loads which may be distributed over the shell or may act at the boundaries of the shell. The thin shell is to be constructed by placing a certain thickness t of a given material at points of A. In the following, no restriction of homogeneity of material is imposed, so that it may be prescribed that different materials are to be used in different specified regions of the middle surface A. The problem is the determination of the variable thickness t so that the shell is just at the limit loading or collapse under the given loads and is such that the design is the optimum one for a given criterion.

It will be assumed here that it is required to design the shell so that the functional

[1] The results presented in this paper were obtained in the course of research sponsored by the Office of Ordnance Research, Department of the Army, under Contract No. DA-19-020-ORD-4564.

[2] Numbers in brackets designate References at end of paper

Contributed by the Applied Mechanics Division and presented at the Annual Meeting, Atlantic City, N. J., November 29–December 4, 1959, of THE AMERICAN SOCIETY OF MECHANICAL ENGINEERS.

Discussion of this paper should be addressed to the Secretary, ASME, 29 West 39th Street, New York, N. Y., and will be accepted until July 10, 1960, for publication at a later date. Discussion received after the closing date will be returned.

NOTE: Statements and opinions advanced in papers are to be understood as individual expressions of their authors and not those of the Society. Manuscript received by ASME Applied Mechanics Division, January 29, 1959. Paper No. 59—A-47.

$$\int_A tf(P)dA \tag{3}$$

is a minimum, where $f(P)$ denotes a non-negative function of the position of a point P on the middle surface A. When minimum volume is required, $f(P) \equiv 1$, and minimum volume coincides with minimum weight for a homogeneous material. In the nonhomogeneous case, minimizing the functional (3) will provide the minimum weight design if $f(P)$ is taken to be the density of the material to be used at the point P of A. Alternatively, if $f(P) = r_P^2$, where r_P denotes distance from an axis, minimizing (3) would design the shell for minimum moment of inertia about the axis in the homogeneous case.

Procedure for Optimum Design

The dissipation rate D_A is a monotonic increasing function of the thickness t of the shell and depends also on the position P in the nonhomogeneous case. It is also a function $D_A(u_i)$ of the velocity components u_i ($i = 1, 2, 3$) of the middle surface from which the generalized strain rates q_n are derived. The components of the applied loads and body force are denoted by T_i and F_i ($i = 1, 2, 3$). For a shell of thickness t_e which is just at the point of collapse under T_i in a deformation rate pattern u_i^e,

$$\int_A D_A(u_i^e)dA = \int_A T_i u_i^e dA + \int_A F_i u_i^e t_e dA \tag{4}$$

The body force F_i per unit volume is assumed to act only if material is present. Equation (4) can be written

$$\int_A \Delta_A(u_i^e)dA = \int_A T_i u_i^e dA, \tag{5}$$

where

$$\Delta_A(u_i^e) = D_A(u_i^e) - F_i u_i^e t_e \tag{6}$$

and $\Delta_A(u_i^e)$ will be called the modified dissipation rate.

We now consider a shell of thickness t_e which is a neighboring shell to the shell of thickness t_e in the sense that $t_e = t_e + \delta t$, where δt is a (small) variation in the terminology of the calculus of variations. Neglecting second and higher-order terms, the modified dissipation rate for the shell of thickness t_e in the deformation-rate pattern u_i^e is equal to

$$\Delta_A(u_i^e) + \delta t \frac{\partial}{\partial t} \Delta_A(u_i^e) \tag{7}$$

provided that $\Delta_A(u_i^e)$ is a continuously differentiable function of t. It is now assumed that the shell of thickness t_e is at or below collapse under the loads T_i. With the value (7) of the modified dissipation rate for the shell t_e it follows that

$$\int_A \left\{ \Delta_A(u_i^e) + \delta t \frac{\partial}{\partial t} \Delta_A(u_i^e) \right\} dA \geq \int_A T_i u_i^e dA, \tag{8}$$

for otherwise the use of the upper-bound theorem (and the collapse mode u_i^e) would predict collapse of the shell t_e under the loads T_i. Subtraction of equation (5) from this inequality gives

$$\int_A \delta t \frac{\partial}{\partial t} \Delta_A(u_i^e)dA \geq 0 \tag{9}$$

An immediate consequence of inequality (9) is that if the shell t_e is such that

$$\frac{\partial}{\partial t} \Delta_A(u_i^e) \Big/ f(P)$$

is constant (and positive) over the middle surface A then

$$\int_A \delta t f(P)dA \geq 0 \tag{10}$$

Thus a shell designed to be just at the point of collapse under the loads T_i and which has a collapse mode such that

$$\frac{1}{f(P)} \frac{\partial \Delta_A}{\partial t} = \text{const} \tag{11}$$

over the middle surface A provides a *relative* minimum of the functional (3) for shells which are at or below collapse under the loads T_i.

We remark that if it were required to minimize the functional

$$\int_A g(t, P)dA,$$

where $g(t, P)$ is continuously differentiable with respect to t, the corresponding condition would be

$$\frac{\partial}{\partial t} \Delta_A(u_i^e) \Big/ \frac{\partial}{\partial t} g(t, P)$$

constant over A.

When minimum volume is desired, i.e., when $f(P) \equiv 1$, the condition (11) has been obtained previously [2] for the particular case of the bending of a plate loaded by transverse pressure and body force, direct stresses being negligible. In this case D_A is proportional to t^3 and condition (11) was interpreted in [2] as requiring the modified dissipation rate Δ *per unit volume* to be constant on the surfaces of the plate. When no body force is present, condition (11) requires D_A/t constant for minimum-volume design of a plate in pure bending, as found previously [7].

The dissipation rate Δ_A per unit area of the middle surface is given by

$$\Delta_A = \int_{-t/2}^{t/2} \Delta dz,$$

where Δ is the modified dissipation rate per unit volume and the co-ordinate z measures distance from the middle surface so that $z = \pm 1/2 t$ are the surfaces of the shell. The derivative $\partial \Delta_A / \partial t$ is therefore given by

$$\frac{\partial \Delta_A}{\partial t} = \frac{1}{2} \left\{ (\Delta)_{z=1/2t} + (\Delta)_{z=-1/2t} \right\},$$

and is the average of the values of the modified dissipation rate Δ per unit volume at the two surfaces of the shell. In pure bending, at a section of the shell, Δ has the same value at each of the surfaces of the shell.

The result of this section applies to a sandwich shell if the appropriate form of the dissipation rate D_A is taken. However, a stronger result can be obtained, and the sandwich shell is considered in detail in the next section.

The Sandwich Shell

The ideal sandwich shell consists of a core of constant or variable thickness H between two thin identical face sheets each of thickness h, where $h \ll H$. The core carries only shear force. Moment and force resultants across a section of the shell are carried by membrane stresses in the face sheets. The thickness H of the core is prescribed and it is required to determine the thickness h of the faces so that the shell is just at the point of collapse under loads T_i and the functional

$$\int_A hf(P)dA \tag{12}$$

has a minimum value, where $f(P)$ is non-negative. Any body force acting on the core which is not negligible is assumed to be included in the applied loads T_i.

Since the thickness H of the core is large compared with the thickness h of the face sheets, the strain rates in each of the faces can be considered to be constant. The dissipation rate $D_A(u_i)$ is then linearly proportional to h.

Consider now a sandwich shell with face sheets of thickness h_e which is just at the point of collapse under the loads T_i in a deformation-rate pattern u_i^e.

$$\int_A \Delta_A(u_i^e)dA = \int_A T_i u_i^e dA, \tag{13}$$

where $\Delta_A(u_i^e) = D_A(u_i^e) - 2F_i u_i^e h_e$. Because of the linear dependence of D_A and therefore Δ_A on h, for any sandwich shell with faces of thickness h_s in the deformation-rate pattern u_i^e the modified dissipation rate is given by $\Delta_A(u_i^e)h_s/h_e$. With equation (13), the assumption that the shell h_s is at or below collapse under T_i requires for the collapse mode u_i^e

$$\int_A \frac{\Delta_A(u_i^e)}{h_e} h_s\, dA \geq \int_A T_i u_i^e\, dA = \int_A \frac{\Delta_A(u_i^e)}{h_e} h_e dA. \tag{14}$$

It follows that

$$\int_A h_s f(P)dA \geq \int_A h_e f(P)dA \tag{15}$$

provided that $\Delta_A(u_i^e)/h_e f(P)$ is constant (and positive) over A. Thus a sandwich shell designed to collapse in a mode such that

$$\Delta_A/hf(P) = \text{const} \tag{16}$$

over the middle surface A provides an *absolute* minimum for the functional (12) for shells which are at or below collapse under the given loads. The quantity Δ_A/h is equal to the sum of the values of the modified dissipation rate Δ per unit volume in the two faces of the sandwich shell.

The condition (16) has been obtained previously [8] for the particular case of a symmetrically loaded circular cylindrical shell with zero body force and $f(P) \equiv 1$ (minimum volume). The analysis of [8] uses the calculus of variations and it is not immediately apparent from this work that the condition (16) provides an *absolute* minimum.

The condition (16) for the optimum design of the sandwich shell is independent of the design thickness because of the linear dependence of Δ_A on the thickness h. For the solid shell of the previous section, however, the condition (11) for optimum design involves the design thickness in general. Thus, in the case of the solid shell, the optimum design is much more difficult to obtain than the corresponding design for a sandwich shell.

The problem of the minimum-volume design of a symmetrically loaded circular cylindrical sandwich shell is relatively straightforward. Some simple problems will be solved in the following sections to illustrate the procedure and to indicate the type of solution obtained. Internal pressure only is considered as failure by buckling is not taken into account in the analysis.

Circular Cylindrical Sandwich Shell

Fig. 1 shows the moment and force resultants acting upon an element of a circular cylindrical shell under axially symmetric loading. In this case the generalized stresses are M the axial bending moment per unit length, N_x the axial force resultant per unit length, and N the circumferential force per unit length. The circumferential bending moment (M_θ) is a passive or induced moment and is omitted from the figure. When the applied load is an internal pressure p, which may vary with the axial co-ordinate x, equilibrium prescribes N_x to be constant and

$$\frac{dM}{dx} = Q, \quad \frac{dQ}{dx} = p(x) - \frac{N}{R}, \tag{17}$$

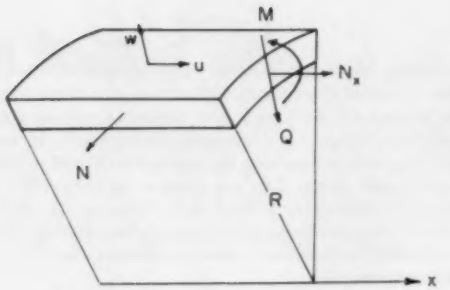

Fig. 1 Element of circular cylindrical shell

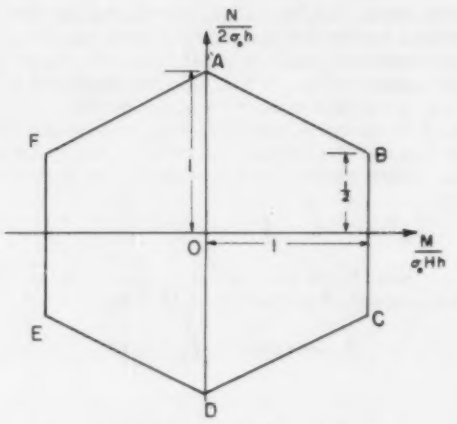

Fig. 2 Yield locus for sandwich shell with zero axial force

where Q is the axial shear force per unit length and R is the radius of the shell. The two equilibrium equations combine to give

$$\frac{d^2M}{dx^2} + \frac{N}{R} = p(x) \tag{18}$$

The radial and axial velocity components of the middle surface are denoted by w and u, respectively. The generalized strain rates are the curvature rate κ and the axial and circumferential strain rates ϵ_x and ϵ, where

$$\kappa = \frac{d^2w}{dx^2}, \qquad \epsilon_x = \frac{du}{dx}, \qquad \epsilon = \frac{w}{R} \tag{19}$$

The rate of internal dissipation of energy per unit area of the middle surface is given by

$$D_A = M\kappa + N_x\epsilon_x + N\epsilon \tag{20}$$

It is assumed that the perfectly plastic material of the face sheets obeys the Tresca yield criterion. When no axial force is present ($N_x = 0$), the limiting combinations of M and N lie on the yield locus shown in Fig. 2. For minimum volume $f(P) \equiv 1$ and with zero body force the condition (16) becomes $D_A/h = \text{const}$. This condition restricts the position of the stress point on the yield hexagon in Fig. 2. For example, the radial velocity w is zero and if this applies over a finite length of the shell, D_A is zero in that region. In fact only the stress states represented by the corners of the hexagon can be associated with a velocity field for which D_A/h is constant for a finite length of the shell. For these stress points, the condition $D_A/h = \text{const}$ can be written:

$$2\sigma_0|\epsilon| = \text{const for } |\epsilon| \geq |\kappa|H, \tag{21}$$

$$\sigma_0\{|\epsilon| + |\kappa|H\} = \text{const for } |\epsilon| \leq |\kappa|H, \tag{22}$$

where σ_0 is the tensile yield stress of the face sheet material.

When the axial force N_x is nonzero, the appropriate yield surface in M, N, N_x space for a sandwich shell has been determined by Hodge [9]. Fig. 3 shows the part of the yield surface for which the force resultants N and N_x are positive.

As for the zero-axial-force case only portions of this surface are such that the condition $D_A/h = \text{const}$ can be satisfied for a finite length of the shell. For the part of the yield surface shown in Fig. 3, only the stress states represented by points on the corners *A-G*, *A-H*, *B-G*, *F-H*, *G-K*, *H-K* and *K-L*, and on the side *A-G-K-H* can be associated with a deformation pattern for which D_A/h is constant. For stress points on the corners *G-K* and *H-K* for example, the condition $D_A/h = \text{const}$ becomes

$$\sigma_0\{2\epsilon + |\kappa|H\} = \text{const}, \tag{23}$$

where for points on *G-K* and *H-K* we must have

$$\epsilon \geq 0 \text{ and } \epsilon_x = {}^1/_2|\kappa|H$$

No Axial Force Examples

We consider now the design for minimum volume of a circular cylindrical sandwich shell of length $2L$ loaded by a known distribution of internal pressure $p(x)$ and carrying no axial force. If the ends of the shell are not restrained, then the membrane design with zero bending moment and the pressure p carried by circumferential force N provides the minimum-volume design. This design is associated with the stress point A in Fig. 2 and the velocity field satisfying $D_A/h = \text{const}$ is the field $w = \text{const}$.

(a) Ends Simply Supported. When conditions of *simple support* apply at both ends of the shell, the bending moment M and the radial velocity w must be zero at the ends. In this case two types of minimum-volume design arise depending on whether the shell is short or long.

For *short* shells, the minimum-volume design is associated with the stress point F in Fig. 2 throughout the shell. The condition $D_A/h = \text{const}$ requires, from equations (19) and (22),

$$\frac{d^2w}{dx^2} - \frac{w}{RH} = -\frac{\alpha}{RH}, \tag{24}$$

where α is a positive constant. For the velocity field w to be associated with the stress point F in Fig. 2 we must have also

$$0 \leq \frac{w}{R} \leq -H\frac{d^2w}{dx^2} \tag{25}$$

Measuring axial distance x from one end of the shell, w must be zero at $x = 0$ and $x = 2L$ so that the appropriate solution of (24) is

$$w = \alpha\{1 - \cosh(l - \xi)/\cosh l\}, \tag{26}$$

where

$$\xi = x/\sqrt{RH}, \qquad l = L/\sqrt{RH}. \tag{27}$$

The inequalities (25) are satisfied throughout the shell by expression (26) for w provided that

$$L \leq \sqrt{(RH)}\cosh^{-1} 2 = 1.317\sqrt{RH} \tag{28}$$

Thus, in the present context, by a short shell is meant a shell such that $L \leq 1.317\sqrt{RH}$. The velocity distribution (26) is shown in Fig. 4(*a*) for $L = \sqrt{RH}$ ($l = 1$).

The thickness distribution is found from the equilibrium equation (18) and the values

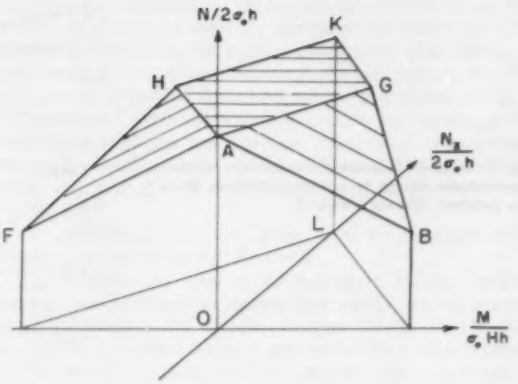

Fig. 3 Portion of yield surface for sandwich shell (N, $N_x \geq 0$)

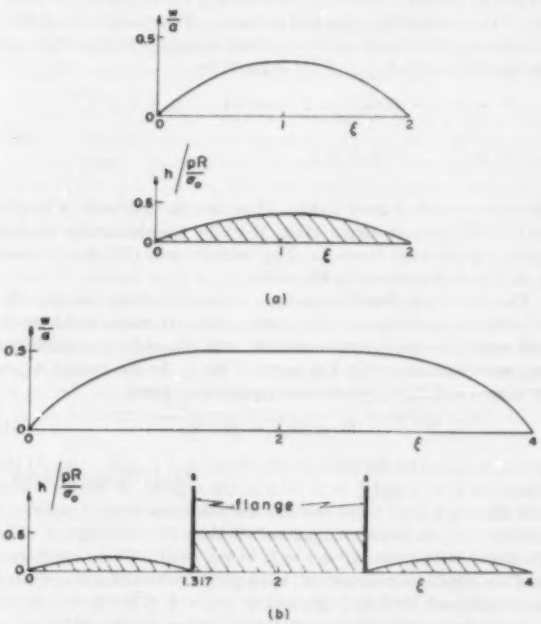

Fig. 4 Simply supported shell: Velocity field and minimum-weight design for (a) short shell ($L/\sqrt{RH} = 1$), and (b) long shell ($L/\sqrt{RH} = 2$) under uniform pressure

$$M = -\sigma_0 Hh, \qquad N = \sigma_0 h, \tag{29}$$

which hold for the stress point F. Substitution of (29) into (18) gives an equation for h which is solved subject to the conditions $h = 0$ at $x = 0$ and $x = 2L$ as M is zero at the ends of the shell. The thickness h for minimum volume can be written in closed form for any distribution of pressure $p(x)$. For illustration, the minimum-volume design in the particular case of constant internal pressure is indicated pictorially in Fig. 4(*a*) for the case $L = \sqrt{RH}$.

For *long* shells ($l \geq 1.317$), a central portion of the shell is stressed by circumferential force N only, stress point A in Fig. 2; the portions of the shell between the central portion and the ends are at the stress state F. The velocity field satisfying $D_A/h = \text{const}$ throughout the shell must satisfy (24) in the end portions and, from (21), $w = \alpha/2$ in the central portion. In addition, no discontinuity in dw/dx is permissible at the junctions of the regions

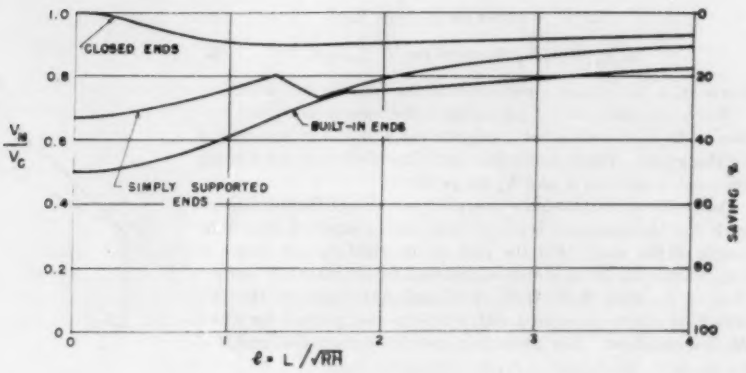

Fig. 5 Ratio of face-sheet volume for minimum-volume design to constant-thickness design (uniform internal pressure)

as this would violate the condition $D_A/h = \text{const}$. The velocity w must be zero at the ends of the shell and such that the inequalities (25) are satisfied in the end portions. It is readily found that the velocity field must be symmetrical about the mid-section and for the half length $0 \leq \xi \leq l$ it is given by

$$\left.\begin{aligned} w &= \alpha\{1 - \cosh(a - \xi)/\cosh a\} \qquad 0 \leq \xi \leq a, \\ w &= \frac{\alpha}{2} \qquad a \leq \xi \leq l, \end{aligned}\right\} \tag{30}$$

where $a = \cosh^{-1} 2 = 1.317$. Thus two end portions of length $1.317\sqrt{RH}$ are at stress state F while the remaining central portion is at stress state A. The velocity field (30) for the case $L/\sqrt{RH} = 2$ is shown in Fig. 4(*b*).

The thickness distribution for minimum volume for any distribution of pressure $p(x)$ can now be found from the yield condition and the equilibrium equation, and closed-form expressions can be written down for h in terms of $p(x)$. In the central region M is zero and $N = 2\sigma_0 h$ so that equilibrium gives

$$N = 2\sigma_0 h = p(x)R, \tag{31}$$

giving at once the thickness in the region $a < \xi < 2l - a$. At the junctions $\xi = a$ and $\xi = 2l - a$ of the regions, M is continuous and therefore zero there so that the thickness h must approach zero as the junctions are approached from the end regions. The thickness is also zero at the ends of the shell. These conditions and the equilibrium equation (18) together with (29) are sufficient to determine h for $0 \leq \xi < a$ and $2l - a < \xi \leq 2l$. It remains to satisfy the condition that the shear force Q, i.e., $dM/dx = -\sigma_0 H\, dh/dx$, be continuous at the junctions $\xi = a$, $\xi = 2l - a$ in the absence of concentrated load. In the central region the shear force is zero but is nonzero, in general, in the end regions. The discontinuity in Q at the junctions is removed by adding flanges of zero width but of finite cross-sectional area to each face sheet at the junctions $\xi = a$, $\xi = 2l - a$. These flanges can be considered as the limit of flanges of finite width stressed to states represented by points on A-F near point A in Fig. 2; in the limit when the flanges become vanishingly thin, the flange is stressed at state A.

To illustrate, in the case of constant pressure the design for the case $L = 2\sqrt{RH}$ is as indicated in Fig. 4(*b*). The infinitely thick flanges[3] can be avoided if an upper limit is placed upon the thickness h of the face sheets. A procedure similar to that used earlier [2] in the minimum-volume design of a rotating disk can be used to obtain the minimum-volume design when the face-sheet thickness is restricted. However, this will not be considered here.

The design with constant face-sheet thickness designed to collapse at the pressure p (ends simply supported) is readily obtained. Fig. 5 compares the volume of the face sheets (including the volume of the flanges) for the minimum-volume design to that for the constant-thickness design. The discontinuity in the slope of the curve at $l = 1.317$ is due to the different forms of the minimum-volume design for short and long shells. The corner in the curve at $l = 1.571$ is due to the change in character of the solution for the collapse of the shell with constant face-sheet thickness. Only for short shells is the saving effected by the minimum-volume design appreciable.

(b) Ends Built In. When the ends of the shell are under conditions of built-in support, the radial velocity w must be zero at the ends as for the case of simple support. In addition, the condition D_A/h constant throughout the shell requires dw/dx to be zero at the ends of the shell. The type of minimum-volume design depends on whether the shell is short or long.

For a shell with built-in ends, the adjective *short* will be used for shells such that $L/\sqrt{RH} \leq 1.691$. For a short shell, two portions of the shell of length $b\sqrt{RH}$ at the ends are at stress point B in Fig. 2 and the remaining central portion of the shell is at stress point F. At the junctions $\xi = b$, $\xi = 2l - b$ of the regions, w and dw/dx are continuous. It is found that w is symmetrical about the mid-section and is given by

$$\begin{aligned} w &= \alpha\{1 - \cos\xi\} \qquad 0 \leq \xi \leq b, \\ w &= \alpha\{1 - \cos b \cosh(l - \xi)/\cosh(l - b)\} \qquad b \leq \xi \leq l, \end{aligned} \tag{32}$$

where, in order that dw/dx be continuous at $\xi = b$, the distance b must be chosen so that

$$\tan b = \tanh(l - b) \tag{33}$$

The velocity field (32) satisfying D_A/h constant for short shells is shown in Fig. 6(*a*) for the case $L/\sqrt{RH} = 1$.

The thickness distribution is found from the equilibrium equation (18) together with the values (29) for M and N in the central portion $b \leq \xi \leq 2l - b$ and the values

$$M = \sigma_0 Hh, \qquad N = \sigma_0 h \tag{34}$$

in the end portions $0 \leq \xi \leq b$ and $2l - b \leq \xi \leq 2l$. As M is negative in the central region and positive in the end regions, the continuity of M requires M to be zero at the junctions of the regions. Thus h is zero at $\xi = b$ and $\xi = 2l - b$. In addition, in the absence of concentrated load, $Q = dM/dx$ must be continuous at the junctions $\xi = b$ and $\xi = 2l - b$.

Closed-form expressions for the minimum-volume thickness can be written down for any distribution of pressure $p(x)$ but will not be done here. When the pressure is constant, the minimum-volume thickness is indicated in Fig. 6(*a*) for the case $L/\sqrt{RH} = 1$.

[3] The author is grateful to a referee for his alternative suggestion that the discontinuities in the shear force could be removed by using transverse ring stiffeners with an idealized T cross section. The idealized T-section would consist of a web of zero thickness and a flange containing all of its area.

When $l \leq 1.691$, the velocity field (32) satisfies D_A/h constant throughout the shell. For *long* shells with values of l greater than 1.691, the condition D_A/h constant can only be satisfied (with nonnegative w) by introducing a central region of constant radial velocity, $w = \alpha/2$, associated with stress point A in Fig. 2. The velocity field is shown in Fig. 6(*b*) for the case $l = 2$. It is again symmetrical about the mid-section of the shell and is given by

$$\begin{aligned} w &= \alpha(1 - \cos \xi) && 0 \leq \xi \leq c, \\ w &= \alpha\{1 - {}^1/_2 \cosh (d - \xi)\} && c \leq \xi \leq d, \\ w &= \alpha/2 && d \leq \xi \leq l \end{aligned} \tag{35}$$

The constants c, d appearing in these equations have the values $c = 0.659$, $d = 1.691$, and are such that

$$\tan c = \tanh(d - c) \qquad \cos c = {}^1/_2 \cosh(d - c) \tag{36}$$

The end regions $0 \leq \xi \leq c$ and $2l - c \leq \xi \leq 2l$ are at stress state B, the regions $c \leq \xi < d$ and $2l - d < \xi \leq 2l - c$ are at stress state F, and the remaining central region is at stress state A.

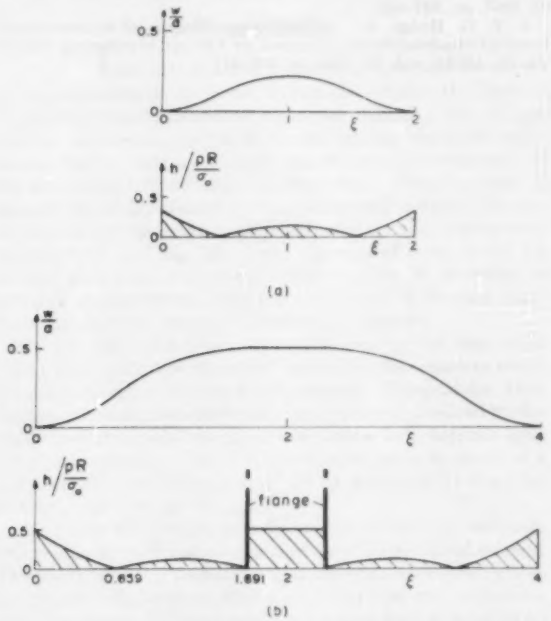

Fig. 6 Built-in shell: Velocity field and minimum-volume design for (*a*) short shell ($L/\sqrt{RH} = 1$) and (*b*) long shell ($L/\sqrt{RH} = 2$) under uniform pressure

The equilibrium equation (18) and the appropriate values for M and N in terms of h serve to determine the minimum-volume thickness distribution for a given distribution of pressure. The thickness h is zero at the junctions $\xi = c$ and $\xi = 2l - c$ of the stress states B and F. As the boundaries $\xi = d$ and $\xi = 2l - d$ of the central region are approached from the regions at stress state F the thickness tends to zero. Flanges or tension rings of zero width but of finite cross-sectional area must be placed at the sections $\xi = d$, $\xi = 2l - d$ in order to make the shear force Q continuous.

For example, for constant pressure p, the minimum-volume design is shown in Fig. 6(*b*) for $l = 2$.

Fig. 5 shows the ratio of the face-sheet volume (including flanges), for the minimum-volume design to that for the constant-thickness design [9] for uniform pressure. The saving effected by the minimum-volume design is greater for the built-in shell than for the simply supported shell, but again is only appreciable for short shells.

(c) Comparison With the Membrane Design. For further comparison, Fig. 7 shows the ratio of the minimum volume to the volume of the face sheets in the membrane design, given by equation (31), for the case of uniform internal pressure with both built-in and simply supported ends. The saving is again only appreciable for short shells.

Also shown in Fig. 7 are the results for loading by a ring of force at the mid-section of the shell. In this case the minimum-volume design coincides with the membrane design for long shells, that is, for $L \geq 1.317\sqrt{RH}$ with simply supported ends and for $L \geq 1.691\sqrt{RH}$ with built-in ends. This is because the minimum-volume design for long shells places material in the face sheets only at the section of application of the load. The ring of force is carried by a tension ring, and the end supports are not used to carry load in the minimum-volume design.

More generally, if the pressure $p(x)$ is nonzero only in the central region (region $a \leq \xi \leq 2l - a$ for the simply supported shell and region $d \leq \xi \leq 2l - d$ for the built-in shell), minimum volume is achieved by the membrane design (31), the supports at the ends of the shell being of no value in carrying load.

Axial Force Present

When end loads produce a constant axial force N_x in the shell, the minimum-volume design can be obtained in an analogous manner. We remark that if $N_x > pR$, a shell with face sheets thick enough to carry the axial force can also carry sufficient circumferential force N to balance the internal pressure p; the minimum-volume design then has face sheets of constant thickness $h = N_x/2\sigma_0$.

For the shell closed at the ends by rigid plates and under constant internal pressure p, the axial force N_x is produced by the in-

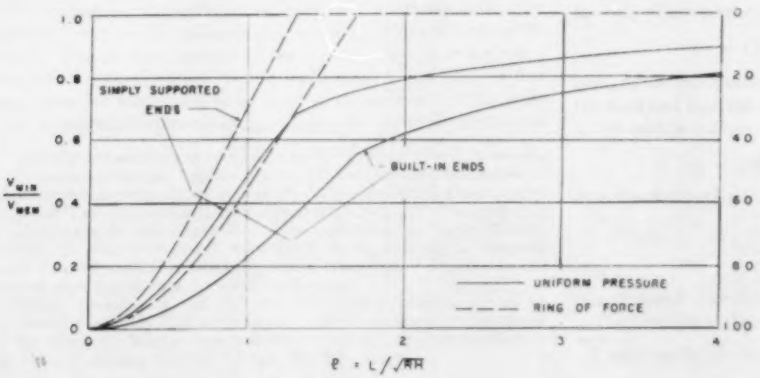

Fig. 7 Ratio of face-sheet volume for minimum-volume design to membrane design: Uniform pressure and ring of force at center section

ternal pressure acting on the end plates, so that $N_x = {}^1/_2 pR$. It is assumed that the rigid plates produce clamped conditions at the ends of the shell. Only stress points on the corners G-K and H-K in Fig. 3 are involved in the minimum-volume design. The design is indicated in Fig. 8 for a shell of half length $L = \sqrt{(2RH)}$. The design for other lengths is similar in form, and no ring stiffeners are necessary. In Fig. 5 is shown the saving in volume effected by the minimum-volume design for the closed-end shell over the design with face sheets of constant thickness [9]. The maximum saving is just over 10 per cent for shells with half length L near $1.4\sqrt{RH}$.

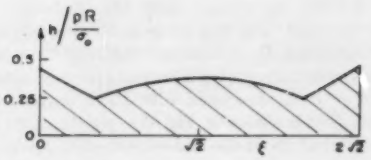

Fig. 8 Closed-end shell: Minimum-volume design (case $L/\sqrt{RH} = \sqrt{2}$) for uniform pressure

References

1 D. C. Drucker and R. T. Shield, "Design for Minimum Weight," Proceedings of the 9th International Congress of Applied Mechanics, Brussels, 1956.

2 D. C. Drucker and R. T. Shield, "Bounds on Minimum Weight Design," *Quarterly of Applied Mathematics*, vol. 15, 1957, pp. 269–281.

3 E. T. Onat, W. Schumann, and R. T. Shield, "Design of Circular Plates for Minimum Weight," *Journal of Applied Mathematics and Physics* (ZAMP), vol. 8, 1957, pp. 485–499.

4 D. C. Drucker, W. Prager, and H. J. Greenberg, "Extended Limit Design Theorems for Continuous Media," *Quarterly of Applied Mathematics*, vol. 9, 1952, pp. 381–389.

5 W. Prager, "General Theory of Limit Design," Sectional Lecture, Proceedings of the 8th International Congress of Applied Mechanics, Istanbul, 1952.

6 D. C. Drucker, "The Effect of Shear on the Plastic Bending of Beams," JOURNAL OF APPLIED MECHANICS, vol. 23, TRANS. ASME, vol. 78, 1956, pp. 509–514.

7 W. Freiberger and B. Tekinalp, "Minimum Weight Design of Circular Plates," *Journal of the Mechanics and Physics of Solids*, vol. 4, 1956, pp. 294–299.

8 W. Freiberger, "On the Minimum Weight Design Problem for Cylindrical Sandwich Shells," *Journal of the Aeronautical Sciences*, vol. 24, 1957, pp. 847–848.

9 P. G. Hodge, Jr., "Rigid-Plastic Analysis of Symmetrically Loaded Cylindrical Shells," JOURNAL OF APPLIED MECHANICS, vol. 21, TRANS. ASME, vol. 76, 1954, pp. 336–342.

Yield Conditions for Rotationally Symmetric Shells Under Axisymmetric Loading[1]

P. G. HODGE, JR.
Professor of Mechanics,
Department of Mechanics,
Illinois Institute of Technology,
Chicago, Ill.
Mem. ASME

The yield condition for a rotationally symmetric shell may be represented as a surface in a four-dimensional stress space. The exact yield surface according to the Tresca yield condition is compared with various approximations. A new approximation is suggested which combines the advantages of mathematical simplicity and reasonable accuracy. The theory is illustrated with reference to a spherical cap under uniform pressure.

1—Introduction

The state of stress in a shell is described by the resulting moments, direct forces, and shears. Within the limits of a thin-shell theory, transverse shears are considered only in relation to equilibrium. If the shell and loading are rotationally symmetric, the twisting moment and the shearing component of the membrane forces vanish by symmetry. Thus the state of stress is essentially defined by four generalized stresses; namely, the principal stress resultants N_1 and N_2 and the principal moment resultants M_1 and M_2. Similarly, the state of strain is defined by four generalized strains which may, in turn, be expressed in terms of displacements. For the rotationally symmetric shell, there are only two such displacements, U and W.

The six unknowns which define the state of the shell must satisfy two equilibrium equations and four further relations which depend upon the properties of the material. In particular, for a rigid-plastic shell, the additional relations are all provided by the yield condition and a flow rule whose precise form depends upon the yield condition. Therefore, the determination or choice of a yield condition will affect four of the six equations for the rotationally symmetric shell.

The plastic yield condition may be represented as a surface in a Cartesian space whose co-ordinates are the generalized stresses. The plastic flow rule then states that the strain-rate vector whose components are the generalized strain rates is normal to this surface. For the general rotationally symmetric shell under axisymmetric loading, this stress space is four dimensional and the yield surface essentially three dimensional. Thus there are certain difficulties in visualization. Partly for this reason and partly due to the inherent complexity of the equations, relatively little work has been done on the general problem of rotationally symmetric shells. The primary purpose of the present paper is to suggest a simplified approximation to the yield surface together with a technique for visualizing it so that future applications to problems of practical interest can be attempted. As an illustration of the relative simplicity achieved, an application is made to a spherical cap under uniform pressure.

The exact yield surface for a uniform shell whose material satisfies the Tresca yield condition is described in the next section. This is followed by a general discussion of approximations to this surface with specific reference to two previously suggested approximations. In Section 4 a new approximation is described in detail. The following two sections apply the new approximate theory to a spherical cap which is subjected to uniform external pressure and is either clamped or simply supported around its edge. Finally, the conclusions to be drawn from the investigation are discussed in Section 7.

2—Exact Tresca Yield Condition

It is convenient to carry out the analysis in terms of dimensionless stress resultants defined by

$$n_1 = N_1/N_0 \quad n_2 = N_2/N_0 \quad m_1 = M_1/M_0 \quad m_2 = M_2/M_0 \tag{1}$$

Here N_0 and M_0 are the maximum uniaxial direct stress and bending moment, respectively. If the uniaxial yield stress of the material is σ_0, then

$$N_0 = 2\sigma_0 H \quad M_0 = \sigma_0 H^2 \tag{2}$$

for a uniform shell of thickness $2H$, and

$$N_0 = 2\sigma_0 h \qquad M_0 = 2\sigma_0 hH \tag{3}$$

for an ideal sandwich shell of face thickness h and core thickness $2H$.

The generalized strain rates λ_1, λ_2, κ_1, κ_2 must be chosen so that the rate of dissipation of energy per unit area has the form [1, 2].[2]

$$D_i = C(\lambda_1 n_1 + \lambda_2 n_2 + \kappa_1 m_1 + \kappa_2 m_2) \tag{4}$$

If λ_1, λ_2 are interpreted as the strain rates of the middle surface of the shell and κ_1, κ_2 are given in terms of the curvature rates K_1, K_2 of the middle surface by

$$\kappa_1 = (M_0/N_0)K_1 \qquad \kappa_2 = (M_0/N_0)K_2 \tag{5}$$

then the dissipation function is

$$D_i = \lambda_1 N_1 + \lambda_2 N_2 + K_1 M_1 + K_2 M_2 = N_0(\lambda_1 n_1 + \lambda_2 n_2 + \kappa_1 m_1 + \kappa_2 m_2) \tag{6}$$

in agreement with Equation (4).

The flow law states that the strain-rate vector

[1] This investigation was sponsored by the Office of Naval Research.

Contributed by the Applied Mechanics Division and presented at the Annual Meeting, Atlantic City, N. J., November 29–December 4, 1959, of The American Society of Mechanical Engineers.

Discussion of this paper should be addressed to the Secretary, ASME, 29 West 39th Street, New York, N. Y., and will be accepted until July 10, 1960, for publication at a later date. Discussion received after the closing date will be returned.

Note: Statements and opinions advanced in papers are to be understood as individual expressions of their authors and not those of the Society. Manuscript received by ASME Applied Mechanics Division, February 11, 1959. Paper No. 59—A-129.

[2] Numbers in brackets designate References at end of paper.

$$\mathbf{E} = (\lambda_1, \lambda_2, \kappa_1, \kappa_2) \tag{7}$$

is directed along the outward normal to the yield surface. At a smooth point on the surface, **E** is uniquely determined to within a magnitude factor; at an edge or corner, **E** will contain one or more parameters. The requirement that **E** be directed outward is equivalent to requiring the dissipation function D_i to be positive.

Historically, the Tresca yield condition was first derived for various special cases of rotationally symmetric shells such as the curved beam [3], the circular plate [4], and the cylindrical shell without [5, 6] and with [6, 7] end load. Here the general result is stated for a rotationally symmetric shell as determined by Onat and Prager [8]. The terminology and viewpoint are slightly different from [8] in order to better serve the present purpose.

The first step is to define the strain-rate vector in terms of a magnitude parameter ν and three direction parameters p, q, and r by

$$p = -\frac{\lambda_1}{4\kappa_1} \qquad r = -\frac{\lambda_2}{4\kappa_2} \qquad q = -\frac{1}{4}\frac{\lambda_1 + \lambda_2}{\kappa_1 + \kappa_2} \tag{8}$$

Therefore the strain-rate vector is

$$\mathbf{E} = \nu[-4p(q - r), -4r(p - q), q - r, p - q] \tag{9}$$

The strain rates in the material are now known in terms of p, q, and r since

$$\epsilon_1 = \lambda_1 + z\kappa_1 \qquad \epsilon_2 = \lambda_2 + z\kappa_2 \tag{10}$$

z being the dimensionless co-ordinate in the thickness direction. Therefore, for any given p, q, and r, ϵ_1 and ϵ_2 can be found for each z. The vector (ϵ_1, ϵ_2) must be normal to the Tresca yield hexagon, hence the stresses are easily found. Finally, an integration yields the stress resultants in terms of the parameters p, q, and r. An ingenious graphical method is used in [8] to reduce the computations. The results are summarized in Table 1 which is subject to the following interpretation:

Table 1 Tresca condition for uniform shell

Intermediate parameter	Stress resultants n_1	n_2	m_1	m_2
p	$\mp(p + q)$	$\mp(q - r)$	$\pm 1 \mp 2(p^2 + q^2)$	$\pm 2(r^2 - q^2)$
q	$\mp(p + q)$	$\mp(q + r)$	$\pm 1 \mp 2(p^2 + q^2)$	$\pm 1 \mp 2(q^2 + r^2)$
r	$\mp(q - p)$	$\mp(q + r)$	$\pm 2(p^2 - q^2)$	$\pm 1 \mp 2(q^2 + r^2)$

In all cases the upper or lower signs must be used consistently in a given line, the correct choice being that which makes D_i positive.

If p, q, and r are all distinct and all within the interval $(-1/2, 1/2)$, then the "intermediate parameter" in Table 1 is that one of p, q, r which lies between the other two.

If p, q, and r are still distinct but one or more is greater than $1/2$, then that parameter must be replaced by $1/2$ in Table 1; similarly if one or more parameter is less than $-1/2$.

If any of the parameters, p, q, or r becomes indeterminate as computed from Equations (8), the other two parameters must necessarily be equal. For example, if $\lambda_2 = \kappa_2 = 0$, r is indeterminate and $r = q$. Either of the first two lines in Table 1 then yields the relation $n_1^2 \pm m_1^2 = 1$; the remaining resultants which contain r are undefined in this case. Similar results hold for other indeterminate possibilities.

Finally, if $p = q = r$, Table 1 can be used with the convention that intermediate parameter corresponds to the absolutely largest numerator of Equations (8).

The various special cases shown in Figs. 1 to 4 may be obtained by setting suitable strain rates or stresses equal to zero; alternatively, they may be obtained directly as was done historically [3 to 7].

3—Approximate Yield Conditions

The exact yield condition obtained in the previous section is nonlinear. If the yield condition is linearized by a suitable approximation, not only are the equations made linear, but also, as pointed out in [9], the stress and velocity equations are uncoupled.

Two linear approximations have been proposed in the literature to date. Hodge [2, 9] has suggested that the exact yield condition for an ideal sandwich shell be used as an approximation for the uniform shell. The yield surface for this case is easily obtained; it consists of the twelve planes shown in Table 2. The signs $\pm$ and $\pm'$ in Table 2 must each be consistent but are independent of each other.

Table 2 Tresca condition for sandwich shell

Stress equation	Strain-rate vector $(\lambda_1, \lambda_2, \kappa_1, \kappa_2)$
$\pm n_1 \pm' m_1 = 1$	$\nu(\pm 1, 0, \pm' 1, 0)$
$\pm n_2 \pm' m_2 = 1$	$\nu(0, \pm 1, 0, \pm' 1)$
$\pm(n_1 - n_2) \pm' (m_1 - m_2) = 1$	$\nu(\pm 1, \mp 1, \pm' 1, \mp' 1)$

Some special cases are shown in Figs. 1 to 4. As with the uniform shell they may be obtained directly [2, 6] or as particular cases in Table 2.

A much simpler approximation has been proposed by Shield and Drucker [10]. They argue that in most rotationally symmetric-shell problems the moments are generally small compared with the direct stresses. Therefore, they ignore completely the hoop moment $m_2 = m_\theta$. The longitudinal moment $m_1 = m_\phi$ must be retained if boundary conditions are to be satisfied, but any interaction between it and the direct stresses is neglected. The resulting yield condition is defined by the eight planes listed in Table 3; it will be referred to as a one-moment limited interaction surface. Typical special cases are shown in Figs. 1 to 4.

Table 3 One-moment limited interaction curve

Face	Equation	Strain-rate vector $(\lambda_\theta, \lambda_\phi, \kappa_\phi)$
1	$n_\theta = 1$	$\nu(1, 0, 0)$
2	$n_\phi = 1$	$\nu(0, 1, 0)$
3	$-n_\theta + n_\phi = 1$	$\nu(-1, 1, 0)$
4	$-n_\theta = 1$	$\nu(-1, 0, 0)$
5	$-n_\phi = 1$	$\nu(0, -1, 0)$
6	$n_\theta - n_\phi = 1$	$\nu(1, -1, 0)$
7	$m_\phi = 1$	$\nu(0, 0, 1)$
8	$m_\phi = -1$	$\nu(0, 0, -1)$

A final assessment of the value of any proposed yield condition can only be made after several examples have been solved and compared with experimental results or with more accurate theories. However, for the sandwich approximation, bounds on the error introduced can be obtained from the theory of limit analysis [2, 11]. The pertinent result here is that if a yield condition A is wholly interior to another yield condition B, then the collapse load computed according to A is not greater than the collapse load computed according to B.

As shown in the Appendix, the sandwich surface is interior to the exact one. If it is multiplied by 1.25, the result will be a sur-

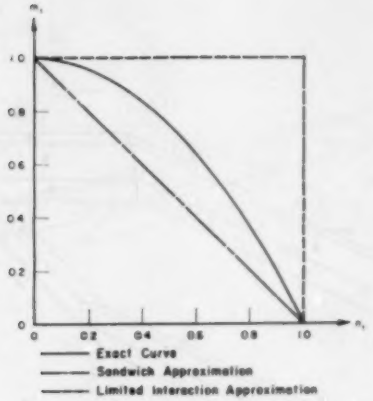

Fig. 1 Yield curves for arches

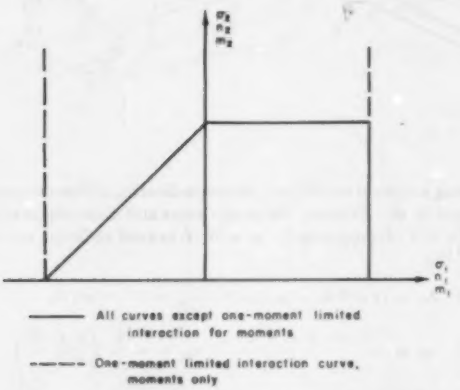

Fig. 2 Yield curves for plane stress, stretching of plates, or bending of plates

face exterior to the actual one. Therefore, if p^* represents the collapse load according to the sandwich surface, the actual load p must satisfy

$$p^* \leq p \leq 1.25p^* \tag{11}$$

In the only examples considered to date [2, 12], the sandwich surface, despite its linearity, leads to complex mathematical problems. On the other hand, although the one-moment linear interaction surface may lead to practically important results in problems for which its assumptions are valid, it is open to certain theoretical objections. In the first place, in order to eliminate m_θ from the problem, the equilibrium equations must be modified. Therefore, the theorems of limit analysis are no longer applicable. Further, it is not clear whether the arguments used to show that moments are unimportant in the case of static loading are equally valid under dynamic loads. Finally, even if the moments are small throughout most of the shell, there may be regions near the axis of symmetry where m_θ is locally important.

For the foregoing reasons, the subject of approximate yield surfaces appears to be worthy of further study. In the next section a surface is proposed which eliminates the major drawbacks of the one-moment limited interaction surface and yet leads to simpler equations than the sandwich approximation.

4—Two-Moment Limited Interaction Yield Surface

The proposed approximate yield surface is based on the premise

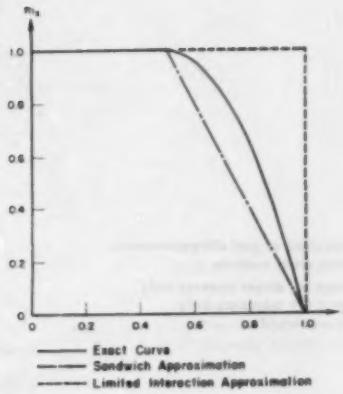

Fig. 3 Yield curves for circular cylindrical shell without end load

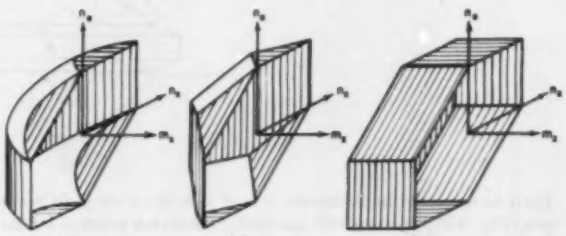

Fig. 4 Yield surfaces for circular cylindrical shell with end load
(a) Exact surface
(b) Sandwich approximation
(c) Limited interaction approximation

that in most shell problems the moments and direct forces will not be of simultaneous importance so that yield relations between moment and force are of limited importance. However, the theory recognizes that either moment or direct force may dominate so that all resultants must be included. Thus all interaction between force and force or between moment and moment is maintained, but all interactions between force and moment are neglected. The result is a linear surface in four-dimensional space defined by the twelve planes listed in Table 4. Evidently the twelve planes represent the six conditions on direct stresses in the absence of moments and the six conditions on moments in the absence of direct stresses. Appropriate special cases in Table 4 are shown in Figs. 1 to 4.

Table 4 Two-moment limited interaction curve

Face	Equation	Strain-rate vector $(\lambda_\theta, \lambda_\phi, \kappa_\theta, \kappa_\phi)$
1	$n_\theta = 1$	$\nu(1, 0, 0, 0)$
2	$n_\phi = 1$	$\nu(0, 1, 0, 0)$
3	$-n_\theta + n_\phi = 1$	$\nu(-1, 1, 0, 0)$
4	$-n_\theta = 1$	$\nu(-1, 0, 0, 0)$
5	$-n_\phi = 1$	$\nu(0, -1, 0, 0)$
6	$n_\theta - n_\phi = 1$	$\nu(1, -1, 0, 0)$
7	$m_\theta = 1$	$\nu(0, 0, 1, 0)$
8	$m_\phi = 1$	$\nu(0, 0, 0, 1)$
9	$-m_\theta + m_\phi = 1$	$\nu(0, 0, -1, 1)$
0	$-m_\theta = 1$	$\nu(0, 0, -1, 0)$
α	$-m_\phi = 1$	$\nu(0, 0, 0, -1)$
β	$m_\theta - m_\phi = 1$	$\nu(0, 0, 1, -1)$

Although the proposed yield condition is a surface in four-dimensional space, it is possible to visualize it partially. Suppose, for example, that the stress point is in the interior of face 2.

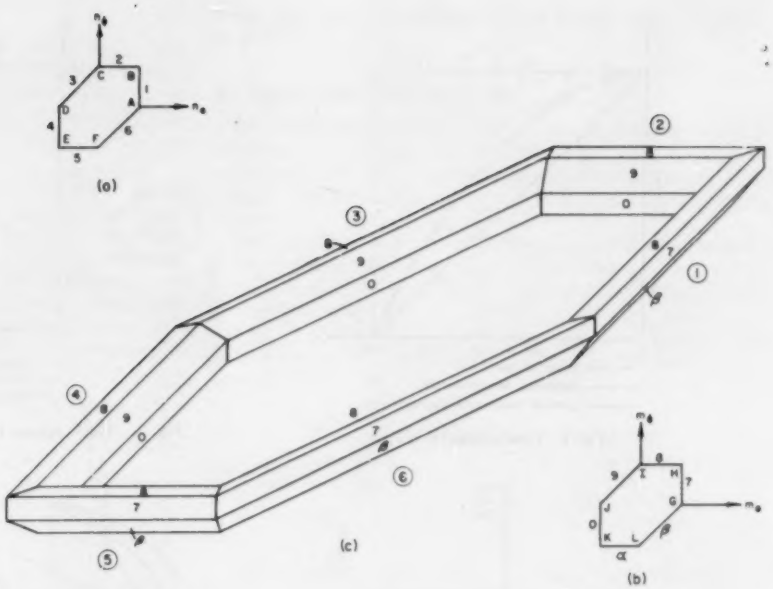

Fig. 5 Representation of part of two-moment limited interaction yield surface
(a) Yield curve for direct stresses only
(b) Yield curve for moments only
(c) Direct stress toroid

Then, in terms of direct stresses, it is on side BC of the yield hexagon, Fig. 5(a); in terms of moments, the stress point is in the interior of the hexagon G-H-I-J-K-L, Fig. 5(b). If the moments remain constant and the direct stresses vary, the stress point may move from the interior of face 2 to its intersection with face 1 or 3. On the other hand, if only the moments vary, the stress point may move to the intersection of face 2 with any of faces 7, 8, 9, 0, α, or β. Therefore, on the yield surface, face 2 is bounded by faces 1, 3, 7, 8, 9, 0, α, and β.

In similar fashion, each of faces 1 to 6 is bounded by the neighboring faces which represent direct stress yielding and by all six faces which represent moment yielding. Since a surface in four-dimensional space is essentially a solid, that part of the yield surface so far described may be schematically represented by an hexagonal toroid as shown in Fig. 5(c). The center line is the hexagon A-B-C-D-E-F drawn to a large scale and the cross section is the hexagon G-H-I-J-K-L. Since any given problem will probably not involve the entire toroid, it may be more convenient to "straighten" the toroid as in Fig. 6(c).

The remaining part of the yield surface is a similar toroid based on the moment hexagon as center line. A straightened version is shown in Fig. 6(d). The two surfaces intersect in all of their common double numbered sides. For example, a continuous stress profile might go from the interior of face 8 to the side 82 in Fig. 6(d) and then into the interior of force 2 in Fig. 6(c).

Further insight into the nature of the yield condition is gained by a qualitative consideration of the shell equations. There are three equilibrium equations which may be written [2]

$$(r_0 n_\phi)' - r_1 n_\theta \cos\phi + r_0 r_1 p_\phi = r_0 s$$
$$r_1 n_\theta \sin\phi + r_0 n_\phi + r_0 r_1 p_r = -(r_0 s)' \qquad (12a)$$

$$k[(r_0 m_\phi)' - r_1 m_\theta \cos\phi] = r_0 r_1 s \qquad (12b)$$

Here physical quantities are defined by capital letters in Fig. 7. Dimensionless quantities, denoted by small letters, are defined by

$$s = S/N_0 \qquad n = N/N_0 \qquad m = M/M_0$$
$$p = PL/N_0 \qquad r = R/L \qquad k = M_0/LN_0 \qquad (13)$$

L being a typical length and primes indicating differentiation with respect to ϕ. Further, the strain rates and dimensionless velocities ($v = V/L$ tangentially, $w = W/L$ inward radially) are related by

$$\lambda_\theta = (v\cot\phi - w)/r_2 \qquad \lambda_\phi = (v' - w)/r_1 \qquad (14a)$$

$$\kappa_\theta = -\frac{k\cot\phi}{r_2}\frac{v + w'}{r_1} \qquad \kappa_\phi = -\frac{k}{r_1}\left(\frac{v + w'}{r_1}\right)' \qquad (14b)$$

For a linear yield surface, the stress and velocity equations are uncoupled. Since there are four stress unknowns and two equilibrium equations after shear is eliminated, there should be two stress yield conditions. Since there are two velocity unknowns there should be two conditions on the strain-rate vector. Both of these requirements are satisfied by a stress point on any plastic side formed by the intersection of two of the faces in Table 4. Therefore, a simple count would indicate that plastic flow can take place only on the boundaries of the toroids in Fig. 5 or 6.

However, a closer examination reveals that there are several exceptions. In the first place, at any of the intersections 78, 89, 90, 0α, $\alpha\beta$, β7, Table 4 shows that $\lambda_\theta = \lambda_\phi = 0$. It then follows from Equations (14a) that, at least for finite radii of curvature, the most general velocity field is the rigid-body motion

$$v = A\sin\phi \qquad w = A\cos\phi \qquad (15)$$

The case $r_2 = \infty$ leads to a cone, cylinder, or flat plate. It can be shown that Equation (15) applies also to the cone and cylinder but not necessarily to the flat plate.

The second exception concerns the plastic faces 1 to 6. On any of these faces, it follows from Table 4 and Equations (14b) that two of the three strain-rate requirements are satisfied by the single relation

$$v + w' = 0. \qquad (16)$$

Therefore, the interior of the toroid in Fig. 5(c) or 6(c) may support plastic flow. In such a case, the yield condition and Equations (12a) determine n_θ and n_ϕ, but the moments are not uniquely

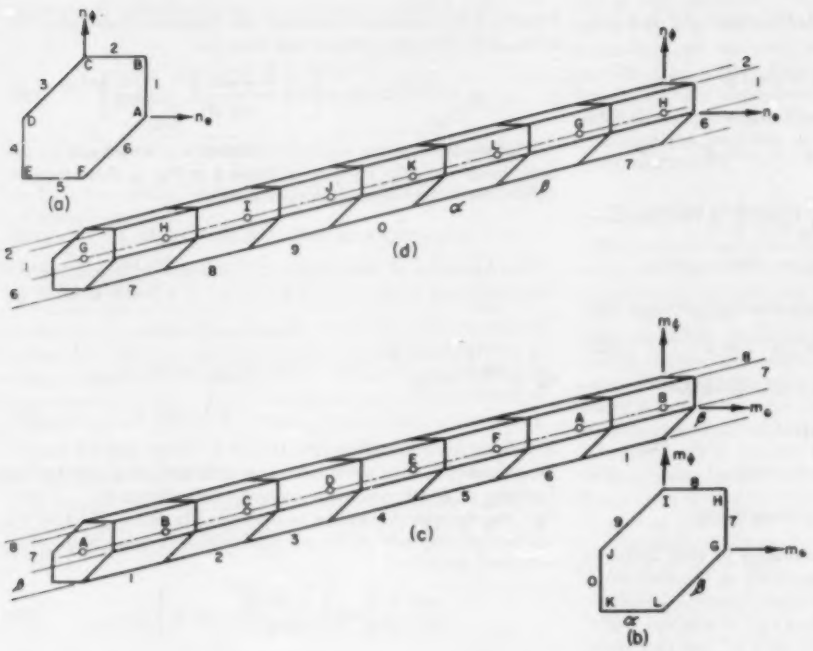

Fig. 6 Representation of two-moment limited interaction surface
(a) Yield curve for direct stresses only
(b) Yield curve for moments only
(c) Direct stress toroid (straightened)
(d) Moment toroid (straightened)

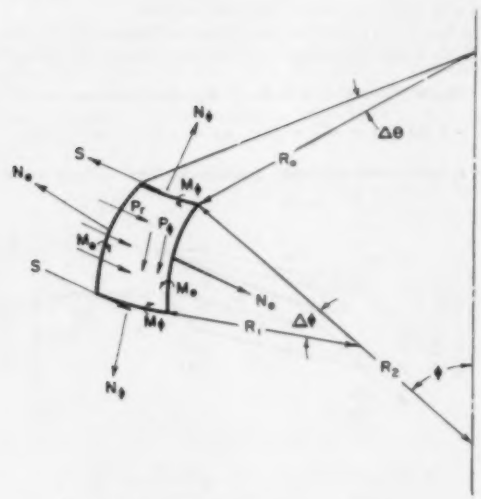

Fig. 7 Element of shell of revolution

determined. It also follows from the foregoing reasoning that no finite portion of the shell can be on any of the intersections 12, 23, 34, 45, 56, or 61.

To summarize, except for a flat plate, plastic flow is possible only when the stress point is on the boundary or interior of the toroid shown in Figs. 5(*c*) and 6(*c*).

The two-moment limited interaction curve can be used to find upper and lower bounds on the exact collapse load. Since the exact yield condition contains all of the restrictions in Table 4, in addition to further interaction requirements, the polyhedron in Table 4 circumscribes the exact surface; hence it provides an upper bound. To obtain a lower bound, it is necessary only to determine a factor f less than 1 such that when the approximate surface is multiplied by f it will lie wholly within the exact one. Since the approximate condition is a convex polyhedron, it will be sufficient to require the vertices to lie on, or within, the exact surface. Further, since both surfaces are symmetric with respect to moments and direct stresses, only 4 of the 36 vertexes need be considered. Therefore, the problem is to determine the largest number f such that the four points

$$P_1 = (f, f, f, f) \qquad P_2 = (f, f, 0, f)$$

$$P_3 = (0, f, f, f) \qquad P_4 = (0, f, 0, f)$$

are all on, or within, the surface defined in Table 1.

Since f is to be positive, the upper signs are appropriate in Table 1. However, it is not known in advance which of the three lines in Table 1 should be used. If any particular point P_i is substituted into each line in Table 1 and resulting equations solved for p, q, r, and f, two of the three solutions will violate the condition of the line in question; the third will give the desired value of f. It is readily verified that if

$$f = (1/2)(\sqrt{5} - 1) = 0.618 \tag{17}$$

then P_1 and P_3 are on the q-surface and P_2 and P_4 are on the r-surface.

Therefore, the yield surface each of whose dimensions is 0.618 times the two-moment limited interaction surface is wholly within the exact yield surface. Thus, if p^* represents the collapse load according to the two-moment surface, the actual collapse load p must satisfy

$$0.618p^* \leq p \leq p^* \tag{18}$$

5—Simply Supported Spherical Cap

If the typical length of the shell is taken to be its radius, the dimensionless radii of the sphere are

$$r_1 = r_2 = 1 \qquad r_3 = \sin \phi \tag{19}$$

Therefore, under a uniform radial load, Equations (12) and (14) become

$$\begin{aligned} &(n_\phi \sin\phi)' - n_\theta \cos\phi = s \sin\phi \\ &(s \sin\phi)' + \sin\phi(p + n_\theta + n_\phi) = 0 \\ &k[(m_\phi \sin\phi)' - m_\theta \cos\phi] = s \sin\phi \end{aligned} \tag{20}$$

and

$$\begin{aligned} \lambda_\theta &= v \cot\phi - w \qquad \lambda_\phi = v' - w \\ \kappa_\theta &= -k \cot\phi(v + w') \qquad \kappa_\phi = -k(v + w')' \end{aligned} \tag{21}$$

At the center of the shell, isotropy and symmetry demand that

$$\phi = 0\text{:}\quad n_\phi = n_\theta \quad m_\phi = m_\theta \quad s = 0 \tag{22}$$

(either $w' = v = 0$ or there is a hinge circle)

At the edge of the simply supported cap

$$\phi = \alpha\text{:}\quad m_\phi = 0 \quad w = 0 \tag{23}$$

(either $v = 0$ or there is a hinge circle)

Hinge circles in shells play a role analogous to yield hinges in beams. By definition, a hinge circle is a circle on the shell across which the slope rate w' and/or extension rate v are discontinuous. If such a circle is regarded as the limiting case of a narrow region across which w' and/or v vary rapidly, then w'' and/or v' must be numerically large compared to all lower derivatives. Therefore, within such a narrow region, the components (21) of the strain-rate vector (7) become

$$\mathbf{E} = (0, v', 0, -kv' - kw'') \tag{24}$$

It follows from Table 4 that if v has a positive discontinuity with increasing ϕ, then the stress point must be on face 2 or its intersection with one or more other faces. Similarly, a negative jump in v corresponds to face 5 and positive and negative jumps in $v + w'$ are associated with hinge circles on faces α and 8, respectively.

The general procedure for finding the collapse load of a plastic structure is first to make a hypothesis as to which plastic regime or regimes are involved. In general, the equilibrium equations and flow law can be solved for any such hypothesis, and the correct hypothesis is distinguished by the fact that all of the associated inequalities are also valid.

In choosing the correct stress profile, it is frequently helpful to begin by considering extreme values of the parameter. If α is very small, the cap is essentially a simply supported circular plate. In the limit, $m_\theta = 1$ throughout [2, 4]; hence the stress profile for a circular plate is everywhere in regime 7. At the other extreme, the solution for the complete sphere [2, 8] is

$$n_\theta = n_\phi = -1 \quad m_\theta = m_\phi = 0 \quad s = 0 \quad p = 2$$

which is everywhere in regime 45. Therefore, in view of the general remarks in Section 4, it appears reasonable to try either of regimes 47 or 57 for the simply supported spherical cap with finite angle α.

It turns out that regime 57 is the correct hypothesis. In view of Table 4, Equations (20), and the stress boundary conditions at $\phi = 0$, the stress solution must be

$$\begin{aligned} &n_\theta = -(1/2)[p - (p-2)\sec^2\phi] \quad n_\phi = -1 \\ &s = -(1/2)(p-2)\tan\phi \qquad m_\theta = 1 \\ &m_\phi = 1 - \frac{p-2}{2k}\left[\frac{1}{\sin\phi}\log\frac{1+\sin\phi}{\cos\phi} - 1\right] \end{aligned} \tag{25}$$

Finally, if this solution is to satisfy the Boundary Condition (23) on m_ϕ at $\phi = \alpha$, the collapse load must be

$$p = 2 + 2k \sin\alpha \left[\log\frac{1+\sin\alpha}{\cos\alpha} - \sin\alpha\right]^{-1} \tag{26}$$

This solution will be statically admissible if it remains on the finite faces 5 and 7. In view of Table 4 or Fig. 6, these requirements mean that the stresses must satisfy

$$-1 \le n_\theta \le 0 \qquad 0 \le m_\phi \le 1 \tag{27}$$

The discussion of Inequalities (27) is begun by expanding the bracketed term in the last Equation (25) in a power series in $\sin\phi$:

$$\frac{1}{\sin\phi}\log\frac{1+\sin\phi}{\cos\phi} - 1 = {}^1/_2 \sin^2\phi + {}^1/_6 \sin^4\phi + {}^1/_7 \sin^6\phi + \ldots. \tag{28}$$

It follows from Equation (26) that p is always greater than 2. Equations (25) then show that n_θ is a monotonically increasing function of ϕ, whereas m_ϕ is monotonically decreasing. Therefore, the stress profile will be as shown in Fig. 8(*b*). Evidently it will be statically admissible provided only that $n_\theta(\alpha) \le 0$. This condition leads to

$$\frac{\cos^2\alpha}{\sin^3\alpha}\left[\log\frac{1+\sin\alpha}{\cos\alpha} - \sin\alpha\right] \ge k \tag{29}$$

Inequality (29) is a restriction on the parameters of the cap; it will be true for most cases of practical interest.

Since the stress profile is everywhere on regime 57, it follows from Table 4 and Equations (21) that the velocity equations are

$$\begin{aligned} \lambda_\theta &= v \cot\phi - w = 0 \qquad \lambda_\phi = v' - w = -\nu_5 \\ \kappa_\theta &= -k \cot\phi(v + w') = \nu_7 \qquad \kappa_\phi = -k(v + w')' = 0 \end{aligned} \tag{30}$$

where ν_5 and ν_7 are arbitrary positive factors. The solution of

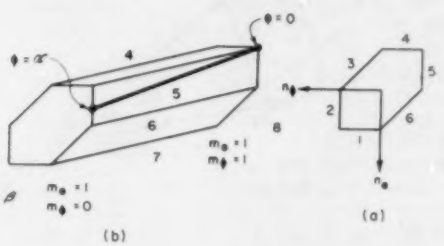

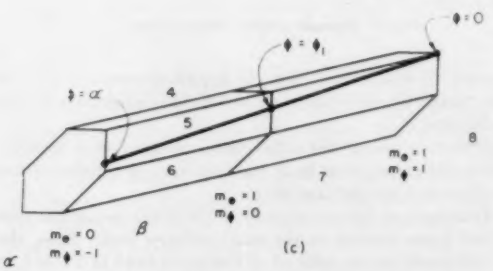

Fig. 8 Stress profiles for spherical cap
(a) Stress plane orientation
(b) Profile for simply supported cap
(c) Profile for clamped cap

Equations (30) which satisfies the boundary condition $w(\alpha) = 0$ is

$$w = w_0 \cos\phi \left[1 - \frac{\log(\sec\phi + \tan\phi)}{\log(\sec\alpha + \tan\alpha)}\right] \quad v = w\tan\phi \quad (31)$$

$$v_b = w_0 \frac{\tan\phi}{\log(\sec\alpha + \tan\alpha)} \qquad v_t = kw_0 \frac{\cot\phi}{\log(\sec\alpha + \tan\alpha)}$$

Here w_0 is the velocity at the center of the shell so that v_b and v_t are evidently positive.

At $\phi = 0$, $v = 0$ and w' has a discontinuity in the proper direction for the hinge circle $m_\phi = 1$. At $\phi = \alpha$, $v = 0$ so that the tangential displacement is continuous.

Therefore, the solution given by Equations (25), (26) and (31) satisfies the equations of equilibrium, the yield condition and associated flow rule, and all the boundary conditions; further, it satisfies all stress inequalities and leads to positive multipliers for the strain-rate vector. Thus it is the desired complete solution according to the two-moment limited interaction yield surface.

6—Clamped Spherical Cap

The only mathematical difference between this problem and the preceding one is that the Boundary Conditions (23) at $\phi = \alpha$ must be replaced by

$$\phi = \alpha\text{: } w = 0 \quad (32)$$

(either $w' = v = 0$ or there is a hinge circle)

The stress profile for the clamped circular plate is in regimes 7 and β [2, 4]. This information, together with the results of the previous section, suggests the stress profile shown in Fig. 8(c).

The complete solution according to this hypothesis is readily computed from Equations (20), (21), (22), and (32) and Table 4. The direct stresses throughout the shell and the moments for $0 \leq \phi \leq \phi_1$ are again given by Equations (25); for $\phi_1 \leq \phi \leq \alpha$ the moments are

$$m_\phi = -1 + \frac{p-2}{2k}\log\frac{\cos\phi}{\cos\alpha} - \log\frac{\sin\alpha}{\sin\phi} \qquad m_\theta = m_\phi + 1 \quad (33)$$

The velocity distribution for the shell is

$$0 \leq \phi \leq \phi_1\text{: } w = C\frac{\cos\phi}{\sin\phi_1}\left[\log\left(\frac{1+\sin\phi_1}{\cos\phi_1}\frac{\cos\phi}{1+\sin\phi}\right) + \sin\phi_1 \log\frac{\tan\alpha}{\tan\phi_1}\right] \quad (34)$$

$$v = w\tan\phi$$

$$v_b = C\tan\phi\csc\phi_1 \qquad v_t = Ck\cot\phi\csc\phi_1$$

$$\phi_1 \leq \phi \leq \alpha\text{: } w = C\cos\phi\log(\tan\alpha/\tan\phi) \quad v = w\tan\phi$$

$$v_b = C\sec\phi \qquad v_\beta = Ck\cos\phi\csc^2\phi$$

The collapse load p and the boundary angle ϕ_1 are defined by the two relations

$$p = 2 + 2k\sin\phi_1\left[\log\frac{1+\sin\phi_1}{\cos\phi_1} - \sin\phi_1\right]^{-1}$$

$$p = 2 + 2k\frac{1+\log(\sin\alpha/\sin\phi_1)}{\log(\cos\phi_1/\cos\alpha)} \quad (35)$$

It may be verified that Equations (25), (33), (34), and (35) satisfy the Equations of Equilibrium (20), the yield condition and flow rule for the profile in Fig. 7(c), and the Boundary Conditions (22) and (32). Further, the stresses, velocities, and velocity slope w' are continuous throughout the shell. The stress inequalities are all valid provided the parameters satisfy Inequality (29). The strain-rate multipliers are all positive. Finally, the only hinge circle is at $\phi = \alpha$ where the discontinuities are of the proper sign. Therefore the foregoing listed equations constitute the complete solution for the two-moment limited interaction surface.

7—Discussion of Results[3]

The spherical cap under uniform pressure is one of the simplest nontrivial examples of a rotationally symmetric shell. Previous bounds on the collapse load have been obtained according to the exact Tresca theory [8] and the Tresca theory for an ideal sandwich shell [2, 12]. Despite the relative simplicity of the problem, none of the previous solutions has been complete and even the bounds have not been very close. Therefore, the outlook for obtaining solutions to more complex rotationally symmetric shell problems according to either Tresca theory is rather bleak.

As previously mentioned, upper and lower bounds according to one theory may be used to find upper and lower bounds according to any other theory by multiplication by a suitable factor. For the sake of defining the problem, let it be assumed temporarily that the Tresca condition for a uniform shell accurately represents the behavior of the shell.

Onat and Prager [8] obtained the first upper and lower bounds by direct consideration of the exact yield surface. Their upper bound for a typical case is shown by the light short-dashed line in Fig. 9; their lower bound is the membrane solution $p = 2$.

In [2], Hodge obtained relatively simple bounds according to the sandwich yield surface. However, if the upper bound is to be interpreted for the exact yield surface, it must be multiplied by 1.25. The resulting upper bund is shown by the light long-dashed curve in Fig. 9. The lower bound may be used directly; for small cap angles it is an improvement over the membrane solution as shown by the heavy long-dashed line in Fig. 9.

[3] The author wishes to thank Mr. L. K. Chatta for carrying out the computations in this section.

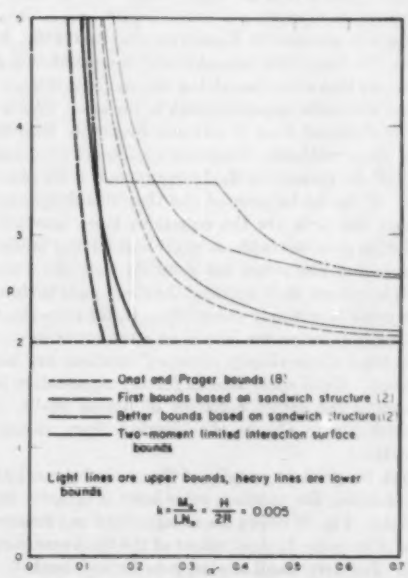
p
α
Onat and Prager bounds [8]
First bounds based on sandwich structure [2]
Better bounds based on sandwich structure [2]
Two-moment limited interaction surface bounds
Light lines are upper bounds, heavy lines are lower bounds
k = M_x/LN_x = H/2R = 0.005

Fig. 9 Upper and lower bounds on collapse load of a clamped spherical cap for different theories

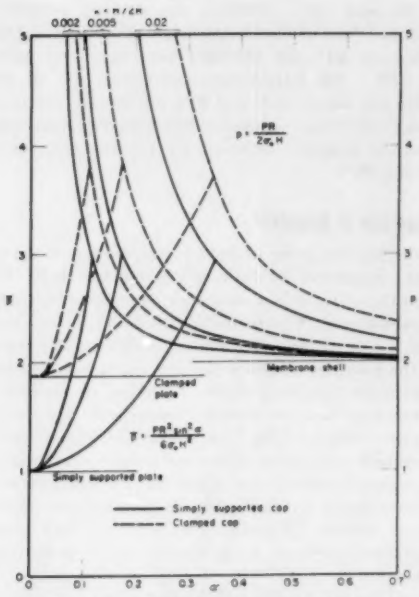

Fig. 10 Collapse load of a spherical cap

Better bounds based on the sandwich yield surface were obtained in [12]. However, as shown by the light and dark dot-dashed lines in Fig. 9, there is still a considerable gap between the upper and lower bounds.

The one-moment limited interaction surface is a very poor approximation, leading to the membrane solution $p = 2$ for all cap angles. Further, this result cannot be interpreted as either an upper or a lower bound.

Finally, the results of the two-moment limited interaction surface are shown by solid lines in Fig. 9. The light curve is plotted from Equations (35). It is the exact solution for the approximate yield surface; hence it is an upper bound on the exact surface. The heavy curve represents a lower bound and is obtained by multiplying the pressure in Equations (35) by 0.618. For large cap angles, the best lower bound is still the membrane solution.

Fig. 9 shows that even though the two-moment limited interaction surface is a crude approximation to the exact Tresca surface, the bounds obtained from it compare favorably with those obtained by other methods. Since the results are comparable, the simplicity of the present method recommends it for practical application. It should be pointed out that this simplicity is twofold in that not only are the equations more tractable, but a single solution provides both an upper and a lower bound.

The preceding discussion has assumed that the Tresca yield surface for a uniform shell is indeed the exact yield surface. However, this point is certainly debatable. If, for example, the shell material really satisfies the Mises' or some other more complex condition, then all previously obtained solutions are merely approximations. Until such time as further information is available concerning the actual behavior of plastic shells, it is certainly justifiable to choose the simplest from among several approximations.

Although the primary purpose of the present paper has been to compare theories, the problem considered is of some interest in its own right. Fig. 10 shows the collapse load as a function of the cap angle α for some typical values of the thickness parameter $k = H/2R$. For very small angles, p as defined tends to infinity; it is more informative to express the results in terms of a different dimensionless pressure

$$\bar{p} = p \sin^2 \alpha/6k = PR^2 \sin^2 \alpha/6\sigma_0 H^2 \tag{36}$$

As α tends to zero, $\bar{p}$ tends to the collapse pressure for a flat plate.

Fig. 10 shows that for relatively large cap angles the effect of the supports is small. The solutions for the clamped and simply supported plates are close to each other and do not differ a great deal from the membrane shell. For very small angles, on the other hand, the curvature of the shell is relatively unimportant and the shells are similar to flat plates. However, there is a rather substantial intermediate range, particularly for the thicker shells, for which both the membrane solution and the plate solution considerably underestimate the collapse load. Thus the present analysis would appear to be particularly valuable for cap angles which lie in this intermediate range.

References

1 W. Prager, "The General Theory of Limit Design," Proceedings Eighth International Congress of Applied Mechanics, Istanbul, vol. 2, 1956, pp. 65–72.

2 P. G. Hodge, Jr., "Plastic Analysis of Structures," McGraw-Hill Book Company, Inc., New York, N. Y., 1959.

3 E. T. Onat and W. Prager, "Limit Analysis of Arches," *Journal of Mechanics and Physics of Solids*, vol. 1, 1953, pp. 77–89.

4 H. G. Hopkins and W. Prager, "The Load Carrying Capacities of Circular Plates," *Journal of Mechanics and Physics of Solids*, vol. 2, 1953, pp. 1–13.

5 D. C. Drucker, "Limit Analysis of Circular Cylindrical Shells Under Axially Symmetric Loading," Proceedings of the First Mid-Western Conference on Solid Mechanics, Urbana, 1954, pp. 158–163.

6 P. G. Hodge, Jr., "The Rigid-Plastic Analysis of Symmetrically Loaded Cylindrical Shells," JOURNAL OF APPLIED MECHANICS, vol. 21, TRANS. ASME, vol. 76, 1954, pp. 336–342.

7 E. T. Onat, "Plastic Collapse of Cylindrical Shells Under Axially Symmetrical Loading," *Quarterly of Applied Mathematics*, vol. 13, 1955, pp. 63–72.

8 E. T. Onat and W. Prager, "Limit Analysis of Shells of Revolution," Proceedings Royal Netherlands Academy of Sciences, series B, vol. 57, 1954, pp. 534–548.

9 P. G. Hodge, Jr., "The Linearization of Plasticity Problems by Means of Nonhomogeneous Materials," *Nonhomogeneity in Elasticity and Plasticity*, Proceedings Symposium in Warsaw, 1958, Pergamon Press, Ltd., London, 1959, pp. 147–156.

10 D. C. Drucker and R. T. Shield, "Limit of a Symmetrically Loaded Thin Shell of Revolution," JOURNAL OF APPLIED MECHANICS, vol. 26, TRANS. ASME, vol. 81, series E, 1959, pp. 61–68.

11 W. Prager and P. G. Hodge, Jr., "Theory of Perfectly Plastic Solids," John Wiley & Sons, Inc., New York, N. Y., 1951.

12 P. G. Hodge, Jr., "The Collapse Load of a Spherical Cap," Proceedings of the Fourth Midwest Conference on Solid Mechanics, Austin, 1959, pp. 108–126.

APPENDIX

Relation Between Exact Surface and Sandwich Approximation

The sandwich approximate yield surface in Table 2 is a convex polyhedron; hence it will be interior to the exact surface in Table 1 if all of its vertexes are in or on the exact yield surface. As shown in [2], there are 36 vertexes. If account is taken of sym-

Table 5 Sandwich yield surface inscribed in exact yield surface

Vertex				Parameters			
n_1	n_2	m_1	m_2	p	q	r	Intermediate
1	0	0	0	1/2	1/2	1/2	p
0	0	1	0	0	0	0	p
1	1	0	0	1/2	1/2	−1/2	p
0	0	1	1	0	0	0	q
1/2	1	−1/2	0	0	1/2	−1/2	p
0	1/2	−1	−1/2	0	0	−1/2	p
1/2	1/2	1/2	−1/2	0	−1/2	0	p
1/2	−1/2	1/2	1/2	−1/2	0	−1/2	p

Table 6 Sandwich yield surface circumscribed on exact yield surface

Plane of inscribed polygon.....	$n_1 + m_1 = 1$	$n_1 - n_2 + m_1 - m_2 = 1$
Strain-rate vector.....	$\nu(1, 0, 1, 0)$	$\nu(1, -1, 1, -1)$
Parameters for exact surface....	$p = q = -1/4$	$p = r = -1/4$
Stresses for exact surface.....	$n_1 = 1/2\, m_1 = 3/4$	$n_1 - n_2 = 1/2\, m_1 - m_2 = 3/4$
Plane of circumscribed polygon.	$n_1 + m_1 = 5/4$	$n_1 - n_2 + m_1 - m_2 = 5/4$

metry, it is sufficient to discuss only the 8 vertexes whose components are listed in the first four columns in Table 5.

It develops that for the two surfaces as defined the vertexes of the sandwich approximation are all on the exact surface. This result is verified by finding values of p, q, and r from Table 1 for each of the eight points. These verifying values are listed in the last four columns of Table 5.

To use the sandwich approximation for an upper bound it is necessary to expand the polyhedron until it is exterior to the actual surface. This will be the case if each of the 12 planes is exterior or tangent to the exact surface at the point where the normals to the two surfaces are the same. Because of symmetry, it is sufficient to consider the two planes listed in Table 6. The strain-rate vector for each plane is given in the second line in Table 6. Values of two of the three parameters are then uniquely defined by Equations (8). The stress point on the exact surface with the same normal is then determined from Table 1. Actually, since there is still a one-parameter family of stress points, the two surfaces are tangent along a line or curve. Finally, the plane through this stress point (or curve) and parallel to the original plane is shown in the last line in Table 6.

It follows from Table 6 that if the approximate surface is multiplied by 1.25 it will be exterior to the exact surface. Evidently the corresponding collapse load will also be multiplied by 1.25. Therefore the exact and approximate collapse loads must satisfy the continued Inequality (11).

An Approximate Analysis of the Influence of Aerodynamic Heating and Initial Twist on the Torsional Stiffness of Thin Wings

LIT S. HAN
Associate Professor,
Department of Mechanical Engineering,
The Ohio State University,
Columbus, Ohio

In the present paper, approximate formulas are derived, based on the "fiber-stress" concept, for the combined influence of aerodynamic heating and initial twist on the torsional stiffness of a thin wing. Criteria are established for calculating the critical temperature difference between that of the edges and that of the mid-chord position, for preventing possible aeroelastic reversals or buckling. Formulas are valid for wings with large aspect ratios.

Introduction

In reference [1],[1] the author and his co-worker derived a simple formula for calculating the thermally induced twist in a thin wing which has an initial twist about its axis. The problem of induced twists is related to the general problem of reduction of torsional stiffness treated in references [2–5]. In this paper a general treatment of the influence of aerodynamic heating and the effects of initial twist on the torsional stiffness are given; the method of approach adopted herein being that of the "fiber-stress" concept.

Analysis

Consider a symmetrical thin wing whose cross section is shown in Fig. 1, and assume that the ends are far removed from the section under consideration. The wing has an initial twist about its axis, θ_i radians per unit length, and has a nonuniform temperature distribution in the chordwise direction as a result of aerodynamic heating. For an approximate treatment, the temperature distribution is assumed symmetrical about the mid-chord axis and uniform in a direction transverse to the chord. It may be easily observed that these restrictions may be removed by performing a similar analysis to the following developments.

We shall employ the inverse method to obtain the characteristic curves relating to the applied moments and the resulting twists; i.e., assuming a new angle of twist θ_f and proceeding to calculate the external torque required to maintain equilibrium.

In Fig. 2, a fiber is shown to assume a new position after a rotation $(\theta_f - \theta_i)$ with the corresponding helix angles γ_i and γ_f. The initial and final lengths of the fiber are therefore given by

$$l_i = (1 + \gamma_i^2)^{1/2} \tag{1}$$

$$l_f = (1 + \gamma_f^2)^{1/2} \tag{2}$$

based on the assertion that ends do not approach each other.

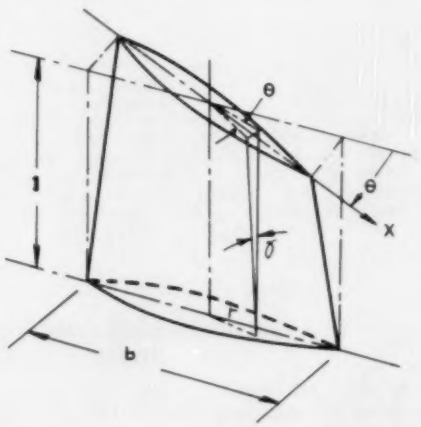

Fig. 1 Co-ordinate system of a symmetrical wing

[1] Numbers in brackets designate References at end of paper.

For presentation at the Summer Conference of the Applied Mechanics Division, University Park, Pa., June 20–22, 1960, of The American Society of Mechanical Engineers.

Discussion of this paper should be addressed to the Secretary, ASME, 29 West 39th Street, New York, N. Y., and will be accepted until July 22, 1960, for publication at a later date. Discussion received after the closing date will be returned.

Note: Statements and opinions advanced in papers are to be understood as individual expressions of their authors and not those of the Society. Manuscript received by ASME Applied Mechanics Division, May 4, 1959. Paper No. 60—APM-13.

Nomenclature

A = area of cross section
b = chord
E = modulus of elasticity
f = subscript, final
G = shear modulus
i = subscript, initial
I_4, I_2, I_{2T} = defined by equations (11)
J = stiffness constant
l = length
M_{ex} = external moment
M_x = moment due to longitudinal stress
r = distance from center to fiber
T = temperature rise
ΔT = differential temperature between edges and mid-chord position
T_a = average temperature rise, defined by equation (11)
ΔT_c = critical value of ΔT, equations (20) and (23)
α = coefficient of thermal expansion
γ = helix angle
ϵ = unit strain
θ = angle of twist
ν = Poisson's ratio
σ = stress (+, tension; −, compression)

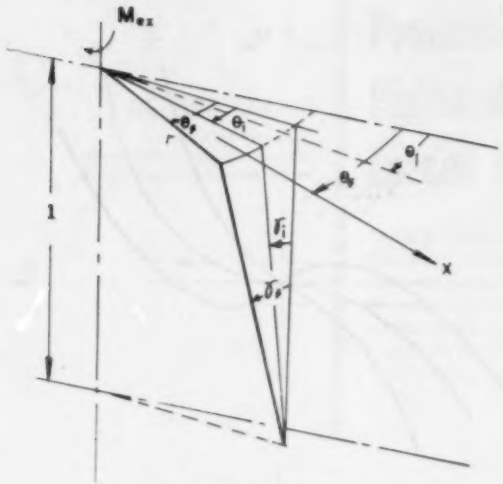

Fig. 2 Positions of a fiber

The strain induced can be approximated by

$$\epsilon = (1/2)r^2(\theta_f^2 - \theta_i^2)/(1 + r^2\theta_i^2)^{1/2} \tag{3}$$

wherein the following approximation is made:

$$\gamma_{i,f} = r\theta_{i,f} \tag{4}$$

If the local fiber temperature is T above the initial temperature, the resulting strain is therefore

$$\epsilon_T = (1/2)\left[\frac{r^2(\theta_f^2 - \theta_i^2)}{(1 + r^2\theta_i^2)^{1/2}}\right] - \alpha T$$

where α is the thermal expansion coefficient. The corresponding stress is

$$\sigma_T = \frac{E}{2}\left[\frac{r^2(\theta_f^2 - \theta_i^2)}{(1 + r^2\theta_i^2)^{1/2}}\right] - \alpha TE \tag{5}$$

In order to maintain self-equilibrium with respect to axial tension, there will be induced a uniform stress, σ_u, along all fibers within the cross section so that the following condition is satisfied:

$$\int_A (\sigma_T + \sigma_u)\cos\gamma_f dA = 0 \tag{6}$$

and the final fiber stress is given by

$$\sigma_r = \sigma_T + \sigma_u \tag{7}$$

Application of condition (6) results in the following expression for σ_r:

$$\sigma_r = \frac{E}{2}(\theta_f^2 - \theta_i^2)\left\{\frac{r^2}{(1 + r^2\theta_i^2)^{1/2}} - \left[\int \frac{r^2 dA}{(1 + r^2\theta_i^2)^{1/2}(1 + r^2\theta_f^2)^{1/2}} \Big/ \int \frac{dA}{(1 + r^2\theta_f^2)^{1/2}}\right]\right\} - \alpha E\left\{T - \left[\int \frac{T dA}{(1 + r^2\theta_f^2)^{1/2}} \Big/ \int \frac{dA}{(1 + r^2\theta_f^2)^{1/2}}\right]\right\} \tag{8}$$

Equation (8) gives the fiber stress which is along the fiber direction in its equilibrium position. These stresses produce a moment given by

$$M_\sigma = \int_A \sigma_r r \sin\gamma_f dA \tag{9}$$

Introducing the following simplifications:

$$\begin{aligned} r &\sim x \\ \sin\gamma_f &\sim x\theta_f \\ x\theta_f &\ll 1 \\ x\theta_i &\ll 1 \end{aligned} \tag{10}$$

and the following notations:

$$\begin{aligned} I_4 &= \int_A x^4 dA \\ I_2 &= \int_A x^2 dA \\ I_{2T} &= \int_A Tx^2 dA \\ T_a &= \frac{1}{A}\int_A T dA \end{aligned} \tag{11}$$

the moment M_σ is accordingly given by

$$M_\sigma = \left(\frac{E}{2}\right)\theta_f(\theta_f^2 - \theta_i^2)[(I_4) - (I_2^2/A)] - \alpha E(I_{2T} - T_a I_2)\theta_f \tag{12}$$

The external moment required to produce equilibrium is therefore the sum of M_σ and that of Saint Venant's moment; i.e.,

$$M_{ex} = \frac{E}{2}\theta_f(\theta_f^2 - \theta_i^2)[I_4 - (I_2^2/A)] - \alpha E(I_{2T} - T_a I_2)\theta_f + GJ(\theta_f - \theta_i) \tag{13}$$

The slope of M_{ex} versus $(\theta_f - \theta_i)$ curve is given by

$$\frac{dM_{ex}}{d\theta_f} = \left(\frac{E}{2}\right)(3\theta_f^2 - \theta_i^2)[I_4 - (I_2^2/A)] - \alpha E(I_{2T} - T_a I_2) + GJ \tag{14}$$

where GJ is Saint Venant's stiffness.

Discussion

Equations (13) and (14) show the combined influence of aerodynamic heating and initial twist on the torsional stiffness of a thin wing. The equations also give the nonlinear effect due to initial twist. A similar analysis without an imposed temperature was treated in references [6] and [7].

In order to arrive at some further observations, regarding the nature of the M-θ curve, a temperature distribution is assumed as follows:

$$T = T_1 + (4\Delta T/b^2)x^2 \tag{15}$$

where T_1 is the mid-chord temperature rise and ΔT represents the differential temperature between the edges and the mid-chord position. Use of equation (15) gives the following results:

$$M_{ex} = E\theta_f[I_4 - (I_2^2/A)]\left[(1/2)(\theta_f^2 - \theta_i^2) - \frac{4\alpha}{b^2}\Delta T\right] + GJ(\theta_f - \theta_i) \tag{16}$$

$$\frac{dM_{ex}}{d\theta_f} = E[I_4 - (I_2^2/A)]\{[(3\theta_f^2 - \theta_i^2)/2] - (4\alpha\Delta T/b^2)\} + GJ \tag{17}$$

In view of equations (16) and (17), the following observations can be made:

(a) Zero Pretwist, $\theta_i = 0$. Since equation (16) is a third-order equation in θ_f; for each M_{ex}, it may have one or three roots for θ_f. The criterion is therefore whether $(dM_{ex}/d\theta_f)$ changes sign or not. This in turn depends on whether the equation

$$\frac{dM_{ex}}{d\theta_f} = 0 \tag{18}$$

possesses a solution or not.

Application of equation (18) shows that it is satisfied when

$$\Delta T > \Delta T_c \tag{19}$$

$$\Delta T_c = \frac{b^2 J}{8\alpha} \Big/ \{(1+\nu)[I_4 - (I_2^3/A)]\} \tag{20}$$

where ν is Poisson's ratio and ΔT_c is defined as the critical temperature differential.

Three typical characteristic curves are shown in Fig. 3 for $\Delta T < \Delta T_c$, $\Delta T = \Delta T_c$ and $\Delta T > \Delta T_c$. It is of significance to observe that for $\Delta T > \Delta T_c$ the torsional characteristic curve exhibits elastic instability and the motion will therefore proceed according to the dashed lines. The reversals of this kind have been discussed for the case of a propeller blade with initial twists in reference [8].

(b) Finite Pretwist ($\theta_i \neq 0$). For a finite pretwist, the condition of buckling can be likewise examined by letting $(dM_{ex}/d\theta_f) = 0$ and determine the roots. This leads to the following expression:

$$E[I_4 - (I_2^3/A)](3\theta_f^2/2) = E\,[I_4 - (I_2^3/A)]\,[(\theta_i^2/2) + (4\alpha\Delta T/b^2)] - GJ \tag{21}$$

Thus the right-hand side must be zero or positive for the existence of real roots for θ_f; i.e.,

$$\Delta T \geqslant \Delta T_c \tag{22}$$

$$\Delta T_c = [(b^2 J/8\alpha)/\{(1+\nu)[I_4 - (I_2^3/A)]\}] - (b^2\theta_i^2/8\alpha) \tag{23}$$

Comparison of equations (20) and (23) leads to the obvious conclusion, that a wing with an initial twist will have a lower buckling temperature differential than one without:

Rewrite equation (16) as

$$M_{ex} = E[I_4 - (I_2^3/A)]\,[(\theta_f^2/2) - (\Delta T - \Delta T_c)(4\alpha/b^2)]\theta_f - GJ\theta_i \tag{24}$$

Representative curves for a fixed θ_i and at various ΔT are shown in Fig. 4. The so-called thermally induced twist is easily calculated by setting $M_{ex} = 0$ in equation (24). For $\Delta T = \Delta T_c$, the induced twist angle $(\theta_f - \theta_i)$ is given by

$$(\theta_f - \theta_i) = \theta_i \left\langle \sqrt[3]{J/\{\theta_i^2(1+\nu)[I_4 - (I_2^3/A)]\}} - 1 \right\rangle \tag{25}$$

which is in a more explicit form than that shown in reference [1].

For a temperature distribution other than that indicated by equation (15), an equation may be written as

$$T = T_1 + C_1 x^2 + C_2 x^4 + \ldots\ldots$$

and an analysis similar to the one contained herein may be easily performed.

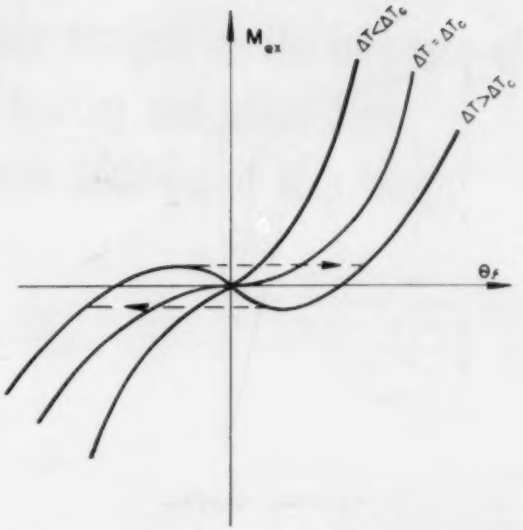

Fig. 3 Torsional characteristics for a thin wing without initial twist

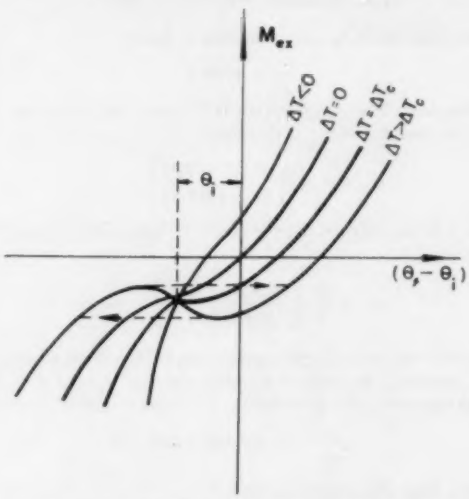

Fig. 4 Torsional characteristics for a thin wing with initial twist

References

1 L. S. Han and K. L. Bergman, "Thermally Induced Twists in Plates of Thin Cross Sections," JOURNAL OF APPLIED MECHANICS, vol. 26, TRANS. ASME, series E, vol. 81, 1959, pp. 134–135.

2 N. J. Goodier, "Elastic Torsion in the Presence of Initial Axial Stress," JOURNAL OF APPLIED MECHANICS, vol. 17, TRANS. ASME, vol. 72, 1950, pp. 383–387.

3 B. Budiansky and J. Mayers, "Influence of Aerodynamic Heating on the Effective Torsional Stiffness of Thin Wings," *Journal of the Aeronautical Sciences*, vol. 23, 1956, pp. 1081–1093.

4 N. J. Hoff, "Approximate Analysis of the Reduction in Torsional Rigidity and of the Torsional Buckling of Solid Wings Under Thermal Stresses," *Journal of the Aeronautical Sciences*, vol. 23, 1956, pp. 603–604.

5 J. Singer, "Thermal Buckling of Solid Wings of Arbitrary Aspect Ratio," *Journal of Aero/Space Sciences*, vol. 25, 1958, pp. 567–572.

6 F. R. Stone and J. O. Schulze, "Calculations of Steady Longitudinal Stresses Arising From Torsional Deflection of a Thin Wing," WADC Technical Report 53-20, March, 1953.

7 Chen Chu, "The Effect of Initial Twist on the Torsional Rigidity of Thin Prismetical Bar and Tubular Members," Proceedings of the First U.S. National Congress of Applied Mechanics, ASME, June, 1951, pp. 265–269.

8 F. W. Niedenfuhr, "On the Possibility of Aeroelastic Reversal of Propeller Blades," *Journal of the Aeronautical Sciences*, 1955, vol. 23, pp. 438–440.

Postbuckling Behavior of Rectangular Plates With Small Initial Curvature Loaded in Edge Compression—(continued)

NOBORU YAMAKI
Assistant Professor,
Institute of High Speed Mechanics,
Tohoku University, Sendai, Japan

In the previous paper [1],[1] the title problem is theoretically treated under eight different boundary conditions and numerical solutions are obtained for the deflection, edge shortening, and effective width of the square plate in edgewise compression. As a continuation of this work, the stress state in the buckled plate is investigated and numerical results for the square plate are given graphically. Further the formulas for the ultimate load of the square plate in each case are derived by using the maximum-shear theory for the beginning of yielding and comparison is made with the previous results and experiments.

THE LARGE deflection problem of the rectangular plate subjected to edgewise compression has been treated theoretically under eight typical boundary conditions [1] and, through numerical calculations, the connections of deflection, edge shortening and effective width of the plate with applied loads are clarified for square plates with and without initial deflection. Continuing this study, the stress state in the buckled plate is here investigated. First, the previous theoretical analysis is outlined for completeness and then the expressions for the stress and strain are derived. Next, using the values of deflection coefficients previously determined, the stress field in the buckled square plate is calculated and the results are presented graphically. Finally, the formulas for the ultimate load of the square plate are derived by using the maximum-shear theory for the beginning of yielding and the results are discussed in some detail.

[1] Numbers in brackets designate References at end of paper.

Presented at the West Coast Conference of the Applied Mechanics Division, Stanford, Calif., September 9–11, 1959, of THE AMERICAN SOCIETY OF MECHANICAL ENGINEERS.

Discussion of this paper should be addressed to the Secretary, ASME, 29 West 39th Street, New York, N. Y., and will be accepted until July 10, 1960, for publication at a later date. Discussion received after the closing date will be returned.

NOTE: Statements and opinions advanced in papers are to be understood as individual expressions of their authors and not those of the Society. Manuscript received by ASME Applied Mechanics Division, March 12, 1959. Paper No. 59—APMW-22.

Basic Equations

For the sake of completeness, we summarize the previous theoretical analysis briefly. The governing equations for the large deflection of the plate with initial curvature have been derived by Marguerre [2], which can be expressed as[2]

$$\nabla^4 F = E(w_{,xy}^2 - w_{,xx}w_{,yy} + 2w_{0,xy}w_{,xy} - w_{0,xx}w_{,yy} - w_{0,yy}w_{,xx}), \quad (1)$$

$$\nabla^4 w = h/D[F_{,yy}(w + w_0)_{,xx} + F_{,xx}(w + w_0)_{,yy} - 2F_{,xy}(w + w_0)_{,xy}] \quad (2)$$

The boundary conditions for this case consist of the supporting and loading conditions, Fig. 1.

For the supporting conditions, we will consider the following four cases: I—All edges simply supported; II—loaded edges simply supported, the other edges clamped; III—loaded edges

[2] Subscripts following a comma stand for differentiation, e.g., $w_{,xy} = \partial^2 w/\partial x \partial y$; $F_{,yy} = \partial^2 F/\partial y^2$, etc.

Nomenclature

x, y, z = rectangular co-ordinates
a = length of plate
b = width of plate
h = thickness of plate
$\beta = a/b$ = aspect ratio
u, v, w = displacements of a point in x, y, and z-directions, respectively
w_0 = initial deflection
a_{mn} = coefficient for initial deflection
b_{mn} = coefficient for net deflection
E = Young's modulus
ν = Poisson's ratio
$D = Eh^3/12(1 - \nu^2)$ = flexural rigidity of plate
F = Airy's stress function
$\nabla^4 = \partial^4/\partial x^4 + 2\partial^4/\partial x^2\partial y^2 + \partial^4/\partial y^4$
P_x, P_y = total loads in x and y-directions, respectively
P_u = ultimate load
$\sigma_u = P_u/ah$ = ultimate average stress
p_y = average compressive stress in y-direction
$\lambda = p_y a^2/\pi^2 Eh^2$
λ_{cr} = critical value of λ corresponding to buckling load
$\sigma_{cr} = \lambda_{cr}\pi^2 Eh^2/a^2$ = buckling stress
σ_{YP} = yield-point stress
τ_m = maximum shearing stress
$\sigma_x, \sigma_y, \tau_{xy}$ = membrane stresses
$\sigma_x', \sigma_y', \tau_{xy}'$ = extreme bending stresses
$\bar{\sigma}_{YP}, \bar{\tau}_m, \bar{\sigma}_x, \bar{\tau}_{xy}'$, etc. = nondimensional stress factors obtained by multiplying $(a^2/\pi^2 Eh^2)$ to original ones
$\epsilon_x, \epsilon_y, \gamma_{xy}$ = membrane strains
$\epsilon_x', \epsilon_y', \gamma_{xy}'$ = extreme bending strains
$\bar{\epsilon}_x, \bar{\gamma}_{xy}'$, etc. = nondimensional strain factors obtained by multiplying $(a^2/\pi^2 h^2)$ to original ones
$X_m = \cos(m\pi/a)x$
$Y_n = \cos(n\pi/b)y$
$x_m = \sin(m\pi/a)x$
$y_n = \sin(n\pi/b)y$
$S_n = \sinh(n\pi/b)x$
$C_n = \cosh(n\pi/b)x$

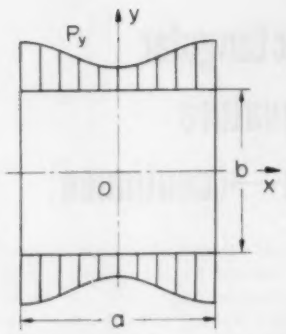

Fig. 1 Rectangular plate loaded in edge compression

clamped, the other edges simply supported; IV—all edges clamped. It is assumed that both the initial and additional deflections satisfy the same supporting conditions in each case.

Concerning the loading conditions, we have along the loaded edges

$$v = \text{const}, \quad P_y = -p_y ah, \quad F_{,xy} = 0, \tag{3}$$

while along the side edges, we consider the following two cases:

$$\begin{aligned} &\text{Case } (a): \quad u = \text{const}, \quad P_x = F_{,xy} = 0, \\ &\text{Case } (b): \quad F_{,yy} = F_{,xy} = 0 \end{aligned} \tag{4}$$

Cases (a) and (b) stand for the straight and stress-free edges, respectively.

The problem consists in finding the solutions of w and F which satisfy Equations (1) and (2) together with the given boundary conditions. To obtain the solution, we first assume the deflections in each case as follows:

$$w_0 = h \sum_m \sum_n a_{mn} f_m(x) g_n(y),$$

$$w = h \sum_m \sum_n b_{mn} f_m(x) g_n(y), \tag{5}$$

where a_{mn} and b_{mn}, respectively, are the prescribed and undetermined constants and where

$$f_m(x) = \begin{cases} \cos(m\pi/a)x, \quad m = 1, 3, 5 \ldots \\ \qquad\qquad \text{for Cases I and III,} \\ (-1)^{m+1} + \cos(2m\pi/a)x, \quad m = 1, 2, 3, \ldots \\ \qquad\qquad \text{for Cases II and IV,} \end{cases}$$

$$g_n(y) = \begin{cases} \cos(n\pi/b)y, \quad n = 1, 3, 5 \ldots \\ \text{or } \sin(n\pi/b)y, \quad n = 2, 4, 6 \ldots \\ \qquad\qquad \text{for Cases I and II,} \\ \vdots \\ (-1)^{n+1} + \cos(2n\pi/b)y, \quad n = 1, 2, 3 \ldots \\ \qquad\qquad \text{for Cases III and IV.} \end{cases} \tag{6}$$

It will be easily seen that these expressions satisfy the related supporting conditions.

Now we will express the stress function F in terms of the deflection coefficients a_{mn} and b_{mn}. Substituting the expressions for the deflections in Equation (1), the results may be expressed in the following form:

$$\nabla^4 F = (\pi^4 Eh^2/a^2b^2) \sum_p \sum_q D_{pq} X_{2p} Y_{2q},$$

$$p, q = 0, 1, 2 \ldots \tag{7}$$

where we have used the abbreviations

$$X_{2p} = \cos(2p\pi/a)x, \quad Y_{2q} = \cos(2q\pi/b)y \tag{8}$$

D_{pq} are the quadratic functions of a_{mn} and b_{mn} obtained in each case. The general solution of Equation (7) is obviously given by adding the biharmonic function F_0 to a particular integral F_1, and after determining F_0 so that the loading conditions are fulfilled, we finally obtain the desired expressions of F as

$$\begin{aligned} F = {} & -\tfrac{1}{2} p_y x^2 + Eh^2 \sum_p \sum_q \varphi_{pq} X_{2p} Y_{2q} \\ & + Eh^2 \sum_{n=1,2\ldots}^{\infty} E_n [(\sinh n\pi\beta + n\pi\beta \cosh n\pi\beta) \cosh (2n\pi/b)x \\ & - (2n\pi/b)x \sinh n\pi\beta \sinh (2n\pi/b)x] \cos (2n\pi/b)y, \end{aligned} \tag{9}$$

where

$$\beta = a/b, \quad \varphi_{pq} = \beta^2 D_{pq}/16(p^2 + q^2\beta^2)^2,$$

$$E_n = \begin{cases} 0 \qquad\qquad \text{for Case } (a), \\ (\sinh n\pi\beta \cosh n\pi\beta + n\pi\beta)^{-1} \displaystyle\sum_{m=0,1,2\ldots}^{\infty} (-1)^{m+1} \varphi_{mn} \quad \text{for Case } (b) \end{cases} \tag{10}$$

Making use of the foregoing expressions for w and F, only the unknowns b_{mn} can now be determined by applying the Galerkin's method to Equation (2). Once b_{mn} are found, w and F are known and the problem is solved.

Stress and Strain in the Buckled Plate

Membrane Stresses and Strains. The membrane stresses σ_x, σ_y, and τ_{xy} are given by the stress function F as

$$\sigma_x = F_{,yy}, \quad \sigma_y = F_{,xx}, \quad \tau_{xy} = -F_{,xy} \tag{11}$$

Hence, letting

$$\begin{aligned} \lambda = p_y a^2/\pi^2 Eh^2, \quad & \bar{\sigma}_x = \sigma_x a^2/\pi^2 Eh^2, \\ & \bar{\sigma}_y = \sigma_y a^2/\pi^2 Eh^2, \quad \bar{\tau}_{xy} = \tau_{xy} a^2/\pi^2 Eh^2, \end{aligned} \tag{12}$$

we obtain from Equation (9)

$$\left.\begin{aligned} \bar{\sigma}_x = {} & -4\beta^2 \sum_p \sum_q q^2 \varphi_{pq} X_{1p} Y_{2q} \\ & - 4\beta^2 \sum_n [G_n C_{2n} - (2n\pi/b)x H_n S_{2n}] Y_{2n}, \\ \bar{\sigma}_y = {} & -\lambda - 4 \sum_p \sum_q p^2 \varphi_{pq} X_{2p} Y_{2q} \\ & + 4\beta^2 \sum_n \{G_n C_{2n} - H_n [2C_{2n} + (2n\pi/b)x S_{2n}]\} Y_{2n}, \\ \bar{\tau}_{xy} = {} & -4\beta \sum_p \sum_q pq \varphi_{pq} x_{1p} y_{1q} \\ & + 4\beta^2 \sum_n \{G_n S_{1n} - H_n [S_{2n} + (2n\pi/b)x C_{2n}]\} y_{2n}, \end{aligned}\right\} \tag{13}$$

where

$$\left.\begin{aligned} & x_{2p} = \sin(2p\pi/a)x, \quad y_{2q} = \sin(2q\pi/b)y, \\ & S_{2n} = \sinh(2n\pi/b)x, \quad C_{2n} = \cosh(2n\pi/b)x, \\ & G_n = n^2(\sinh n\pi\beta + n\pi\beta \cosh n\pi\beta)E_n, \\ & \qquad H_n = n^2 E_n \sinh n\pi\beta \end{aligned}\right\} \tag{14}$$

Defining the corresponding strains by ϵ_x, ϵ_y, and γ_{xy}, and letting

$$\bar{\epsilon}_x = \epsilon_x a^2/\pi^2 h^2, \quad \bar{\epsilon}_y = \epsilon_y a^2/\pi^2 h^2, \quad \bar{\gamma}_{xy} = \gamma_{xy} a^2/\pi^2 h^2, \tag{15}$$

we have

$$\bar{\epsilon}_x = \bar{\sigma}_x - \nu\bar{\sigma}_y, \quad \bar{\epsilon}_y = \bar{\sigma}_y - \nu\bar{\sigma}_x, \quad \bar{\gamma}_{xy} = 2(1+\nu)\bar{\tau}_{xy} \tag{16}$$

Table 1 Formulas for extreme bending strains in each case

Case	$\bar{\epsilon}_x'$	$\bar{\epsilon}_y'$	$\bar{\gamma}_{xy}'$	m	n
I	$^1/_2\Sigma\Sigma m^2 b_{mn} X_m \begin{pmatrix} Y_n \\ y_n \end{pmatrix}$	$^1/_2\beta^2\Sigma\Sigma n^2 b_{mn} X_m \begin{pmatrix} Y_n \\ y_n \end{pmatrix}$	$\mp\beta\Sigma\Sigma mn b_{mn} x_m \begin{pmatrix} y_n \\ Y_n \end{pmatrix}$	$1, 3, 5 \ldots$	$\begin{pmatrix} 1, 3, 5 \ldots \\ 2, 4, 6 \ldots \end{pmatrix}$
II	$2\Sigma\Sigma m^2 b_{mn} X_{2m} \begin{pmatrix} Y_n \\ y_n \end{pmatrix}$	$^1/_2\beta^2\Sigma\Sigma n^2 b_{mn} [(-1)^{m+1} + X_{2m}] \begin{pmatrix} Y_n \\ y_n \end{pmatrix}$	$\mp 2\beta\Sigma\Sigma mn b_{mn} x_{2m} \begin{pmatrix} y_n \\ Y_n \end{pmatrix}$	$1, 2, 3 \ldots$	$\begin{pmatrix} 1, 3, 5 \ldots \\ 2, 4, 6 \ldots \end{pmatrix}$
III	$^1/_2\Sigma\Sigma m^2 b_{mn} X_m [(-1)^{n+1} + Y_{2n}]$	$2\beta^2\Sigma\Sigma n^2 b_{mn} X_m Y_{2n}$	$-2\beta\Sigma\Sigma mn b_{mn} x_m y_{2n}$	$1, 3, 5 \ldots$	$1, 2, 3 \ldots$
IV	$2\Sigma\Sigma m^2 b_{mn} X_{2m} [(-1)^{n+1} + Y_{2n}]$	$2\beta^2\Sigma\Sigma n^2 b_{mn} [(-1)^{m+1} + X_{2m}] Y_{2n}$	$-4\beta\Sigma\Sigma mn b_{mn} x_{2m} y_{2n}$	$1, 2, 3 \ldots$	$1, 2, 3 \ldots$

NOTE: In Cases I and II, the upper and lower letters, respectively, correspond with each other.

Extreme Bending Stresses and Strains. Denoting by ϵ_x', ϵ_y', and γ_{xy}' the bending strains at the surface of the plate, $z = h/2$, we have

$$\epsilon_x' = -(h/2)w_{,xx}, \quad \epsilon_y' = -(h/2)w_{,yy}, \quad \gamma_{xy}' = -hw_{,xy} \quad (17)$$

Hence, letting

$$\bar{\epsilon}_x' = \epsilon_x' a^2/\pi^2 h^2, \quad \bar{\epsilon}_y' = \epsilon_y' a^2/\pi^2 h^2, \quad \bar{\gamma}_{xy}' = \gamma_{xy}' a^2/\pi^2 h^2, \quad (18)$$

we obtain, from Equations (5) and (6), the formulas shown in Table 1.

The corresponding stresses σ_x', σ_y', and τ_{xy}' are given by

$$\bar{\sigma}_x' = \frac{1}{1-\nu^2}(\bar{\epsilon}_x' + \nu\bar{\epsilon}_y'), \quad \bar{\sigma}_y' = \frac{1}{1-\nu^2}(\bar{\epsilon}_y' + \nu\bar{\epsilon}_x'),$$

$$\bar{\tau}_{xy}' = \frac{1}{2(1+\nu)}\bar{\gamma}_{xy}', \quad (19)$$

where

$$\bar{\sigma}_x' = \sigma_x' a^2/\pi^2 E h^2, \quad \bar{\sigma}_y' = \sigma_y' a^2/\pi^2 E h^2,$$

$$\bar{\tau}_{xy}' = \tau_{xy}' a^2/\pi^2 E h^2 \quad (20)$$

Stress Field in the Buckled Square Plate

Now we will investigate the postbuckling stress state of the square plate under eight different boundary conditions, combining four kinds of supporting conditions and two kinds of loading conditions. First we assume the nonzero deflection coefficients are those as shown in Table 2 and take the values of a_{mn} in each case so that both cases can be treated where the plate is initially flat and initially deflected, the deviation of which is one tenth of its thickness. Poisson's ratio ν is taken as 1/3. Under these conditions, values of b_{mn} for various values of λ in each case have been calculated, with the results shown in Tables 2 to 5 of the previous paper [1]. Making use of these results together with the formulas given in the foregoing, we can calculate the stresses at any point in the plate.

Here we will observe the stresses at the four principal points in the plate as shown in Fig. 2. These points correspond to A, B, C, and D in the Cases except for Case II, where they are chosen as E, B, C, and F.[2] The results of the calculation for the membrane stresses are given in Figs. 3(*a–h*), while those for the bending stresses are shown in Figs. 4(*a–h*). In these figures, solid and dotted curves correspond to the initially flat and deflected plates, respectively, and the meaning of the marks labeled on the curves are as follows: e.g., $A_x = \bar{\sigma}_x$ at A, $B_y' = \bar{\sigma}_y'$ at B, $C_{xy}' = \bar{\tau}_{xy}'$ at C, etc. Further, the stresses which are not shown in the figures, for instance, $\bar{\sigma}_x$ at C or D in Case I(*b*), are to be understood as identically zero.

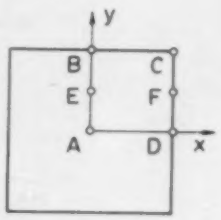

Fig. 2 Positions in the plate where stresses are calculated

From these figures, it will be seen that the stresses in the buckled plate are remarkably affected not only by the supporting

Table 2 Nonzero deflection coefficients in each case

Case	a_{mn}	b_{mn}			
I	a_{11}	b_{11},	b_{11},	b_{31},	b_{33}
II	a_{12}	b_{12}	b_{32},	b_{52}	b_{14}
III	a_{11}	b_{11},	b_{13},	b_{31},	b_{12}
IV	a_{11}	b_{11},	b_{13},	b_{31}	b_{22}

Table 3 Values of λ_{cr}, k_1, and k_2 in Equations (25)

	Case	I	II	III	IV
	λ_{cr}	0.375	0.724	0.632	0.956
Case (*a*)	k_1	0.253	0.149	0.281	0.191
	k_2	2.76	6.08	4.48	7.63
Case (*b*)	k_1	0.177	0.141	0.199	0.183
	k_2	3.05	6.14	5.00	7.71

[2] In Case II, it is to be noted that the plate buckles in two half-waves in the y-direction, which is antisymmetric about the x-axis.

Table 4 Comparison of ultimate loads obtained by various formulas with test results

Material		Duralumin V-groove plates			Brass Square tubes		
Test condition							
Width, a, in.		4.00	3.515	10.01	1.0	1.0	2.0
Thickness, h, in.		0.0893	0.0356	0.0322	0.0065	0.0056	0.0065
E, 10^7 psi		1.06	1.0	1.0	1.64	1.60	1.64
σ_{YP}, 10^4 psi		4.1	4.5	4.5	3.14	2.86	3.14
$\bar{\sigma}_{YP}$		0.786	4.44	44.1	4.59	5.77	18.4
P_u, lb	Test	7,300	1,175	1,270	290	210	340
	Timoshenko	10,200	2,700	6,375	391	300	726
	Karman	9,990	1,620	1,310	231	161	231
	Author	8,350	1,390	2,670	2[illegible]	193	438

Table 5 Values of σ_u/σ_{cr} calculated by various formulas

σ_{YP}/σ_{cr}		1	2	3	4	5	6	8	10
Formulas (28), with $\alpha = 0.78$, $n = 0.8$		1	1.358	1.878	2.364	2.827	3.271	4.117	4.922
Formulas (28), with $\alpha = 0.8$, $n = 0.58$		1	1.196	1.513	1.788	2.035	2.262	2.672	3.042
Formulas (29)	Case I(*a*)	1	1.253	1.506	1.759	2.012	2.265	2.771	3.277
	Case I(*b*)	1	1.177	1.354	1.531	1.708	1.885	2.239	2.593

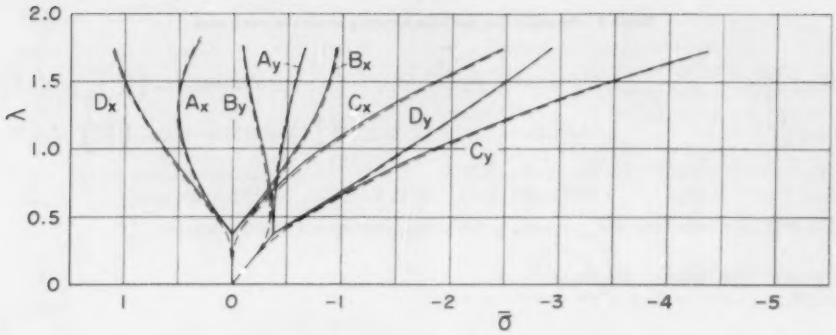

Fig. 3(a) Membrane stresses versus applied load for Case I(a)

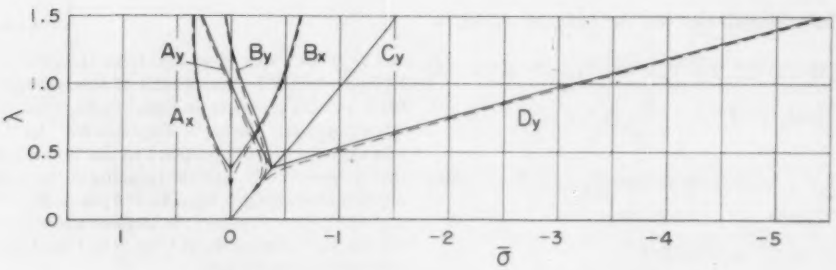

Fig. 3(b) Membrane stresses versus applied load for Case I(b)

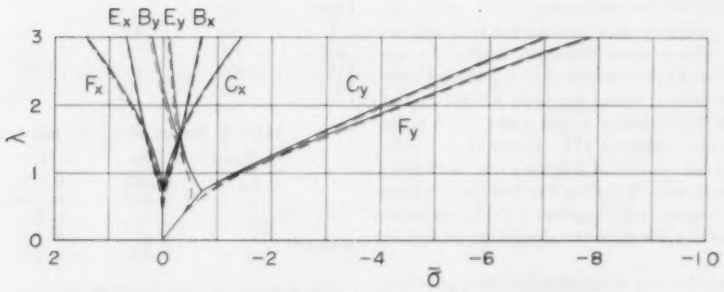

Fig. 3(c) Membrane stresses versus applied load for Case II(a)

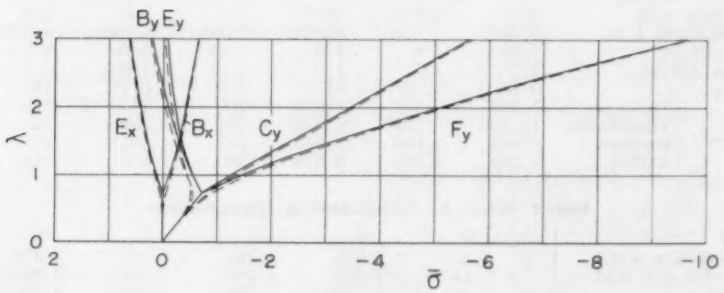

Fig. 3(d) Membrane stresses versus applied load for Case II(b)

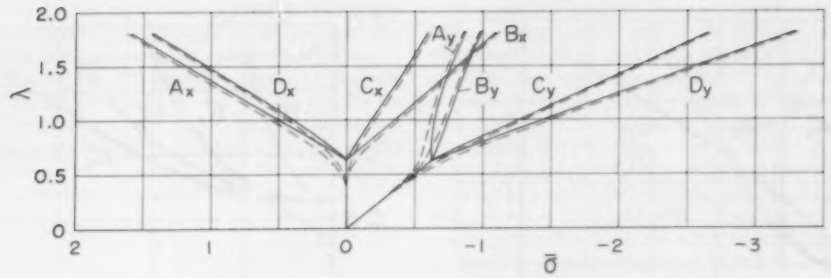

Fig. 3(e) Membrane stresses versus applied load for Case III(a)

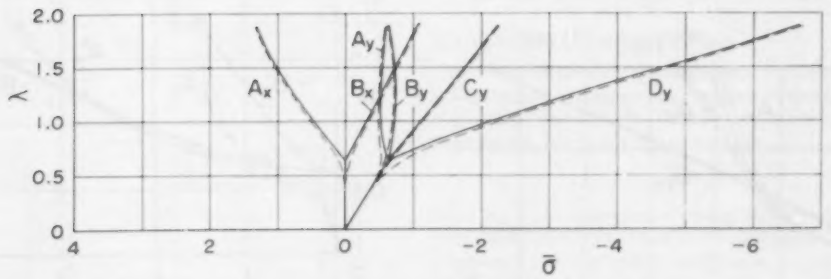

Fig. 3(f) Membrane stresses versus applied load for Case III(b)

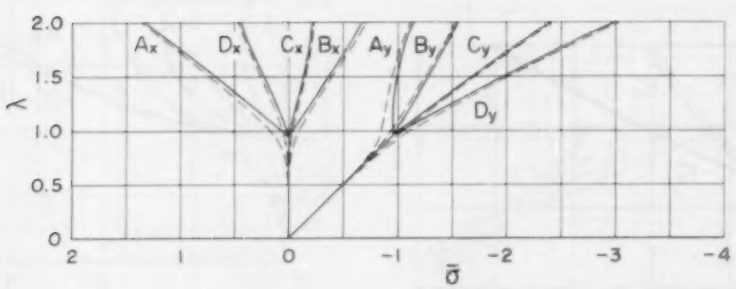

Fig. 3(g) Membrane stresses versus applied load for Case IV(a)

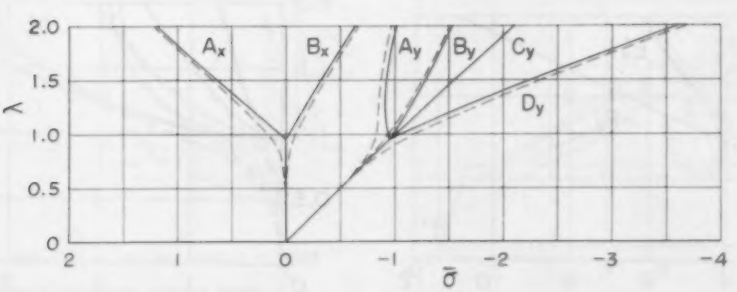

Fig. 3(h) Membrane stresses versus applied load for Case IV(b)

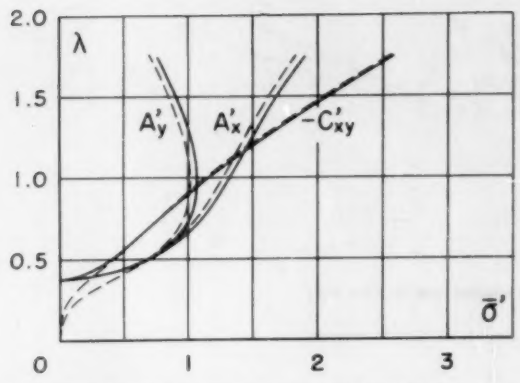

Fig. 4(a) Bending stresses versus applied load for Case I(a)

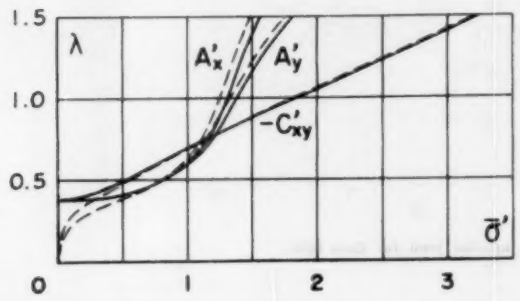

Fig. 4(b) Bending stresses versus applied load for Case I(b)

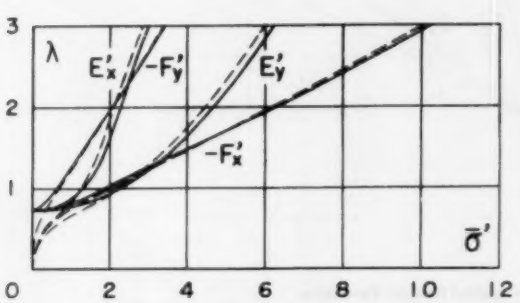

Fig. 4(c) Bending stresses versus applied load for Case II(a)

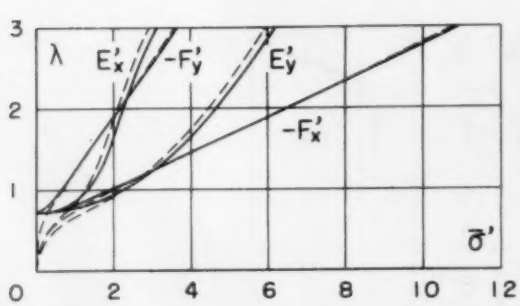

Fig. 4(d) Bending stresses versus applied load for Case II(b)

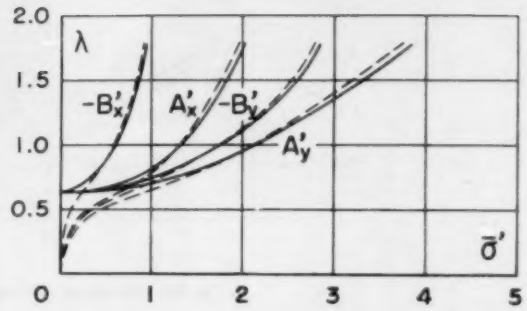

Fig. 4(e) Bending stresses versus applied load for Case III(a)

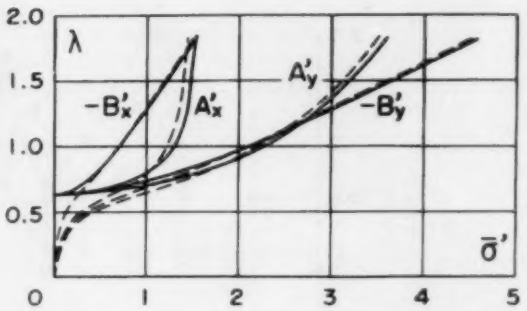

Fig. 4(f) Bending stresses versus applied load for Case III(b)

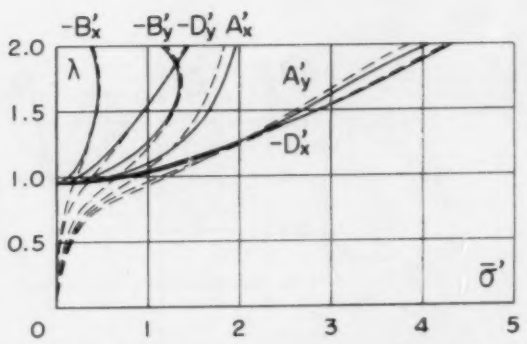

Fig. 4(g) Bending stresses versus applied load for Case IV(a)

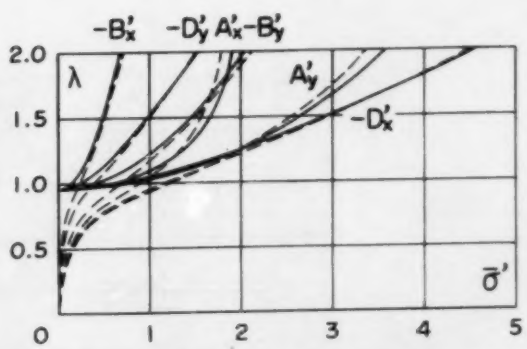

Fig. 4(h) Bending stresses versus applied load for Case IV(b)

conditions but also by the loading conditions along the side edges. On the contrary, the slight initial deflections considered here may be seen to have minor effects on the post-critical stress state.

For Case I(a), Levy [3] has calculated the stresses at the same points as here for the initially flat square plate, by taking the six nonzero deflection coefficients, i.e., b_{11}, b_{13}, b_{31}, b_{33}, b_{15}, and b_{51}, and by assuming the value of ν as 0.316. It is found that the results here obtained by taking $\nu = 1/3$, namely, Figs. 3(a) and 4(a), are in good agreement with those obtained by Levy.

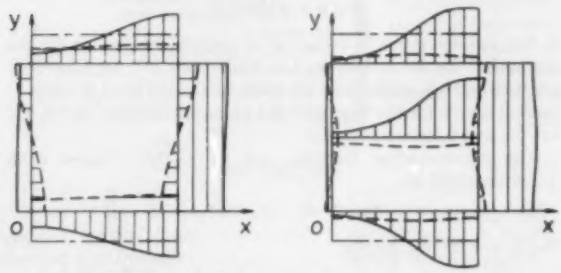

(a) Case I(a), $\lambda = 0.839$ (b) Case II(a), $\lambda = 1.646$

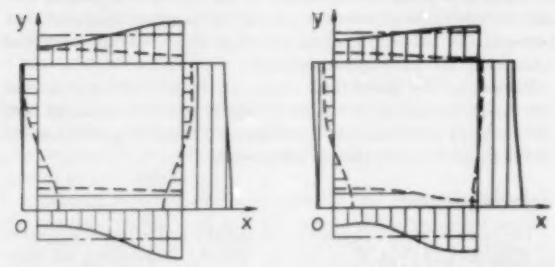

(c) Case III(a), $\lambda = 1.419$ (d) Case IV(a), $\lambda = 2.036$

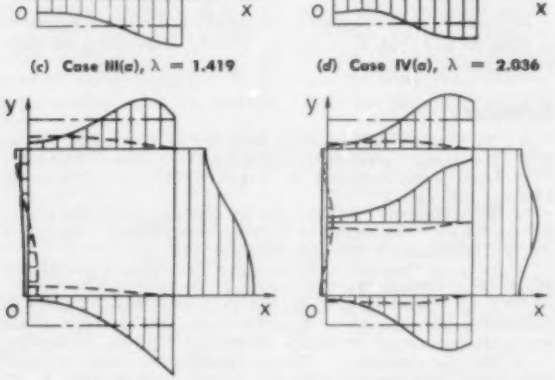

(e) Case I(b), $\lambda = 0.798$ (f) Case II(b), $\lambda = 1.637$

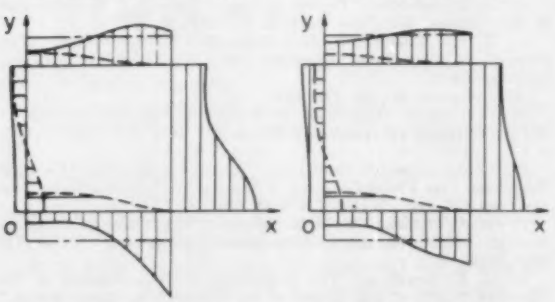

(g) Case III(b), $\lambda = 1.392$ (h) Case IV(b), $\lambda = 2.098$

Fig. 5 Distribution of membrane stresses along boundaries and symmetrical axes of square plates

Next, we will consider the stress distribution along the boundaries and symmetrical axes of the initially flat square plate, at some fixed loads several times the critical ones. Numerical results for the membrane stresses[4] in each case are presented graphically in Figs. 5(a–h). Owing to the symmetrical nature, only a quarter of the square plate is shown. In these figures, solid and dotted lines correspond to σ_y and σ_x,[5] respectively, and dashed lines represent the average compressive stress p_y. Further, positive and negative stresses are drawn inward and outward with respect to the square region, respectively. For Case II, the stress distribution along $y = b/4$ is added, since the plate buckles in two half-waves in this case. It will be noted that the stress distribution differs measurably according to the variation of the side edge conditions.

For Case I(b), Coan [4] has reported the load-strain relations and stress distributions of the square plate, with $\nu = 0.316$. The accuracy of his results seems to be somewhat insufficient, as only the three nonzero deflection coefficients were used.

Ultimate Load of the Square Plate

Here we will determine the ultimate load which can be carried by the initially flat square plate without yielding. As the criterion of yielding, we will use Tresca's condition or the maximum-shear theory, which can be expressed as

$$\tau_m = 1/2\,\sigma_{YP}, \tag{21}$$

where τ_m is the maximum shearing stress and σ_{YP} is the yield point stress in simple tension. Introducing the dimensionless quantities $\bar{\tau}_m = \tau_m a^2/\pi^2 Eh^2$ and $\delta_{YP} = \sigma_{YP}\, a^2/\pi^2 Eh^2$, the foregoing condition becomes

$$\bar{\tau}_m = 1/2\delta_{YP} \tag{22}$$

[4] Those for bending stresses are omitted to save space. It is comparatively easy to calculate them by using the values of b_{mn} together with Table 1 and Equations (19).

[5] Membrane shearing stress τ_{xy} always vanishes along these lines.

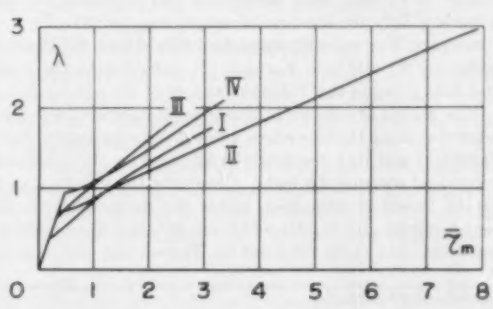

Fig. 6(a) Maximum shearing stresses versus applied load for Case (a)

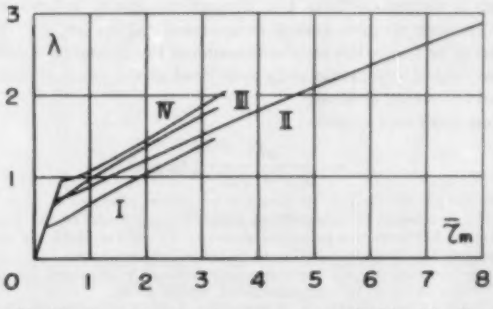

Fig. 6(b) Maximum shearing stresses versus applied load for Case (b)

Now, from the numerical results in the preceding section, the positions which give the maximum shearing stress[6] in the buckled square plate are found to be the point C in Case I, F in Case II, and D in other cases. Performing the calculations, we obtain the relations between λ and $\bar{\tau}_m$ as shown in Figs. 6(a) and (b). It will be noted that before the plate buckles, $\tau_m = 1/2p_y$ or $\bar{\tau}_m = 1/2\lambda$.

Making use of these figures, the ultimate load can be determined for any given material, dimensions, and boundary conditions of the square plate. That is, first calculate the value of $\bar{\sigma}_{YP}$ by the given data and find the value of λ at which $\bar{\tau}_m = 1/2\bar{\sigma}_{YP}$, on the curve corresponding to the given boundary conditions. Then the ultimate load P_u will be given by

$$P_u = \lambda \pi^2 E h^3/a \tag{23}$$

Next, we will derive the simple formulas for the ultimate loads in each case. For this purpose, we approximate the relations between λ and $\bar{\tau}_m$ as follows:

$$\left.\begin{aligned} 0 \leqq \bar{\sigma}_{YP} \leqq \lambda_{cr}&: \quad \bar{\tau}_m = 1/2\lambda \\ \lambda_{cr} \leqq \bar{\sigma}_{YP} \leqq \lambda_m&: \quad \bar{\tau}_m = c_1 + c_2\lambda \end{aligned}\right\} \tag{24}$$

λ_{cr} is the critical value of λ corresponding to the buckling load and λ_m is the upper bound of $\bar{\sigma}_{YP}$, within which these relations are considered to be valid. From Figs. 6(a) and (b) it will be seen that the value of λ_m can be taken as 20 in Case II and 10 in the other cases. c_1 and c_2 are constants. Then, recalling Condition (22), we obtain from Equations (24) the following formulas:

$$\begin{aligned} 0 \leqq \bar{\sigma}_{YP} \leqq \lambda_{cr}&: \quad P_u = \sigma_{YP} a h, \\ \lambda_{cr} \leqq \bar{\sigma}_{YP} \leqq \lambda_m&: \quad P_u = a h [k_1 \sigma_{YP} + k_2 E (h/a)^2], \end{aligned} \tag{25}$$

where $k_1 = 1/(2c_2)$ and $k_2 = -\pi^2 c_1/c_2$. Values of λ_{cr}, k_1, and k_2 in each case are listed in Table 3.

As is well known, the estimation of the ultimate load is of considerable importance for the design of airplane construction, and a number of studies, both theoretical and experimental, have been made chiefly for the case of simple support [5]. First, we will compare the present formulas with those obtained by Timoshenko [6] and von Karman [7], referring to the experimental data given in the Tables 48 and 49 of Timoshenko's book [8]. The results are shown in Table 4. Considering the degree of constraint along the side edges, present formulas corresponding to Cases I(b) and I(a), respectively, are used for the cases of the V-groove and square-tube tests. Observing the values of $\bar{\sigma}_{YP}$ in the table, it will be seen that, within the range of application, present formulas give results which are in better agreement with experiments than those obtained by Timoshenko and von Karman.

Timoshenko's formula

$$P_u = a h [0.434 \sigma_{YP} + 2.04 E (h/a)^2], \tag{26}$$

which is derived for Case I(a) through the similar procedure as here, is seen to give always exaggerated values for P_u. This seems to be due to the underestimation of the maximum shearing stress, which is approximately calculated at the point D making use of the energy method.[7]

Von Karman's formula

$$P_u = \frac{\pi h^2}{[3(1-\nu^2)]^{1/2}} (E\sigma_{YP})^{1/2} \tag{27}$$

is derived under a rough assumption on the postcritical stress state, but is known to give fairly good estimation.

Another comparison will be made with the formulas proposed by Gerard [9]. They can be expressed as

$$\begin{aligned} \sigma_{YP} < \alpha^{-1/n}\sigma_{cr}&: \quad \sigma_u = \sigma_{cr}, \\ \sigma_{YP} \geqq \alpha^{-1/n}\sigma_{cr}&: \quad (\sigma_u/\sigma_{cr}) = \alpha(\sigma_{YP}/\sigma_{cr})^n, \end{aligned} \tag{28}$$

where $\sigma_u (= P_u/ah)$ is the ultimate average stress and

$$\sigma_{cr} (= \lambda_{cr}\pi^2 E h^2/a^2)$$

is the critical stress. Values of α and n obtained from the theoretical results of Mayers and Budiansky [10] for Case I(a) are 0.78 and 0.8, while those obtained by Gerard from the experimental results for the V-groove and square-tube tests [11, 12, 13] are 0.8 and 0.58, respectively.

The corresponding formulas can be easily obtained from Equations (25) as

$$\begin{aligned} \sigma_{YP} \leqq \sigma_{cr}&: \quad \sigma_u = \sigma_{YP}, \\ \sigma_{cr} \leqq \sigma_{YP} \leqq (\lambda_m/\lambda_{cr})\sigma_{cr}&: \\ &(\sigma_u/\sigma_{cr}) = 1 - k_1 + k_1(\sigma_{YP}/\sigma_{cr}) \end{aligned} \tag{29}$$

In Table 5 is given a comparison of the values of σ_u/σ_{cr} as calculated by using each formula. It will be seen that the agreement between the present formula for Case I(a) and the empirical formula by Gerard is quite excellent.

Both from the theoretical nature of the derivation and from the discussions given in the foregoing, it will be recognized that the accuracy of the present formulas may be fairly good, in so far as the range of application is not exceeded.

Acknowledgment

The author wishes to express his thanks to Professor Emeritus S. Higuchi and Prof. F. Numachi, Tōhoku University, for their invaluable advice during the course of the present work.

References

1 N. Yamaki, "Postbuckling Behavior of Rectangular Plates With Small Initial Curvature Loaded in Edge Compression," JOURNAL OF APPLIED MECHANICS, vol. 26, TRANS. ASME, vol. 81, series E, 1959, pp. 407–414.

2 K. Marguerre, "Zur Theorie der gekrümmten Platte grosser Formänderung," Proceedings of the Fifth International Congress for Applied Mechanics, Cambridge, England, 1938, pp. 93–101.

3 S. Levy, "Bending of Rectangular Plates With Large Deflections," NACA Report No. 737, 1942, pp. 139–157.

4 J. M. Coan, "Large Deflection Theory for Plates With Small Initial Curvature Loaded in Edge Compression," JOURNAL OF APPLIED MECHANICS, vol. 18, TRANS. ASME, vol. 73, 1951, pp. 143–151.

5 See, for example, F. Bleich, "Buckling Strength of Metal Structures," McGraw-Hill Book Company, Inc., New York, N. Y., 1952, pp. 459–480.

6 S. Timoshenko, "Theory of Elastic Stability," McGraw-Hill Book Company, Inc., New York, N. Y., 1936, p. 390.

7 T. von Karman, E. E. Sechler, and L. H. Donnell, "The Strength of Thin Plates in Compression," TRANS. ASME, vol. 54, 1932, pp. 53–57.

8 Reference [6], pp. 397–398.

9 G. Gerard, "Handbook of Structural Stability, Part IV—Failure of Plates and Composite Elements," NACA TN 3784, 1957, p. 13.

10 J. Mayers and B. Budiansky, "Analysis of Behavior of Simply Supported Flat Plates Compressed Beyond the Buckling Load Into the Plastic Range," NACA TN 3368, 1955.

11 R. A. Anderson and M. S. Anderson, "Correlation of Crippling Strength of Plate Structures With Material Properties," NACA TN 3600, 1956.

12 J. F. Besseling, "The Experimental Determination of the Effective Width of Flat Plates in the Elastic and Plastic Range," Nationaal Luchtvaartlaboratorium, Rep. S. 414, 1953.

13 M. Botman, "The Experimental Determination of the Effective Width of Flat Plates in the Elastic and Plastic Range (Part II)," Nationaal Luchtvaartlaboratorium, Rep. S. 438, 1954.

[6] The maximum shearing stress is given by one half of the largest difference between two principal stresses. Of course, both the membrane and bending stresses should be taken into account.

[7] For comparison, the corresponding formula is obtained by using the values of $\bar{\tau}_m$ at D here calculated, which gives

$$P_u = a h [0.374 \sigma_{YP} + 2.32 E (h/a)^2]$$

D. H. CHENG
The City College of New York; Consultant, The M. W. Kellogg Company, New York, N. Y.

N. A. WEIL
Mechanics Research Division, Armour Research Foundation, Chicago, Ill.
Formerly: The M. W. Kellogg Company, New York, N. Y.
Mem. ASME

The Junction Problem of Solid-Slotted Cylindrical Shells

This paper presents a solution for the problem of three cylindrical shells, one of which is slotted lengthwise. With slot length as one of the parameters, the solution includes the solid three-shell problem as a particular case. The results are applicable to the stress problem of a closed-end vessel supported either by a slotted or an ordinary skirt, or one that is mounted on top of another vessel. It is shown that slotting substantially reduces the critical stress at the junction.

Introduction

One of the safest and most general methods of support for vertical closed-end pressure vessels (towers) is to set them on a comparatively short continuous cylindrical shell, commonly referred to as the skirt. In usual practice, the junction between the tower and the skirt is made by a continuous fillet weld.

Ordinarily, stresses at this junction are very high; if calculated by elastic theory, they are usually found to exceed 10^5 psi. While this may be of little consequence under steady-state conditions, the overwhelming portion of these stresses being of a bending character and therefore subject to relaxation, under cyclic conditions these stresses may rapidly induce fatigue failures, especially at service conditions associated with high pressures or temperatures [1].[1]

A detailed treatment [2] was recently presented, dealing with the analysis, design, and recommended fabrication practices for solid skirt supports. It was shown that the most effective method of reducing the critical junction stresses is achieved through a lowering of thermal gradients by means of rearranging the insulation about the junction. While this should be sufficient for most practical cases, under extremely severe operating conditions even these improvements may not suffice. It is then necessary to reduce stresses still further. This can be achieved most conveniently by means of slotting the skirt and thereby reducing its stiffness. This concept is gaining increasing acceptance in the process industry.

Examples of such a slotted-skirt construction are shown in Figs. 1 and 2. The slots are spaced evenly around the circumference and terminate in drilled holes (generally $^1/_2$ in. diam) in order to minimize stress concentrations at the change of section from slotted to solid construction. The slots are generally narrow in relation to their circumferential spacing; in a representative case, slots 16 in. long and $^3/_{16}$ in. wide would be cut on a 12-in. spacing around the circumference. The slots terminate about 1 in. short of the top of the skirt, as shown in Fig. 2, retaining a narrow intact band which allows for the deposition of a continuous skirt-attachment weld.

This paper considers the solution of the slotted-skirt-attachment problem. Since the slot length is retained as a parameter in the analysis, the general solution reduces to the particular case of the solid skirt [2], as the slot length is permitted to vanish.

Assumptions and Method of Analysis

The actual physical case of a tower supported on a slotted skirt represents a highly complex problem. It is necessary to make admissible simplifying assumptions in order to arrive at a reasonably tractable solution.

In the analysis presented here, the system is idealized as the axisymmetric problem of three cylindrical shells joined at a common junction. Shell 1, the skirt, is then replaced by a series of flat cantilevers, representing the slotted portion, which frame into

[1] Numbers in brackets designate References at end of paper.

For presentation at the Summer Conference of the Applied Mechanics Division, University Park, Pa., June 20–22, 1960, of The American Society of Mechanical Engineers.

Discussion of this paper should be addressed to the Secretary, ASME, 29 West 39th Street, New York, N. Y., and will be accepted until July 22, 1960, for publication at a later date. Discussion received after the closing date will be returned.

Note: Statements and opinions advanced in papers are to be understood as individual expressions of their authors and not those of the Society. Manuscript received by ASME Applied Mechanics Division, May 21, 1958. Paper No. 60—APM-2.

Nomenclature

a_i = mean radius of cylinder, in.
h_i = wall thickness, in.
E_i = modulus of elasticity, psi
ν = Poisson's ratio
M_i, Q_i = distributed internal moment (lb), and internal shear (lb/in.) at junction, respectively, positive as shown in Fig. 4
θ_i, w_i = rotation and deflection (in.) at junction, respectively, positive as shown in Fig. 4
e_1, e_2 = center-of-wall distances between cylinders 1 and 2, and 2 and 3, respectively, in.
d_1, d_2 = free-body deflection of cylinders 1 and 2 with respect to cylinder 3 at junction, in., positive as shown in Fig. 5
φ_1, φ_2 = free-body rotation of cylinder 1 related to cylinder 3, and cylinder 2 to 3, at junction, positive as shown in Fig. 5
M, Q, P = external distributed moment (lb), shear and thrust (lb/in.) applied at junction, positive as shown in Fig. 4
$I_i = h_i^3/12$
$\mu_1 = h_1/h_3$
$\mu_2 = h_2/h_3$
$D_i = E_iI_i/(1-\nu^2)$
$\beta_i = [3(1-\nu^2)]^{1/4}/(ah_i)^{1/2}$
$K_1 = \beta_1D_1/E_1I_1 = \beta_1/(1-\nu^2)$
i = subscripts to be replaced by 1, 2, 3 for reference to component cylinders

Subscripts l and c denote quantities acting in longitudinal and circumferential directions, respectively. Subscript x indicates quantities occurring at a distance x from junction. Auxiliary functions are as defined in text.

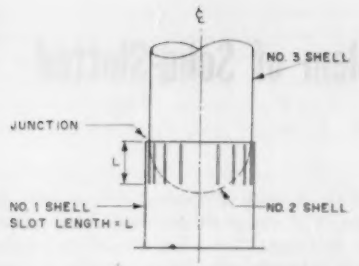

Fig. 1 Junction of three cylindrical shells, one slotted lengthwise

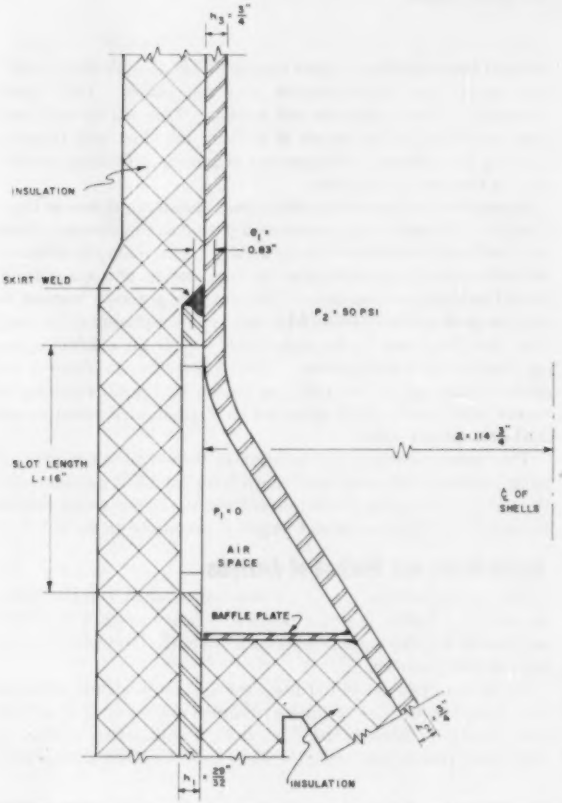

Fig. 2 Dimensional details for numerical example

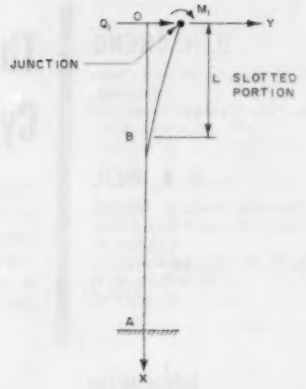

Fig. 3 A slotted skirt subjected to end moment and shear

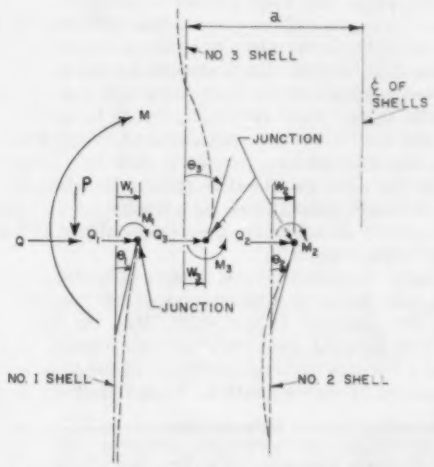

Fig. 4 Junction moments, shears, and associated displacements

a solid cylinder representing the intact bottom portion of the skirt. The effect of curvature on the stiffness of the cantilevers is neglected, since practical problems generally deal with large-diameter vessels (10 ft $< D <$ 50 ft). Also neglected is the reduction in circumference resulting from removal of material at the slots, this effect generally being small as mentioned before. If warranted, this condition could be readily considered, as explained later in the text.

The stiffening effect of the skirt-attachment weld and the narrow continuous band retained at the top of the skirt is ignored, the slots being assumed to penetrate to the junction. This is entirely admissible, since the rotational stiffness of a ring with the dimensions considered here is completely negligible as compared to that of the shells, so that the inclusion of this effect would merely serve to make the analysis far more intricate.

Apart from the necessity of determining the dilatational and rotational stiffness of the slotted skirt, presented in the Appendix, the analysis follows the familiar lines established in [2]. The free-body cylinder displacements are first determined from known conditions of internal pressure and thermal gradients [2, 4, 5]. Next, compatibility of the structure is restored by the application of suitable end-moment and shear distributions. The effect of local axisymmetric moments, shears, and thrusts at the junction, if any, are then superposed on the results to complete the solution.

Analysis for Differential Expansions and Rotations

Shell 1, with lengthwise slots, behaves as a series of cantilevers. The "fixed" ends of the cantilevers, however, must maintain continuity with the cylindrical shell at a distance L below the junction where the slots end, Fig. 3.

Fig. 4 shows the final displacements due to the application of moment and shear in each shell. Then, by Equation (25) of the Appendix, the radial and angular displacements at the end of Shell 1 may be related to the applied moment and shear as follows:

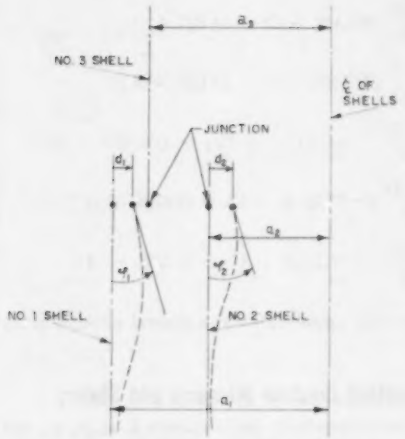

Fig. 5 Relative displacements at free end

$$w_1 - d_1 = \frac{1}{2\beta_1^3 D_1}\left[(1 + 2\beta_1 L + 2\beta_1^2 L^2 + {}^2/_3 K_1\beta_1^3 L^3)Q_1 + \beta_1(1 + 2\beta_1 L + K_1\beta_1 L^2)M_1\right] \tag{1}$$

$$\theta_1 + \varphi_1 = \frac{1}{2\beta_1^2 D_1}\left[(1 + 2\beta_1 L + K_1\beta_1 L^2)Q_1 + 2\beta_1(1 + K_1 L)M_1\right.$$

Similarly, for shells 2 and 3 [3]:

$$\left.\begin{aligned} w_2 - d_2 &= \frac{1}{2\beta_2^3 D_2}(Q_2 + \beta_2 M_2) \\ \theta_2 + \varphi_2 &= \frac{1}{2\beta_2^2 D_2}(Q_2 + 2\beta_2 M_2) \end{aligned}\right\} \tag{2}$$

$$\left.\begin{aligned} w_3 &= \frac{1}{2\beta_3^3 D_3}(Q_3 + \beta_3 M_3) \\ \theta_3 &= -\frac{1}{2\beta_3^2 D_3}(Q_3 + 2\beta_3 M_3) \end{aligned}\right\} \tag{3}$$

Continuity and equilibrium of forces at the junction require that:

$$\left.\begin{aligned} w_i &= w \\ \theta_i &= \theta \\ \sum_i Q_i &= 0 \end{aligned}\right\} \quad i = 1, 2, 3 \qquad M_1 + M_2 - M_3 = 0 \tag{4}$$

If the amount of material removed by the slots is substantial, the last two of Equations (4) should be replaced by

$$\left.\begin{aligned} \frac{nb}{2\pi a_1} Q_1 + Q_2 + Q_3 &= 0 \\ \frac{nb}{2\pi a_1} M_1 + M_2 - M_3 &= 0 \end{aligned}\right\} \tag{5}$$

where n is the number of flat plate elements between slots of width b. The results will be an intensification of moments, shears, and stresses in Shell 1 by a factor of $2\pi a_1/nb$.

The system represented by Equations (1, 2, 3, 4) can be reduced to eight equations in eight unknowns: w, θ, M_i, Q_i. The closed-form solution of these simultaneous equations yields:

$$\left.\begin{aligned}
w &= \frac{1}{K}\left[\beta_1^3 D_1\left(2Bt + A\frac{r}{\beta_1}\right)d_1 + \beta_2^3 D_2(2B\beta_2 + A)d_2 + \beta_1^3 D_1\left(Br + \frac{s}{\beta_1}\right)\varphi_1 + \beta_2 D_2(B\beta_2 + A)\varphi_2\right] \\
\theta &= -\frac{1}{K}\left[\beta_1^2 D_1\left(2At + C\frac{r}{\beta_1}\right)d_1 + \beta_2^2 D_2(2A\beta_2 + C)d_2 + \beta_1^2 D_1\left(Ar + C\frac{s}{\beta_1}\right)\varphi_1 + \beta_2 D_2(A\beta_2 + C)\varphi_2\right] \\
M_1 &= -\frac{2\beta_1 D_1}{K}\left\{\beta_1^2 D_1[2\beta_1 t(B\beta_1 r + As) + A\beta_1 r^2 + r(Cs - K/\beta_1 D_1)]d_1 + \beta_2^2 D_2[2\beta_2(B\beta_1 r + As) + A\beta_1 r + Cs]d_2 + \beta_1 D_1[\beta_1 r(B\beta_1 r + 2As) + s(Cs - K/\beta_1 D_1)]\varphi_1 + \beta_2 D_2[\beta_2(B\beta_1 r + As) + A\beta_1 r + Cs]\varphi_2\right\} \\
M_2 &= -\frac{2\beta_2 D_2}{K}\left\{\beta_1^2 D_1[2\beta_1 t(B\beta_2 + A) + r(A\beta_2 + C)]d_1 + \beta_2^2 D_2[\beta_2(2B\beta_2 + 3A) + C - K/\beta_2 D_2]d_2 + \beta_1 D_1[\beta_1 r(B\beta_2 + A) + s(A\beta_2 + C)]\varphi_1 + \beta_2 D_2[\beta_2(B\beta_2 + 2A) + C - K/\beta_2 D_2]\varphi_2\right\} \\
M_3 &= -\frac{2\beta_3 D_3}{K}\left\{\beta_1^2 D_1[\beta_3(2B\beta_1 t + Ar) - (2A\beta_1 t + Cr)]d_1 + \beta_2^2 D_2[\beta_2(2B\beta_2 + A) - (2A\beta_2 + C)]d_2 + \beta_1 D_1[\beta_3(B\beta_1 r + As) - (A\beta_1 r + Cs)]\varphi_1 + \beta_2 D_2[\beta_2(B\beta_2 + A) - (A\beta_2 + C)]\varphi_2\right\} \\
Q_1 &= \frac{2\beta_1^3 D}{K}\left\{\beta_1^2 D_1[4\beta_1 t(B\beta_1 t + Ar) + Cr^2 - 2Kt/\beta_1 D_1]d_1 + \beta_2^3 D_2[2\beta_2(2B\beta_1 t + Ar) + 2A\beta_1 t + Cr]d_2 + \beta_1 D_1[2\beta_1 t(B\beta_1 r + As) + A\beta_1 r^2 + r(Cs - K/\beta_1 D_1)]\varphi_1 + \beta_2 D_2[\beta_2(2B\beta_1 t + Ar) + 2A\beta_1 t + Cr]\varphi_2\right\} \\
Q_2 &= \frac{2\beta_2^3 D_2}{K}\left\{\beta_1^3 D_1[2\beta_1 t(2B\beta_2 + A) + r(2A\beta_2 + C)]d_1 + \beta_2^3 D_2[4\beta_2(B\beta_2 + A) + C - 2K/\beta_2 D_2]d_2 + \beta_1 D_1[\beta_1 r(2B\beta_2 + A) + s(2A\beta_2 + C)]\varphi_1 + \beta_2 D_2[\beta_2(2B\beta_2 + 3A) + C - K/\beta_2 D_2]\varphi_2\right\} \\
Q_3 &= \frac{2\beta_3^3 D_3}{K}\left\{\beta_1^3 D_1[2\beta_3(2B\beta_1 t + Ar) - (2A\beta_1 t + Cr)]d_1 + \beta_2^3 D_2[2\beta_3(2B\beta_2 + A) - (2A\beta_2 + C)]d_2 + \beta_1 D_1[2\beta_3(B\beta_1 r + As) - (A\beta_1 r + Cs)]\varphi_1 + \beta_2 D_2[2\beta_3(B\beta_2 + A) - (A\beta_2 + C)i\varphi_2\right\}
\end{aligned}\right\} \tag{6}$$

where

$$
\left.\begin{aligned}
A &= -(\beta_1^3 D_1 r + \beta_2^3 D_2 - \beta_3^3 D_3)\\
B &= (\beta_1 D_1 s + \beta_2 D_2 + \beta_3 D_3)\\
C &= 2(\beta_1^3 D_1 t + \beta_2^3 D_2 + \beta_3^3 D_3)\\
K &= BC - A^2
\end{aligned}\right\} \tag{7}
$$

and

$$
\left.\begin{aligned}
r &= \frac{1 + 2\beta_1 L + \beta_1 K_1 L^2}{1 + 2K_1 L + 2K_1\beta_1 L^2 + (4\,K_1\beta_1^2 L^3/3) + (K_1^2\beta_1^2 L^4/3)}\\
s &= \frac{1 + 2\beta_1 L + 2\beta_1^2 L^2 + (2\,K_1\beta_1^2 L^4/3)}{1 + 2K_1 L + 2K_1\beta_1 L^2 + (4\,K_1\beta_1^2 L^3/3) + (K_1^2\beta_1^2 L^4/3)}\\
t &= \frac{1 + K_1 L}{1 + 2K_1 L + 2K_1\beta_1 L^2 + (4\,K_1\beta_1^2 L^3/3) + (K_1^2\beta_1^2 L^4/3)}
\end{aligned}\right\} \tag{8}
$$

It should be noted that Equations (6, 7, 8) are perfectly general as long as only cylindrical shells are considered; they permit the treatment of component shells of different mean radii made of different materials. Also, when Shell 1 is not slotted, $L = 0$, $r = s = t = 1$, and the solution reduces to the solid-cylinder intersection problem [2].

In most practical cases Shell 2, the bottom head, will not be a cylinder; rather, it will be hemispherical, torispherical, conical, or toriconical in shape. Nonetheless, the results obtained here for cylindrical shells are still expected to hold with good accuracy, as explained in detail for the solid-skirt problem [2]. If Shell 1, the skirt, is conical rather than cylindrical, the "equivalent-cylinder" approach, with suitable corrections for shear, affords a satisfactory approximation [2].

Analysis for External Moments and Shears Applied to Junction

Since the center lines of Shells 1, 2, and 3 are at slightly different radial distances, the internal pressure, weight, and wind loads may give rise to distributed moments which can be considered as external moments applied to the junction. Distributed shear will be introduced, in turn, if any of the shells deviates from the cylindrical shape. These local forces will be represented by axisymmetric moment and shear distributions—the wind-induced effects are taken as constants with values equal to those of their maximum intensity. Then, from the condition of continuity and equilibrium of forces:

$$
\left.\begin{aligned}
w_i &= w\\
\theta_i &= \theta\\
\sum_i Q_i &= Q
\end{aligned}\right\} \; i = 1, 2, 3 \tag{9}
$$

$$
M_1 + M_2 - M_3 = M
$$

Displacements, moments, and shears are obtained by solving the familiar set of simultaneous equations:

$$
\left.\begin{aligned}
w &= \frac{1}{2K}(BQ - AM)\\
\theta &= \frac{1}{2K}(CM - AQ)\\
M_1 &= \frac{\beta_1 D_1}{K}\,[M(A\beta_1 r + Cs) - Q(B\beta_1 r + As)]\\
M_2 &= \frac{\beta_2 D_2}{K}\,[M(A\beta_2 + C) - Q(B\beta_2 + A)]\\
M_3 &= \frac{\beta_3 D_3}{K}\,[M(A\beta_3 - C) - Q(B\beta_3 - A)]\\
Q_1 &= \frac{\beta_1^3 D_1}{K}\,[-M(2A\beta_1 t + Cr) + Q(2B\beta_1 t + Ar)]\\
Q_2 &= \frac{\beta_2^3 D_2}{K}\,[-M(2A\beta_2 + C) + Q(2B\beta_2 + A)]\\
Q_3 &= \frac{\beta_3^3 D_3}{K}\,[-M(2A\beta_3 - C) + Q(2B\beta_3 - A)]
\end{aligned}\right\} \tag{10}
$$

Equations (10) again represent a general solution for cylindrical shells.

The Resultant Junction Moments and Shears

With known free-body displacements d_1, d_2, φ_1, φ_2, and external forces M and Q, the solution for the junction moments and shears can be simply obtained by superposing the results of Equations (6) and (10).

Considerable simplifications can be achieved in the treatment of the problem if all three shells are cylindrical with identical junction radii and moduli of elasticity. For this case $E_i = E$, $a_i = a$, $i = 1, 2, 3$, with

$$
\left.\begin{aligned}
\frac{\beta_1 D_1}{\beta_2 D_2} &= \mu_1^{5/3}, \qquad \frac{\beta_2 D_2}{\beta_3 D_3} = \mu_2^{5/3}\\
\frac{\beta_1}{\beta_3} &= \mu_1^{-1/3}, \qquad \frac{\beta_2}{\beta_3} = \mu_2^{-1/3}\\
\frac{\beta_2}{\beta_1} &= \left(\frac{\mu_1}{\mu_2}\right)^{1/3}
\end{aligned}\right\} \tag{11}
$$

The resulting expressions are, after simplification:

$$
\left.\begin{aligned}
w &= r_{12}d_1 + r_{22}d_2 + \frac{1}{\beta_1}r_{11}\varphi_1 + \frac{1}{\beta_2}r_{21}\varphi_2\\
&\quad + \frac{1}{2\beta_2^2 D_2}\,[(r_{22} - r_{21})Q - \beta_2(p_{22} - p_{21})M]\\
\theta &= -(\beta_1 p_{12}d_1 + \beta_2 p_{22}d_2 + p_{11}\varphi_1 + p_{21}\varphi_2)\\
&\quad + \frac{1}{2\beta_2^2 D_2}\,[(r_{22} - 2r_{21})Q - \beta_2(p_{22} - 2p_{21})M]\\
M_1 &= 2\beta_1 D_1[\beta_1(k_{11}d_1 - k_{12}d_2) + l_{11}\varphi_1 - l_{12}\varphi_2]\\
&\quad - \frac{1}{\beta_1}r_{11}Q + p_{11}M\\
M_2 &= 2\beta_2 D_2[\beta_2(k_{21}d_1 - k_{22}d_2) + (\mu_1/\mu_2)^{5/3}l_{12}\varphi_1 - l_{22}\varphi_2]\\
&\quad - \frac{1}{\beta_2}r_{21}Q + p_{21}M\\
M_3 &= M_1 + M_2 - M\\
Q_1 &= -2\beta_1^3 D_1[\beta_1(m_{12}d_1 - m_{12}d_2) + k_{11}\varphi_1\\
&\quad - (\mu_2/\mu_1)^2 k_{21}\varphi_2] + r_{12}Q - \beta_1 p_{12}M\\
Q_2 &= 2\beta_2^3 D_2\{\beta_2[(\mu_1/\mu_2)^{5/3}m_{12}d_1 - m_{22}d_2]\\
&\quad + (\mu_1/\mu_2)^2 k_{12}\varphi_1 - k_{22}\varphi_2\} + r_{22}Q - \beta_2 p_{22}M\\
Q_3 &= Q - Q_1 - Q_2
\end{aligned}\right\} \tag{12}
$$

where,

$$
\left.
\begin{aligned}
k_{11} &= \frac{1}{q}\,[\mu_1{}^2(\mu_2{}^2-1)(2st-r^2) \\
&\quad +(\mu_2{}^2+1)^2r+2\mu_2{}^{2/3}(\mu_2+1)r] \\
k_{12} &= \frac{\mu_2{}^2}{q}\,[\mu_1{}^2(2st-r^2)+(\mu_2{}^2-1)r \\
&\quad +2(\mu_1{}^{1/3}s+r)(\mu_2{}^{-1/3}+1)] \\
k_{21} &= \frac{\mu_1{}^2}{q}\,[\mu_1{}^2(2st-r^2)+(\mu_2{}^2-1)r \\
&\quad +2(\mu_2{}^{1/3}+1)(\mu_1{}^{-1/3}t+r)] \\
k_{22} &= \frac{1}{q}\,[\mu_2{}^2(\mu_1{}^2r-1)+\mu_1{}^4(2st-r^2) \\
&\quad +2\mu_1{}^2r+1+2\mu_1{}^{2/3}(\mu_1s+t)] \\
l_{11} &= \frac{1}{q}\,[\mu_1{}^{2/3}(\mu_2{}^{2/3}+1)(2st-r^2)+(\mu_2{}^2+1)^2s \\
&\quad +2\mu_2{}^{2/3}(\mu_2+1)s] \\
l_{12} &= \frac{\mu_2{}^{2/3}}{q}\,[\mu_1{}^{2/3}(2st-r^2)+(\mu_2{}^{2/3}+1)s \\
&\quad +(\mu_1{}^{-1/3}r+s)(\mu_2{}^{-1/3}-1)] \\
l_{22} &= \frac{1}{q}\,[\mu_2{}^{2/3}(\mu_1{}^{2/3}s+1)+\mu_1{}^4(2st-r^2) \\
&\quad +2\mu_1{}^2r+1+2\mu_1{}^{2/3}(\mu_1s+t)] \\
m_{11} &= \frac{2}{q}\,[\mu_1{}^{2/3}(\mu_2{}^{2/3}+1)(2st-r^2)+(\mu_2{}^2+1)^2t \\
&\quad +2\mu_2{}^{2/3}(\mu_2+1)t] \\
m_{12} &= \frac{2\mu_2{}^{2/3}}{q}\,[\mu_1{}^{2/3}(2st-r^2)+(\mu_2{}^{2/3}+1)t \\
&\quad +(\mu_1{}^{1/3}r+t)(\mu_2{}^{1/3}+1)] \\
m_{22} &= \frac{2}{q}\,[\mu_2{}^{2/3}(\mu_1{}^{2/3}t+1)+\mu_1{}^4(2st-r^2) \\
&\quad +2\mu_1{}^2r+1+2\mu_1{}^{2/3}(\mu_1s+t)] \\
p_{11} &= \frac{\mu_1{}^2}{q}\,[\mu_1{}^2(2st-r^2)-(\mu_2{}^2-1)r+2\mu_1{}^{1/3}(\mu_2{}^{2/3} \\
&\quad +1)s] \\
p_{12} &= \frac{2\mu_1{}^2}{q}\,[\mu_1{}^{1/3}(\mu_2{}^{2/3}+1)r-(\mu_2{}^2-1)t] \\
p_{21} &= \frac{\mu_2{}^2}{q}\,[2\mu_2{}^{1/3}(\mu_2{}^{2/3}+\mu_1{}^{2/3}t+1)-\mu_2{}^2-\mu_1{}^2r+1] \\
p_{22} &= \frac{2\mu_2{}^2}{q}\,[\mu_2{}^{1/3}(\mu_1{}^{2/3}t+1)-\mu_1{}^2r+1] \\
r_{11} &= \frac{\mu_1{}^{2/3}}{q}\,[(\mu_2{}^{2/3}+1)r-\mu_1{}^{1/3}(\mu_2{}^2-1)s] \\
r_{12} &= \frac{\mu_1{}^{2/3}}{q}\,[\mu_1{}^{2/3}(2st-r^2)+2(\mu_2{}^{2/3}+1)t-\mu_1{}^{1/3}(\mu_2{}^2 \\
&\quad -1)r] \\
r_{21} &= \frac{\mu_2{}^{2/3}}{q}\,[\mu_1{}^{2/3}s-\mu_2{}^{1/3}(\mu_1{}^2r-1)+1] \\
r_{22} &= \frac{\mu_2{}^{2/3}}{q}\,[\mu_2{}^{1/3}(\mu_2{}^2-\mu_1{}^2r+1)+2(\mu_1{}^{2/3}s+1)] \\
q &= 2(\mu_2{}^{2/3}+\mu_1{}^{2/3}s+1)(\mu_2{}^{2/3}+\mu_1{}^{2/3}t+1) \\
&\quad -(\mu_2{}^2+\mu_1{}^2r-1)^2
\end{aligned}
\right\} \qquad (13)
$$

In problems of a recurring nature, the functions of Equations (13) may be arranged conveniently in chart-form solutions.

Stresses at and Away From the Junction

Unslotted Shells. When the displacement, moment, and shear at the end of each shell are determined, the longitudinal and circumferential stresses at any point along the shell can be evaluated by the expressions:

$$
\left.
\begin{aligned}
\sigma_{lx} &= \mp\frac{6}{h_i{}^2}\left(\varphi M_i+\frac{\zeta}{\beta_i}\,Q_i\right) \\
\sigma_{cx} &= \nu\sigma_{lx}-\frac{[12(1-\nu^2)]^{1/2}}{h_i{}^2}\left(\psi M_i+\frac{\xi}{\beta_i}\,Q_i\right)
\end{aligned}
\right\} \qquad (14)
$$

where

$$
\left.
\begin{aligned}
\varphi &= e^{-\beta_i x}(\cos\beta_i x+\sin\beta_i x) \\
\psi &= e^{-\beta_i x}(\cos\beta_i x-\sin\beta_i x) \\
\zeta &= e^{-\beta_i x}\sin\beta_i x \\
\xi &= e^{-\beta_i x}\cos\beta_i x \\
i &= 1,\ 2,\ 3
\end{aligned}
\right\} \qquad (15)
$$

Membrane stresses resulting from internal pressure are additive to those given in Equations (14). According to the functions of Equations (15) the stresses die out in an exponential fashion; hence the stresses must be localized near the end of shell. A tensile stress is designated as positive and the upper signs refer to internal surfaces in Equations (14).

The stresses at the junction ($x = 0$), which normally are maximum for unslotted cylindrical shells, can be deduced from Equations (14). Assuming Poisson's ratio ν to be 0.3, one gets:

$$
\left.
\begin{aligned}
\sigma_{li} &= \mp\frac{6M_i}{h_i{}^2}+\frac{a\Delta p}{2h_i} \\
\sigma_{ci} &= (0.3\pm 0.551)\sigma_{li}-\frac{3.305}{\beta_i h_i{}^2}\,Q_i+(1.7\mp 0.551)\,\frac{a\Delta p}{2h_i} \\
& \qquad i = 1,\ 2,\ 3
\end{aligned}
\right\} \qquad (16)
$$

where Δp denotes pressure differential, assumed positive if the pressure inside is larger than outside of the shell.

It should be pointed out that the stress created by the vessel load P is considered negligible in comparison with that induced by the internal pressure. If Shell 1 is a skirt, the vessel load induces a compressive stress uniformly distributed around the circumference, whereas the pressure difference vanishes, so that the stresses in the solid skirt can be described as follows:

$$
\left.
\begin{aligned}
\sigma_{l1} &= \mp\frac{6M_1}{h_1{}^2}-\frac{P}{h_1} \\
\sigma_{c1} &= (0.3\pm 0.551)\left(\sigma_{l1}+\frac{P}{h_1}\right)-\frac{3.305}{\beta_1 h_1{}^2}\,Q_1
\end{aligned}
\right\} \qquad (17)
$$

The Slotted Skirt. The stress condition in the slotted portion of the skirt is uniaxial. At the junction, the stresses take the following form:

$$
\left.
\begin{aligned}
\sigma_{l1} &= \mp\frac{6M_1}{h_1{}^2}-\frac{P}{h_1} \\
\sigma_{c1} &= 0
\end{aligned}
\right\} \qquad (18)
$$

Numerical Example

The skirt support selected to illustrate the treatment of the problem is shown in Fig. 2. The applicable numerical values are as follows:

Dimensional Data

$a = 114.75$ in.,	$e_1 = 0.83$ in.,	$h_1 = 0.9063$ in.
$E = 25.5 \times 10^6$ psi,	$e_2 = 0$,	$h_2 = h_3 = 0.75$ in.

Table 1 Values of junction forces

Component	Moments, in-lb/in.			Shears, lb/in.		
	Solid skirt	Slotted skirt	Per cent reduction	Solid skirt	Slotted skirt	Per cent reduction
Shell 1 (skirt)	4063	3060	24.7	−647	−214	66.9
Shell 2.....	−3405	−2130	37.4	496	212	57.3
Shell 3.....	−752	−480	36.2	151	2	98.7

Table 2 Comparison of junction stresses, psi

Component	Surface	Longitudinal			Circumferential		
		Solid skirt	Slotted skirt	Per cent reduction	Solid skirt	Slotted skirt	Per cent[a] reduction
Shell 1 (skirt)	Inner	−31560	−24280	23.1	−4560	0	100.0
	Outer	27800	20520	26.2	13250	0	100.0
Shell 2.....	Inner	40125	25525	36.4	17575	17195	2.2
	Outer	−32475	−18875	41.9	−4260	4350	(2.1)
Shell 3.....	Inner	11825	8940	24.4	8110	11910	(46.9)
	Outer	−4175	−1290	69.1	3275	8850	(170.2)

[a] Numbers in parentheses designate per cent increases.

Loading Parameters

$\varphi_1 = 0.558 \times 10^{-2}$; $M = 1410$ in-lb/in.,

$\varphi_2 = 1.325 \times 10^{-2}$; $Q = 0$,

$d_1 = 2.926 \times 10^{-2}$ in.; $P = 1700$ lb/in.

$d_2 = -0.585 \times 10^{-2}$ in.; $p_1 = 0$

$p_2 = 50$ psi

This numerical example, representing the skirt-support problem of an actual refinery vessel, already incorporates the improvements obtainable from a redistribution of insulation around the crotch [2]. The problem was to determine the added advantages to be gained from a slotting of the skirt. Comparative results for the cases of a solid skirt ($L = 0$) and a slotted skirt ($L = 16$ in.) are presented in Table 1 for the junction forces and in Table 2 for the junction stresses.

The numerical example points up the pronounced benefits obtained by slotting the skirt. Not only are the junction forces and stresses substantially reduced by the added flexibility imparted to the skirt through slotting, but the reduction is greatest in the highest stressed elements, notably the skirt and Shell 2 (the bottom portion of the vessel). Comparable reductions were obtained in a number of other cases analyzed by the authors.

Conclusions

The practical stress problem of three shells, one of which is slotted, is solved in this paper in general form. The solution given, though explicit, is rather tedious. However, with high-speed digital computers, the auxiliary functions that are prerequisite to the solution can be expediently tabulated numerically for design applications. With tables so constructed, the relative merits of different designs can be studied with ease.

A numerical example is presented, dealing with a vertical refinery vessel in cyclic service and examining both alternatives of a solid and slotted-skirt support. The merits of slotting the skirt for greater flexibility and lower junction stresses are well brought out by this example. For average conditions, a minimum slot length with a $\beta_1 L$ value of 2.0 is suggested for an effective reduction of junction stresses.

Design criteria and recommended fabrication practices for skirt supports on towers subject to high pressure and temperature as well as cyclic service have been discussed in another paper [2].

References

1 N. A. Weil and F. S. Rapasky, "Experiences With Vessels of Delayed Coking Units," *Proceedings*, American Petroleum Institute, vol. 38, section 3, Refining, 1958, pp. 214–232.

2 N. A. Weil and J. J. Murphy, "Design and Analysis of Welded Pressure Vessel Skirt Supports," *Journal of Engineering for Industry*—Trans. ASME, vol. 82, series B, 1960, pp. 1–14.

3 S. Timoshenko, "Theory of Plates and Shells," McGraw-Hill Book Company, Inc., New York, N. Y., 1940, p. 393.

4 W. E. Cooper, M. T. Roche, and J. L. Noble, "Stresses in a Semi-Infinite Thin-Walled Cylinder Caused by an Exponential Temperature Distribution," KAPL Report No. 973, March, 1955.

5 N. A. Weil and D. H. Cheng, "Steady-State Thermal Stresses in Thin Cylinders," to be published.

APPENDIX

Slotted Skirts Subjected to End Moments and Shears

Owing to slotting, the continuity of the cylindrical skirt in the hoop direction is destroyed. If a uniformly distributed moment or shear is applied at the end of the slotted skirt, the slotted portion will behave like a series of cantilever beams with their far ends framed into a continuous cylindrical shell. The cantilever also has a mild curvature, but this will be neglected in the subsequent analysis for sake of simplicity.

As the slotted portion must maintain continuity with the adjoining cylindrical shell, certain moments and shears are generated in the shell. It can be shown that stresses and deflection so induced are local in nature. Hence, for practical purposes, the problem can be treated as a cantilever of finite length framed into a cylindrical shell of infinite length assuming, of course, the unslotted portion is not too short.

The differential equation governing the curvature and the bending moment takes the following form:

$$E_1 I_1 \frac{d^2y}{dx^2} = M_1 + Q_1 x \qquad \text{where} \qquad 0 \leq x \leq L \tag{19}$$

Equation (19) can be integrated to get

$$E_1 I_1 \frac{dy}{dx} = M_1 x + Q_1 \frac{x^2}{2} + C_1 \tag{20}$$

$$E_1 I_1 y = M_1 \frac{x^2}{2} + Q_1 \frac{x^3}{6} + C_1 x + C_2 \tag{21}$$

At $x = L$, the slotted skirt and the shell have a common tangent, therefore [3]:

$$\frac{1}{2\beta_1^2 D_1}(2\beta_1 M_B + Q_B) = \frac{-1}{E_1 I_1}\left(M_1 L + Q_1 \frac{L^2}{2} + C_1\right)$$

But

$$M_B = M_1 + Q_1 L$$

$$Q_B = Q_1$$

Hence

$$C_1 = \frac{-E_1I_1}{2\beta_1^2D_1}\left[(2\beta_1L + 1)Q + 2\beta_1M_1\right] - M_1L - Q_1\frac{L^2}{2}$$

Equation (20) then becomes

$$-E_1I_1\frac{dy}{dx} = \frac{E_1I_1}{2\beta_1^2D_1}\left[(2\beta_1L + 1)Q_1 + 2\beta_1M_1\right] + M_1(L - x) - \frac{Q_1}{2}(L^2 - x^2)$$

or, denoting

$$K_1 = \frac{\beta_1D_1}{E_1I_1} = \frac{\beta_1}{(1 - \nu^2)},$$

$$\frac{dy}{dx} = -\frac{1}{2\beta_1^2D_1}\left[(2\beta_1L + 1)Q_1 + 2\beta_1M_1\right] - \frac{K_1(L - x)}{\beta_1D_1}\left[M_1 + \frac{Q_1}{2}(L + x)\right] \quad (22)$$

Also, at $x = L$, the slotted skirt and the shell should deflect the same amount, so that

$$\frac{1}{2\beta_1^2D_1}\left[(\beta_1L + 1)Q_1 + \beta_1M_1\right] = \frac{1}{E_1I_1}\left[M_1\frac{L^2}{2} + Q_1\frac{L^3}{6} + C_1L + C_2\right]$$

or

$$C_2 = \frac{E_1I_1}{2\beta^2D_1}\left[(2\beta_1^2L^2 + 2\beta_1L + 1)Q_1 + \beta_1(2\beta_1L + 1)M_1\right] + M_1\frac{L^2}{2} + Q_1\frac{L^3}{3}$$

Substituting the constants back into Equation (21),

$$E_1I_1y = M_1\frac{x^2}{2} + Q_1\frac{x^3}{6} - \frac{E_1I_1}{2\beta_1^2D_1}\left[(2\beta_1L + 1)Q_1 + 2\beta_1M_1\right]x - M_1Lx - Q_1\frac{L^2}{2}x + \frac{E_1I_1}{2\beta_1^2D_1}\left[(2\beta_1^2L^2 + 2\beta_1L + 1)Q_1 + \beta_1(2\beta_1L + 1)M_1\right] + M_1\frac{L^2}{2} + Q_1\frac{L^3}{3}$$

After simplification, the equation of the elastic curve becomes

$$y = \frac{-1}{2\beta_1^2D_1}\left\{\left[(2\beta_1^2L(x - L) + \beta_1(x - 2L) - 1\right]Q_1 - \beta_1\left[2\beta_1(L - x) + 1\right]M_1\right\} + \frac{K_1}{\beta_1D_1}\left\{\left[x^2 - 3L^2x + 2L^2\right]\frac{Q_1}{6} + (L - x)^2\frac{M_1}{2}\right\} \quad (23)$$

If $x = L$, Equation (23) reduces to

$$y = \frac{1}{2\beta_1^2D_1}\left[(\beta_1L + 1)Q_1 + \beta M_1\right] \quad (24)$$

It may be observed that when L and x are set equal to zero, the results reduce to the case of a solid skirt.

For the slotted skirt with a moment and shear applied at the end, the angular and the radial displacements at the free end may be evaluated by setting $x = 0$ in Equations (22) and (23)

$$\frac{dy}{dx} = -\frac{1}{2\beta_1^2D_1}\left[(2\beta_1L + 1)Q_1 + 2\beta_1M_1\right] - \frac{K_1L}{\beta_1D_1}\left(M_1 + \frac{Q_1}{2}L\right)$$

$$y = \frac{1}{2\beta_1^2D_1}\left[(2\beta_1^2L^2 + 2\beta_1L + 1)Q_1 + \beta_1(2\beta_1L + 1)M_1\right] + \frac{K_1L^2}{6\beta_1D_1}(2Q_1L + 3M_1) \quad (25)$$

Journal of APPLIED MECHANICS

Brief Notes

On the recommendation of the Executive Committee of the ASME Applied Mechanics Division, it was decided to initiate a section devoted to brief notes on technical matters in mechanics. These notes must not be longer than 750 words (about 2½ double-spaced typewritten pages, including figures) and will be subject to the usual review procedure prior to publication. After approval such notes will be published as soon as possible, normally in the next issue of the Journal. The notes should be submitted to the Technical Editors of the Journal of Applied Mechanics.

A Method of Numerical Evaluation of a Large Determinant

F. R. E. CROSSLEY[1] and ÜSTÜN GERMEN[2]

When solving problems in the vibration of a close-coupled system, there arises the need to expand a tridiagonal determinant of the type of equation (1). A very quick and accurate means of accomplishing this expansion is provided by the following numerical procedure, which can readily be adapted to computer programming.

IN FINDING the natural frequencies of torsional oscillation of a multicylinder engine, or the eigenvalues in an electric ladder network, one encounters a determinant which has the form:

$$\Delta \equiv \begin{vmatrix} (\alpha_1 + \beta_1 - \omega^2) & -\beta_1 & 0 & 0 & 0 \\ -\alpha_2 & (\alpha_2 + \beta_2 - \omega^2) & -\beta_2 & 0 & 0 \\ 0 & -\alpha_3 & (\alpha_3 + \beta_3 - \omega^2) & -\beta_3 & 0 \\ 0 & 0 & -\alpha_4 & (\alpha_4 + \beta_4 - \omega^2) & -\beta_4 \\ 0 & 0 & 0 & -\alpha_5 & (\alpha_5 + \beta_5 - \omega^2) \end{vmatrix} \quad (1)$$

In this, all terms α and β are presumed to be known, while ω is unknown. The determinant is typical of a class and, if it is of an order higher than the third, it becomes rather laborious to expand it by minors, although this is a common approach. The order of the determinant will agree with the number of degrees of freedom, which is also the number of characteristic values in the system; in the determinant shown, five have been taken merely as an example. When expanded, the determinant will yield a polynomial in ω^2; and the roots of this polynomial are the desired natural frequencies.

The equation of fifth order, obtained when the determinant is set equal to zero, will arise in the analysis of the ladder-type system of five masses and five or six springs, such as is shown in Fig. 1.

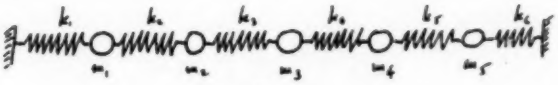

Fig. 1

From a consideration of the forces on each mass in succession, the five simultaneous linear equations are:

$$\left.\begin{aligned} m_1\ddot{x}_1 &= k_2(x_2 - x_1) - k_1x_1 \\ m_2\ddot{x}_2 &= k_3(x_3 - x_2) - k_2(x_2 - x_1) \\ &\cdots \quad \cdots \quad \cdots \\ m_5\ddot{x}_5 &= -k_6x_5 - k_5(x_5 - x_4) \end{aligned}\right\} \quad (2)$$

In these, we first define $\alpha_n = k_n/m_n$ and $\beta_n = k_{n+1}/m_n$ and then assume in the usual manner that each co-ordinate varies harmonically with a different amplitude but the same circular frequency ω; in this manner we come immediately to the Lagrangian determinant in equation (1). It is also clear that if this determinant is multiplied out, there will appear a quintic equation in ω^2, such as

$$\omega^{10} - A\omega^8 + B\omega^6 - C\omega^4 + D\omega^2 - E = 0 \quad (3)$$

The five coefficients, A through E, are all sums of products of the known parameters α_n and β_n. These can readily be evaluated by using a table, Table 1. In the first column we list the known ratios α_1, β_1, α_2, β_2, α_3, and so on, in order: here they are given round-number values in order to present the process as simply as possible. That the last term β_5 is zero indicates that the spring k_6 (Fig. 1) is absent.

[1] Associate Professor, School of Engineering, Yale University, New Haven, Conn.

[2] Graduate Student.

Manuscript received by ASME Applied Mechanics Division, October 28, 1959.

Table 1

$\alpha_1 = 5$	19	95	108	540	168	840	24	120
$\beta_1 = 2$	15	30	60	120	60	120	0	0
$\alpha_2 = 4$	12	48	27	108	6	24		
$\beta_2 = 3$	11	33	18	54	0	0		
$\alpha_3 = 1$	9	9	6	6				
$\beta_3 = 2$	6	12	0	0				
$\alpha_4 = 3$	2	6						
$\beta_4 = 4$	0	0						
$\alpha_5 = 2$								
$\beta_5 = 0$								
$A = 26$		$B = 233$		$C = 828$		$D = 984$		$E = 120$

We then proceed as follows:

Column 2: Add the numbers in column 1 from the bottom up, putting the successive sums two rows higher. Thus in the eighth row put 0, in the seventh $0 + 2$, in the sixth $0 + 2 + 4$, and so on.

Column 3: Multiply the numbers in column 2 by those in column 1, row by row. Thus $5 \times 19 = 95$, $2 \times 15 = 30$, and so on.

Column 4: Add the numbers of column 3 from the bottom up and set two rows higher, in a similar process to that for column 2.

Column 5, and all odd-number columns: Multiply the numbers of the preceding column by those in column 1 in the same row.

Column 6, and all even-number columns: as with columns 2 and 4.

Lastly, add the total of all numbers in each odd-number column. These will be the coefficients of the polynomial.

For this example, therefore, equation (3) has the form

$$\omega^{10} - 26\omega^8 + 233\omega^6 - 828\omega^4 + 984\omega^2 - 120 = 0$$

The roots of this equation can then be found by synthetic division, or by a procedure such as Graeffe's.

It may be noted that this process involves only a little more computation for a twentieth-order determinant, and is certainly no more complicated, than for one of tenth order. In fact, the larger the determinant, the greater the advantage of this method.

APPENDIX

The algebraic proof of the method needs demonstration. The expansion of a determinant Δ of n^{th} order such as equation (1) yields

$$\begin{aligned}
\Delta = {} & (\alpha_1 + \beta_1 - \omega^2)(\alpha_2 + \beta_2 - \omega^2)(\alpha_2 + \beta_2 - \omega^2)(\alpha_4 + \beta_4 - \omega^2)(\alpha_5 + \beta_5 - \omega^2)(\ldots) \\
& -\beta_1 \quad \alpha_2 \quad (\alpha_2 + \beta_2 - \omega^2)(\alpha_4 + \beta_4 - \omega^2)(\alpha_5 + \beta_5 - \omega^2)(\ldots) \\
& -(\alpha_1 + \beta_1 - \omega^2)\beta_2 \quad \alpha_3 \quad (\alpha_4 + \beta_4 - \omega^2)(\alpha_5 + \beta_5 - \omega^2)(\ldots) \\
& -(\alpha_1 + \beta_1 - \omega^2)(\alpha_2 + \beta_2 - \omega^2)\beta_3 \quad \alpha_4 \quad (\alpha_5 + \beta_5 - \omega^2)(\ldots) \\
& -(\alpha_1 + \beta_1 - \omega^2)(\alpha_2 + \beta_2 - \omega^2)(\alpha_2 + \beta_2 - \omega^2)\beta_4 \quad \alpha_5 \quad (\ldots) \\
& - \ldots\ldots \\
& + \beta_1 \quad \alpha_2 \quad \beta_3 \quad \alpha_4 \quad (\alpha_5 + \beta_5 - \omega^2)(\ldots) \\
& + \beta_1 \quad \alpha_2 \quad (\alpha_2 + \beta_3 - \omega^2)\beta_4 \quad \alpha_5 \quad (\ldots) \\
& +(\alpha_1 + \beta_1 - \omega^2)\beta_2 \quad \alpha_3 \quad \beta_4 \quad \alpha_5 \quad (\ldots) \\
& + \ldots\ldots
\end{aligned} \tag{4}$$

We observe that the two highest-order terms in the polynomial expansion can only arise from the first product term cited; that the next two polynomial terms can only issue from the first and second types of product terms (i.e. from the first five terms in the foregoing case), and so forth. We note also that those individual parameters, which "escape" from the brackets with ω^2, escape in pairs (such as $\beta_1\alpha_2$ in the second term cited), and that these pairs are the "bend sinister" terms of the determinant. They may be recognized in the physical system as the two derived from the same spring acting on neighboring masses. In the expansion, all polynomial coefficients involving products of neighboring parameters, either $\alpha_n\beta_n$ or $\beta_n\alpha_{n+1}$, are always eliminated.

Proceeding then to multiply out the products cited, one can obtain

$$\begin{aligned}
(-1)^n\Delta = {} & \omega^{2n} - [\alpha_1 + \beta_1 + \alpha_2 + \beta_2 + \ldots\ldots + \beta_n]\omega^{2n-2} \\
& + [\alpha_1(\alpha_2 + \beta_2 + \alpha_3 + \ldots + \beta_n) \\
& + \beta_1(\beta_2 + \alpha_3 + \ldots\ldots + \beta_n) \\
& + \alpha_2(\alpha_3 + \beta_3 + \ldots + \beta_n) + \ldots + \alpha_{n-2}(\alpha_n + \beta_n) \\
& + \beta_{n-2}\beta_n]\omega^{2n-4} - \ldots\ldots
\end{aligned} \tag{5}$$

To simplify the coefficients of this second term and subsequent terms we define

$$\begin{aligned}
S_1 &= \alpha_2 + \beta_2 + \alpha_3 + \beta_3 + \ldots\ldots + \beta_n \\
S_2 &= \beta_2 + \alpha_3 + \beta_3 + \ldots\ldots + \beta_n \\
S_3 &= \alpha_3 + \beta_3 + \ldots\ldots + \beta_n \\
S_4 &= \beta_3 + \ldots\ldots + \beta_n, \text{ and so forth}
\end{aligned}$$

and with these, equation (5) is written

$$\begin{aligned}
(-1)^n\Delta = {} & \omega^{2n} - [\alpha_1 + \beta_1 + \alpha_2 + \beta_2 + \ldots\ldots + \beta_n]\omega^{2n-2} \\
& + [\alpha_1 S_1 + \beta_1 S_2 + \alpha_2 S_2 + \beta_2 S_4 + \ldots]\omega^{2n-4} \\
& - [\alpha_1(S_2 + S_4 + S_5 + \ldots) + \beta_1(S_4 + S_5 + \ldots) \\
& + \alpha_2(S_5 + S_6 + \ldots) + (\ldots) + \ldots]\omega^{2n-6} \\
& + [\ldots \quad \ldots]\omega^{2n-8} - \ldots\ldots
\end{aligned} \tag{6}$$

To simplify the third coefficient in this we let

$$\begin{aligned}
T_1 &= S_2 + S_4 + S_5 + S_6 + \ldots\ldots \\
T_2 &= S_4 + S_5 + S_6 + \ldots\ldots \\
T_3 &= S_5 + S_6 + \ldots\ldots \text{ and so forth}
\end{aligned}$$

so that the equation appears more neatly as:

$$\begin{aligned}
(-1)^n\Delta = {} & \omega^{2n} - [\alpha_1 + \beta_1 + \alpha_2 + \beta_2 + \ldots + \beta_n]\omega^{2n-2} \\
& + [\alpha_1 S_1 + \beta_1 S_1 + \alpha_2 S_3 + \ldots]\omega^{2n-4} \\
& - [\alpha_1 T_1 + \beta_1 T_2 + \alpha_2 T_3 + \ldots]\omega^{2n-6} \\
& + [\alpha_1(T_3 + T_4 + T_5 + \ldots) + \beta_1(T_4 + T_5 + \ldots) \\
& + \alpha_2(T_5 + \ldots) + \ldots]\omega^{2n-8} + \ldots
\end{aligned}$$

From these it is plain that the successive coefficients of the polynomial terms are

$$\begin{aligned}
A &= \alpha_1 + \beta_1 + \alpha_2 + \beta_2 + \ldots \\
B &= \alpha_1 S_1 + \beta_1 S_2 + \alpha_2 S_3 + \ldots \\
C &= \alpha_1 T_1 + \beta_1 T_2 + \alpha_2 T_3 + \ldots \quad \text{and so forth}
\end{aligned}$$

and these were found by the table.

On the Griffith-Irwin Fracture Theory

J. L. SANDERS, JR.[1]

THE purpose of the present paper is to give a new mathematical formulation of the criterion for crack extension according to the Griffith-Irwin theory in terms of a path-independent line integral. The derivation will be made for the case of a crack in a plate where the plane-stress theory applies, but it may be generalized easily to other cases (three-dimensional elasticity, shells, etc.). An account of the Griffith-Irwin theory as such may be found in [1][2] and in the papers referred to in that paper.

Analysis

Suppose we have a plate with arbitrary boundaries on which we prescribe arbitrary boundary conditions (possibly time-dependent). The plate is supposed to contain a crack of length $L(\alpha)$ where α is some parameter which increases when L increases. The edges of the crack itself are assumed stress-free and all inertia effects are neglected. We will assume that the (quasistatic) solution of this plane-stress problem is known, that is, σ_{ij}, ϵ_{ij}, and u_i are known functions of x, y, t, and α. Let C be some simple closed curve surrounding the crack. According to the Griffith-Irwin theory, the following energy balance must hold during a (virtual) extension of the crack:

> The rate at which work is being done by forces acting across C equals the rate of increases of strain energy stored in the material inside C plus the rate at which energy is dissipated by the growing crack.

The last term in this equality is assumed to be proportional to

$$\frac{dL}{dt} = \frac{dL}{d\alpha}\frac{d\alpha}{dt} = L'\dot{\alpha}$$

In symbols the equality reads:

$$\int_C T_i \frac{du_i}{dt}\,ds = \frac{1}{2}\frac{d}{dt}\int_C T_i u_i\,ds + GL'\dot{\alpha} \tag{1}$$

where T_i are the boundary tractions, and G is a constant which depends on the power required to extend the crack at a given rate. Equation (1) may be transformed into

$$\frac{1}{2}\dot{\alpha}\int_C \left(T_i\frac{\partial u_i}{\partial \alpha} - u_i\frac{\partial T_i}{\partial \alpha}\right)ds + \frac{1}{2}\int_C (T_i\dot{u}_i - u_i\dot{T}_i)ds = GL'\dot{\alpha} \tag{2}$$

where

$$\frac{du_i}{dt} = \dot{u}_i + \dot{\alpha}\frac{\partial u_i}{\partial \alpha}$$

and similarly for dT_1/dt. Now the second integral on the left is easily shown to vanish, and so we have the result:

$$\left[\frac{1}{2}\int_C \left(T_i\frac{\partial u_i}{\partial \alpha} - u_i\frac{\partial T_i}{\partial \alpha}\right)ds - GL'\right]\dot{\alpha} = 0 \tag{3}$$

Ordinarily equation (3) has no solution other than $\dot{\alpha} = 0$ and we have here a kind of eigenvalue problem. For certain values of the crack length (or load level) which may be called critical the following equation holds:

$$I = \frac{1}{2}\int_C \left(T_i\frac{\partial u_i}{\partial \alpha} - u_i\frac{\partial T_i}{\partial \alpha}\right)ds = GL' \tag{4}$$

In the usual case a crack length longer than that determined by (4) would extend and lead to failure of the structure. However, in other cases the solution of equation (4) may determine the conditions under which a running crack would be arrested (neglecting inertia effects) and so the proper physical interpretation of the solution to (4) must be left to depend on the case at hand. The most useful feature of the present form of the criterion (4) is that the integral I is independent of the path C (by the manner of its derivation). One obvious advantage is that there will be no difficulties connected with calculating the strain energy in infinite regions. A simple modification of (4) is that C need not necessarily be a closed path but may begin and end on a free boundary in such a way as to enclose the tip of the crack.

Since the integral I is independent of the path C, one might expect it to take a simple form if the solution of the plane-stress problem is known in terms of the two analytic functions ϕ and ψ of the Muskhelishvili formulation of plane-stress theory [2]. This is indeed the case. According to Muskhelishvili,

$$E(u - iv) = (3 - \nu)\bar{\phi} - (1 + \nu)z\phi' - (1 + \nu)\psi \tag{5}$$

where $u_1 = u$, $u_2 = v$, and a bar over a quantity denotes the complex conjugate. Let $T_1 ds = dX$, $T_2 ds = dY$, and let a subscript α denote differentiation with respect to α. The integral I may be written

$$\begin{aligned} I &= \frac{1}{2}\,\mathrm{Re}\left\{\int_C [(u_\alpha + iv_\alpha)d(X - iY) - (u + iv)d(X_\alpha - iY_\alpha)]\right\} \\ &= \frac{1}{2E}\,\mathrm{Im}\left\{\int_C [(1 + \nu)z\bar{\phi}_\alpha' - (3 - \nu)\phi_\alpha \right. \\ &\qquad + (1 + \nu)\psi_\alpha]d(\bar{z}\phi' + \bar{\phi} + \psi) \\ &\qquad \left. - [(1 + \nu)z\bar{\phi}' - (3 - \nu)\phi + (1 + \nu)\psi]d(\bar{z}\phi_\alpha' + \bar{\phi}_\alpha + \psi_\alpha)\right\} \end{aligned} \tag{6}$$

where Re or Im means the real or imaginary part of, and where $d(X - iY) = id(\bar{z}\phi' + \bar{\phi} + \psi)$. After some manipulation (6) becomes:

$$I = -\frac{2}{E}\,\mathrm{Im}\left\{\int_C (\psi_\alpha\phi' + \psi'\phi_\alpha)dz\right\} \tag{7}$$

If the path C begins at point A and ends at point B on a free boundary where the boundary condition is $\bar{z}\phi' + \bar{\phi} + \psi = 0$, then equation (7) must be modified to read:

$$I = -\frac{2}{E}\,\mathrm{Im}\left\{[\bar{z}\phi'\phi_\alpha]_A^B + \int_A^B (\psi_\alpha\phi' + \psi'\phi_\alpha)dz\right\} \tag{8}$$

Applications

The following two examples are not new results but are presented to illustrate the application of the criterion (4).

Consider the problem of a cracked rectangular plate loaded on two opposite edges which are constrained to remain straight and free on the other two edges. On the first loaded edge let $u_1 = u_2 = 0$. Let C be the boundary of the plate; then the only contribution to I comes from the second loaded edge. We have:

$$I = \frac{1}{2}\frac{\partial U}{\partial \alpha}\int T_2\,ds - \frac{1}{2}U\frac{\partial}{\partial \alpha}\int T_2 f ds$$

or

$$= \frac{1}{2}\frac{\partial U}{\partial \alpha}F - \frac{1}{2}U\frac{\partial F}{\partial \alpha} \tag{9}$$

[1] Gordon McKay Lecturer on Structural Mechanics, Division of Engineering and Applied Physics, Harvard University, Cambridge, Mass.

[2] Numbers in brackets indicate References at end of Note.

Manuscript received by ASME Applied Mechanics Division, October 2, 1959.

where $F = \int T_x ds$, $u_1 = 0$, and $u_2 = U$ on the second loaded edge. For the present purpose, all we need to know about the solution of the plane-stress problem is that, for a fixed value of α, there exists a linear relation between the resultant load F and the displacement U, namely

$$F = k(\alpha)U \tag{10}$$

From the foregoing we can show that the critical crack length for a fixed grip test ($\partial U/\partial\alpha = 0$) is the same as for a dead load test ($\partial F/\partial\alpha = 0$). In the first case we have from (9) and (10)

$$I = -\frac{1}{2}U\frac{\partial F}{\partial\alpha} = -\frac{1}{2}U^2k' \tag{11}$$

In the second case from (9) and (10)

$$I = \frac{1}{2}F\frac{\partial U}{\partial\alpha} = -\frac{1}{2}\left(\frac{F}{k}\right)^2 k' = -\frac{1}{2}U^2k' \tag{12}$$

The value of I is the same in both cases and hence so is the critical crack length. This result has been noted before by several authors.

For another example, consider the problem of an infinite plate with a periodic array of cracks of length $2a$ along the x-axis with a distance l between the centers of the cracks. The plate is subjected to a uniform stress $\sigma_y = \sigma$ at infinity. The problem of determining the distribution in this case was solved by Westergaard [3]. In terms of the Muskhelishvili functions the solution is:

$$\phi = -\frac{\sigma}{4}\left[z + \frac{2il}{\pi}\cosh^{-1}\left(\frac{\cos\dfrac{\pi z}{l}}{\cos\dfrac{\pi a}{l}}\right)\right] \tag{13}$$

$$\psi = -z\phi' + \phi + \frac{1}{2}\sigma z \tag{14}$$

Let C enclose the crack which extends from $z = -a$ to $z = a$. By using (14) we have

$$\begin{aligned} I &= -\frac{2}{E}\,\mathrm{Im}\left\{\int_C (\bar{\psi}_o\phi' + \psi'\bar{\phi}_o)dz\right\} \\ &= -\frac{2}{E}\,\mathrm{Im}\left\{\int_C \left(2\phi' + \frac{1}{2}\sigma\right)\bar{\phi}_o dz\right\} \\ &= -\frac{\sigma^2}{E}\tan\frac{\pi a}{l}\,\mathrm{Im}\left\{\int_C \frac{\sin\dfrac{\pi z}{l}\cos\dfrac{\pi z}{l}}{\cos^2\dfrac{\pi z}{l} - \cos^2\dfrac{\pi a}{l}}dz\right\} \end{aligned} \tag{15}$$

The path C encloses the two simple poles at $z = a$ and $z = -a$ so the integral may be evaluated easily. After the calculations have been performed the criterion reads

$$\frac{2\sigma^2 l}{E}\tan\frac{\pi a}{l} = 2G \tag{16}$$

and hence the critical stress for a crack length $L = 2a$ is

$$\sigma = \left[\frac{GE}{l}\cot\frac{\pi a}{l}\right]^{1/2} \tag{17}$$

Conclusions

The Griffith-Irwin criterion for crack extension has been expressed in the form of a contour integral. The path independence of the integral makes it clear that the amount of strain energy available in the cracked structure is irrelevant. The quantity that does matter is the strength of the square-root singularity at the tip of the crack. This strongly suggests that the Griffith-Irwin approach to fracture mechanics via energy concepts is equivalent to an approach via stress-concentration factors (which reinforces a conclusion reached in Ref. [4]).

References

1 G. R. Irwin, "Analysis of Stresses and Strains Near the End of a Crack Traversing a Plate," JOURNAL OF APPLIED MECHANICS, vol. 24, TRANS. ASME, vol. 79, 1957, pp. 361–364.

2 N. I. Muskhelishvili, "Some Basic Problems of the Mathematical Theory of Elasticity," P. Noordhoff Ltd., Groningen, 1953.

3 H. M. Westergaard, "Bearing Pressures and Cracks," JOURNAL OF APPLIED MECHANICS, vol. 6, TRANS. ASME, vol. 61, 1939, pp. A-49–A-53.

4 G. E. Irwin, J. A. Kies, and H. L. Smith, "Fracture Strengths Relative to Onset and Arrest of Crack Propagation," Proceedings of the ASTM, vol. 58, 1958, pp. 640–660.

On the Flexure of Plastic Plates[1]

S. LERNER[2] and W. PRAGER[3]

IN THEIR pioneering work on bending of rigid, perfectly plastic plates, Hopkins and Prager[4] used the yield condition of Tresca and the associated flow rule. Hopkins and Wang[5] later extended the analysis to arbitrary yield conditions and the associated flow rules. On account of the mathematical difficulties presented by other shapes, work in this area has been almost exclusively concerned with circular plates under rotationally symmetric loading. Attempts at experimental verification of the theory have likewise been restricted to circular plates under rotationally symmetric loading.[6] Such tests can at best provide indirect verification of the theory because they deal with the over-all deformation of the circular plate under a nonuniform distribution of radial and circumferential bending moments. The purpose of the present note is to draw attention to a simple test that provides a direct check on the fundamental assumptions of the theory, when the two principal bending moments have opposite signs.

Analysis

Fig. 1 illustrates the proposed test: A horizontal rhomboid plate of the uniform thickness h and semidiagonals of the lengths a and b is subjected to four vertical loads of the same intensity P, two of which act downward at the end points of one diagonal, while the remaining two act upward at the end points of the other diagonal. As was first pointed out by Kelvin and Tait, this type of loading is compatible with a distribution of bending and twist-

[1] The results presented in this Note were obtained in the course of research sponsored by the Office of Naval Research under Contract Nonr 562(10).

[2] Associate Professor of Engineering, Brown University, Providence, R. I.

[3] L. Herbert Ballou University Professor, Brown University, Providence, R. I.

[4] H. G. Hopkins and W. Prager, "The Load-Carrying Capacity of Circular Plates," *Journal of the Mechanics and Physics of Solids*, vol. 2, 1952, pp. 1–13.

[5] H. G. Hopkins and A. J. Wang, "Load-Carrying Capacities for Circular Plates of Perfectly Plastic Material With Arbitrary Yield Conditions," *Journal of the Mechanics and Physics of Solids*, vol. 3, 1954, pp. 117–129.

[6] R. M. Haythornthwaite and E. T. Onat, "The Load-Carrying Capacity of Initially Flat Circular Steel Plates Under Reversed Loading," *Journal of the Aeronautical Sciences*, vol. 22, 1955, pp. 867–869.

Manuscript received by ASME Applied Mechanics Division, Sept. 21, 1959.

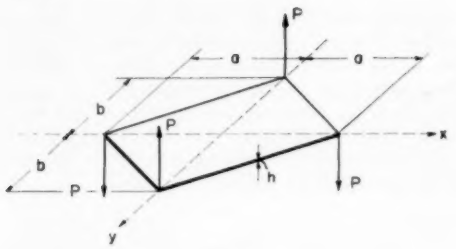

Fig. 1

ing moments that is uniform over all of the plate except narrow strips along the edges in which all shear forces are transmitted.

As the intensity P of the loads is increased slowly, starting from zero, the plate remains rigid until a critical value P^* of the load intensity is reached and plastic flow sets in. The rate of deflection for this incipient plastic flow can be assumed to be given by

$$w = \frac{c}{2}(x^2 - \gamma^2 y^2), \tag{1}$$

where c and γ are constants. The corresponding rates of curvature and twist are

$$\left.\begin{aligned} \kappa_x &= -\partial^2 w/\partial x^2 = -c, \\ \kappa_y &= -\partial^2 w/\partial y^2 = \gamma^2 c, \\ \kappa_{xy} &= -\partial^2 w/\partial x \partial y = 0. \end{aligned}\right\} \tag{2}$$

According to the general theory of limit analysis, the bending and twisting moments associated with these rates of curvature and twist can be written as follows:

$$M_x = -\lambda c, \qquad M_y = \lambda \gamma^2 c, \qquad M_{xy} = 0; \tag{3}$$

here λ is a positive factor of proportionality, which can be determined from the yield condition of the plate. The vanishing of the twisting moment M_{xy} in (3) shows that M_x and M_y are principal bending moments.

If, for instance, the plate material obeys the yield condition of von Mises, these principal bending moments must satisfy the relation

$$M_x^2 + M_y^2 - M_x M_y = M_0^2, \tag{4}$$

(see Hopkins and Wang),[5] where M_0 is the yield moment in simple flexure. In terms of the yield stress σ_0 in simple tension and the thickness h of the plate, this yield moment is given by

$$M_0 = \sigma_0 h^2/4. \tag{5}$$

Substitution of (3) into (4) and use of the resulting value of λ in (3) furnishes

$$\left.\begin{aligned} M_x &= -M_0(1 + \gamma^2 + \gamma^4)^{-1/2}, \\ M_y &= \gamma^2 M_0(1 + \gamma^2 + \gamma^4)^{-1/2}. \end{aligned}\right\} \tag{6}$$

The critical load intensity P^* can now be determined by equating the moment of a corner load with respect to a diagonal to the total bending moment transmitted along this diagonal; one finds

$$P^* = -2\frac{b}{a}M_x = 2\frac{a}{b}M_y. \tag{7}$$

Comparison of the values of M_y/M_x obtained from (3) and (7) shows that

$$\gamma = b/a. \tag{8}$$

For the yield condition (4), the critical load intensity (7) can therefore be written as

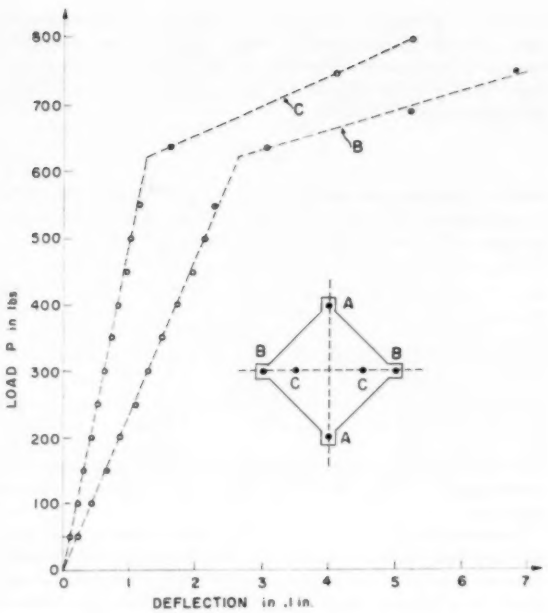

Fig. 2

$$P^* = \frac{2\gamma M_0}{(1 + \gamma^2 + \gamma^4)^{1/2}}, \tag{9}$$

where γ is given by (8) and M_0 by (5).

The preceding analysis starts from an assumed yield condition (4) and furnishes the critical load intensity P^* in dependence on the shape parameter $\gamma = b/a$. Conversely, for a given value of this shape parameter, the experimentally determined value of the critical load intensity P^* furnishes, by means of (7), the coordinates M_x and M_y of a point on the "yield locus," which represents the yield condition of the plate. By using rhomboid plates of different shapes, those parts of the yield locus may be determined that lie in the second and fourth quadrants of the M_x, M_y-plane.

Experiment

As budget limitations ruled out a complete test series of this kind, only a single test was performed with a square plate of mild steel with the following dimensions: $a = b = 9$ in., $h = 0.25$ in. To determine the yield stress σ_0 in simple tension and check the isotropy of the plate, two strips were cut in each diagonal direction from the same sheet as the plate and tested in simple tension. The observed yield stresses had the mean value $\sigma_0 = 34{,}700$ psi, from which they differed by at most 1 per cent. The diagrams in Fig. 2 show the load intensity P versus the deflection of the points B and C with respect to the points A (see inset). Each set of observations closely fits two straight lines; the ordinate of the point of intersection of these lines gives the critical load intensity $P^* = 620$ lb. This agrees well with the yield condition of von Mises, because for a square plate ($\gamma = 1$), Equations (9) and (5) furnish

$$P^* = \frac{2}{\sqrt{3}}M_0 = \frac{1}{2\sqrt{3}}\sigma_0 h^2$$

$$= \frac{1}{2\sqrt{3}} \times 34{,}700 \times 0.25^2 = 625 \text{ lb}.$$

Induced Velocities in the Two-Dimensional Cascade Theory

J. POLÁŠEK[1]

In a paper,[2] M. J. Schilhansl described an approximate method for calculating the velocity component induced on a section of a two-dimensional cascade by vortexes distributed on the remaining sections.[3] This method gives good results only in the case of small solidities ($\sigma < 1$), since for $\sigma > 1$ the expansions in his equations (35) and (36) diverge. For greater solidities, the method can be employed so that the effect of one or two adjacent pairs of blade sections is calculated directly, as stated in Prof. Schilhansl's paper. However, the calculation by means of the Simpson's rule, as mentioned in the paper, is time-consuming; for this reason we would like to point out that relatively simple expressions for exact calculation can be obtained by the use of the function of complex variable.

Analysis

The basic distributions on two blade sections with the ordinal numbers $+\nu$ and $-\nu$ induce on the chord of the blade section zero velocities which can be written in a complex form:

$$\frac{(v_\gamma)_{n,\nu}}{u_m} + i\frac{(u_\gamma)_{n,\nu}}{u_m} = \frac{1}{\pi}\int_{-1}^{1}\left[\frac{1}{\xi - x + \frac{2\nu}{\sigma}e^{-i\beta}} + \frac{1}{\xi - x - \frac{2\nu}{\sigma}e^{-i\beta}}\right]\gamma_n(\xi)d\xi \quad (1)$$

where

$$\gamma_0(\xi) = \left(\frac{1-\xi}{1+\xi}\right)^{1/2}, \quad \gamma_n(\xi) = \xi^{n-1}(1-\xi^2)^{1/2}, \quad n = 1, 2, \ldots \quad (2)$$

Equation (1) contains integrals of the type

$$\frac{1}{\pi}\int_{-1}^{1}\frac{\gamma_n(\xi)}{\xi - a}\,d\xi \quad (3)$$

which can be calculated by considering ξ a complex variable and by selecting the integration path as shown in Fig. 1. Since the integrand of Equation (3) has for finite values of the argument ξ only a pole of the first order for $\xi = a$ and branch points of second order for $\xi = 1$ and $\xi = -1$, the following applies according to the residue theorem:

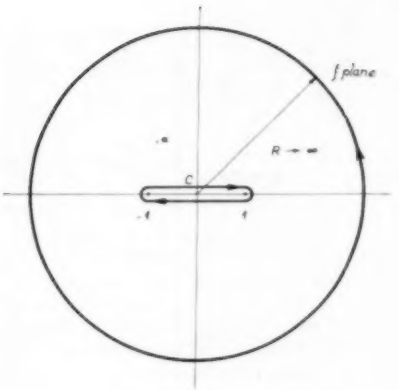

Fig. 1

$$\frac{1}{\pi}\int_{-1}^{1}\frac{\gamma_n(\xi)}{\xi - a}\,d\xi = \frac{1}{2\pi}\int_{c}\frac{\gamma_n(\xi)}{\xi - a}\,d\xi = i[\text{res } f(a) - \text{res } f(\infty)] \quad (4)$$

Other details of the calculation which can be performed quite easily are not included, only the results being presented herein.

Denoting

$$\omega_1 = -x + \frac{2\nu}{\sigma}e^{-i\beta} - \left(\frac{4\nu^2}{\sigma^2}e^{-2i\beta} - 2x\frac{2\nu}{\sigma}e^{-i\beta} + x^2 - 1\right)^{1/2} \quad (5)$$

$$\omega_2 = -x - \frac{2\nu}{\sigma}e^{-i\beta} + \left(\frac{4\nu^2}{\sigma^2}e^{-2i\beta} + 2x\frac{2\nu}{\sigma}e^{-i\beta} + x^2 - 1\right)^{1/2} \quad (6)$$

where the signs of the roots are selected so as to yield $|\omega_1| < 1$, $|\omega_2| < 1$, it follows that

$$\frac{(v_\gamma)_{0,\nu}}{u_m} + i\frac{(u_\gamma)_{0\nu}}{u_m} = \frac{1+\omega_1}{\left(\frac{4\nu^2}{\sigma^2}e^{-2i\beta} - 2x\frac{2\nu}{\sigma}e^{-i\beta} + x^2 - 1\right)^{1/2}} - \frac{1+\omega_2}{\left(\frac{4\nu^2}{\sigma^2}e^{-2i\beta} + 2x\frac{2\nu}{\sigma}e^{-i\beta} + x^2 - 1\right)^{1/2}} \quad (7)$$

$$\frac{(v_\gamma)_{1,\nu}}{u_m} + i\frac{(u_\gamma)_{1,\nu}}{u_m} = \omega_1 + \omega_2, \quad (8)$$

$$\frac{(v_\gamma)_{2,\nu}}{u_m} + i\frac{(u_\gamma)_{2,\nu}}{u_m} = -\frac{1}{2}(\omega_1^2 + \omega_2^2), \quad (9)$$

$$\frac{(v_\gamma)_{3,\nu}}{u_m} + i\frac{(u_\gamma)_{3,\nu}}{u_m} = \frac{1}{4}(\omega_1 + \omega_2 + \omega_1^3 + \omega_2^3), \quad (10)$$

$$\frac{(v_\gamma)_{4,\nu}}{u_m} + i\frac{(u_\gamma)_{4,\nu}}{u_m} = -\frac{1}{4}(\omega_1^2 + \omega_2^2) - \frac{1}{8}(\omega_1^4 + \omega_2^4). \quad (11)[4]$$

The velocity components $(v_\gamma)_{n,\nu}$ and $(u_\gamma)_{n,\nu}$ are then the real and the imaginary part, respectively, of the expression on the right-hand sides of equations (7) to (11). In a numerical calculation all operations are carried out with complex numbers, the

---

[1] Aeronautical Research Scientist, Státni vyzkumný ústav tepelné techniky, Prague, Czechoslovakia.

[2] M. J. Schilhansl, "A Simple Approach to an Approximate Two-Dimensional Cascade Theory," Journal of Applied Mechanics, vol. 25, Trans. ASME, vol. 80, 1958, pp. 607–612.

[3] Several printing errors appear in the text of Prof. Schilhansl's paper:

(*a*) Equations (30) and (31) should read: $i_2 = +\frac{2u_m}{\pi}\ldots$

(*b*) In Table 1, the individual items should read: $F_{22} = -1/4$, $F_{42} = -1/8 - 3/4\,x^2$, $F_{24} = -1/8$, $F_{44} = -3/64 - 3/8\,x^2$.

(*c*) Equation (36) should read: $\frac{(v_\gamma)_n}{u_m} = \frac{\pi^2}{6}(1/2\sigma)^2\cos 2\beta.F_{2n} + \frac{\pi^4}{90}(1/2\sigma)^4\cos 4\beta.F_{4n} + \ldots$

(*d*) Page 611, 2nd column, 2nd line should read: $\lambda = 60$ deg.

Manuscript received by ASME Applied Mechanics Division, November 25, 1959.

[4] For small values of σ/ν it is possible to develop the foregoing expressions into power series and to obtain relations (35) and (36) of the original paper directly.

Table 1 $(u_\gamma)_0/u_m$

	σ/x	−1	−1/2	0	1/6	5/6	1
$\beta = 120$ deg	1/2	0.0846	−0.0009	−0.0863	−0.1138	−0.2143	−0.2361
	$1/\sqrt{2}$	0.1607	−0.0036	−0.1672	−0.2151	−0.3872	−0.4191
	1	0.2935	−0.0134	−0.3136	−0.4005	−0.6473	−0.6843
	$\sqrt{2}$	0.5093	−0.0457	−0.5546	−0.6845	−0.9977	−1.0363
	2	0.8431	−0.1314	−0.8999	−1.0713	−1.4674	−1.5115
$\beta = 150$ deg	1/2	0.0935	0.0009	−0.0918	−0.1236	−0.2604	−0.2975
	$1/\sqrt{2}$	0.1948	0.0035	−0.1889	−0.2567	−0.5554	−0.6341
	1	0.4016	0.0122	−0.3978	−0.5458	−1.1135	−1.2085
	$\sqrt{2}$	0.7607	0.0234	−0.8488	−1.1382	−1.7485	−1.8012
	2	1.3138	−0.0400	−1.6096	−1.9223	−2.5232	−2.6079

Table 2 $(v_\gamma)_0/u_m$

	σ/x	−1	−1/2	0	1/6	5/6	1
$\beta = 90$ deg	1/2	0.0981	−0.0010	−0.0998	−0.1318	−0.2505	−0.2773
	$1/\sqrt{2}$	0.1885	−0.0036	−0.1941	−0.2541	−0.4649	−0.5092
	1	0.3528	−0.0125	−0.3687	−0.4761	−0.8249	−0.8914
	$\sqrt{2}$	0.6387	−0.0398	−0.6753	−0.8553	−1.3909	−1.4825
	2	1.1152	−0.1118	−1.1780	−1.4593	−2.2372	−2.3569
$\beta = 120$ deg	1/2	0.0535	0.0005	−0.0528	−0.0710	−0.1468	−0.1664
	$1/\sqrt{2}$	0.1091	0.0015	−0.1080	−0.1457	−0.3008	−0.3392
	1	0.2205	0.0038	−0.2223	−0.2996	−0.5933	−0.6575
	$\sqrt{2}$	0.4302	0.0048	−0.4529	−0.6007	−1.0806	−1.1965
	2	0.7979	−0.0142	−0.8759	−1.1211	−1.8124	−1.9261
$\beta = 150$ deg	1/2	−0.0481	0.0006	0.0497	0.0653	0.1186	0.1281
	$1/\sqrt{2}$	−0.0867	0.0029	0.0952	0.1225	0.1815	0.1754
	1	−0.1278	0.0147	0.1696	0.2030	0.1050	0.0270
	$\sqrt{2}$	−0.1240	0.0701	0.2270	0.1904	−0.2534	−0.3388
	2	−0.0484	0.2256	0.0121	−0.1933	−0.6532	−0.7470

separation into the real and the imaginary part being performed at the end.

When calculating the velocity induced by the two blade sections with the ordinal numbers +1 and −1 according to the exact formulae (7) to (11) and the remaining according to the modified expressions (35) and (36), results are obtained with arbitrarily small errors. (For yet larger solidities, the effect of blade sections with ordinal numbers +2 and −2, or possibly +3 and −3, must be calculated in accordance with the exact formulas.)

Tables 1 and 2 contain certain values of the components of $(u_\gamma)_0$ and $(v_\gamma)_0$ for various β and σ, calculated by the described method; the error of the values thus obtained is smaller than 0.0001.

The Relation Between Stress Concentration and Boundary Displacement for Simple Openings

J. S. BROCK[1]

In this note an interesting relation between stress concentration and boundary displacement is pointed out which applies for openings in the form of circles and ellipses loaded parallel to a semiaxis.

It is well-known that both the boundary and field stresses around a general opening in a uniformly stressed infinite plate of homogeneous isotropic material are independent of the elastic constants. First, let us show that the boundary displacements for a given strain in a plate are also independent of the material constants. The familiar condition for a boundary free of externally applied forces is,[2]

$$\phi(\sigma) + \frac{\omega(\sigma)}{\bar{\omega}'(\bar{\sigma})}\,\bar{\phi}'(\bar{\sigma}) + \bar{\psi}(\bar{\sigma}) = 0 \qquad (1)$$

where $\phi(\sigma)$ and $\psi(\sigma)$ denote the values of the potential functions on the boundary, which is described by the mapping function $\omega(\sigma)$. The displacement of points on the boundary of the opening is given by

$$2\mu(g_1 + ig_2) = k\phi(\sigma) - \frac{\omega(\sigma)}{\bar{\omega}'(\bar{\sigma})}\,\bar{\phi}'(\bar{\sigma}) - \bar{\psi}(\bar{\sigma}) \qquad (2)$$

where g_1 and g_2 are the Cartesian co-ordinate components of the displacement (see Fig. 1), and for plane stress,

$$k = \frac{3 - \nu}{1 + \nu}.$$

Substituting $\bar{\psi}(\bar{\sigma})$ from (1) in (2) yields

$$g_1 + ig_2 = \frac{(k+1)}{2\mu}\,\phi(\sigma) = \frac{4}{E}\,\phi(\sigma) \qquad (3)$$

Thus, for a general opening, the boundary displacements are independent of Poisson's ratio. They depend only upon the ϕ-function and inversely on Young's modulus. Therefore, for a given strain applied to the plate, the unit displacements of the boundary of an opening are independent of the elastic constants.

Equation (3) will now be applied to the consideration of the deformation of an elliptical opening to show the relation existing between the boundary displacements and the stress concentration. The mapping function for an ellipse whose semiaxes, a and b, lie on the co-ordinate axes is

$$\omega(\zeta) = \frac{1}{2}\,(a + b)\zeta + (a - b)/2\zeta \qquad (4)$$

For a uniform stress acting in the direction of the y-axis the ϕ-function is simply

$$\phi(\zeta) = \frac{S_y}{4}\left[\frac{(a+b)\zeta}{2} - \frac{(3a+b)}{2\zeta}\right] \qquad (5)$$

The boundary displacements, easily obtained from (3) and (5), are given by

$$g_1 + ig_2 = \frac{S_y}{E}\,[-a\cos\beta + i(2a + b)\sin\beta] \qquad (6)$$

[1] Department of the Navy, David Taylor Model Basin, Washington, D. C.

[2] I. S. Sokolnikoff, "Mathematical Theory of Elasticity," McGraw-Hill Book Co., Inc., New York, N. Y., 1956.

Manuscript received by ASME Applied Mechanics Division, August 7, 1959.

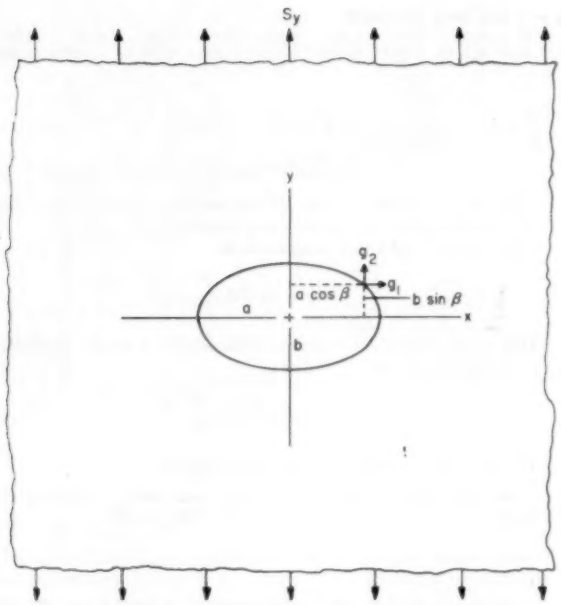

Fig. 1 Directions of load and displacements

and the unit displacements or "strains" are

$$\frac{g_1}{a\cos\beta} = -\frac{S_y}{E}$$

$$\frac{g_2}{b\sin\beta} = \left(1 + 2\frac{a}{b}\right)\frac{S_y}{E} \tag{7}$$

Thus we have the somewhat surprising result that all horizontal chords of the ellipse experience uniform "compressive strain" equal in magnitude to the minimum strain around the boundary of the opening. Likewise, all chords in the direction of the applied load experience uniform "tensile strain" equal to the maximum strain around the boundary of the opening. Stated differently, the coefficients of S_y/E in (7) are equal, respectively, to the well-known minimum and maximum stress-concentration factors for this opening and load.

This result holds for any ellipse in a plate which is uniformly stressed by loads which are parallel to the semiaxes of the ellipse.

Bending of an Isotropic Triangular Plate, Two of Whose Edges Are Simply Supported and the Third Clamped

B. D. AGGARWALA[1]

We consider an equilateral triangular plate OAB whose sides OA and OB are simply supported and the side AB is clamped. An isolated load of intensity P is assumed to be acting at the center G of the triangle so that OG $= 1/\sqrt{3} = a$. (OA $= 1$).

The equation giving the deflection w at any point except G of the triangle is

$$\nabla^4 w = 0 \tag{1}$$

with the boundary conditions

$$w = \nabla^2 w = 0 \qquad \text{on } \theta = \pm\pi/6 \tag{2a}$$

$$w = \partial w/\partial x = 0 \qquad \text{on AB} \tag{2b}$$

Solution

We write

$$w = w_0 - w_1 \tag{3}$$

where w_0 is a solution of (1) satisfying (2a).

To obtain w_0, we notice that $\Delta^2 w_0$ is a harmonic function which vanishes on $\theta = \pm\pi/6$ and (because of a singular load) has a logarithmic singularity at $r = 1/\sqrt{3}$, $\theta = 0$. Such a function may be considered as the stream function due to a rectilinear vortex inside a cylinder bounded by $\theta = \pm\pi/6$. Satisfying the condition that the load at the point of application is P, one obtains[2]

$$\nabla^2 w_0 = -\frac{P}{4\pi D}\log\frac{z^3 - a^3\bar{z}^3 - a^3}{z^3 + a^3\bar{z}^3 + a^3}$$

Integrating this equation and adding to the integral a harmonic function in such a fashion that the integral will have a singularity of the type $r^2\log r$ at the point of application of the load and at the images of this point in the lines $\theta = \pm\pi/6$, one obtains

$$\begin{aligned}\frac{w_0}{R} &= (z-a)(\bar{z}-a)\ln(z-a)(\bar{z}-a)\\ &- (z+a\epsilon^2)(\bar{z}+a\epsilon)\ln(z+a\epsilon^2)(\bar{z}+a\epsilon)\\ &- (z+a\epsilon)(\bar{z}+a\epsilon^2)\ln(z+a\epsilon)(\bar{z}+a\epsilon^2)\\ &- (z+a)(\bar{z}+a)\ln(z+a)(\bar{z}+a)\\ &+ (z-a\epsilon^2)(\bar{z}-a\epsilon)\ln(z-a\epsilon^2)(\bar{z}-a\epsilon)\\ &+ (z-a\epsilon)(\bar{z}-a\epsilon^2)\ln(z-a\epsilon)(\bar{z}-a\epsilon^2)\end{aligned} \tag{4}$$

where

$$R = -P/16\pi D$$

$$z = x + iy$$

and 1, ϵ, ϵ^2 are the three cube roots of unity. Equation (4) gives

$$\begin{aligned}\frac{\partial w_0}{\partial x} &= 2Rx\ln\frac{(z^3-a^3)(\bar{z}^3-a^3)}{(z^3+a^3)(\bar{z}^3+a^3)}\\ &- 2iRa\ln(z^3-a^3)(\bar{z}^3-a^3)\\ &+ Ra\ln(z^4+a^3z^3+a^4)(\bar{z}^4+a^3\bar{z}^3+a^4)\end{aligned} \tag{5}$$

We require w_1 to nullify w_0 and $\partial w_0/\partial x$ on the straight line $x = \sqrt{3}/2$, while keeping the moments and deflections on $\theta = \pm\pi/6$ zero.

We could proceed by writing

$$\frac{w_1}{R} = \sum_{n=0}^{\infty}(A_n r^{6n+3} + B_n r^{6n+5})\cos(6n+3)\theta \tag{6}$$

and then determine A_n and B_n so as to nullify w_0 and $\partial w_0/\partial x$ at $x = \sqrt{3}/2$. This, however, would be cumbersome.

Instead, we shall write

$$\frac{w_1}{R} = (Ar^3\cos 3\theta + Br^9\cos 9\theta) + (Cr^3\cos 3\theta + Dr^{11}\cos 9\theta) \tag{7}$$

and demand

[1] Assistant Professor, Department of Mechanics, Rensselaer Polytechnic Institute, Troy, N. Y.

Manuscript received by ASME Applied Mechanics Division, February 4, 1959; final draft received August 6, 1959.

[2] B. D. Aggarwala, "Singularly Loaded Rectilinear Plates—1," *Zeitschrift für angewandte Mathematik und Mechanik*, vol. 34, 1954, pp. 226–237.

Table 1 Deflection w along $y = 0$ in units of $P/16\pi D$

γ	0	0.05	0.1	0.15	0.2	0.25	0.3	0.35	0.4	0.45	0.5	0.55	0.6	0.65	0.7	0.85	0.86	0.866
W	0	0.0003	0.0019	0.0066	0.015	0.0279	0.0453	0.0666	0.0906	0.1146	0.1358	0.1491	0.1420	0.1135	0.0785	0.00165	0.00076	0.0006

$$\int_0^{1/2} w dy = 0 \qquad \text{at } x = \sqrt{3}/2 \tag{8a}$$

$$\int_0^{1/2} \frac{\partial w}{\partial x} dy = 0 \qquad \text{at } x = \sqrt{3}/2 \tag{8b}$$

$$w(\sqrt{3}/2, 0) = \frac{\partial w}{\partial x}(\sqrt{3}/2, 0) = 0 \tag{8c}$$

This gives the equations

$$2.25A + 2.8477B + 2.8125C + 2.610D = .186201$$
$$0.6495A + 0.274B + 0.4872C + 0.2005D = -0.3472$$
$$0.2165A + 0.0866B + 0.1732C - 0.0787D = -0.1049$$
$$A - B + 1.2C - 1.0909D = -0.0654$$

Solving these and substituting in (7), one gets

$$\frac{w_1}{R} = (-1.4277r^3 \cos 3\theta + 0.0301r^9 \cos 9\theta) + (1.1699r^5 \cos 3\theta + 0.0095r^{11} \cos 9\theta) \tag{9}$$

In fact, r is less than unity throughout the region and therefore only the first terms in the two series need be kept.

The central deflection is found to be

$$w_c = (0.003)\frac{P}{D}$$

This compares with the central deflection for a simply supported plate, in which case[3]

$$w_c = (0.0043)\frac{P}{D}$$

The deflection along $y = 0$ is given in Table 1.

[3] S. Timoshenko, "Theory of Plates and Shells," McGraw-Hill Book Company, Inc., New York, N. Y., 1940, p. 295

Simplified Analysis of a Thrust-Augmentation System

K. L. BERGMAN[1]

Von Karman[2] has made some theoretical remarks on thrust augmentation concerning the system shown in Fig. 1 with the omission of the diffuser. The purpose of this note is to show that with a diffuser on the exit larger values of thrust augmentation are possible, and that these values are very sensitive to the secondary nozzle and diffuser efficiencies. Incompressible, one-dimensional flow is assumed.

The thrust-augmentation factor α is defined as the ratio of the thrust produced by the thrust-augmentation system to the thrust produced by the primary jet if it were discharging into the environment with the same mass rate and combustion chamber pressure. Thus, applying the momentum law,

$$\alpha = \frac{V_4\left(1 + \frac{V_2A_2}{V_1A_1} - \frac{V_0V_2A_2}{V_1A_1}\right)}{V_R} \tag{1}$$

where V_4, V_2, V_1, V_0, and V_R are the fluid velocities at the following places, respectively: at exit from the system, at the entrance to the mixing chamber from the secondary nozzle, at entrance to the mixing chamber from the primary nozzle, at entrance to the secondary nozzle, and at the exit from the primary nozzle if it were discharging into the environment. A_1 and A_2 are the primary and secondary jet areas at entrance to the mixing chamber, respectively.

Equation (1) can be reduced to equation (2) by applying conservation of energy, conservation of mass, and the momentum law with shear stress neglected on the mixing chamber walls. The pressure decrease in the secondary nozzle is required to equal the pressure increase in the mixing chamber plus the pressure increase in the diffuser to allow expulsion of the fluid to the environment. Defining $\beta = A_1/A_2$, $\lambda = V_2/V_1$, $\gamma = V_0/V_1$

$$\alpha = \frac{\left(1 + \frac{\lambda}{\beta}\right)\sqrt{\frac{\eta_D\left(\frac{\beta + \lambda}{\beta + 1}\right)^2 + 2\beta\left(\frac{\lambda - 1}{\beta + 1}\right)^2 - \frac{1}{\eta_N}(\lambda^2 - \gamma^2)}{\eta_D}} - \frac{\gamma\lambda}{\beta}}{\sqrt{\frac{\eta_1}{\eta_2} - \frac{\eta_1}{\eta_N}(\lambda^2 - \gamma^2)}} \tag{2}$$

where η_1, η_2, η_D, and η_N are the efficiencies of the following, respectively: primary nozzle when it is discharging into the environment, primary nozzle when it is discharging in the thrust-augmentation system, the diffuser, and the secondary nozzle.

The form of equation (2) suggests the terms under the radical in the numerator could be in a critical balance between the positive terms with η_D and the negative term with η_N. Computation with an electronic computer has shown this to be true. Curves have been calculated for the case $\eta_1 = \eta_2 = 1$, $\gamma = 0$, and $\eta_D =$

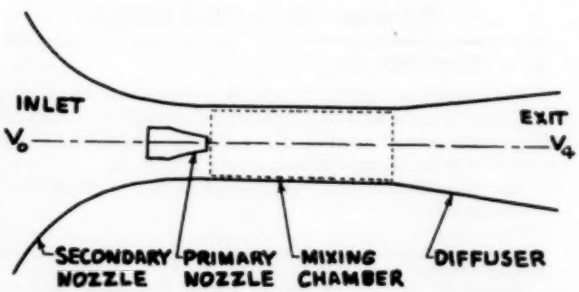

Fig. 1 Thrust-augmentation system

[1] Mechanical Engineer, Aeronautical Research Laboratory, Wright-Patterson Air Force Base, Ohio. Currently, Instructor, Mechanical Engineering Department, The Ohio State University, Columbus, Ohio.

[2] Th. von Karman, "Theoretical Remarks on Thrust Augmentation," Reissner Anniversary Volume, J. W. Edwards, Ann Arbor, Mich., 1949, pp. 461–468.

Manuscript received by ASME Applied Mechanics Division, March 20, 1959; final draft received August 18, 1959.

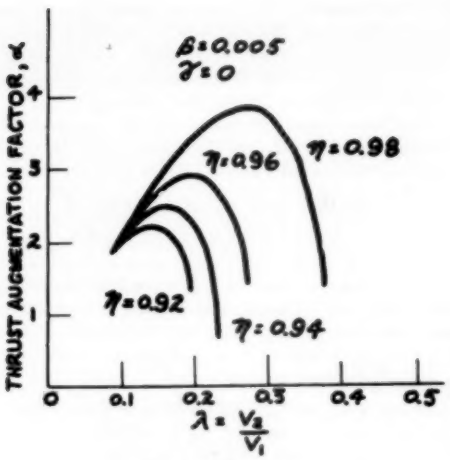

Fig. 2 Sample curves

$\eta_N = \eta$. Shown in Fig. 2 is a sample of the curves. The critical dependence of the thrust-augmentation factor upon η can plainly be seen since a change in η of two per cent produces a significant change in the thrust-augmentation factor.

For

$$\lambda < \frac{1}{1 + \sqrt{\frac{(\beta+1)^2}{2\eta_N\beta}}} \tag{3}$$

the curves in Fig. 2 have been terminated because this is the condition at which the pressure decrease in the secondary nozzle is less than the pressure increase in the mixing chamber plus the pressure increase in the diffuser. Clearly, this situation is physically impossible, and a nozzle rather than a diffuser is required on the exit.

For

$$\lambda = \frac{1}{1 + \sqrt{\frac{(\beta+1)^2}{2\eta_N\beta}}} \tag{4}$$

von Karman's analysis applies, and it is seen that the thrust-augmentation factor is larger to the right of the value of λ given by equation (4). Thus, placing a diffuser on the exit of the system allows the thrust-augmentation factor to be larger than it is otherwise.

Stress Concentration in a Rotating Disk With a Central Hole and Two Additional Symmetrically Located Holes[1]

TA-CHENG KU[2]

THE two-dimensional problem of stresses in a rotating disk with noncentral holes has been investigated photoelastically by Hetényi[3], Newton[4], and Barnhart, et al.[5] An approximate solution, in which the hole is treated as if it were in an infinite region and subjected to biaxial stresses, was used separately in each of the latter two references to verify the experimental results.

The purpose of the present paper is to develop a theoretical solution for the plane-stress problem of a rotating circular disk with a central hole and two additional holes located on the same diameter of the disk and equidistant from the center, Fig. 1. The solution in the present paper is obtained by a convergent combination of stress functions, and the procedure used is parallel to that adopted by Howland in his paper.[6] A numerical example is worked out to make possible a comparison with Hetényi's photoelastic results obtained on a disk with the same dimensions. With minor changes, the solution presented in the following can be adapted to other loading conditions (such as press-fit pressure, internal or external fluid pressure, contact pressure, friction force, and so on) of a disk having the hole system shown in Fig. 1 or other symmetrical hole systems with more than two noncentral holes.

A stress-concentration factor K is defined as the ratio of the circumferential stress σ_ϕ at any point in a rotating disk with the two noncentral holes to the circumferential stress at the inner boundary of a rotating disk with the central hole only. The values of K across a section GHIK are plotted in Fig. 1, where comparison is made between the theoretical solution for Poisson's ratios of $\nu = 0.3$ and $\nu = 0.5$. Fig. 2 shows the comparison between the results obtained by making only one approximation, those obtained by five successive approximations, those from the photoelastic method, and those from the approximate solution. The stress concentration factors by the photoelastic method are calculated from the data given by Hetényi[3] in his

[1] The results presented in this Note are based upon a dissertation submitted by the author to the Graduate Division of the University of California, Berkeley, Calif., in partial fulfillment of the requirements for the degree of Doctor of Philosophy, June, 1953.

[2] International Business Machines Corporation, Products Development Laboratory, Endicott, N. Y.

Manuscript received by ASME Applied Mechanics Division, February 27, 1959.

[3] M. Hetényi, "The Application of Hardening Resins in Three-Dimensional Photoelasticity," *Journal of Applied Physics*, vol. 10, 1939, p. 295.

[4] R. E. Newton, "A Photoelastic Study of Stresses in Rotating Disks," JOURNAL OF APPLIED MECHANICS, vol. 7, TRANS. ASME, vol. 62, 1940, p. 57.

[5] K. E. Barnhart, Jr., A. L. Hale, and J. L. Meriam, "Stresses in Rotating Disks Due to Noncentral Holes," Proceedings of the Society for Experimental Stress Analysis, vol. 9, 1951, p. 35.

[6] R. C. J. Howland, "On the Stresses in the Neighborhood of a Circular Hole in a Strip Under Tension," Transactions, Royal Society of London, series A, vol. 229, 1930, p. 49.

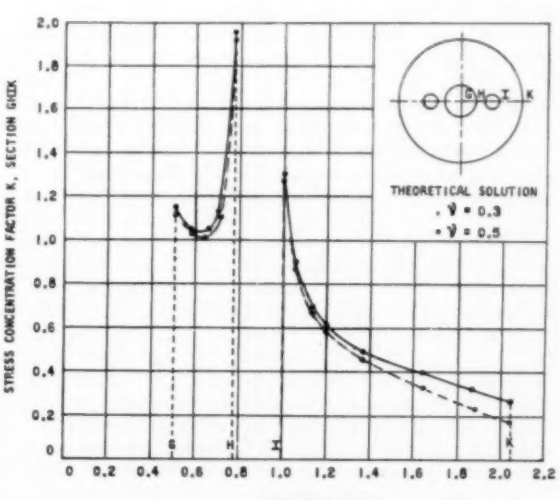

Fig. 1 Values of stress-concentration factor K from theoretical solutions for $\nu = 0.3$ and $\nu = 0.5$

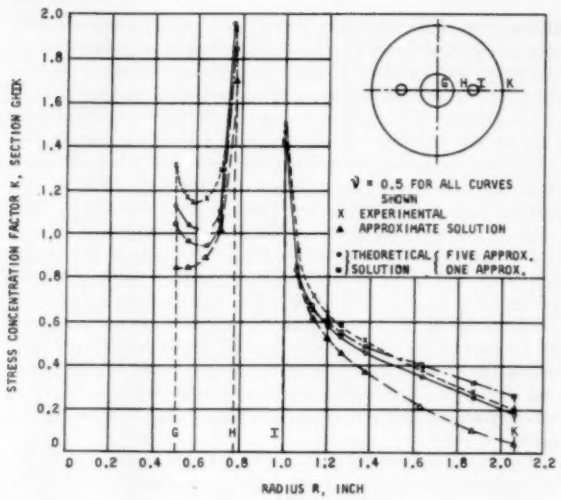

Fig. 2 Comparison of values of stress-concentration factor K from experimental results, approximate and theoretical solutions

Fig. 10. The values from the approximate solution are based on the method proposed by Barnhart, Hale, and Meriam.[5]

From the close agreement of the curves for $\nu = 0.3$ and $\nu = 0.5$ in Fig. 1, it can be seen that the effect of Poisson's ratio is very small and can be neglected for practical purposes.

There is a general good agreement between the theoretical and Hetényi's experimental values of the stress concentration factor K for $\nu = 0.5$ throughout the section GHIK (Fig. 2), except in the region between G and H.

The error due to not proceeding beyond the fifth approximation in the numerical example of this paper is much less than 1 per cent. The error in K max from a single approximation is only 4.65 per cent of K max at point H. The approximate solution by Barnhart, Hale, and Meriam[5] is acceptable in most engineering problems with an expected error in the neighborhood of 11 per cent.

Acknowledgment

The author wishes to express his sincere appreciation of the guidance and criticism received from Professors C. W. Nelson and J. L. Meriam of the University of California at Berkeley, and is indebted to Mr. J. E. Brophy of International Business Machines Corporation, Endicott, N. Y., for many helpful suggestions.

Viscous Damping in Flexural Vibrations of Bars[1]

J. M. McCORMICK, Jr.[2] One of the curves given by the author in his Fig. 2 (that for the upper mode for large damping) appears to be incorrect. The author shows the phase velocity, c_2, decreasing monotonically as the reciprocal of the wave length, $K\mu_2$, increases. Further, the author asserts in the text that "if the range of $K\mu_2$ is extended indefinitely, c_2 tends to zero producing short-wave-length vibration cutoffs." It would seem, however, that while c_2 initially decreases with increasing $K\mu_2$, it eventually reaches a minimum and then increases monotonically and without a bound as $K\mu_2$ increases indefinitely.

That this is so may be seen by a rather simple calculation [putting a wave form with real frequency and complex wave number into the governing differential equation, the author's Equation (7), and solving for the ratio of the frequency to the real part of the wave number as a function of the frequency], but it is perhaps more illuminating to reason qualitatively from consideration of the way in which the viscoelasticity is brought into the problem.

The author has assumed the extensional law to be of the Kelvin type while retaining the elastic law for the shear components. (These two laws are consistent with each other only if they are derivable from three-dimensional stress-strain laws, which must then exhibit viscoelastic compressibility, whereas most recent work in viscoelasticity seems to favor using viscoelastic deviatoric relations with elastic compressibility.) It is thus to be expected that the viscoelastic effects will be evident only where the extensional law substantially influences the behavior. The author's damping curves (Fig. 3) tend to confirm this view.

As the author points out in his introduction, the damping in both modes increases at first with increasing $K\mu_2$, but as the lower mode becomes more and more a pure shear mode, the damping decreases and becomes negligible. The upper mode, however, continues to be influenced strongly by the extensional law and the damping continues to increase with increasing $K\mu_2$. Qualitative predictions can also be made concerning the dispersion curves (Fig. 2). The lower mode becomes essentially a shear mode for large values of $K\mu_2$ and the phase velocity accordingly approaches the velocity of shear waves in an infinite medium. The upper mode, on the other hand, approaches a velocity $[(E/\rho)^{1/2}$ in the elastic case] which depends on the complex modulus, a quantity proportional to the real part of the wave number for Kelvin-type damping. Thus the phase velocity for this mode, with Kelvin-type damping, must increase without limit if $K\mu_2$ is taken large enough, as long as the viscosity is nonzero. The author's curves for the upper mode in Fig. 2 do not indicate behavior of this type; his low damping curve is not extended far enough to tell and his high-damping curve exhibits a quite different behavior.

The author's choice of stress-strain laws was apparently motivated by a desire to obtain damping curves which agree with experimental results, like those for the lower mode in Fig. 3. Accordingly, it is noted that the same behavior for the lower mode, namely, the hump-backed damping curves and the phase velocity approaching c_2 for large values of $K\mu_2$, is obtained if, instead of putting Kelvin damping in the extensional law, one were to put Maxwell-type damping in the shear law. In this case, then, the behavior of the upper mode would also be acceptable. The author's approach, Laplace transform, would probably be unmanageable for Maxwell-type damping and the objection would again have to be made concerning the necessity of viscoelastic compressibility in the three-dimensional laws if the Maxwell-type shear relation and an elastic extensional law are to be consistent. To assume that both laws have standard-solid type behavior seems to be the only simple, physically meaningful representation for the viscoelasticity. Again the Laplace-transform approach would probably be unmanageable mathematically for this type of law.

[1] By M. K. Newman, published in the September, 1959, issue of the JOURNAL OF APPLIED MECHANICS, vol. 26, TRANS. ASME, vol. 81, series E, pp. 367–376.

[2] Institute of Flight Structures, Department of Civil Engineering and Engineering Mechanics, Columbia University, New York, N. Y.

Author's Closure

The solution of the beam equation presented in this paper is written for specified initial and boundary conditions, the excitation chosen being that of a half-period sine wave impact. The response consists of the sum of the transient vibrations and the forced vibrations.

The emphasis in the analysis is on the free vibrations since they represent the really significant part of the boundary-value problem.

The object of the dispersion curves shown in Fig. 2, including the one for large damping, is to exhibit the effect of damping on the free vibrations of the system. This can be done effectively by plotting as a continuous curve the wave velocity of free vibrations as function of a real wave number. The wave velocity of free damped vibrations is simply defined as the product of the frequency of damped free vibrations and the corresponding wave length as given in Equations (38) and (39) of the paper.

Damped frequencies of free vibrations are the imaginary parts of the roots $z_{1,2}$ and $z_{3,4}$ of the quartic equation (36*b*). These roots are defined in Equation (37*a*), where $z_{1,2}$ corresponds to the lower mode of wave motion and $z_{3,4}$ to the upper mode of wave motion.

These so-called frequencies of damped vibrations are not the natural frequencies but form, when plotted as a continuous curve, the locus for the discrete frequency spectrum characteristic of a particular beam. The characteristic values are governed by the boundary conditions and determined as explained in the paper.

The discussion and analysis of the quartic equation (36*b*) for real values of $K\mu_2$ are therefore essentially an analysis of the effects of damping on the frequency response in free vibrations of the system. The terminology used when referring to "short-wave-length vibration cutoffs," or to "frequency cutoffs" means of course "cutoffs of free vibrations."

The object of Fig. 2 and of Fig. 3 thus is to show that, no matter how small the damping is, as long as $\rho_1 > 0$, the upper mode c_2 will eventually reach critical damping as the wave length is diminished indefinitely. This means, of course, that wave velocities of free vibrations, which are the object of this discussion, tend to zero as wave lengths are diminished indefinitely.

It is also to be noted that frequency cutoffs may occur in the case of the wave velocities c_1 of the lower mode of wave motion, provided $\rho_1 \geqslant M_1$. In that case, there will exist a range of wave

numbers $K\mu_2$ for which the damping factor $\beta_1 \geq 1$. In other words, the humpbacked β_1-curve in Fig. 3 may cross the value $\beta_1 = 1$ twice. For the range of values of $K\mu_2$ where $\beta_1 \geq 1$, no free vibrations exist. It was, however, pointed out in the paper that the values of the viscosity coefficients ζ corresponding to values of $\rho_1 < M_1$ cover a very large range of values that can be made to satisfy every conceivably practical condition of damping.

All this is in no way in contradiction to the argument advanced by the discusser. A wave form with real frequency and complex wave number presupposes a forced excitation of the system, When substituted into the governing differential equation (7), wave velocities will be obtained that tend to infinity as the real part of the wave number is allowed to increase indefinitely. The effect of damping, however, is, in this case, completely obscured because the forced frequency response of the viscoelastic system is insensitive to damping, or, in other words, the viscoelastic dispersion curve in forced excitation is the same for all values of damping.

The same result can also be obtained by substituting $p = i\omega$ into Equation (20*a*) of the paper and allowing ω to become very large. The complex wave number μ_1 will then be of the form

$$\mu_1 = \frac{1+i}{\sqrt{2}} \frac{\omega^{1/2}}{c_1 f_i^{1/2}}$$

The wave velocity c_2 which is the ratio of the frequency to the real part of the wave number is then seen to tend to infinity as wave lengths are diminished indefinitely. This can also be seen by noting that the wave velocity c_2 of the upper mode depends on the complex modulus, a quantity proportional to the real part of the wave number for Voigt or Kelvin-type damping.

The choice of extensional viscoelasticity of the Voigt type together with elastic shear components of stress is an approximation made necessary by the fact that viscoelastic damping in shear introduces into the partial differential equations of motion, Equations (5) and (6) of the paper, coupling terms which make it impossible to eliminate the rotational co-ordinate ψ and thus to combine Equations (5) and (6) into one Equation (7).

In viscoelasticity of the Voigt-Kelvin type, the coefficients of viscosity are derived from the three-dimensional stress-strain laws as coefficients of first-order approximations in the time rates of strain. These coefficients of viscosity cannot be expressed in a consistent manner as is the case with the elastic constants for a homogeneous, isotropic, and perfectly elastic solid. This is inherent in the assumption of viscoelasticity.

Nevertheless, viscoelasticity can be looked upon as a reasonable approximation to the processes of dissipation of mechanical energy.

For example, in a specific case, viscous energy dissipation in shear may be negligible when compared to energy dissipation in normal strain. This may happen over a whole band of frequencies where some particular phenomenon such as the thermoelastic effect is to be approximated and where transmission of shearing strain is insignificant.

In addition, it may happen that the phenomenon to be approximated does not extend over that part of the frequency spectrum where the shearing strains transmitted are the predominant part of the wave motion.

The aim in this problem is to devise a viscoelastic model of thermoelastic damping in flexural vibrations of reeds.

In the case of thermoelasticity, the friction arises from temperature relaxation across the reed. Irreversible conversion of mechanical energy into heat appears as internal friction in the range of frequencies where periods of vibrations are comparable with the relaxation time for conduction of heat across a specimen.

In the viscoelastic model, a similar mechanism is used. Friction arises from strain relaxation in extensional viscoelasticity. Dissipation occurs in the region of the frequency spectrum where periods of vibrations are comparable with the time of relaxation of extensional strain.

The governing differential equation (7) of the paper, with damping taken zero, is known to be a good approximation to flexural wave propagation up to the very high frequencies.

The relative content of extensional and shearing strain transmitted by the lower mode of wave motion depends on the wave length or frequency.

In the range of frequencies starting at zero, and where the wave velocities exhibit considerable dispersion, the strains propagated are predominantly extensional. The shearing strains that are transmitted in this range of frequencies are of the order of small corrections. Consequently, neglecting viscoelastic damping in shear in this range can have only small effects even though the coefficient of shear viscosity is not zero.

An approximation to thermoelastic damping in flexure can therefore be obtained by relying entirely on extensional viscoelasticity provided the relaxation period of the strain is properly chosen to fall within the range of frequencies where the extensional strain is the predominant component of the wave.

Beyond this range, as wave lengths diminish still further, this mode tends to become more and more a pure shear mode. Thermoelastic damping in pure shear is zero when steady vibrations are applied.

Very few solids behave in fact, even approximately, like the Voigt or the Maxwell model. For this reason, it has been suggested that the dynamic behavior of materials might be approximated more adequately in terms of a spectrum of relaxation times rather than by a single relaxation time.

In the simpler model described in this paper, advantage is taken of the dispersion characteristics in the lower mode of wave motion of the Timoshenko beam equation in conjunction with a properly chosen single relaxation of extensional strain. The governing differential equation (7) may therefore be considered, in the absence of the coefficient of shear viscosity, as an approximation to thermoelastic damping in flexure which applies in the region of the spectrum where propagation of shearing strain is negligible.

An estimate of the range of validity of this analysis can be established by a comparison of the damping curves, obtained for various materials using extensional relaxation, with the results obtained from thermoelasticity in flexure.

On Supersonic Wind Tunnels With Low Free-Stream Disturbances[1]

THOMAS VREBALOVICH.[2] The author describes clearly the problem of trying to reduce and determine the causes of free-stream disturbances in supersonic wind tunnels. He has much experimental evidence to indicate some of the sources of these disturbances, and describes the manner in which many of these disturbance sources may be eliminated, or at least minimized.

Some of the results of a series of experiments conducted at the Jet Propulsion Laboratory[3] in the 12-in. and 20-in. supersonic

[1] By M. V. Morkovin, published in the September, 1959, issue of the JOURNAL OF APPLIED MECHANICS, vol. 26, TRANS. ASME, vol. 81, series E, pp. 319–324.

[2] Jet Propulsion Laboratory, California Institute of Technology, Pasadena, Calif.

[3] This paper presents the results of one phase of research carried out at the Jet Propulsion Laboratory, California Institute of Technology, under joint sponsorship of the Department of the Army, Ordnance Corps (under Contract No. DA-04-459-Ord 18), and the Department of the Air Force.

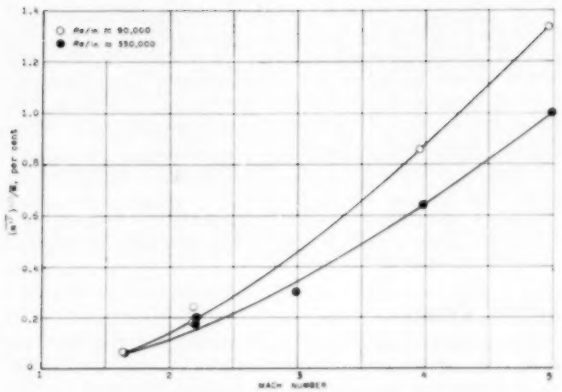

Fig. 1 Mass-flow fluctuations in test section

wind tunnels add proof to the ideas presented in the paper. Other results indicate that our understanding is not complete.

The supply section of the Jet Propulsion Laboratory supersonic wind tunnels has velocity fluctuations of less than 1 per cent at all Mach numbers, and all other fluctuations are small compared to this. Increasing the supply-section turbulence level to about 6 per cent caused the transition Reynolds number to decrease at Mach numbers below 2.5 and had no effect on transition above $M = 2.5$, references [1, 2].[4]

From hot-wire measurements in the test section of these wind tunnels, it is possible to determine the types of fluctuations that are present [3, 4]. The result of the free-stream fluctuation measurements was that the mass-flow fluctuations $(\overline{m'^2})^{1/2}/\bar{m}$ increased with Mach number and with turbulent wall boundary-layer thickness, as can be seen in Fig. 1 of this discussion. In addition, the mass flow and total temperature fluctuations had a minus one correlation coefficient [5, 6]. Sound waves satisfy this rather restrictive condition, and it would seem probable that the turbulent wall boundary layers do radiate sound energy. Assuming then that these fluctuations are sound waves, it is found that the sound intensity $\overline{p'^2}/\bar{p}^2$ is proportional to M^4. Details of these measurements will be found in [6].

Recently it was found possible to operate the 12-in. supersonic wind tunnel at such low supply pressures that the wall boundary layers became laminar. By placing tripping devices upstream of the sonic throat, it was also possible to have a turbulent wall boundary layer at the same pressure level. Preliminary results show that the free-stream fluctuation levels are much smaller when the wall boundary layer is laminar than when it is turbulent. This indicates that the turbulent wall boundary layer in a supersonic wind tunnel is indeed a major source of disturbances in the free stream at high Mach numbers. As was expected, the fully turbulent tripped boundary layer introduced less fluctuations into the wind-tunnel free stream than the case in which transition from laminar to turbulent wall boundary layer occurred between the sonic throat and the test section of the tunnel. Further work is being done in order to determine the source of the fluctuations when the wall boundary layers are laminar.

Obviously it is difficult to reduce any fluctuations originating from the turbulent wall boundary layers; but the large amplitude of these fluctuations at the higher Mach numbers may have significant effects on supersonic wind-tunnel model testing and should be investigated. The author's suggestions for reducing disturbance levels and their effects in wind tunnels should be considered as part of good supersonic wind-tunnel design.

[4] Numbers in brackets designate References at end of this discussion.

References

1 J. Laufer and J. Marte, "Results and a Critical Discussion of Transition-Reynolds-Number Measurements on Insulated Cones and Flat Plates in Supersonic Wind Tunnels," Report No. 20-96, Jet Propulsion Laboratory, California Institute of Technology, November 30, 1955.

2 J. Laufer, "Factors Affecting Transition Reynolds Numbers on Models in Supersonic Wind Tunnels," Readers' Forum, *Journal of the Aeronautical Sciences*, vol. 21, 1954, pp. 497–498.

3 L. S. G. Kovasznay, "Turbulence in Supersonic Flow," *Journal of the Aeronautical Sciences*, vol. 20, 1953, pp. 657–674.

4 M. V. Morkovin, "Fluctuations and Hot-Wire Anemometry in Compressible Flows," AGARDograph No. 24, NATO, November, 1956, p. 102.

5 J. Laufer and T. Vrebalovich, "Stability of a Supersonic Laminar Boundary Layer on a Flat Plate," Report No. 20-116, Jet Propulsion Laboratory, California Institute of Technology, December, 1958.

6 J. Laufer, "Aerodynamic Noise in Supersonic Wind Tunnels," Progress Report No. 20-378, Jet Propulsion Laboratory, California Institute of Technology, May, 1959.

Author's Closure

The author wishes to thank Dr. Vrebalovich for his most informative discussion. In fact, his and Dr. Laufer's delicate experimentation provide the most complete and consistent source of information on disturbances in supersonic wind tunnels, keeping in mind that their tunnels belong to an "aristocratic" class in that they are extraordinarily smooth and aerodynamically clean.

The reported experiment in which the only "external" change was in the nature of the tunnel-wall boundary layer proves conclusively that at higher Mach numbers even in their smooth facility the aerodynamic sound from the wall layer is a dominant source of free-stream disturbances. The details of their measurements (discusser's Ref. [6]) indicate that in their tunnel the sound waves appear to be generated by pressure sources moving along the tunnel walls with 40 to 50 per cent of free-stream velocity. Although the source velocity is rather low, the presence of relative motion identifies this sound as primarily of Lighthill type. Actually, the experiment of Fig. 13 of same reference suggests that the hot wire may not resolve well enough the signals from a superposition of moving sound waves and shivering Mach waves so that the measurements in question may well correspond to Lighthill sources traveling with *higher* speed together with a smaller contribution from nonmoving shivering waves. In less clean facilities the contribution from the nonmoving waves is larger and often dominates.

Whatever the actual distribution of the types of sound, Vrebalovich's Fig. 1 indicates that the net sound level increases as the wall boundary layer thickens. This finding suggests that, for smooth walls, lengthening of the nozzle and test section would not help to decrease the free-stream sound disturbances even though the mean shear in the boundary layer would be less.

Since the publication of the original paper, the author has had some queries about "free-stream" disturbances in shock tubes which are erroneously assumed to be absent because the conditions ahead of the shock are indeed very uniform. The nonuniformities here come from two sources of sound, one being again the wall boundary layer growing behind the moving shock. Except for the difference in the boundary-layer profiles, most of the comments of the paper on the various types of generated sound are applicable. The second source is a tail of the Mach Y reflection of the original nonplane "explosive" shock. As the shock straightens and proceeds down tube, this tail becomes increasingly more lateral and bounces back and forth from the sides of the tube, while keeping an umbilical connection to the principal shock.

Since the original paper was written in 1946, interest has shifted toward *hot* supersonic wind tunnels in which the nonuniformities in the settling chamber are again likely to be the major offenders. To the author's knowledge, no one as yet has measured the steady and unsteady disturbances in either the settling chamber or the test section of a hot facility. Without such information, the precautions counseled in the paper remain as the main guide for design or improvement of such a facility. However, the low-speed study of Mills and Corrsin[5] (Fig. 11) furnish some experimental information on decay of temperature-density-entropy disturbances relevant to the conditions in the settling chamber and associated ducts in supersonic tunnels. These authors found no effect of density spottiness upon the turbulence dynamics when the flow was accelerated from 14 ft/sec to 56 ft/sec, as one would expect at these "incompressible" speeds and low density changes. By contrast, Rudinger and Somers[6] observe experimentally and calculate approximately the buoyancy effects of accelerated, isolated density spots produced by a spark discharge. The application of these lessons to nonisolated density spots produced by differential heating in hot supersonic tunnels as they are accelerated through the nozzle has yet to be made. This interaction may have been negligible for cold supersonic tunnels, as the original paper suggests, but should definitely be examined as an additional source of sound and vorticity for hot supersonic tunnels.

In the hot tunnels, the location of transition from laminar to turbulent boundary layer again assumes increased importance. Many a design depends critically on local heat-transfer rates which may reach a maximum in the transition region. Besides this important though indirect influence of free-stream disturbances, the high level of random pressure fluctuations (sound of all types) is likely to affect directly the mechanical abrasion of materials in hot facilities. It is very probable that ablation of re-entry vehicles is less than would be indicated in hot facilities such as rocket exhausts, arc jets, etc., because of the absence of the free-stream "differential pounding and scrubbing" in flight.

The Determination of Safe Loads of Beams Subjected to Combined Twisting and Biaxial Bending Moments[1]

L. E. MALVERN.[2] The authors are to be congratulated for their excellent contribution to the literature on limit analysis. The writer would like to raise one question and make a few comments. Would it be difficult to extend this work to cross sections more common in structures than the square cross section considered? In practice, of course, a designer would have to be more cautious about lateral instability of members subjected to bending and twist, if thinner sections were used. However, it would not seem too difficult to make the plastic-limit analysis, even though the bending interaction curve would be more complicated.

It was tacitly assumed that the areas on the two sides of the curve $y = f(x)$ in Fig. 1 were equal, in order that the resultant of the axial stress would be merely a couple, which could be evaluated by taking moments about the co-ordinate axes. Fortunately, the optimum curve $f(x) = -\lambda x$ satisfies this condition, though no such restriction was put on admissible functions $f(x)$.

If the Mises condition were used instead of the Tresca, as suggested in footnote 3 of the paper, the expression for T_0 in Equation (5*b*) would also be different.

A factor t was omitted in the last term of the formula for D_i given at the end of p. 443 of the paper.

It is not clear from the statement of the example that the force P acts in a plane parallel to the yz-plane, although the solution evidently assumes that it does.

Authors' Closure

The authors would like to thank Professor Malvern for his comments and questions. It should be reasonably straightforward to find the interaction curve for biaxial bending for any section and then to find bounds on the interaction surface when twist is present. As long as the resulting surface can reasonably be approximated by the same or fewer number of planes, the resulting analysis of a problem would be no more difficult.

It is intuitively evident that the maximum resistance to bending will be accompanied by zero axial force, hence no explicit mention of this requirement was made. If appreciable net axial force is present it can, of course, be treated by imposing an additional condition. In the example, since axial force is not considered, any component of P in the x-direction would be ignored.

Finally, the authors apologize for the two misprints and thank the discusser for pointing them out.

Determination of the Creep Deflection of a Rivet in Double Shear[1]

J. E. GRIFFITH.[2] The comments by the writer are offered for constructive purposes only. A number of intricate effects are involved which may require close examination before application is made of the author's creep-deflection equation.

First, the inflection point is determined from a moment diagram based on an assumed uniform load, uniform support, and end moments applied to the rivet. Certainly the inflection points and the resulting deflections based on this assumed loading condition are valid. However, the bearing stresses between the plates and the rivet are complex and involve the properties of the plates as well as the rivet. In a practical case, the actual loading on the rivet may be quite different from that illustrated by the author. In fact, concentrated loads would appear to be a closer approximation to the initial loading pattern between rivet and plates. With the progress of time these loads tend to become distributed and approach as a limit the uniform load condition employed by the author. Thus the load pattern is a function of time and the creep deflection thereby is dependent on this function.

Another important consideration is the effect of highly localized stresses. For short beams, these stresses produce large localized strains which in turn affect the deflection. In addition, such localized stresses in the inelastic range of the material may produce a discontinuous neutral plane which forms the deflection curve. Therefore a restriction of the theory might be provided by defining a range of ratio values of $L/_D$, rivet half-length to rivet

[5] R. R. Mills and S. Corrsin, "Effect of a Contraction on Turbulence and Temperature Fluctuations Generated by a Warm Grid," NASA Memo 5-5-59W, May, 1959.

[6] G. Rudinger and L. Somers, "Behavior of Small Regions of Different Gases Carried in Accelerated Gas Flows," Cornell Aero Lab Rept. 76-P, March, 1958.

[1] By P. G. Hodge, Jr., and R. Sankaranarayanan, published in the September, 1959, issue of the JOURNAL OF APPLIED MECHANICS, vol. 26, TRANS. ASME, vol. 81, series E, pp. 442–447.

[2] Professor of Applied Mechanics, Michigan State University, East Lansing, Mich.

[1] By Joseph Marin, published in the June, 1959, issue of the JOURNAL OF APPLIED MECHANICS, vol. 26, TRANS. ASME, vol. 81, series E, pp. 285–290.

[2] Assistant Professor of Engineering Mechanics, University of Florida, Gainesville, Fla. Assoc. Mem. ASME.

diameter, for which the analysis is valid. Some principle might be employed for the inelastic range which would determine the regions of the rivet where end effects are negligible (similar to Saint Venant's principle in the theory of elasticity).

Imposing the condition of plane sections produced by an applied bending moment, which has been verified for many materials in the inelastic range, does not necessarily imply similar material behavior in tension and compression. This dissimilarity also may be exhibited in the stress relaxation which occurs in the outer portions. These dissimilarities will shift the neutral axis. For large deflections, however, this shift is probably of negligible magnitude.

A reader of this interesting paper becomes aware of the complexity of inelastic problems. Assumptions, which are sometimes questionable, and approximations are usually needed to solve a practical problem. Even for elastic theory many problems involving connections remain to be solved. The author has provided a reasonable approach for determining the creep deflection of a rivet and perhaps for solving many other practical engineering problems concerned with inelastic behavior.

Author's Closure

The author appreciates the comments by Prof. Griffith regarding the complexities of the problem considered. It should be noted, however, that in order to obtain an engineering answer, assumptions of the nature made in the paper are necessary. There are many other assumptions involved in such a problem as the one considered, which may lead to greater error than the ones noted by Prof. Griffith.

Production of Rotation in a Confined Liquid Through Translational Motion of the Boundaries[1]

E. W. GRAHAM.[2] This paper presents an interesting analogy between the motion of a conical pendulum and the motion of liquid in a circular cylindrical tank. In this analogy the rotary motion of the conical pendulum is compared to the rotary motion of the CG (center of gravity) of the liquid about the axis of the tank.

This analogy says nothing directly about rotational motions of the liquid (rotation of the liquid particles as distinguished from a rotary motion of the CG of the liquid). The rotary motion of the CG about the axis does not necessarily imply rotation of the liquid particles. For example, if the amplitudes are small the rotary motion of the CG can be produced by the superposition of two properly phased oscillatory motions lying (essentially) in planes at right angles to each other. These oscillatory motions may be individually (vanishing viscosity is assumed) irrotational and, if so, their sum is irrotational. If the amplitudes are large it is still possible theoretically to obtain a rotary motion of the CG of the liquid without rotation of the liquid particles.

At this point it is not clear why the author introduces a vortex into the liquid to produce rotational kinetic energy and angular momentum for comparison with the pendulum. Such energy and momentum are already theoretically available in the irrotationally moving liquid just as in the pendulum, and that is the analogy. If a vortex is introduced into the liquid then the corresponding feature in the pendulum would probably be a rotation of the pendulum mass about its own axis.

It may well be that rotary motion of the CG of the liquid produces rotation of the liquid particles, but this relationship has not been established quantitatively. Possibly it might be necessary to go to the walls of the cylindrical tank to see how rotation of the liquid particles is actually generated. It is believed that the explanation of some such mechanism was the stated purpose of the paper, although the author's use of the word "rotation" makes this uncertain.

G. E. RANSLEBEN, JR.,[3] **AND H. N. ABRAMSON.**[4] According to the results given in the paper, a tank with a fluid depth-to-diameter ratio of 1.0 and an excitation amplitude-to-diameter ratio of 0.0083 (which corresponds to a peak-to-peak amplitude of 0.2 in. in Fig. 2 of the paper) should exhibit rotational fluid motions for frequencies in the range $0.94\omega_b < \omega < 1.22\omega_b$. The larger value is reduced to $1.16\omega_b$ if the conical pendulum boundary is employed. In a rather extensive series of experiments, we have consistently been able to narrow the range of frequencies resulting in rotational fluid motions to $0.97\omega_b < \omega < 1.04\omega_b$. This was accomplished by approaching the resonant frequency from both above and below very slowly and carefully, and by our fortunate circumstance of possessing a test facility in which all components are very carefully aligned and in which the excitation is a sinusoid of high quality. We have had equally good results with a tank of considerably larger size. Consequently, in addition to the implications regarding the effects of viscosity given by the author in his Conclusions, we should like to emphasize that the stability boundaries will be greatly influenced by the mechanical design of the test equipment and the resulting quality of the translational motion. The implications for prediction of "in-flight" characteristics are obvious.

We also would like to point out that for a 1.0-ft-diam tank the fundamental resonant frequency is 1.73 cps, whereas the author gives the maximum driving frequency attainable with his equipment as only 1.2 cps. The latter figure must be incorrect.

Author's Closure

The author thanks Messrs. Graham, Ransleben, and Abramson for their comments on his paper. The 1.2 cps figure challenged by the latter two is indeed an error.

Concerning the point raised by Graham as to the necessity of introducing a vortex into the liquid to produce angular momentum, the author does not agree that such momentum can be produced by the superposition of two properly phased oscillatory motions lying in planes at right angles to each other. Since each wave by itself contains no angular momentum, the superposition cannot create any such momentum. The analogy in this case is with two linear pendulums swinging at right angles and 90 deg out of phase. Then the CG will rotate about the center line but there will be no angular momentum associated with the motion of this mathematical point. For a conical pendulum there will, of course, be angular momentum, and it is for this reason that a vortex has to be added to the linear wave motion to carry this momentum.

The author had previously examined the question of the importance of the walls in producing the observed rotation and does not believe they are responsible for the phenomenon. Some rotation could be produced in a single oscillation and the only place where the viscous stresses are of sufficient magnitude for this is at the vortex core, where the velocity gradients approach infinity.

[1] By R. R. Berlot, published in the December, 1959, issue of the JOURNAL OF APPLIED MECHANICS, vol. 26, TRANS. ASME, vol. 81, series E, pp. 513–516.

[2] Shaw Island, Wash.

[3] Senior Research Engineer, Department of Applied Mechanics, Southwest Research Institute, San Antonio, Tex.

[4] Director, Department of Applied Mechanics, Southwest Research Institute, San Antonio, Tex. Mem. ASME.

The author congratulates Messrs. Ransleben and Abramson on the quality of their equipment and hopes that, by publishing their results, they will make their tantalizingly obvious implications for predicting "in-flight" characteristics even more obvious.

Transient Analysis of Stress-Wave Penetration in Plates[1]

K. B. BROBERG.[2] The analysis carried out by the author is quite interesting and shows the advantage of Cagniard's method, which enables solution of rather complicated boundary-value problems in dynamic elasticity. The first part of the paper, which deals with load-time functions not specified, seems to be correct, whereas in the second part, where particular cases are studied, a delta-function singularity has been omitted. It is the writer's opinion that this delta function is essential for the conclusions of the possibility of spalling in the plate. On the other hand, the inclusion of the delta function does not change the author's numerical results for the nonsingular parts of the stress waves.

When comparing equations (48), (50), and (51) in the paper, it is evident that the function

$$f(t(0))\delta(t - t(0))$$

should be added to equations (50) and (51). This means, for instance, a delta-function singularity in the front of the waves shown in Fig. 5 of the paper.

The physical meaning of this delta function is somewhat obscure. The writer believes that an understanding of such a singularity in this case is achieved either by widening the front of the load-time relation or by widening the area of application of the load. Let us study these two cases for a step-pulse input and a semi-infinite solid.

Widening of the Front of the Load-Time Relation. For a step pulse input

$$P(t) = P_0 H(t)$$

where $H(t)$ is the unit step function, we obtain on the line of symmetry of the semi-infinite solid, $z \geq 0$, the following expression:

$$\frac{2\pi z^2}{P_0}\sigma_z = -\delta(\tau - 1) - H(\tau - 1)\frac{d}{d\tau}Q(\tau) + H\left(\tau - \frac{1}{k}\right)\frac{d}{d\tau}R(\tau) \quad (1)$$

where

$$\tau = c_d t/z$$

(c_d = velocity of irrotational waves)

$$k = c_r/c_d$$

(c_r = velocity of equivoluminal waves)

$$Q(\tau) = \frac{\tau\left(\tau^2 + \frac{1}{2k^2} - 1\right)^2}{\left(\tau^2 - \frac{1}{2k^2}\right)^2 - \tau(\tau^2 - 1)\left(\tau^2 + \frac{1}{k^2} - 1\right)^{1/2}}$$

and

$$R(\tau) = \frac{\tau^2\left(\tau^2 - \frac{1}{k^2}\right)\left(\tau^2 - \frac{1}{k^2} + 1\right)^{1/2}}{\left(\tau^2 - \frac{1}{2k^2}\right)^2 - \tau\left(\tau^2 - \frac{1}{k^2}\right)\left(\tau^2 - \frac{1}{k^2}\right)^{1/2} + 1}$$

This is in agreement with the author's results (although in a different form) after the delta function has been included.

If now the input is changed to

$$P(t) = \begin{cases} 0 & t < 0 \\ qt & 0 < t > \Delta t \\ q\Delta t & \Delta t < t \end{cases}$$

the response obviously will be

$$\frac{2\pi c_d z}{q}\sigma_z = -H(\tau - 1)Q(\tau) - H(\tau - \Delta\tau - 1)Q(\tau - \Delta\tau) + H\left(\tau - \frac{1}{k}\right)R(\tau) - H\left(\tau - \Delta\tau - \frac{1}{k}\right)R(\tau - \Delta\tau)$$

where

$$\Delta\tau = \frac{c_d \Delta t}{z}.$$

Comparing this equation with equation (2) we detect that the part of the stress wave that corresponds to the delta function is approximately when $\Delta t \ll z/c_d$

$$\frac{2\pi c_d z}{P_0}\sigma_z = -\frac{H\left(t - \frac{z}{c_d}\right) - H\left(t - \Delta t - \frac{z}{c_d}\right)}{\Delta t} \quad (2)$$

if $q\Delta t = P_0$. This means a compressive rectangular stress wave, the amplitude of which decreases like $1/z$ and the duration of which is constant $= \Delta t$.

Widening the Area of Application of the Load. Instead of the point load, characterized by the function

$$A(r) = \frac{\delta(r)}{\pi r} \quad (3)$$

we change to

$$A(r) = \frac{r_0}{2\pi(r^2 + r_0^2)^{3/2}} \quad (4)$$

which means that the load is essentially spread over a circular area of radius r_0 [when $r_0 \to 0$, equation (4) $\to$ equation (3)]. Then making use of the relation

$$\int_0^\infty \frac{r r_0}{2\pi(r^2 + r_0^2)^{3/2}} J_0(\gamma r)dr = e^{-\gamma r_0}$$

we can use the author's method of calculating σ_z. The result shows that the part of σ_z that corresponds to the delta function in equation (1) of this discussion will be, approximately, for $(c_d t/z) - 1 \ll 1$:

$$\frac{2\pi}{P_0}\sigma_z = -H(\tau - 1)\frac{r_0}{[c_d^2 t^2 - z^2 + r_0^2]^{3/2}}$$

Writing $\rho_0 = r/z$ and $\sigma_0 = P_0/2\pi r_0^2$, we obtain for $\tau - 1 \ll 1$:

$$\sigma_z = -\sigma_0 \frac{1}{\left[\left(\frac{\tau - 1}{\rho_0}\right)^2 + \frac{2}{\rho_0}\left(\frac{\tau - 1}{\rho_0}\right) + 1\right]^{3/2}} \quad (5)$$

[1] By Norman Davids, published in the December, 1959, issue of the JOURNAL OF APPLIED MECHANICS, vol. 26, TRANS. ASME, vol. 81, series E, pp. 651–660.

[2] The Royal Institute of Technology, Stockholm, Sweden.

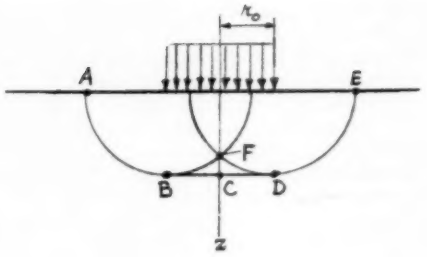

Fig. 1

We observe that $\sigma_z = -\sigma_0$ for $\tau = 1 + 0$ and that σ_z has decreased to $\sigma_0/2\sqrt{2}$ when $\tau - 1 \approx \rho_0^2/2$; i.e., the "duration" of this part of the stress waves is approximately equal to $r_0^2/2c_d z$.

The two different methods to avoid the delta-function singularity thus give different results: Widening of the front of the load-time relation gives a pulse with constant duration and an amplitude that decreases like $1/z$, whereas widening of the area of application gives a pulse with a constant amplitude and a duration that decreases like $1/z$. It may be observed that the character of the later pulse can be interpreted without complicated analysis (this fact has been pointed out to the writer by Prof. J. S. Rinehart). Consider a step-pulse input, producing uniform stress $-\sigma_0$ inside a circular area with radius r_0 as shown in Fig. 1 of this discussion. A simple geometric construction shows the wave front A-B-C-D-E at a certain time. In the region B-C-D-F-B there exists a plane wave with the stress $\sigma_z = -\sigma_0$ and a duration (at the z-axis) which is approximately $r_0^2/2c_d z$ for $z \gg r_0$.

In a real material short pulses with very high stress amplitude cannot exist, and other mechanisms than the afore-mentioned will also be responsible for widening of the delta function. Assuming that in any case the product of the duration and the stress amplitude decreases like $1/z$, the important question regards how "dangerous" such a short pulse is, when it has been converted into a tensile-stress pulse after reflection at a free surface. At a certain position, the impulse is known, whereas there can be some doubt as regards the amplitude and the duration. In the absence of experimental data of fracturing produced by very short pulses, it can be interesting to study the initiation of yielding by pulses of the same impulse but different duration. Then data, obtained by Clark and Wood[3] for mild steel, indicate that the pulse will be less dangerous when its duration increases. This fact indicates that short pulse peaks cannot be neglected in studies of spalling, at least not without further investigation about the fracture behavior for such pulses.

Finally, it may be noted that delta-function singularities also occur for the displacements in a plate when the pulse input is a delta function. This fact has been studied theoretically and experimentally by the writer in a recent paper.[4]

Author's[5] Closure

The author thanks Prof. Broberg for correctly pointing out the role of the δ-function and feels that his calculations on the widened time front and area substantially extend our understanding about this problem. One of the issues that have been raised, and which is implied in the use of the δ-function idealization, is how sensitive the wave is to slight changes of distribution near the source. This would be essentially the question of extending Saint Venant's principle (which postulates static equilibrium) to dynamic conditions. One can attack this problem by extending Boussinesq's method of replacing the infinite stress (and displacement) of a concentrated load by a small, statically equivalent hemisphere cut out of the material. The extension in question, which can be shown to reduce to the Boussinesq solution as the radius or the time tends to zero, is built up from solutions to the Pochhammer equations in spherical co-ordinates of orders $n = 1$ and $n = 0$:

$$\Delta = \gamma_1^2 A_0 h_0(i\gamma_1 R) + \gamma_1^2 A_1 h_1(i\gamma_1 R)\cos\theta \qquad (1a)$$

$$\omega_\phi = \gamma_2^2 B_0 h_0(i\gamma_2 R)(1 - \cos\theta)/2\sin\theta - \gamma_2^2 B_1 h_1(i\gamma_2 R)(\sin\theta)/2 \qquad (1b)$$

where R, θ are spherical polar co-ordinates, Δ the dilatation, ω_ϕ a component of the rotation, h_i the spherical Hankel functions, and the remaining symbols defined as in the paper. The term containing B_0 is a distortion wave of exceptional type, since the θ-factor is not of the form $dP_0/d\theta$. However, it plays its part in providing the additional independent function needed to construct the proper boundary stresses. When the coefficients are chosen as

$$A_1 = iP/2\pi(\lambda + \mu) \qquad A_0 = i\gamma_1 A_1/2\gamma_2$$

$$B_1 = \gamma_2^2 A_1/\gamma_1^2 \qquad B_0 = -iA_1/2$$

all terms in the stresses containing R^{-2} and R^{-4} vanish close to the origin, and the resulting stresses are given by

$$\sigma_{RR} \sim -iA_1[\mu - (3\lambda + 4\mu)\cos\theta]/R^3$$

$$\sigma_{\theta\theta} \sim -i\mu A_1[\cos\theta - 1 + (1 - \cos\theta)/\sin^2\theta]/R^2$$

$$\sigma_{R\theta} \sim -i\mu A_1[\sin\theta + (\cos\theta - 1)/\sin\theta]/R^2$$

$$\sigma_{\phi\phi} \sim -i\mu A_1[\cos\theta + (\cos\theta - 1)/\sin^2\theta]/R^3$$

which are precisely in agreement with the stresses given by Boussinesq (see, e.g., Timoshenko and Goodier, "Theory of Elasticity," pp. 362–365) when converted to spherical co-ordinates.

The construction of this wave implies physically that the resulting stress is insensitive to the small area over which the stress is distributed—but after some time interval has passed. This qualification unfortunately affects the transient zone between the dilatation and distortion fronts. Here the inverse Laplace transform of equation (1) leads to δ-function fronts in some of the stress components, all of which decay as $1/R$, as well as step-function fronts decaying as $1/R^3$. This is in accordance with Broberg's comments also.

The work described here is under further study.

[3] D. S. Clark and D. S. Wood, "The Time Delay for the Initiation of Plastic Deformation at Rapidly Applied Constant Stress," *Proceedings of the American Society for Testing Materials*, vol. 49, 1949, p. 717.

[4] K. B. Broberg, "A Problem on Stress Waves in an Infinite Elastic Plate," *Transactions*, The Royal Institute of Technology, Stockholm, Sweden, 1959.

[5] Department of Engineering Mechanics, The Pennsylvania State University.

The Drag on Spheres and Cylinders in a Stream of Dust-Laden Air[1]

A. R. KRIEBEL.[2] As the authors state, the drag force on targets due to suspended particles is of current interest and ap-

[1] By Thomas Gillespie and A. W. Gunter, published in the December, 1959, issue of the JOURNAL OF APPLIED MECHANICS, vol. 26, TRANS. ASME, vol. 81, series E, pp. 584–586.

[2] Mechanical Engineer, Physics Department, Stanford Research Institute, Menlo Park, Cal.

parently has received little previous study. Work similar to that of the authors is mentioned in reference [1][2] of this discussion, however, and a project has been initiated at SRI with the sponsorship of the Defense Atomic Support Agency, Department of Defense, which includes detailed investigation of the pressure distribution about a cylinder in a heavily dust-laden air stream.

The authors appear to have assumed that in their tests the suspended particles had the same vertical velocity into the test section as the air stream. This assumption is criticized as follows: The terminal velocity of a spherical particle (for free fall with gravity through a fluid where drag force is equal to weight) is given by

$$V^2 = \frac{4g\rho_p d}{3\rho C}$$

where

V = particle terminal velocity (relative to air)
ρ_p = particle density = 2.5 gm/cc for glass
ρ = air density = 0.0765 pcf
d = particle diameter
C = particle drag coefficient
g = acceleration of gravity = 32.2 ft/sec^2

To make use of measured values of C, reference [2] suggests rearranging the equation to be

$$C\left(\frac{\rho V d}{\mu}\right)^2 = C\mathbf{R}^2 = \frac{4g\rho\rho_p d^3}{3\mu^2} = x$$

where

$\mathbf{R}$ = Reynolds number
μ = air viscosity = 3.72×10^{-7} slug/ft-sec

By plotting x versus $\mathbf{R}$, $\mathbf{R}$ (and V) then may be found for a given value of x. From such a plot based on data from [3] and [4], for $1.5 < \mathbf{R} < 500$

$$\mathbf{R} = \left(\frac{x}{20}\right)^{5/7} \pm 15 \text{ per cent}$$

Thus, within the indicated range of Reynolds number and accuracy, the terminal velocity may be found simply from the foregoing equation, which when rearranged gives

$$V = \left(\frac{\rho d}{\mu}\right)^{3/7}\left(\frac{\rho_p d g}{15\rho}\right)^{5/7}$$

For glass beads in air

$$V - \frac{\text{ft}}{\text{sec}} = 0.765\left(\frac{d - \text{microns}}{47.6}\right)^{5/7}$$

and

$$\mathbf{R} = \frac{d - \text{microns}}{47.6} \times V - \frac{\text{ft}}{\text{sec}}$$

For the conditions indicated in the authors' Fig. 5 (Table 1, herewith) U_p is the upward velocity of the particle in the air-stream which moves upward with velocity U_a = 426 cm/sec ($U_p = U_a - V$).

Table 1

d, microns	V, fps	R	V, cm/sec	U_p, cm/sec
470	10.4	10.3	317	109
155	2.9	9.6	89	337
55	0.9	1.1	27	399

The total force on their targets correlated with the authors' equation (1), "provided that the two-phase density ρ^*, is used for ρ," and "there were no particle size effects" on the measured force. Thus the target drag coefficient for each phase (C_{Da} for air and C_{Dp} for particles) apparently was equal to that for a fluid with the same total density. However, for these conclusions C_{Dp} is based on the air velocity U_a.

If C_{Dp} is based on the actual particle velocity in the free stream, U_p, there is a marked effect of particle size on C_{Dp}, and $C_{Dp} > C_{Da}$. The ratio C_{Dp}/C_{Da} is then proportional to $(U_a/U_p)^2$ for Fig. 5 as follows:

d, microns	C_{Dp}/C_{Da}
470	15
155	1.6
55	1.1

The fact that C_{Dp} for the 470-micron particles is unreasonably large indicates that the actual value of V was less than calculated in the foregoing (possibly due to free-stream turbulence or mutual interaction of particles). Nevertheless, it does not appear reasonable to neglect V in interpreting the test results.

The conclusions of the authors (that drag force can be calculated for dust-laden air by replacing ρ by ρ^* and neglecting the effect of particle size) can be made only under the identical test conditions used by the authors (upward flow, velocity range, particle-size range, target size, and so on.) In fact, their results indicate that these conclusions cannot hold under other conditions. It is suggested that some of their tests should be repeated with flow downward through the test section to determine the effect of terminal velocity V.

Since the authors do not state what the particle size was, except in Fig. 5, it is not possible to judge the importance of V in the remainder of their tests. Since they also do not give the diameters of their target cylinder and sphere, the customary inertia parameter [5] cannot be calculated. However, the targets appear to be small enough (and the particles large enough) that particles probably impinged on the targets without appreciable deceleration or deflection by the air stream before impingement (judging from the results of [5]). Furthermore, the effect of radial variation of free-stream velocity and/or particle distribution during their tests is not discussed by the authors.

Thus the interesting but inconclusive results reported by the authors indicate a need for further study of the flow of heavily dust-laden air over bluff bodies to determine drag force during specific conditions.

References

1 J. R. Bannister, "Particulate Dynamic Research at Sandia Laboratory," 6th Midwestern Conference on Fluid Mechanics, University of Texas, September, 1959.

2 J. H. Perry, Editor, "Chemical Engineers Handbook," McGraw-Hill Book Company, Inc., New York, N. Y., third edition, 1950.

3 I. Langmuir and K. B. Blodgett, "A Mathematical Investigation of Water Droplet Trajectories," Technical Report No. 5418 Air Material Command, AAF, February, 1956.

4 G. C. Williams, "Heat Transfer, Mass Transfer, and Friction for Spheres," ScD Thesis, Massachusetts Institute of Technology, 1942.

5 R. J. Brun, Lewis, Perkins, and Serafine, "Impingement of Cloud Droplets on a Cylinder and Procedure for Measuring Liquid-Water Content and Droplet Sizes in Super-Cooled Clouds by a Rotating Multicylinder Method," NACA Report 1215, 1955.

Authors' Closure

The possibility of a significant difference between U_p and U_a

[2] Numbers in brackets designate References at end of discussion.

is of importance in analyzing the data in Fig. 5 and makes the conclusion that there were no particle size effects doubtful. All of the other data presented were obtained using 55-micron particles at relatively high air velocities. For these, the difference between U_a and the calculated value of U_p is too small to affect the results significantly.

One cannot calculate the ratio D_{D_p}/C_{D_a} as indicated because the dust-concentration values given in Fig. 5 would be incorrect if U_a/U_p is much greater than unity. The dust concentration was determined by dividing the measured value for the dust flow in gms/sec by the quantity of air pushed through the tube per sec. To be correct, each value should be multiplied by U_a/U_p. Taking this factor into account, the values of D_{D_p}/D_{D_a} calculated by assuming there are no particle interaction effects would be as follows:

d (microns)	C_{D_p}/C_{D_a}
470	3.8
155	1.26
55	1.03

U_p for the 470 micron particles must be about one quarter of the theoretical value for dust-free air or there is some particle size effect or some experimental error. Repeat experiments in which U_p is measured are needed.

The Reynolds number for flow in the tube leading to the sensing unit was always greater than 4000. This would indicate that it would not be necessary to take into account the velocity profile.

A Photoelastic Approach to Transient Stress Problems Employing Low-Modulus Materials[1]

E. VOLTERRA.[2] The authors are to be congratulated upon their excellent paper which represents a very important contribution in the field of dynamic photoelasticity. Since the early 1940's much work has been done on the dynamic characteristics of low-modulus materials. Perhaps it is correct to state that the study of this subject started in Cambridge, England, during the Second World War when, under the supervision of Sir Geoffrey Taylor, research on the dynamic properties of some plastics and rubberlike materials under impact loading was carried out for the British Admiralty [1, 2, 3].[3]

The main object of the early experiments was to derive, from a rheological point of view, the dynamic stress-strain relationships of these materials under impact loading. This was the object also of experiments which were carried out in later years at the Illinois Institute of Technology and at Rensselaer Polytechnic Institute in this country under the sponsorship first of the Office of Naval Research and later of the Air Force Office of Scientific Research [4–8].

In all the earlier experiments mentioned, the apparatus used to produce impact loading on the specimens was the same as that used by the authors of the present paper. On the other hand, in all the experiments, methods of recording stress and strain were continually being improved. In fact, whereas in the early Cambridge experiments optical methods were used to record the distance between the pendulums during impact (which involved a double differentiation to be performed in order to derive the stress-strain relationship), in more recent experiments, performed at Rensselaer Polytechnic Institute, a more exact method based on the use of an accelerometer fixed to one of the pendulums was used to record stresses and strains. In this paper the authors, in addition to the accelerometer, use a linear differential transformer mounted between the pendulums and a Fastex motion-picture camera. It is interesting to learn that the three methods give the same results as to stress-strain curves. However, there are three questions in which the writer requests comment:

1 What is the influence of the end conditions of the specimen? How were the ends of the specimens lubricated?

2 During impact did barreling of the specimens occur and, if so, how did it affect the assumption of uniform stress distribution in the specimen?

3 Is the assumption justifiable that lateral inertia of the specimen during impact can be neglected?

References

1 G. I. Taylor, "The Testing of Materials at High Rates of Loading," *Journal of the London Institution of Civil Engineers*, vol. 26, 1946, pp. 486–519.

2 E. Volterra, "Sulla Relazione Dinamica tra Sforzi Specifici e Deformazioni Specifiche per i Materiali Elastici e Plastici," *Giornale del Genio Civile*, Fasc. 3, May and June, 1946.

3 E. Volterra, "Alcuni Risultati di Prove Dinamiche Sui Materiali," *La Rivista del Nuovo Cimento*, vol. 4, 1948, pp. 1–28.

4 E. Volterra, "A Mathematical Interpretation of Some Experiments on Plastics and Rubber-Like Materials," Proceedings of the Second International Congress on Rheology, Oxford, England, July, 1953, pp. 73–78.

5 E. Volterra, R. A. Eubanks, and D. Muster, "Some Experiments at High Rates of Loading," Proceedings of the Eighth International Congress of Applied Mechanics, Istanbul, Turkey, August, 1952.

6 E. Volterra, R. A. Eubanks, and D. Muster, "An Investigation of the Dynamic Properties of Plastics and Rubber-Like Materials," *Proceedings of the Society for Experimental Stress Analysis*, vol. 8, 1950, pp. 85–96.

7 D. Muster and E. Volterra, "A Rotating Drum Camera for Recording Impact Loading Deformations," *Proceedings*, American Society of Motion Picture and Television Engineers, vol. 59, 1952, pp. 44–48.

8 E. Volterra and C. S. Barton, "An Impact Testing Machine for Plastics and Rubber-Like Material," *Proceedings of the Society for Experimental Stress Analysis*, vol. 16, 1958, pp. 157–166.

Authors' Closure

The authors are very grateful to Prof. Volterra for his kind comments and constructive criticisms.

The validity of the dynamic stress strain determination from the double pendulum method depends upon the assumption that the stress distribution is uniform over the entire specimen. Three factors may influence the validity of this assumption:

1 Frictional constraint at the ends of the specimen.
2 Lateral inertia of the specimen.
3 Viscoelastic characteristics of the specimen material.

The first factor is strongly dependent on the lubrication at the interface between the specimen and the pendulums. In this experiment a liberal quantity of a silicone grease was applied to the right-hand pendulum and a thin layer of the same grease to the left-hand pendulum. The photographs shown in Fig. 4 indicated almost no frictional constraint on the right-hand side, yet they do indicate some effects of friction on the left-hand side. Barreling will be dependent on frictional effects at the ends, and the magnitude of the strain applied to the specimen. The photoelastic fringe patterns were obtained at low values of strain and

[1] By J. W. Dally, W. F. Riley, and A. J. Durelli, published in the December, 1959, issue of the JOURNAL OF APPLIED MECHANICS, vol. 26, TRANS. ASME, vol. 81, series E, pp. 613–620.

[2] Professor of Engineering Mechanics, The University of Texas, Austin, Tex. Mem. ASME.

[3] Numbers in brackets designate References at end of discussion.

the barreling of the specimen were not large enough to be noticeable.

The authors believe the effects of lateral inertia are small and much less serious than the end conditions. Referring again to Fig. 4, the 1.5, 4.5, 6.5, and 7.5 fringes are nearly uniformly distributed over the width of the specimen. The other fringes are not as well distributed, but it is believed that the conditions at the ends of the specimen produced the irregularities rather than lateral inertia effects.

If the material were perfectly elastic and if one neglected lateral inertia effects, the fringes would build up as a consequence of wave propagation and reflection. Thus a difference in the fringe order over the length of the specimen would always exist. Inspection of Fig. 4 shows this wave-propagation effect for the first 6 frames as the one-half fringe propagates down the specimen and reflects from the right-hand pendulum. However, from frame 7 on there is little evidence of wave propagation and the fringe order at both ends of the specimen is equal. Any local differences in the fringe order at the ends of the specimen may be attributed to frictional effects.

It is the authors belief that lateral inertia and wave propagation effects will not influence the distribution of the stress in a specimen of a low-modulus material to any appreciable extent. Frictional constraint is the greatest factor which introduces experimental error and it should be the first concern of the investigator.

Response of a Nonlinear String to Random Loading[1]

R. H. LYON.[2] In his paper, Caughey has presented calculations for the mean square displacement of a string governed by the equation of motion (his notation)

$$\rho\left(\frac{\partial^2 u}{\partial t^2}+\beta\frac{\partial u}{\partial t}\right)=\left[T_0+\frac{AE}{2L}\int_0^L\left(\frac{\partial u}{\partial x}\right)^2 dx\right]\frac{\partial^2 u}{dx^2}+f(x,t) \quad (1)$$

where $f(x, t)$ is governed by the correlation function

$$\overline{f(x,t_1)f(\eta,t_2)}=4D\delta(x-\eta)(\sin\omega_c\tau)/\tau. \quad (2)$$

It is the purpose of this discussion to show that his results may be obtained by elementary considerations and to suggest that recent work of the present author[3] has discounted the validity of using equation (1) in this problem.

The mean square displacement of the i^{th} linear mode may be easily found to be [see Caughey's equation (21)]

$$\sigma_{i,0}^2=2DL/i^2\pi^2\beta T_0. \quad (3)$$

The effect of the total motion is merely to increase the average tension by an amount

$$\overline{\Delta T}=\frac{EA\pi^2}{4L^2}\sum_{i=1}^{N}i^2\sigma_{i,0}^2=\frac{EAD}{2\beta T_0 L}N. \quad (4)$$

Since

$$\overline{U_0^2}=\sum_{i=1}^{\infty}\sigma_{i,0}^2=\frac{DL}{3\beta T_0}$$

and

$$\overline{U^2}=\sum_{i=1}^{\infty}\sigma_i^2=\frac{DL}{3\beta(T_0+\overline{\Delta T})},$$

one has

$$\overline{U^2}/\overline{U_0^2}=(1+\overline{\Delta T}/T_0)^{-1}=(1+\alpha\sigma_{1,0}^2N)^{-1} \quad (5)$$

which is Caughey's result for $\alpha\sigma_{1,0}^2N$ small, which it must be for the analysis to be consistent. It is obvious that the new linear system with tension $T_0+\overline{\Delta T}$ will satisfy equipartition.

The work just referred to does not use equation (1) but rather more general equations similar to those developed by Carrier.[4] Although the assumption is made that $EA \gg T_0$, the result does not reduce to (5) but rather

$$\sigma_i^2/\sigma_{i,0}^2=(1+2Q_i\overline{\Delta T}/T_0)^{-1} \quad (6)$$

where Q_i is the quality factor for the i^{th} mode. Since for a large number of systems $Q_i \gg 1$, the reduction in displacement is stronger than (5) would indicate. This result, when traced back, occurs by an interaction between longitudinal and transverse motions of the string.

Author's Closure

The author wishes to thank Dr. Lyon for his interesting comments on the paper. The author would like to refute the claim that equation (1) of the above paper is invalid. To this end, consider Carrier's equations for the string,[4] modified to include damping and external forces.

$$f(x,t)=\rho u_{tt}+ru_t-\partial_x[T\sin\theta] \quad (1)$$

$$O=\rho V_{tt}+\eta V_t-\partial_x[T\cos\theta] \quad (2)$$

where

$$\sin\theta=\frac{u_x}{1+e} \quad (3)$$

and the local strain e is given by

$$e=((1+V_x)^2+u_x^2)^{1/2}-1 \quad (4)$$

$$T=T_0+EAe \quad (5)$$

If the following assumptions are made:

(a) $V_x=O(u_x^2)\ll 1$

(b) $T_0\ll EA$

(c) $w_c<\Omega_1$

where w_c is the highest frequency excited in transverse vibration and Ω_1 is the lowest eigen value for longitudinal vibrations.

If assumption (c) is satisfied, the time derivative terms in (2) may be neglected. Hence,

$$\partial_x[T\cos\theta]=0 \quad (6)$$

$$\therefore\ T\cos\theta=g(t) \quad (7)$$

where $g(t)$ is independent of x.

Using assumption (a) and equations (3) and (4),

$$T\simeq T_0+EA\left(V_x+\frac{1}{2}u_x^2\right) \quad (8)$$

[1] By T. K. Caughey, published in the September, 1959, issue of the JOURNAL OF APPLIED MECHANICS, vol. 26, TRANS. ASME, series E, vol. 81, pp. 341–344.

[2] Associate Professor of Electrical Engineering, University of Minnesota, Minneapolis, Minn. Currently on leave as National Science Foundation Postdoctoral Fellow at the Department of Mathematics, The University, Manchester, England.

[3] R. H. Lyon, "The Random Vibration of Elastic Strings—Theoretical," WADC Technical Report 58-570, September, 1958.

[4] G. F. Carrier, "On the Nonlinear Vibration Problem of the Elastic String," *Quarterly of Applied Mathematics*, vol. 3, 1945, pp. 157–165.

$$\cos\theta \simeq 1 - \frac{1}{2}u_x^2 \tag{9}$$

$$\therefore T\cos\theta \simeq T_0 + EAV_x + (EA - T_0)^1/_2 u_x^2 = g(t) \tag{10}$$

Now the boundary conditions require that the axial displacement V vanish at both ends of the string.

$$\therefore \int_0^l V_x dx = 0 \tag{11}$$

Thus, integrating (10),

$$g(t) \simeq T_0 + \frac{EA - T_0}{2l}\int_0^l u_x^2 dx \tag{12}$$

Using assumption (*b*),

$$g(t) \simeq T_0 + \frac{EA}{2l}\int_0^l u_x^2 dx \tag{13}$$

Substituting (7) into (1),

$$f(x,t) = \rho u_{tt} + ru_t - g(t)\partial_x(\tan\theta) \tag{14}$$

Using assumption (*a*) and equation (3),

$$\tan\theta = \frac{u_x}{1+V_x} \simeq u_x \tag{15}$$

Hence, equation (14) becomes

$$f(x,t) = \rho u_{tt} + ru_t - \left[T_0 + \frac{EA}{2l}\int_0^l u_x^2 dx\right]u_{xx} \tag{16}$$

Equation (16) is identical to equation (1) of Caughey.[1] This result was first proved by Carrier[5] in a somewhat different manner.

Having established the validity of equation (1) of the paper, it is necessary to explain the differences between the results obtained in Caughey[1] and those obtained by Lyon.[3] If equation (2.11) of Lyon[3] is examined in the light of the assumptions (*a*), (*b*), and (*c*) above, it may easily be shown that:

$$V_x^{(3)} = -\frac{1}{2}u_x^{2(1)} + b(t) \tag{17}$$

where

$$b(t) = \frac{1}{2l}\int_0^l u_x^{2(1)} dx \tag{18}$$

If equations (17) and (18) are substituted into equation (2.11) of Lyon,[3] there results the equation:

$$\rho u_{tt}^{(3)} + ru_t^{(3)} - T_0 u_{xx}^{(3)} = \left[\frac{EA}{2l}\int_0^l u_x^{2(1)} dx\right]u_{xx}^{(1)} \tag{19}$$

This equation is exactly what one would expect by applying Lyon's perturbation scheme to equation (16). Hence, the differences between the two theories cannot be explained by the coupling between the transverse and longitudinal motions as suggested by Lyon. The difference must therefore be due to the perturbation method used by Lyon.

Examination of the perturbation scheme used by Lyon reveals the following disturbing facts:

1 Examination of equation (2.10) of Lyon[3] reveals that the quantities are not all of the same magnitude. For example, ru_t^1 is retained in the equation along with ρu_{tt}^1 and $T_0 u_{xx}^1$ despite the fact that r is assumed very small, making ru_t^1 a quantity of second order, whereas ρu_{tt}^1 and $T_0 u_{xx}^1$ are quantities of first order. Similar remarks apply to equations (2.11) and (2.12).

2 The perturbation scheme used by Lyon perturbs the transverse and longitudinal displacements; however, the frequency is left unperturbed. This is highly unusual in nonlinear problems unless one retains all the secular terms as Carrier did.[4] For further discussion of this point, the reader is referred to J. J. Stokes.[6]

It would therefore appear that the methods used by Lyon are somewhat questionable.

[5] G. F. Carrier, "A Note on the Vibrating String," *Quarterly of Applied Mathematics*, vol. 7, 1949, pp. 97–101.

[6] J. J. Stokes, "Nonlinear Vibrations," Pure and Applied Mathematics, vol. II, Interscience Publishers, Inc., New York, N. Y., 1950.

Nonlinear Creep Deformations of Columns of Rectangular Cross Section[1]

H. G. McCOMB, JR.[2] The contribution of this paper is the development of easily calculated upper and lower bounds for the creep collapse time of rectangular section columns. In recent work at the Langley Research Center, NASA [1],[3] the variational theorem referred to by the authors has been utilized with direct methods to make some very accurate calculations for this problem. In [1] the power creep law was used as in the present paper. In addition, the stress distribution through the thickness was allowed to take on a nonlinear shape. The results of [1], therefore, represent a refinement of the previous work mentioned by the authors [2] which utilized the variational theorem but in conjunction with a linear stress distribution. An interesting comparison between the results of [1] and the authors' results is shown in Fig. 1 of this discussion. This figure is like Fig. 4 of the paper where τ_{CR} is plotted against z_0/h, the initial deflection parameter. Only the case $k = 3$ is shown. The dashed and solid lines are the upper and lower bounds for τ_{CR} from the authors' paper. The dash-dot lines are from [1]; the upper one is for $\sigma_0/\sigma_E = 0.2$ and the lower for $\sigma_0/\sigma_E = 0.8$. The results of [1] lie between the authors' bounds, and therefore are consistent with them. The figure gives some idea of the accuracy of the authors' conjecture that for $\sigma_0/\sigma_E < 0.2$ the upper bound should be a good approximation to the collapse time and for $\sigma_0/\sigma_E > 0.8$ the lower bound should be a good approximation.

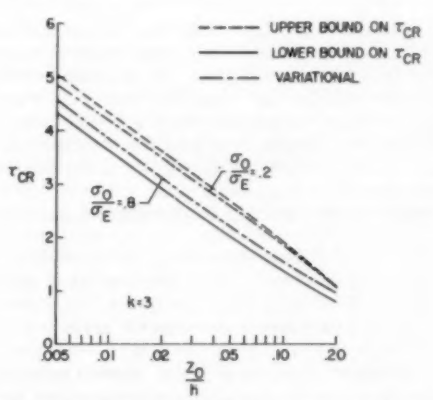

Fig. 1 Comparison between variational results and bounds on τ_C

[1] By H. H. Bleich and O. W. Dillon, Jr., published in the December, 1959, issue of the JOURNAL OF APPLIED MECHANICS, vol. 26, TRANS. ASME, vol. 81, series E, pp. 517–525.

[2] Langley Research Center, National Aeronautics and Space Administration, Langley Field, Va.

[3] Numbers in brackets designate References at end of discussion.

DISCUSSION

Substantial discrepancies in collapse time exist between creep-buckling theories such as this one and experiments. Calculations based on rather simple creep-buckling hypotheses such as those proposed by Shanley [3] and Gerard [4] show up just as well or better in comparisons between theory and experiment as the more refined analysis, even though these simple hypotheses seem to have relatively little physical or rational basis. The analysis of this paper and of [1] and of the great majority of other papers on this problem (and there are many) are based on creep relations which are really only valid for creep under constant stress. That is, the constants in the creep relation (λ and k in this paper) are determined from constant stress-creep data. Actually, of course, the stress at some points in the column varies considerably as creep progresses. In [3] and in Libove's papers, [5] and [6], an effort was made to account for this fact that the stress varies during creep of the column. Perhaps it is time to reappraise the creep relations that are being used in analyses of this type and determine whether or not they adequately represent the material behavior.

References

1 F. R. Schlechte, "Theoretical Analysis of the Creep Collapse of Columns," NASA TN D-95, September, 1959.

2 J. L. Sanders, H. G. McComb, Jr., and F. R. Schlechte, "A Variational Theorem for Creep With Applications to Plates and Columns," NACA Report 1342, 1958, supersedes NACA TN 4003.

3 F. R. Shanley, "Weight-Strength Analysis of Aircraft Structures," McGraw-Hill Book Company, Inc., New York, N. Y., 1952, pp. 343–357.

4 George Gerard, "A Creep Buckling Hypothesis," *Journal of the Aeronautical Sciences*, vol. 23, 1956, pp. 879–882, 887.

5 Charles Libove, "Creep Buckling of Columns," *Journal of the Aeronautical Sciences*, vol. 19, 1952, pp. 459–467.

6 Charles Libove, "Creep Buckling Analysis of Rectangular-Section Columns," NACA TN 2956, June 1953.

Analysis of Plane Stress in Polar Co-ordinates and With Varying Thickness[1]

V. S. MUSICK.[2] In May, 1958, the writer submitted in partial fulfillment for a Master of Science degree in Engineering at Union College, Schenectady, N. Y., a thesis entitled, "On the General Solution of Variable Thickness Plane-Stress Problems in Polar Co-ordinates With a Special Solution of a Variable Thickness Stodala Type Disk With Nonuniform, Radial Boundary Loading." The solution given in the present paper closely parallels the writer's earlier work.

The author has observed that the characteristic equation

$$\lambda^4 + 2(m-2)\lambda^3 + (4 - 5m - \nu m - 2n^2 + m^2)\lambda^2 - (m-2)(m + \nu m + 2n^2)\lambda - n^2(4 + \nu m - 3m - \nu m^2 - n^2) = 0 \qquad (13)$$

is easily factorable for $m = 2$. In the writer's investigation of this same characteristic equation, it was discovered, for $n = 2$ and $\nu = 0.3$, in the cases checked, the roots were real for $0 < m \leq 2$ and for $m > 2$ some roots were found to be conjugate complex of the form:

$$\lambda_1 = a_n + b_n i$$
$$\lambda_2 = a_n - b_n i$$
$$\lambda_3 = c_n + b_n i$$
$$\lambda_4 = c_n - b_n i$$

Hence the form of equation

$$R_n = (A_n r^{\lambda_1} + B_n r^{\lambda_2} + C_n r^{\lambda_3} + D_n r^{\lambda_4}) \qquad (22)$$

will change to

$$R_n' = A_n' r^{a_n} \cos(b_n \ln r) + B_n' r^{a_n} \sin(b_n \ln r) + C_n' r^{c_n} \text{les}(b_n \ln v) + D_n' r^{c_n} \sin(b_n \ln r)$$

As a point in passing, one should make note of the fact that $m > 2$ represents a fairly high flare of cross section.

Direct Determination of Stresses in Plane Elasticity Problems Based on the Properties of Isostatics[1]

GUSTAV MESMER.[2] It is well known (references [4, 5, 7] of this paper) that all systems of equipotential lines and the corresponding orthogonal streamlines can be considered to be isostatics (stress trajectories) of certain elastic plane-stress systems. These stress systems belong obviously to a peculiar limited class, fulfilling specific boundary conditions. This means that the trajectories of only a few exceptional cases of elastic problems can be considered to be potential lines or, which is equivalent, of the "square" type (differential parameters h_1 and h_2 being equal). To mention one important point; the "closed" type of internal isotropic points, very often appearing in stress trajectories, has no counterpart in the potential network. The method of the author can therefore be used with reliability only in some peculiar cases. The circular plate between two singular forces belongs to this group. Most real problems, for example, the problems of the simple tension and bending bar with holes or notches, do not belong to this class, and one cannot expect accuracy or reliability in the stress results based upon a partly similar but nonetheless wrong network of trajectories. Some comparative numbers of Table 3 of the paper are significant.

Author's Closure

The author wishes to thank Professor G. Mesmer for his comments. As it was pointed out in the paper, and it was mentioned in the discussion, the necessary and sufficient condition for a network of isostatics of a plane-stress elastic system to be represented by a network of equipotentials and the corresponding stream lines is to be isometric. This restricts the rigorous application of this analogy only to those cases fulfilling this condition.

But, following Wegner,[3] we can express the Cartesian stress components in a plane-stress elastic field by the following relations:

$$\sigma_x = -r^2 R \cdot [F(z)] + R \cdot \left[\int_{z_0}^{z} zF(z)dz + p\right] - R \cdot [N(z)]$$

$$\sigma_y = r^2 R \cdot [F(z)] + R \cdot \left[\int_{z_0}^{z} zF(z)dz + p\right] + R[N(z)]$$

$$\tau_{xy} = r^2 I \cdot [F(z)] + I \cdot [N(z)]$$

---

[1] By H. D. Conway, published in the September, 1959, issue of the JOURNAL OF APPLIED MECHANICS, vol. 26, TRANS. ASME, vol. 81, series E, pp. 437–439.

[2] Turbine Bucket and Rotor Engineering, Large Steam Turbine-Generator Department, General Electric Company, Schenectady, N. Y. Assoc. Mem. ASME.

[1] By P. S. Theocaris, published in the June, 1959, issue of the JOURNAL OF APPLIED MECHANICS, vol. 26, TRANS. ASME, vol. 81, series E, pp. 227–234.

[2] Washington University, St. Louis, Mo.

[3] Reference [5] of the paper.

Fig. 1

where $R\cdot$ and $I\cdot$ denote the real and imaginary parts of two arbitrary analytic functions $F(z)$ and $N(z)$ of the complex variable z.

Therefore any plane-stress elastic field with no body forces can be considered as resulting from two independent *isometric* stress systems, one of which, defined by the function $N(z)$, is a harmonic stress system whose first invariant $2\sigma = (\sigma_1 + \sigma_2)$ is everywhere zero. The superposition of the two systems is possible only if certain criteria exist relating either the functions $F(z)$ and $N(z)$ or the difference of the principal stresses.

However, it may be noted that, in general, the contribution of the analytic function $N(z)$ on the resultant stress field is secondary and its influence in deviating the principal stress field corresponding to the analytic function $F(z)$ is negligible in regions far from singularities. This explains the isometric character of the field of isostatics in these regions. In cases of plane-stress fields containing singularities, these can be determined accurately from a photoelastic fringe pattern. The singularities correspond either to points of transition from one isostatic to its orthogonal or to isolated points belonging to one type of isostatic surrounded by the two extreme isostatics of the other family.

The determination of the isotropic points or lines on the boundaries or in the interior of the field allows the separation of the boundaries into two groups from which each belongs to one family of isostatics and the determination of the extreme isostatics. Each family of isostatics can be traced by using the extreme isostatics of the family as electrodes of application of the potential in the electrical analogy method. The parts of the boundaries corresponding to this family and not belonging to the extreme isostatics must have also electrodes. The potential of these electrodes is regulated to correspond to a limiting value of potential which makes this electrode an equipotential.

Since the boundaries of the traced field of isostatics are compelled to correspond to those of the real problem, and since the greater discrepancies due to the function $N(z)$ are encountered in the vicinity of the singularities, which are forced to correspond to those of the rigorous problem by the placing of the electrodes, the deviations from the correct network are insignificant. Therefore the traced network of isostatics, by this analogy, is in many cases more accurate than the corresponding network constructed by a purely graphical process on the basis of isoclinics which, moreover, are, in general, very badly determined photoelastically. As an example, we give in Fig. 1 the one family of isostatics traced by this analogy in the case of a circular ring subjected to a diametral compression because this case contains all kinds of singularities. For the sake of comparison, the same network of isostatics, traced graphically, is given in the book by M. M. Frocht, "Photoelasticity," vol. 1, page 209.

Velocity and Temperature Fluctuation Measurements in a Turbulent Boundary Layer Downstream of a Stepwise Discontinuity in Wall Temperature[1]

S. J. KLINE[2] and P. W. RUNSTADLER.[3] The author has indicated that perhaps the most novel result of this investigation is the observed intermittency of the temperature fluctuations within one region of the fully turbulent boundary layer as distinguished from measurements of the velocity fluctuations. This intermittency is shown in Fig. 6 of the paper for a value of $y = 2.2$ in. A possible explanation of this phenomenon may lie in the results of studies performed at Stanford University and described in a recent paper.[4] These visual studies have indicated that a repeated instability exists in the wall layers of the turbulent boundary layer; this instability gives rise to a flow model which is repeated over the entire wall and in turn creates the large fluctuations which are responsible for the continuance of the turbulent shear layer over a solid surface.

In order for this flow model of the wall layers to explain the phenomenon reported by the author, it must account for the following observations: (*a*) The intermittency of the thermal measurements; (*b*) the one-sided spikes of the thermal intermittent measurements; (*c*) the lack of intermittency in the velocity measurements at the same place where there is intermittency in the thermal measurements.

The author's test plate is heated on only the last 6 ft of the 20-ft test section, giving a thermal boundary layer which does not reach the free stream at the downstream end of the plate. Over the heated portion of the wall, the part of the flow extremely close to the wall contains very slowly moving fluid which is heated by thermal conduction from the plate. Some of this high-temperature fluid is then displaced away from the wall by the vortex-like motion of the "tail" of the flow model. These vortex tails of fluid break up farther out into "bursts" of typical turbulent motion. These bursts are then carried away from the wall and downstream by the mean motion of the fluid. At any given location, away from the wall, the fluctuations represent the integrated history of bursts created upstream near the wall. Since the bursts are moved away from the wall by the mean flow, it seems reasonable to assume that far from the wall, near the edge of the boundary layer, the fluctuations are bursts which have originated far upstream; nearer the wall one would expect a mixture of bursts, some from far upstream and some originating nearby; close to the wall most bursts will come from the nearby wall section.

In terms of this concept of the turbulent shear layer, it is then relatively easy to rationalize the author's results. At the downstream end of the plate, very near the wall, most of the bursts will have originated on the heated section of the plate; in the middle of the boundary layer some bursts will have come from the heated and some from the unheated portion of the plate; in the outermost portion of the layer almost all of the bursts will have come from the unheated section of the plate. Thus for

[1] By D. S. Johnson, published in the September, 1959, issue of the JOURNAL OF APPLIED MECHANICS, vol. 26, TRANS. ASME, vol. 81, series E, pp. 325–336.

[2] Associate Professor, Department of Mechanical Engineering, Stanford University, Stanford, Calif. Mem. ASME.

[3] Research Assistant, Department of Mechanical Engineering, Stanford University, Stanford, Calif.

[4] S. J. Kline and P. W. Runstadler, "Some Preliminary Results of Visual Studies of the Flow Model of the Wall Layers of the Turbulent Boundary Layer," JOURNAL OF APPLIED MECHANICS, vol. 26, TRANS. ASME, vol. 81, series E, June, 1959, pp. 166–170.

the y-location of the intermittent thermal measurements shown in Fig. 6, which corresponds to the middle portion of the layer just described, the velocity fluctuations are not intermittent since bursts from the whole plate cover this region; but since only some of these bursts originated on the heated portion of the plate, thermal intermittency is observed. Moreover, the author's "base line" represents the energy of the cold fluid and all of the thermal intermittencies are due to the arrival of random high-temperature bursts and hence are one-sided.

The writers feel that the author's results are useful in two regards: (a) The work gives strong further evidence of the close relation between wall effects and the origin of turbulent bursts in the wake portion of the turbulent boundary layer. In particular, it tends to verify that the primary origin of bursts is in the wall layers and is not due to free-stream interactions. (b) The results suggest the use of thermal elements mounted in the wall as a means for tracking the history of one or more turbulent bursts originating in the wall layers. Such information should be of aid in describing the path of fluctuations and in determining the size and frequency of single bursts as well as the frequencies and angle with respect to the wall of the generating vortex system.

Slow Rotatory Motion of a Circular Disk About One of Its Diameters in a Viscous Fluid[1]

E. M. SPARROW.[2] The author is to be congratulated on his solution of an interesting problem in fluid mechanics. In the interests of a concise presentation, a definition of the parameter α and a discussion of its characteristics have been omitted from the paper. Apparently, α is a kind of eigenvalue; but it takes on a continuous spectrum rather than the discrete spectrum of values as is frequently encountered in boundary-value problems. Further remarks about the properties of α would be of interest.

It would appear that equations (19) to (23) provide the velocity and pressure results corresponding to a given α. To achieve the final solution, integration over α seems necessary, and this has been done for w and p in the plane $z = 0$. However, the integrations have not been carried out for $z \neq 0$; and in this sense, the solution is not complete. Whatever remarks the author may wish to make about the integrated results for the condition when $z \neq 0$ would be helpful.

Author's Closure

Professor Sparrow's comments are very much appreciated. His remarks about the parameter α are quite correct. It may, however, be added that this method of solving the boundary-value problems is essentially the method of Hankel transforms.

The reason that the integration of the main results have been carried out only in the plane $z = 0$ is that the couple on the disk is thereby completely determined. Second, the value of w turns out to be given in an elegant closed form. The values of the pressure and the velocity components can also be derived for the case $z \neq 0$. We shall demonstrate it by evaluating the pressure.

Observing that the expression $\left(\frac{\sin \alpha r_0}{\alpha r_0} - \cos \alpha r_0\right)$ is related to the Bessel function $J_{3/2}(\alpha r_0)$, as

$$\left(\frac{\sin \alpha r_0}{\alpha r_0} - \cos \alpha r_0\right) = \pi/2 \sqrt{\alpha r_0}\, J_{3/2}(\alpha r_0), \qquad (1)$$

the value of the pressure, as given by the relations (23) and (26) of the original paper, is

$$p = \frac{4\sqrt{2}\mu\omega_0 r_0^{3/2}}{\sqrt{\pi}} \sin\theta \int_0^\infty \alpha J_{3/2}(\alpha r_0) J_1(\alpha r) e^{-\alpha z}\, d\alpha \qquad (2)$$

The quantity $\sqrt{\alpha}\, J_{3/2}(\alpha r_0) J_1(\alpha r)$, can be expanded in the series in α, as[3]

$$\alpha^{1/2} J_{3/2}(\alpha r_0) J_1(\alpha r) = \frac{4\sqrt{2}\,(r_0)^{3/2} r}{3\sqrt{\pi}} \times \sum_{n=0}^{\infty} \{(2n+3)(n+2)(n+1) F_4(-n, 3+n;\ 5/2, 2;\ r_0^2, r^2) \times J_{2n+3}(\alpha)\}. \qquad (3)$$

Therefore

$$p = \frac{32\mu\omega_0 r_0^3 r \sin\theta}{3\pi} \sum_{n=0}^{\infty} \{(2n+3)(n+2)(n+1) F_4(-n, 3+n;\ 5/2, 2;\ r_0^2, r^2) \times \int_0^\infty J_{2n+3}(\alpha) e^{-\alpha z}\, d\alpha. \qquad (4)$$

But[4]

$$\int_0^\infty J_{2n+3}(\alpha) e^{-\alpha z}\, d\alpha = \frac{\left(\sqrt{z^2+1} - z\right)^{2n+3}}{\sqrt{z^2+1}}. \qquad (5)$$

Substituting the relation (5) in (4), we have the complete evaluation of the pressure.

Incidently, now that the method of evaluation of the velocity components for the case $z \neq 0$, has been demonstrated in the foregoing analysis, one can investigate the shearing stresses experienced by the disk.

A New Theory of Elastic Sandwich Plates—One-Dimensional Case[1]

J. M. FRANKLAND.[2] For homogeneous plates, coupling of thickness-shear and thickness-stretch modes with the simpler forms of extensional and flexural vibration does not occur below very high frequencies. These phenomena are therefore of minor interest in the dynamic analysis of structures. If sandwich plates are used, however, this paper shows that the coupling can be of importance down to much lower frequencies. Sandwich structures subjected to acoustic excitation, for example, might show a more complicated behavior than a homogeneous structure. The subject deserves further study to make clear

[1] By R. P. Kanwal, published in the December, 1959, issue of the JOURNAL OF APPLIED MECHANICS, vol. 26, TRANS. ASME, vol. 81, series E, pp. 485–487.

[2] Professor of Mechanical Engineering, University of Minnesota, Minneapolis, Minn.

[3] Bateman Manuscript Project, "Higher Transcendental Functions," vol. 2, page 99, formula 7.

[4] G. N. Watson, "Theory of Bessel Functions," Cambridge, 1944, page 386.

[1] By Yi-Yuan Yu, published in the September, 1959, issue of the JOURNAL OF APPLIED MECHANICS, vol. 26, TRANS. ASME, vol. 81, series E, pp. 415–421.

[2] National Bureau of Standards, U. S. Department of Commerce, Washington, D. C.

the conditions under which these effects will be important. In particular, the writer hopes that the author will consider more customary sandwich proportions where the facings are less thick than in his numerical example.

Author's Closure

The author wishes to thank Dr. Frankland for his comments and agrees with his opinion that the subject deserves further study. The numerical example discussed during the presentation of the paper was for a ratio of $h_2/h_1 = 1/2$. Since then, another example in which $h_2/h_1 = 1/10$ has been calculated, and both examples have been included in a forthcoming paper.[3] The simple thickness-shear frequency in the case of $h_2/h_1 = 1/10$ is somewhat higher than that in the case of $h_2/h_1 = 1/2$ but is still much lower than that of a homogeneous plate.

Thermal Stress Owing to a Hot Spot in a Rectangular Strip[1]

CHIH-BING LING.[2] In this paper the author gives a solution of the interesting thermoelastic problem of a hot spot in an infinite strip. It is appreciated that the author also in a footnote points out a typographical error in the table of one of the writer's recent papers.

The writer wishes to show that the same problem can be solved by using the method of images. This method has been used by the writer with advantage in solving many an elastic problem. For generality, let λ denote the radius of the hot spot, which may be less than, or equal to, a. Consider a series of such identical hot spots uniformly distributed in an infinite plate along the y-axis with their centers at $y = 2na$, where n takes all positive and negative integral values including zero. By symmetry, the tangential stress along the lines $y = \pm a$ vanishes identically and only traction along these lines is a normal stress given by

$$(\sigma_{x1})_{y=\pm a} = CE\alpha \sum_{n=-\infty}^{\infty} \frac{x^2 - (2n-1)^2a^2}{\{x^2 + (2n-1)^2a^2\}^2} \tag{1}$$

$$= -\frac{\pi^2 CE\alpha}{4a^2} \operatorname{sech}^2 \frac{\pi x}{2a}$$

where

$$C = \int_0^{\lambda} T(r) r dr \tag{2}$$

The series are summed with the aid of the following relations[3]

$$\sum_{n=1}^{\infty} \frac{1}{x^2 + (2n-1)^2a^2} = \frac{\pi}{4ax} \tanh \frac{\pi x}{2a} \tag{3}$$

$$\sum_{n=1}^{\infty} \frac{1}{\{x^2 + (2n-1)^2a^2\}^2} = \frac{\pi}{8ax^2} \left(\tanh \frac{\pi x}{2a} - \frac{\pi x}{2a} \operatorname{sech}^2 \frac{\pi x}{2a} \right)$$

The foregoing boundary stress can be annulled by introducing a Howland's integral[4] of type 1.

$$\chi_1 = \frac{4}{\pi} \int_0^{\infty} \frac{f(m) \sinh ma}{m^2(\sinh 2ma + 2ma)} \{my \sinh my - (1 + ma \coth ma) \cosh my\} \cos mx \, dm \tag{4}$$

where[5]

$$f(m) = \frac{\pi^2 CE\alpha}{4a^2} \int_0^{\infty} \operatorname{sech}^2 \frac{\pi x}{2a} \cos mx \, dx$$

$$= \frac{m\pi CE\alpha}{2 \sinh ma} \tag{5}$$

Therefore

$$\chi_1 = 2CE\alpha \int_0^{\infty} \left\{ \frac{my \sinh my - (1 + ma \coth ma) \cosh my}{m(\sinh 2ma + 2ma)} \times \cos mx + \frac{1}{2m^2a} \right\} dm \tag{6}$$

in which the term $1/2m^2a$ is added to the integrand in order to render the integral convergent at the lower limit.

Consequently, the stresses in the strip outside the hot spot are given by

$$\sigma_x = \frac{\partial^2 \chi_1}{\partial y^2} - CE\alpha \sum_{n=-\infty}^{\infty} \frac{x^2 - (y - 2na)^2}{\{x^2 + (y - 2na)^2\}^2}$$

$$= \frac{\partial^2 \chi_1}{\partial y^2} - \frac{\pi^2 CE\alpha}{2a^2} \left(\cosh \frac{\pi x}{a} \cos \frac{\pi y}{a} - 1 \right) \Big/ \left(\cosh \frac{\pi x}{a} - \cos \frac{\pi y}{a} \right)^2 \tag{7}$$

$$\sigma_y = \frac{\partial^2 \chi_1}{\partial x^2} + \frac{\pi^2 CE\alpha}{2a^2} \left(\cosh \frac{\pi x}{a} \cos \frac{\pi y}{a} - 1 \right) \Big/ \left(\cosh \frac{\pi x}{a} - \cos \frac{\pi y}{a} \right)^2 \tag{8}$$

$$\tau_{xy} = -\frac{\partial^2 \chi_1}{\partial x \partial y} - 2CE\alpha \sum_{n=-\infty}^{\infty} \frac{x(y - 2na)}{\{x^2 + (y - 2na)^2\}^2}$$

$$= -\frac{\partial^2 \chi_1}{\partial x \partial y} - \frac{\pi^2 CE\alpha}{2a^2} \sinh \frac{\pi x}{a} \sin \frac{\pi y}{a} \Big/ \left(\cosh \frac{\pi x}{a} - \cos \frac{\pi y}{a} \right)^2 \tag{9}$$

where the series is summed with the aid of the relation[6]

$$\sum_{n=-\infty}^{\infty} \frac{1}{x^2 + (y - 2na)^2} = \frac{\pi}{2ax} \sinh \frac{\pi x}{a} \Big/ \left(\cosh \frac{\pi x}{a} - \cos \frac{\pi y}{a} \right) \tag{10}$$

and its derivatives.

The stresses in the strip inside a hot spot of constant temperature are also given by the foregoing expressions provided that the following quantities are added, respectively:

---

[3] Yi-Yuan Yu, "Flexural Vibrations of Elastic Sandwich Plates," to be published in the *Journal of Aero/Space Sciences*.

[1] By C. W. Nelson, published in the December, 1959, issue of the JOURNAL OF APPLIED MECHANICS, vol. 26, TRANS. ASME, vol. 81, series E, pp. 488–490.

[2] Director, Institute of Mathematics, Academia Sinica, Taiwan, China.

[3] The first relation is obtained by replacing θ with $i\pi x/2a$ in Formula (421), L. B. W. Jolly, "Summation of Series," Chapman and Hall, Limited, 1925, p. 126. The second follows at once by differentiation.

[4] R. C. J. Howland, "Stress Systems in an Infinite Strip," *Proceedings of The Royal Society of London*, series A, vol. 124, 1929, pp. 89–119. The function has been modified in conformity with the present notation.

[5] Cf. Formula (3), in Table 267 for $p = 0$, D. Bierens de Haan, "Nouvelles Tables D'Intégrales Définies," G. E. Stechert and Company, 1939, p. 390.

[6] Cf. Formula (521a), L. B. W. Jolly, ibid., p. 158.

$$CE\alpha\left\{\frac{x^2-y^2}{(x^2+y^2)^2}-\frac{1}{\lambda^2}\right\},\quad -CE\alpha\left\{\frac{x^2-y^2}{(x^2+y^2)^2}+\frac{1}{\lambda^2}\right\},\quad \frac{2CE\alpha xy}{(x^2+y^2)^2}$$

Author's Closure

The author wishes to thank Dr. Ling for demonstrating the solution of the author's problem by another method, namely, the method of images.

Since Dr. Ling's solution differs in form from that derived by the author, an outline of the main steps in a proof of the exact equivalence of the two solutions appears to be worth while and is given in the following.

Subtraction of σ_x given by one solution from σ_x given by the other solution yields a result which reduces to zero if the following equation is true

$$\int_0^\infty \frac{\frac{w}{2}e^{-\frac{w}{2}}}{\sinh\frac{w}{2}}\cosh\frac{wy}{2a}\cos\frac{wx}{2a}\frac{dw}{2} = \frac{a^2(x^2-y^2)}{(x^2+y^2)^2}-\frac{\pi^2}{2}\frac{\left(\cosh\frac{\pi x}{a}\cos\frac{\pi y}{a}-1\right)}{\left(\cosh\frac{\pi x}{a}-\cos\frac{\pi y}{a}\right)^2} \quad (1)$$

It will be shown that this equation is true. It can be shown that Equation (1) is also obtained by specifying that expressions for σ_y from the two solutions are equivalent. In a similar way, it can be shown that equivalent expressions for τ_{xy} are obtained from the two solutions if the following equation is true:

$$\int_0^\infty \frac{\frac{w}{2}e^{-\frac{w}{2}}}{\sinh\frac{w}{2}}\sinh\frac{wy}{2a}\sin\frac{wx}{2a}\frac{dw}{2} = \frac{2a^2xy}{(x^2+y^2)^2}-\frac{\pi^2}{2}\frac{\sinh\frac{x\pi}{a}\sin\frac{\pi y}{a}}{\left(\cosh\frac{\pi x}{a}-\cos\frac{\pi y}{a}\right)^2} \quad (2)$$

It will be shown that Equation (2) is also true.

The correctness of Equation (1) follows from the known formulas[7]

$$\int_0^\infty ze^{-\frac{zy}{a}}\cos\frac{zx}{a}dz = -\frac{a^2(x^2-y^2)}{(x^2+y^2)^2} \quad (3)$$

and

$$\int_0^\infty \frac{z\cosh\left(1-\frac{y}{a}\right)z\cdot\cos\frac{x}{a}z\cdot dz}{\sinh z} = -\frac{\pi^2}{2}\frac{\left(\cosh\frac{\pi x}{a}\cos\frac{\pi y}{a}-1\right)}{\left(\cosh\frac{\pi x}{a}-\cos\frac{\pi y}{a}\right)^2} \quad (4)$$

Similarly, Equation (2) is seen to be correct because

$$\int_0^\infty ze^{-\frac{zy}{a}}\sin\frac{zx}{a}dz = \frac{2a^2xy}{(x^2+y^2)^2} \quad (5)$$

and

$$\int_0^\infty \frac{z\sinh\left(1-\frac{y}{a}\right)z\cdot\sin\frac{xz}{a}\cdot dz}{\sinh z} = \frac{\pi^2}{2}\frac{\sinh\frac{\pi x}{a}\sin\frac{\pi y}{a}}{\left(\cosh\frac{\pi x}{a}-\cos\frac{\pi y}{a}\right)^2} \quad (6)$$

Thus the expected equivalence of Dr. Ling's solution and the author's solution has been demonstrated by showing that the two solutions give exactly equivalent expressions for σ_x, σ_y, and τ_{xy}.

[7] Equations (3) and (5) may be derived by differentiating with respect to the proper parameter both sides of Formula 521 or Formula 522, p. 69, "A Short Table of Integrals," Fourth Edition, Peirce and Foster, Ginn and Company, 1956. Equations (4) and (6) may be derived by differentiating both sides of Formula (4), Table 265, p. 388, "Nouvelles Tables D'Integrales Definies," by D. Bierens de Haan, Edition of 1867-corrected, Hafner Publishing Co., New York, 1957. Formulas (5) and (8) of the same table (265) both contain errors. Otherwise they could have been used for deriving Equations (1) and (2) of this Closure.

Symmetric Vortex Separation on Circular Cylinders and Cones[1]

NICHOLAS ROTT.[2] The author's treatment of the separation problem by the "concentrated-vortex" approximation contains an empirical constant, namely, the position of the separation point. Previous applications of this method were restricted to cases involving sharp corners, which were identified with the separation points (Kutta condition) so that the treatment appeared to be free of empiricism. However, comparison of these theories with experiments revealed that the concentrated-vortex approximation is in general inadequate because of the so-called "secondary" vortex separation at the sharp corners. A possible way out here is to relax the Kutta condition and to replace it with empirical information. From this point of view it is evident that in spite of the necessity of using some experimental information, the author's work is in the same category as the previous applications.

[1] By A. E. Bryson, published in the December, 1959, issue of the JOURNAL OF APPLIED MECHANICS, vol. 26, TRANS. ASME, vol. 81, series E, pp. 643–648.

[2] Professor, Department of Aeronautical Engineering, Cornell University, Ithaca, N. Y.

Journal of APPLIED MECHANICS

Book Reviews

Heat Exchangers

Compact Heat Exchangers. By W. M. Kays and A. L. London. McGraw-Hill Book Company, Inc., New York, N. Y., 1958. 156 pp. $6.

REVIEWED BY E. R. G. ECKERT[1]

THE book presents friction factors and Stanton numbers for 88 heat-exchanger configurations together with a text explaining the parameters and their use in design calculations. This extensive compilation is the result of research which has been conducted chiefly at Stanford University since 1945. The book contains the following chapters: 1 Introduction; 2 Heat exchanger analysis; 3 Effects of temperature dependent fluid properties; 4 Abrupt contraction and expansion, pressure loss coefficients; 5 Analytical solutions for flow in tubes; 6 Summaries of analyses and experiments for simple geometries; 7 Experimental methods; 8 Heat transfer surface geometry; 9 Heat transfer and flow friction design data.

Chapter 2 contains tables and diagrams for the effectiveness of heat exchangers with various flow arrangements. The designer of heat-transfer equipment can either use the results in Chap. 9 if his geometry is identical with one of the investigated surfaces, or he can deduce heat-transfer performance and pressure loss from the information contained in Chaps. 4 and 6. The presentation of the data for a wide variety of geometries on a unified basis is of great help to the user; it makes, however, some arbitrary decisions unavoidable. Some of the following remarks have to be considered in this light. Others concern a few minor shortcomings in the text which can easily be corrected in a new edition.

The Prandtl numbers and heat conductivities for air contained in Table 25 and Figure 114 are too small, especially at higher temperatures, according to recent investigations. Nothing has been mentioned in Chaps. 5 and 6 on the circumferential distribution of the wall temperature in the rectangular ducts. Recent research has shown that for some duct shapes even average heat-transfer coefficients depend strongly on this boundary condition, especially in laminar flow. Two methods are today primarily in use to account for a temperature dependence of the properties appearing in the dimensionless parameters—to introduce the properties at a reference temperature, or to include a temperature ratio in the relation describing Nusselt number and friction factor. The reference temperature method has proved its value in high-temperature heat transfer for boundary-layer flow and it has also been successfully applied to duct flow. The critical remarks about this method contained in the book appear, therefore, unjustified. The term "number of exchanger heat transfer units" and the notation NTU appear somewhat lengthy and may even lead to confusion in equations. This reviewer feels that it would be very desirable to replace it by a simpler name and notation.

The reports and publications on which this book is based are being used extensively by companies manufacturing heat-exchanger equipment. Design engineers will therefore certainly welcome that this valuable information is now conveniently available in book form.

[1] Professor, Department of Mechanical Engineering, University of Minnesota, Minneapolis, Minn.

Structures

Hyperstatic Structures, Vol. 1. By J. A. L. Matheson. Academic Press, Inc., New York, N. Y., 1959. $15.50.

REVIEWED BY D. C. DRUCKER[2]

THE student of the theory of structures taught in the conventional way as a myriad collection of unrelated theorems and techniques will welcome this text. As the author states, "the purpose of this book is to show how all these theorems fit together into a coherent pattern," some based on equilibrium and some on compatibility approaches.

A knowledge of the elementary theory of structures is assumed and the principle of minimum potential energy for conservative systems is chosen as the starting point. Although inelastic action is then somewhat troublesome to handle and the reviewer much prefers to start instead with the general theorem of virtual work, there is no question but that this is one of the outstanding texts on structures written in English.

The main part of the book consists of the interrelated sections on Castigliano's, Bettis', Mohr's, and Maxwell's theorems, moment distribution, slope deflection, and plastic collapse techniques, and the discussion of trusses, frames, and arches. They are supplemented by a chapter on elastic stability written by N. W. Murray, and a chapter on matrix and computing methods by R. K. Livesley.

Volume 2 will contain worked examples and problems for solution.

Mechanisms

Mechanism and Motion. By K. H. Hunt. John Wiley & Sons, Inc., New York, N. Y., 1959. Cloth, 5½ × 9 in., xiv and 114 pp., illus. $4.25.

REVIEWED BY BURTON PAUL[3]

IN REFERENCE to the study of mechanisms the author states in his preface: "This small subject has been becoming smaller; it has been suffering a decline at a time when nearly every part of the engineering curriculum has been going through a process of active rationalization. The work in kinematic analysis of mechanisms is often uninspired and antiquated. . . ." This quotation reflects a state of affairs equally true of the situation in this country as it is of the British universities, for which the book has been primarily designed. Therefore any attempt to correct the situation will be warmly welcomed by all those seriously concerned with the teaching or practice of mechanical analysis and design.

The book commences with a chapter on vector methods and consistently uses Gibbsian vector notation in the following chapters which cover the vector equations of relative motion, velocity and acceleration images, criteria of freedom and constraint, analysis of specific plane mechanisms, and space mechanisms. The concluding chapter deals with additional topics in plane

[2] Professor, Division of Engineering, Brown University, Providence, R. I.

[3] Assistant Professor of Engineering, Brown University, Providence, R. I.

mechanisms and includes discussions of instant centers, the Euler-Savary equations, substitute mechanisms and the acceleration center.

The most important aim of the book (as stated in the preface) is "to show that our conventional methods of mechanism analysis may be rationalized." That the book is only partially successful in achieving this goal is due in a large measure to its extremely modest size (slightly over 100 pages of text and problems) which precludes coverage of many important topics. For example, there is no treatment of the complex number (phasor) notation which is so prevalent in the current literature. There is, by intent, extremely little material on the central problem of the designer, viz., direct synthesis of mechanisms. Finally, there is a very concise discussion of the Euler-Savary equation and the inflection circle, but there is practically no indication of what use these tools may be put to.

The book contains an interesting assortment of exercises which are intended to supplement the text, as well as a number of "extended exercises" or drawing room projects.

Hypersonic Flow

Hypersonic Flow Theory. By Wallace D. Hayes and Ronald F. Probstein. Academic Press, New York and London, 1959. Cloth, $6^1/_4 \times 9^1/_4$ in., xiv and 469 pp., illus. $11.50.

Hypersonic Aerodynamics. By Robert Wesley Truitt. Ronald Press, New York, N. Y., 1959. Cloth, $6^1/_4 \times 9^1/_4$ in., xii and 462 pp. $10.

REVIEWED BY MILTON VAN DYKE[4]

THESE first two books on hypersonic flow to appear represent, despite their outward similarity, the extremes between which all others now in preparation will certainly fall. One is a scholarly monograph, concerned with fundamental concepts and avoiding empirical results no matter how accurate, and might be used in an advanced graduate course. The other is a textbook suitable for undergraduate instruction, which emphasizes an engineering approach to a variety of practical aerodynamic problems.

The difference between these aims is illustrated by the attitude to that bulwark of hypersonic-flow theory, the Newtonian approximation. Truitt enthusiastically embraces simple Newtonian impact theory which, neglecting Busemann's correction for centrifugal forces, predicts surface pressures proportional to the sine squared of the local angle of incidence. This simple rule can fairly be said to be his basic weapon (although he discusses many other methods), and in writing chapters on complete configurations and on stability and control he has, of course, no other. By contrast, Hayes and Probstein immediately dismiss that rule as having no logical basis in theory, and hence erroneous. Instead, they analyze in detail the somewhat more complicated Newton-Busemann theory, which yields the limit of the exact solution as Mach number becomes infinite and the adiabatic exponent approaches unity. In so doing, they uncover some extraordinary anomalies. The hypersonic engineer has become accustomed to the thought that, in Newton's approximation or its more sophisticated successor, the oncoming fluid condenses into a sheet of zero thickness and infinite density wrapped about the nose of his body. He may be startled to learn, however, that this sheet may in some circumstances undergo a further condensation into a line, and finally even into a point. Hayes and Probstein stoutly defend the theory and, although admitting that such predictions are unrealistic, suggest that they may correspond to significant real phenomena.

[4] Professor of Aeronautical Engineering, Stanford University, Stanford, Calif.

Aside from this basic difference in attitude, both books treat the same subjects to a considerable extent, particularly for inviscid flows. Each devotes a chapter to hypersonic small-disturbance theory and the associated similarity rules and simple solutions, to the notorious blunt-body problem as attacked by both approximate analytical and numerical methods, and to minimum-drag bodies using their respective Newtonian approximations. Hayes and Probstein cover viscous hypersonic flows much more thoroughly, and include a chapter on the numerical method of characteristics and related methods. Truitt considers real-gas effects (including magnetohydrodynamics), and is alone in attacking complete configurations and stability and control.

Hayes and Probstein have written with care and discrimination; the result is a sound scholarly treatment bearing the strong mark of their own personalities. They are particularly to be commended for having critically covered the recent literature, including the Russian. On the other hand, Truitt has to some extent simply assembled his book, which is always hazardous. Thus the hypersonic similarity rule is deduced early in the book by reproducing Tsien's old faulty derivation, and again much later when a paper of the reviewer appears almost verbatim as chapter 8. There are a number of inexact or misleading statements and infelicities of expression; to cite only one, the governing differential equations for inviscid flow are on page 34 termed the Navier-Stokes equations.

The difference in level is so great that few prospective readers will buy both books. The advanced student and researcher need not hesitate: he will reject Truitt as elementary and unsound, and choose Hayes and Probstein to study and criticize. The practicing engineer, on the other hand, will find the latter book completely unreadable, and applaud Truitt for giving him the answers he needs.

Structures

Plastic Analysis of Structures. By P. G. Hodge. McGraw-Hill Book Co., Inc., New York, N. Y., 1959. Cloth, 6×9 in., xiv and 364 pp., illus. $10.50.

REVIEWED BY ARIS PHILLIPS[5]

THIS excellent text is the newest of a number of books on plastic analysis and design of structures which have appeared during recent years. The appearance of these books shows the increasing interest of engineers toward plastic methods of structural analysis.

The book of Professor Hodge is based on the concept of collapse of a structure of a perfectly plastic material. Contained plastic deformations and strain hardening are not discussed. Therefore its scope is more narrow than the scope of the previous texts on plasticity by Hill, Prager-Hodge, and Phillips. On the other hand, its coverage is much wider than that of the books by Beedle and Neal because it covers plates and shells also.

This is a well-written book and it proceeds at a brisk pace so that in its 364 pages a considerable amount of material is covered.

The book is divided into two parts. The first part considers the plastic analysis and design of beams, frames, and arches from the point of view of the elementary bending theory. It includes seven chapters on limit analysis of beams and frames, displacements of plastic beams and frames, general loading, limit design, and axial forces on frames and arches. The first part should be useful to practicing civil engineers.

The second part is devoted to the collapse of structures under combined stresses. In this part the following topics are covered: General theory of combined stresses, beams under combined stresses, bending of plates, limit analysis of shells, problems in

[5] Professor, Yale University, New Haven, Conn.

plane stress, impact loading of plastic structures. Due to the nature of the subject the second part is written at a level considerably more advanced than the first part. It is based on recent research work and should be of great interest to research engineers.

The extensive bibliography and abundant problems add to the value of this book.

Photoelasticity

Praktische Spannungsoptik. By L. Föppl and E. Mönch. Springer Verlag, 1959. Cloth, 6½ × 9½ in., illus., vii and 209 pp. DM 30.

REVIEWED BY GUSTAV MESMER[6]

THE second edition of this book is thoroughly revised and completed. As before, the authors describe their own pertinent research at some length, reporting more briefly on other publications.

Chapter I of Part 1 deals with the instruments (including a new projectory arrangement of lenses and mirrors) and the basic photoelastic facts and measurements. The materials Araldit (made by CIBA, Basel, Switzerland) and VP 1527 (made by Dynamit, Troisdorf, Germany) are recommended and discussed.

Chapter II covers three-dimensional photoelasticity, especially the use of Araldit B in the freezing method.

Chapter III discusses some theoretical and practical aspects of model-similarity, the choice of scale, and the magnitude of errors.

The second part of the book includes short paragraphs concerning mechanical and optical measurements of the sum of the principal stresses, measurement of bending moments in plates, and photoplasticity.

The third part describes some test methods and results of the Munich Photoelastic Laboratory. Some stress problems in gears, foundations, and a plexiglas dome are repeated from the first edition. New tests deal with three-dimensional stresses in helical gears, in the area of a pipe intersection, in a three-dimensional part of the block of a turbine. Interesting two-dimensional examples are a swaybracing wall, gravity stresses in a gelatine model of a dam, and stresses in reinforced concrete.

Summarizing, the reviewer recommends the book to the photoelastic beginner as containing a short, clear, reliable, and rather complete introduction, and to the expert as fairly presenting the present (1959) state of photoelasticity in Germany.

Statistical Physics

Statistical Physics. By Landau and Lifshitz. Addison-Wesley Reading, Mass., and Pergamon Press, New York, N. Y., 1958. Cloth, 6 × 9 in., viii and 484 pp. $12.50.

REVIEWED BY JOHN ROSS[7]

THIS is one of a series of volumes on theoretical physics by Landau and Lifshitz in an English translation. Other volumes available include "Quantum Mechanics," "Fluid Mechanics," and "The Classical Theory of Fields." It has been said, with merit, that these volumes are the most brilliant and authoritative work on theoretical physics since the classical compendium of A. Sommerfeld.

The topics discussed in this volume include not only the standard ones of the Gibbs ensemble distribution, the perfect gas, the real gas and condensation, solids, and solutions, but also excellent vignettes of topics such as quantum fluids and superfluidity, the properties of matter at very high temperatures, fluctuations and their relations to equilibrium as well as transient phenomena, the symmetry of macroscopic bodies, and surfaces. In addition, there are chapters on the thermodynamics of homogeneous and heterogeneous systems. The breadth of applications of statistical mechanics in physics is remarkable and given full display in the book, from the completely ionized gas to the creation of nuclei (in the chapter on surfaces, of course!).

The authors reject the proposition that statistical physics is the least well-founded branch of theoretical physics. They ignore the fact that the formulation of its foundations is disputed and discussed by a large number of physicists, and dismiss the entire issue with the sentence, "We believe that the difficulties are created artificially because the problems are often not stated sufficiently rationally." There is no fooling around here. The critical point is the role of ergodic theory in statistical mechanics. The authors accept the Gibbsian axioms of ensemble theory, and deny the need for solutions of the ergodic problem, at least in physics. (My sentiments are with them until they seek a rationale for the use of ensembles in a thinly disguised ergodic theory.)

Fortunately, the structure and predictions of statistical physics are independent of the arguments surrounding its foundations, and this, the main concern of the book, is given in precise and logical sequence. The depth of understanding by the authors and their ability to convey this on the written page elicit admiration. The highest praise is due the excellent book by Landau and Lifshitz, and it is recommended for its astuteness, insight, and clear presentation.

Heat Transfer

Turbulent Flows and Heat Transfer. Vol. V of High Speed Aerodynamics and Jet Propulsion. Edited by C. C. Lin. Princeton University Press, Princeton, N. J., 1959. Cloth, xvi and 549 pp. $15.

REVIEWED BY J. KESTIN[8]

THIS is vol. 5 of the twelve volumes of the "Princeton Series" which now needs no special introduction to the readers of this Journal. As its title lays down, it deals with:

A Transition from Laminar to Turbulent Flow (H. L. Dryden)
B Turbulent Flow (G. B. Schubauer and C. M. Tchen)
C Statistical Theories of Turbulence (C. C. Lin)
D Conduction of Heat (M. Yachter and E. Mayer)
E Convective Heat Transfer and Friction in Flow of Liquids (R. G. Deissler and R. H. Sabersky)
F Convective Heat Transfer in Gases (E. R. van Driest)
G Cooling by Protective Fluid Films (S. W. Yuan)
H Physical Basis of Thermal Radiation (S. S. Penner)
I Engineering Calculations of Radiant Heat Exchange (H. C. Hottel)

Most reviewers of the series have agreed that, with the number of busy and highly competent contributors, it was not possible to attempt to weld the sections in a particular volume into an organic treatise. In many of the previous volumes it lead to excessive repetition as well as to serious omissions. The present volume is a happy exception in the first respect. It is much more unified than the others and does not suffer from being repetitive. It is not, however, comprehensive and does not give an exhaustive treatment under each heading.

[6] Professor, Department of Applied Mechanics, Washington University, St. Louis, Mo.

[7] Professor, Department of Chemistry, Brown University, Providence, R. I.

[8] Professor, Division of Engineering, Brown University, Providence, R. I.

The existence of turbulent flows was discovered nearly one hundred years ago by O. Reynolds, and yet it is still impossible to indicate a unified theory of transition. The first article by H. L. Dryden pinpoints the reasons for it with great lucidity and in minute detail. In particular, the essentially three-dimensional character of transition and the relation of transition to boundary-layer instability are discussed in simple and clear terms. His conclusions carry with them the weight of authority and one cannot but agree when he states: "... the principal outlines are reasonably clear and the apparently rival ideas are not contradictory but complimentary," and: "Progress in the development of a satisfactory conceptual picture and theory is dependent on progress in the study of nonstationary solutions of the Navier-Stokes equations."

The second section gives a thoughtful description of fully developed turbulent motions, the aim being to "... understand the reason for their behavior, not only to formulate laws for practical use, but to satisfy our desire to know and to be able to explain...". Wherever possible, the presentation is carried out in terms of compressible flows, but often the authors are compelled to revert to the more conventional, incompressible presentation, because many of the fundamental concepts have not yet become satisfactorily transposed to embrace compressible fluids. The contribution includes a well-written section on Reynolds' analogy, a thoughtful discussion of the various empirical laws of wall and wake friction, and an excellent bibliography. It is very complete and informative and constitutes an admirable presentation of the subject. It may be inadequate as a handy reference for practical engineers, but this would be impossible to achieve even in the space alloted to the whole volume.

The reviewer must refrain from making any comments on Section C. On the one hand, the mathematical equipment required is beyond the grasp of average engineers, and on the other, it is difficult to see which contributions from the statistical theories of turbulence can be turned into practical use (in the widest sense of the meaning of the word).

Section D does not attempt to give a general theory of conduction, and readers who expect it might be disappointed, because "the problems discussed ... have been selected on the basis of their immediate applicability to heat flow in combustion chambers and nozzles, in skins of high speed aircraft, turbine blades, etc. Emphasis is placed on simple ...model problems...". If the reader bears this in mind, he will find much to interest him, but the reviewer is surprised that not a single chapter is devoted to dimensional analysis and that the presentation is couched in almost exclusively analytic terms.

Section E is rather disappointing and far too short for its scope; it ends with a discussion of nucleate boiling. Problems of forced convection in gases, i.e., compressible fluids, have been concentrated in Section F. Their treatment is not comprehensive but the most important results for laminar and turbulent compressible boundary layers have been included. The subject is developed analytically with careful comparisons with experimental measurements discussed at every step. Chapter 2 is devoted to engineering applications (aerodynamic heating, heat transfer in rocket motors) and to a very brief discussion of dissociation effects. Problems of transpiration cooling are discussed in Section G.

The very short Section H gives a brief summary of the laws of radiation as derived from Planck's distribution law and then concentrates on theoretical calculations of gas emissivities presented in the form of a qualitative outline. Section I concentrates on the conventional and most practical methods of calculating the exchange of heat by radiation. This section too, is very short.

The volume, as a whole, is very useful and worth having. The reviewer regrets that the phrase "space does not permit" occurs far too frequently for a 12-volume work running well into 8000 pages.

Journal of APPLIED MECHANICS

Information for Authors

• Manuscripts should be submitted in final form to the Technical Editors. Each manuscript must be accompanied by a statement that it has not been published elsewhere nor has it been submitted for publication elsewhere. A paper which would occupy more than five pages of the Journal may be returned to the author for abridgment.

• The author should state his business connection, the title of his position, and his mailing address. A short abstract (50 to 100 words) should be included on the first page immediately preceding the introductory paragraph of the paper.

• Three copies of the manuscript are required. One of these must be a carefully prepared printer's copy, typed in double spacing, on one side of the page only, with wide margins, on $8^1/_2$ by 11-in. opaque white paper. Mimeographed manuscripts, if prepared with exceptional care, can be accepted provided they are completely edited.

• As far as possible, all mathematical expressions should be typewritten. Greek letters and other symbols not available on the typewriter should be carefully inserted in ink. Care should be taken to distinguish between capital and lowercase letters, between zero (0) and the letter (*O*), between the numeral (1) and the letter (*l*), etc. A letter representing a vector cannot be printed with an arrow above or below it. The letter should be underscored with a single wavy line, wherever it appears in the text, to designate boldface type. A list of symbols carefully marked for the use of the editor (thus: κ, Greek l.c. kappa), if it has not been included in the body of the paper, should accompany the manuscript on a separate page.

• Before preparing a manuscript the author should study printed articles in the Journal, with special attention to the form and style of mathematical expressions, tables, footnotes, references, and abstract. Numbers that identify mathematical expressions should be enclosed in parentheses. Numbers that identify references at the end of the paper should be enclosed in brackets. Care should be taken to arrange all tables and mathematical expressions in such a way that they will fit into a single column when set in type. Equations that might extend beyond the width of one column (fractions that should not be broken or long expressions enclosed in parentheses) should be rephrased to go on two or more lines within column width. Fractional powers are preferred to root signs and should always be used in more elaborate formulas. The solidus should be used instead of the horizontal line for fractions wherever possible.

• A normal paper should not exceed five pages in the Journal. It is about 6000 words or twenty to twenty-five double-spaced typewritten pages inclusive of drawings. A Brief Note should not exceed 750 words or about one column in the Journal inclusive of drawings.

• Originals and two copies of figures must accompany the manuscript. Line drawings should not be larger than $8^1/_2 \times 11$ inches and should be planned for reduction to column width. Lettering should be large enough to be clearly legible when the illustration is reduced. The originals of line drawings must be in India ink on white or pale blue tracing paper or tracing cloth. Photographs of equipment or test specimens must be glossy prints and should be used sparingly. Captions for figures should be typed double-spaced and included as the last page of the manuscript. The figure number and author's name should be written in the margin or on the back of each illustration.

• Titles of papers should be brief.

• Authors can obtain copies of the ASME Manual MS-4, "An ASME Paper," from the Technical Editors and are urged to do so before drafting their papers in final form.

• Papers published in the Journal of Applied Mechanics must be presented at a Meeting, either in person or by title. Scheduling of papers is in the hands of the Secretary of the Applied Mechanics Division. Authors should indicate their preference in this respect to the Technical Editors when submitting a paper.

• An author is entitled to 25 preprints free of charge (in the case of two authors, 15 each; three or more authors, 10 each). Larger quantities of preprints or reprints can be ordered from Editorial Department, The American Society of Mechanical Engineers, 29 West 39th Street, New York 18, N. Y. Quotations will be sent on request.

ASME Publications Committee

Please address all communications to:

Technical Editors

Journal of Applied Mechanics, ASME

Division of Engineering

Brown University

Providence 12, R. I.

Journal of ENGINEERING FOR POWER

Series A of the ASME Transactions

The subjects covered by this Journal are: Power generation and usage; conversion of energy sources to power generation; hydraulic prime movers; pumping machinery; compressors; design, operation, and application of all types of gas turbine prime movers; preparation and use of fuels; fuel burning equipment design and operation; control and utilization of the products of burning processes; application of nuclear energy; reactor design, components and techniques; reactor safeguards; waste disposal and radiation hazards; internal combustion engines and auxiliaries—their design construction, application, and operation; air pollution problems; solar energy application.

Published in January, April, July, and October. Annual subscription price: $10* to nonmembers, $5* to ASME members.

Journal of HEAT TRANSFER

Series C of the ASME Transactions

Covers the activities of the heat transfer field and particularly important problems associated with radiation, conduction, convection, complex systems, phase changes and mixtures, transient phenomena, thermophysical properties, experimental techniques, thermometry, analog methods, analytical and numerical methods, applications, design techniques, heat exchangers, insulation, economic factors, biotechnology, astronautics.

Published in February, May, August, and November. Annual subscription price: $10* to nonmembers, $5* to ASME members.

***NOTE: Annual subscription price of any two of the ASME Transactions Series $18, of any three $25, of any four $30, of all five $33. To ASME members prices are 50% less. Additional postage outside the U.S.: 50¢ for each Journal.**

Journal of BASIC ENGINEERING

Series D of the ASME Transactions

Provides authoritative information on developments in the following areas of the mechanical engineering field: Lubrication; fluid mechanics; water hammer; cavitation; fundamental researches in hydrodynamics; instruments and automatic controls; new metals, metal-forming processes and testing procedures, and better engineering application of metals. Research reports on automatic regulation theory, effect of temperature on the properties of metals, mechanical pressure elements, fluid meters, prevention of fracture in metals, and plastic flow of metals will also be published in this quarterly.

Published in March, June, September, and December. Annual subscription price: $10* to nonmembers, $5* to ASME members.

Journal of ENGINEERING FOR INDUSTRY

Series B of the ASME Transactions

Here will be found reports of major advances and original information on certain aspects of aircraft and missile design; machine design; mechanical engineering phases of process industries, with emphasis on unit operations; maintenance and plant engineering; management procedures and skills; human engineering factors; materials handling equipment and techniques; machining and assembly of metal parts, with their related problems; manufacture and use of rubber and plastics relating to mechanical engineering; special areas of the petroleum field; safety; textile machinery and procedures; wood utilization and wood working machinery, and operation.

Published in February, May, August, and November. Annual subscription price: $10* to nonmembers, $5* to ASME members.

Engineers everywhere find these eight ASME technical publications unsurpassed in their usefulness. The timely, authoritative information in their pages enables each reader to keep abreast of developments in his own highly specialized field and to have the broadest possible grasp of significant progress throughout the mechanical engineering field.

If you are not taking advantage of the help these recognized leaders offer, ASME invites you to do so. Your instructions should be sent to:

THE AMERICAN SOCIETY OF MECHANICAL ENGINEERS
29 W. 39th St., New York 18, N. Y.

Journal of APPLIED MECHANICS

Series E of the ASME Transactions

Here will be found fundamental analytical and experimental studies in the fields of elasticity, plasicity, dynamics, vibration, impact, flow and fracture, structures, stress analysis, mechanical properties of materials, hydraulics, aerodynamics, internal flow, turbulence, boundary layers, aeroelasticity, thermodynamics, heat transfer, lubrication and wear, and computing devices and methods.

Where subjects overlap the fields covered by the other publications of this Series, the Journal of Applied Mechanics will deal with the basic laws and the more advanced methods of studying problems.

Published in March, June, September, and December. Annual subscription price: $10* to nonmembers, $5* to ASME members.

MECHANICAL ENGINEERING

This magazine is of prime interest to mechanical engineers regardless of their own specialized line or industry because it gives them the essence of the things that really count in engineering practice. The information is presented in clear, concise, and well illustrated articles; news items drawn from current engineering periodicals and other sources; surveys of engineering progress in the British Isles and Western Europe; digests of papers presented at ASME Meetings; annotated photographs which transmit useful information on equipment location and arrangement, materials and other engineering tools; letters from readers on a variety of subjects; and comprehensive book reviews.

Published monthly. Annual subscription price: $7 to nonmembers. Price of one subscription is included in membership dues. For each additionel subscription, member's price is $5.60. Extra postage outside of U. S.: $1.50.

APPLIED MECHANICS Reviews

The unique, unmatched, reviewing service offered by this magazine enables engineers to keep posted on worldwide developments in applied mechanics, both in its established boundaries and wherever it cuts through other fields of scientific and engineering endeavor. The technical contributions reviewed in this magazine are selected from over a thousand sources, including 750 engineering periodicals in 37 countries devoted wholly or in part to the field, new books containing pertinent information, and reports of industrial specialists everywhere. Over 400 reviews, are published monthly, highlighted by an article which surveys and evaluates progress in a specialized area.

Published monthly. Annual subscription price: $25 to nonmembrs, $10 to ASME members.

PMM Journal of APPLIED MATHEMATICS AND MECHANICS

This bimonthly contains the important findings of Russian scientists and engineers working in the fields of applied mathematics, fluid and solid mechanics, aeronautical sciencies, astronautics, rocketry and space flight. It is a cover-to-cover translation of the Journal entitled "Prikladnaya Matematika i Mekhanika" which has been for over two decades one of the leading Soviet periodicals in the fields.

This translation series began with Volume 22 (1958) and is being published bimonthly or corresponding to the number of original Russian issues per annum. All subscriptions are on a calendar year basis.

Annual subscription price: $35 to nonmembers, $28 to ASME members.